BENEATH THE TIP OF THE ICEBERG – EMPHASIZING THE ROLE OF METABOLITES IN PHYSIOLOGICALLY BASED PHARMACOKINETIC MODEL DEVELOPMENT

DISSERTATION

zur Erlangung des Grades des Doktors der Naturwissenschaften
der Naturwissenschaftlich-Technischen Fakultät
der Universität des Saarlandes

von
Fatima Zahra Marok
Diplom-Apothekerin (Dipl.-Pharm.)

Saarbrücken
2024

Die vorliegende Arbeit wurde von April 2019 bis September 2022 unter Anleitung von Herrn Professor Dr. Thorsten Lehr in der Fachrichtung Klinische Pharmazie der Naturwissenschaftlich-Technischen Fakultät der Universität des Saarlandes angefertigt.

Tag des Kolloquiums:	05.11.2024
Dekan:	Prof. Dr.-Ing Dirk Bähre
Berichterstatter:	Prof. Dr. Thorsten Lehr Prof. Dr. Markus R. Meyer Prof. Dr. Matthias Schwab
Vorsitz:	Prof. Dr. Marc Schneider
Akad. Mitarbeiterin:	Priv.-Doz. Dr. Jessica Hoppstädter

INCLUDED PUBLICATIONS

The following research articles [1–3] published in peer reviewed journals were included in this thesis:

RESEARCH ARTICLE I – BUPROPION: Marok FZ, Fuhr LM, Hanke N, Selzer D, and Lehr T. Physiologically Based Pharmacokinetic Modeling of Bupropion and Its Metabolites in a CYP2B6 Drug-Drug-Gene Interaction Network. *Pharmaceutics*. 2021; 13(3):331. https://doi.org/10.3390/pharmaceutics13030331.

RESEARCH ARTICLE II – KETOCONAZOLE: Marok FZ, Wojtyniak JG, Fuhr LM, Selzer D, Schwab M, Weiss J, Haefeli WE, and Lehr T. A Physiologically Based Pharmacokinetic Model of Ketoconazole and its Metabolites as Drug-Drug Interaction Perpetrators. *Pharmaceutics*. 2023; 15(2):679. https://doi.org/10.3390/pharmaceutics15020679.

RESEARCH ARTICLE III – 5-FLUOROURACIL AND URACIL: Marok FZ, Wojtyniak JG, Selzer D, Dallmann R, Swen JJ, Guchelaar HJ, Schwab M, and Lehr T. Personalized Chronomodulated 5-Fluorouracil Treatment: A Physiologically Based Pharmacokinetic Precision Dosing Approach for Optimizing Cancer Therapy. *Clinical Pharmacology and Therapeutics*. 2024; 0:1–11. https://doi.org/10.1002/cpt.3181.

CONTRIBUTION REPORT

According to the contributor roles taxonomy (contributor roles taxonomy (CRediT)) [4], the author Fatima Zahra Marok would like to declare her contributions to the above mentioned research articles included in this thesis:

RESEARCH ARTICLE I – BUPROPION: Conceptualization, Investigation, Visualization, Writing-Original Draft, Writing-Review and Editing.

RESEARCH ARTICLE II – KETOCONAZOLE: Conceptualization, Investigation, Visualization, Writing-Original Draft, Writing-Review and Editing.

RESEARCH ARTICLE III – 5-FLUOROURACIL AND URACIL: Conceptualization, Investigation, Visualization, Writing-Original Draft, Writing-Review and Editing.

ABSTRACT

Metabolites can provide unique insights for drug discovery and development (D3) processes and their roles are well reflected and addressed in several respective regulatory guidance documents. Currently, there is no explicit guidance for investigating metabolites in the context of physiologically based pharmacokinetic (PBPK) modeling with no mention thereof in dedicated regulatory PBPK modeling guidelines. With PBPK modeling becoming an integral part in D3, its usefulness in estimating various drug interaction scenarios is well recognized in several clinical guidance documents by regulatory agencies. Consequently, understanding the contributions of a parent drug's metabolite(s) is helpful for a thorough and mechanistic model development. To highlight the significance of metabolites in PBPK model analyses, particularly for drug interactions, parent-metabolites PBPK models were developed for the antidepressant bupropion, the antimycotic ketoconazole and the anticancer drug 5-fluorouracil alongside its endogenous biomarker uracil. In this context, inclusion of metabolites was crucial to implement and evaluate drug interactions and subsequent model applications such as model-based dose adjustments. This thesis outlines a blueprint for determination of a metabolite's role and need for its inclusion in PBPK model development, drawing insights from the presented projects.

ZUSAMMENFASSUNG

Metabolite können wichtige Einblicke in die Entdeckung und Entwicklung von Arzneimitteln (AM) liefern. Ihre Rolle wird in mehreren einschlägigen regulatorischen Leitfäden gut reflektiert und behandelt. Derzeit gibt es keine explizite Anleitung für die Untersuchung von Metaboliten im Rahmen der Physiologie-basierten pharmakokinetischen (PBPK) Modellierung. Auch in den speziellen regulatorischen PBPK-Modellierungsleitlinien werden sie nicht erwähnt. Da die PBPK-Modellierung mittlerweile ein integraler Bestandteil der Arzneimittelentwicklung ist, wird ihre Nützlichkeit bei der Abschätzung verschiedener AM-Interaktionen in mehreren klinischen Leitfäden der Zulassungsbehörden anerkannt. Daher ist es für eine ausführliche und mechanistische Modellentwicklung hilfreich, die Metaboliten einer Ausgangssubstanz zu verstehen. Um die Bedeutung von Metaboliten in PBPK-Modellanalysen hervorzuheben, wurden entsprechende PBPK-Modelle für das Antidepressivum Bupropion, das Antimykotikum Ketoconazol und das Zytostatikum 5-Fluorouracil sowie dessen endogenen Biomarker Uracil entwickelt. Hier war die Einbeziehung von Metaboliten entscheidend AM-Interaktionen zu implementieren und zu bewerten sowie Modellanwendungen wie modellbasierte Dosierungsanpassungen abzuleiten. Diese Arbeit präsentiert ein Konzept zur Bestimmung der Rolle eines Metaboliten und Notwendigkeit seiner Einbeziehung in die Entwicklung von PBPK-Modellen unter Verwendung der Erkenntnisse aus den vorgestellten Projekten.

GRAPHICAL ABSTRACT

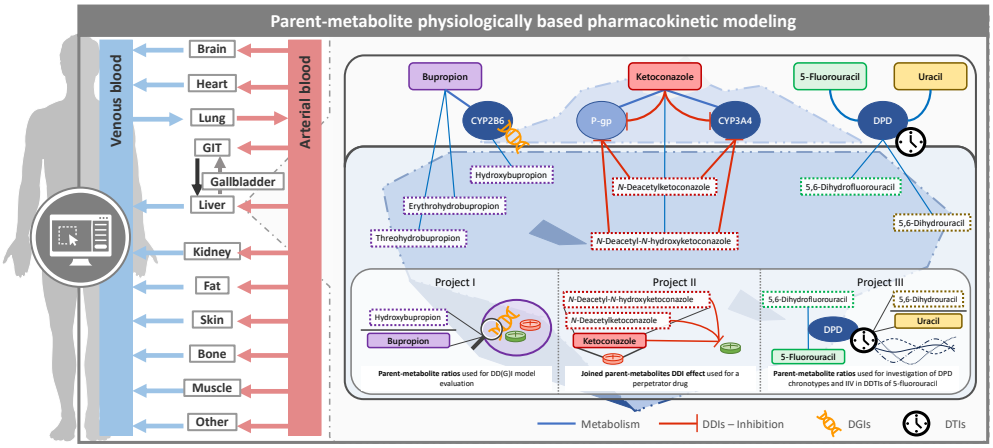

Figure 1: Graphical abstract. CYP: cytochrome P450, DD(G)I: drug-drug-gene interaction, DDTI: drug-daytime interaction, DPD: dihydropyrimidine dehydrogenase, IIV: interindividual variability, P-gp: P-glycoprotein.

CONTENTS

LIST OF FIGURES

ACRONYMS

AADAC	arylacetamide deacetylase
ADME	absorption, distribution, metabolism, and elimination
ADRs	adverse drug reactions
AUC	area under plasma concentration-time curve
BCRP	breast cancer resistant protein
CNVs	copy number variations
CPIC	Clinical Pharmacogenetics Implementation Consortium
CRediT	contributor roles taxonomy
CYP	cytochrome P450
DDIs	drug-drug-interactions
DDGIs	drug-drug-gene interactions
DDTIs	drug-daytime interactions
DGIs	drug-gene-interactions
DHU/U	ratio of dihydrouracil and uracil
DNA	deoxyribonucleic acid

DPD	dihydropyrimidine dehydrogenase
DPH	dihydropyrimidinase
DPWG	Dutch Pharmacogenetics Working Group
DPYD	gene coding for DPD
D3	drug discovery and development
EMA	European Medicines Agency
FDA	Food & Drug Administration
FdUMP	5-fluoro-desoxy-uridine monophosphate
FdUTP	5-fluoro-desoxy-uridine triphosphate
FMO	flavin-containing monooxygenases
FUTP	5-fluoro-uridine triphosphate
GMFE	geometric mean fold error
HBup/Bup	ratio of hydroxybupropion to bupropion
HSD	hydroxysteroid-dehydrogenase
IC50	half maximal inhibitory concentration
InDels	insertions and deletions
IIV	Interindividual variability
MID3	model informed D3
MRD	multi-drug-resistance protein
mRNA	messenger ribonucleic acid (RNA)
MSA	median symmetric accuracy
OATP	organic anion transporting polypeptides
PGx	pharmacogenetics
P-gp	P-glycoprotein
PBMCs	peripheral blood mononuclear cells
PBPK	physiologically based pharmacokinetic modeling
PD	pharmacodynamics
PK	pharmacokinetics
QSAR	quantitative structure-activity relationship
RNA	ribonucleic acid
SLC	solute carrier transporter
SNPs	single nucleotide polymorphisms
SULT	sulfotransferase
UGT	uridine diphosphate-glucuronosyltransferase
U-PGx	Ubiquitous Pharmacogenomics

1 INTRODUCTION

1.1 MOTIVATION: METABOLITES – TRASH OR TREASURE?

Metabolites, commonly perceived as simple byproducts of drug metabolism meant for degradation and elimination, hold significant biological importance beyond their initial characterization. While metabolites couldn't be further from biological "trash", the investigation into their roles are often limited, overlooked, or misinterpreted. This is especially the case for metabolite-metabolites, which are rarely considered in drug investigation. However, their contribution to understanding, developing and improving drug design could be very beneficial. A prime example would be pharmacologically active metabolites, that not only add to a parent's therapeutic effect but help understand occurrence for adverse drug reactions (ADRs) [5].
For example in case of tamoxifen, used in breast cancer therapy, its metabolite endoxifen exhibited strong antiestrogenic activity [6]. Therefore, understanding tamoxifen's efficacy and safety is closely linked to understanding its metabolite endoxifen, especially its formation via the highly polymorphic cytochrome P450 (CYP) 2D6 [6, 7]. Currently under investigation as an administered anticancer drug itself, endoxifen was also tested for oral treatment of mania in bipolar disorders [6, 8].
Another example is terfenadine and its metabolite fexofenadine. Terfenadine, a second-generation antihistaminic drug and CYP3A4 substrate, is prone to drug interactions with its potentially elevated exposure linked to cardiotoxic side effects, prolongation of QT interval in particular [9–11]. Its pharmacologically active metabolite fexofenadine not only showed great therapeutic efficacy and tolerability, as it doesn't cross the blood-brain barrier, it's also not associated with the cardiotoxic side effects of its parent. As fexofenadine has been successfully used as an antihistamine for decades, it illustrates the pivotal role metabolites could possess in their parent's pharmacodynamics [12, 13].
Likewise, metabolites demonstrate significant pharmacokinetic relevance, including active roles in drug-drug-interactions (DDIs) as enzyme or transporter perpetrators, or as biomarkers for assessing drug metabolism, such as of phenotyping methods [14–17]. This highlights their rather treasurable role for drug discovery and development.

1.2 CREATION OF METABOLITES AND METABOLIZING ENZYMES

Metabolism and Metabolic Reactions

Metabolism represents our body's fundamental engine consisting of various biochemical processes. The creation of metabolites, whether of endogenous or administered substances, mainly entails the parent's its hydrophilic break down in order to facilitate its elimination from the body or its bioactivation to active compounds. The biodegradation, so called catabolism, and the bioactivation, known as anabolism, can be seen as two sides of the same coin representing an organisms' profound ability and necessity of maximizing the accumulation of energy and minimizing the loss of energy [18].

Alongside the liver, the most prominent site of metabolism in mammals, metabolism occurs in many organs and tissues, such as the intestines, skin, lung, or blood [19]. Here, expression and activity of several enzymes catalyzing metabolic reactions have been identified. These have historically been categorized as phase-I-, and phase-II-biotransformations. More recently, additional categories, such as phase-0 and phase-III, have been discussed. These biotransformations can occur sequentially or simultaneously [20].

Phase-I metabolic reactions mainly aim to increase the water solubility and the polarity of a compound through hydrolysis, oxidation and reduction [21, 22]. Enzymes catalyzing phase-I-transformations include CYP enzymes or flavin-containing monooxygenases (FMO) [18].

Cytochrome P450 Enzymes

Prominent examples of CYP enzymes are CYP3A4 and CYP2B6. CYP3A4, a key CYP enzyme, metabolizes a broad range of drugs. It is responsible for about 40% of the CYP-mediated metabolism of the top 200 prescribed drugs as well as 64% of drugs approved by the Food & Drug Administration (FDA) from 2005 to 2016 [23]. CYP3A4 is known for its key role in DDIs, which can occur when multiple drugs are given concomitantly. Another example is CYP2B6, as it plays an important role in project I. Similar to CYP3A4, CYP2B6 is prone to DDIs. On average, CYP2B6 contributes around 2–10% to total hepatic CYP contents [24]. Furthermore, CYP2B6 is subject to genetic polymorphisms causing significant changes in its activity [25].

Dihydropyrimidine dehydrogenase

An interesting example of an enzyme known for phase-I-reactions other than CYP enzymes is dihydropyrimidine dehydrogenase (DPD). DPD is the rate-limiting enzyme in the metabolism of uracil and a key element in regulation of nucleobase levels [26]. Moreover, DPD is mainly responsible for the detoxification of 5-fluorouracil, a well-established anticancer agent [26]. Similarly, DPD can be affected by several drug-interactions, where it's most known to be affected by drug-gene-interactions (DGIs), which often necessitate dose adaptations for anticancer agents such as 5-fluorouracil and its prodrug capecitabine [15].

Uridine diphosphate-glucuronosyltransferase enzymes

Conversely, phase-II-reactions typically form conjugates for excretion through processes such as glucuronidation, methylation or sulfation [21, 22]. For instance, the uridine diphosphate-glucuronosyltransferase (UGT) and the sulfotransferase (SULT) as metabolizing enzymes are responsible for phase-II-transformations [18]. These processes constitute the majority of non-CYP-mediated metabolism, with UGT enzymes covering 45% of the metabolism for the 200 most prescribed drugs [23]. UGTs are primarily expressed in liver cells, but they are also found in other organs such as the intestines and kidney [27]. Similar to CYP enzymes, they exhibit a wide substrate specificity, illustrating their versatility. Prominent examples are the UGT1A isoforms, such as UGT1A1 or UGT1A4, as well as UGT2B7 [27].

P-glycoprotein

Phase-0 and phase-III interactions mainly describe detoxification or excretion processes compared to the metabolic reaction of phase-I- and phase-II-reactions. Here, compounds are actively transported for uptake and elimination for example by the multi-drug-resistance protein (MRD) or solute carrier transporter (SLC) families [20]. For example, MRD1, or also known as P-glycoprotein (P-gp), is a vital efflux transporter extensively distributed across various tissues, such as the intestines and kidney. It plays a key role in the body's blood-brain barrier forming an essential defense mechanism against potentially harmful compounds [20, 28].

This work includes several examples from phase-I, -II, as well as -0 and -III reactions in the presented projects. These reactions were relevant, as they describe the formation of metabolites and are often involved in drug interactions occurring due to genetic polymorphisms, co-medication, as well as time-of-day variations. While (patho-)physiological implications such as hepatic or renal impairment, as well as age-related factors, such as enzyme expression in pediatric patients, can gravely impact the formation and activity of metabolites [29], the main focus of the presented work lies upon drug-interactions occurring regardless of a patient's disease state or age, such as DGIs, DDIs, drug-drug-gene interactions (DDGIs) as well as drug-daytime interactions (DDTIs).

1.3 ROLE AND IMPACT OF METABOLITES WITHIN DRUG INTERACTION SCENARIOS

Several factors, including genetic polymorphisms, polymedication and diurnal variations, can contribute to drug interactions impacting the formation of metabolites as shown in Figure 1.1. Especially, for understanding a drug's efficacy and safety, primarily the risk for adverse drug reactions (ADRs), investigating the interactive role of

metabolites within these scenarios is crucial.

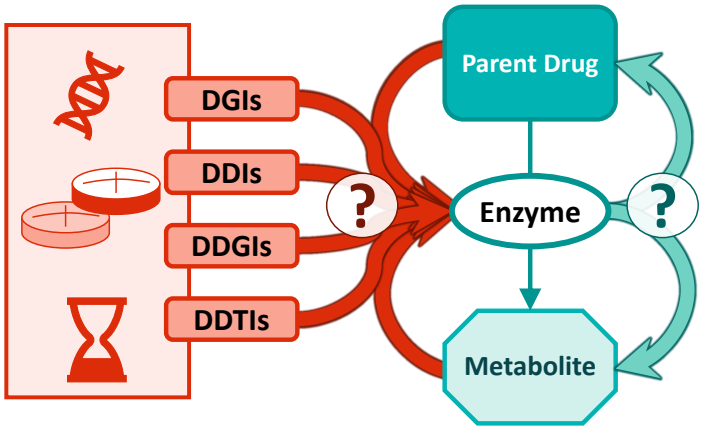

Figure 1.1: Overview on drug interaction scenarios. Drug interactions which occur due to genetic polymorphisms, polymedication or diurnal variations can result in unknown effects on drug metabolism. Moreover, parent drugs and metabolites themselves can impact the respective metabolizing enzyme as well. The outcome of all of these factors especially when occuring at the same time is often unknown and complex to assess [1–3, 30]. DDIs: drug-drug interactions, DDGIs: drug-drug-gene interactions, DDTIs: drug-daytime interactions, DGIs, drug-gene interactions.

1.3.1 *Drug-Gene Interactions*

Drug-Gene-Interactions and Adverse Drug Reactions

DGIs describe the occurrence of genetic alterations that can impact the pharmacokinetics (PK) or pharmacodynamics (PD) of a compound. As a global phenomenon, genetic polymorphisms can occur in all ethnicities with varying distributions [30, 31]. Here, genetic alterations can affect protein expressions relevant to absorption, distribution, metabolism, and elimination (ADME) processes [30]. DGIs can pose a concerning risk for ADRs, potentially resulting in hospitalizations and fatalities. Approximately, 60% of ADRs occurring annually are attributed to pharmacogenomics, meaning the drug response affected by the genome [32].

Although, drug labels increasingly incorporate information on DGIs, and organizations such as the Clinical Pharmacogenetics Implementation Consortium (CPIC) or the Dutch Pharmacogenetics Working Group (DPWG) regularly publish pharmacogenetic guidelines, genetic testing prior to treatment remains mandatory only for a few drugs. This oversight of potential DGIs can lead to inappropriate drug prescriptions in 60–80% of cases [15, 32, 33].

Genetic Testing and Genotype-Guided Drug Therapy

However, genetic testing holds an invaluable potential in reducing the incidence of ADRs, as shown by Swen et al. [33], wherein the prospective clinical trial (PREPARE study under the Ubiquitous Pharmacogenomics (U-PGx) project), patients were tested for genetic variants for a variety of pharmacogenes before undergoing drug treatment. Here, a genotype-guided drug therapy led to a significant reduction in ADRs compared to the control group (odds ratio of 0.70 [95% CI 0.61-0.79]; p <0.0001; 3342 patients receiving genotype-guided treatment and 3602 patients receiving standard care) [33]. Given that a majority of metabolism-related proteins are associated with DGIs, Swen et al. included genes coding for metabolizing enzymes – such as CYP2B6, CYP2C9, CYP2C19, CYP2D6, CYP3A5, DPD and UGT1A1, in the gene panel tested within the PREPARE study [33].

Genetic Polymorphisms of CYP2B6 and Resulting Parent/Metabolite Ratios

Polymorphisms underlying these genetic variants can include single nucleotide polymorphisms (SNPs), copy number variations (CNVs) or insertions and deletions (InDels) [34]. SNPs for example are responsible for genetic alteration in the highly polymorphic gene expressing CYP2B6 (*CYP2B6)* and can lead to decreased and increased enzyme activity. As a result, poor, intermediate, normal and rapid metabolizer CYP2B6 phenotypes have been observed, with the *CYP2B6*1*, **4*, **5* and **6* variants being prevalent in European populations. Here, they occur with frequencies of 49%, 4%, 12% and 23% respectively [25, 35].
Table 1.1 lists CYP2B6 genotypes with their corresponding phenotypes according to CPIC, while the distributions of the resulting phenotypes are illustrated for multiple populations in Figure 1.2.

Table 1.1: *CYP2B6* Genotype – Phenotype Relationship

CYP2B6 genotype	CYP2B6 phenotype
**6* | **6*	Poor Metabolizer
**1* | **6*, **4* | **6*, **5* | **6*	Intermediate Metabolizer
**1* | **1*, **1* | **5*, **5* | **5*	Normal Metabolizer
**1* | **4*, **4* | **5*	Rapid Metabolizer
**4* | **4*	Ultrarapid Metabolizer

Information gathered from [25, 35, 36]. CYP: cytochrome P450

In the case of bupropion, identified as a sensitive substrate of CYP2B6 [37], variations in plasma levels of hydroxybupropion, a pharmacologically active metabolite primarily formed by CYP2B6-mediated metabolism, have been observed. For example, homogenous or even heterogenous expression of the *CYP2B6*4* haplotype could lead to an up to 153% higher ratio of hydroxybupropion to bupropion (HBup/Bup) area under plasma concentration-time curve (AUC)($AUC_{HBup/Bup}$), while homozygous *CYP2B6*6* expression resulted in to 31% lower $AUC_{HBup/Bup}$ compared to wildtype [25, 38].

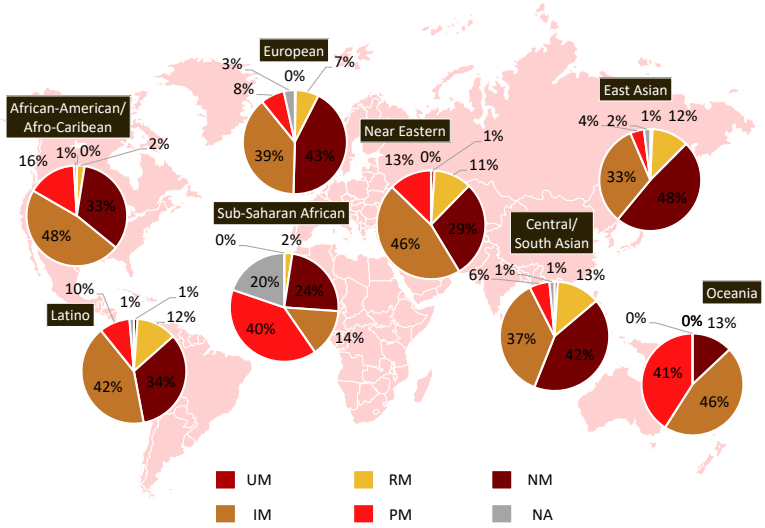

Figure 1.2: Global CYP2B6 phenotype distribution [31]. *IM: CYPB6 intermediate metabolizer, NA: not determined CYP2B6 metabolizer, NM: CYP2B6 normal metabolizer, PM: CYP2B6 poor metabolizer, RM: CYP2B6 rapid metabolizer, UM: CYP2B6 ultrarapid metabolizer.*

1.3.2 *Drug-Drug Interactions*

Drug-Drug-Interactions and Adverse Drug Reactions

The interaction of two or more drugs is often referred to as DDIs. Similar to DGIs, DDIs can pose a serious threat to a patient's health. According to an analysis by Magro et al. (2021) 72% of reported ADRs were related to DDIs, of which 73% were classified as serious ADRs [39]. Geriatric patients are particularly susceptible to DDIs, as multimorbidity and resulting polymedication can create a convenient environment. Here, an analysis by Bronskill et al. (2012) found that the majority of older adults between 75 and 85 years received at least five prescribed drugs [40]. Especially patients in long-term care are vulnerable towards DDIs, as they received around nine or more medications [40].

Role of Drug-Drug-Interaction Partners by Regulatory Agencies

Here, different roles can be attributed to a drug within a DDIs scenario, such as substrate, inhibitor and inducer [30]. Inhibitors can operate in reversible and irreversible mechanisms, which can include competitive, uncompetitive or mechanism-based inhibitions as well as down regulation, whereas inducer drugs lead to an increased amount of the respective protein by amplifying its gene expression [14, 30]. The US American FDA lists clinically relevant substrates, inhibitors and inducers [37, 41]. Alongside its "Guidance for Industry", the FDA provides considerations for evaluating pharmacokinetic CYP- and transporter-mediated DDIs for investigation of new drug applications during drug development and communication of essential information in drug labelling [41]. Moreover, food ingredients were observed to participate in drug interactions as well, e.g. *grapefruit juice* is known to mediate

down-regulations of enzymes, namely CYP3A4, as it is the case for plenty drug-grapefruit interaction scenarios, for example with CYP3A4 victim drugs felodipine or midazolam [42, 43].

Ketoconazole's Joined Parent-Metabolites DDI Effect

Among clinically relevant perpetrator drugs, some have been observed to inhibit their own metabolism (auto-inhibition), for example ketoconazole or auto-inductions such as carbamazepine [2, 14, 44]. In case of ketoconazole, it inhibits its own metabolism via CYP3A4 and its own transport via P-gp. Here, CYP3A4 and P-gp-mediated auto-inhibition can be partially attributed to ketoconazole's metabolite N-deacetlyketoconazole, as reversible inhibition of CYP3A4 and P-gp among other proteins was observed by both parent and metabolite *in-vitro* [14].
When administered with other CYP3A4 or P-gp victim drugs, ketoconazole can lead to significant changes in victim drug exposure, deserving its title as an index inhibitor of CYP3A4-mediated metabolism for use in clinical DDIs studies as suggested by the FDA [37, 45].
For example, bidaily administration of ketoconazole led to an increase of midazolam AUC by 12-fold when given concomitantly [46]. Even with dosing time gaps between perpetrator and victim drug, ketoconazole showed great inhibitory potential, as shown by a reported AUC increase by 6–8-fold of oral alfentanil given in the morning with the last ketoconazole administration the evening before [45].

1.3.3 *Drug-Drug-Gene Interactions*

Unknown Impact of Drug-Drug-Gene-Interactions

DDGIs describe the often very complex interplay of DGIs and DDIs. Here, perpetrator drugs alongside the occurrence of pharmacokinetically relevant polymorphisms can result in unforeseen effects on a drug's exposure and potentially pharmacological efficacy and toxicity. Dosing guidelines seldom address DDGIs and such interactions are frequently overlooked in clinical drug safety assessment. Usually, either DGIs or DDIs are investigated separately as both simultaneously could result in a vast number of potential combinations, infeasible in testing in a clinical setting [30]. Regardless of the combinatorial explosion of DDGIs scenarios, extrapolating DDGIs from a clinical setting (e.g. healthy male adults) to real-world patients, poses limitations, as additional unknown DDIs and DGIs could occur. An approach to investigate, understand and predict the risk of ADRs due to DDGIs is the currently ongoing European-wide project SafePolyMed. The project aims to develop software tools using real-world data to help patients manage their medication and educate them regarding DDGIs [47].
To illustrate the possibilities for DDGIs to occur, Figure 1.3 provides a ranking of top genes impacted by pharmacogenetics (PGx) and CYP enzymes related to DDIs.

For instance, CYP enzymes, such as CYP2D6, CYP2C19, CYP2C9, CYP3A5 as well as CYP2B6 have been identified in both rankings,

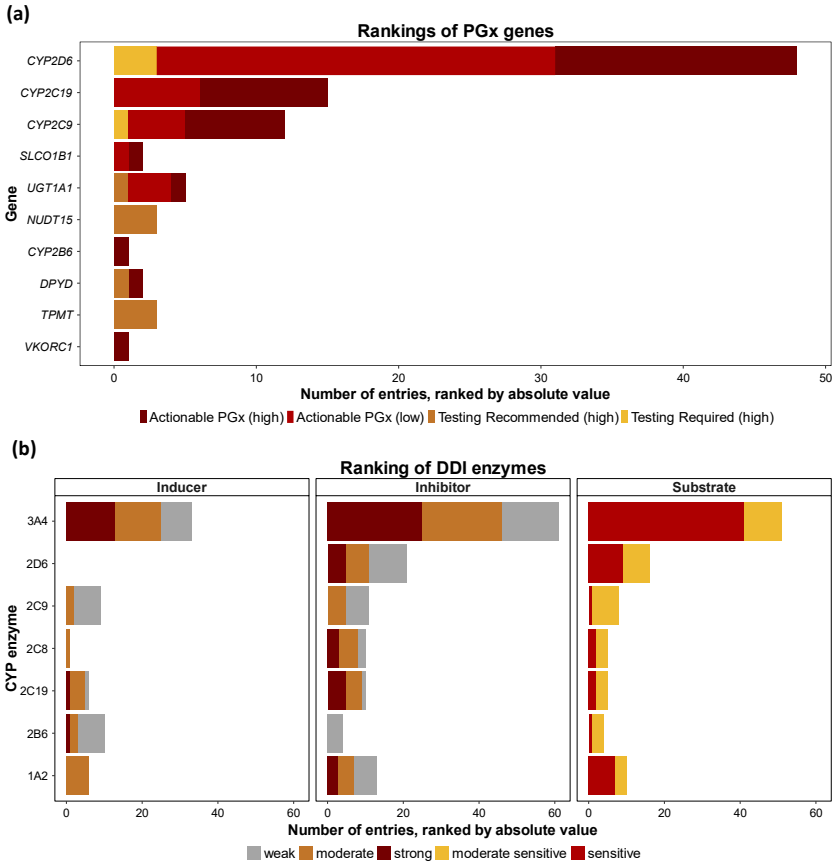

Figure 1.3: Enzymes susceptible for DDGIs (a) Based on clinical guideline annotations (CPIC), which were summarized and made publicly accessible on pharmgkb [48], enzymes for which genetic annotations by CPIC were available, were ranked based on the number of drugs linked to them. These were classified as to whether actionable PGx existed and testing was required or recommended. Moreover, the list provided levels of evidence which are illustrated in the figure as high or low in brackets. (b) Based on the DDIs-list provided by the FDA recommending DDIs perpetrator and substrate drugs [37, 49], CYP enzymes were ranked by the number of drugs associated with DDIs related to them. These drugs were classified within the different roles of inhibitors, inducers or substrates. *ABCG*: adenosine triphosphate-binding cassette super-family G protein gene, CYP: cytochrome P450 enzyme, DDI: drug-drug interaction, *DPYD*: dihydropyrimidine dehydrogenase gene, *NUDT*: nudix hydrolase gene, PGx: pharmacogenetics, *SLCO*: solute carrier organic anion transporter gene, *TMPT*: thiopurine methyltransferase gene, *UGT*: uridine diphosphate-glucuronosyltransferase gene, *VKORC*: vitamin K epoxide reductase complex gene

indicating a significant potential for DDGIs. Several different factors can add to the complexity of DDGIs, for example a perpetrator's effect on protein activity may vary based on genetic variations. As

such, voriconazole-mediated inhibition of efavirenz hydroxylation catalyzed by CYP2B6 was described to be stronger in-vitro for underlying *CYP2B6*6* haplotypes than for the *CYP2B6*1* wildtype [50]. Complexity of DDGIs additionally increases with the number of involved enzymes and perpetrators. For example, quinidine, which is a CYP3A4 substrate and, therefore, prone to be affected by DDIs, is able to inhibit the highly polymorphic CYP2D6 enzyme. Here, quinidine's metabolite, 3-hydroxyquinidine,was reported to inhibit CYP2D6 as well, resulting in very complex DDGIs scenarios [51].

Phenoconversion

In general, depending on the nature of the coadministered drug and the respective genetic polymorphism, effects can be notably increased, for example when a perpetrator drug induces expression of a metabolizing enzyme and is given to a *rapid metabolizer* which already exhibited increased enzyme activity compared to *normal metabolizers*. Alternatively, when the same perpetrator drug – inducing expression of a metabolizing enzyme – is given to a *poor metabolizer*, who initially exhibited reduced enzyme activity, could then show comparable enzyme activity to a *normal metabolizer*. This scenario, where simultaneous DDIs and DGIs could lead to a different apparent phenotype (e.g. *normal metabolizer*) compared to the original one (e.g.*poor metabolizer*), is also known as a "phenoconversion" [30, 34]. For example, similar observations could be found when patients with various CYP2B6 genotypes are pretreated with the CYP2B6 inducer rifampicin. The respective parent/metabolite ratio for bupropion was reported for genotypes including the haplotypes **1*, **4*, **5*, and **6* [36] and illustrated in Figure 1.4.

Parents and Metabolites during DDGIs

Patients who were *CYP2B6 intermediate metabolizer* (expressed by *CYP2B6*1|*6*) showed comparable $AUC_{HBup/Bup}$ ratios to *CYP2B6 poor metabolizer* (expressed as *CYP2B6 *6|*6*) receiving rifampicin pretreatment. Similarly, the same *CYP2B6 intermediate metabolizer* exhibited greater $AUC_{HBup/Bup}$ ratios under rifampicin therapy than the *CYP2B6 rapid metabolizers* without rifampicin intake (expressed as *CYP2B6 *1|*4*) [36].

Not only does the existence of CYP2B6 polymorphisms contribute to bupropion's involvement in DDGIs, but its metabolites also play an important role as well. Bupropion was observed to irreversibly inhibit CYP2D6, which is why the FDA lists it as a clinical DDIs perpetrator drug for CYP2D6 [37, 49]. Here, it can lead to a down regulation of CYP2D6 enzymes, leading to a notable loss in CYP2D6 activity. Since, CYP2D6 is also highly polymorphically expressed, the potential bupropion holds in participating in DDGIs is vast [52–55].

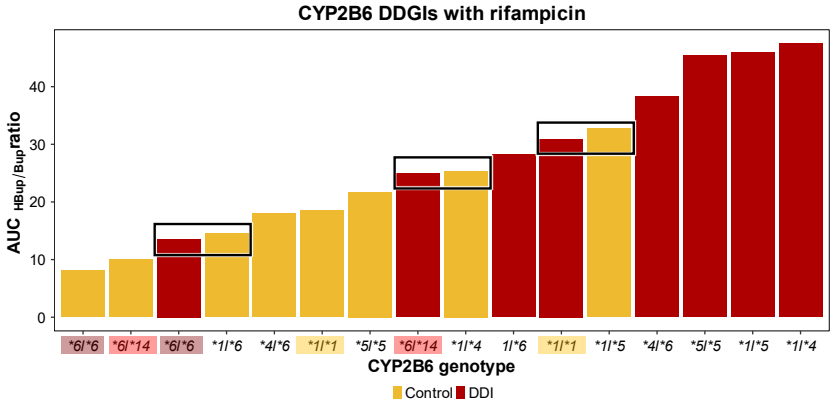

Figure 1.4: Phenoconversion illustrated for *CYP2B6* on $AUC_{HBup/Bup}$ ratios. $AUC_{HBup/Bup}$ ratios as an example of a potential phenoconversion were observed by Loboz et al. [36], surrounding the enzyme CYP2B6. Here, individuals exhibiting various *CYP2B6* polymorphisms received rifampicin, a CYP2B6 inducer, and bupropion, a CYP2B6 substrate. The marked bars in the boxes illustrate potential phenoconversion, where for example *poor metabolizer*, (expressed as *CYP2B6*6 | *6*), receiving rifampicin appear to be *intermediate metabolizer* (equivalent to *CYP2B6*1 | *6*), or *normal metabolizer* (expressed as *CYP2B6*1 | *1*) receiving rifampicin exhibit a similar $AUC_{HBup/Bup}$ ratio to *rapid metabolizer* (equivalent to *CYP2B6*1 | *5*). $AUC_{HBup/Bup}$: ratio of the area under the plasma concentration-time curve of hydroxybupropion to bupropion, CYP: cytochrome P450, DDI: drug-drug interaction

1.3.4 *Drug-Daytime Interactions*

Chronopharmacokinetics

Circadian rhythmicity is involved in a multitude of physiological processes. With regards to pharmaceutical compounds, DDTIs occur in most ADME processes, as illustrated in Figure 1.5. Here, diurnal variations can affect a drug's PK, which can be referred to its chronopharmacokinetics, as cellular clocks lead to fluctuations in various physiological processes. These include gastric motility and pH, renal and hepatic blood flow rates as well as expression and activity of transporters or enzymes [56].

In general, several different processes simultaneously attribute to a drug's chronopharmacokinetic profile. As an example, Tuerk et al. investigated, if and which pathways could play a role in the PK of metformin by using a physiologically based pharmacokinetic modeling (PBPK) model to simulate circadian rhythmicity on a variety of parameters to describe the varying metformin exposure after administration in the morning and evening [51]. Here, various – for metformin relevant – elimination pathways were examined, revealing that incorporating diurnal variations into their respective parameters improves model predictions [51].

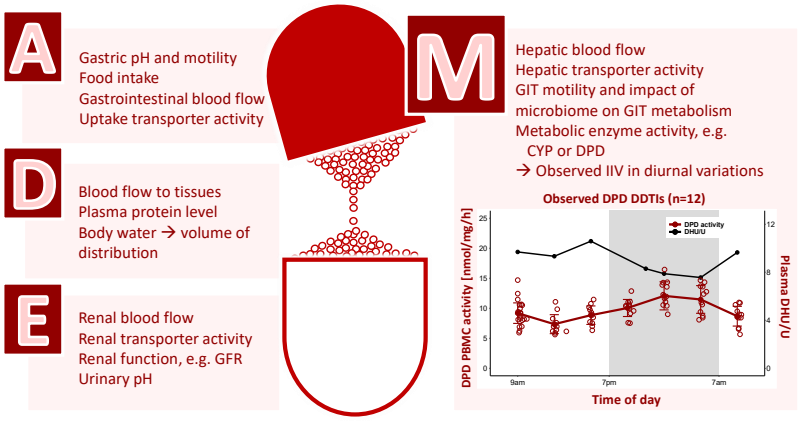

Figure 1.5: Chronopharmacokinetics. Several different pathways of the ADME profile of a drug can be influenced by circadian clocks [26, 51, 56]. With regards to metabolites impacted by the varying DPD activity, oscillating DPD activities measured in peripheral blood mononuclear cells (PBMCs) together with plasma ratio of dihydrouracil and uracil (DHU/U) ratios of healthy individuals are shown throughout the day on the bottom right. Observed mean data (connected by lines) are shown as dots, while individual data are illustrated as open circles. The shaded areas indicate nighttime [26]. CYP: cytochrome P450, DDTIs: drug-daytime interaction, DHU/U: ratio of dihydrouracil and uracil, DPD: dihydropyrimidine dehydrogenase, GFR: glomerular filtration rate, GIT: gastro-intestinal tract, IIV: interindividual variability, n: number of individuals, PBMC: peripheral blood mononuclear cells.

Diurnal Formation of Metabolites

Especially regarding metabolism, metabolizing enzymes can exhibit fluctuation in their enzyme activity, as it was observed for several CYP enzymes and DPD, resulting in diurnal variations in the formation of metabolites [26, 57]. As an example of such DDTIs, Figure 1.5 illustrates DPD activities, alongside parent-metabolite ratios of endogenous uracil, a substrate of DPD, as DHU/U plasma ratios observed throughout a day in healthy subjects [26]. Similarly, a drug's pharmacological target can be influenced by diurnal variations as well. Chronopharmacodynamics are becoming increasingly relevant, particularly in oncology with chronotherapy as a rapidly expanding field of research in recent years. Here, the timing of drug administration is adapted specifically to improve a drug's efficacy and minimize its toxicity [26, 58, 59]. These so called chronomodulated treatments are established therapy approaches for a variety of anticancer agents, such as the chronoFLO4 treatment which includes 5-fluorouracil with peak delivery at 4 a.m. alongside leucovorin and oxaliplatin, which is further elaborated in Section 3.6.3 [58].

Chronopharmacodynamics

Inter-individual Chronotypes

Interindividual variability (IIV) can be a key factor in understanding DDTIs, as individual chronotypes are reported in literature. Differences in lifestyles, such as sleeping patterns, long-distance travelling,

shift work, underlying diseases or simply genetics can result in individually different chronotypes [60, 61]. While two extremes of chronotypes have been known for a while, *the night owl* and *the early bird*, a bimodal type was investigated more recently, which illustrated characteristics of both extremes [61, 62]. The majority of people, however, are intermediate types and can be classified somewhere within the spectrum between *the night owl* and *the early bird* [61, 62].
As DDTIs are still under-investigated in comparison to other drug interactions, they are becoming more and more relevant for personalized medicine approaches due to their susceptibility towards IIV [61, 62].

While the single effect of DGIs, DDIs, or DDTIs are already complex and challenging to address in clinical drug development, a combination of several effects occuring at the same time, such as DDGIs scenarios including several perpetrator drugs, are often impossible to assess and, thus, bear a great unknown risk. Especially, investigating treatment scenarios where toxic drug levels could easily be reached or toxic metabolites could accumulate, may be ethically concerning. Here, *in silico* approaches enable an investigation of various drug interaction scenarios, which would be infeasibale to test *in vivo*. In the presented work, PBPK modeling was used to investigate several parent drugs and their metabolites within various drug interaction scenarios.

1.4 PBPK MODELING

1.4.1 *Scope and Purpose*

PBPK is a mathematical modeling approach with which the ADME behavior of a substance can be investigated, simulated and predicted [63]. Originally developed for the use in toxicology, PBPK modeling today is an established method to guide and inform drug discovery and development (D_3) processes, as well as regulatory assessment. Both the European Medicines Agency (EMA) and FDA recognize the value that PBPK modeling adds towards D_3 and reference potential applications of model informed D3 (MID_3) strategies [64, 65]. PBPK modeling allows for a mechanistic description of anatomical and physiological aspects, particularly in whole-body PBPK models, where it describes various organs and tissues as compartments, that are connected by blood flow rates. Naturally, these models are data driven, consisting of a wide range of parameters. Consequently, they require extensive and detailed data on the organism's anatomy and (patho-)physiology (system-dependent data), along with the physicochemical and biochemical properties of the investigational drug (drug-dependent data) [30]. Moreover, they are built upon clinical study data, that ideally includes drug exposure, such as of parent and metabolites, in various

tissues, namely plasma or urine. Figure 1.6 gives an overview of the PBPK model development process.

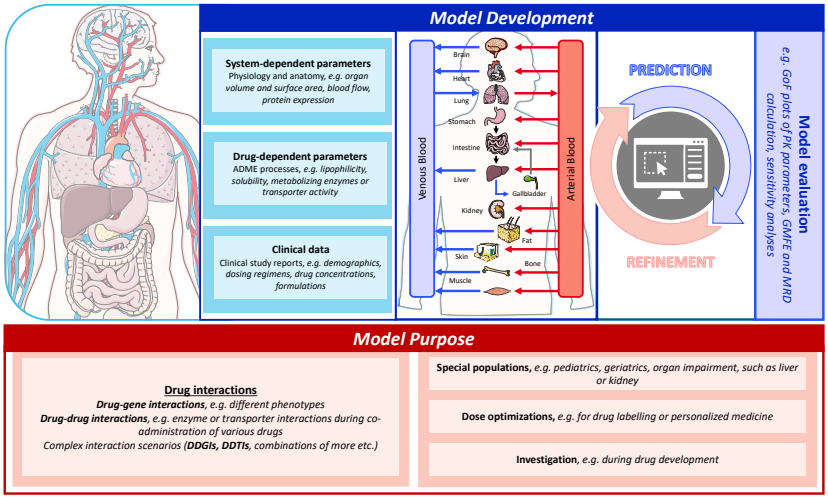

Figure 1.6: Physiologically based pharmacokinetic modelling and its applications. Whole-body PBPK models are built upon large number of parameters, that include system-dependent and drug-dependent parameters as well as clinical data (shown in cyan in the left). Here, the PBPK model framework, where parameters can be implemented into, consists of mathematical compartments describing organs, which are further divided into sub-compartments, such as tissue cells, red blood cells, blood and interstitial space. These organ compartments are connected through blood flow rates. During PBPK model development, observed data, such as plasma concentration-time profiles, are predicted and used to refine model parameters. The model performance is evaluated through various measures based on defined quality criteria (indicated blue of top half), which are further detailed in Section 3.5. PBPK models are generally built for a specific purpose, of which some examples are listed in the bottom half in red [63–66]. ADME: absorption, distribution, metabolism and elimination, DDGIs: drug-drug-gene interactions, DDTIs: drug-daytime interactions, GMFE: geometric mean fold error, GoF: goodness-of-fit, MRD: mean relative deviation, PK: pharmacokinetics.

1.4.2 *Drug Discovery and Development*

Within D_3, clinical trials are performed to evaluate newly developed chemical entities, with focus on their safety, tolerability and efficacy. The clinical trial process is conducted in different phases (I–IV) [67, 68] and regulated by authorities like the FDA and EMA, who issue relevant guidelines.
Phase I, usually involving a small cohort, focuses on drug safety, especially most common side effects and highest tolerable doses [68].

Both PD and PK are examined to provide potential initial dosing for the respective target population [69]. Upon these findings, phase II studies, conducted in the pharmacological target cohort, examine preliminary therapeutic effectiveness for a particular condition. Risk assessments as well as further dose and treatment optimizations are tested through comparison of placebo and standard treatment [67, 68, 70]. Similarly, phase III trials investigate larger cohorts to confirm previous findings and observe potential occurrence of rare or long-term side effects and ADRs, for example in multicenter trials over a longer period of time [67, 68]. Lastly, in phase IV, the post-approval and marketing stage, drug safety and efficacy is continuously assessed as wider groups of populations are treated under real-world conditions over prolonged periods of time [68, 70].

1.4.3 *Investigation of Metabolites in Drug Discovery and Development*

Metabolites are an important aspect of D_3 and are already tested for in a preclinical setting, like *in vitro* drug interaction assays or *in vivo* animal PK studies [71]. Figure 1.7 gives a brief overview on their role in D_3.

In clinical trials, especially early on in phase I trials, metabolites are investigated towards their contribution to a parent's safety profile, regardless of their pharmacological activity. Within these first-in-human trials, occurrence of metabolites is evaluated in comparison to nonclinical findings, e.g. metabolite exposure observed in animals like rodents, dogs or monkeys [69]. The FDA recommends further nonclinical testing, if metabolites occur to be *disproportionate* [71]. This is the case when metabolites are observed solely or at a higher plasma exposure in humans, for example within early PK studies such as in phase I, compared to animals tested in the preceding nonclinical studies. In particular, "if they account for plasma levels greater than 10 % of total drug-related exposure, measured as AUC at steady state", according to the FDA [71], they are classified as *disproportionate*. Additional nonclinical testing is recommended by administering the metabolite itself, if feasible, or by testing in an animal species that forms the metabolite to a similar extent as observed in humans. Here, it's important to understand the behavior of *disproportionate* metabolites as they represent an investigational drug's major metabolic pathways potentially most susceptible towards different sources of variabilities [71]. Furthermore, metabolites are of relevance in phase II and III trials, where the clinical effectiveness can be impacted by the metabolites themselves, especially if tested in special populations. For example, age-related (e.g. pediatrics and elderly) or disease-related (e.g. liver or kidney diseases) differences in drug metabolism could lead to metabolite exposure in pharmacodynamically relevant ranges [64, 69, 72].

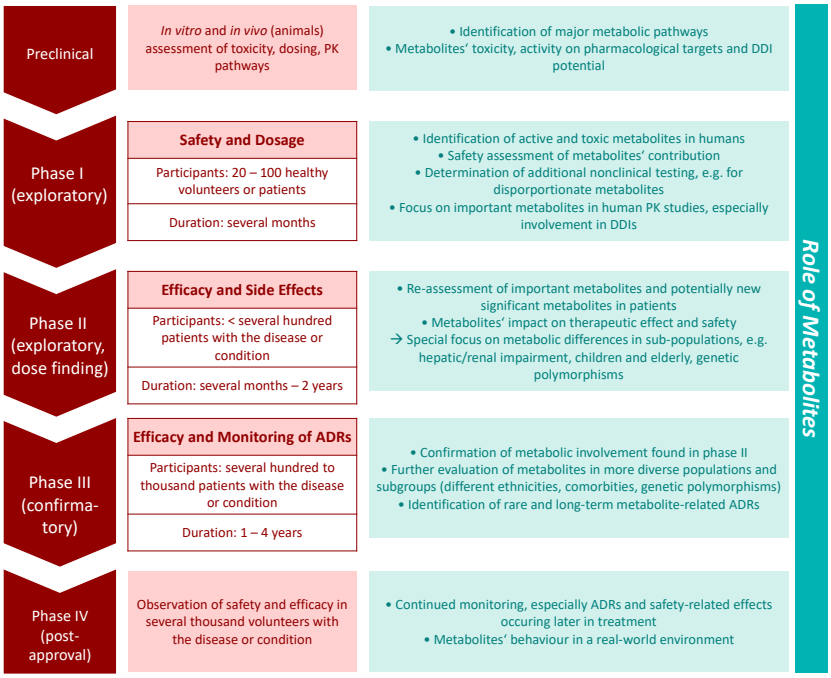

Figure 1.7: Role of Metabolites in D3. Overview of the studies conducted during drug development. In yellow on the left the different phases are briefly explained regarding their focus and extent. On the right in turquoise the role of the metabolites is demonstrated for the various phases. Here, information were gathered mainly from regulatory guidelines provided by the FDA and EMA that mention the testing of metabolites in relation to drug development or conduction of clinical studies, e.g. drug interaction studies [29, 67–74]. ADRs: adverse drug reactions, DDIs: drug-drug interactions, PK: pharmacokinetics.

Additionally, drug interactions, namely DGIs and DDIs, are tested for in clinical trial periods, where investigating active and –to some extent– inactive metabolites becomes crucial [29, 73]. In various guidelines by the EMA, investigation of metabolites is recommended [29, 69, 72, 73]. Pharmacologically active metabolites should, for example, be included in dosing recommendations for genetic sub-populations. Here, the EMA recommends deriving alternative dosing accounting for the active metabolites drug exposure alongside their parent by adapting the dose to match the sum of all active drug moieties [73]. However, inactive metabolites should also be carefully explored. The EMA highlights the risk of metabolite exposure elevated to toxic levels, for instance, in genetic sub-populations, as well as those with hepatic or renal impairment. This concern extends to conducting clinical DDIs trials [29, 72–74]. In general, the EMA suggests comprehensive directives on metabolite testing during the investigation on drug interactions in nonclinical and clinical trials. These include (i) identification of

active metabolites and their role during drug interactions, (ii) assessment of metabolic pathways *in vitro* and *in vivo* and how these are impacted during drug interactions, (iii) evaluation of inhibitory or inductive effects by metabolites, and, (iv) if the data indicates inhibitory or inductive effects, even conduction of clinical DDIs trials with said metabolites. To summarize, four different characteristics of metabolites which imply their role for D_3 can be observed, namely PD activity, PK interactivity, disproportionality and overall inactivity. In phase III but especially phase IV trials, involvement of metabolites is further tested in more diverse cohorts, allowing for identifying rare or long-term metabolite-related effects especially in different ethnicities [70].

1.4.4 *PBPK Modeling in Model-informed Drug Discovery and Development*

In several guidelines of the EMA and FDA, PBPK modeling as a means of MID_3 is reflected. Both agencies not only provide dedicated guidance documents on the use and reporting of PBPK models, but they also highlight the method's value throughout various guidelines, especially with focus on clinical study design and drug labeling, thus, acknowledging the significant utility of the technique. As a mechanistic approach, PBPK modeling is extensively used for the prediction of drug interactions. Particularly for investigation of DDIs, the regulatory bodies emphasize their usefulness in predicting and assessing complex DDIs scenarios revolving around metabolizing enzymes and transporters [29]. Furthermore, PBPK modeling is recommended to be applied across different populations, with a variety in age, gender, ethnicity, genetic differences, and disease state [72–74]. Moreover, developed and validated PBPK models can help guide dose optimizations for various use-cases, for example as recommended by the EMA for patients with liver impairment or with genetic polymorphisms [72, 73]. Figure 1.6 lists a few possible fields of applications for PBPK modelling. Although, both the EMA and FDA guidance documents for PBPK modeling do not specifically address the modeling of metabolites [64, 65], they stress the importance of ensuring the model's quality and validation. This is crucial for the effective contribution of MID_3 towards understanding a drug's PK and PD. Overall, with the growing acceptance of PBPK modeling in D_3 as well as in regulatory decision-making, PBPK modeling is a powerful tool which can help to enhance the safety and efficacy of the investigational drug with MID_3 being encouraged by regulatory agencies in new drug applications.

2 OBJECTIVES

The objectives of the presented thesis were to investigate and highlight the role of metabolites for PBPK modelling, which includes their impact on their parents' pharmacokinetic behavior, demonstrated within various drug-interaction scenarios. The presented compounds bupropion, ketoconazole, 5-fluorouracil and uracil, as well as their corresponding parent-metabolites PBPK models exemplify the significance in including the respective metabolites on all levels of PBPK model development. Here, project I and II were developed as part of the OSMOSES project, which tackled the further development of the "Open Source Pharmacology Suite" (OSPS) [75], that is used for complex PBPK modeling analyses. Project I and II were developed with the aim to establish a publicly available PBPK compound library for use in simulation and prediction of DDIs. Project III was developed under the U-PGx project funded by the European Commission to understand and investigate genotype-guided personalized medicine [76].

2.1 PROJECT I – PHYSIOLOGICALLY BASED PHARMACOKINETIC MODELING OF BUPROPION AND ITS METABOLITES IN A CYP2B6 DRUG-DRUG-GENE INTERACTION NETWORK

Project I aimed to establish a first CYP2B6 DDGIs network as part of the publicly available compound library established in OSMOSES. The main objectives were the development of a PBPK model for the antidepressant bupropion, a sensitive substrate of CYP2B6, as well as its most relevant metabolites to describe and predict CYP2B6 DGIs, DDIs and DDGIs. Moreover, project I investigated the usefulness of parent-metabolite ratios of bupropion and its metabolite formed by CYP2B6 to evaluate the effect model for several CYP2B6 DD(G)I scenarios [1].

2.2 PROJECT II – A PHYSIOLOGICALLY BASED PHARMACOKINETIC MODEL OF KETOCONAZOLE AND ITS METABOLITES AS DRUG-DRUG INTERACTION PERPETRATORS

Similarly, project II aimed to build a PBPK for the antimycotic ketoconazole, a prominent DDIs perpetrator drug, which inhibits several enzymes and transporters. Here, project II investigated the contribution of its metabolites to the overall DDIs potential by simulating DDIs with ketoconazole alone compared to DDIs with

ketoconazole and its metabolites as perpetrators with a variety of DDIs victim drugs [2].

2.3 PROJECT III – PERSONALIZED CHRONOMODULATED 5-FLUOROURACIL TREATMENT: A PHYSIOLOGICALLY BASED PHARMACOKINETIC PRECISION DOSING APPROACH FOR OPTIMIZING CANCER THERAPY

Project III aimed to investigate time-dependent DPD-mediated metabolism and related DDTIs. For this, the primary objective of project III was to develop a PBPK model for the anticancer drug 5-fluorouracil and its endogenous counterpart uracil as well as their metabolites formed by DPD. The parent-metabolites PBPK models were used to assess IIV of DPD chronotypes, as well as to develop a novel personalized dosing approach of infusional chronomodulated 5-fluorouracil treatment [3].

3

METHODS

3.1 PBPK MODELING SOFTWARE

The open-source modeling software PK-Sim® and MoBi® as part of the Open Systems Pharmacology Suite (version 9–11) was used for model development. This software is released under the GPLv2 license by the Open Systems Pharmacology Community (www.open-systems-pharmacology.org [66]). Model input parameters were optimized by minimizing the sum of least squares between simulated and observed values using Monte Carlo and Levenberg-Marquardt optimizations, and tested in local sensitivity analyses. Both model optimizations and sensitivity analsyses were performed in PK-Sim® and MoBi®. For digitization of published clinical data, GetData Graph Digitizer 2.26.0.20 (© S.Federov) was used. R (3.6.3 – 4.1.3, the R Foundation for Statistical Computing, Vienna, Austria) using RStudio (RStudio PBC, Boston, MA, USA) was used to compile the PK analyses, model performance measures and plots.

3.2 PBPK – LITERATURE SEARCH

For model development, a broad literature search was performed to gather drug-dependent parameters, e.g. through information on physicochemical properties, as well as ADME-relevant processes of the investigated compounds. Additionally, the literature search focused on clinical studies that reported exposure data for parent drugs and their metabolite in various tissues, including plasma, urine or feces. These data were used to inform system-dependent parameters and adjust drug-dependent parameters.

3.2.1 *Drug-dependent Parameters | Physicochemical Properties and Biochemical Processes*

For model building, physicochemical properties, such as molecular weight, lipophilicity or solubility were gathered from measured data reported in literature, if available. In case of missing information, especially with regards to under-investigated metabolites, physicochemical properties were also calculated by the online tool Chemicalize [77] to provide input parameters for the respective compounds.
Biochemical processes were investigated to inform important ADME

processes. These included data on transporter activity, metabolizing enzymes, as well as inhibitory or inducive activities. Especially with regards to the respective interaction models, literature data served as a source for parameter input values, where possible. These could include (i) different Michaelis-Menten constant values for various *CYP2B6* haplotypes in the CYP2B6 D(D)GI modeling of bupropion, (ii) inhibition constants for CYP3A4 and P-gp autoinhibition for the DDIs modeling of ketoconazole or (iii) the amplitude in oscillation of diurnal variations in DPD activity for DDTIs modeling of 5-fluorouracil and uracil.

3.2.2 *System-dependent Parameters | Clinical Data*

System-dependent data, such as tissue compositions, blood flow rates, as well as organ volumes and surface areas are predefined in the modeling software based on population databases describing various demographics and ethnicities. Clinical data encompassed demographic data, as well as data on drug exposure, such as measured tissue concentration-time profiles or AUC values, derived from published clinical studies reporting on the investigational drugs, as well as their metabolites. All clinical data were divided into a training dataset used for model building and a test dataset used for model evaluation. Here, the training dataset included metabolite exposure, different formulations, as well as a broad dosing range in various administration protocols. Moreover, studies were assigned to the dataset with a balance of sexes to account for differences between male and female individuals.

3.3 PBPK MODEL BUILDING

Based on the gathered data, virtual individuals, compounds and respective administrations were defined to simulate the reported clinical studies. Model parameters that either could not be adequately informed by the literature or were involved in important quantitative structure-activity relationship (QSAR) model estimates of permeability and distribution processes were optimized by fitting the model simultaneously to all plasma concentration-time profiles of the training dataset [1–3].

3.3.1 *Virtual Individuals*

Mean and mode demographic data (age, ethnicity, sex, body height and weight) were used according to the respective clinical study

reports to create virtual individuals for each study. In case of missing information; i.e., lacking information on height or weight, demographics were described based on the suggested value provided by PK-Sim® based on the respective implemented population databases. If no data were available, a virtual standard individual with default values was created [1, 2]. For project III, rather than using default values, which failed to accurately reflect the typical 5-fluorouracil patient, a mean individual was estimated based on the available data [3]. Tissue distributions of enzymes were implemented according to the PK-Sim® expression database [78–80].

3.3.2 *Virtual Populations*

To create virtual populations, 500 virtual individuals were simulated within the ranges of the demographic information (age range, sex composition, ethnicity) derived from the respective clinical study report. If no information on the study population was available, a European male population with an age range of 20–50 years was assumed [1]. System-dependent parameters were varied by the implemented algorithm in PK-Sim® based on the limits of the following databases: American: Third National Health and Nutrition Examination Survey (NHANES) [81] database, Asian: Tanaka model [82], European: International Commission on Radiological Protection (ICRP) database [83]. The reference concentrations of the metabolizing enzymes and transporters, listed in the respective supplementary materials, were log-normally distributed according to the variabilty reported in the ontogeny database implemented in PK-Sim® [84]. If no information was available, reference concentrations were distributed with a variability of 35% (geometric standard deviation of 1.4) [3].

3.3.3 *Virtual Formulations*

Within the scope of the projects represented in this thesis, oral formulations were simulated using different hypotheses and models to account for the individual liberation and absorption kinetics of the investigational drugs. These approaches included: (i) dissolved formulations for rapid drug absorption utilized in project III, (ii) Weibull models to characterize different release kinetics (immediate, sustained and extended release) in project I, and (iii) particle dissolution methods incorporating literature-informed particle size distributions to address for solubility-restricted absorption, applied in project II.

3.4 PBPK EFFECT MODEL BUILDING

Several different effects and interactions were simulated within the presented projects.

3.4.1 *Drug-Gene Interactions*

DGIs were implemented in project I for the enzyme CYP2B6. To model the effect of *CYP2B6* genetic variants, CYP2B6 metabolism was split into two pathways to allow combinations of different haplotypes, e.g. *CYP2B6*1* (wildtype), *CYP2B6*4*, *CYP2B6*5*, and *CYP2B6*6*. Difference in enzyme activity was expressed by variation of the Michaelis-Menten (K_M) and catalytic rate constant (k_{cat}) values for various genotypes and haplotypes, which were either described by literature values or estimated in parameter optimizations with clinical data based on a population with the respective genotype. If no data on genotype or phenotype of the investigated subjects was available, *CYP2B6 wildtype* was assumed. If mean plasma concentration-time profiles of a population with mixed genotypes were reported, the most frequent genotype was used for model simulations [1].

3.4.2 *Drug-Drug and Drug-Drug-Gene Interactions*

DDIs were described by implementation of induction (project I) and reversible inhibitions (project II) processes. For project II, effects were simulated with and without involvement of the metabolites. In case of DDGIs, both effects of DGIs and DDIs were simulated concomitantly.

3.4.3 *Drug-Daytime Interactions*

Time-of-day variations during DDTIs were implemented using a time-dependent sine function to simulate oscillation in enzyme activity or chronomodulated drug infusion over 24 hours, as shown in Equation 3.1. For the majority of DDTIs, DPD amplitude could be derived from literature. Otherwise, the amplitude had to be estimated individually based in the observed 5-fluorouacil plasma concentrations. A mean phase shift was adapted individually for all DDTIs [3].

Diurnal variation

$$f(t) = (1 + Amp * sin(\frac{2\pi(t + T_{Acr})}{24})) * V \tag{3.1}$$

Amp = amplitude
t = simulation time [hours]
T_{Acr} = phase shift [hours]
V = enzyme activity or infusion rate

3.4.3.1 *PBPK Model Adaptation – Individualization of Chronomodulated Treatment*

Individual DPD chronotypes were assessed, by estimation of the diurnal parameters, Amp and T_{Acr} used in Equation 3.1, for (i) the *in vitro* measurements of DPD activities in PBMCs or (ii) for DPD activities estimated from measured *gene coding for DPD (DPYD)* messenger RNA (mRNA) expressions. Subsequently, the individual diurnal parameter sets served as input parameters for the daytime-dependent DPD-mediated biotransformation of 5-fluorouracil in individual model simulations. Here, novel chronomodulated administrations were derived by varying the diurnal parameters (Equation 3.1) for the chronomodulated administrations [3].

3.5 PBPK MODEL EVALUATION

PBPK model evaluation was performed using several methods, which included (i) graphical comparisons of model-predicted concentration-time profiles to observed profiles from the respective clinical studies, (ii) goodness-of-fit plots of predicted compared to observed concentration values, AUC_{last} and C_{max} values, as well as (iii) quantitative measures for model performance, namely MRD and median symmetric accuracy (MSA) for predicted compared to observed concentration values, as well as geometric mean fold error (GMFE) for predicted compared to observed PK parameters. Overall MRD and GMFE values of $\leq$ 2 were considered reasonable predictions. The respective equations are listed below [1–3].

Mean relative deviation

$$MRD = 10^x \text{ with } x = \sqrt{\frac{1}{n}\sum_{i=1}^{n}(\log_{10}\hat{c}_i - \log_{10} c_i)^2} \tag{3.2}$$

c_i = the i^{th} observed plasma concentration
$\hat{c}_i$ = the respective predicted plasma concentration
n = number of observed values

Median symmetric accuracy

$$MSA = 100(e^{(M(|\log_e(x_i)|))} - 1) \text{ with } x_i = c_i/\hat{c}_i \tag{3.3}$$

c_i = the i^{th} observed plasma concentration
$\hat{c}_i$ = the respective predicted plasma concentration
M = median

Geometric mean fold error

$$GMFE = 10^x \text{ with } x = \frac{1}{n}\sum_{i=1}^{n}|\log_{10}(\frac{\hat{a}_i}{a_i})| \tag{3.4}$$

a_i = observed AUC_{last} or C_{max} value
$\hat{a}_i$ = predicted AUC_{last} or C_{max} value
n = number of studies

3.5.1 *Effect Model Evaluation*

For the effect model evaluations, the quantitative measures were applied for effect ratios between the PK parameters calculated in case of the effect and without the effect according to Equation 3.5 [1, 2].

Effect ratios of PK parameter values

$$Effect\ PK\ ratio = \frac{PK_{effect}}{PK_{control}} \tag{3.5}$$

PK = PK parameter, such as AUC
$PK_{control}$ = PK parameter without the effect
PK_{effect} = PK parameter during the effect, such as DGIs or DDIs

In case of project I, parent-metabolite ratios of the respective PK parameters were included, as shown in Equation 3.7. As a quantitative measure of DGIs, DDIs, and DDGIs model performance for project I, GMFE values of the predicted $PK_{HBup/Bup}$ values as well as their effect ratios were calculated [1].

Hydroxybupropion/bupropion ratio

$$HBup/Bup = \frac{PK(HBup)}{PK(Bup)} \tag{3.6}$$

$$EffectPK_{HBup/Bup} = \frac{HBup/Bup_{effect}}{HBup/Bup_{control}} \tag{3.7}$$

Bup = bupropion
$control$ = no effect
$effect$ = effect, such as DGIs or DDIs
$HBup$ = hydroxybupropion

3.5.2 *Sensitivity analysis*

Local sensitivity analyses were performed to assess the sensitivity of model predictions, here calculated as the relative change in AUC_{last}, towards single parameter changes. A relative perturbation of 1000% or 3000% for transporter-mediated process parameters was used (variation range 10.0 or 30.0, maximum number of 9 steps). Focus of the analyses was on parameters that are likely to have an impact due to their involvement of a variety of calculations, as well as parameters that are uncertain, e.g. that had to be optimized or are linked to optimized parameters. Local sensitivity was calculated according to Equation 3.8. For all projects the local sensitivity analyses were performed for parent and metabolites exposure with different administration formulations [1–3].

Equation: Sensitivity analysis

$$S = \frac{\Delta AUC_{last}}{\Delta p} * \frac{p}{AUC_{last}} \tag{3.8}$$

S = sensitivity of the AUC to the examined model parameter
ΔAUC = change of the AUC
AUC = simulated, AUC with the original parameter value
Δp = change of the examined parameter value
p = original parameter value

A sensitivity of + 1.0 signifies that a 10% increase of the examined parameter value causes a 10% increase of the simulated AUC.

3.6 PARENT-METABOLITES PBPK MODELS

To underline the role of metabolites for PBPK modeling, several different parent-metabolites PBPK models were developed. Therefore, various metabolite characteristics were investigated, which include (i) PD activity and disproportionality as bupropion and its metabolites hydroxybupropion, erythrohydrobupropion and threohydrobupropion (project I), (ii) PK interactivity as ketoconazole and its metabolites *N*-deacetylketoconazole and *N*-deacetyl-*N*-hydroxyketoconazole (project II), as well as (iii) inactivity as 5-fluorouracil and uracil with their respective metabolites dihydrofluorouracil and dihydrofluorouracil (project III).

3.6.1 *Bupropion*

Metabolism and Role of Metabolites

Bupropion is an antidepressant agent which is also used to support smoking cessation, by administration as oral immediate release, sustained release or extended release tablets [85, 86]. Its PD effects can partly be attributed to its metabolites, such as hydroxybupropion, erythrohydrobupropion and threohydrobupropion [85], showed different affinities and binding kinetics to, for example, dopamine and noradrenaline reuptake or muscarinic as well as nicotinic acetylcholine receptors [87–89].
ADRs especially in case of bupropion intoxication [5] can be attributed to its metabolites, such as occurrence of seizures (stronger than bupropion itself) [38], as well as insomnia and dry mouth [90].
Bupropion is metabolized by CYP2B6 to hydroxybupropion, while erythrohydrobupropion and threohydrobupropion are formed by the 11β-hydroxysteroid-dehydrogenase (HSD) [91–93]. An overview of

bupropion's metabolic pathways is shown in Figure 3.1.

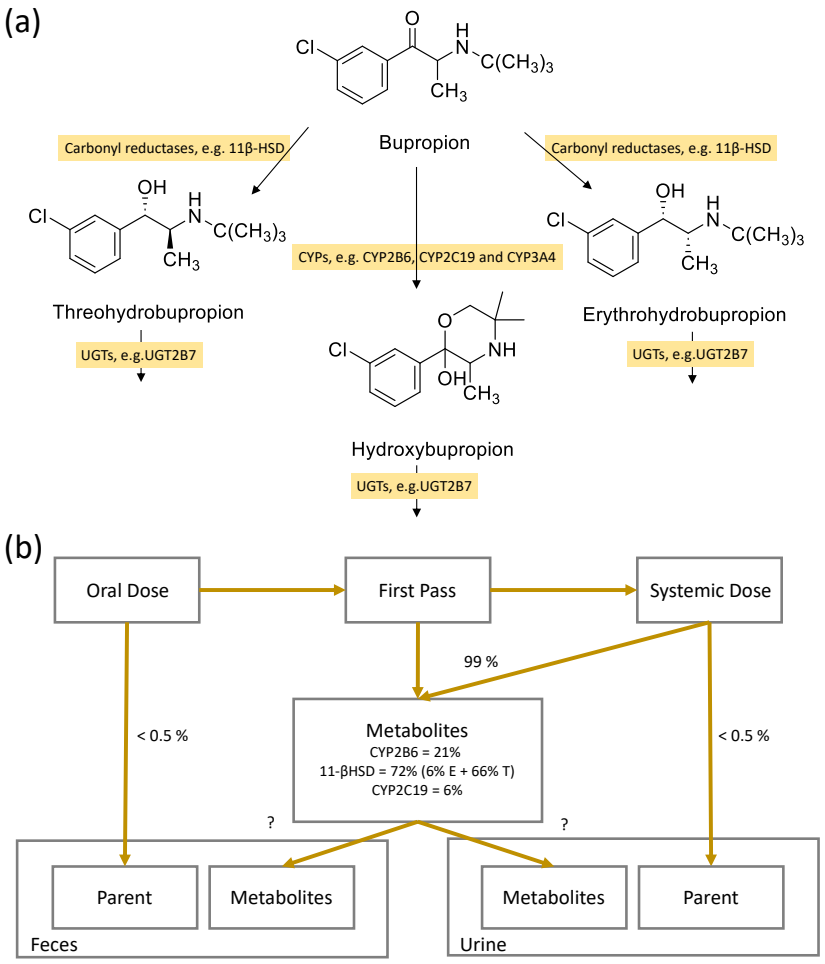

Figure 3.1: **Metabolic and elimination pathways of bupropion.** (a) Bupropion is metabolized via CYP enzymes, namely CYP2B6, CYP2C19 and CYP3A4 to hydroxybupropion and via carbonyl reductases, such as 11β-HSD to erythrohydrobupropion and threohydrobupropion. The metabolites are further degraded by UGT2B7 [91–94]. (b) Quantitative mass-balance diagram of the elimination pathways of bupropion, where metabolism via CYP2B6, via 11β-HSD and CYP2C19 accounts for roughly 99% of total bupropion [95]. Less than 0.5 % of unchanged bupropion is excreted into urine and feces [96]. 11β-HSD: 11β-hydroxysteroid dehydrogenase, CYP: cytochrome P450, E: erythrohydrobupropion, T: threohydrobupropion

Drug Interaction Potential

Bupropion's metabolites also play a role during its drug interactions[96]. DGIs surrounding CYP2B6 led to minimal differences in bupropion plasma levels across phenotype groups, whereas hydroxybupropion exposure, e.g. in form of plasma AUC, is sensitive to

changes in CYP2B6 activity [25].
Furthermore, the FDA lists bupropion as a strong inhibitor of CYP2D6 [37], as it reversibly inhibits CYP2D6 and down regulates its expression [52–55]. Here, bupropion and its three metabolites individually attribute to the CYP2D6 down regulation, with erythrohydrobupropion showing the strongest effect on CYP2D6 reversible inhibition, e.g. half maximal inhibitory concentration (IC_{50}) values of 13.3 µM and 2.9 µM for bupropion and erythrohydrobupropion respectively [52].

3.6.2 *Ketoconazole*

The antimycotic ketoconazole is mainly used in treatment of dermal infections [97]. Systematic use of ketoconazole is limited, due its severe hepatotoxicity and increased risk for torsades de pointes tachycardia resulting from prolonged QT intervals [98, 99]. Moreover, ketoconazole is one of the most prominent CYP3A4 and P-gp inhibitor drugs and the FDA lists ketoconazole as a selective CYP3A4 and P-gp inhibitor for use in clinical DDIs studies and drug labeling [37]. Next to CYP3A4 and P-gp, ketoconazole was also shown to inhibit further enzymes and transporters, such as CYP2C9, breast cancer resistant protein (BCRP) or organic anion transporting polypeptides (OATP) 1B1 [14]. It's important to note, that despite ketoconazole short half-life of roughly 160 minutes [100] and reversible inhibition of protein activity [14], it showed remarkable, long-lasting inhibitory effects. A part of ketoconazole's inhibitory potential can be attributed to its metabolite formed by arylacetamide deacetylase (AADAC), UGT1A4 and CYP3A4 [14, 101, 102]. The first metabolite *N*-deacetylketoconazole formed by AADAC was successfully quantified in plasma and observed to inhibit similar proteins like ketoconazole itself, as reported in literature [14, 103]. Figure 3.2 shows the metabolic pathways of ketoconazole, assumed in the results [2] of the presented work.

Metabolism and Role of Metabolites

Drug Interaction Potential

N-Deacetylketoconazole is assumed to accumulate intracellularly, as its plasma exposure was significantly smaller compared to ketoconazole, e.g. C_{max} of *N*-deacetylketoconazole was of 6.07 ng/ml, while C_{max} of ketoconazole was 4956.03 ng/ml [14]. *N*-Deacetylketoconazole is further metabolized to structurally similar compounds, which have yet to be quantified in plasma [103]. In general, several more (consecutive) metabolites have been identified *in vitro* (human and mice data) [105]. As reversible inhibition of several enzymes and transporters was observed for both ketoconazole and *N*-deacetylketoconazole [14], a cumulation of parent and metabolites inhibitory activity could explain the long-lasting DDIs effect.

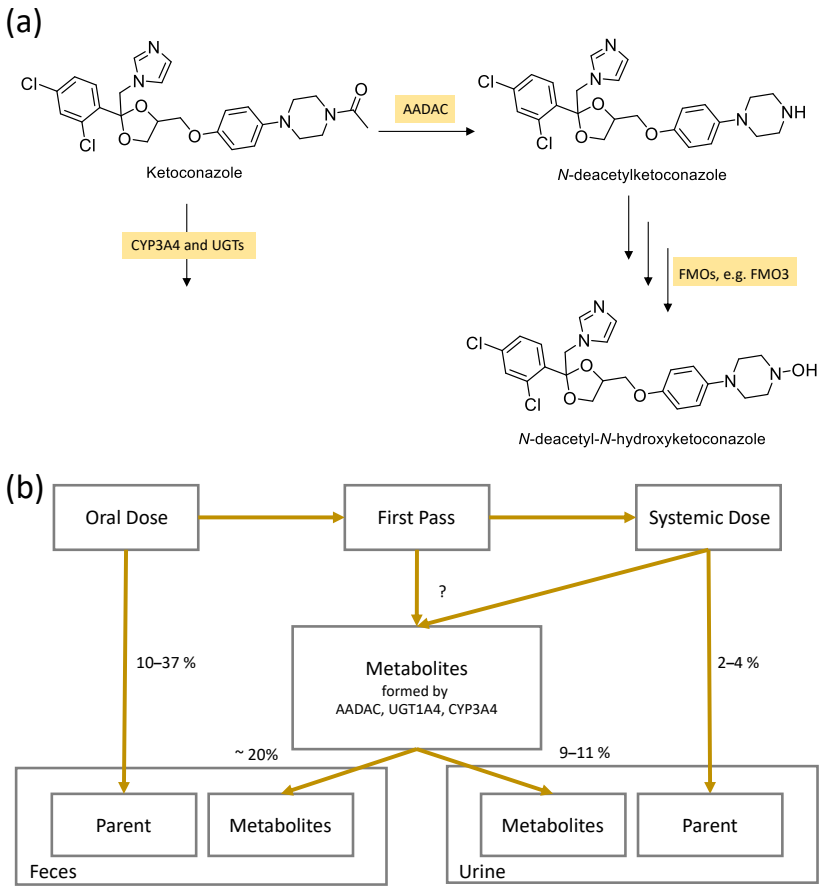

Figure 3.2: **Metabolic and elimination pathways of ketoconazole.** (a) Ketoconazole is metabolized via CYP3A4 and UGT1A4, as well as AADAC which forms *N*-deacetylketoconazole and consecutively *N*-deacetyl-*N*-hydroxyketoconazole through the FMO3 [101–103]. (b) Quantitative mass-balance diagram of the elimination pathways of ketoconazole, where 2–4 % and 10–37% of unchanged ketoconazole is excreted into urine and feces [97, 104]. Fraction metabolized were not found in literature. AADAC: arylacetamide deacetylase, CYP: cytochrome P450, UGT: uridine diphosphate-glucuronosyltransferases

3.6.3 *5-Fluorouracil and Uracil*

Metabolism and Role of Metabolites

5-Fluorouracil is a prominent antitumor agent and part of first-line treatment regimens, for example for colorectal or breast cancer [106–108]. Mimicking the endogenous uracil, two of its anabolites , 5-fluoro-desoxy-uridine triphosphate (FdUTP) and 5-fluoro-uridine triphosphate (FUTP), are incorporated into deoxyribonucleic acid (DNA) and RNA, respectively, while a third anabolite, 5-fluoro-desoxy-uridine monophosphate (FdUMP), inhibits the thymidylate synthase [109]. 5-Fluorouracil's catabolism is mediated by DPD responsible for detoxi-

fication, with its resulting catabolites mainly eliminated renally [15]. Formed by DPD, dihydrofluorouracil is further transformed via the dihydropyrimidinase (DPH) [109], as shown in Figure 3.3.

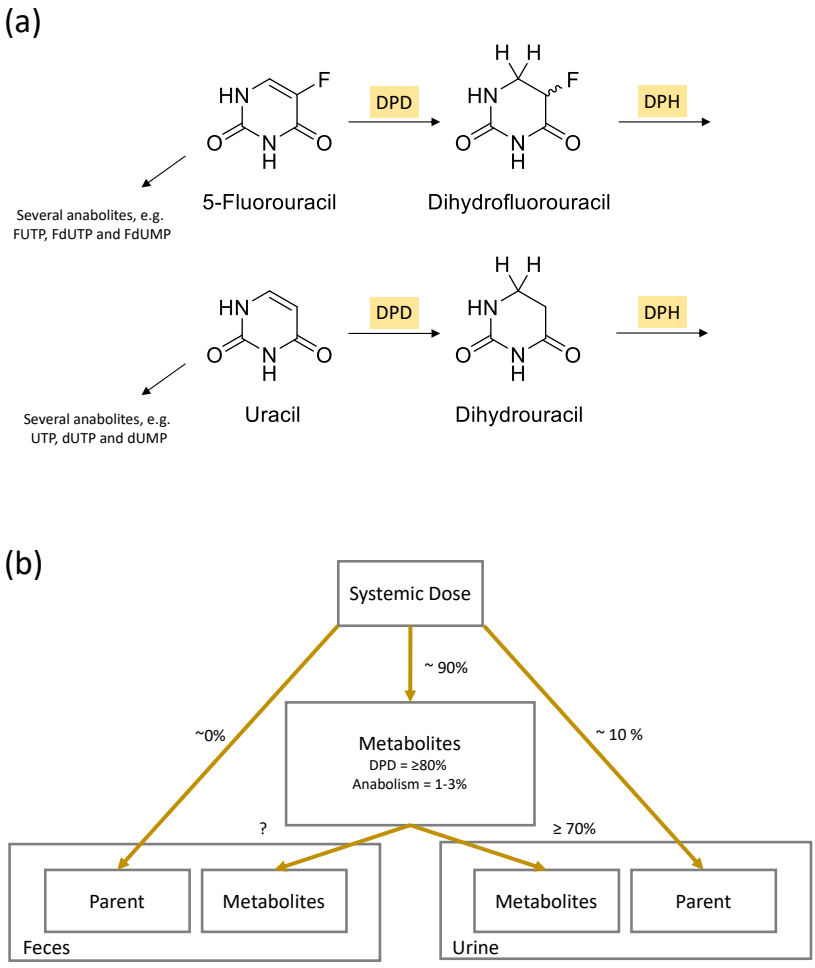

Figure 3.3: **Metabolic and elimination pathways of 5-fluorouracil and uracil.** (a) 5-Fluorouracil and uracil are metabolized to several active anabolites, namely their uridine phosphate analogues, as well as to their inactive DPD metabolites, dihydrofluorouracil and dihydrouracil, which are further metabolized by DPH [109]. (b) Quantitative mass-balance diagram of the elimination pathways of 5-fluorouracil, where around 10% of unchanged 5-fluorouracil is excreted in urine and nearly no elimination is expected in feces [110]. Fractions metabolized were reported to be at least 80%, with the overwhelming majority mediated by DPD [106]. DPD: Dihydropyrimidine dehydrogenase, DPH: dihydropyrimidinase, dUMP: desoxy-uridine monophosphate, dUTP: desoxy-uridine triphosphate, UTP: uridine triphosphate, FdUMP: 5-fluoro-desoxy-uridine monophosphate, FdUTP: 5-fluoro-desoxy-uridine triphosphate, FUTP: 5-fluoro-uridine triphosphate.

Drug Interaction Potential

As 5-fluorouracil clearance strongly correlates with DPD activity and there is an established link between plasma AUC and clinical outcomes, genetic polymorphisms or diurnal variations impacting DPD enzyme activity are a crucial part for 5-fluorouracil safety and efficacy [15, 26, 93, 111]. Assessment of DGIs through genotyping and phenotyping methods is mandatory with genotype-guided 5-fluorouracil treatment recommended through several guidelines such as CPIC and DPWG [15–17]. However, circadian rhythmicity affecting 5-fluorouracil metabolism and resulting variability in cellular exposure in healthy and cancerous tissues is more complex to estimate [26, 59, 112, 113]. While chronomodulated 5-fluorouracil treatment which typically involves intravenous long-term continuous infusions with peak 5-fluorouracil delivery at 4 am [58, 107, 108, 114], strong IIV poses a noteworthy clinical challenge. For example, patients receiving chronomodulated 5-fluorouracil exhibited varying individual plasma exposure (e.g. up to 12-fold differences in C_{max}), although receiving similar relative doses at the same peak delivery [114]. Moreover, sex-related difference in tolerability of chronomodulated 5-fluorouracil were observed, with female patients suffering from more grade 3–4 toxicities, decreased response rates and less overall survival than male patients [113].

4 RESULTS

4.1 PUBLICATION I – PHYSIOLOGICALLY BASED PHARMACOKINETIC MODELING OF BUPROPION AND ITS METABOLITES IN A CYP2B6 DRUG-DRUG-GENE INTERACTION NETWORK

4.1.1 *Reference*

Marok FZ, Fuhr LM, Hanke N, Selzer D, and Lehr T. Physiologically Based Pharmacokinetic Modeling of Bupropion and Its Metabolites in a CYP2B6 Drug-Drug-Gene Interaction Network. *Pharmaceutics*. 2021; 13(3):331. https://doi.org/10.3390/pharmaceutics13030331.

4.1.2 *Supplementary Materials*

The related electronic supplementary materials can be found on the accompanying compact disk or accessed online via: https://www.mdpi.com/1999-4923/13/3/331/s1.

4.1.3 *Author Contributions*

Following, the author contributions are listed according to CRediT [4].

Fatima Zahra Marok:	Conceptualization, Investigation, Visualization, Writing-Original Draft, Writing-Review and Editing.
Laura Maria Fuhr:	Conceptualization, Investigation, Writing-Review and Editing.
Nina Hanke:	Conceptualization, Writing- Review and Editing.
Dominik Selzer:	Conceptualization, Writing- Review and Editing.
Thorsten Lehr:	Conceptualization, Funding Acquisition, Writing- Review and Editing.

4.1.4 *Copyright*

pharmaceutics

MDPI

Article

Physiologically Based Pharmacokinetic Modeling of Bupropion and Its Metabolites in a CYP2B6 Drug-Drug-Gene Interaction Network

Fatima Zahra Marok, Laura Maria Fuhr, Nina Hanke, Dominik Selzer and Thorsten Lehr *

Clinical Pharmacy, Saarland University, 66123 Saarbrücken, Germany; fatima.marok@uni-saarland.de (F.Z.M.); laura.fuhr@uni-saarland.de (L.M.F.); n.hanke@mx.uni-saarland.de (N.H.); dominik.selzer@uni-saarland.de (D.S.)
* Correspondence: thorsten.lehr@mx.uni-saarland.de; Tel.: +49-681-3027-0255

Abstract: The noradrenaline and dopamine reuptake inhibitor bupropion is metabolized by CYP2B6 and recommended by the FDA as the only sensitive substrate for clinical CYP2B6 drug–drug interaction (DDI) studies. The aim of this study was to build a whole-body physiologically based pharmacokinetic (PBPK) model of bupropion including its DDI-relevant metabolites, and to qualify the model using clinical drug–gene interaction (DGI) and DDI data. The model was built in PK-Sim® applying clinical data of 67 studies. It incorporates CYP2B6-mediated hydroxylation of bupropion, metabolism via CYP2C19 and 11β-HSD, as well as binding to pharmacological targets. The impact of CYP2B6 polymorphisms is described for normal, poor, intermediate, and rapid metabolizers, with various allele combinations of the genetic variants *CYP2B6*1*, **4*, **5* and **6*. DDI model performance was evaluated by prediction of clinical studies with rifampicin (CYP2B6 and CYP2C19 inducer), fluvoxamine (CYP2C19 inhibitor) and voriconazole (CYP2B6 and CYP2C19 inhibitor). Model performance quantification showed 20/20 DGI ratios of hydroxybupropion to bupropion AUC ratios (DGI $AUC_{HBup/Bup}$ ratios), 12/13 DDI $AUC_{HBup/Bup}$ ratios, and 7/7 DDGI $AUC_{HBup/Bup}$ ratios within 2-fold of observed values. The developed model is freely available in the Open Systems Pharmacology model repository.

Keywords: physiologically based pharmacokinetic modeling; bupropion; hydroxybupropion; cytochrome P450 2B6 (CYP2B6); drug-drug-interactions (DDIs); drug-gene-interactions (DGIs)

check for updates

Citation: Marok, F.Z.; Fuhr, L.M.; Hanke, N.; Selzer, D.; Lehr, T. Physiologically Based Pharmacokinetic Modeling of Bupropion and Its Metabolites in a CYP2B6 Drug-Drug-Gene Interaction Network. *Pharmaceutics* **2021**, *13*, 331. https://doi.org/10.3390/pharmaceutics13030331

Academic Editors: Marival Bermejo and Xavier Declèves

Received: 31 December 2020
Accepted: 27 February 2021
Published: 4 March 2021

1. Introduction

Bupropion is used for the treatment of major depressive disorders and to support smoking cessation [1]. Nearly one out of 10 prescriptions among psychotherapeutics was attributed to bupropion in 2018 [2]. In the treatment of depressive disorders, it is either used as monotherapy or in combination with other antidepressant agents, and is administered as oral immediate release, sustained release or extended release tablets [1,3].

Bupropion and various of its metabolites are pharmacologically active [4]. Hydroxybupropion is one of the major metabolites and is formed by cytochrome P450 (CYP) 2B6-mediated hydroxylation of bupropion. Bupropion and hydroxybupropion are known inhibitors of dopamine and noradrenaline reuptake transporters. Furthermore, they act as antagonists to various acetylcholine receptors and serotonin reuptake transporters [5–7]. Erythrohydrobupropion and threohydrobupropion are further metabolites of bupropion and formed via 11β-hydroxysteroid-dehydrogenase (11β-HSD) as the rate-limiting step in the reaction pathway [8]. After administration of a single dose of 200 mg bupropion, nearly 97% of total bupropion was recovered in urine (87%) and feces (10%). However, only 0.5% of unchanged bupropion was found in urine [9]. Adverse drug events or symptoms of bupropion intoxications, i.e., insomnia, vomiting, dry mouth or seizures, can be attributed to bupropion and its metabolites [10]. It was observed that erythrohydrobupropion plasma levels significantly correlate with insomnia, while threohydrobupro-

pion is assumed to be responsible for dry mouth [11]. Moreover, hydroxybupropion induced seizures more potently than bupropion in rodent experiments [12] and immediate release administration of bupropion was associated with a higher incidence of seizures than a sustained release administration in humans [10,13,14]. All three metabolites are further metabolized via glucuronidation by uridine 5′-diphospho-glucuronosyltransferase (UGT) 2B7 [15].

According to the United States Food and Drug Administration (FDA), bupropion is listed as a sensitive substrate of CYP2B6 in clinical drug–drug interaction studies (DDIs), ref. [16] and it is subject to various CYP2B6 DDIs, when inducers or inhibitors of CYP2B6 are administered concomitantly [17,18]. For example, HIV patients that are on bupropion medication exhibited a 57% decrease in bupropion AUC at the initiation of antiviral therapy with ritonavir, an inducer of CYP2B6 [19,20]. Clopidogrel, an antiplatelet drug and known CYP2B6 inhibitor, was reported to decrease hydroxybupropion AUC by 60% after pretreatment with 75 mg clopidogrel [21]. Even short-term use of CYP2B6 perpetrator drugs can seriously affect bupropion hydroxylation, as shown for the administration of fluvoxamine and voriconazole shortly before bupropion administration that caused a 90% reduction in the hydroxybupropion to bupropion AUC plasma ratio ($AUC_{HBup/Bup}$) [22]. In addition to its CYP2B6 interaction potential, bupropion is also listed as a strong clinical inhibitor of CYP2D6 [16]. However, the inhibitory effect is primarily attributed to its metabolites hydroxybupropion, erythrohydrobupropion, and threohydrobupropion [23].

In addition to its DDI potential, bupropion is also subject to CYP2B6 drug–gene interactions (DGIs). Polymorphisms in the *CYP2B6* gene can result in rapid, normal, intermediate, or poor metabolizer phenotypes. Important genetic variants of *CYP2B6* include *CYP2B6*1, *4, *5,* and **6* with frequencies of 49%, 4%, 12%, and 23% in European populations, respectively [17,24]. It has been shown that hydroxybupropion plasma levels and hydroxybupropion to bupropion plasma ratios are significantly altered in rapid or poor metabolizers, with 153% higher or 31% lower hydroxybupropion to bupropion AUC ratios compared to wildtype [17]. However, the clinical relevance for CYP2B6 polymorphic patients is still unclear and dose adjustment guidelines have yet to be developed.

Considering the DDI, DGI and drug–drug–gene interaction (DDGI) potential, the complex pharmacokinetics of bupropion should be thoroughly investigated. Here, physiologically based pharmacokinetic modeling (PBPK) can be a valuable tool to grasp the high level of complexity and implications of genetic polymorphisms and perpetrator drugs on the pharmacokinetics of bupropion [25]. However, a robust bupropion PBPK model connected to a strong DDGI CYP2B6 network has not been developed yet.

The aim of the presented work was the development of a PBPK model of bupropion including its three most relevant metabolites for the prediction of CYP2B6 DDI, DGI, and DDGI scenarios, and the qualification of this model using clinical data of CYP2B6 polymorphic individuals and DDI studies with different perpetrator drugs in the first published CYP2B6 DDGI network. The final model is shared with the modeling and drug development community in the Open Systems Pharmacology model repository (www.open-systems-pharmacology.org, December 2020) [26]. A transparent and comprehensive documentation of model development and evaluation is provided in the Supplementary Materials.

2. Materials and Methods

2.1. Software

The PBPK model was developed with the open-source modeling software PK-Sim® and MoBi® (Open Systems Pharmacology Suite 9.1, released under the GPLv2 license by the Open Systems Pharmacology community, www.open-systems-pharmacology.org (accessed on 31 December 2020)) [26]. GetData Graph Digitizer 2.26.0.20 (© S. Fedorov) was used to digitize published clinical study data according to best practices [27]. Model input parameters were optimized by application of the Levenberg–Marquardt algorithm with multiple starting values. Local sensitivity analyses were performed within PK-Sim®.

Non-compartmental analyses, model performance measures, and plots were compiled in R 3.6.3 (The R Foundation for Statistical Computing, Vienna, Austria) with RStudio 1.2.5033 (RStudio PBC, Boston, MA, USA).

2.2. Clinical Data

Clinical studies of bupropion in single-and multiple-dose regimens were gathered and digitized from the literature [27]. The collected profiles were divided into a training (n = 19) and a test dataset (n = 48), used for model building and model evaluation, respectively [3,17–22,28–57]. Studies in the training dataset were selected to include metabolite concentration-time profiles, a wide dosing range, and different oral formulations. To minimize bias, the distribution of data on female and male populations was balanced as well. The whole dataset is documented in the clinical study tables, with their respective clinical data shown in semilogarithmic as well as linear plots in Sections 2–4 of the Supplementary Materials.

2.3. PBPK Model Building

Model building was started with an extensive literature search for physicochemical properties and information regarding absorption, distribution, metabolism, and excretion (ADME) processes of bupropion and its investigated metabolites.

Averaged demographic information about age, sex, ethnicity, body weight, and height listed in clinical study reports was used to create virtual individuals. If data on demographics was missing, a virtual standard individual with default values was created. Details on standard individuals are listed in Table S1.2 of the Supplementary Materials. Virtual populations of 500 individuals were created based on the demographic information provided in the clinical study reports. If no data was available, a male European population with an age distribution of 20–50 years was assumed.

Tissue distribution of enzymes and binding proteins used for the ADME processes of bupropion and its metabolites was implemented according to the PK-Sim® expression database [58]. Information on their expression is provided in Table S1.1 of the Supplementary Materials.

Tablet formulations with different bupropion release kinetics were simulated using a Weibull model (Section 1.1 in the Supplementary Materials). The Weibull shape and Weibull time parameters (50% dissolved) were derived, if available, from dissolution profiles reported in the literature. Model parameters that either could not be sufficiently informed from the literature or were involved in important QSAR model estimates of permeability and distribution processes were optimized by fitting the model simultaneously to all plasma concentration-time profiles of the training dataset.

2.4. PBPK Model Evaluation

PBPK model evaluation was performed using several methods. Model predictions of plasma concentration-time profiles were graphically compared to observed profiles from the respective clinical studies. Subsequently, predicted plasma concentrations from all studies were plotted against their corresponding observed values in goodness-of-fit plots. The model performance was further evaluated by comparison of predicted to observed area under the plasma concentration-time curve (AUC) and maximum plasma concentration (C_{max}) values. AUC values (predicted as well as observed) were calculated from the time of drug administration to the time of the last concentration measurement (AUC_{last}). If measured profiles were missing, predicted AUC was calculated as reported in the corresponding study. As quantitative measures of the model performance, mean relative deviation (MRD) of all predicted and observed plasma concentrations and geometric mean fold error (GMFE) of all predicted and observed AUC_{last} and C_{max} values were calculated

according to Equations (1) and (2). Predictions with MRD and GMFE values ≤ 2 were considered successful model predictions.

$$\text{MRD} = 10^{x}; \quad x = \sqrt{\frac{\sum_{i=1}^{k} \left(\log_{10}\hat{c}_i - \log_{10}c_i\right)^2}{k}} \tag{1}$$

where c_i = the ith observed plasma concentration, $\hat{c}_i$ = the corresponding predicted plasma concentration, and k = the number of observed values.

$$\text{GMFE} = 10^{x}; \quad x = \frac{\sum_{i=1}^{m} \left| \log_{10}\left(\frac{\text{predicted PK parameter}_i}{\text{observed PK parameter}_i}\right)\right|}{m} \tag{2}$$

where predicted PK parameter$_i$ = the ith predicted AUC_{last} or C_{max} value, observed PK parameter$_i$ = the corresponding observed AUC_{last} or C_{max} value, and *m* = the number of studies.

Local sensitivity of the AUC of bupropion, hydroxybupropion, erythrohydrobupropion, and threohydrobupropion to single parameter changes was analyzed for bupropion multiple dose administrations of the three different release formulations. Analyses included parameters that were either optimized or assumed to have an impact on AUC. A detailed description is provided in the Supplementary Materials Section 2.5.5.

2.5. DGI, DDI and DDGI Modeling

To model the effect of CYP2B6 genetic variants, difference in enzyme activity was expressed by variation of the Michaelis-Menten (K_M) and catalytic rate constant (kcat) values for *CYP2B6*1/*1 (wildtype)*, *CYP2B6*1|*4*, *CYP2B6*1|*6*, *CYP2B6*5|*5*, and *CYP2B6*6|*6* genotypes. Parameters that could not be informed from literature were optimized by fitting the model to clinical data based on a population with the respective genotype. If no data on genotype or phenotype of the investigated subjects was available, *CYP2B6* wildtype was assumed. If mean plasma concentration-time profiles of different genotypes were reported, the most frequent one was used for model simulations.

To model the effect of DDIs, different interaction processes (competitive inhibition or induction) were incorporated into the perpetrator PBPK model with the corresponding in vitro interaction parameters values extracted from the literature. The different interaction types are described in the Supplementary Materials Section 1.6. Previously published PBPK models of the CYP2B6 perpetrator drugs rifampicin, voriconazole, and fluvoxamine were used to simulate DDI scenarios with bupropion [59–61].

To predict the rifampicin-bupropion DDGIs in carriers of different *CYP2B6* alleles, inhibition and induction parameters for wildtype DDI simulations were assumed.

2.6. DGI, DDI and DDGI Model Evaluation

DGI, DDI, and DDGI model performance was evaluated by comparison of predicted to observed plasma concentration-time profiles of bupropion (Bup) and its CYP2B6 metabolite hydroxybupropion (HBup) after single administration and during concomitant administration of CYP2B6 perpetrator drugs (rifampicin or fluvoxamine and voriconazole). In addition, the metabolite–parent ratio HBup/Bup of the PK parameters AUC (AUC_{last} or AUC_{inf} [AUC extrapolated to infinity]) and C_{max} was calculated for predicted and observed effect and control profiles according to Equation (3). HBup/Bup AUC and C_{max} ratios were used to calculate DGI, DDI, and DDGI effect ratios according to Equation (4).

$$PK_{HBup/Bup} = \frac{HBup_{\ PK}}{Bup_{\ PK}} \tag{3}$$

where Bup_{PK} = PK parameter of bupropion, and $HBup_{PK}$ = PK parameter of hydroxybupropion.

$$\text{DGI, DDI or DDGI } PK_{HBup/Bup} = \frac{PK_{HBup/Bup}\ (\text{DGI, DDI or DDGI})}{PK_{HBup/Bup}\ (\text{reference})} \quad (4)$$

where $PK_{HBup/Bup}$ = Hydroxybupropion-bupropion PK parameter ratio.

As a quantitative measure of DGI, DDI, and DDGI model performance, *GMFE* values of the predicted and observed $PK_{Hbup/Bup}$ values as well as $PK_{Hbup/Bup}$ effect ratios were calculated according to Equation (2).

3. Results

3.1. Model Building and Evaluation

A PBPK model for bupropion and its three metabolites, hydroxybupropion, erythrohydrobupropion, and threohydrobupropion was developed. A total of 48 clinical studies in which bupropion was administered in a wide dosing range (20–300 mg) as immediate, sustained, and extended release tablets in single or multiple dose regimens were used in the model development process. In total, all 48 studies included plasma concentration-time profiles of bupropion, 40 of hydroxybupropion, and 17 of erythro- and threohydrobupropion. Study details are listed in Table S2.1 of the Supplementary Materials. For the extended release tablet formulation, Weibull parameters were calculated from dissolution profiles from the literature according to Langenbucher et al. [62]. For additional formulations, parameters were fitted to plasma concentration-time profiles of the training dataset. Dissolution details are listed in Table S2.2 of the Supplementary Materials.

Figure 1a illustrates the basic structure of the developed whole-body PBPK model and implemented DGI and DDI processes. Figure 1b summarizes the implemented metabolism of bupropion via CYP2B6 to hydroxybupropion and via 11β-HSD to erythro- and threohydrobupropion. Moreover, CYP2B6 metabolism is influenced by genetic variants and perpetrator drugs, such as the CYP2B6 inducer and inhibitor rifampicin [63,64] and the CYP2B6 inhibitor voriconazole [65]. Bupropion metabolism via CYP2C19 was modeled to reflect minor metabolic pathways of bupropion covered by other CYPs. Since binding to therapeutic targets might influence the PK of bupropion, binding to a surrogate protein representing various neurotransmitter transporters was implemented. Furthermore, the model applied glucuronidation of the three metabolites via UGT2B7. UGT2B7 and CYP2C19 metabolism were also considered in DDI predictions, as fluvoxamine and voriconazole inhibit CYP2C19 [65,66] and rifampicin induces CYP2C19. Moreover, both compounds induce and inhibit UGT2B7 [64,67]. In summary, the simulated effects include: (i) CYP2B6 polymorphisms; (ii) induction of CYP2B6, CYP2C19 and UGT2B7, and inhibition of CYP2B6 and UGT2B7 by rifampicin; and (iii) inhibition of CYP2C19 by fluvoxamine as well as inhibition of CYP2B6 and CYP2C19 by voriconazole.

Tables 1 and 2 provide an overview of the drug-dependent model parameters as well as details on the implemented metabolic processes. A description of all implemented processes and formulations with their respective model parameters is listed in the drug-dependent parameter table in the Supplementary Materials.

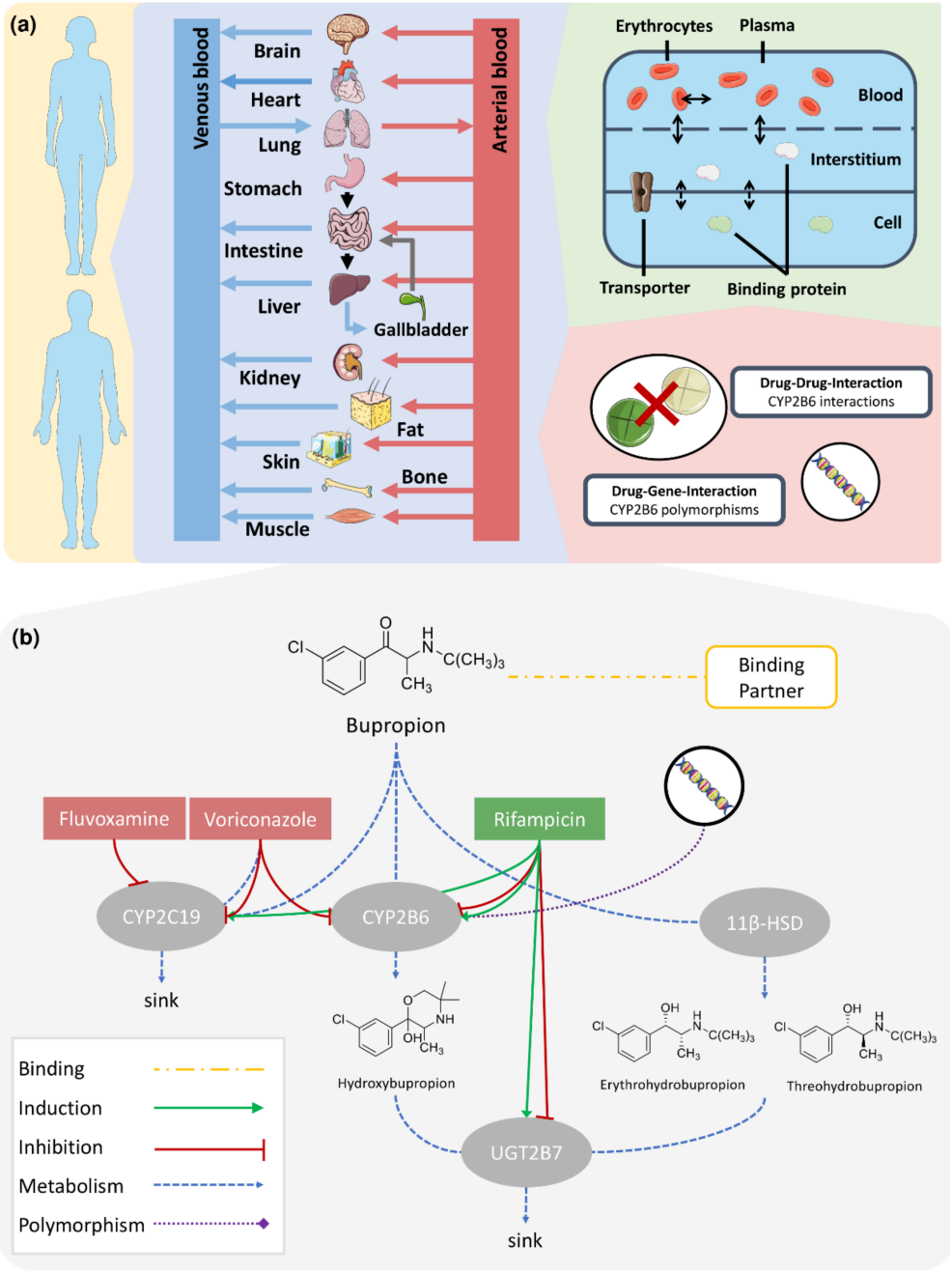

Figure 1. Modeling overview of the CYP2B6 DDGI Network. A whole-body PBPK model was augmented for the simulation of CYP2B6 drug–drug, drug–gene, and drug–drug–gene interactions (**a**). The model describes bupropion's metabolism via CYP2B6, CYP2C19, and 11β-HSD (**b**). Its metabolites hydroxybupropion, erythro- and threohydrobupropion are transformed via UGT2B7. Binding to an unspecific binding protein, representing bupropion's pharmacological targets, was implemented. Several effects on the bupropion PK were modeled, i.e., effects of genetic polymorphisms on CYP2B6; induction of CYP2C19 by rifampicin; induction and inhibition of CYP2B6 and UGT2B7 by rifampicin; inhibition of CYP2C19 by fluvoxamine; and inhibition of CYP2B6 and CYP2C19 by voriconazole. Drawings by Servier, licensed under CC BY 3.0 [68]. 11β-HSD: 11β-hydroxysteroid-dehydrogenase, CYP2B6: cytochrome P450 2B6, CYP2C19: cytochrome P450 2C19, UGT2B7: uridine 5′-diphospho-glucuronosyltransferase 2B7.

Table 1. Drug-dependent parameters of the bupropion PBPK model.

Parameter	Value	Unit	Source	Literature	Reference	Description
MW	239.74	g/mol	lit.	239.74	[69]	Molecular Weight
pKa	8.75	-	lit.	8.75	[70]	Acid dissociation constant
Solubility (pH = 7.40)	365.56	mg/mL	lit.	365.56	[71]	Solubility
log P	2.57	-	fit.	3.27	[69]	Lipophilicity
fu	16.00	%	lit.	16.00	[23]	Fraction unbound
Intestinal perm.	2.76×10^{-5}	cm/min	fit.	-	-	Transcellular intestinal permeability
Partition coefficients	Diverse	-	calc.	Berez.	[72]	Cell to plasma partitioning
Cellular Perm.	-	-	fit.	PK-Sim	[73]	Permeability into the cellular space
GFR fraction	1.00	-	asm.	-		Filtered drug in urine
EHC cont. fraction	1.00	-	asm.	-		Bile fraction continuously released
K_M *CYP2B6*1* → HBup	‡ 25.80	µmol/L	lit.	‡ 25.80	[74]	Michaelis-Menten constant
k_{cat} *CYP2B6*1* → HBup	* 10.87	1/min	fit.	-	-	Catalytic rate constant
K_M *CYP2B6*6* → HBup	‡ 61.26	µmol/L	lit.	‡ 61.26	[74]	Michaelis-Menten constant
k_{cat} *CYP2B6*6* → HBup	* 9.52	1/min	fit.	-	-	Catalytic rate constant
K_M *CYP2B6*4* → HBup	12.70	µmol/L	lit.	12.70	[75]	Michaelis-Menten constant
k_{cat} *CYP2B6*4* → HBup	[a] 18.13	1/min	lit.	* 18.13	[75]	Catalytic rate constant
K_M 11β-HSD → EBup	39.10	µmol/L	lit.	39.10	[76]	Michaelis-Menten constant
k_{cat} 11β-HSD → EBup	2.15	1/min	fit.	-	-	Catalytic rate constant
K_M 11β-HSD → TBup	39.10	µmol/L	lit.	39.10	[76]	Michaelis-Menten constant
k_{cat} 11β-HSD → TBup	8.18	1/min	fit.	-	-	Catalytic rate constant
K_M CYP2C19	8.30	µmol/L	lit.	8.30	[77]	Michaelis-Menten constant
k_{cat} CYP2C19	2.59	1/min	fit.	-	-	Catalytic rate constant
K_D Binding partner	0.44	µmol/L	fit.	[b] 0.35–0.60	[78–80]	Dissociation constant for binding
k_{off} Binding partner	0.05	1/min	fit.	-	-	Dissociation rate constant for binding

‡ in vitro values corrected for binding in the assay using fraction unbound to microsomal protein measurements from the same study, * half of the optimized parameter, [a] calculated mean of enantiomer selective degradation, [b] also includes inhibition constant values (Ki), 11β-HSD: 11β-hydroxysteroid-dehydrogenase, asm.: assumed, Berez.: Berezhkovskiy calculation method, calc.: calculated, cont.: continuous, CYP2B6: cytochrome P450 2B6, CYP2C19: cytochrome P450 2C19, EBup: erythrohydrobupropion, EHC: enterohepatic circulation, fit.: optimized parameter, GFR: glomerular filtration rate, HBup: hydroxybupropion, lit.: literature, perm.: permeability, PK-Sim: PK-Sim® standard calculation method, TBup: threohydrobupropion.

Table 2. Drug-dependent parameters of the hydroxybupropion, erythrohydrobupropion and threohydrobupropion PBPK models.

Parameter	Value	Unit	Source	Literature	Reference	Value	Unit	Source	Literature	Reference	Description
	Hydroxybupropion					Erythro-and Threohydrobupropion					
MW	255.74	g/mol	lit.	255.74	[81]	241.76	g/mol	lit.	241.76	[82]	Molecular Weight
pKa	7.65	-	lit.	7.65	[81]	9.71	-	lit.	9.71	[82]	Acid dissociation constant
Solubility (pH = 7.40)	0.91	mg/mL	lit.	0.91	[81]	82.98	mg/mL	lit.	82.98	[82]	Solubility
log P	1.90	-	fit.	2.20	[83]	1.89	-	fit.	2.98	[82]	Lipophilicity
fu	23.00	%	lit.	23.00	[23]	58.00	%	lit.	58.00	[23]	Fraction unbound
Partition coefficients	Diverse	-	calc.	Berez.	[72]	Diverse	-	calc.	Berez.	[72]	Cell to plasma partitioning
Cellular Perm.	-	-	fit.	Ch.d.S.	[84]	-	-	fit.	Ch.d.S.	[84]	Permeability into the cellular space
GFR fraction	1.00	-	asm.	-	-	1.00	-	asm.	-	-	Filtered drug in urine
EHC cont. fraction	1.00	-	asm.	-	-	1.00	-	asm.	-	-	Bile fraction continuously released
K_M UGT2B7	‡ 14.64	µmol/L	lit.	14.64	[15]	(E) ‡ 9.33 (T) ‡ 6.22	µmol/L	lit.	(E) ‡ 9.33 (T) ‡ 6.22	[15]	Michaelis-Menten constant
k_{cat} UGT2B7	1.09	1/min	fit.	-	-	(E) 0.63(T) 0.10	1/min	fit.	-	-	Catalytic rate constant

‡ in vitro values corrected for binding in the assay using fraction unbound to microsomal protein measurements from the same study, asm.: assumed, Berez.: Berezhkovskiy calculation method, calc.: calculated, Ch.d.S.: Charge dependent Schmitt calculation method, cont.: continuous, E: erythrohydrobupropion, EHC: enterohepatic circulation, GFR: glomerular filtration rate, fit.: optimized parameter, lit.: literature, perm.: permeability, T: threohydrobupropion, UGT2B7: uridine 5′-diphospho-glucuronosyltransferase 2B7.

Figure 2a–i presents simulations of bupropion administration as immediate, sustained, and extended release tablets. The bupropion PBPK model accurately described and predicted plasma concentration-time profiles of bupropion and its metabolites after single and multiple dose administrations for the three different formulations. Predicted concentration-time profiles of all 48 clinical studies compared to observed data are provided on linear and semi-logarithmic scale in Figures S2.4.1–S2.4.14 in the Supplementary Materials. All simulated plasma profiles were in good agreement with their respective observed data.

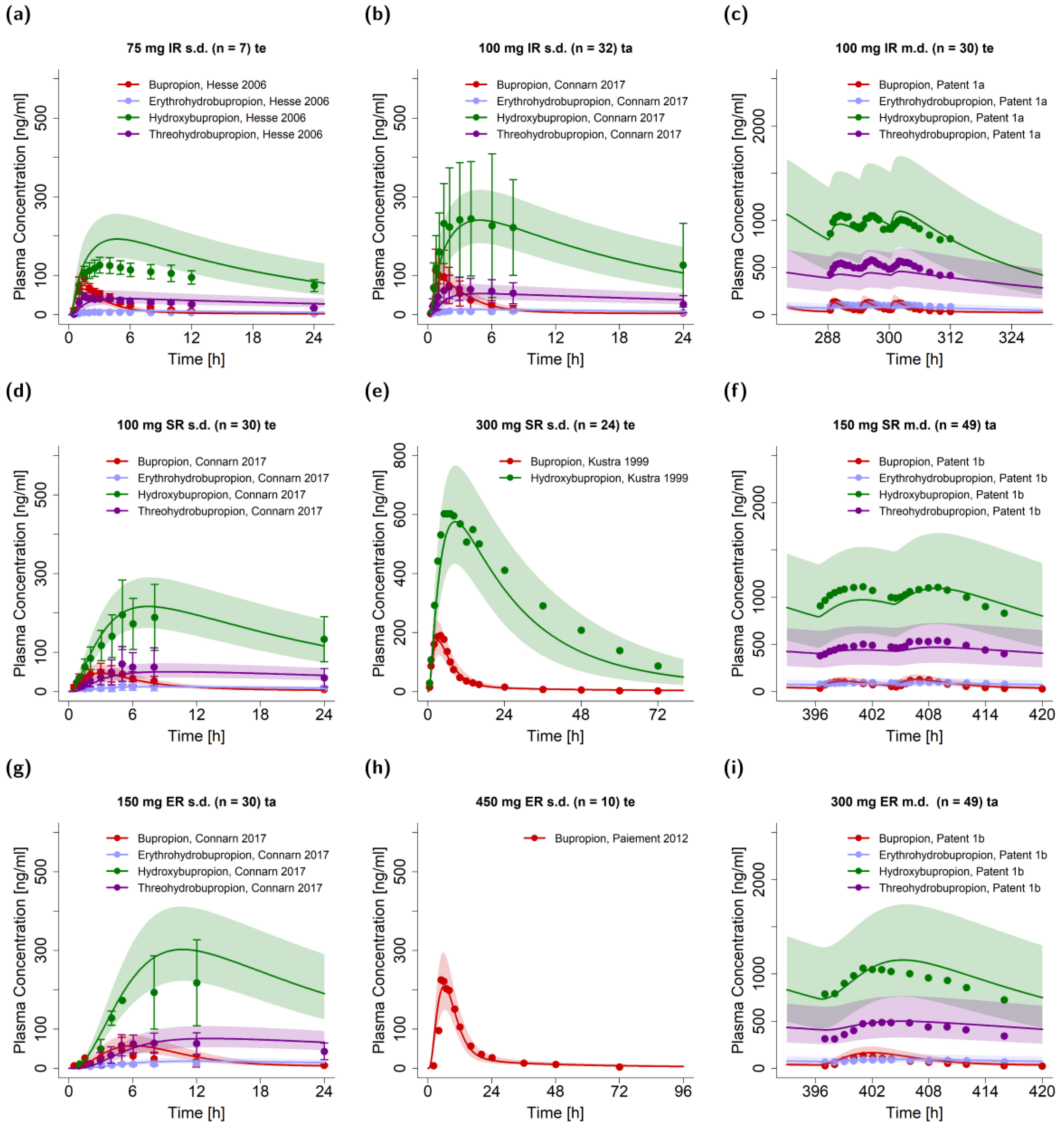

Figure 2. Predicted plasma concentration-time profiles of selected clinical studies from test and training datasets for bupropion, hydroxybupropion, erythro- and threohydrobupropion after application of single and multiple oral tablets with immediate release (**a**–**c**), sustained release (**d**–**f**) and extended release (**g**–**i**) kinetics compared to observed data [3,28,32,51,54]. The geometric means of the population predictions (n = 500) are shown as solid lines and corresponding observed data as dots (arithmetic mean ± standard deviation, if available). The shaded areas indicate the geometric standard deviation. Detailed information on study protocols is provided in Table S2.1 of the Supplementary Materials. ER: extended release, IR: immediate release, m.d.: multiple dose, n: number of participants, s.d.: single dose, SR: sustained release, ta: training dataset, te: test dataset.

Model performance is demonstrated in Figure 3 as comparisons of predicted to observed AUC_{last} (a) and C_{max} values (b). Both training and test data were well predicted for all four compounds. In addition, Table 3 provides MRDs of plasma concentration-time profiles and GMFEs of AUC_{last} and C_{max} for the four compounds. With 119/124 of the predicted AUC_{last} and 121/124 of the predicted C_{max} values within the 2-fold acceptance limits, total GMFEs of 1.31 (range 0.43–3.06) for predicted AUC_{last} values and 1.29 (range 0.55–2.87) for C_{max} values further confirmed an adequate model performance. Individual MRD and GMFE values for all plasma profiles are listed in Tables S2.3 and S2.4 in the Supplementary Materials.

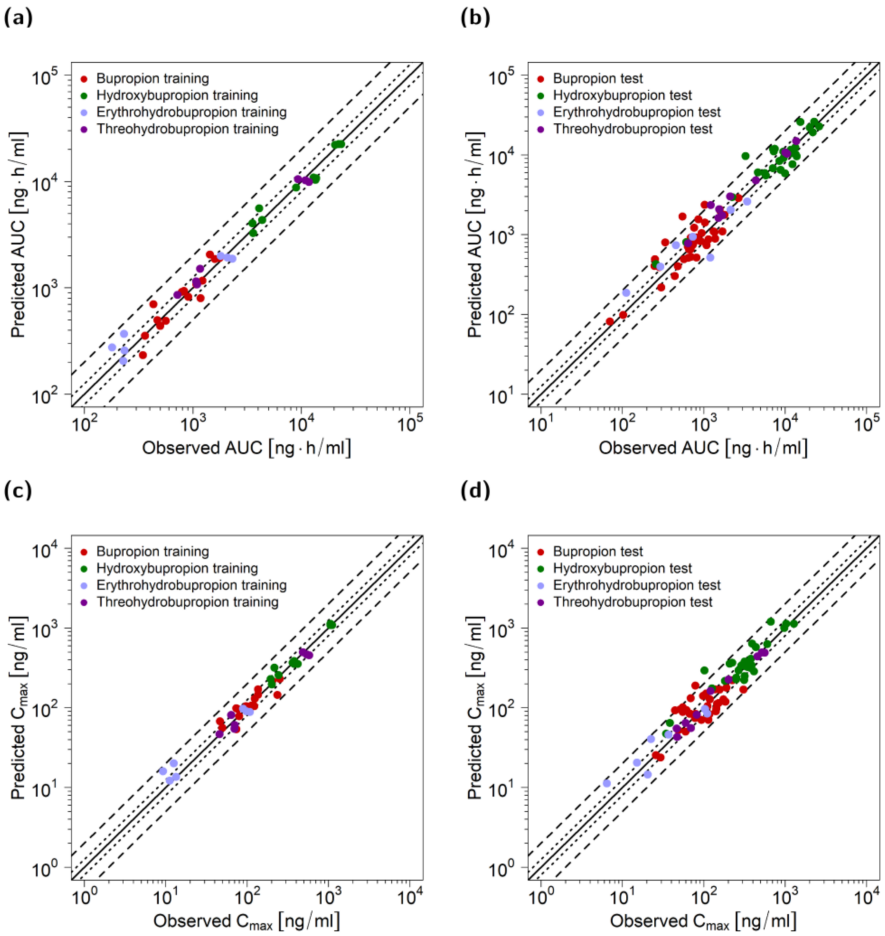

Figure 3. Goodness-of-fit plots of PK parameters for bupropion and metabolites. Predicted AUC of the training (**a**) and test dataset (**b**) as well as C_{max} values of the training (**c**) and test dataset (**d**) compared to observed values. The solid line marks the line of identity, dotted lines indicate 1.25-fold, and dashed lines indicate 2-fold deviation. AUC: area under the plasma concentration-time curve from the time of drug administration to the time of the last concentration measurement, C_{max}: maximum plasma concentration.

Table 3. Summary of quantitative measures of model performance for bupropion and its metabolites, separated by training and test dataset.

	Mean MRD		**Mean GMFE$_{AUC}$**		**Mean GMFE$_{Cmax}$**	
	training	test	training	test	training	test
Bupropion	1.62	1.90	1.20	1.42	1.20	1.41
Hydroxybupropion	1.16	1.30	1.14	1.34	1.10	1.32
Erythrohydrobupropion	1.48	1.38	1.25	1.46	1.26	1.38
Threohydrobupropion	1.36	1.21	1.36	1.23	1.17	1.30
Overall	1.51		1.31		1.29	
Profiles with measure ≤ 2	103/124		119/124		121/124	
Range	1.01–6.21		0.43–3.06		0.55–2.87	

AUC: area under the plasma concentration-time curve from the time of drug administration to the time of the last concentration measurement, C_{max}: maximum plasma concentration, GMFE: geometric mean fold error, MRD: mean relative deviation.

Sensitivity analysis of a 14-day multiple dose simulation of either 100 mg immediate release three times daily, 150 mg sustained release twice daily, or 300 mg extended release once daily, revealed that regardless of the bupropion formulation, the highest impact on bupropion AUC can be attributed to the fraction unbound of bupropion, a fixed literature value. Of the optimized parameters, the most impactful parameter was CYP2B6 kcat for immediate and sustained release formulations. For the extended release formulation, AUC was more sensitive to bupropion lipophilicity than to CYP2B6 kcat. A detailed assessment of model sensitivity is provided in Section 2.5.5 of the Supplementary Materials.

3.2. DGI Modeling and Evaluation

The developed model was extended to describe effects of polymorphism in the CYP2B6 gene on CYP2B6 activity and interaction with CYP2B6 perpetrator drugs. Most published studies only reported mean profiles of populations, often exhibiting multiple different genotypes, or only the respective AUC or HBup/Bup ratio of plasma AUC or single concentrations at specific time points after administration. However, plasma concentration-time profiles of four genetic variants could be gathered from the literature. These included: *CYP2B6*1* (or wildtype), *CYP2B6*4, CYP2B6*5,* and *CYP2B6*6*. Three studies reporting profiles of bupropion and hydroxybupropion were used for development of DGI predictions. Michaelis Menten constants (K_M) were obtained from the literature and corrected for binding in the microsomal assay, if necessary. The rate constant k_{cat} was optimized for the *CYP2B6*6* haplotype. Table 1 provides bupropion K_M and k_{cat} values for the implemented *CYP2B6* alleles. Prediction of *CYP2B6*4 heterozygous* expression was simulated by splitting the implemented CYP2B6-mediated pathway in two clearance processes. In vitro parameters representing the CYP2B6 partition not produced by the *CYP2B6*4* allele were assumed to be equal to parameters for homozygous expression of the respective allele (i.e., *CYP2B6*1/*1* or *CYP2B6*6/*6*). For example, the *CYP2B6*1* allele was simulated with a K_M value of 25.80 µmol/l from the literature and half of the optimized *CYP2B6*1|*1* kcat value of 21.74 1/min. Figure 4 demonstrates the performance of the bupropion DGI model with Figure 4a–c illustrating model-based simulations of 150 mg bupropion as an immediate release tablet alongside their respective observed profiles of three different polymorphisms in comparison to *CYP2B6*1|*1* (wildtype). The effect of DGIs, especially on hydroxybupropion plasma levels, was well described for rapid (*CYP2B6*1|*4*), normal (*CYP2B6*1|*1* or wildtype), intermediate (*CYP2B6*1|*6)* and poor metabolizers (*CYP2B6*6|*6*). Plots documenting the model performance for all modeled bupropion DGIs are provided in Figures S3.4.1 and S3.4.2 of the Supplementary Materials. Figure 4d–e shows predicted compared to observed DGI HBup/Bup ratios calculated for AUC (d) and C_{max} (e). Predicted DGI HBup/Bup ratios were in good agreement with observed ratios, with 20/20 of DGI $AUC_{HBup/Bup}$ and 8/8 of DGI $C_{max\ HBup/Bup}$ values within the 2-fold acceptance limits and 18/20 of DGI $AUC_{HBup/Bup}$ and 7/8 of DGI $C_{max\ HBup/Bup}$ values within the prediction success limits suggested by Guest et al. with

1.25-fold variability [85]. Predicted and observed DGI $AUC_{HBup/Bup}$ ratios showed an overall GMFE of 1.25 (range 0.64–1.77) and DGI $C_{max\ HBup/Bup}$ of 1.35 (range 0.41–1.29). Tables S3.3 and S3.4 of the Supplementary Materials list all calculated MRD and GMFE values of predicted and observed plasma concentration-time profiles and the corresponding AUC and C_{max} values along with the DGI HBup/Bup ratios.

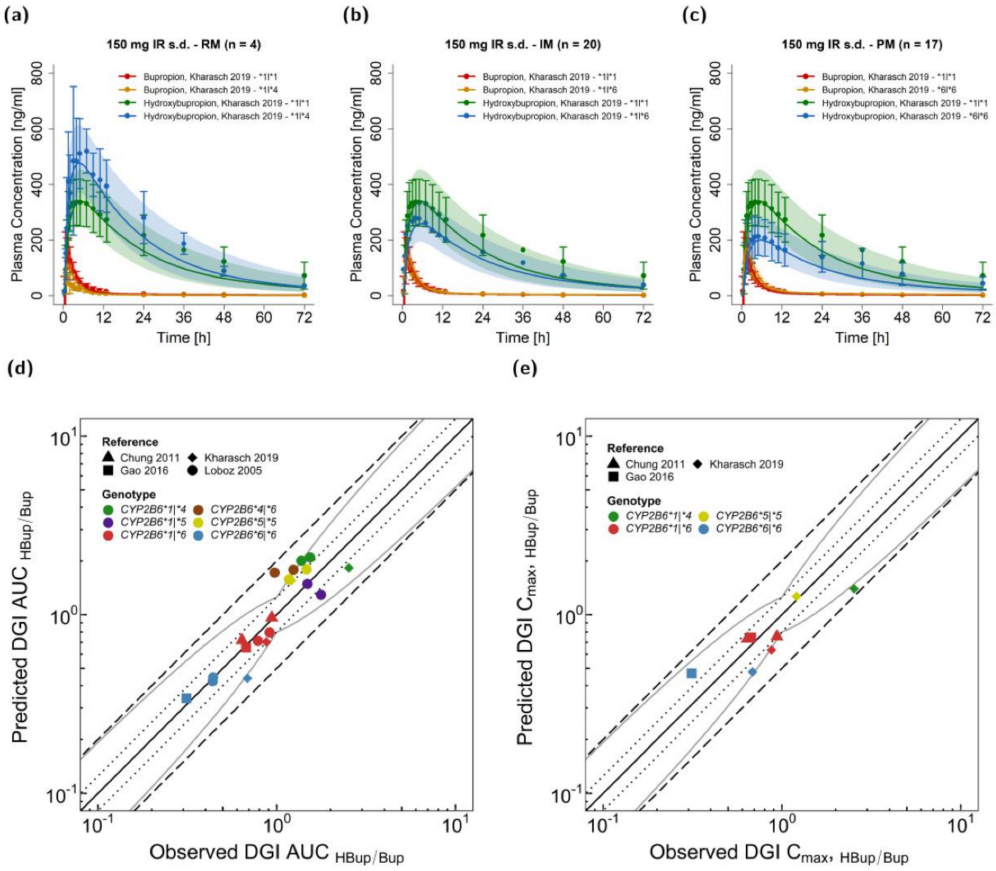

Figure 4. Bupropion CYP2B6 DGI model evaluation. Predicted compared to observed plasma concentration-time profiles are illustrated for *CYP2B6*1/*4* (**a**), *CYP2B6*1/*6* (**b**) and *CYP2B6*6/*6* (**c**) genotypes [17] in comparison to the *CYP2B6*1/*1* genotype (wildtype, n = 21). The effects of respective genetic variants of CYP2B6 are shown in orange and blue for bupropion and hydroxybupropion, respectively; the corresponding profiles of the *CYP2B6*1/*1* genotype are shown in red and green for bupropion and hydroxybupropion, respectively. The solid line illustrates the geometric mean of the population predictions (n = 500) and the shaded area the geometric standard deviation. Predicted compared to observed DGI effect ratios are shown for hydroxybupropion–bupropion ratios of AUC (**d**) and C_{max} (**e**) with different colors indicating the genotypes and different shapes the respective studies [17,35,40,44]. The straight solid line marks the line of identity, the curved solid lines show the prediction acceptance limits proposed by Guest et al. including 1.25-fold variability [85]. Dotted lines indicate 1.25-fold and dashed lines indicate 2-fold deviation. Details on the study protocols and DGI ratios are provided in the Supplementary Materials. AUC: area under the plasma concentration-time curve, C_{max}: maximum plasma concentration, DGI: drug–gene interaction, HBup/Bup: hydroxybupropion–bupropion ratio, IM: intermediate metabolizer, IR: immediate release, PM: poor metabolize, RM: rapid metabolizer, s.d.: single dose.

3.3. Bupropion DDI Modeling and Evaluation

The bupropion DDI model was established and evaluated using a total of five clinical DDI studies with the perpetrator drugs fluvoxamine together with voriconazole (one study) and rifampicin (four studies). Details on the previously developed PBPK models for

rifampicin [60], fluvoxamine [61], and voriconazole [59] are listed in the parameter tables in Section 4 of the Supplementary Materials.

The rifampicin-bupropion DDI was predicted as an induction of CYP2B6, CYP2C19, and UGT2B7 with interaction parameters obtained from the literature [63,64,67]. Additionally, competitive inhibition of CYP2B6 and UGT2B7 by rifampicin was included as well [86,87].

The fluvoxamine-voriconazole-bupropion DDI was predicted as competitive inhibition of CYP2B6 and CYP2C19 metabolism by voriconazole and competitive inhibition of CYP2C19 by fluvoxamine. Literature CYP2C19 K_i values were used for both fluvoxamine and voriconazole [65,66]. CYP2B6 K_i of voriconazole was adjusted via parameter optimization.

Figure 5a–c illustrates predicted plasma concentration-time profiles before and during DDI scenarios in comparison to the corresponding observed data from clinical DDI studies. Induction by rifampicin and inhibition via fluvoxamine and voriconazole are shown for bupropion and hydroxybupropion plasma levels on linear scale for three representative studies (two for rifampicin DDIs with different bupropion release formulations and one for fluvoxamine and voriconazole). In Section 4 of the Supplementary Materials, predicted compared to observed profiles of all investigated rifampicin–bupropion DDIs are presented. In the DDI studies, 600 mg rifampicin were administered daily with 150 mg bupropion given once either as immediate release (Figure 5a) or sustained release tablets (shown in Figure 5b, Figure 6 and in Section 4 of the Supplementary Materials). Plasma concentration-time profiles during CYP2B6 inhibition were only provided in one DDI study with a single dose of bupropion as a cocktail capsule [22]. For the fluvoxamine–voriconazole–bupropion DDI scenario, fluvoxamine and voriconazole were administered concomitantly, 2 h before the bupropion cocktail capsule. Further details on regimens and population characteristics of the DDI studies are listed in Tables S4.4 and S4.5 of the Supplementary Materials.

HBup/Bup ratios were calculated via Equations (4) and (5) for AUC and C_{max} values and are depicted in Figure 5d–e. Here, 12/13 DDI $AUC_{HBup/Bup}$ and 6/6 DDI $C_{max\ HBup/Bup}$ values were within the limits proposed by Guest et al. assuming 1.25-fold variability [85] with overall GMFE values of 1.23 (range 0.74–1.73) for DDI $AUC_{HBup/Bup}$ and 1.46 (range 0.56–1.44) for DDI $C_{max\ HBup/Bup}$. Calculated MRD and GMFE values of all predicted DDI studies are listed in Tables S4.6 and S4.7 of the Supplementary Materials.

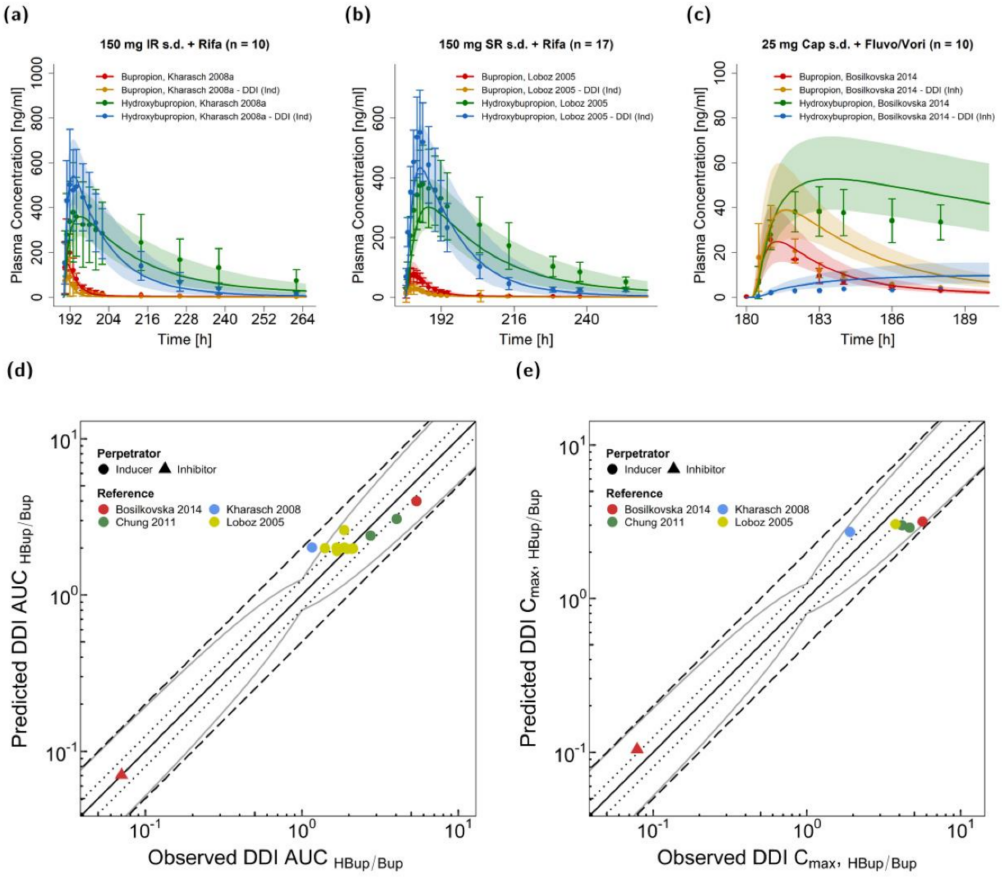

Figure 5. Victim drug plasma concentrations and DDI HBup/Bup ratios for AUC and C_{max} of the modeled bupropion DDIs. Predicted compared to observed plasma concentration-time profiles of bupropion and hydroxybupropion are shown for interactions with rifampicin (**a**,**b**) as well as fluvoxamine and voriconazole (**c**). The profiles during administration of CYP2B6 perpetrator drugs are shown in orange and blue for bupropion and hydroxybupropion, respectively, and the corresponding profiles without DDI are shown in red and green for bupropion and hydroxybupropion, respectively. The solid line illustrates the geometric mean of the population predictions (n = 500) and the shaded area the geometric standard deviation. Predicted compared to observed effect ratio plots for the hydroxybupropion–bupropion ratios of AUC (**d**) and C_{max} (**e**) show data of four CYP2B6 inducer and one CYP2B6 inhibitor studies. Different shapes indicate the perpetrators and different colors the respective studies [19,22,35,44]. The straight solid line marks the line of identity; the curved solid lines show the prediction acceptance limits proposed by Guest et al. including 1.25-fold variability [85]. Dotted lines indicate 1.25-fold and dashed lines indicate 2-fold deviation. Details on the study protocols and the values of all DDI ratios are provided in the Supplementary Materials. AUC: area under the plasma concentration-time curve, Cap: capsule (Geneva Capsule [22]), C_{max}: maximum plasma concentration, DDI: drug-drug interaction, Fluvo/Vori: fluvoxamine and voriconazole, HBup/Bup: hydroxybupropion–bupropion ratio, Ind: inducer, Inh: inhibitor, IR: immediate release, Rifa: rifampicin, s.d.: single dose, SR: sustained release.

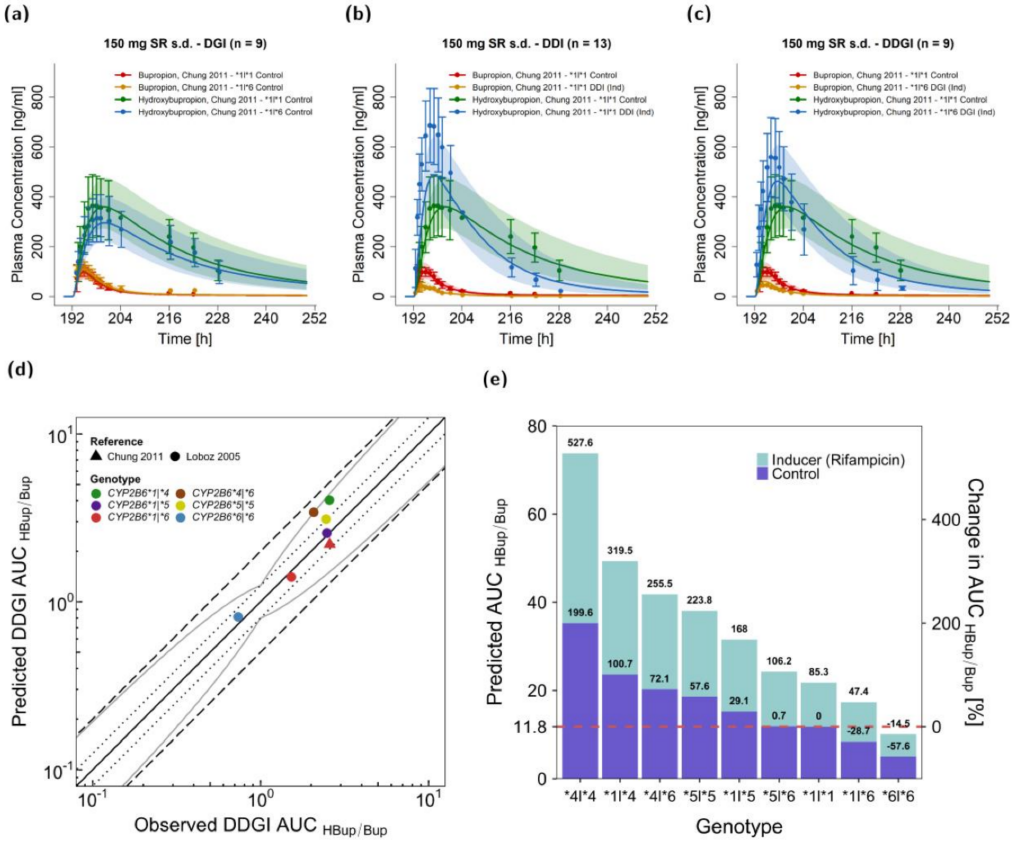

Figure 6. Rifampicin–bupropion CYP2B6 DDGI. Predicted compared to observed plasma concentration-time profiles are illustrated for the CYP2B6 bupropion DGI (*CYP2B6*1* | **6* compared to *CYP2B6*1* | **1*) (**a**), for rifampicin–bupropion DDI in individuals with the *CYP2B6*1* | **1* genotype (**b**) and for the rifampicin–bupropion DDGI for individuals with the *CYP2B6*1* | **6* genotype compared to carriers of the *CYP2B6*1* | **1* genotype (**c**). The predicted and observed plasma concentrations under the combined effects of CYP2B6 genetic polymorphism and perpetrators are shown in orange and blue, respectively, while the control is shown in red and green. The solid line illustrates the geometric mean of the population predictions (n = 500) and the shaded area the geometric standard deviation. Predicted compared to observed effect ratio plot for the hydroxybupropion–bupropion ratio of AUC values are shown for six different genotypes after rifampicin induction (**d**). Different colors indicate the genotypes and different shapes the respective studies ([35,44]). The straight solid line marks the line of identity, the curved solid lines show the prediction acceptance limits proposed by Guest et al. including a 1.25-fold variability [85]. Dotted lines indicate 1.25-fold and dashed lines indicate 2-fold deviation. Predicted effects of rifampicin-bupropion DDGIs on the hydroxybupropion-bupropion AUC ratios were compared to *CYP2B6*1* | **1* without co-administration of rifampicin (**e**). Details on study protocols and DDGI ratios are provided in the Supplementary Materials. AUC area under the plasma concentration-time curve, DGI: drug–gene interaction, DDI: drug–drug interaction, DDGI: drug drug gene interaction, HBup/Bup: hydroxybupropion–bupropion ratio, Ind: inducer, po: oral, s.d.: single dose, SR: sustained release.

3.4. Bupropion DDGI Modeling and Evaluation

DDGIs, combinations of DGIs and DDIs, were predicted for the polymorphisms *CYP2B6*1*, *CYP2B6*4*, *CYP2B6*5*, and *CYP2B6*6* for bupropion intake in DDI scenarios with concomitant rifampicin administration. Rifampicin was administered in multiple oral doses of 600 mg (daily) before a single oral dose of 150 mg bupropion (sustained release) was administered [35,67]. One DDGI study reported plasma concentration-time profiles of bupropion and hydroxybupropion for *CYP2B6*1* | **1* and *CYP2B6*1* | **6* either with or without rifampicin. Figure 6a–c shows predicted compared to observed profiles for a DGI in *CYP2B6*6 heterozygous* subjects (a), a DDI with rifampicin in *CYP2B6 wildtype* subjects

(b), and a DDGI with rifampicin in *CYP2B6*6 heterozygous* subjects (c) compared to *CYP2B6* wildtype subjects receiving bupropion solely. Furthermore, HBup/Bup ratios of AUC_{inf} after rifampicin induction were reported for several CYP2B6 polymorphic individuals [44]. Figure 6d illustrates predicted compared to observed DDGI $AUC_{HBup/Bup}$ values for several genetic variants of *CYP2B6*.

Figure 6e shows predicted $AUC_{HBup/Bup}$ values for all possible allele combinations of the modeled *CYP2B6* variants with or without rifampicin interaction. HBup/Bup ratios were decreased in carriers of the variant *CYP2B6*6* allele. A homozygous *CYP2B6*6* expression with inducer was predicted to be lower in CYP2B6 activity than wildtype CYP2B6 without inducer resulting in a ~15% decrease in $AUC_{HBup/Bup}$. *CYP2B6*5*|**6* individuals were predicted to exhibit $AUC_{HBup/Bup}$ ratios similar to wildtype individuals, with or without inducer. The highest $AUC_{HBup/Bup}$ was simulated for homozygous expression of the gene variant *CYP2B6*4* after rifampicin intake. However, it should be noted that for predictions of the genotypes *CYP2B6*4*|**4* and *CYP2B6*5*|**6*, no observed data for validation were available. In summary, DDGI predictions showed overall DDGI $AUC_{HBup/Bup}$ GMFE values of 1.27 (range 0.85–1.60) with 7/7 of the predicted DDGI $AUC_{HBup/Bup}$ within the acceptance limits of Guest et al., assuming 1.25-fold variability [85].

4. Discussion

In the presented work, a whole-body PBPK model of bupropion and its metabolites hydroxybupropion, threohydrobupropion and erythrohydrobupropion was built and evaluated to predict drug plasma concentrations over a wide dosing range (20–300 mg) for three different oral formulations. Furthermore, the model was extended to describe the effects of CYP2B6 DGIs, DDIs, and rifampicin-bupropion CYP2B6 DDGIs on the PK of bupropion and its metabolites.

So far, only one other bupropion PBPK model has been published yet [88]. Despite demonstrating reasonable performance, in comparison to the presented work, the model did not incorporate a similarly large amount of data for building and evaluation and did not reflect the effects of different genetic alterations of CYP2B6. These shortcomings, which we consider as necessary elements to qualify the bupropion PBPK model as a part of the CYP2B6 network, were addressed in our model.

Bupropion is predominantly metabolized to hydroxybupropion in the liver and, to some extent, also in the gut [10]. Even though CYP2B6 hydroxylation plays a major role in the metabolism of bupropion, the implementation of CYP2C19 as minor metabolic pathway was important to sufficiently describe the data including DDIs and DGIs [17,77]. In addition to CYP2B6 and CYP2C19 metabolism, carbonyl reductases transform bupropion to erythrohydrobupropion and threohydrobupropion [10]. In the presented model, the metabolic pathway along several carbonyl reductases was reduced to the rate-limiting enzymatic step via 11β-HSD for the formation of erythrohydrobupropion and threohydrobupropion. Here, the respective K_M values for all implemented enzymes could be informed from the literature. After a single dose of 150 mg bupropion, the bupropion fractions metabolized were predicted as 58%, 28%, and 13% via CYP2B6, 11β-HSD, and CYP2C19, respectively (Figure S2.1.1 of the Supplementary Materials). Furthermore, the model predicts an extensive metabolism of bupropion (99%) after complete absorption with small fractions excreted unchanged to urine and feces (~1%), which is consistent with the literature [9]. Reported bupropion fractions metabolized varied with measurements from in vitro clearance data of 56% or 12% for hydroxybupropion formation and 40% or 68% for threohydrobupropion formation [8,89], which are in reasonable agreement with predicted values.

Bupropion shows affinity to a variety of therapeutic targets, such as numerous acetylcholine receptors and dopamine and noradrenaline reuptake transporters [10]. Target binding was incorporated into our model as it improved the description of the concentration-time profiles. To simplify the complex binding of bupropion to several targets, only binding to the noradrenaline reuptake transporter was implemented, as it covers the expression in all relevant organs, such as brain or gastro-intestinal tract, where noradrenaline and

dopamine reuptake transporters, as well as nicotinic acetylcholine receptors are expected. The applied K_D value is in good agreement with literature values describing binding or inhibition of the different relevant targets [78–80].

The bupropion metabolism is especially sensitive to genetic polymorphisms in CYP2B6 [17]. Unfortunately, documentation on genetic polymorphisms of participants was poor in most clinical studies. Either mean profiles of mixed populations were presented or no genotype information was reported. Nevertheless, gene variants *CYP2B6*1*, **4*, **5*, and **6* were included in our model and described the available plasma concentration-time profiles of bupropion and hydroxybupropion sufficiently well. Dose adjustment guidelines for genetic polymorphisms have not been implemented yet. However, as hydroxybupropion might play an important role in the occurrence and onset of seizures after rapid bupropion absorption [10,12–14], the presented model could support a rational individualized CYP2B6 polymorphism-guided dose selection.

The presented DDI network includes interactions via CYP2B6, CYP2C19, and UGT2B7. The rifampicin–bupropion DDI covers the induction of CYP2B6, CYP2C19, and UGT2B7, with simultaneous competitive inhibition of CYP2B6 and UGT2B7. All rifampicin–bupropion interaction parameters were derived from the literature [45–48]. However, inhibition is relatively weak with inhibition constants (K_i) of 118.50 µmol/L and 554.87 µmol/L for CYP2B6 and UGT2B7 [86,87] and presumably negligible; especially after multiple dose applications of rifampicin. For single dose administrations, rifampicin's inhibitory activity on bupropion could not be evaluated, due to a lack of clinical bupropion DDI data.

Voriconazole is a known CYP2B6 inhibitor that displayed interactions with bupropion and efavirenz [74]. The reported K_i value of voriconazole was not strong enough to fully describe the observed in vivo effects. This seems reasonable, since the metabolite voriconazole N-oxide is also responsible for the inhibitory effect on CYP2B6 [90], but was not implemented in the published PBPK model [59]. Moreover, a polymorphism-dependent CYP2B6 inhibition of voriconazole was previously described for efavirenz hydroxylation, where lower K_i values were reported for *CYP2B6*6* than for *CYP2B6*1* [74]. In the DDI study conducted by Bosilkovska et al. [22], six of 10 subjects exhibited a *CYP2B6*6* polymorphism, which could potentially explain a deviation in prediction. Due to the lack of relevant clinical data, the K_i value of voriconazole for CYP2B6 had to be optimized and could not be validated yet. Hence, further in vitro studies are needed to optimize and evaluate the voriconazole DDI. Inhibition of CYP2C19 was implemented, as fluvoxamine and voriconazole are listed as strong and weak inhibitors for CYP2C19 by the FDA, respectively [16]. As bupropion is also a known CYP2D6 inhibitor, we assumed that the inhibitory effect on CYP2D6-mediated fluvoxamine metabolism is negligibly small, as fluvoxamine is given 2 h prior to bupropion administration, and as bupropion's strong CYP2D6 inhibition potential is predominately attributed to its metabolites and a CYP2D6 downregulation after long-term bupropion intake [91].

The model correctly predicted DDGI plasma profiles of bupropion co-administered with rifampicin in *CYP2B6*6* heterozygous subjects. Furthermore, DDGI model performance was successfully evaluated by comparison of predicted and reported HBup/Bup AUC ratios. Subsequently, potential DDGIs were simulated for combinations of the genetic *CYP2B6* variants *CYP2B6*1*, *CYP2B6*4*, *CYP2B6*5*, and *CYP2B6*6*. The simulated scenarios illustrate the models' potential to investigate the effect of DDGIs on bupropion and hydroxybupropion plasma levels. Whether the simulated DDGI combinations lead to the predicted changes in HBup/Bup ratios, especially the profound increase in rapid metabolizers receiving the CYP2B6 inducer rifampicin, should be carefully evaluated in clinical studies. Moreover, pharmacological implications of bupropion intake, with or without perpetrator, in CYP2B6 polymorphic patients, are still unclear. While clinical efficacy or tolerability can be correlated to plasma levels of bupropion or its metabolites, guidelines regarding bupropion dosing have yet to be established. Our presented model demonstrated its flexibility in simulations of various DDGI scenarios and can be applied to

develop rational dosing recommendations for bupropion drug labeling or clinical study design.

5. Conclusions

A comprehensive parent-metabolite PBPK model of bupropion including whole-body PBPK models of bupropion and the metabolites hydroxybupropion, erythrohydrobupropion, and threohydrobupropion was developed. Bupropion pharmacokinetics were thoroughly described for tablets with different release formulations in single and multiple dose regimens. The established CYP2B6 network incorporates reliable prediction of DGIs with several polymorphisms, DDIs and DDGIs as combinations of DGIs and DDIs. A transparent and detailed documentation of the model development and performance further underlines the model quality. The final PBPK model files are freely available in the Open Systems Pharmacology repository (www.open-systems-pharmacology.org, December 2020) [26] to assist the development of bupropion dosing guidelines and to support DDI studies in drug discovery and development.

Supplementary Materials: The following are available at https://www.mdpi.com/1999-4923/13/3/331/s1, Electronic Supplementary Materials: A comprehensive reference manual, providing documentation of the complete model performance assessment.

Author Contributions: Conceptualization, F.Z.M., L.M.F., N.H., D.S. and T.L.; funding acquisition, T.L.; investigation, F.Z.M., L.M.F., N.H., D.S. and T.L.; visualization, F.Z.M.; writing—original draft, F.Z.M.; writing—review and editing, F.Z.M., L.M.F., N.H., D.S. and T.L. All authors have read and agreed to the published version of the manuscript.

Funding: This work has received support from the project "Open-source modeling framework for automated quality control and management of complex life science system models" (OSMOSES), which is funded by the German Federal Ministry of Education and Research (BMBF, grant ID:031L0161C). We acknowledge support by the Deutsche Forschungsgemeinschaft (DFG, German Research Foundation) and Saarland University within the funding program Open Access Publishing.

Institutional Review Board Statement: Not applicable.

Informed Consent Statement: Not applicable.

Data Availability Statement: All modeling files including utilized clinical study data can be found at https://github.com/Open-Systems-Pharmacology (accessed on 31 December 2020).

Acknowledgments: We thank Elizaveta Burgakova for her work during her internship at Saarland University.

Conflicts of Interest: Thorsten Lehr has received research grants from the German Federal Ministry of Education and Research (grant 031L0161C). Fatima Zahra Marok, Laura Maria Fuhr, Nina Hanke and Dominik Selzer declare no conflict of interest. The funders had no role in the design of the study; in the collection, analyses, or interpretation of data; in the writing of the manuscript, or in the decision to publish the results.

References

1. Fava, M.; Rush, A.J.; Thase, M.E.; Clayton, A.; Stahl, S.M.; Pradko, J.F.; Johnston, J.A. 15 Years of Clinical Experience with Bupropion HCl. *Prim. Care Companion J. Clin. Psychiatry* **2005**, *07*, 106–113. [CrossRef] [PubMed]
2. DrugStats, C. Multum Therapeutic Class Comparison, United States, 2018—Total Prescribtions in 2018. Available online: https://clincalc.com/DrugStats/TC/PsychotherapeuticAgents (accessed on 17 December 2020).
3. Connarn, J.N.; Flowers, S.; Kelly, M.; Luo, R.; Ward, K.M.; Harrington, G.; Moncion, I.; Kamali, M.; McInnis, M.; Feng, M.R.; et al. Pharmacokinetics and Pharmacogenomics of Bupropion in Three Different Formulations with Different Release Kinetics in Healthy Human Volunteers. *AAPS J.* **2017**, *19*, 1513–1522. [CrossRef] [PubMed]
4. Fokina, V.M.; Xu, M.; Rytting, E.; Abdel-Rahman, S.Z.; West, H.; Oncken, C.; Clark, S.M.; Ahmed, M.S.; Hankins, G.D.V.; Nanovskaya, T.N. Pharmacokinetics of bupropion and its pharmacologically active metabolites in pregnancy. *Drug Metab. Dispos.* **2016**, *44*, 1832–1838. [CrossRef]
5. Slemmer, J.E.; Martin, B.R.; Damaj, M.I. Bupropion is a nicotinic antagonist. *J. Pharmacol. Exp. Ther.* **2000**, *295*, 321–327. [PubMed]

6. Stahl, S.M.; Pradko, J.F.; Haight, B.R.; Modell, J.G.; Rockett, C.B.; Learned-Coughlin, S. A Review of the Neuropharmacology of Bupropion, a Dual Norepinephrine and Dopamine Reuptake Inhibitor. *Prim. Care Companion J. Clin. Psychiatry* **2004**, *06*, 159–166. [CrossRef]
7. Eriksson, O.; Långström, B.; Josephsson, R. Assessment of receptor occupancy-over-time of two dopamine transporter inhibitors by [11C]CIT and target controlled infusion. *Ups. J. Med. Sci.* **2011**, *116*, 100–106. [CrossRef]
8. Sager, J.E.; Price, L.S.L.; Isoherranen, N. Stereoselective Metabolism of Bupropion to OH-bupropion, Threohydrobupropion, Erythrohydrobupropion, and 4′-OH-bupropion in vitro. *Drug Metab. Dispos.* **2016**, *44*, 1709–1719. [CrossRef]
9. Biovial Corporation. Wellbutrin XL ®®(Bupropion Hydrochloride Extended-Release Tablets)—Medicine Guide. Available online: https://www.accessdata.fda.gov/drugsatfda_docs/label/2010/021515s022lbl.pdf (accessed on 22 January 2021).
10. Costa, R.; Oliveira, N.G.; Dinis-Oliveira, R.J. Pharmacokinetic and pharmacodynamic of bupropion: Integrative overview of relevant clinical and forensic aspects. *Drug Metab. Rev.* **2019**, *51*, 293–313. [CrossRef] [PubMed]
11. Johnston, J.A.; Fiedler-Kelly, J.; Glover, E.D.; Sachs, D.P.L.; Grasela, T.H.; De Veaugh-Geiss, J. Relationship between drug exposure and the efficacy and safety of bupropion sustained release for smoking cessation. *Nicotine Tob. Res.* **2001**, *3*, 131–140. [CrossRef]
12. Silverstone, P.H.; Williams, R.; McMahon, L.; Fleming, R.; Fogarty, S. Convulsive liability of bupropion hydrochloride metabolites in Swiss albino mice. *Ann. Gen. Psychiatry* **2008**, *7*, 19. [CrossRef] [PubMed]
13. Davidson, J. Seizures and bupropion: A review. *J. Clin. Psychiatry* **1989**, *50*, 256–261. [CrossRef]
14. Dunner, D.L.; Zisook, S.; Billow, A.A.; Batey, S.R.; Johnston, J.A.; Ascher, J.A. A Prospective Safety Surveillance Study for Bupropion Sustained-Release in the Treatment of Depression. *J. Clin. Psychiatry* **1998**, *59*, 366–373. [CrossRef]
15. Gufford, B.T.; Lu, J.B.L.; Metzger, I.F.; Jones, D.R.; Desta, Z. Stereoselective glucuronidation of bupropion metabolites in vitro and in vivo. *Drug Metab. Dispos.* **2016**, *44*, 544–553. [CrossRef]
16. U.S. Food and Drug Administration. Drug Development and Drug Interactions: Table of Substrates, Inhibitors and Inducers. FDA. Available online: https://www.fda.gov/drugs/drug-interactions-labeling/drug-development-and-drug-interactions-table-substrates-inh (accessed on 31 December 2020).
17. Kharasch, E.D.; Crafford, A. Common Polymorphisms of CYP2B6 Influence Stereoselective Bupropion Disposition. *Clin. Pharmacol. Ther.* **2019**, *105*, 142–152. [CrossRef]
18. Masters, A.R.; Gufford, B.T.; Lu, J.B.L.; Metzger, I.F.; Jones, D.R.; Desta, Z. Chiral Plasma Pharmacokinetics and Urinary Excretion of Bupropion and Metabolites in Healthy Volunteers. *J. Pharmacol. Exp. Ther.* **2016**, *358*, 230–238. [CrossRef] [PubMed]
19. Khrarasch, E.D.; Bedynek, P.S.; Walker, A.; Whittington, D.; Hoffer, C.; and Park, S. Mechanism of ritonavir changes in methadone pharmacokinetics and pharmacodynamics. II. Ritonavir effects on CYP3A and P- glycoprotein activities. *Clin. Pharmacol. Ther.* **2008**, *84*, 506–512. [CrossRef] [PubMed]
20. Hogeland, G.W.; Swindells, S.; McNabb, J.C.; Kashuba, A.D.M.; Yee, G.C.; Lindley, C.M. Lopinavir/ritonavir Reduces Bupropion Plasma Concentrations in Healthy Subjects. *Clin. Pharmacol. Ther.* **2007**, *81*, 69–75. [CrossRef] [PubMed]
21. Turpeinen, M.; Tolonen, A.; Uusitalo, J.; Jalonen, J.; Pelkonen, O.; Laine, K. Effect of clopidogrel and ticlopidine on cytochrome P450 2B6 activity as measured by bupropion hydroxylation. *Clin. Pharmacol. Ther.* **2005**, *77*, 553–559. [CrossRef]
22. Bosilkovska, M.; Samer, C.F.; Déglon, J.; Rebsamen, M.; Staub, C.; Dayer, P.; Walder, B.; Desmeules, J.A.; Daali, Y. Geneva Cocktail for Cytochrome P450 and P-Glycoprotein Activity Assessment Using Dried Blood Spots. *Clin. Pharmacol. Ther.* **2014**, *96*, 349–359. [CrossRef]
23. Reese, M.J.; Wurm, R.M.; Muir, K.T.; Generaux, G.T.; St. John-Williams, L.; Mcconn, D.J. An in Vitro Mechanistic Study to Elucidate the Desipramine/Bupropion Clinical Drug-Drug Interaction. *Drug Metab. Dispos.* **2008**, *36*, 1198–1201. [CrossRef]
24. Desta, Z.; Gammal, R.S.; Gong, L.; Whirl-Carrillo, M.; Gaur, A.H.; Sukasem, C.; Hockings, J.; Myers, A.; Swart, M.; Tyndale, R.F.; et al. Clinical Pharmacogenetics Implementation Consortium (CPIC) Guideline for CYP2B6 and Efavirenz-Containing Antiretroviral Therapy. *Clin. Pharmacol. Ther.* **2019**, *106*, 726–733. [CrossRef]
25. Wojtyniak, J.; Selzer, D.; Schwab, M.; Lehr, T. Physiologically Based Precision Dosing Approach for Drug-Drug-Gene Interactions: A Simvastatin Network Analysis. *Clin. Pharmacol. Ther.* **2020**, cpt.2111. [CrossRef]
26. Lippert, J.; Burghaus, R.; Edginton, A.; Frechen, S.; Karlsson, M.; Kovar, A.; Lehr, T.; Milligan, P.; Nock, V.; Ramusovic, S.; et al. Open Systems Pharmacology Community—An Open Access, Open Source, Open Science Approach to Modeling and Simulation in Pharmaceutical Sciences. *CPT Pharmacomet. Syst. Pharmacol.* **2019**, *8*, 878–882. [CrossRef] [PubMed]
27. Wojtyniak, J.; Britz, H.; Selzer, D.; Schwab, M.; Lehr, T. Data Digitizing: Accurate and Precise Data Extraction for Quantitative Systems Pharmacology and Physiologically-Based Pharmacokinetic Modeling. *CPT Pharmacomet. Syst. Pharmacol.* **2020**, *9*, 322–331. [CrossRef] [PubMed]
28. Hesse, L.M.; Greenblatt, D.J.; von Moltke, L.L.; Court, M.H. Ritonavir Has Minimal Impact on the Pharmacokinetic Disposition of a Single Dose of Bupropion Administered to Human Volunteers. *J. Clin. Pharmacol.* **2006**, *46*, 567–576. [CrossRef]
29. Yamazaki, T.; Desai, A.; Goldwater, R.; Han, D.; Howieson, C.; Akhtar, S.; Kowalski, D.; Lademacher, C.; Pearlman, H.; Rammelsberg, D.; et al. Pharmacokinetic Effects of Isavuconazole Coadministration With the Cytochrome P450 Enzyme Substrates Bupropion, Repaglinide, Caffeine, Dextromethorphan, and Methadone in Healthy Subjects. *Clin. Pharmacol. Drug Dev.* **2017**, *6*, 54–65. [CrossRef]
30. Posner, J.; Bye, A.; Jeal, S.; Peck, A.W.; Whiteman, P. Alcohol and bupropion pharmacokinetics in healthy male volunteers. *Eur. J. Clin. Pharmacol.* **1984**, *26*, 627–630. [CrossRef] [PubMed]

31. Posner, J.; Bye, A.; Dean, K.; Peck, A.W.; Whiteman, P.D. The disposition of bupropion and its metabolites in healthy male volunteers after single and multiple doses. *Eur. J. Clin. Pharmacol.* **1985**, *29*, 97–103. [CrossRef]
32. Oberegger, W.; Eradiri, O.; Zhou, F.; Maes, P. Modified Release Tablet of Bupropion Hydrochloride. U.S. Patent No. US 2006/0228415 A1, 12 October 2006.
33. Kharasch, E.D.; Mitchell, D.; Coles, R.; Blanco, R. Rapid Clinical Induction of Hepatic Cytochrome P4502B6 Activity by Ritonavir. *Antimicrob. Agents Chemother.* **2008**, *52*, 1663–1669. [CrossRef]
34. Benowitz, N.L.; Zhu, A.Z.X.; Tyndale, R.F.; Dempsey, D.; Jacob, P. Influence of CYP2B6 genetic variants on plasma and urine concentrations of bupropion and metabolites at steady state. *Pharmacogenet. Genom.* **2013**, *23*, 135–141. [CrossRef]
35. Chung, J.Y.; Cho, J.Y.; Lim, H.S.; Kim, J.R.; Yu, K.S.; Lim, K.S.; Shin, S.G.; Jang, I.J. Effects of pregnane X receptor (NR1I2) and CYP2B6 genetic polymorphisms on the induction of bupropion hydroxylation by rifampin. *Drug Metab. Dispos.* **2011**, *39*, 92–97. [CrossRef]
36. Dennison, J.; Puri, A.; Warrington, S.; Endo, T.; Adeloye, T.; Johnston, A. Amenamevir: Studies of Potential CYP2C8- and CYP2B6-Mediated Pharmacokinetic Interactions with Montelukast and Bupropion in Healthy Volunteers. *Clin. Pharmacol. Drug Dev.* **2018**, *7*, 860–870. [CrossRef]
37. Fan, L.; Wang, J.C.; Jiang, F.; Tan, Z.R.; Chen, Y.; Li, Q.; Zhang, W.; Wang, G.; Lei, H.P.; Hu, D.L.; et al. Induction of cytochrome P450 2B6 activity by the herbal medicine baicalin as measured by bupropion hydroxylation. *Eur. J. Clin. Pharmacol.* **2009**, *65*, 403–409. [CrossRef] [PubMed]
38. Farid, N.A.; Payne, C.D.; Ernest, C.S.; Li, Y.G.; Winters, K.J.; Salazar, D.E.; Small, D.S. Prasugrel, a new thienopyridine antiplatelet drug, weakly inhibits cytochrome P450 2B6 in humans. *J. Clin. Pharmacol.* **2008**, *48*, 53–59. [CrossRef] [PubMed]
39. Gao, L.C.; Huang, X.; Tan, Z.R.; Fan, L.; Zhou, H.H. The effects of sodium ferulate on the pharmacokinetics of bupropion and its active metabolite in healthy men. *Eur. Rev. Med. Pharmacol. Sci.* **2012**, *16*, 1192–1196.
40. Gao, L.-C.; Liu, F.-Q.; Yang, L.; Cheng, L.; Dai, H.-Y.; Tao, R.; Cao, S.P.; Wang, D.; Tang, J. The P450 oxidoreductase (POR) rs2868177 and cytochrome P450 (CYP) 2B6*6 polymorphisms contribute to the interindividual variability in human CYP2B6 activity. *Eur. J. Clin. Pharmacol.* **2016**, *72*, 1205–1213. [CrossRef]
41. Hsyu, P.-H.; Singh, A.; Giargiari, T.D.; Dunn, J.A.; Ascher, J.A.; Johnston, J.A. Pharmacokinetics of Bupropion and its Metabolites in Cigarette Smokers versus Nonsmokers. *J. Clin. Pharmacol.* **1997**, *37*, 737–743. [CrossRef]
42. Lei, H.; Ji, W.; Lin, J.; Chen, H.; Tan, Z.; Hu, D.; Liu, L.; Zhou, H. Effects of Ginkgo biloba extract on the pharmacokinetics of bupropion in healthy volunteers. *Br. J. Clin. Pharmacol.* **2009**, *68*, 201–206. [CrossRef]
43. Lei, H.-P.; Yu, X.-Y.; Xie, H.-T.; Li, H.-H.; Fan, L.; Dai, L.-L.; Chen, Y.; Zhou, H.-H. Effect of St. John's wort supplementation on the pharmacokinetics of bupropion in healthy male Chinese volunteers. *Xenobiotica* **2010**, *40*, 275–281. [CrossRef]
44. Loboz, K.; Gross, A.; Williams, K.; Liauw, W.; Day, R.; Blievernicht, J.; Zanger, U.; McLachlan, A. Cytochrome P450 2B6 activity as measured by bupropion hydroxylation: Effect of induction by rifampin and ethnicity. *Clin. Pharmacol. Ther.* **2006**, *80*, 75–84. [CrossRef]
45. Palovaara, S.; Pelkonen, O.; Uusitalo, J.; Laine, K. Inhibition of cytochrome P450 2B6 activity by hormone replacement therapy and oral contraceptive as measured by bupropion hydroxylation. *Clin. Pharmacol. Ther.* **2003**, *74*, 326–333. [CrossRef]
46. Li, B.; Nangia, A.; Ming, C.; Cheng, X.X. Controlled Release Oral Dosage Form. U.S. Patent No. US 8,545,880 B2, 30 September 2013.
47. Qin, W.; Zhang, W.; Liu, Z.; Chen, X.; Tan, Z.; Hu, D.; Wang, D.; Fan, L.; Zhou, H. Rapid clinical induction of bupropion hydroxylation by metamizole in healthy Chinese men. *Br. J. Clin. Pharmacol.* **2012**, *74*, 999–1004. [CrossRef] [PubMed]
48. Robertson, S.M.; Maldarelli, F.; Natarajan, V.; Formentini, E.; Alfaro, R.M.; Penzak, S.R. Efavirenz induces CYP2B6-mediated hydroxylation of bupropion in healthy subjects. *J. Acquir. Immune Defic. Syndr.* **2008**, *49*, 513–519. [CrossRef]
49. Turpeinen, M.; Koivuviita, N.; Tolonen, A.; Reponen, P.; Lundgren, S.; Miettunen, J.; Metsärinne, K.; Rane, A.; Pelkonen, O.; Laine, K. Effect of renal impairment on the pharmacokinetics of bupropion and its metabolites. *Br. J. Clin. Pharmacol.* **2007**, *64*, 165–173. [CrossRef] [PubMed]
50. Turpeinen, M.; Uusitalo, J.; Lehtinen, T.; Kailajärvi, M.; Pelkonen, O.; Vuorinen, J.; Tapanainen, P.; Stjernschantz, C.; Lammintausta, R.; Scheinin, M. Effects of Ospemifene on Drug Metabolism Mediated by Cytochrome P450 Enzymes in Humans in Vitro and in Vivo. *Int. J. Mol. Sci.* **2013**, *14*, 14064–14075. [CrossRef] [PubMed]
51. Kustra, R.; Corrigan, B.; Dunn, J.; Duncan, B.; Hsyu, P.H. Lack of effect of cimetidine on the pharmacokinetics of sustained-release bupropion. *J. Clin. Pharmacol.* **1999**, *39*, 1184–1188.
52. Schmid, Y.; Rickli, A.; Schaffner, A.; Duthaler, U.; Grouzmann, E.; Hysek, C.M.; Liechti, M.E. Interactions between Bupropion and 3,4-Methylenedioxymethamphetamine in Healthy Subjects. *J. Pharmacol. Exp. Ther.* **2015**, *353*, 102–111. [CrossRef] [PubMed]
53. Woodcock, J.; Khan, M.; Yu, L.X. Withdrawal of Generic Budeprion for Nonbioequivalence. *N. Engl. J. Med.* **2012**, *367*, 2461–2463. [CrossRef]
54. Paiement, N.; Noonan, P.K.; González, M.A.; Zerbe, H. Steady State Plasma Levels of Bupropion After Administration of 3×150 Mg Extended Release Reference Tablets and Switching to 1x450 Mg Extended Release 450ER Tablets. *Int. J. Clin. Pharmacol. Toxicol.* **2012**, *1*, 26–31. [CrossRef]
55. Bosilkovska, M.; Samer, C.; Déglon, J.; Thomas, A.; Walder, B.; Desmeules, J.; Daali, Y. Evaluation of Mutual Drug-Drug Interaction within Geneva Cocktail for Cytochrome P450 Phenotyping using Innovative Dried Blood Sampling Method. *Basic Clin. Pharmacol. Toxicol.* **2016**, *119*, 284–290. [CrossRef]

56. Findlay, J.W.A.; Van Wyck Fleet, J.; Smith, P.G.; Butz, R.F.; Hinton, M.L.; Blum, M.R.; Schroeder, D.H. Pharmacokinetics of bupropion, a novel antidepressant agent, following oral administration to healthy subjects. *Eur. J. Clin. Pharmacol.* **1981**, *21*, 127–135. [CrossRef]
57. Zahner, C.; Kruttschnitt, E.; Uricher, J.; Lissy, M.; Hirsch, M.; Nicolussi, S.; Krähenbühl, S.; Drewe, J. No Clinically Relevant Interactions of St. John's Wort Extract Ze 117 Low in Hyperforin with Cytochrome P450 Enzymes and P-glycoprotein. *Clin. Pharmacol. Ther.* **2019**, *106*, 432–440. [CrossRef]
58. Open Systems Pharmacology Suite Community. PK-Sim®®Ontogeny Database Documentation, Version 7.3. Available online: https://github.com/Open-Systems-Pharmacology/OSPSuite.Documentation/blob/master/PK-Sim%20Ontogeny%20Database%20Version%207.3.pdf (accessed on 31 December 2020).
59. Li, X.; Frechen, S.; Moj, D.; Lehr, T.; Taubert, M.; Hsin, C.-H.; Mikus, G.; Neuvonen, P.J.; Olkkola, K.T.; Saari, T.I.; et al. A Physiologically Based Pharmacokinetic Model of Voriconazole Integrating Time-Dependent Inhibition of CYP3A4, Genetic Polymorphisms of CYP2C19 and Predictions of Drug–Drug Interactions. *Clin. Pharmacokinet.* **2020**, *59*, 781–808. [CrossRef]
60. Hanke, N.; Frechen, S.; Moj, D.; Britz, H.; Eissing, T.; Wendl, T.; Lehr, T. PBPK Models for CYP3A4 and P-gp DDI prediction: A modeling network of rifampicin, itraconazole, clarithromycin, midazolam, alfentanil, and digoxin. *CPT Pharmacometrics Syst. Pharmacol.* **2018**, *7*, 647–659. [CrossRef]
61. Britz, H.; Hanke, N.; Volz, A.; Spigset, O.; Schwab, M.; Eissing, T.; Wendl, T.; Frechen, S.; Lehr, T. Physiologically-based pharmacokinetic models for CYP1A2 drug–drug interaction prediction: A modeling network of fluvoxamine, theophylline, caffeine, rifampicin, and midazolam. *CPT Pharmacomet. Syst. Pharmacol.* **2019**, *8*, 296–307. [CrossRef] [PubMed]
62. Langenbucher, F. Linearization of dissolution rate curves by the Weibull distribution. *J. Pharm. Pharmacol.* **1972**, *24*, 979–981. [CrossRef]
63. Ramamoorthy, A.; Liu, Y.; Philips, S.; Desta, Z.; Lin, H.; Goswami, C.; Gaedigk, A.; Li, L.; Flockhart, D.A.; Skaar, T.C. Regulation of microRNA expression by rifampin in human hepatocytes. *Drug Metab. Dispos.* **2013**, *41*, 1763–1768. [CrossRef] [PubMed]
64. Zhang, J.G.; Patel, R.; Clark, R.J.; Ho, T.; Trisdale, S.K.; Fang, Y.; Stresser, D.M. Effect of Fifteen CYP3A4 in vitro Inducers on the Induction of Hepatocytes: A Trend Analysis. Poster Presented at 20th North American ISSX Meeting, Orlando FL, USA, 18–22 October 2015.
65. Jeong, S.; Nguyen, P.D.; Desta, Z. Comprehensive in vitro analysis of voriconazole inhibition of eight cytochrome P450 (CYP) enzymes: Major effect on CYPs 2B6, 2C9, 2C19, and 3A. *Antimicrob. Agents Chemother.* **2009**, *53*, 541–551. [CrossRef] [PubMed]
66. Foti, R.S.; Wahlstrom, J.L. CYP2C19 Inhibition: The Impact of Substrate Probe Selection on in Vitro Inhibition Profiles. *Drug Metab. Dispos.* **2008**, *36*, 523–528. [CrossRef]
67. Soars, M.G.; Petullo, D.M.; Eckstein, J.A.; Kasper, S.C.; Wrighton, S.A. An assessment of UDP-glucuronosyltransferase induction using primary human hepatocytes. *Drug Metab. Dispos.* **2004**, *32*, 140–148. [CrossRef] [PubMed]
68. Les Laboratoires Servier. Servier Medical At. Available online: https://smart.servier.com/ (accessed on 27 November 2020).
69. ChemAxon Bupropion. Available online: https://chemicalize.com/app/calculation/bupropion (accessed on 27 November 2020).
70. Takayanagi, T.; Itoh, D.; Mizugushi, H. Analysis of Acid Dissociation Equilibrium of Bupropion by Capillary Zone Electrophoresis after the Heat-Degradation. *Chromatography* **2016**, *37*, 105–109. [CrossRef]
71. Muralidhar, P.; Bhargav, E.; Srinath, B. Formulation and optimization of bupropion HCl in microspongesby 2^3 factorial design. *Int. J. Pharm. Sci. Res.* **2017**, *8*, 1134–1144. [CrossRef]
72. Berezhkovskiy, L.M. Volume of distribution at steady state for a linear pharmacokinetic system with peripheral elimination. *J. Pharm. Sci.* **2004**, *93*, 1628–1640. [CrossRef]
73. Open Systems Pharmacology Suite Community. Open Systems Pharmacology Suite Manual, Version 7.0.0. 2017. Available online: http://www.open-systems-pharmacology.org/ (accessed on 31 December 2020).
74. Xu, C.; Ogburn, E.T.; Guo, Y.; Desta, Z. Effects of the CYP2B6*6 allele on catalytic properties and inhibition of CYP2B6 in vitro: Implication for the mechanism of reduced efavirenz metabolism and other CYP2B6 substrates in vivo. *Drug Metab. Dispos.* **2012**, *40*, 717–725. [CrossRef] [PubMed]
75. Wang, P.F.; Neiner, A.; Kharasch, E.D. Stereoselective Bupropion Hydroxylation by Cytochrome P450 CYP2B6 and Cytochrome P450 Oxidoreductase Genetic Variants. *Drug Metab. Dispos.* **2020**, *48*, 438–445. [CrossRef]
76. Wang, X.; Abdelrahman, D.R.; Zharikova, O.L.; Patrikeeva, S.L.; Hankins, G.D.V.; Ahmed, M.S.; Nanovskaya, T.N. Bupropion metabolism by human placenta. *Biochem. Pharmacol.* **2010**, *79*, 1684–1690. [CrossRef] [PubMed]
77. Chen, Y.; Liu, H.F.; Liu, L.; Nguyen, K.; Jones, E.B.; Fretland, A.J. The in vitro metabolism of bupropion revisited: Concentration dependent involvement of cytochrome P450 2C19. *Xenobiotica* **2010**, *40*, 536–546. [CrossRef] [PubMed]
78. Arias, H.R.; Gumilar, F.; Rosenberg, A.; Targowska-Duda, K.M.; Feuerbach, D.; Jozwiak, K.; Moaddel, R.; Wainer, I.W.; Bouzat, C. Interaction of Bupropion with Muscle-Type Nicotinic Acetylcholine Receptors in Different Conformational States. *Biochemistry* **2009**, *48*, 4506–4518. [CrossRef]
79. Simonsen, U.; Comerma-Steffensen, S.; Andersson, K.E. Modulation of Dopaminergic Pathways to Treat Erectile Dysfunction. *Basic Clin. Pharmacol. Toxicol.* **2016**, *119*, 63–74. [CrossRef]
80. Carroll, F.I.; Blough, B.E.; Abraham, P.; Mills, A.C.; Holleman, J.A.; Wolckenhauer, S.A.; Decker, A.M.; Landavazo, A.; McElroy, K.T.; Navarro, H.A.; et al. Synthesis and biological evaluation of bupropion analogues as potential pharmacotherapies for cocaine addiction. *J. Med. Chem.* **2009**, *52*, 6768–6781. [CrossRef]

81. ChemAxon Hydroxybupropion. Available online: https://chemicalize.com/app/calculation/Hydroxybupropion (accessed on 27 November 2020).
82. ChemAxon Erythro- and Threohydrobupropion. Available online: https://chemicalize.com/app/calculation/CC(NC(C)(C)C)C(O)C1%3DCC%3DCC(Cl)%3DC1%20|lp%3A2%3A1%2C8%3A2%2C14%3A3| (accessed on 27 November 2020).
83. PubChem Hydroxybupropion. Available online: https://pubchem.ncbi.nlm.nih.gov/compound/446 (accessed on 27 November 2020).
84. Kawai, R.; Lemaire, M.; Steimer, J.L.; Bruelisauer, A.; Niederberger, W.; Rowland, M. Physiologically based pharmacokinetic study on a cyclosporin derivative, SDZ IMM 125. *J. Pharmacokinet. Biopharm.* **1994**, *22*, 327–365. [CrossRef] [PubMed]
85. Guest, E.J.; Aarons, L.; Houston, J.B.; Rostami-Hodjegan, A.; Galetin, A. Critique of the Two-Fold Measure of Prediction Success for Ratios: Application for the Assessment of Drug-Drug Interactions. *Drug Metab. Dispos.* **2011**, *39*, 170–173. [CrossRef] [PubMed]
86. Shimokawa, Y.; Yoda, N.; Kondo, S.; Yamamura, Y.; Takiguchi, Y.; Umehara, K. Inhibitory Potential of Twenty Five Anti-tuberculosis Drugs on CYP Activities in Human Liver Microsomes. *Biol. Pharm. Bull.* **2015**, *38*, 1425–1429. [CrossRef] [PubMed]
87. Rajaonarison, J.F.; Placidi, M.; Lacarelle, B. Screening in Human Liver Interactions for Inhibitors. *Drug Metab. Dispos.* **1994**, *20*.
88. Xue, C.; Zhang, X.; Cai, W. Prediction of drug-drug interactions with bupropion and its metabolites as CYP2D6 inhibitors using a physiologically-based pharmacokinetic model. *Pharmaceutics* **2018**, *10*, 1. [CrossRef]
89. Connarn, J.N.; Zhang, X.; Babiskin, A.; Sun, D. Metabolism of Bupropion by Carbonyl Reductases in Liver and Intestine. *Drug Metab. Dispos.* **2015**, *43*, 1019–1027. [CrossRef]
90. Giri, P.; Naidu, S.; Patel, N.; Patel, H.; Srinivas, N.R. Evaluation of In Vitro Cytochrome P450 Inhibition and In Vitro Fate of Structurally Diverse N-Oxide Metabolites: Case Studies with Clozapine, Levofloxacin, Roflumilast, Voriconazole and Zopiclone. *Eur. J. Drug Metab. Pharmacokinet.* **2017**, *42*, 677–688. [CrossRef] [PubMed]
91. Sager, J.E.; Tripathy, S.; Price, L.S.L.; Nath, A.; Chang, J.; Stephenson-Famy, A.; Isoherranen, N. In vitro to in vivo extrapolation of the complex drug-drug interaction of bupropion and its metabolites with CYP2D6; simultaneous reversible inhibition and CYP2D6 downregulation. *Biochem. Pharmacol.* **2017**, *123*, 85–96. [CrossRef]

4.2 PUBLICATION II – A PHYSIOLOGICALLY BASED PHARMACOKINETIC MODEL OF KETOCONAZOLE AND ITS METABOLITES AS DRUG-DRUG INTERACTION PERPETRATORS

4.2.1 *Reference*

Marok FZ, Wojtyniak JG, Fuhr LM, Selzer D, Schwab M, Weiss J, Haefeli WE, and Lehr T. A Physiologically Based Pharmacokinetic Model of Ketoconazole and its Metabolites as Drug-Drug Interaction Perpetrators. *Pharmaceutics*. 2023; 15(2):679. https://doi.org/10.3390/pharmaceutics15020679.

4.2.2 *Supplementary Materials*

The related electronic supplementary materials can be found on the accompanying compact disk or accessed online via: https://www.mdpi.com/article/10.3390/pharmaceutics15020679/s1.

4.2.3 *Author Contributions*

Following, the author contributions are listed according to CRediT [4].

Fatima Zahra Marok:	Conceptualization, Investigation, Visualization, Writing-Original Draft, Writing-Review and Editing.
Jan-Georg Wojtyniak:	Conceptualization, Investigation, Writing-Original Draft, Writing- Review and Editing.
Laura Maria Fuhr:	Writing-Original Draft, Writing- Review and Editing.
Dominik Selzer:	Writing-Original Draft, Writing- Review and Editing.
Matthias Schwab:	Funding Acquisition, Writing- Review and Editing.
Johanna Weiss:	Conceptualization, Writing- Review and Editing.
Walter Emil Haefeli :	Conceptualization, Writing- Review and Editing.
Thorsten Lehr :	Conceptualization, Funding Acquisition, Writing-Original Draft, Writing- Review and Editing.

4.2.4 *Copyright*

pharmaceutics

Article

A Physiologically Based Pharmacokinetic Model of Ketoconazole and Its Metabolites as Drug–Drug Interaction Perpetrators

Fatima Zahra Marok [1], Jan-Georg Wojtyniak [1,2], Laura Maria Fuhr [1], Dominik Selzer [1], Matthias Schwab [2,3,4], Johanna Weiss [5,6], Walter Emil Haefeli [5,6] and Thorsten Lehr [1,*]

1 Clinical Pharmacy, Saarland University, 66123 Saarbruecken, Germany
2 Dr. Margarete Fischer-Bosch-Institut of Clinical Pharmacology, 70376 Stuttgart, Germany
3 Departments of Clinical Pharmacology, and of Biochemistry and Pharmacy, University Hospital Tuebingen, 72076 Tuebingen, Germany
4 Cluster of Excellence iFIT (EXC2180) "Image-Guided and Functionally Instructed Tumor Therapies", University Tuebingen, 72076 Tuebingen, Germany
5 Department of Clinical Pharmacology and Pharmacoepidemiology, University of Heidelberg, 72076 Tuebingen, Germany
6 German Center for Infection Research (DZIF), Heidelberg Partner Site, 69120 Heidelberg, Germany
* Correspondence: thorsten.lehr@mx.uni-saarland.de; Tel.: +49-681-302-70255

Abstract: The antifungal ketoconazole, which is mainly used for dermal infections and treatment of Cushing's syndrome, is prone to drug–food interactions (DFIs) and is well known for its strong drug–drug interaction (DDI) potential. Some of ketoconazole's potent inhibitory activity can be attributed to its metabolites that predominantly accumulate in the liver. This work aimed to develop a whole-body physiologically based pharmacokinetic (PBPK) model of ketoconazole and its metabolites for fasted and fed states and to investigate the impact of ketoconazole's metabolites on its DDI potential. The parent–metabolites model was developed with PK-Sim® and MoBi® using 53 plasma concentration-time profiles. With 7 out of 7 (7/7) DFI AUC_{last} and DFI C_{max} ratios within two-fold of observed ratios, the developed model demonstrated good predictive performance under fasted and fed conditions. DDI scenarios that included either the parent alone or with its metabolites were simulated and evaluated for the victim drugs alfentanil, alprazolam, midazolam, triazolam, and digoxin. DDI scenarios that included all metabolites as reversible inhibitors of CYP3A4 and P-gp performed best: 26/27 of DDI AUC_{last} and 21/21 DDI C_{max} ratios were within two-fold of observed ratios, while DDI models that simulated only ketoconazole as the perpetrator underperformed: 12/27 DDI AUC_{last} and 18/21 DDI C_{max} ratios were within the success limits.

Keywords: physiologically based pharmacokinetic (PBPK) modeling; ketoconazole; cytochrome P450 3A4 (CYP3A4); P-glycoprotein (P-gp); reversible inhibition; metabolites; drug–food interaction; drug–drug interaction

check for updates

Citation: Marok, F.Z.; Wojtyniak, J.-G.; Fuhr, L.M.; Selzer, D.; Schwab, M.; Weiss, J.; Haefeli, W.E.; Lehr, T. A Physiologically Based Pharmacokinetic Model of Ketoconazole and Its Metabolites as Drug–Drug Interaction Perpetrators. *Pharmaceutics* **2023**, *15*, 679. https://doi.org/10.3390/pharmaceutics15020679

Academic Editor: Im-Sook Song

Received: 23 December 2022
Revised: 6 February 2023
Accepted: 13 February 2023
Published: 17 February 2023

1. Introduction

The imidazole derivative ketoconazole is used topically for the treatment of dermal fungal infections and systemically as therapy for Cushing's syndrome [1,2]. For systemic applications, ketoconazole is administered as oral tablets in dose ranges of 200–400 mg [3]. For doses below 400 mg, pronounced drug–food interactions (DFIs) have also been observed for the biopharmaceutical classification system (BCS) class II compound as its oral bioavailability is highly limited by its poor solubility of 0.006 mg/mL (at a pH of 7.5) [4,5]. In contrast, at higher doses, DFIs do not significantly modulate ketoconazole exposure [6].

Upon absorption, ketoconazole is mainly bound to albumin and blood cells, and only 1% is unbound in plasma [1]. Moreover, ketoconazole has been discussed as a substrate of the efflux transporter P-glycoprotein (P-gp) as well as a substrate of cytochrome

P450 3A4 (CYP3A4), arylacetamide deacetylase (AADAC), and uridine diphosphate glucuronosyltransferase 1A4 (UGT1A4) [7–11]. Roughly 10–37% of unchanged ketoconazole is eliminated in feces, while 2–4% can be found in urine [5].

A systemic administration of ketoconazole for the treatment of fungal infections is not recommended, as oral ketoconazole intake might result in liver injury and can lead (similar to other azole antifungals) to prolonged QT intervals; therefore, an increased risk for torsades de pointes tachycardia [11,12]. The efficacy of ketoconazole in reducing cortisol levels for the treatment of Cushing's disease may outweigh the risk of potential side effects [2]. The likelihood of experiencing severe adverse drug reactions can be further amplified due to ketoconazole's strong drug–drug interaction (DDI) potential. Here, the exposure of the co-administered drug might be increased via inhibition of its drug metabolism [12,13].

Based on its strong DDI potential, ketoconazole is systematically administered in clinical studies as a DDI perpetrator drug [14,15]. Here, it serves as a potent inhibitor of CYP3A4 and P-gp, among other proteins, with substantial increases in drug exposure of victim compounds being reported in the literature. For example, the administration of 400 mg of ketoconazole over four days led to a 15-fold increase in the area under the plasma concentration-time curve (AUC) of midazolam [16], while pretreatment with 200 mg of ketoconazole twice daily over three days increased the AUC of triazolam 11-fold [17]. However, since ketoconazole inhibits CYP3A4 and P-gp reversibly and has a mean half-life of only 160 min (after a 400 mg dose) [18], long-term inhibitory effects cannot be explained by the involvement of the parent compound alone [19]. In the case of itraconazole, which is also an azole antimycotic as well as a potent DDI perpetrator drug, its metabolites contribute to its DDI activity; e.g., by reversibly inhibiting CYP3A4 [20]. Equivalently, some of ketoconazole's inhibitory potential can also be attributed to its metabolites. One important metabolite, *N*-deacetylketoconazole (M1), which is formed via AADAC, was reported to inhibit the same enzymes and transporters as ketoconazole itself, including CYP3A4 and P-gp [13]. As for itraconazole, because three of its metabolites are involved in DDIs, it might be reasonable to assume that M1 is not the only metabolite responsible for ketoconazole-mediated DDIs; for example, the structurally similar *N*-deacetyl-*N*-hydroxyketoconazole (M2) among other metabolites might also contribute [7,21]. However, the individual contributions of ketoconazole's metabolites to the observed DDI effects are still unknown, especially regarding their long-term inhibitory effects. To investigate the involvement of a perpetrator's metabolites in DDIs, model simulations can be performed to assess their contributions and impact on their parent's overall DDI potential. Here, physiologically based pharmacokinetic (PBPK) modeling can assist in testing hypotheses regarding the potential impacts of metabolites on ketoconazole's strong observed DDI potential. The usefulness of parent–metabolite PBPK modeling for the investigation of drug interactions by imidazole derivatives was previously demonstrated in the application of an itraconazole–metabolites PBPK model within an extensive CYP3A4–P-gp–DDI network by Hanke et al. [22]. In general, the application of PBPK modeling is recommended by both the European Medicines Agency (EMA) and the U.S. Food and Drug Administration (FDA) for the different stages of the drug development pipeline [23–25].

Thus, the aims of the present study were (i) to build a PBPK model for ketoconazole under fasted and fed conditions and (ii) to investigate the contributions of its metabolites; i.e., M1 and M2, to ketoconazole's DDI potential by predicting DDIs with the parent alone in comparison to DDIs with the parent alongside its metabolites as perpetrators impacting the pharmacokinetics of the victim drugs alfentanil, alprazolam, midazolam, triazolam (CYP3A4 victim drugs), and digoxin (P-gp victim drug). The developed parent–metabolites PBPK model files will be made publicly available at http://models.clinicalpharmacy.me.

2. Materials and Methods

2.1. Software

The PBPK model was developed with the open-source modeling software PK-Sim® and MoBi® (Open Systems Pharmacology Suite 11 released under the GPLv2 license by the Open Systems Pharmacology community; www.open-systems-pharmacology.org (accessed on 20 April 2022)) [26]. Published clinical study data were digitized using GetData Graph Digitizer 2.26.0.20 (© S. Federov) according to best practices [27]. Model input parameter estimation using Monte Carlo or Levenberg–Marquardt optimizations, by minimizing the sum of squares between the simulation and measurements from all included studies, and local sensitivity analyses were performed within PK-Sim®. Pharmacokinetic parameter analysis, model performance measures, and plots were compiled in R 4.1.3 (The R Foundation for Statistical Computing, Vienna, Austria) using RStudio 1.2.1335 (RStudio PBC, Boston, MA, USA).

2.2. Clinical Data

Clinical trials of ketoconazole with single-dose and multiple-dose regimens in fasted and fed participants were gathered and digitized from the literature [27]. Moreover, additional mean and individual plasma concentration-time profiles for ketoconazole and M1 were kindly provided by Weiss et al. [13]. Collected plasma concentration-time profiles were divided into a training dataset for model building and a test dataset for model evaluation. Studies in the training dataset were selected to include ketoconazole and M1 plasma concentration-time profiles and a wide ketoconazole dosing range administered in different formulations. No plasma concentration-time profiles of the metabolite M2 could be found in the literature. The compiled training and test datasets are documented in clinical study tables in Sections S2 and S3 of the Supplementary Materials.

2.3. PBPK Model Building

The model-building process began with an extensive literature search for physicochemical properties and information about the absorption, distribution, metabolism, and excretion processes of ketoconazole and its metabolites.

Mean and mode demographic information (age, sex, ethnicity, body weight, and height) listed in clinical study reports was used to create virtual individuals for each study. If entries were partially missing; i.e., lacking information on weight or height, data were informed based on the suggested value provided by PK-Sim® computed from the respective implemented population databases. If no data were available, a virtual standard individual with default values was created (see Section S1.2).

Tissue distributions of enzymes were implemented according to the PK-Sim® expression database and are listed in Table S1.1 in the Supplementary Materials.

Model parameters that either could not be adequately informed by the literature or were involved in important QSAR model estimates of permeability and distribution processes were optimized by fitting the model simultaneously to all plasma concentration-time profiles of the training dataset.

2.4. Drug–Food Interaction Modeling

The compiled clinical studies included data on ketoconazole administration under fasted or fed conditions. Data on particle size distributions were gathered from the literature to inform the parametrization of formulation models for oral ketoconazole solutions and tablets for simulations with and without the intake of food. To simulate the effect of DFIs on oral ketoconazole absorption, intestinal permeabilities were estimated based on the fasted and fed datasets, and gastric emptying time was adapted for the fed state. If no information about fasted or fed study conditions was provided, the fed state was assumed if (i) a delay in the time of maximum plasma concentration (T_{max}) of more than two hours could be observed, (ii) multiple doses were administered within a day (as a continuous fasted state was considered unlikely), or if (iii) single doses as oral tablets of 800 mg or

higher were administered (as differences in ketoconazole plasma exposure were found to be negligible for higher doses between fasted and fed states) [6].

2.5. Drug–Drug Interaction Modeling

To model the effect of DDIs, reversible inhibition of CYP3A4 and P-gp using ketoconazole and its metabolites was implemented into the parent–metabolites PBPK model using the respective in vitro data derived from the literature (if available). Previously published PBPK models of the CYP3A4 victim drugs alfentanil, alprazolam, midazolam, and triazolam as well as the P-gp victim drug digoxin were used to simulate DDI scenarios with ketoconazole co-administration [22,28,29]. The victim drug PBPK models were used to evaluate the performance of the ketoconazole model in DDI scenarios. Interaction partner models were selected if (i) the FDA listed them as sensitive or moderately sensitive substrates for CYP3A4 and P-gp [30], (ii) the evaluation as CYP3A4 and P-gp victim models was thoroughly investigated in DDI networks [22,31], (iii) models were developed in the Open System Pharmacology Suite, and (iv) model files were publicly available and accessible. Here, simulations were performed with and without the inclusion of ketoconazole metabolites.

2.6. PBPK Model Evaluation

Model evaluations included graphical comparisons of (i) predicted and observed plasma concentration-time profiles by plotting model predictions alongside their respective observed data, (ii) predicted and observed plasma concentration values in goodness-of-fit plots, and (iii) predicted and observed area under the plasma concentration-time curve calculated from the time of drug administration to the time of the last concentration measurement (AUC_{last}) and maximum plasma concentration (C_{max}) values. Additionally, as quantitative measures of the model performance, the mean relative deviation (MRD) of all predicted plasma concentrations and geometric mean fold error (GMFE) of all predicted AUC_{last} and C_{max} values were calculated according to Equations (1) and (2). Predictions with MRD and GMFE values ≤ 2 were considered successful model predictions.

$$MRD = 10^x;\ x = \sqrt{\frac{\sum_{i=1}^{k} \left(\log_{10}\hat{c}_i - \log_{10}c_i\right)^2}{k}} \quad (1)$$

where c_i = the ith observed plasma concentration, $\hat{c}_i$ = the corresponding predicted plasma concentration, and k = the number of observed values.

$$GMFE = 10^x;\ x = \frac{\sum_{i=1}^{m} \left|\log_{10}\left(\frac{\hat{PK}_i}{PK_i}\right)\right|}{m} \quad (2)$$

where $\hat{PK}_i$ = the ith predicted AUC_{last} or C_{max} value, PK_i = the corresponding observed AUC_{last} or C_{max} value, and m = the number of studies.

Local model sensitivity to single parameter changes was analyzed for the AUC of ketoconazole and M1 after multiple dose administrations in fasted and fed states. Analyses included parameters that were either optimized or assumed to impact the AUC. Section S2.6 of the Supplementary Materials provides a detailed description of the performed local sensitivity analyses.

2.7. Drug–Food and Drug–Drug Interaction Model Evaluation

To assess the model performance of DFI and DDI effects, model predictions were evaluated with graphical comparisons of plasma concentration-time profiles, AUC_{last}, and

C_{max} values. Furthermore, effect ratios were calculated for the PK parameters AUC_{last} and C_{max} according to Equation (3):

$$\text{DFI or DDI PK} = \frac{PK_{effect}}{PK_{reference}} \quad (3)$$

where PK = PK parameter (AUC_{last} or C_{max}) either of the DFI or DDI effect profile (PK_{effect}) or of the respective control or placebo profile as the reference ($PK_{reference}$).

In the case of DFIs, comparisons between fed (effect) and fasted (reference) conditions were only conducted for self-controlled studies with equal-dose regimens. In the case of DDIs, victim-drug plasma concentration-time profiles and PK parameters during co-administration of ketoconazole as the perpetrator drug (effect) were compared to respective measures without ketoconazole administration (reference).

As a quantitative measure of the effect model performance, *GMFE* values of the predicted AUC_{last} and C_{max} values as well as their effect ratios were calculated according to Equation (2).

3. Results

3.1. Model Building

Whole-body PBPK models for ketoconazole and its metabolites M1 and M2 were developed in PK-Sim® and MoBi®. The compiled clinical dataset consisted of 53 studies with a dosing range of 100–1200 mg administered as solutions, capsules, or tablets to 492 participants in total. The respective population characteristics and details of the clinical trials are listed in Table S2.2 in the Supplementary Materials.

As depicted in Figure 1, ketoconazole is metabolized by CYP3A4, AADAC, and UGT1A4. Here, AADAC catalyzes the formation of M1, which is further metabolized by flavin-containing monooxygenase 3 (FMO3) to M2. These processes were implemented via Michaelis–Menten kinetics using Michaelis–Menten constants (K_M) for AADAC and FMO3 transformations from the literature. As no K_M value for CYP3A4 metabolism of ketoconazole was found in the literature, the inhibition constant (K_i) of ketoconazole's CYP3A4 inhibition was used as a surrogate value for K_M [13]. M2 metabolism via FMO3 was implemented as FMO3-mediated first-order clearance, as no data on this process were available. The developed parent–metabolites model included reversible autoinhibition of CYP3A4 and P-gp. DDIs with the CYP3A4 victim drugs alfentanil, alprazolam, midazolam, and triazolam as well as the P-gp victim drug digoxin were simulated. An overview of the drug-dependent parameters and the respective implemented metabolic processes is summarized in Table 1 and listed in more detail in Table S1.3 in the Supplementary Materials.

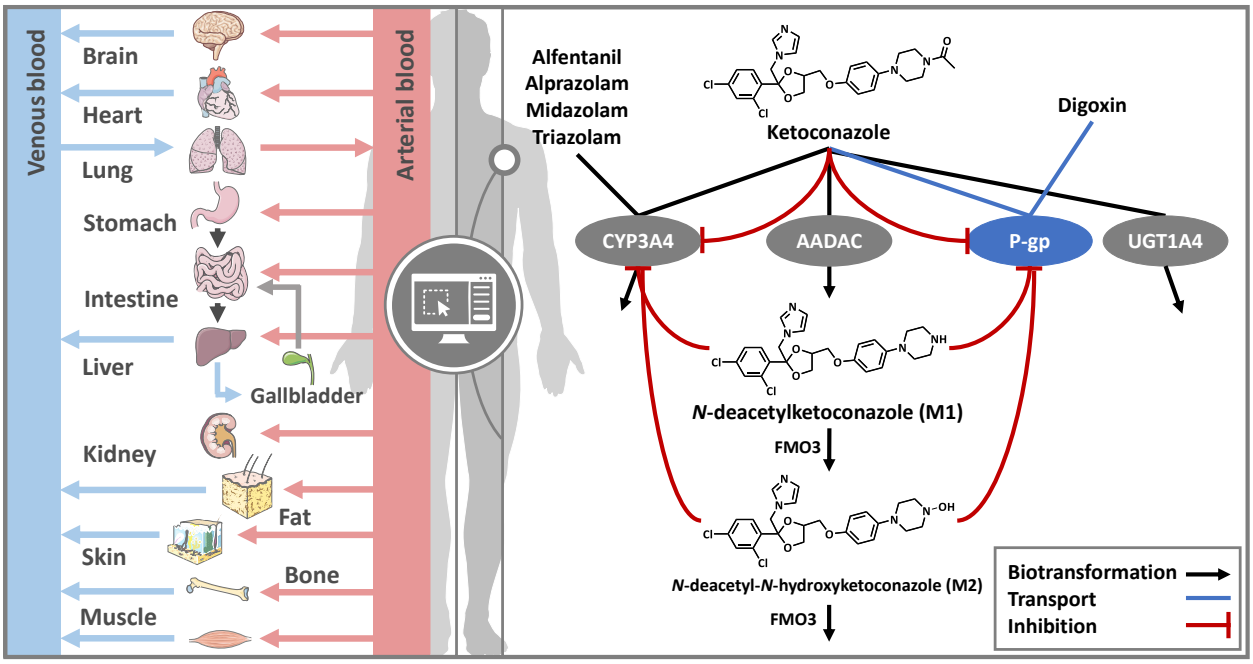

Figure 1. DDI PBPK modeling overview. Whole-body PBPK models for ketoconazole and its metabolites were established and used to simulate the inhibitory effect of ketoconazole, which is substrate of CYP3A4, AADAC, UGT1A4, and P-gp. Its metabolite M1, which is formed by AADAC biotransformation, is metabolized by FMO3 to M2, which is metabolized via FMO3 as well. Both the parent compound and the metabolites concomitantly inhibit CYP3A4 and P-gp. CYP3A4-related DDIs were simulated with the CYP3A4 victim drugs alfentanil, alprazolam, midazolam, and triazolam. P-gp DDIs were simulated with the P-gp victim drug digoxin. Drawings by Servier (licensed under CC BY 3.0) [32]. AADAC: arylacetamide deacetylase, CYP3A4: cytochrome P450 3A4, FMO3: flavin-containing monooxygenase 3, M1: *N*-deacetylketoconazole, M2: *N*-deacetyl-*N*-hydroxyketoconazole, P-gp: P-glycoprotein, UGT1A4: uridine diphosphate glucuronosyltransferase 1A4.

Table 1. Drug-dependent parameters of the parent–metabolite PBPK models for ketoconazole, M1 and M2.

Parameter	Unit	Value	Literature	Value	Literature	Value	Literature	Reference	Description
		Ketoconazole		M1		M2			
MW	g/mol	531.43	531.43	489.40	489.40	505.40	505.40	[33–35]	Molecular weight
pKa	-	2.94 6.51	2.94 6.51	0.20 6.42 8.90	0.20 6.42 8.90	3.42 6.42	3.42 6.42	[33–35]	Acid dissociation constant
Solubility (pH)	mg/L	$2.03 \cdot 10^4$ (1.2) $4.3 \cdot 10^4$ (3) 7.00 (6.8). 5.40 (7), 6.00 (7.5)	$2.03 \cdot 10^4$ (1.2) $4.3 \cdot 10^4$ (3) 7.00 (6.8). 5.40 (7), 6.00 (7.5)	$1.24 \cdot 10^3$ (6.5)	$1.24 \cdot 10^3$ (6.5)	$4.40 \cdot 10^3$ (6.5)	$4.40 \cdot 10^3$ (6.5)	[4,34,35]	Solubility
log P	-	[o] 2.52	2.73	[o] 3.75	4.58	4.20	4.20	[34–36]	Lipophilicity
fu	%	1.00	1.00	[a] 1.00	-	[a] 1.00	-	[1]	Fraction unbound
Partition coefficients	-	Various	Berez.	Various	R&R	Various	Berez.	-	Cell-to-plasma partitioning
Cellular perm.	-	-	PK-Sim	-	Ch.d.S.	-	Ch.d.S.		Permeability into the cellular space

Table 1. *Cont.*

Parameter	Unit	Value	Literature	Value	Literature	Value	Literature	Reference	Description
		Ketoconazole		M1		M2			
GFR fraction	-	1.00	-	1.00	-	1.00	-	-	Fraction of filtered drug in urine
EHC cont. fraction	-	1.00	-	1.00	-	1.00	-	-	Bile fraction continuously released
Intest. perm. fasted	cm/min	[o] $1.56 \cdot 10^{-5}$	[c] $4.28 \cdot 10^{-6}$	-	-	-	-	[37]	Transcellular intestinal permeability
Intest. perm. fed	cm/min	[o] $9.95 \cdot 10^{-6}$	[c] $4.28 \cdot 10^{-6}$	-	-	-	-	[37]	Transcellular intestinal permeability
GET fasted	min	15	[d] 15	-	-	-	-	[37]	Gastric emptying time
GET fed	min	[a] 45	45–120	-	-	-	-	[38]	Gastric emptying time
K_M AADAC	µmol/L	1.88	1.88	-	-	-	-	[7]	Michaelis–Menten constant
k_{cat} AADAC	1/min	[o] 0.87	-	-	-	-	-	-	Catalytic rate constant
K_M CYP34	µmol/L	[a] 0.008	-	-	-	-	-	-	Michaelis–Menten constant
k_{cat} CYP34	1/min	[o] 0.10	-	-	-	-	-	-	Catalytic rate constant
K_M UGT1A4	µmol/L	7.00	7.00	-	-	-	-	[10]	Michaelis–Menten constant
k_{cat} UGT1A4	1/min	[o] 0.31	-	-	-	-	-	-	Catalytic rate constant
K_M FMO3	µmol/L	-	-	1.77	1.77	-	-	[39]	Michaelis–Menten constant
k_{cat} FMO3	1/min	-	-	[o] 378.65	-	-	-	-	Catalytic rate constant
Cl FMO3	l/µmol/min	-	-	-	-	[o] 0.09	-	-	First order clearance rate constant
K_M P-gp	µmol/L	[a] 0.035	-	-	-	-	-	-	Michaelis–Menten constant
k_{cat} P-gp	1/min	[o] 0.33	-	-	-	-	-	-	Catalytic rate constant
K_i CYP3A4	µmol/L	0.008	‡ 0.008	0.022	‡ 0.022	[a] 0.022	-	[13]	Conc. for half-maximal inhibition
K_i P-gp	µmol/L	0.035	‡ 0.035	0.119	‡ 0.119	[a] 0.119	-	[13]	Conc. for half-maximal inhibition

‡ In vitro values calculated from respective IC50 values. [a] Assumed; [c] calculated; [d] default value; [o] optimized value. AADAC: arylacetamide deacetylase; Berez.: Berezhkovskiy calculation method [40]; Ch.d.S.: charge-dependent Schmitt calculation method [41]; conc.: concentration; cont.: continuous; CYP3A4: cytochrome P450 3A4; EHC: enterohepatic circulation; FMO3: flavin-containing monooxygenase 3; GET: gastric emptying time; GFR: glomerular filtration rate; intest.: intestinal; KTZ: ketoconazole; M1: *N*-deacetylketoconazole; M2: *N*-deacetyl-*N*-hydroxylketoconazole; perm.: permeability; P-gp: P-glycoprotein; PK-Sim: PK-Sim® standard calculation method [37]; R&R: Rodgers and Rowland calculation method [42]; UGT1A4: uridine diphosphate glucuronosyltransferase 1A4.

3.2. Drug–Food Interaction Model Evaluation

The PK of ketoconazole was investigated under both fasted and fed conditions, as clinical data showed considerable influences of food intake on the plasma levels of ketoconazole, especially for doses below 400 mg. To simulate oral solutions, capsules, and tablets, particle dissolution was simulated either with negligible particle radii under 0.002 µm for immediately dissolved particles or with a particle size distribution extrapolated from in vitro data [43] as described in Table S1.3 in the Supplementary Materials. Exemplary simulations of ketoconazole administrations as single and multiple doses under fasted conditions are presented in Figure 2. For this, the observed plasma concentration-time profiles were well described for ketoconazole and its metabolite M1. Model predictions and observations of all plasma concentration-time profiles can be found in Sections S2.1 and S2.2 of the Supplementary Materials.

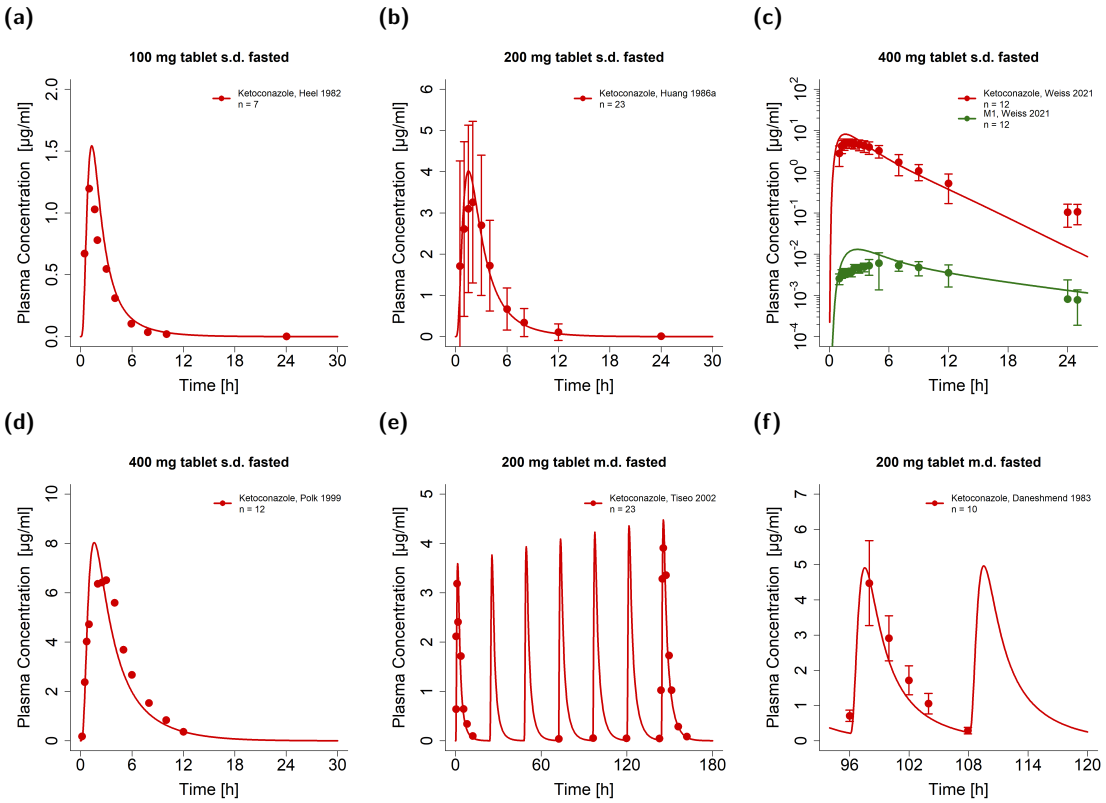

Figure 2. Graphical comparison of predicted and observed plasma concentration-time profiles of exemplary clinical trials of ketoconazole under fasted and fed conditions. (**a**–**d**) Single-dose administrations of tablets in fasted state with metabolite measurements; (**e**,**f**) multiple-dose administrations of capsules and tablets in fasted state [1,13,44–48]. The model predictions are shown as solid lines and the corresponding observed data as dots (arithmetic mean ± standard deviation (if available)). Detailed information on study protocols is provided in Table S1.2 in the Supplementary Materials. fasted: fasted condition, fed: fed conditions, M1: *N*-deacetylketoconazole, n: number of study participants.

To model the effect of food intake, the gastric emptying time was optimized to 45 min, which was three times higher than for fasted simulations. Additionally, the intestinal permeability was adapted for fed simulations separately by optimizing the parameter to observed data. Here, the adapted permeability for fed simulations was 1.6-fold lower compared to the fasted state ($9.95 \cdot 10^{-6}$ versus $1.56 \cdot 10^{-5}$ cm/min) as listed in Table 1.

To further underline the impact of DFIs, Figure 3a–c show exemplary plasma concentration-time profiles of ketoconazole administrations under fed conditions, while Figure 3d,e depict comparisons of participants in fasted and fed states. For this, the participants either received ketoconazole after an overnight fast or at the end of a standard breakfast [6,49]. Model-predicted plasma concentration-time profiles were illustrated for doses of 200, 400, and 600 mg during the fasted and fed state alongside their respective observed data. Here, the effect of DFIs was well predicted, especially for the delayed plasma concentrations in fed conditions. Comparisons of observed and predicted plasma concentration-time profiles of 800 mg ketoconazole are shown in Figures S2.17 and S2.18 in the Supplementary Materials. Graphical comparisons of all predicted and observed plasma concentration-time profiles are shown on a linear and semi-logarithmic scale in Figures S2.1–S2.14 in the Supplementary Materials.

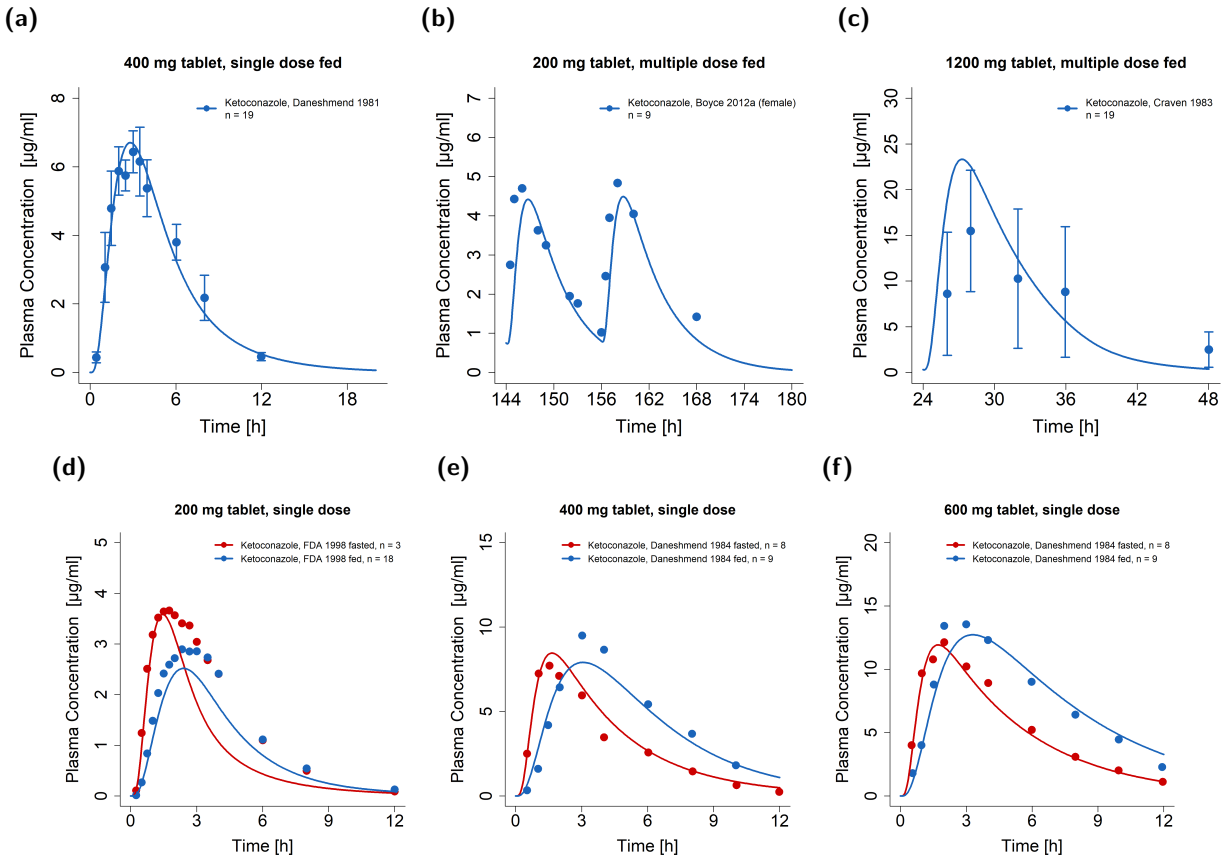

Figure 3. Ketoconazole DFI model performance. Illustrated are plasma concentration-time profiles of exemplary clinical trials of (**a**–**c**) single- and multiple-dose administrations of tablets in fed state [46,48,50]. Moreover, comparisons of fasted (red) and fed (blue) predicted and observed plasma concentration-time profiles are illustrated for 200 mg (**d**), 400 mg (**e**), and 600 mg (**f**) single-dose administrations of ketoconazole [6,49]. The model predictions are shown as solid lines and the corresponding observed data as dots (arithmetic mean). Detailed information on the study protocols is provided in Table S1.2 in the Supplementary Materials. fasted: fasted condition; fed: fed condition; n: number of participants.

The general model performance is shown in Figure 4 as the comparison of the predicted and observed AUC_{last} and C_{max} values for the training (a,b) and test dataset (c,d). The PK of ketoconazole and its metabolite M1 was well predicted for fasted, fed, and unknown food states. As shown in Table 2, the overall MRD of 1.45 and the respective GMFEs of 1.37 for AUC_{last} (1.00–2.57) and 1.26 for C_{max} (1.00–2.15) underlined an adequate model performance. Here, 69/77 of the predicted AUC_{last} and the predicted C_{max} values were within the two-fold acceptance limits.

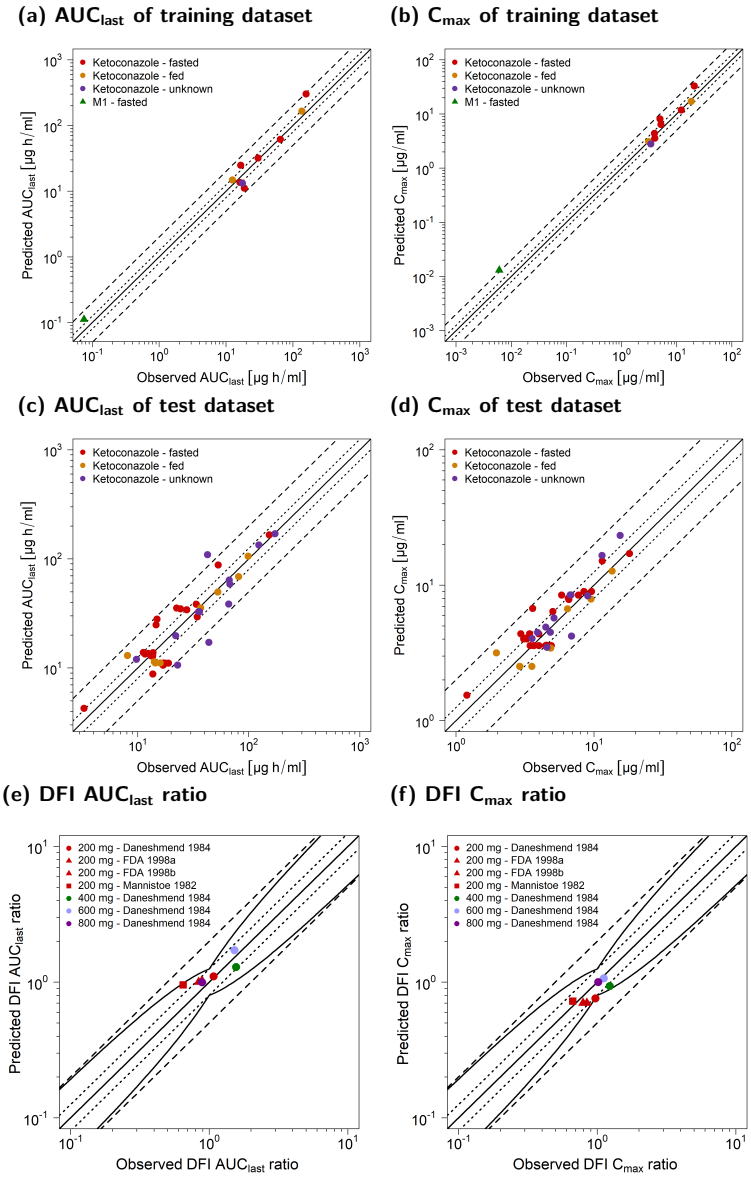

Figure 4. Goodness-of-fit plots of PK parameters for ketoconazole and M1. Predicted AUC_{last} values of the training (**a**) and test dataset (**c**) as well as C_{max} values of the training (**b**) and test dataset (**d**) were compared to the respective observed data. Predicted (as compared to observed) DFI effect ratios of AUC_{last} (**e**) and C_{max} (**f**) are shown for the single doses of 200, 400, 600, and 800 mg [6,49,51]. The straight solid line marks the line of identity, dotted lines indicate 1.25-fold, and dashed lines indicate 2-fold deviation. The curved solid lines show the prediction acceptance limits proposed by Guest et al. (including 1.25-fold variability) [52]. Detailed information on the study protocols is provided in Table S1.2 in the Supplementary Materials. AUC_{last}: area under the plasma concentration-time curve calculated from the first to the last concentration measurement; C_{max}: maximum plasma concentration; DFI: drug–food interaction; fasted: fasted condition; fed: fed condition, M1: *N*-deacetylketoconazole; n: number of study participants; unknown: unknown food intake.

Table 2. Summary of quantitative measures of model performance for ketoconazole and its metabolite M1.

Compound (n)	Mean MRD	Mean GMFE AUC_{last}	Mean GMFE C_{max}
Ketoconazole (52)	1.42	1.37	1.24
M1 (1)	2.51	1.48	2.15
Overall	1.45	1.37	1.26
Profiles with measure ≤ 2	49/53	50/53	52/53
Range	1.09–2.69	1.00–2.57	1.00–2.15

AUC_{last}: area under the plasma concentration-time curve from the time of drug administration to the time of the last concentration measurement; C_{max}: maximum plasma concentration; GMFE: geometric mean fold error; M1: *N*-deacetylketoconazole; MRD: mean relative deviation; n: number of mean plasma concentration-time profiles.

Figure 4e,f depict the predicted compared to observed DFI ratios calculated for AUC_{last} (e) and C_{max} (f). Table 3 lists the mean GMFEs of the predicted compared to observed DFI PK ratios stratified according to the administered dose. For AUC_{last}, DFIs were more pronounced for single doses of 400 and 600 mg of ketoconazole and showed an approximately 50% increase in the observed AUC_{last} [6]. For C_{max}, the impact of DFIs decreased with increasing doses; the strongest effect was predicted and observed for single doses of 200 mg. Here, C_{max} decreased up to 33% under DFIs [6,49,51]. For the administration of 800 mg, the DFI effect on C_{max} was negligible. With an overall GMFE of 1.19 (1.02–1.47) for AUC_{last} and 1.15 (1.02–1.32) for C_{max}, the model predictions for the DFI ratios were in good agreement with the observed data. Here, 7/7 of the AUC_{last} and C_{max} ratios were within the prediction success limits suggested by Guest et al. with a 1.25-fold variability [52]. Implemented DFIs are further documented in Tables S2.4 and S2.5 in the Supplementary Materials. Moreover, Table S2.6 in the Supplementary Materials lists the calculated GMFE values of the predicted and observed plasma concentration-time profiles and the corresponding AUC_{last} and C_{max} values along with the respective DFI PK ratios.

Table 3. Predicted and observed DFI PK ratios alongside quantitative measures of DFI model performance.

Single-Dose Ketoconazole (mg) (n)	Mean GMFE DFI AUC_{last}	Mean GMFE DFI C_{max}
200 (4)	1.21	1.12
400 (1)	1.20	1.23
600 (1)	1.13	1.12
800 (1)	1.13	1.02
Overall GMFE	1.19	1.15
DFIs within guest limits	7/7	7/7
Range	1.02–1.47	1.02–1.32

AUC_{last}: area under the plasma concentration-time curve from the time of drug administration to the time of the last concentration measurement; C_{max}: maximum plasma concentration; DFI: drug–food interaction; GMFE: geometric mean fold error; n: number of DFI ratios.

Sensitivity analyses for a 7-day multiple-dose simulation of 200 mg of ketoconazole once daily showed that ketoconazole AUC was especially sensitive to changes in the parent's lipophilicity and fraction unbound. Moreover, changes in the gastric emptying time as well as metabolism via and inhibition of CYP3A4 were among the model parameters to which the AUC was most sensitive. Further details on the performed sensitivity analyses are provided in Section S2.8 of the Supplementary Materials.

3.3. Drug–Drug Interaction Modeling and Evaluation

For DDI model performance evaluation, 31 clinical DDI studies covering the CYP3A4 victim drugs alfentanil, alprazolam, midazolam, and triazolam as well as the P-gp victim drug digoxin were used. The collected DDI studies investigated the concomitant treatment of the respective perpetrator alongside the victim drug as well as time-delayed

administrations of the perpetrator and victim drugs. Information about the used PBPK models of the victim drugs with the respective model parameters are listed in Section S3 of the Supplementary Materials.

First, CYP3A4 and P-gp DDIs with (auto)inhibition by ketoconazole were simulated with a reversible inhibition via the parent compound alone (DDI scenario: P). For this, the respective K_i values that described the inhibition of CYP3A4 and P-gp were extracted from the literature [13]. Here, ketoconazole DDIs were simulated for perpetrator and victim drug administration without and with a dosing time gap.

Second, to examine the possible effects of ketoconazole's metabolites, the DDIs were extended to include reversible inhibition by M1 (DDI scenario: P + M1) and M2 (DDI scenario: P + M1 + M2) as well. While M1 was reported to inhibit CYP3A4 and P-gp and implemented K_i values for M1 could be derived from the literature [13], the inhibition by further metabolites was described via inclusion of M2 with K_i values for inhibition by M2 surrogated by M1 K_i values, as no in vitro data were available (see Table 1).

To investigate the impact of these metabolites (especially for the (long-lasting) DDI potential of ketoconazole), the DDI model performance was compared between simulations with an inhibitory effect by the parent alone (P), the parent with first metabolite (P + M1), and the parent with both metabolites (P + M1 + M2).

Figure 5a demonstrates the predicted concentrations of ketoconazole and its metabolites after a single oral ketoconazole dose in liver cells. The second metabolite (M2) showed a T_{max} roughly 10 h later and a 3.7-fold higher half-life ($t_{1/2}$) in the liver than ketoconazole itself (T_{max}: 13.05 vs. 2.20 h; $t_{1/2}$: 45.94 vs. 12.31 h). While the model predicted low concentrations of M1 in plasma (see Figure 2c), thereby indicating minor extracellular distribution, no M2 was simulated to distribute into the plasma.

Figure 5b–e illustrate the plasma concentration-time profiles of the victim drugs given for the case of concomitant dosing with ketoconazole alongside their respective observed data. Here, representative studies of midazolam (Figure 5b,c), alprazolam (Figure 5d), and digoxin (Figure 5e) are depicted and the three DDI scenarios P, P + M1, and P + M1 + M2 compared. In contrast to DDIs with ketoconazole alone (DDI scenario P), model predictions with all three compounds as perpetrators (DDI scenario P + M1 + M2) performed better for the ketoconazole–midazolam and ketoconazole–alprazolam DDIs. Here, the DDI AUC_{last} ratio of the ketoconazole–alprazolam DDI was 0.97 for the DDI scenario P + M1 + M2, while it was only 0.67 for the scenarios P + M1 and P. Here, the DDI scenarios P + M1 and P were very similar, and simulations without dosing time gaps between the victim and perpetrator could not be distinguished by the naked eye. All three scenarios simulated a similar DDI effect for the ketoconazole–digoxin interaction.

Similarly, Figure 6 shows the exemplary plasma concentration-time profiles of the victim drugs given in DDIs with a dosing time gap between victim and perpetrator for alfentanil (Figure 6a,b), midazolam (Figure 6c,d), alprazolam (Figure 6e), and triazolam (Figure 6f) alongside their respective observed data. Again, DDIs were simulated for the three DDI scenarios (P, P + M1, and P + M1 + M2).

Simulations of scenario P performed worst in all illustrated DDIs by underpredicting most of the DDI plasma concentration-time curves. In particular, for the ketoconazole–alfentanil DDIs, predictions with ketoconazole alone showed no effect, as the simulated concentrations were comparable to the respective reference simulation; e.g., alfentanil administration without perpetrator intake. For DDIs with dosing time gaps of 8 h and longer, simulations that included only M1 (DDI scenario P + M1) performed better compared to simulations of ketoconazole alone (DDI scenario P). For example, the DDI AUC_{last} ratios were 0.25 (DDI scenario P + M1) and 0.18 (DDI scenario P) for the ketoconazole–alfentanil DDIs (see Figure 6b). For the remaining simulations, the performance of scenarios P and P + M1 was comparable (as shown in Figure 6d–f).

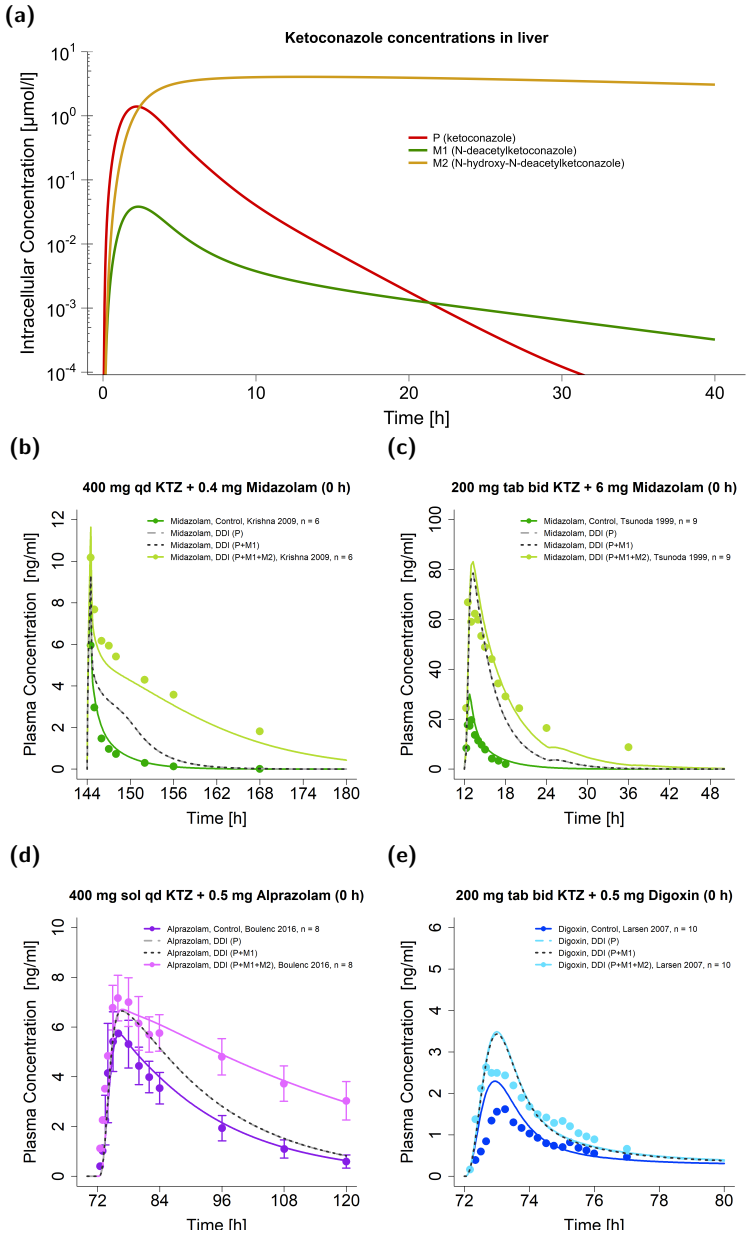

Figure 5. Ketoconazole DDI model simulations without a dosing time gap between victim and perpetrator. Predicted intracellular concentrations in liver cells are illustrated for ketoconazole and its metabolites (M1 and M2) on a semi-logarithmic scale (**a**). Predicted compared to observed plasma concentration-time profiles are illustrated for DDIs with the victim drugs midazolam (**b**,**c**), alprazolam (**d**), and digoxin (**e**) [15,53–55]. Illustrated are DDI predictions (i) with the parent alone (P) (long dashed line in grey), (ii) with the parent and M1 (P + M1) (dashed line in black), and (iii) with the parent and both metabolites (P + M1 + M2) (solid line in a brighter colored shade) alongside their respective reference profile (solid line in a darker colored shade). Corresponding observed data are shown as dots (arithmetic mean ± standard deviation (if available)). Detailed information on the study protocols is provided in Table S3.7 in the Supplementary Materials. bid: twice daily; DDI: drug–drug interaction; KTZ: ketoconazole; M1: *N*-deacetylketoconazole; M2: *N*-hydroxy-*N*-deacetylketoconazole; n: number of participants; P: ketoconazole alone; qd: once daily; sd: single dose, sol: solution; tab: tablet.

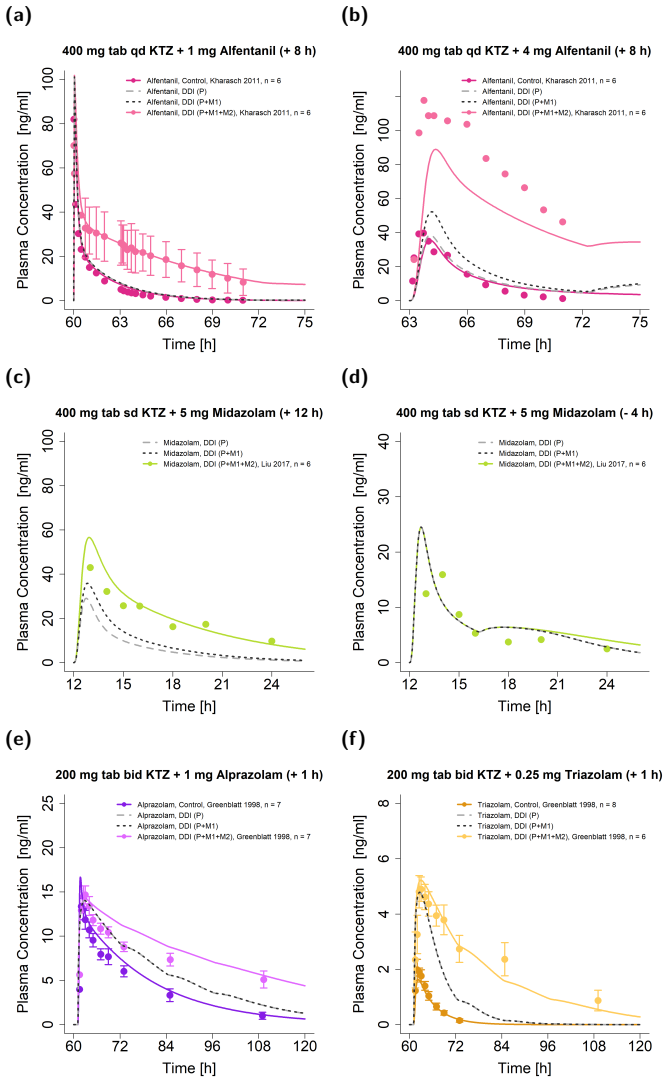

Figure 6. Ketoconazole DDI model simulations. Predicted (as compared to observed) plasma concentration-time profiles are illustrated for DDIs with the victim drugs alfentanil (**a**,**b**), midazolam (**c**,**d**), alprazolam (**e**), and triazolam (**f**) [17,19,56]. The time of victim drug intake was 8 or 12 h after (**a**–**c**), 4 h before (**d**), and 1 h after (**e**,**f**) ketoconazole administration. Illustrated are DDI predictions (i) with the parent compound alone (P) (long dashed line in grey), (ii) with the parent compound and M1 (P + M1) (dashed line in black), and (iii) with the parent compound and both metabolites (P + M1 + M2) (solid line in a brighter colored shade) alongside their respective reference profiles (solid line in a darker colored shade). Corresponding observed data are shown as dots (arithmetic mean ± standard deviation (if available)). The dosing of ketoconazole–alfentanil DDIs (**a**,**b**) was normalized to the respective control to highlight the comparison of DDI and control, while the Supplementary Materials show the data from the respective studies that were simulated as described in their clinical trials reports for the DDI model evaluation and documentation [19]. Detailed information on the study protocols is provided in Table S3.7 in the Supplementary Materials. For the DDI studies illustrated in (**c**,**d**), no reference profiles were available. Note: bid: twice daily; DDI: drug–drug interaction; KTZ: ketoconazole; M1: *N*-deacetylketoconazole; M2: *N*-hydroxy-*N*-deacetylketoconazole; n: number of participants; P: ketoconazole alone; qd: once daily; sd: single dose; tab: tablet.

Overall, the joint parent–metabolites DDI model (DDI scenario P + M1 + M2) demonstrated the most convincing performance compared to the models that included either one or no metabolite (DDI scenarios P + M1 and P) for the prediction of long-lasting DDI effects, especially if ketoconazole was administered several hours before the victim drug.

All simulated DDI profiles with their respective observed data are shown in Section S3.3.1 of the Supplementary Materials together with a detailed description of regimens and population characteristics in Table S3.7.

Figure 7 illustrates the comparison of the predicted and observed DDI ratios for the AUC_{last} and C_{max} of all victim drugs. Figure 7a–c show the calculated DDI AUC_{last} ratios, whereas Figure 7c–e depict the respective calculated DDI C_{max} ratios. Goodness-of-fit plots were stratified for the three DDI scenarios (P, P + M1, and P + M1 + M2).

Here, 26/27 of the predicted DDI AUC_{last} ratios of the P + M1 + M2 DDI model were within the limits proposed by Guest et al. [52], while only 12/27 of the DDI ratios were well predicted for the P and P + M1 DDI models. All predicted DDI AUC_{last} ratios for DDI simulations with dosing time gaps between victim and perpetrator administration were outside of the acceptance limits. For DDI C_{max} predictions, all 21/21 of the DDI ratios of the joint P + M1 + M2 model were within the limits proposed by Guest et al. [52], while only 19/21 and 18/21 met the acceptance criterion if DDIs were simulated for P + M1 and P, respectively.

The mean GMFE values of the calculated DDI PK ratios of all victim drugs are shown in Figure 7g,h for existing dosing time gaps stratified according to the three DDI scenarios (P, P + M1, and P + M1 + M2).

The overall GMFEs for the DDI performance that included both metabolites (P + M1 + M2) were 1.35 (1.01–2.41) for DDI AUC_{last} and 1.27 (1.02–1.96) for DDI C_{max}. For the DDI model that included only M1 (P + M1), the mean GMFEs for DDI AUC_{last} and DDI C_{max} were 2.44 (1.01–5.34) and 1.42 (1.02–3.28), respectively. For DDI prediction without metabolite inhibition (P), the mean GMFEs were 2.64 (1.01–6.75) for DDI AUC_{last} and 1.52 (1.02–4.15) for DDI C_{max}. In general, the DDI model performance was the best for DDI P + M1 + M2 compared to DDI P + M1 and DDI P, and there was a larger impact on DDI AUC_{last} than on DDI C_{max} ratios. The calculated AUC_{last} and C_{max} ratios as well as the GMFE values of all predicted DDI studies are listed in Table S3.9 in the Supplementary Materials.

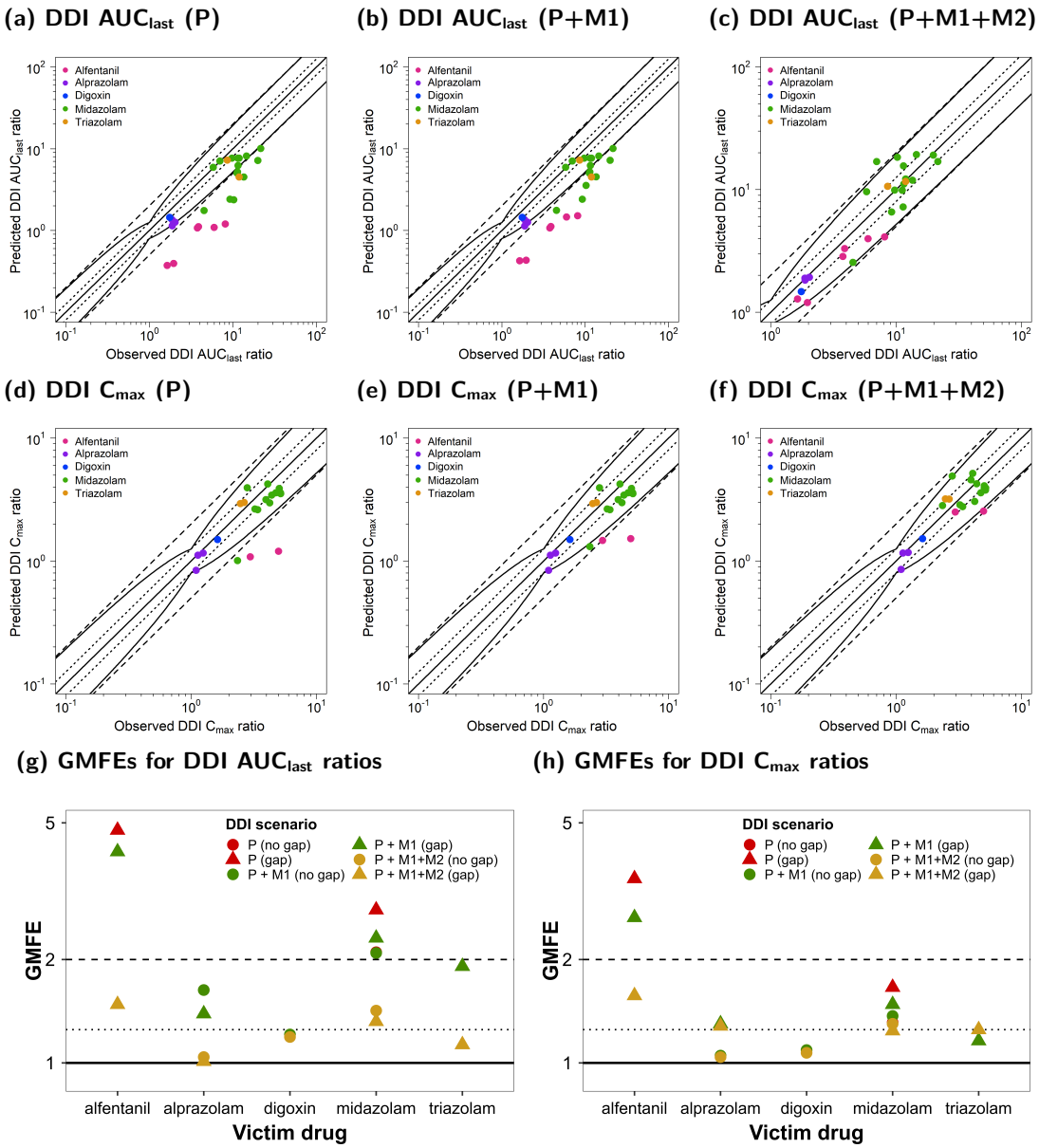

Figure 7. Ketoconazole DDI model evaluation. Predicted DDI AUC_{last} ratios of DDI simulations of three scenarios (P (**a**), P + M1 (**b**), and P + M1 + M2 (**c**)), as well as DDI C_{max} ratios of three scenarios (P (**d**), P + M1 (**e**), and P + M1 + M2 (**f**)) were compared to the respective observed data. The straight solid line marks the line of identity, and the curved solid lines show the prediction acceptance limits proposed by Guest et al. (including 1.25-fold variability) [52]. Calculated mean GMFE values for DDI AUC_{last} (**g**) and DDI C_{max} ratios (**h**) for the three scenarios (P, P + M1, and P + M1 + M2) stratified according to victim with or without a dosing time gap between ketoconazole administration. Dotted lines indicate 1.25-fold and dashed lines indicate two-fold deviation. Detailed information on the study protocols is provided in Table S3.7 in the Supplementary Materials. AUC_{last}: area under the plasma concentration-time curve calculated from the first to the last concentration measurement; C_{max}: maximum plasma concentration; DDI: drug–drug interaction; GMFE: geometric mean fold error; KTZ: ketoconazole; M1: *N*-deacetylketoconazole; M2: *N*-hydroxy-*N*-deacetylketoconazole; P: ketoconazole alone.

4. Discussion

A whole-body PBPK model for ketoconazole and its metabolites M1 and M2 was built and evaluated to cover ketoconazole administrations as oral solutions, capsules, or tablets for a wide dosing range of 100–1200 mg to model DFIs and CYP3A4 and P-gp DDIs.

The available literature lacked studies on ketoconazole intravenous injections or infusions in humans, and only data on oral or dermal applications were available [3]. For oral intake, the absorption of ketoconazole is highly limited by its poor solubility, which rapidly decreases with increasing pH [4]. As food consumption can influence gastric pH, it is reasonable to assume that this might also modulate the oral bioavailability of ketoconazole [6]. The liberation of oral ketoconazole formulations was described as a particle-dissolution process. For oral solutions, particles were assumed to be immediately dissolved; in the case of oral tablets, particle radii and distribution were estimated from observed data [57]. Moreover, supersaturation of the poorly soluble ketoconazole over the modeled dosing range (up to 1200 mg) was assumed, since in the current literature, potential oversaturation was discussed for ketoconazole and other imidazole derivatives with known poor solubility [58].

Generally, the intake of food might lead to delayed gastric emptying times of up to two hours depending on the meal composition [38]. Thus, ketoconazole's residence time in the gut (and therefore at the absorption site) can be prolonged during DFIs. This can result in an increased absorption as well as a delay in T_{max}. To model ketoconazole absorption in the fed state, a specific intestinal permeability was estimated, and the transit time in the stomach compartment was prolonged to describe the delay in T_{max} compared to the fasted state. Here, the gastric emptying time was set to 15 min (default value) for fasted simulations. For all fed simulations, a gastric emptying time of 45 min was optimal to describe the observed data, although the relative time of food intake varied in the investigated studies; i.e., either simultaneous intake or 0.5–1 h before or after ketoconazole administration. For doses of 200–600 mg, T_{max} was delayed by 1–1.5 h compared to ketoconazole administered in a fasted state [6]. Observed C_{max} values were not affected by food intake, while the respective AUC_{last} values were higher for fasted scenarios [6]. With increasing doses of administration, differences in plasma exposure were less pronounced for ketoconazole. For AUC_{last}, the impact of DFIs was especially relevant for doses of 400 and 600 mg with observed DFI ratios of 1.59 and 1.45, respectively, while only unnoticeable differences in the plasma concentration-time curves between 800 mg ketoconazole in the fasted and fed states could be observed [6].

If the intake of food was not specified in the clinical study protocol, a DFI was assumed if fasted simulations were not appropriate to describe the respective data. This was the case in the following scenarios: First, if T_{max} was observed more than two hours after ketoconazole administration. Second, if multiple doses were administered within a day or over several days, as it was assumed that participants were not in a fasted state throughout the entirety of their study protocol. Third, if doses of orally administered ketoconazole were higher than 600 mg, as differences in absorption between the fasted and fed states substantially decrease with increasing dose (e.g., differences in the observed T_{max} and C_{max} of 800 mg ketoconazole were unnoticeable in both cases) [6]. This can be explained by a delayed absorption of higher doses due to ketoconazole's limited solubility rather than the intake of food alone.

The developed ketoconazole PBPK model included metabolism via AADAC and UGT1A4 [7,10]. Here, K_M values could be extracted from the literature. Implementation of AADAC-mediated metabolism was essential to describe the formation of M1 and M2. UGT1A4 was implemented to cover ketoconazole degradation irrespective of inhibitory DDI effects, as it was neither involved in the formation of the modeled metabolites nor affected by ketoconazole's autoinhibition.

Moreover, ketoconazole metabolism via CYP3A4 and transport via P-gp also were implemented as discussed in the literature [8,9,59]. Although CYP3A4-mediated metabolism and P-gp-mediated transport have not been fully investigated for ketoconazole and no

information guiding kinetic parametrization (e.g., K_M or V_{max}) has been reported yet, metabolism via CYP3A4 was implemented to describe a potential accumulation of ketoconazole during multiple-dose administrations due to its autoinhibition [5]. The K_i that described the CYP3A4 autoinhibition by ketoconazole was used as a surrogate value for a missing K_M of CYP3A4 since a similar parametrization strategy was already successfully applied during the PBPK model development of the imidazole derivative itraconazole by Hanke et al. [22]. The implementation of P-gp as an efflux transporter was included to thoroughly describe ketoconazole excretion, as between 10–37% of unchanged ketoconazole could be found in feces [5]. For this, the presented model predicted a fraction excreted to feces of around 27% after a single-dose administration of 200 mg of ketoconazole as an oral tablet in the fasted state. The K_M for P-gp transport was also taken from the K_i value used to describe the autoinhibition of P-gp.

The metabolite M1, which is formed by AADAC transformation of ketoconazole, is further metabolized to M2 via FMO3 [7,39]. The K_M value of FMO3-mediated metabolism was derived from the literature [39], while k_{cat} was optimized to fit the observed data. However, only one study by Weiss et al. reported plasma concentration-time profiles of M1 [13]; its exposure in plasma was only a fraction of its parent with observed C_{max} values of 6.07 ng/mL compared to 4956.03 ng/mL for ketoconazole after a single dose of 400 mg in the fasted state [13]. As metabolite concentrations are low in plasma, the authors assumed M1 accumulation in the liver [13]. In previous studies, M1 could not even be detected in plasma [60], and its metabolite M2, which is also metabolized by FMO3, was never reported to appear in plasma. Thus, in the present parent–metabolites PBPK model, M2 accumulation in liver cells was assumed, and permeation into plasma was prevented to account for the lack of reported M2 quantification in plasma. However, to precisely assess M2 disposition kinetics, more research is required. For the FMO3-mediated metabolism of M2 in the cell [39] no in vitro measurements were available. Hence, an FMO3-mediated clearance was implemented and optimized to thoroughly predict the respective DDIs. It should be noted that the implementation of M2-mediated inhibition captured the potential involvement of several metabolites, which could be important to ketoconazole's inhibitory effect. Here, M2 served as a representative metabolite of various metabolites that are not fully understood and also need to be further investigated [21,39].

While M1 has also been observed to inhibit CYP3A4 and P-gp [7,13] (with respective K_i values available in the literature), M2-mediated inhibition was not reported. To investigate the importance of both M1 and M2, which may account for further unknown metabolites, for ketoconazole's inhibitory effect, DDIs were simulated for the parent alone (P), with only M1 (P + M1), and with both metabolites (P + M1 + M2). For M2-mediated inhibition of CYP3A4 and P-gp, the respective K_i values were surrogated from literature K_i values used for M1 inhibition. CYP3A4 and P-gp DDIs were simulated with the victim drugs alfentanil, alprazolam, midazolam, triazolam, and digoxin.

In general, the modeling of both metabolites (P + M1 + M2) outperformed predictions without metabolites (scenarios P and P + M1), and apparent differences were most notable in the following two scenarios: First, if victim drug exposure was observed over a long time. Here, victim drug plasma concentrations measured 10 hours after administration were better predicted if modeling of M1 and M2 was included (Figure 5). Second, DDI performance of P + M1 + M2 was superior if the perpetrator and victim drug were administered at different times. This was especially apparent when comparing the DDI AUC_{last} and C_{max} ratios in evaluations without modeling M1 and M2. In the case of dosing time gaps between the victim and perpetrator, the inclusion of only M1 performed slightly better than modeling the DDIs with only the parent compound. For the remaining model scenarios, P + M1 and P performed equally well. Moreover, the modeling of M1 or M2 did not impact ketoconazole exposure.

Simulations of various DDI scenarios illustrated that reversible inhibition via ketoconazole alone was not sufficient to describe the impact on AUC_{last} and C_{max} of the victim compounds, especially if dosing time gaps of several hours between the victim

and perpetrator were considered. Similarly, a successfully developed parent–metabolites PBPK model for itraconazole included its three metabolites that participated in the DDIs as well [22]. Hence, it is reasonable to assume that ketoconazole is not solely responsible for its DDI effect. For ketoconazole, a potential mechanism-based inhibition; e.g., of CYP3A4, was discussed, but the contributions of ketoconazole's metabolites were not investigated [61,62]. In more recent studies, a reversible rather than a mechanism-based inhibition was reported [13,63]. In the present work, all inhibitions were described as reversible inhibitions, as it could be assumed that the supposed mechanism-based inhibition of ketoconazole might be a sequence of reversible inhibitions by ketoconazole and its metabolites intracellularly.

Overall, the developed parent–metabolites PBPK model of ketoconazole was capable of describing and predicting DDIs with CYP3A4 and P-gp victims successfully, especially for dosing time gaps between perpetrator and victim drug administration. There were potential biases when it came to the model development and application. Potential sources of bias might have included: (i) the selection of clinical study reports for the training and test datasets from publicly available data sources; (ii) the demographic distribution of modeled individuals due to the inclusion criteria of the respective clinical trials and thus potential heterogeneities in the respective physiology of the investigated participants; (iii) heterogeneities in the modeled pathophysiology (mostly healthy individuals were covered in our analysis); and (iv) the potential to miss the implementation of important but yet unknown metabolism or transport processes. Moreover, several assumptions had to be made to inform the implemented processes; for example, assuming K_M values to estimate k_{cat} values for CYP3A4 metabolism or P-gp transport. A previously published PBPK model of ketoconazole discussed its impact as a perpetrator on DDIs with alprazolam and midazolam [15]. For this, only ketoconazole administrations of 200 mg twice daily and 400 mg once daily as oral solutions in the fed state were investigated. In addition, our modeling work also investigated the inhibition of P-gp and the potential involvement of ketoconazole metabolites in DDIs to cover a broad dosing regimen with multiple victim drugs. Based on the presented simulations, the modeled metabolites might play a crucial and important role in the overall inhibitory effect of ketoconazole. The developed PBPK models can serve to generate hypotheses regarding the impact of metabolites on a drug's interaction potential, especially in polymedicated individuals. Moreover, since ketoconazole is classified by the FDA as a strong inhibitor of CYP3A4 and P-gp, the presented PBPK models can be coupled with further victim models to simulate different DDI scenarios and also to interpret the extensive DDI evidence already collected using this compound.

5. Conclusions

A parent–metabolites PBPK model for ketoconazole and its metabolites M1 and M2 was developed. The comprehensive PBPK model was capable of predicting the effect of DFIs on ketoconazole. Moreover, the presented model captured the potential importance of metabolites for ketoconazole's prominent inhibitory effect as a CYP3A4 and P-gp perpetrator drug in various investigated DDI scenarios. The PBPK model files are freely available at http://models.clinicalpharmacy.me to support further DDI studies in drug development and discovery.

Supplementary Materials: The following supporting information can be downloaded at: https://www.mdpi.com/article/10.3390/pharmaceutics15020679/s1, S1: PBPK Model Building; S2: Ketoconazole—PBPK model evaluation; S3: Ketoconazole—DDI Modeling.

Author Contributions: Conceptualization, F.Z.M., J.-G.W., J.W., W.E.H. and T.L.; funding acquisition, M.S. and T.L.; investigation, F.Z.M. and J.-G.W.; visualization, F.Z.M.; writing—original draft, F.Z.M., J.-G.W., L.M.F., D.S. and T.L.; writing—review and editing, F.Z.M., J.-G.W., L.M.F., D.S., M.S., J.W., W.E.H. and T.L. All authors have read and agreed to the published version of the manuscript.

Funding: M.S. was supported by the Robert Bosch Stiftung (Stuttgart, Germany), a European Commission Horizon 2020 UPGx grant (668353), a grant from the German Federal Ministry of Education and Research (BMBF; 031L0188D), and the Deutsche Forschungsgemeinschaft (DFG; German Research Foundation) under Germany's Excellence Strategy (EXC 2180—390900677). T.L. was supported by the project "Open-source modeling framework for automated quality control and management of complex life science system models" (OSMOSES) funded by the German Federal Ministry of Education and Research (BMBF; grant ID: 031L0161C).

Institutional Review Board Statement: Not applicable.

Informed Consent Statement: Not applicable.

Data Availability Statement: All modeling files (including the clinical study data utilized) can be found at http://models.clinicalpharmacy.me.

Conflicts of Interest: J.-G.W. has been an employee of Boehringer Ingelheim Pharma GmbH and Co., KG, since January 2020. All other authors declare no conflict of interest.

References

1. Heel, R.C.; Brogden, R.N.; Carmine, A.; Morley, P.A.; Speight, T.M.; Avery, G.S. Ketoconazole: A Review of its Therapeutic Efficacy in Superficial and Systemic Fungal Infections. *Drugs* **1982**, *23*, 1–36. [CrossRef] [PubMed]
2. Castinetti, F.; Guignat, L.; Giraud, P.; Muller, M.; Kamenicky, P.; Drui, D.; Caron, P.; Luca, F.; Donadille, B.; Vantyghem, M.C.; et al. Ketoconazole in Cushing's Disease: Is It Worth a Try? *J. Clin. Endocrinol. Metab.* **2014**, *99*, 1623–1630. [CrossRef] [PubMed]
3. Janssen Pharmaceuticals Nizoral(R) (Ketoconazole) Tablets. *Drug Label* **2013**.
4. Ghazal, H.S.; Dyas, A.M.; Ford, J.L.; Hutcheon, G.A. The impact of food components on the intrinsic dissolution rate of ketoconazole. *Drug Dev. Ind. Pharm.* **2015**, *41*, 1647–1654. [CrossRef]
5. Daneshmend, T.K.; Warnock, D.W. Clinical Pharmacokinetics of Ketoconazole. *Clin. Pharmacokinet.* **1988**, *14*, 13–34. [CrossRef]
6. Daneshmend, T.K.; Warnock, D.W.; Ene, M.D.; Johnson, E.M.; Potten, M.R.; Richardson, M.D.; Williamson, P.J. Influence of food on the pharmacokinetics of ketoconazole. *Antimicrob. Agents Chemother.* **1984**, *25*, 1–3. [CrossRef]
7. Fukami, T.; Iida, A.; Konishi, K.; Nakajima, M. Human arylacetamide deacetylase hydrolyzes ketoconazole to trigger hepatocellular toxicity. *Biochem. Pharmacol.* **2016**, *116*, 153–161. [CrossRef]
8. Fitch, W.; Tran, T.; Young, M.; Liu, L.; Chen, Y. Revisiting the Metabolism of Ketoconazole Using Accurate Mass. *Drug Metab. Lett.* **2009**, *3*, 191–198. [CrossRef]
9. Schwab, D.; Fischer, H.; Tabatabaei, A.; Poli, S.; Huwyler, J. Comparison of in Vitro P-Glycoprotein Screening Assays: Recommendations for Their Use in Drug Discovery. *J. Med. Chem.* **2003**, *46*, 1716–1725. [CrossRef]
10. Bourcier, K.; Hyland, R.; Kempshall, S.; Jones, R.; Maximilien, J.; Irvine, N.; Jones, B. Investigation into UDP-Glucuronosyltransferase (UGT) Enzyme Kinetics of Imidazole- and Triazole-Containing Antifungal Drugs in Human Liver Microsomes and Recombinant UGT Enzymes. *Drug Metab. Dispos.* **2010**, *38*, 923–929. [CrossRef]
11. European Medicines Agency European European Medicines Agency Recommends Suspension of Marketing Authorisations for Oral Ketoconazole. Available online: https://www.ema.europa.eu/documents/press-release/european-medicines-agency-recommends-suspension-marketing-authorisations-oral-ketoconazol (accessed on 1 January 2013).
12. Nix, D.E. Cardiotoxicity Induced by Antifungal Drugs. *Curr. Fungal Infect. Rep.* **2014**, *8*, 129–138. [CrossRef]
13. Weiss, J.; Foerster, K.I.; Weber, M.; Burhenne, J.; Mikus, G.; Lehr, T.; Haefeli, W.E. Does the circulating ketoconazole metabolite N-deacetyl ketoconazole contribute to the drug-drug interaction potential of the parent compound? *Eur. J. Pharm. Sci.* **2022**, *169*, 106076. [CrossRef] [PubMed]
14. Janssen Pharmaceutics Nizoral(R) (Ketoconazole) 2% Shampoo. *Drug Label* **2013**.
15. Boulenc, X.; Nicolas, O.; Hermabessière, S.; Zobouyan, I.; Martin, V.; Donazzolo, Y.; Ollier, C. CYP3A4-based drug-drug interaction: CYP3A4 substrates' pharmacokinetic properties and ketoconazole dose regimen effect. *Eur. J. Drug Metab. Pharmacokinet.* **2016**, *41*, 45–54. [CrossRef] [PubMed]
16. Olkkola, K.T.; Backman, J.T.; Neuvonen, P.J. Midazolam should be avoided in patients receiving the systemic antimycotics ketoconazole or itraconazole. *Clin. Pharmacol. Ther.* **1994**, *55*, 481–485. [CrossRef]
17. Greenblatt, D.J.; Wright, C.E.; Von Moltke, L.L.; Harmatz, J.S.; Ehrenberg, B.L.; Harrel, L.M.; Corbett, K.; Counihan, M.; Tobias, S.; Shader, R.I. Ketoconazole inhibition of triazolam and alprazolam clearance: Differential kinetic and dynamic consequences. *Clin. Pharmacol. Ther.* **1998**, *64*, 237–247. [CrossRef]
18. Daneshmend, T.K.; Warnock, D.W.; Turner, A.; Roberts, C.J.C. Pharmacokinetics of ketoconazole in normal subjects. *J. Antimicrob. Chemother.* **1981**, *8*, 299–304. [CrossRef]
19. Kharasch, E.D.; Vangveravong, S.; Buck, N.; London, A.; Kim, T.; Blood, J.; Mach, R.H. Concurrent assessment of hepatic and intestinal cytochrome P450 3A activities using deuterated alfentanil. *Clin. Pharmacol. Ther.* **2011**, *89*, 562–570. [CrossRef]
20. Isoherranen, N.; Kunze, K.L.; Allen, K.E.; Nelson, W.L.; Thummel, K.E. Role of itraconazole metabolites in CYP3A4 inhibition. *Drug Metab. Dispos.* **2004**, *32*, 1121–1131. [CrossRef]

21. Kim, J.-H.; Choi, W.-G.; Lee, S.; Lee, H. Revisiting the Metabolism and Bioactivation of Ketoconazole in Human and Mouse Using Liquid Chromatography–Mass Spectrometry-Based Metabolomics. *Int. J. Mol. Sci.* **2017**, *18*, 621. [CrossRef]
22. Hanke, N.; Frechen, S.; Moj, D.; Britz, H.; Eissing, T.; Wendl, T.; Lehr, T. PBPK Models for CYP3A4 and P-gp DDI prediction: A modeling network of rifampicin, itraconazole, clarithromycin, midazolam, alfentanil, and digoxin. *CPT Pharmacomet. Syst. Pharmacol.* **2018**, *7*, 647–659. [CrossRef]
23. U.S. Food and Drug Administration. Physiologically Based Pharmacokinetic Analyses—Format and Content. Available online: https://www.fda.gov/media/101469/download (accessed on 14 July 2022).
24. European Medicines Agency. Guideline on the reporting of physiologically Based Pharmacokinetic (PBPK) Modelling and Simulation. Available online: https://www.ema.europa.eu/en/documents/scientific-guideline/guideline-reporting-physiologically-based-pharmacokinetic-pbpk-modelling-simulation_en.pdf (accessed on 14 July 2022).
25. Türk, D.; Fuhr, L.M.; Marok, F.Z.; Rüdesheim, S.; Kühn, A.; Selzer, D.; Schwab, M.; Lehr, T. Novel models for the prediction of drug-gene interactions. *Expert Opin. Drug Metab. Toxicol.* **2021**, *17*, 1293–1310. [CrossRef]
26. Lippert, J.; Burghaus, R.; Edginton, A.; Frechen, S.; Karlsson, M.; Kovar, A.; Lehr, T.; Milligan, P.; Nock, V.; Ramusovic, S.; et al. Open Systems Pharmacology Community—An Open Access, Open Source, Open Science Approach to Modeling and Simulation in Pharmaceutical Sciences. *CPT Pharmacomet. Syst. Pharmacol.* **2019**, *8*, 878–882. [CrossRef]
27. Wojtyniak, J.; Britz, H.; Selzer, D.; Schwab, M.; Lehr, T. Data Digitizing: Accurate and Precise Data Extraction for Quantitative Systems Pharmacology and Physiologically-Based Pharmacokinetic Modeling. *CPT Pharmacomet. Syst. Pharmacol.* **2020**, *9*, 322–331. [CrossRef]
28. Solodenko, J.; Frechen, S.; Dallmann, A. Building and Evaluation of a PBPK Model for Triazolam in Healthy Adults. Available online: https://github.com/Open-Systems-Pharmacology/OSP-PBPK-Model-Library/blob/master/Triazolam/Triazolam_evaluation_report.pdf (accessed on 30 June 2022).
29. Frechen, S.; Dallmann, A. Building and Evaluation of a PBPK Model for Alprazolam in Healthy Adults. Available online: https://github.com/Open-Systems-Pharmacology/OSP-PBPK-Model-Library/blob/v9.1/Alprazolam/Alprazolam_evaluation_report.pdf (accessed on 30 June 2022).
30. Drug Development and Drug Interactions | Table of Substrates, Inhibitors and Inducers. Available online: https://www.fda.gov/drugs/drug-interactions-labeling/drug-development-and-drug-interactions-table-substrates-inhibitors-and-inducers (accessed on 20 June 2022).
31. Frechen, S.; Solodenko, J. CYP3A4 DDI Qualification Plan. Available online: https://github.com/Open-Systems-Pharmacology/OSP-Qualification-Reports/blob/master/DDI_Qualification_CYP3A4/report.pdf (accessed on 20 January 2023).
32. Les Laboratoires Servier. Servier Medical at. Available online: https://smart.servier.com/ (accessed on 14 July 2022).
33. Chemicalize Ketoconazole Entry. Available online: https://chemicalize.com/app/calculation/ketoconazol (accessed on 1 May 2021).
34. Chemicalize N-deactylketoconazole Entry. Available online: https://chemicalize.com/app/calculation/ClC1%3DCC%3DC(C(Cl)%3DC1)[C%40]1(CN2C%3DCN%3DC2)OC[C%40%40H](COC2%3DCC%3DC(C%3DC2)N2CCNCC2)O1%7Clp%3A0%3A3%2C6%3A3%2C10%3A1%2C13%3A1%2C15%3A2%2C19%3A2%2C26%3A1%2C29%3A1%2C32%3A2%7C (accessed on 1 May 2021).
35. Chemicalize N-Deacetyl-N-Hydroxy-Ketoconazole Entry. Available online: https://chemicalize.com/app/calculation/ON1CCN(CC1)C1%3DCC%3DC(OCC2COC(CN3C%3DCN%3DC3)(O2)C2%3DC(Cl)C%3DC(Cl)C%3DC2)C%3DC1%7Clp%3A0%3A2%2C1%3A1%2C4%3A1%2C11%3A2%2C15%3A2%2C18%3A1%2C21%3A1%2C23%3A2%2C26%3A3%2C29%3A3%7C (accessed on 1 May 2021).
36. Taneri, F.; Güneri, T.; Aigner, Z.; Kata, M. Improvement in the Physicochemical Properties of Ketoconazole through Complexation with Cyclodextrin Derivatives. *J. Incl. Phenom. Macrocycl. Chem.* **2002**, *44*, 257–260. [CrossRef]
37. Open Systems Pharmacology Suite Community Open Systems Pharmacology Suite Manual. Available online: https://docs.open-systems-pharmacology.org/ (accessed on 20 April 2022).
38. Fisher, R.S.; Rock, E.; Malmud, L.S. Effects of meal composition on gallbladder and gastric emptying in man. *Dig. Dis. Sci.* **1987**, *32*, 1337–1344. [CrossRef] [PubMed]
39. Rodriguez, R.J.; Acosta, D. Metabolism of ketoconazole and deacetylated ketoconazole by rat hepatic microsomes and flavin-containing monooxygenases. *Drug Metab. Dispos.* **1997**, *25*, 772–777. [PubMed]
40. Berezhkovskiy, L.M. Volume of Distribution at Steady State for a Linear Pharmacokinetic System with Peripheral Elimination. *J. Pharm. Sci.* **2004**, *93*, 1628–1640. [CrossRef]
41. Kawai, R.; Lemaire, M.; Steimer, J.L.; Bruelisauer, A.; Niederberger, W.; Rowland, M. Physiologically based pharmacokinetic study on a cyclosporin derivative, SDZ IMM 125. *J. Pharmacokinet. Biopharm.* **1994**, *22*, 327–365. [CrossRef]
42. Rodgers, T.; Rowland, M. Physiologically based pharmacokinetic modelling 2: Predicting the tissue distribution of acids, very weak bases, neutrals and zwitterions. *J. Pharm. Sci.* **2006**, *95*, 1238–1257. [CrossRef]
43. Dallmann, A. IVIC with the Particle Dissolution Module Implemented in OSP. Available online: https://github.com/AndreDlm/IVIVC-with-particle-dissolution-module-in-OSP (accessed on 30 June 2022).
44. Huang, Y.-C.; Colaizzi, J.L.; Bierman, R.H.; Woestenborghs, R.; Heykants, J.J.P. Pharmacokinetics and Dose Proportionality of Domperidone in Healthy Volunteers. *J. Clin. Pharmacol.* **1986**, *26*, 628–632. [CrossRef]

45. Polk, R.E.; Crouch, M.A.; Israel, D.S.; Pastor, A.; Sadler, B.M.; Chittick, G.E.; Symonds, W.T.; Gouldin, W.; Lou, Y. Pharmacokinetic interaction between ketoconazole and amprenavir after single doses in healthy men. *Pharmacotherapy* **1999**, *19*, 1378–1384. [CrossRef]
46. Boyce, M.J.; Baisley, K.J.; Warrington, S.J. Pharmacokinetic interaction between domperidone and ketoconazole leads to QT prolongation in healthy volunteers: A randomized, placebo-controlled, double-blind, crossover study. *Br. J. Clin. Pharmacol.* **2012**, *73*, 411–421. [CrossRef]
47. Tiseo, P.J.; Perdomo, C.A.; Friedhoff, L.T. Concurrent administration of donepezil HCl and ketoconazole: Assessment of pharmacokinetic changes following single and multiple doses. *Br. J. Clin. Pharmacol.* **2002**, *46*, 30–34. [CrossRef] [PubMed]
48. Daneshmend, T.K.; Warnock, D.W.; Ene, M.D.; Johnson, E.M.; Parker, G.; Richardson, M.D.; Roberts, C.J.C. Multiple dose pharmacokinetics of ketoconazole and their effects on antipyrine kinetics in man. *J. Antimicrob. Chemother.* **1983**, *12*, 185–188. [CrossRef] [PubMed]
49. U.S. Food and Drug Administration Bioequivalence—Application Number: 74–971. 1998, pp. 1–33. Available online: https://www.accessdata.fda.gov/drugsatfda_docs/anda/99/74-971_Ketoconazole.cfm (accessed on 21 December 2022).
50. Craven, P.C.; Graybill, J.R.; Jorgensen, J.H.; Dismukes, W.E.; Levine, B.E. High-dose ketoconazole for treatment of fungal infections of the central nervous system. *Ann. Intern. Med.* **1983**, *98*, 160–167. [CrossRef] [PubMed]
51. Männistö, P.T.; Mäntylä, R.; Nykänen, S.; Lamminsivu, U.; Ottoila, P. Impairing effect of food on ketoconazole absorption. *Antimicrob. Agents Chemother.* **1982**, *21*, 730–733. [CrossRef]
52. Guest, E.J.; Aarons, L.; Houston, J.B.; Rostami-Hodjegan, A.; Galetin, A. Critique of the two-fold measure of prediction success for ratios: Application for the assessment of drug-drug interactions. *Drug Metab. Dispos.* **2011**, *39*, 170–173. [CrossRef]
53. Tsunoda, S.M.; Velez, R.L.; von Moltke, L.L.; Greenblatt, D.J. Differentiation of intestinal and hepatic cytochrome P450 3A activity with use of midazolam as an in vivo probe: Effect of ketoconazole. *Clin. Pharmacol. Ther.* **1999**, *66*, 461–471. [CrossRef]
54. Krishna, G.; Moton, A.; Ma, L.; Savant, I.; Martinho, M.; Seiberling, M.; McLeod, J. Effects of oral posaconazole on the pharmacokinetic properties of oral and intravenous midazolam: A phase I, randomized, open-label, crossover study in healthy volunteers. *Clin. Ther.* **2009**, *31*, 286–298. [CrossRef]
55. Larsen, U.L.; Olesen, H.L.; Nyvold, G.C.; Eriksen, J.; Jakobsen, P.; Østergaard, M.; Autrup, H.; Andersen, V. Human intestinal P-glycoprotein activity estimated by the model substrate digoxin. *Scand. J. Clin. Lab. Investig.* **2007**, *67*, 123–134. [CrossRef] [PubMed]
56. Liu, B.; Crewe, H.K.; Ozdemir, M.; Rowland Yeo, K.; Tucker, G.; Rostami-Hodjegan, A. The absorption kinetics of ketoconazole plays a major role in explaining the reported variability in the level of interaction with midazolam: Interplay between formulation and inhibition of gut wall and liver metabolism. *Biopharm. Drug Dispos.* **2017**, *38*, 260–270. [CrossRef] [PubMed]
57. Elder, E.J.; Evans, J.C.; Scherzer, B.D.; Hitt, J.E.; Kupperblatt, G.B.; Saghir, S.A.; Markham, D.A. Preparation, characterization, and scale-up of ketoconazole with enhanced dissolution and bioavailability. *Drug Dev. Ind. Pharm.* **2007**, *33*, 755–765. [CrossRef] [PubMed]
58. Cristofoletti, R.; Patel, N.; Dressman, J.B. Differences in Food Effects for 2 Weak Bases With Similar BCS Drug-Related Properties: What Is Happening in the Intestinal Lumen? *J. Pharm. Sci.* **2016**, *105*, 2712–2722. [CrossRef] [PubMed]
59. European Medicines Agency Summary of Product Characteristics. 2014. Available online: https://www.ema.europa.eu/documents/product-information/ketoconazole-hra-epar-product-information_en.pdf (accessed on 20 November 2022).
60. Badcock, N.R.; Bartholomeusz, F.D.; Frewin, D.B.; Sansom, L.N.; Reid, J.G. The pharmacokinetics of ketoconazole after chronic administration in adults. *Eur. J. Clin. Pharmacol.* **1987**, *33*, 531–534. [CrossRef]
61. Baumann, P.; Van den Heuvel, M.W.; Sitsen, J.M.A.; Eap, C.B.; Peeters, P.A.M. P.1.157 Effect of the CYP3A4 inhibitor ketoconazol on the pharmacokinetics of mirtazapine in healthy volunteers. *Eur. Neuropsychopharmacol.* **2003**, *13*, S241. [CrossRef]
62. Von Moltke, L.L.; Durol, A.L.B.; Duan, S.X.; Greenblatt, D.J. Potent mechanism-based inhibition of human CYP3A in vitro by amprenavir and ritonavir: Comparison with ketoconazole. *Eur. J. Clin. Pharmacol.* **2000**, *56*, 259–261. [CrossRef]
63. Greenblatt, D.J.; Zhao, Y.; Venkatakrishnan, K.; Duan, S.X.; Harmatz, J.S.; Parent, S.J.; Court, M.H.; Von Moltke, L.L. Mechanism of cytochrome P450-3A inhibition by ketoconazole. *J. Pharm. Pharmacol.* **2011**, *63*, 214–221. [CrossRef]

4.3 PUBLICATION III – PERSONALIZED CHRONOMODULATED 5-FLUOROURACIL TREATMENT: A PHYSIOLOGICALLY BASED PHARMACOKINETIC PRECISION DOSING APPROACH FOR OPTIMIZING CANCER THERAPY.

4.3.1 *Reference*

Marok FZ, Wojtyniak JG, Selzer D, Dallmann R, Swen JJ, Guchelaar HJ, Schwab M, and Lehr T. Personalized Chronomodulated 5-Fluorouracil Treatment: A Physiologically Based Pharmacokinetic Precision Dosing Approach for Optimizing Cancer Therapy. *Clinical Pharmacology and Therapeutics*. 2024; 0, 1–11. https://doi.org/10.1002/cpt.3181.

4.3.2 *Supplementary Materials*

The related electronic supplementary materials can be found on the accompanying compact disk or accessed online via: https://ascpt.onlinelibrary.wiley.com/action/downloadSupplement?doi=10.1002%2Fcpt.3181&file=cpt3181-sup-0001-Supinfo.pdf.

4.3.3 *Author Contributions*

Following, the author contributions are listed according to CRediT [4].

Fatima Zahra Marok:	Conceptualization, Visualization, Investigation, Writing-Original Draft, Writing-Review and Editing
Jan-Georg Wojtyniak:	Conceptualization, Writing- Review and Editing.
Dominik Selzer:	Conceptualization, Investigation, Writing-Review and Editing.
Robert Dallmann:	Conceptualization, Funding Acquisition, Writing- Review and Editing.
Jesse J Swen:	Conceptualization, Funding Acquisition, Writing- Review and Editing.
Henk-Jan Guchelaar :	Conceptualization, Funding Acquisition, Writing- Review and Editing.
Matthias Schwab:	Conceptualization, Funding Acquisition, Writing- Review and Editing.
Thorsten Lehr :	Conceptualization, Funding Acquisition, Writing- Review and Editing.

4.3.4 *Copyright*

Personalized Chronomodulated 5-Fluorouracil Treatment: A Physiologically-Based Pharmacokinetic Precision Dosing Approach for Optimizing Cancer Therapy

Fatima Zahra Marok[1], Jan-Georg Wojtyniak[1,2], Dominik Selzer[1], Robert Dallmann[3], Jesse J. Swen[4], Henk-Jan Guchelaar[4], Matthias Schwab[2,5,6] and Thorsten Lehr[1,*]

The discovery of circadian clock genes greatly amplified the study of diurnal variations impacting cancer therapy, transforming it into a rapidly growing field of research. Especially, use of chronomodulated treatment with 5-fluorouracil (5-FU) has gained significance. Studies indicate high interindividual variability (IIV) in diurnal variations in dihydropyrimidine dehydrogenase (DPD) activity – a key enzyme for 5-FU metabolism. However, the influence of individual DPD chronotypes on chronomodulated therapy remains unclear and warrants further investigation. To optimize precision dosing of chronomodulated 5-FU, this study aims to: (i) build physiologically-based pharmacokinetic (PBPK) models for 5-FU, uracil, and their metabolites, (ii) assess the impact of diurnal variation on DPD activity, (iii) estimate individual DPD chronotypes, and (iv) personalize chronomodulated 5-FU infusion rates based on a patient's DPD chronotype. Whole-body PBPK models were developed with PK-Sim(R) and MoBi(R). Sinusoidal functions were used to incorporate variations in enzyme activity and chronomodulated infusion rates as well as to estimate individual DPD chronotypes from *DPYD* mRNA expression or DPD enzymatic activity. Four whole-body PBPK models for 5-FU, uracil, and their metabolites were established utilizing data from 41 5-FU and 10 publicly available uracil studies. IIV in DPD chronotypes was assessed and personalized chronomodulated administrations were developed to achieve (i) comparable 5-FU peak plasma concentrations, (ii) comparable 5-FU exposure, and (iii) constant 5-FU plasma levels via "noise cancellation" chronomodulated infusion. The developed PBPK models capture the extent of diurnal variations in DPD activity and can help investigate individualized chronomodulated 5-FU therapy through testing alternative personalized dosing strategies.

Study Highlights

WHAT IS THE CURRENT KNOWLEDGE ON THE TOPIC?

☑ 5-Fluorouracil (5-FU) is a widely used anticancer drug, that is influenced by diurnal variations and often administered as chronomodulated intravenous infusions. Pronounced interindividual variability (IIV) of dihydropyrimidine dehydrogenase (DPD) chronotypes was shown in patients with cancer.

WHAT QUESTION DID THIS STUDY ADDRESS?

☑ The presented study aimed to question the use of uniformed chronomodulated 5-FU treatment on an individual patient level.

WHAT DOES THIS STUDY ADD TO OUR KNOWLEDGE?

☑ Physiologically-based pharmacokinetic (PBPK) models of endogenous uracil and 5-FU together with their respective metabolites formed by DPD were developed to include the impact of diurnal variations on DPD and to investigate the influence of IIV in DPD chronotypes for 5-FU exposure during various treatment scenarios.

HOW MIGHT THIS CHANGE CLINICAL PHARMACOLOGY OR TRANSLATIONAL SCIENCE?

☑ With help of the successfully developed PBPK models, the study proposes a new and personalized treatment approach of 5-FU therapy based on an individuals' DPD chronotype.

[1]Clinical Pharmacy, Saarland University, Saarbruecken, Germany; [2]Dr. Margarete Fischer-Bosch-Institut of Clinical Pharmacology, Stuttgart, Germany; [3]Division of Biomedical Sciences, Warwick Medical School, University of Warwick, Coventry, UK; [4]Department of Clinical Pharmacy & Toxicology, Leiden University Medical Center, RC Leiden, The Netherlands; [5]Departments of Clinical Pharmacology, and of Biochemistry and Pharmacy, University Tuebingen, Tuebingen, Germany; [6]Cluster of excellence iFIT (EXC2180) "Image-Guided and Functionally Instructed Tumor Therapies", University Tuebingen, Tuebingen, Germany. *Correspondence: Thorsten Lehr (thorsten.lehr@mx.uni-saarland.de)

Received August 4, 2023; accepted January 3, 2024. doi:10.1002/cpt.3181

5-Fluorouracil (5-FU) is a potent anticancer agent that is extensively used in treatment of various cancers, for example, as first-line treatment in combinations with other anticancer drugs.[1,2] Given its structural similarity to the endogenous nucleobase uracil, 5-FU effectively inhibits tumor growth by interfering with the synthesis of DNA, RNA, and other nucleosides. Due to its highly variable oral bioavailability (ranging from 0 to 80%[2]), narrow therapeutic window,[2] and improved toxicity profile, 5-FU is commonly administered as a combination of an intravenous bolus injection followed by a continuous infusion, or solely as a continuous infusion over a period of 22–96 hours, in repeated cycles covering several months of treatment.[3]

Dihydropyrimidine dehydrogenase (DPD) catalyzes the rate-limiting reaction in the conversion of 5-FU to inactive metabolites. Several genetic variants within the gene coding for DPD (*DPYD*) have been identified that lead to altered enzyme activity and subsequently result in reduced 5-FU metabolism.[4] Thus, considering the narrow therapeutic window,[2] certain *DPYD* alleles are associated with potentially life-threatening toxicities during chemotherapy.[1,4,5] Furthermore, cellular circadian clocks strongly modulate 5-FU metabolic pathways, which can affect both catabolic pathways, such as DPD metabolism, as well as anabolic pathways, for example, mediated by the uridine monophosphate synthase. Specifically, diurnal variation significantly influences the expression of *DPYD* messenger RNA (mRNA) and, hence, DPD biosynthesis. This leads to pronounced diurnal patterns in plasma levels of its endogenous substrate uracil, as well as the ratio of dihydrouracil-to-uracil (DHU/U).[6-9] Additionally, studies have indicated diurnal variations in plasma concentrations of 5-FU during continuous constant-rate infusions, as reported in the literature.[10-13] Notably, these studies have documented inter- and intraindividual variability regarding both the time and extent of peak DPD activity.[8,14,15] Chronomodulated 5-FU treatment schedules have peak infusion rates at 4 AM,[6] often in various combinations with chronomodulated irinotecan and oxaliplatin like the chronoFLO4 treatment.[6,16,17] Compared with constant-rate infusions, chronomodulated infusions with peak delivery at 4 AM were better tolerated by male patients, whereas female patients experienced more grade 3–4 toxicities and demonstrated decreased response rates and overall survival under chronomodulated treatment.[16,17] Mathematical analyses using semimechanistic models unveiled considerable interpatient variability in the pharmacokinetics (PK) during chronomodulated therapy with 5-FU.[18] Despite all patients receiving 5-FU treatment (combined with irinotecan and oxaliplatin) with the same peak delivery rate and relative dose per body surface area, significant differences in maximum plasma concentrations (C_{max}) and areas under plasma concentration-time curves (AUC) could be observed.[18,19] As 5-FU clearance strongly correlates with DPD activity, interindividual variability (IIV) regarding diurnal DPD-mediated 5-FU metabolism could attribute significantly to the variability observed in 5-FU plasma exposure.[20]

In order to better understand the intricate interplay between the circadian clock and the time-of-day dependent variation in 5-FU therapy, our primary objective in this study was to formulate a personalized strategy for chronomodulated 5-FU treatment. We achieved this by using physiologically-based pharmacokinetic (PBPK) modeling, a mathematical technique to describe and predict a drug's behavior in various physiological tissues. Here, the versatility of the whole-body PBPK framework enables the exploration of various treatment scenarios, including intravenous, intra-arterial, or oral administrations of 5-FU.

Thus, the objectives of this study are as follows: (i) to predict the impact of diurnal variation on time-dependent DPD-mediated metabolism by developing whole-body PBPK models for 5-FU, uracil, and their metabolites dihydrofluorouracil (DHFU) and dihydrouracil (DHU); (ii) to simulate continuous infusions of 5-FU with chronomodulated administration rates; (iii) to estimate individual DPD chronotypes based on observed mRNA expressions, enzyme activities, or endogenous uracil levels; and (iv) to ultimately derive personalize chronomodulated 5-FU treatment tailored to the estimated individual DPD chronotypes.

METHODS

Software

For model development, PK-Sim and MoBi (Open Systems Pharmacology Suite 9.1, released under the GPLv2 license by the Open Systems Pharmacology community, www.open-systems-pharmacology.org)[21] were utilized. Model parameter estimation was carried out using Monte Carlo and Levenberg–Marquardt algorithms implemented in PK-Sim(R) and MoBi(R). Published concentration-time profiles of 5-FU, uracil, and their metabolites were digitized using GetData Graph Digitizer (version 2.26.0.20, S. Fedorov). PK parameter analysis, model performance evaluation, and figures were generated using the R programming language (version 3.6.3, R Core Team; R: A Language and Environment for Statistical Computing. R Foundation for Statistical Computing, Vienna, Austria, 2021).

Clinical data

Data from clinical studies of 5-FU and uracil were obtained from the literature and digitized following the approach of Wojtyniak and coworkers.[22] Plasma concentration-time profiles of endogenous uracil, [2-^{13}C] uracil after oral administration in healthy subjects, and 5-FU during and after intravenous administration in patients with cancer were compiled and divided into a training and a test data set used for model building and model evaluation, respectively. The training data set included metabolite concentration-time profiles, a broad dosing range, and various administration protocols. To account for the known sex differences, studies were assigned to the respective training and test data sets for a balanced distribution of female and male subjects. Demographic information of all collected profiles can be found in the clinical study tables in **Sections S2** and **S3** of the Supplementary Materials.

PBPK model building

An extensive literature search was conducted to gather data on the physicochemical properties, PK processes, as well as clinical studies. Whole-body PBPK models were built with virtual individuals based on the mean and mode of reported demographic information, including age, body weight, height, ethnicity, and sex for each study. If demographic data were unavailable for a study, virtual standard individuals were created with details listed in **Table S1.3**. Tissue distributions of relevant enzymes

and transporters were implemented, using the PK-Sim(R) expression database.[23] Detailed information on the used expression profiles derived from the PK-Sim(R) expression database is provided in **Tables S1.1** and **S1.2**.

Model input parameters that could not be sufficiently informed from the literature or were involved in important quantitative structure–activity relationship model estimates of permeability and distribution processes were optimized by fitting the models simultaneously to all plasma concentration-time profiles of the training data set.

Implementation of diurnal variations

For simulations of continuous infusions, a time-dependent sine function was used to describe oscillation over 24 hours (Eq. 1) accounting for diurnal variations in enzyme activity of DPD and dihydropyrimidinase (DPH), which catalyzes biotransformations of 5-FU and uracil metabolites. Similarly, variations in chronomodulated infusion rates were also calculated according to (Eq. 1):

$$f(t) = \left(1 + \mathrm{Amp} * \sin\left(\frac{2\pi\left(t + T_{\mathrm{Acr}}\right)}{24}\right)\right) * V \qquad (1)$$

where Amp is the amplitude, t represents the simulation time in hours, T_{Acr} is the phase shift, and V is the respective enzymatic activity rate or infusion rate.

The amplitude was either derived from studies reporting mean DPD activities over a period of 24 hours[7,9] for the majority of studies, or adjusted to fit the respective observed plasma concentrations, as listed in **Table S3.3**. Because the time of peak DPD activity (acrophase) and resulting minimal 5-FU plasma concentrations differed between several studies,[15,18,20,24] a mean phase shift parameter T_{Acr} could not be derived from the literature. Hence, if no data on DPD activity of patients were available and their respective acrophase was unknown, T_{Acr} was estimated. This estimation was also necessary if information regarding the time-of-day for the start of 5-FU administration or plasma concentration measurements was missing. When incorporating diurnal variations in DPH activity, values for Amp and T_{Acr} (Eq. 1) were estimated, as no activity profiles were available in the existing literature.

PBPK model evaluation

Model performance was evaluated by visual predictive checks of predicted and observed profiles from the corresponding clinical studies. Moreover, goodness-of-fit plots of predicted vs. observed plasma concentrations, AUC calculated from the time of the first to the last concentration measurement (AUC_{last}) as well as C_{max} values were generated. To quantify the descriptive and predictive performance of the models, mean relative deviation (MRD) and median symmetric accuracy (MSA) of all plasma concentration predictions together with geometric mean fold error (GMFE) of all AUC and C_{max} predictions were computed. For this, MRD and GMFE values ≤ 2 were considered successful model predictions. Details on the quantitative model evaluation can be found in **Section S1.1**.

Local sensitivity to single parameter changes was analyzed for the AUC of 5-FU, uracil, and their metabolites as described in **Section S1.2** with visualized results in **Section S2.4.5** and **S3.4.5**.

In vitro–in vivo-extrapolation of individual DPD chronotypes for dose individualizations

To estimate individual DPD chronotypes, diurnal patterns were derived from *in vitro* measurements of DPD activities or from *in vitro* measurements of *DPYD* mRNA expressions, which were then translated into DPD activities.[7,8] Next, the Amp and T_{Acr} of the diurnal pattern (see Eq. 1) were estimated to fit the observed DPD activities. Subsequently, the estimated diurnal parameters served as input for the DPD-mediated biotransformation in *in vivo* predictions of 5-FU or uracil plasma concentrations with the developed PBPK models.

RESULTS

PBPK model development: Implementation of diurnal variations

Whole-body PBPK models for 5-FU, uracil, and their metabolites DHFU and DHU were developed based on clinical data from 41 5-FU studies involving 777 patients and 10 uracil studies involving 104 volunteers. The administered doses of 5-FU ranged from 140 to 600 mg/m^2 for injections, 250–1750 mg/m^2/day for infusions and 300–580 mg/m^2 for oral solutions. Oral [2-^{13}C]uracil studies involved dosing ranging from 50 to 1,000 mg. Overall, 16 profiles were compiled in the training data set and 89 profiles were used for the test data set. All clinical studies used for model development are listed in **Tables S2.1**, **S3.1**, and **S4.1**.

A structure of the whole-body 5-FU and uracil PBPK models is depicted in **Figure 1a**. The biotransformation of 5-FU and uracil via DPD to DHFU and DHU, respectively, which are then further metabolized via DPH or transported via multidrug resistance-associated protein 4 (MRP4) are illustrated in **Figure 1b**.

Cellular endogenous uracil synthesis was simulated with a constant rate for each intracellular compartment, which was optimized to fit the observed data of endogenous plasma concentrations measured throughout the day. For DPD- and DPH-mediated metabolism, Michaelis–Menten kinetics were assumed, with the Michaelis–Menten constants derived from literature[26,27] and respective activity rates optimized to fit the observed data. Diurnal rhythms were implemented for DPD and DPH-mediated metabolism according to Eq. 1. Additionally, active transport of 5-FU and uracil via MRP4 was implemented and optimized as well. The respective drug-dependent parameters of the models are summarized in **Tables S2.2**, **S2.3**, **S3.2**, **S3.3**, and **S4.2**.

The model predictions of observed plasma concentrations of uracil as [2-^{13}C]uracil from oral solutions, 5-FU from intravenous bolus and continuous administrations, and their metabolites are shown in selected profiles in **Figure 2**. Diurnal variations in DPD activity were implemented with $\mathrm{Amp}_{\mathrm{DPD}}$ (0.124) derived from literature[7] and $T_{\mathrm{Acr,DPD}}$ optimized to fit the observed plasma concentrations. The impact of diurnal variation in DPD activity is further detailed in **Figure 3** with exemplary plasma concentration-time profiles of endogenous uracil, DHU and their corresponding parent-metabolite plasma ratio (DHU/U; often used to assess DPD phenotypes), as well as profiles of 5-FU and DHFU during continuous infusions of 5-FU with constant and chronomodulated rates.

For all model simulations presented in **Figure 3**, a literature value for Amp_{DPD} (0.124)[7] was used, appropriate to capture the extent of diurnal variations in mean uracil and 5-FU plasma concentrations, whereas $T_{\mathrm{Acr,DPD}}$ was optimized individually. Because both the constant rate infusion (**Figure 3b**) and the chronomodulated infusion (**Figure 3c**) were administered in the same cohort,[36] $T_{\mathrm{Acr,DPD}}$ of 1,285 min resulting in an acrophase at 7 PM was used for both simulations. To simulate chronomodulated infusions (**Figure 3c,d**), variations in administration rates described with the parameters Amp and T_{Acr} (here $\mathrm{Amp}_{\mathrm{INF}}$ and $T_{\mathrm{Acr,INF}}$) according to Eq. 1 were estimated based on the observed plasma concentration-time profiles. Overall, patients received ~ 60% of the daily 5-FU dose during the night with a peak delivery rate at 4 AM.

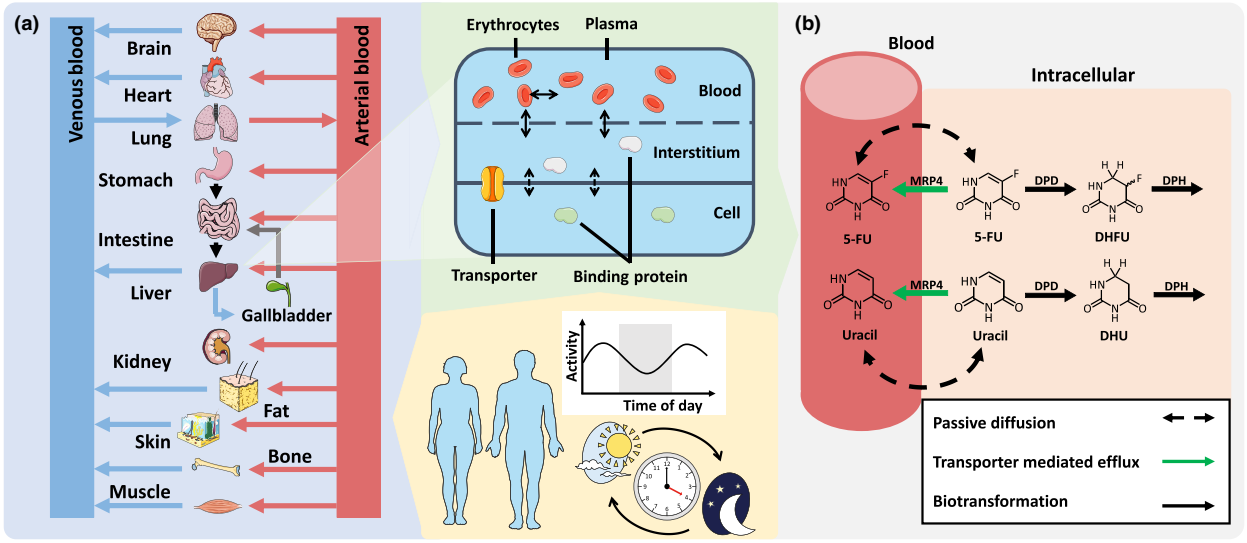

Figure 1 Schematic overview of the PBPK models of 5-FU and uracil. (**a**) The whole-body PBPK model comprises compartments representing organs and tissues, interconnected via blood flow. Each organ compartment is further divided into four subcompartments: plasma, red blood cells, and interstitial and intracellular space. Multi-compartment models were built to describe and predict the PKs of 5-FU and uracil considering drug-clock time interactions. (**b**) An illustrative depiction of the implemented processes: 5-FU is inactivated by DPD to DHFU. DHFU is subsequently metabolized by DPH. Similarly, uracil is transformed to DHU via DPD with subsequent metabolism of DHU via DPH. Drawings by Servier, licensed under CC BY 3.0.[25] 5-FU, 5-fluorouracil; DHFU, dihydrofluorouracil; DHU, dihydrouracil; DHP, dihydropyrimidinase; DPD, dihydropyrimidine dehydrogenase; DPH, dihydropyrimidinase; DHU, dihydrouracil; MRP4, multidrug resistance-associated protein 4; PBPK, physiologically-based pharmacokinetic; U, uracil.

Additionally, diurnal variations in DPH activity were simulated based on the assumption that clock genes may influence DPH as well. The diurnal parameters for DPH activity (Amp_{DPH} and $T_{Acr,DPH}$) were optimized to match the respective metabolite profiles (**Figure 3a,b**). By considering diurnal DPH activity, the diurnal patterns observed in the metabolite plasma concentrations were well-predicted, particularly in the case of DHFU, whose plasma levels substantially exceeded the oscillation of the parent plasma levels. MRD values for the metabolite predictions with a diurnal DPH activity were 1.06 and 1.68 for DHU and DHFU, respectively. Predictions of metabolite plasma concentrations with a constant DPH activity are shown in **Sections S2.3** and **S4.4**.

Overall, the assessed performance of the models predicting observed plasma concentrations of 5-FU and uracil as well as their metabolites are shown in goodness-of-fit plots with selected plasma concentration-time profiles in **Sections S2.4.3**, **S3.4.3**, and **S4.5.3**. All predictions were in good agreement with the observed data, with 96 of 98 of predicted AUC_{last} and 27 of 28 of predicted C_{max} values within the 2-fold acceptance limits. Total GMFEs for the 5-FU and uracil model performance were 1.23 and 1.12 (1.00–2.43) for AUC_{last} values as well as 1.20 and 1.20 (1.00–2.06) for C_{max} values, respectively.

All predicted compared with observed plasma concentration-time profiles on a linear and semilogarithmic scale, as well as AUC_{last} and C_{max} values for the test and training data sets are given in **Sections S2.4**, **S3.4**, and **S4.5**, and MRD, MSA, and GMFE values summarized in **Tables S2.4**, **S2.5**, **S3.4**, **S3.5**, **S4.3**, and **S4.4**.

PBPK model adaptation: Personalized dosing based on individual DPD chronotypes

To investigate the extent of IIV in DPD activity and its impact on 5-FU therapy, individual DPD chronotypes were estimated for patients with cancer and healthy subjects. DPD chronotypes in patients with cancer were derived from two different groups. First, individual DPD chronotypes were estimated from observed 5-FU plasma concentration-time profiles reported by Lévi *et al.*[19] (Lévi group) by adapting Amp_{DPD} and $T_{Acr,DPD}$ to match the observed 5-FU plasma profiles for every individual (**Figure 4a**). Here, all 10 patients received chronomodulated 5-FU with a peak delivery rate at 4 AM. The administration rates were obtained from the respective study. Individual 5-FU plasma levels were observed to vary greatly, with peak concentrations differing by up to 12-fold between patients, despite receiving the same dose and infusion rate. Second, DPD chronotypes were extrapolated from *DPYD* mRNA expression profiles reported from cancer patients by Raida *et al.*[8] (Raida group). Here, the parameters Amp_{DPD} and $T_{Acr,DPD}$ were estimated from leukocyte *DPYD* mRNA expressions, neglecting the short translation time of 1.7 minutes (translation rate of 10 amino acids per seconds[38] for a 1,025 amino acid long DPD protein[39]).

The respective values for Amp_{DPD} and $T_{Acr,DPD}$ for the Lévi and Raida groups were used according to (Eq. 1) to calculate DPD activity over time, based on V_{DPD} (baseline DPD activity) as shown in **Figure 4b,c**.

DPD chronotypes in healthy individuals were determined from measured DPD enzyme activities[7] (**Figure 4e**). In healthy subjects, acrophase and extent of enzyme activity exhibited greater

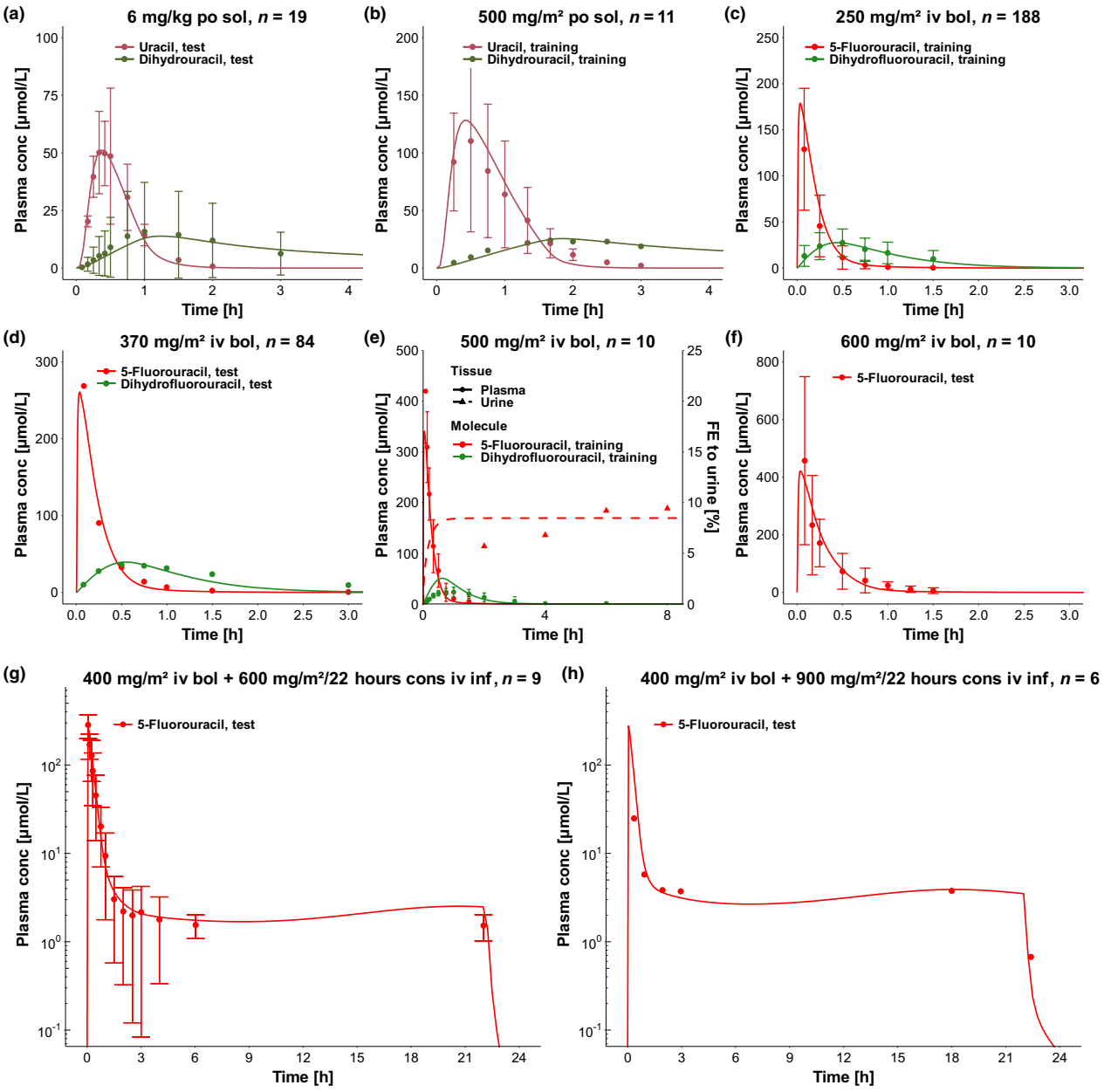

Figure 2 PBPK model performance. (**a,b**) Predicted (solid lines) and observed (dots) plasma concentration-time profiles of [2-^{13}C]uracil and dihydrouracil after application of 6 mg/kg body weight and 500 mg/m^2 body surface area [2-^{13}C]uracil as an oral solution with observed data from Mattison *et al.*[28] and Van Staveren *et al.*[29] (**c—f**) Predicted (solid lines) and observed (dots) plasma concentration-time profiles of 5-FU and dihydrofluorouracil after intravenous bolus injections of 250 mg/m^2, 370 mg/m^2, 500 mg/m^2 and 600 mg/m^2 5-FU with observed data from Bocci *et al.*,[30] Paolo *et al.*,[31] and Bardakji *et al.*[32] Additionally predicted (dashed line) and observed (triangles) fractions excreted in urine after administration of 500 mg/m^2 5-FU as bolus injections.[33] (**g,h**) Predicted (solid lines) and observed (dots) plasma concentration-time profiles of 5-FU after intravenous bolus injections of 400 mg/m^2 as loading dose and intravenous continuous infusions at a constant rate of 600 and 900 mg/m^2 over 22 hours as maintenance dose with observed data from Joel *et al.*[34] and Joulia *et al.*[35] 5-FU, 5-fluorouracil; bol, bolus injection; conc, concentration; cons, constant rate continuous infusion; inf, infusion; iv, intravenous; n, number of subjects; PBPK, physiologically-based pharmacokinetic; po, oral; sol, solution.

homogeneity, whereas both cancer patient groups displayed more pronounced IIV. This distinction is further emphasized when comparing the individual DPD maximum activity at their acrophases between healthy subjects and patients with cancer throughout the day (**Figure 4d**). DPD acrophases in healthy subjects were observed during the night between 1 and 5 AM, whereas in both patients with cancer groups they were distributed across the entire day, with the majority occurring during daytime hours. The standard deviation of mean DPD acrophases for patients with cancer was 3.6-fold higher than for the healthy group (9:53 AM ±5.29 hours for patients with

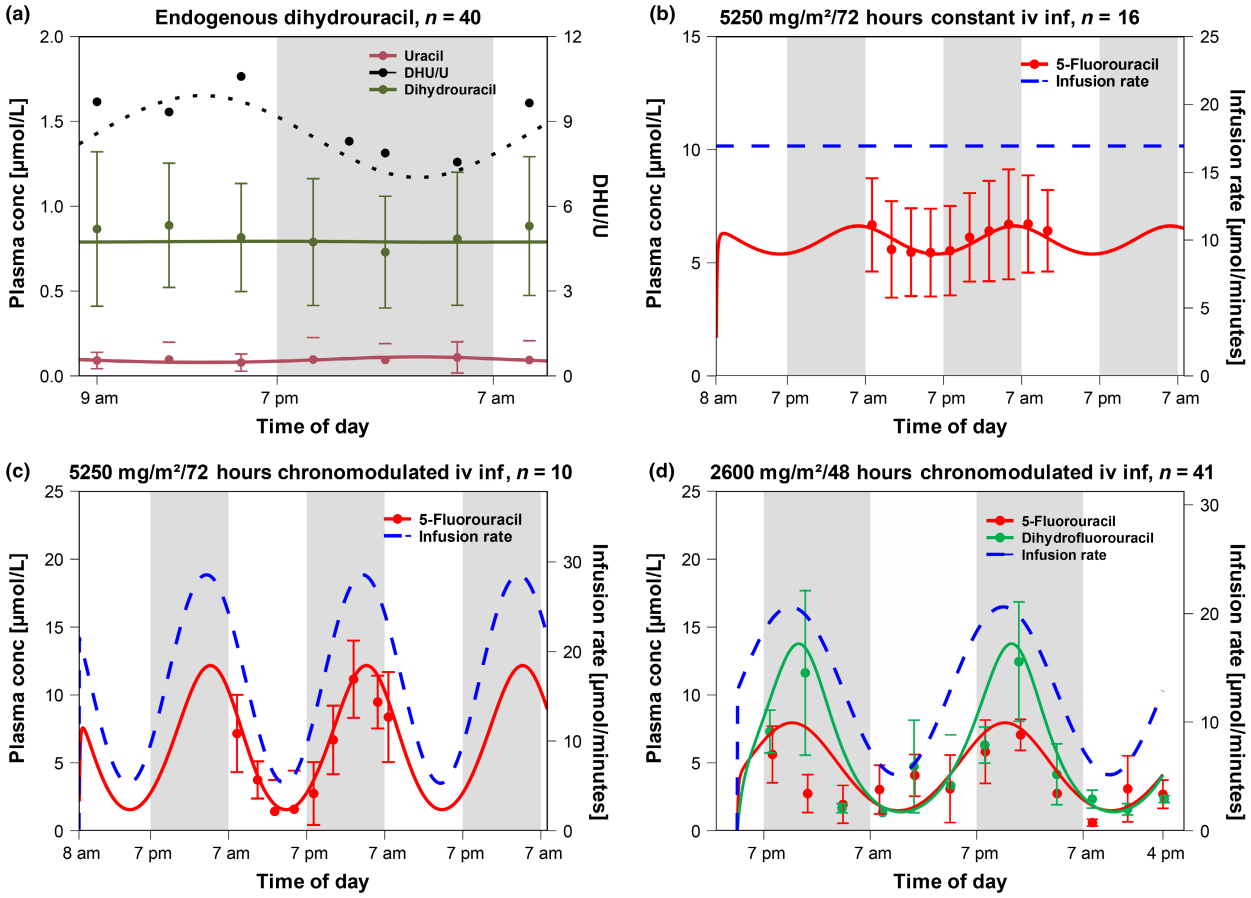

Figure 3 Physiologically-based chronopharmacokinetic model performance. (**a**) Predicted (lines) and observed mean (dots) plasma concentration-time profile of endogenous uracil (U, dark red) and dihydrouracil (DHU, dark green) with respective DHU/U ratios (black).[7] (**b**) Predicted (solid line) and observed (dots) mean 5-FU plasma concentration-time profile after a constant rate infusion of 5,250 mg/m^2 5-FU over 3 days (dashed line).[36] (**c**) Predicted (solid line) and observed (dots) mean 5-FU plasma concentration-time profile after a chronomodulated infusion of 5,250 mg/m^2 5-FU over 3 days (dashed line).[36] (**d**) Predicted (solid lines) and observed (dots) mean 5-FU and dihydrofluorouracil plasma concentration-time profiles after a chronomodulated infusion of 2,600 mg/m^2 5-FU over 48 hours (dashed line).[37] Dihydrouracil and dihydrofluorouracil were simulated with a DPH-mediated metabolism with an adapted diurnal activity rate. Parameters describing circadian DPD activity were derived from reported activity measurements in peripheral blood mononuclear cells (PBMCs).[7] 5-FU, 5-fluorouracil; conc, concentration; DHU/U, dihydrouracil to uracil plasma ratio; inf, infusion; iv, intravenous; n, number of subjects; PBMC, peripheral blood mononuclear cells; PBPK, physiologically-based pharmacokinetic.

cancer vs. 2:49 AM ±1.45 hours for healthy subjects). The estimated maximum DPD enzyme activity for both patients with cancer and healthy subjects was more uniformly distributed in the range of 10 and 20 nmol/mg/hour (12.94 ± 1.89 nm/mg/hour for healthy subjects vs. 12.50 ± 2.13 nmol/mg/hour for patients with cancer).

Overall, the importance of diurnal variations and their impact on individual plasma concentrations led to the development of a potential model-informed precision dosing approach for chronomodulated 5-FU treatment, as illustrated in **Figure 5** based on 3 representative individuals from the Raida group (shown in **Figure 4c**). Individual DPD chronotype estimation can be performed using measured *DPYD* mRNA expressions, DPD enzyme activities (e.g., in PBMC cells) or DPD substrate concentrations, such as endogenous uracil or 5-FU plasma levels. After estimating the amplitude and acrophase (Amp_{DPD} and $T_{Acr,DPD}$) required to describe diurnal DPD activity, the PBPK models were used to introduce alternative modified infusion rates for different chronomodulated infusion scenarios. As demonstrated in **Figure 5**, these include (i) a chronomodulated infusion rate with peak delivery at 4 AM, resulting in comparable peak plasma concentrations, (ii) a chronomodulated infusion rate with peak rate at an individual time, resulting in comparable shapes, peak plasma concentrations and AUCs, and finally (iii) a "noise canceling" infusion rate, resulting in constant linear plasma levels.

DISCUSSION

5-FU is a widely used and potent anticancer agent with complex PKs, which were captured and assessed by our developed PBPK models, providing a ground for further examination. In this study, both 5-FU and uracil, as well as their metabolites DHFU and DHU, were simulated to comprehensively characterize the impact of diurnal variations and their (interpatient) variability in DPD activity on drug exposure. The models are capable of predicting various administrations of intravenous and oral 5-FU across a

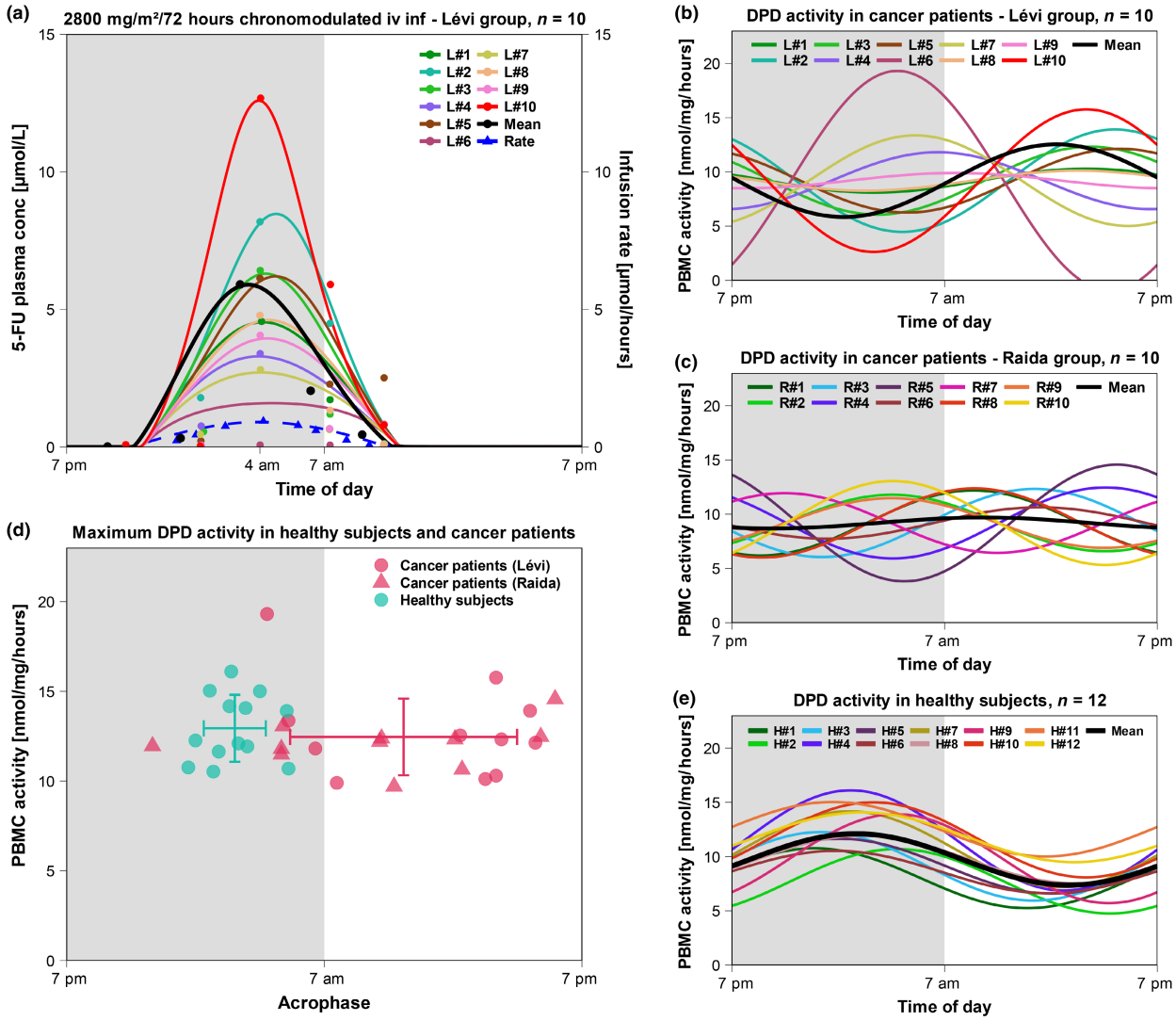

Figure 4 IIV of DPD chronotypes in healthy subjects and patients with cancer. (**a**) Predicted (solid lines) and observed (dots) mean and individual 5-FU plasma concentration-time profiles after a chronomodulated hepatic arterial infusion of 2,800 mg/m^2 over 3 days.[19] The corresponding administration rate (dashed line) was simulated to fit the reported (triangles) administration rate. (**b**) Mean and individual DPD chronotypes in patients with cancer estimated from observed 5-FU plasma concentration-time profiles reported by Lévi *et al.*[19] (Lévi group). Individual DPD enzyme activities were adapted to fit the observed plasma concentration-time profiles and are shown in (a). (**c**) Mean and individual DPD chronotypes in cancer patients estimated from observed relative *DPYD* mRNA expression reported Raida *et al.*[8] (Raida group). (**d**) Maximum DPD activity at its respective acrophase estimated in cancer patients derived from Lévi *et al.*[19] and Raida *et al.*[8] compared with healthy subjects compiled from Jacobs *et al.*[7] The lines indicate mean ± SD of maximum activity and acrophase. (**e**) Mean and individual DPD chronotypes as enzyme activities estimated from observed DPD activities in healthy subjects reported by Jacobs *et al.*[7] 5-FU, 5-fluorouracil; chrono, chronomodulated; conc, concentration; DPD, dihydropyrimidine dehydrogenase; H#, healthy individual; inf, infusion; iv, intravenous; L#, patient with cancer from the Lévi group; *n*, number of individuals; PBMC, peripheral blood mononuclear cells; R#, patient with cancer from the Raida group.

broad dosing range (143—2,800 mg/m^2), as well as orally administered and endogenous uracil and were successfully evaluated by comparing predicted and observed plasma concentration-time profiles and fractions excreted in urine, AUC_{last} and C_{max} values and calculations of their respective MRDs, MSAs, and GMFEs.

Several PK models have previously been published to describe the PK of 5-FU or uracil. For example, one approach focused on predictions of 5-FU as a metabolite of capecitabine,[40] whereas also describing 2 intermediate metabolites. Additionally, a PBPK model was developed to describe the 3-step metabolism for orally administered [2-^{13}C]uracil.[41] A previously published semimechanistic PK model, which assessed interpatient variability for PK parameters, modeled chronomodulated infusions of 5-FU with irinotecan and oxaliplatin.[18] Our study builds on the concepts of these previously published models and incorporates a broad dosing range for various administrations, including constant and chronomodulated infusions of 5-FU, endogenous synthesis of uracil, and diurnal variations in DPD and DPH activity, as well as 5-FU and uracil metabolites. Moreover, our

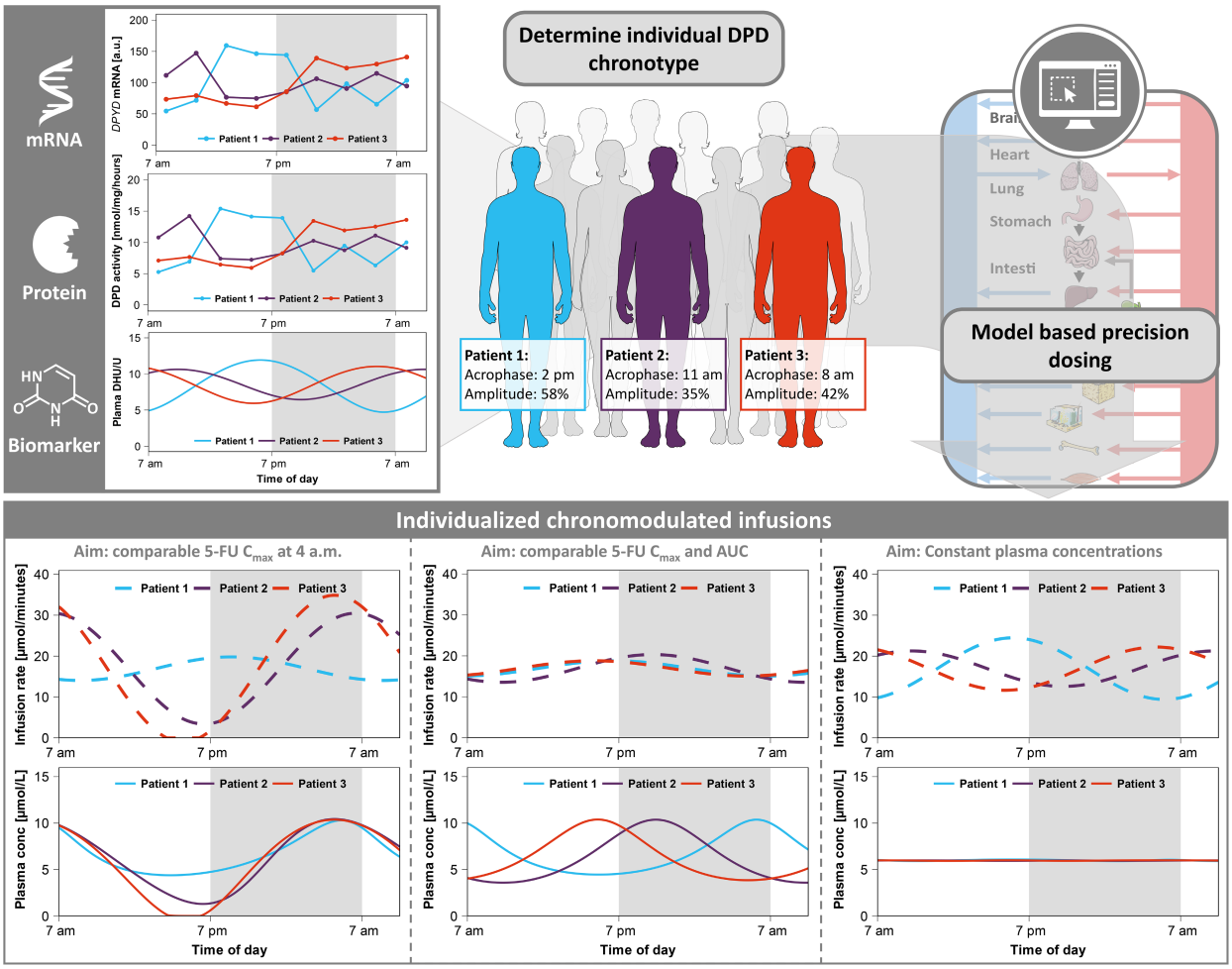

Figure 5 Model-based chronomodulated precision dosing. To address the prevalent interindividual variability in diurnal variations concerning 5-FU treatment, a model-based precision dosing approach was developed using the presented PBPK models. The DPD chronotype can be determined through measurements of *DPYD* mRNA expressions, DPD enzyme activities, or endogenous plasma levels of dihydrouracil and uracil. Upon estimating the T_{Acr} and Amp_{DPD} (in this example, for 3 individuals), the respective parameters can be utilized to simulate diurnal DPD activities according to Eq. 1. Here, 3 scenarios were simulated: individual chronomodulated infusion of 5,250 mg/m^2 5-FU over 3 days with (left) individual peak rates at 4 AM to achieve similar C_{max} at 4 AM; (middle) individual peak rates at individual clock times to achieve similar C_{max} and AUC with a similar shape in the plasma concentration–time profiles; (right) "noise canceling" infusion rates to achieve constant plasma concentrations. The infusion rates are illustrated in the top row (dashed lines) and the respective 5-FU plasma concentrations are shown in the bottom row (solid lines). 5-FU, 5-fluorouracil; a.u., arbitrary units; AUC, area under plasma concentration-time curve; C_{max}, maximum plasma concentration; conc, concentration; DPD, dihydropyrimidine dehydrogenase; *DPYD*, gene coding for dihydropyrimidine dehydrogenase; DHU/U: dihydrouracil to uracil plasma ratio, mRNA: messenger ribonucleic acid; PBPK, physiologically-based pharmacokinetic.

models incorporate an efflux transporter mimicking MRP4's active transport,[42] as both 5-FU and uracil are subject to a variety of transporter proteins,[43-46] of which MRP4 and its associated *ABCC4* gene polymorphisms were discussed to impact on treatment efficacy for colorectal cancer in 5-FU and capecitabine chemotherapy.[24]

As fluctuating plasma levels were observed in literature,[7,37] diurnal variations in DPD activity were effectively incorporated using a time-dependent sine function. Additionally, diurnal activity in DPH was simulated, based on the assumption that human cellular clocks influence DPH, similarly to observed diurnal patterns in DPH activity in mice.[47] In the case of endogenous uracil, differences in the oscillation of metabolite plasma levels between the simulated constant and circadian DPH activities were negligible, although these data were measured in healthy subjects.[7] In patients with cancer, oscillations in plasma concentrations were more pronounced for DHFU than for 5-FU, the parent, itself.[37] Here, the metabolite plasma levels were successfully predicted only when assuming diurnal variations to impact DPH as well. However, it remains unclear if and to what extent DPH is under circadian control and whether differences in diurnal activity exist between healthy subjects and patients with cancer, or between endogenous uracil and administered 5-FU.

Nonetheless, the impact on DPH activity may be of relevance, for instance, when using endogenous uracil or DHU/U ratios as biomarkers for DPD activity. Before initiating treatment with fluoropyrimidine-based medications, it is suggested to undertake

alternative or complementary testing for DPD phenotyping in addition to *DPYD* genotyping. These recommendations are in accordance with the guidelines proposed by the European Medicines Agency and various international guidelines.[4,48] Phenotyping methods often include single measurements of DHU/U ratios.[4,48] Regardless of the phenotyping method, such as DHU/U plasma or DPD PBMC activity measurements, clinicians should generally consider conducting repeated measurements over 24 hours when phenotyping for DPD. This would enable a more accurate prediction of its activity in polymorphic patients and consequently improve efficacy and safety in fluoropyrimidine treatment.

Within the framework of 5-FU treatment, simulations were conducted to model diurnal variations for both average and individual DPD chronotypes. For the underlying DPD chronotypes of observed mean plasma concentrations in study populations, Amp_{DPD} could be described by two values derived from literature (0.124[9] and 0.245[7]), whereas T_{Acr} differed for most study populations and had to be estimated for each profile.[7,9] When simulating plasma concentrations for individual patients, parameters Amp_{DPD} and T_{Acr} had to be adapted individually, as patients showed pronounced IIV in their DPD chronotypes.

In general, DPD chronotypes could be estimated (i) retrospectively from observed DPD substrate concentrations, such as 5-FU plasma concentrations, (ii) from observed DPD enzyme activities, or (iii) from observed *DPYD* mRNA expressions in leukocytes. Although, whereas DPD activity perfectly correlates with 5-FU clearance,[20] knowledge on the correlation between 5-FU clearance and *DPYD* mRNA expression is missing. In this analysis, the correlation between 5-FU clearance and *DPYD* mRNA expression was explored, acknowledging the challenges in establishing a direct relationship. Although a calculated very short translation rate (1.7 minutes) was used to extrapolate DPD enzyme activity from *DYPD* mRNA expression, the timing and extent of this correlation, particularly considering the enzyme's activity, require further investigation, as studies such as Barrat *et al*.,[49] which observed circadian variations in DPD activity in specific tissues (e.g., oral mucosa, suggested that this relationship might be complex and tissue-dependent). Understanding these nuances is essential before confidently using such correlations to chronotype patients for DPD in a clinical setting.

Lévi *et al*.[19] treated patients with 5-FU via a hepatic artery infusion with a peak rate at 4 AM. Although individual plasma concentrations showed a consistent time to reach C_{max} (T_{max}) due to uniform drug administration rates, there was still significant variability between individuals in C_{max} with an up to a 12-fold difference between minimum and maximum observed C_{max} values. Similarly, interpatient variability was apparent among individual DPD chronotypes extrapolated from the patients' 5-FU plasma concentration-time profiles, particularly concerning their respective acrophases, which is comparable to IIV estimated from DPD chronotypes extrapolated from *DPYD* mRNA expressions measured in patients with cancer. A lower IIV was observed in DPD activities measured in healthy volunteers.[8] When comparing estimated DPD chronotypes in healthy subjects and patients with cancer, acrophases were homogenous within nighttime for healthy individuals. In contrast, acrophases for the patients with cancer groups were distributed throughout the day. Although the presented modeling approach successfully captured IIV in diurnal DPD function, inherent limitations may exist in estimating diurnal parameters (Amp and T_{Acr}) from sparse PK data. Future studies with more extensive data sets are required to validate and refine these estimations, ensuring a more robust understanding of the circadian rhythm of DPD function in patients with cancer. However, recent advances in circadian biology introduce methods to determine an individual's circadian phase without frequent biosamples. These techniques use biomolecular markers and computational analyses, offering a less invasive patient chronotyping.[50] Although, extension of these established methods to assess the DPD chronotype would have to be investigated further.

The notable IIV in DPD chronotypes among patients with cancer suggests that a uniform chronomodulated infusion rate could result in varying efficacy. For instance, Takimoto *et al*.[51] reported no major differences in toxicity for 5-FU therapy between constant and chronomodulated infusions. Conversely, in a phase III trial comparing conventional to chronomodulated chemotherapy conducted in 2006, the treatment efficacy of infusional 5-FU administered with a constant rate and a chronomodulated rate was investigated.[16] Here, an increase in response rates and overall survival as well as a decrease in grade 3–4 toxicities was observed in men receiving chronomodulated cancer therapy. However, women experienced lower response rates and overall survival along with increased toxicities.[16] In case of chronomodulated therapy with other anticancer drugs, irinotecan is widely discussed regarding differences in tolerability between men and women.[52] One approach for personalizing chronomodulated irinotecan treatment was based on the patient's sex. Here, Innominato *et al*. investigated the time of lowest toxicity of irinotecan, finding that men tolerated irinotecan better when receiving peak delivery in the morning, whereas women experienced the least toxicity in the afternoon.[52] In this case, patients would benefit from receiving irinotecan treatment tailored to their respective sex. Similarly, this could suggest a potential advantage of personalized dosing for anticancer treatment with 5-FU.

To offer an alternative to chronomodulated 5-FU infusions with uniformed peak rate at 4 AM, different scenarios were simulated in virtual individuals exhibiting estimated DPD activities from the Raida cancer patient group.[8] Instead of a common peak rate at 4 AM, infusion rates were simulated to achieve comparable peak concentrations at 4 AM. Additionally, infusion rates were adapted to reach comparable 5-FU peak concentrations at individual clock times to maintain comparable shapes in their plasma concentration-time curves. We accomplished this by adjusting the peak rate during periods of minimum DPD enzyme activity to prevent excessively high infusion rates. Additionally, we tested an individualized "noise-canceling" infusion rate to maintain constant plasma levels of 5-FU.

The clinical impact of achieving peak 5-FU plasma levels at different clock times compared with 4 AM on therapy efficacy and tolerability for individual patients remains to be determined in dedicated studies specifically designed to examine personalized chronomodulated 5-FU treatment. Relevant chronopharmacodynamic pathways which involve the formation of intracellular active metabolites or target enzyme activity, such as thymidylate synthase, were not implemented, as relevant data were unavailable. These factors deserve further investigation and consideration in future adaptations of 5-FU treatment strategies. Moreover, several assumptions

had to be made for model development and its application for personalized chronomodulated treatment simulations. This might lead to potential sources of bias as well as related limitations and risks including (i) missing data from clinical study reports on time of administration and thus description of related diurnal DPD parameters, (ii) on demographic data mainly body surface area leading to potentially inadequately estimated simulated dosing, (iii) inclusion criteria of the clinical trials resulting in heterogenous distributions in the study demographics and the respective physiology, and (iv) pathophysiology and co-administration of the included patients, as well as (v) the pharmacological implications of the chronopharmacodynamic processes of 5-FU treatment. Nonetheless, the presented PBPK models might be useful to guide the design of dosing adaptation by simulating various 5-FU treatment scenarios based on individual DPD chronotypes.

In summary, the developed whole-body PBPK models effectively describe and predict the complexity of 5-FU PKs, as they account for the significant interpatient variability in DPD chronotypes and their impact on 5-FU therapy. The developed models might be particularly impactful for the future practice of cancer medicine as they provide an innovative framework for precision dosing of 5-FU based on patients' unique DPD chronotypes. The Open Systems Pharmacology (OSP) framework was utilized for a detailed mechanistic implementation of 5-FU PKs inside a whole-body PBPK framework and, thus, the flexibility to address 5-FU chronopharmacology at both organ and cellular levels. In contrast, Bayesian frameworks in population PK approaches might be superior capturing IIV but require specific individual data sets and typically lack mechanistic depth. Future advancements may pave the way for more integrative modeling methods that could improve our mechanistical understanding on a patient-individual level. For this, the developed PBPK models are publicly available for open access (GitHub repository on http://models.clinicalpharmacy.me). [Correction added on 31 January 2024, after first online publication: In the above sentence, URL to GitHub repository has been corrected in this version.] However, they could guide design and dosage adaptations in future clinical trials, emphasizing their translational relevance in the field of oncology.

SUPPORTING INFORMATION

Supplementary information accompanies this paper on the *Clinical Pharmacology & Therapeutics* website (www.cpt-journal.com).

FUNDING

R.D.'s work is supported by a grant from Cancer Research UK (C53720/A29468) and Anglo American Platinum. J.J.S., H.J.G., and M.S. were supported by the European Commission Horizon 2020 UPGx grant 668353. Moreover, M.S. was funded by the Robert Bosch Stiftung (Stuttgart, Germany), a grant from the German Federal Ministry of Education and Research (BMBF 031L0188D), and the Deutsche Forschungsgemeinschaft (DFG, German Research Foundation) under Germany's Excellence Strategy—EXC 2180—390900677. T.L. was supported by the project "Open-source modeling framework for automated quality control and management of complex life science system models" (OSMOSES) funded by the German Federal Ministry of Education and Research (BMBF, grant ID:031L0161C).

CONFLICTS OF INTEREST

Since January 2020, J.-G.W. is an employee of Boehringer Ingelheim Pharma GmbH and Co. KG. All other authors declared no competing interests for this work.

AUTHOR CONTRIBUTIONS

All authors wrote the manuscript and designed the research. F.Z.M. performed the research. F.Z.M. and D.S. analyzed the data.

ACKNOWLEDGMENT

Open Access funding enabled and organized by Projekt DEAL.

1. Sara, J.D. *et al*. 5-fluorouracil and cardiotoxicity: a review. *Ther. Adv. Med. Oncol.* **10**, 175883591878014 (2018).
2. Diasio, R.B. & Harris, B.E. Clinical pharmacology of 5-fluorouracil. *Clin. Pharmacokinet.* **16**, 215–237 (1989).
3. Meta-Analysis Group In Cancer *et al*. Toxicity of fluorouracil in patients with advanced colorectal cancer: effect of administration schedule and prognostic factors. *J. Clin. Oncol.* **16**, 3537–3541 (1998).
4. Amstutz, U. *et al*. Clinical pharmacogenetics implementation consortium (CPIC) guideline for Dihydropyrimidine dehydrogenase genotype and fluoropyrimidine dosing: 2017 update. *Clin. Pharmacol. Ther.* **103**, 210–216 (2017).
5. Deenen, M.J. *et al*. Upfront genotyping of DPYD*2A to individualize fluoropyrimidine therapy: a safety and cost analysis. *J. Clin. Oncol.* **34**, 227–234 (2016).
6. Mormont, M.C. & Levi, F. Cancer chronotherapy: principles, applications, and perspectives. *Cancer* **97**, 155–169 (2003).
7. Jacobs, B.A.W. *et al*. Pronounced between-subject and circadian variability in thymidylate synthase and dihydropyrimidine dehydrogenase enzyme activity in human volunteers. *Br. J. Clin. Pharmacol.* **82**, 706–716 (2016).
8. Raida, M. *et al*. Circadian variation of dihydropyrimidine dehydrogenase mRNA expression in leukocytes and serum cortisol levels in patients with advanced gastrointestinal carcinomas compared to healthy controls. *J. Cancer Res. Clin. Oncol.* **128**, 96–102 (2002).
9. Jiang, H., Lu, J. & Ji, J. Circadian rhythm of dihydrouracil/uracil ratios in biological fluids: a potential biomarker for dihydropyrimidine dehydrogenase levels. *Br. J. Pharmacol.* **141**, 616–623 (2004).
10. Harris, B., Song, R., Soong, S.-J. & Diasio, R. Relationship between dihydropyrimidine dehydrogenase activity and plasma 5-fluorouracil levels with evidence for circadian variation of enzyme activity and plasma. *Cancer Res.* **50**, 197–201 (1990).
11. Metzger, G. *et al*. Spontaneous or imposed circadian changes in plasma concentrations of 5-fluorouracil coadministered with folinic acid and oxaliplatin: relationship with mucosal toxicity in patients with cancer. *Clin. Pharmacol. Ther.* **56**, 190–201 (1994).
12. Lévi, F., Giacchetti, S., Adam, R., Zidani, R., Metzger, G. & Misset, J.L. Chronomodulation of chemotherapy against metastatic colorectal cancer. *Eur. J. Cancer* **31**, 1264–1270 (1995).
13. Petit, E. *et al*. Circadian rhythm-varying plasma concentration of 5-fluorouracil during a five-day continuous venous infusion at a constant rate in cancer patients. *Cancer Res.* **48**, 1676–1679 (1988).
14. Lévi, F., Okyar, A., Dulong, S., Innominato, P.F. & Clairambault, J. Circadian timing in cancer treatments. *Annu. Rev. Pharmacol. Toxicol.* **50**, 377–421 (2010).
15. Zeng, Z.L. *et al*. Circadian rhythm in dihydropyrimidine dehydrogenase activity and reduced glutathione content in peripheral blood of nasopharyngeal carcinoma patients. *Chronobiol. Int.* **22**, 741–754 (2005).
16. Giacchetti, S. *et al*. Phase III trial comparing 4-day chronomodulated therapy versus 2-day conventional delivery of fluorouracil, leucovorin, and oxaliplatin As first-line chemotherapy

of metastatic colorectal cancer: the European organisation for research and treatment of can. *J. Clin. Oncol.* **24**, 3562–3569 (2006).
17. Giacchetti, S. *et al*. Sex moderates circadian chemotherapy effects on survival of patients with metastatic colorectal cancer: a meta-analysis. *Ann. Oncol. Off. J. Eur. Soc. Med. Oncol.* **23**, 3110–3116 (2012).
18. Hill, R.J.W., Innominato, P.F., Lévi, F. & Ballesta, A. Optimizing circadian drug infusion schedules towards personalized cancer chronotherapy. *PLoS Comput. Biol.* **16**, e1007218 (2020).
19. Lévi, F. *et al*. Pharmacokinetics of irinotecan, oxaliplatin and 5-fluorouracil during hepatic artery chronomodulated infusion: a translational European OPTILIV study. *Clin. Pharmacokinet.* **56**, 165–177 (2017).
20. Fleming, R.A. *et al*. Correlation between dihydropyrimidine dehydrogenase activity in peripheral mononuclear cells and systemic clearance of fluorouracil in cancer patients. *Cancer Res.* **52**, 2899–2902 (1992).
21. Lippert, J. *et al*. Open systems pharmacology community—an open access, open source, Open Science approach to modeling and simulation in pharmaceutical sciences. *CPT Pharmacometrics Syst. Pharmacol.* **8**, 878–882 (2019).
22. Wojtyniak, J., Britz, H., Selzer, D., Schwab, M. & Lehr, T. Data digitizing: accurate and precise data extraction for quantitative systems pharmacology and physiologically-based pharmacokinetic modeling. *CPT Pharmacometrics Syst. Pharmacol.* **9**, 322–331 (2020).
23. Meyer, M., Schneckener, S., Ludewig, B., Kuepfer, L. & Lippert, J. Using expression data for quantification of active processes in physiologically based pharmacokinetic modeling. *Drug Metab. Dispos.* **40**, 892–901 (2012).
24. Chen, Q. *et al*. A polymorphism in ABCC4 is related to efficacy of 5-FU/capecitabine-based chemotherapy in colorectal cancer patients. *Sci. Rep.* **7**, 7059 (2017).
25. Les Laboratories Servier. Servier Medical At <https://smart.servier.com/> (assessed on 10 Feburary 2022).
26. Hishinuma, E. *et al*. Functional characterization of 21 allelic variants of dihydropyrimidinase. *Biochem. Pharmacol.* **143**, 118–128 (2017).
27. Yamazaki, S., Hayashi, M., Toth, L.N. & Ozawa, N. Lack of interaction between bropirimine and 5-fluorouracil on human dihydropyrimidine dehydrogenase. *Xenobiotica* **31**, 25–31 (2001).
28. Mattison, L.K. The uracil breath test in the assessment of dihydropyrimidine dehydrogenase activity: pharmacokinetic relationship between expired 13CO2 and plasma [2-13C] dihydrouracil. *Clin. Cancer Res.* **12**, 549–555 (2006).
29. Van Staveren, M.C., Theeuwes-Oonk, B., Guchelaar, H.J., Van Kuilenburg, A.B.P. & Maring, J.G. Pharmacokinetics of orally administered uracil in healthy volunteers and in DPD-deficient patients, a possible tool for screening of DPD deficiency. *Cancer Chemother. Pharmacol.* **68**, 1611–1617 (2011).
30. Bocci, G. *et al*. A pharmacokinetic-based test to prevent severe 5-fluorouracil toxicity. *Clin. Pharmacol. Ther.* **80**, 384–395 (2006).
31. Di Paolo, A. *et al*. Relationship between 5-fluorouracil disposition, toxicity and. *Ann. Oncol.* **12**, 1301–1306 (2001).
32. Bardakji, Z., Jolivet, J., Langelier, Y., Besner, J.-G. & Ayoub, J. 5-Fluorouracil-metronidazole combination therapy in metastatic colorectal cancer. *Cancer Chemother. Pharmacol.* **18**, 140–144 (1986).
33. Heggie, G.D., Sommadossi, J.P., Cross, D.S., Huster, W.J. & Diasio, R.B. Clinical pharmacokinetics of 5-fluorouracil and its metabolites in plasma, urine, and bile. *Cancer Res.* **47**, 2203–2206 (1987).
34. Joel, S.P. *et al*. Lack of pharmacokinetic interaction between 5-fluorouracil and oxaliplatin. *Clin. Pharmacol. Ther.* **76**, 45–54 (2004).
35. Joulia, J.M., Pinguet, F., Ychou, M., Duffour, J., Astre, C. & Bressolle, F. Plasma and salivary pharmacokinetics of 5-fluorouracil (5-FU) in patients with metastatic colorectal cancer receiving 5-FU bolus plus continuous infusion with high-dose Folinic acid. *Eur. J. Cancer* **35**, 296–301 (1999).
36. Grem, J.L. *et al*. N-(phosphonacetyl)-l-aspartate and calcium leucovorin modulation of fluorouracil administered by constant rate and circadian pattern of infusion over 72 hours in metastatic gastrointestinal adenocarcinoma. *Ann. Oncol.* **12**, 1581–1587 (2001).
37. Falcone, A. *et al*. 5-fluorouracil administered as a 48-hour Chronomodulated infusion in combination with leucovorin and cisplatin: a randomized phase II study in metastatic colorectal cancer. *Oncology* **61**, 28–35 (2001).
38. Shamir, M., Bar-On, Y., Phillips, R. & Milo, R. SnapShot: timescales in cell biology. *Cell* **164**, 1302–1302.e1 (2016).
39. Genecards entry for DPD. <https://www.genecards.org/cgi-bin/carddisp.pl?gene=DPYD&keywords=dpd> (accessed on 15.02.2022).
40. Tsukamoto, Y. *et al*. A physiologically based pharmacokinetic analysis of capecitabine, a triple prodrug of 5-FU, in humans: the mechanism for tumor-selective accumulation of 5-FU. *Pharm. Res.* **18**, 1190–1202 (2001).
41. Ito, S. *et al*. Physiologically based pharmacokinetic modelling of the three-step metabolism of pyrimidine using13C-uracil as an in vivo probe. *Br. J. Clin. Pharmacol.* **60**, 584–593 (2005).
42. Protein-Atlas entry for ABCC4. <https://www.proteinatlas.org/ENSG00000125257-ABCC4/tissue> (assessed on 10 Feburary 2022).
43. Mata, J.F. *et al*. Role of the human concentrative nucleoside transporter (hCNT1) in the cytotoxic action of 5[prime]-deoxy-5-fluorouridine, an active intermediate metabolite of capecitabine, a novel oral anticancer drug. *Mol. Pharmacol.* **59**, 1542–1548 (2001).
44. Kobayashi, Y., Ohshiro, N., Sakai, R., Ohbayashi, M., Kohyama, N. & Yamamoto, T. Transport mechanism and substrate specificity of human organic anion transporter 2 (hOat2 [SLC22A7]). *J. Pharm. Pharmacol.* **57**, 573–578 (2005).
45. Lostao, M.P., Mata, J.F., Larrayoz, I.M., Inzillo, S.M., Casado, F.J. & Pastor-Anglada, M. Electrogenic uptake of nucleosides and nucleoside-derived drugs by the human nucleoside transporter 1 (hCNT1) expressed in Xenopus laevis oocytes. *FEBS Lett.* **481**, 137–140 (2000).
46. Yuan, J.-H. *et al*. Breast cancer resistance protein expression and 5-fluorouracil resistance. *Biomed. Environ. Sci.* **21**, 290–295 (2008).
47. Zhang, R., Lahens, N.F., Ballance, H.I., Hughes, M.E. & Hogenesch, J.B. A circadian gene expression atlas in mammals: implications for biology and medicine. *Proc. Natl. Acad. Sci. U. S. A.* **111**, 16219–16224 (2014).
48. European Medicines Agency (EMA). 5-Fluorouracil (i.v.), capecitabine and tegafur containing products: Pre-treatment testing to identify DPD-deficient patients at increased risk of severe toxicity Patients with partial or complete dihydropyrimidine dehydrogenase (DPD) deficiency ar (2020).
49. Barrat, M.A., Renée, N., Mormont, M.C., Milano, G. & Levi, F. Étude des variations circadiennes de l'activité de la dihydropyrimidine déshydrogénase (DPD) dans la muqueuse buccale chez des sujets volontaires sains. *Pathol. Biol.* **51**, 191–193 (2003).
50. Woelders, T. *et al*. Machine learning estimation of human body time using metabolomic profiling. *Proc. Natl. Acad. Sci.* **120**, 2017 (2023).
51. Takimoto, C.H. *et al*. High inter- and intrapatient variation in 5-fluorouracil plasma concentrations during a prolonged drug infusion. *Clin. Cancer Res.* **5**, 1347–1352 (1999).
52. Innominato, P.F. *et al*. Sex-dependent least toxic timing of irinotecan combined with chronomodulated chemotherapy for metastatic colorectal cancer: randomized multicenter EORTC 05011 trial. *Cancer Med.* **9**, 4148–4159 (2020).

5 DISCUSSION

During the investigation and development of projects I–III, the necessity to include metabolites for the PBPK modeling process became more and more evident. While the drugs investigated in project I (bupropion), project II (ketoconazole) and project III (5-fluorouracil) were completely different in their pharmacodynamic nature, as well as their drug interaction behavior, parent-metabolites PBPK modeling crystallized itself to be the key element in all of the presented projects. The underlying importance of metabolites for PBPK modeling was, therefore, thoroughly elaborated in the presented thesis.

5.1 LEVERAGING INVALUABLE METABOLITE-RELATED KNOWLEDGE

5.1.1 *Exploiting Existing Metabolite-related Data*

Metabolites harbor an invaluable amount of data, that once properly investigated, should be excessively exploited. Especially in case of PBPK modelling, where data is key to a model's reliability and capabilities, metabolites provide an extended view into the investigational drug's profile. As a prime example for this, project I illustrated the great potential of existing metabolites' data, especially regarding their PK and associated drug interactions [1].
As hydroxybupropion was observed to be impacted by changes in CYP2B6 activity to a greater extent than bupropion [25], modelling the metabolite was helpful in effectively implementing and evaluating several CYP2B6 interactions, namely CYP2B6 DGIs including *CYP2B6 intermediate metabolizer* and *CYP2B6 rapid metabolizer* and related CYP2B6 DDGIs. Here, CYP2B6 DGIs could go unnoticed when only observing the parent compound alone, as bupropion's metabolism could be compensated by further enzymes [91–93]. However, as the formation of hydroxybupropion is mainly mediated by CYP2B6 [92], data related to hydroxybupropion was useful in implementing several CYP2B6 interactions. These especially included CYP2B6 DDGIs, that were only reported through the HBup/Bup AUC ratios in the literature. By considering metabolite data early on in the modeling development process, several genetic variants could be investigated and reflected in the developed parent-metabolites interaction PBPK model.
Moreover, two further metabolites, erythrohydrobupropion and threohydrobupropion, were included in the analyses within the scope of project I [1]. These bear a great potential in expanding the existent

model to cover a magnitude of complex D(D)GI scenarios surrounding CYP2D6, as all three metabolites alongside bupropion showed comparable potency in down regulation of CYP2D6 expression [52–55]. Therefore, regardless of their relation to CYP2B6, the existing data on erythrohydrobupropion and threohydrobupropion allowed for the model's flexibility and adaptability to various different use-cases outside of the already established and published model-predicted CYP2B6 interaction scenarios, which could focus around CYP2D6 and its substrates [52].
Further use-cases could also be of pharmacodynamic nature, as bupropion's metabolites showed pharmacological activity, especially with contributions to the occurrence of ADRs. Overall, the PBPK interaction model performance benefitted greatly from acknowledging, exploiting and integrating existing metabolite data throughout the entire model development process, as they complemented the already existing parent data perfectly [1].
While bupropion is an exceptional case of well investigated and documented PK data on an investigational drug, it does not represent the norm especially considering publicly available clinical data. For some drugs, several potential interactions they could partake are underinvestigated, and respective data are hardly available, which could bear many challenges especially for whole-body PBPK model development. Here, knowledge gaps could make or break a model's capability in describing and predicting complex drug interactions.

5.1.2 *Closing Knowledge Gaps of Parent Drugs*

Missing data and expected knowledge gaps could impede PBPK model development, especially when focusing on mechanistically describing and predicting complex drug interactions. However, upon focusing beyond the investigational drug itself, metabolites could help bridging knowledge gaps, that couldn't be explained through the parent compound alone. Here, project II (ketoconazole) was especially interesting regarding how parent-metabolites modeling played an integral part in covering blind spots of a drug's PK profile. In this project, a whole-body PBPK model of ketoconazole was developed focusing on its strong DDIs potential [2].
Based on the literature, ketoconazole was observed to impact victim drug exposure significantly long after its administration even in single dose regimens, illustrating its long-lasting inhibitory effects. For example, in a reported ketoconazole-alfentanil DDIs study, where ketoconazole was administered the evening before an alfentanil dose in the next morning, ketoconazole managed to increase alfentanil exposure as the plasma AUC by up to 8-fold [45]. However, ketoconazole was also observed to inhibit target proteins such as CYP3A4 or P-gp reversibly, while "only" exhibiting a relatively short half-life of around

160 minutes [14, 100]. When looking at ketoconazole's interaction profile, a reversible inhibition by ketoconazole alone would therefore be unlikely. Upon focusing on its metabolite *N*-deacetylketoconazole, which was quantified for the first time in 2022 in human plasma during *in vivo* ketoconazole studies, ketoconazole's ambiguous DDIs profile became a bit clearer, as *N*-deacetylketoconazole was reported to inhibit similar proteins as ketoconazole itself, although reversibly as well [14]. As ketoconazole was shown to have a range of chemically similar metabolites, including *N*-deacetylketoconazole [103], it was assumed during the PBPK model development process, that further metabolites could be potentially involved in the long-lasting effect of ketoconazole-mediated reversible inhibition, as focusing on ketoconazole alone did not lead to satisfying DDIs model performance.

For example, a former approach to model ketoconazole DDIs by implementing irreversible inhibition of CYP3A4 and P-gp would not only be wrong contrary to recent findings [14], it would also lead to implications in simulating and predicting ketoconazole disposition in various tissues, particularly its observed excretion into feces of up to 37% [97, 104] which would contradict an irreversible-autoinhibition of ketoconazole own P-gp-mediated elimination.

To test the hypothesis of a cumulative and concomitant reversible inhibitory effect by parent and metabolites, an approach to effectively include ketoconazole's metabolite *N*-deacetylketoconazole as well as the following metabolite *N*-hydroxy-*N*-deacetylketoconazole [103], as a surrogate for remaining underreported metabolites, was considered, where both metabolites were implemented to inhibit CYP3A4 and P-gp reversibly to cover effects that could not be explained by the parent alone. As such, the cumulative effect of parent's and metabolites' reversible inhibition was sufficient to describe and predict DDIs, particularly long-lasting DDIs effects with dosing time gaps of several hours between ketoconazole and victim drugs [2, 115, 116].

With regards to the antimycotic imidazol derivate itraconazole, similar decisions were made for its PBPK model development by Hanke et al., which performed well in predicting several DDIs for a variety of victim drugs. The reported itraconazole PBPK model includes three modeled metabolites, which all reversibly inhibit CYP3A4. However, biochemical data for their activity were available in literature, providing a level of certainty for its metabolites' DDI effects [117].

Of course, with the implementation of the second surrogate metabolite of ketoconazole purely based on the assumption that it inhibits target proteins similarly to its precursors, this approach might include sources of bias. However, the similarities in the chemical structures of ketoconazole, *N*-deacetylketoconazole and *N*-hydroxy-*N*-deacetylketoconazole, as well as the observed inhibitory effects of ketoconazole and *N*-deacetylketoconazole indicate a potential ground for the hypothesized reversible inhibition by remaining metabolites

such as *N*-hydroxy-*N*-deacetylketoconazole [14, 103].
While the versatility of parent-metabolites PBPK modeling was especially helpful in testing such hypotheses, it's even more important to emphasize the need for further investigation on that subject, as there is a tremendous potential in thoroughly describing ketoconazole-mediated DDIs, as ketoconazole has been used regularly clinical DDIs studies with ketoconazole being a prominent DDIs perpetrator drug recommended by the FDA [37]. The parent-metabolites PBPK model development process of ketoconazole and the assumption made along its way illustrated, that considering metabolites, especially early on, could help overcome knowledge gaps towards the parent's PK behavior.
In principle, closing knowledge gaps with the help of investigation of metabolites should be considered during PBPK model development, as well as during drug development in general. However, taking a closer look towards an investigational drug's metabolites behavior can also help identifying new knowledge gaps altogether.

5.1.3 *Identifying Knowledge Gaps in Drug Behavior*

PBPK modeling is an exceptional tool for investigation of a drug's behavior, as it allows for a very flexible approach to simulate and predict drug disposition in various different drug interaction scenarios. Here, a model-based investigation of a metabolite's behavior can reveal knowledge gaps, and raise questions that should be addressed to thoroughly understand and assess the parent drug's safety, efficacy and toxicity, not only within the drug development process but also after drug approval.
In project III, a novel approach to personalize 5-fluorouracil treatment was developed, where parent-metabolites PBPK modeling was an essential part [3]. Investigating and simulating the inactive metabolites (i) dihydrofluorouracil in cancer patients receiving 5-fluorouracil and (ii) endogenous dihydrouracil in healthy subjects, led to several questions, that could not be informed by existing literature. For example, as the key enzyme DPD is coordinated by diurnal variations [26], one approach to individualize 5-flurouracil treatment proposed in the project III was chronotyping individuals for DPD activity, by analyzing DHU/U ratios in the respective patients [3].
However, metabolite modeling revealed that the oscillation of the inactive metabolite's drug exposure in plasma could be described by solely implementing circadian variation in DPD activity for dihydrouracil, but not for dihydrofluorouracil, where it's elimination via DPH had to be varied throughout the day, as well. Here, according to parameter estimates, DPD and DPH showed different patterns of diurnal variation [3]. This poses the question whether these differences in diurnal variations of inactive metabolite's plasma levels depend

on (i) the pathophysiological implications on DPD in cancer patients compared to healthy subjects, (ii) the kinetic differences between infusional 5-fluorouracil compared to endogenous uracil, (iii) diurnal variations impacting DPD and DPH through different circadian clocks, (iv) unknown mechanisms, or (v) a complex interplay of all of these hypotheses.
Although, as measuring DHU/U ratios is also a clinically established phenotyping method for DPD and 5-fluorouracil treatment is associated with a high risk for to some extent even life-threatening ADRs [15–17, 107], addressing the before-mentioned questions is not only relevant to the newly developed and innovative dosing approach, but also to re-assess the already existing ones. Here, parent-metabolites PBPK modeling was especially helpful in personalizing chronomodulated treatment as presented in project III, where it was used to generate novel dose adaptations. Especially, since generating these approaches in a clinical setting could be unethical due to 5-fluorouracil's severe toxicity, parent-metabolites PBPK modeling can bear a great potential for novel dosing strategies.

5.2 PARENT-METABOLITES MODELING DURING MID3 AND FUTURE DIRECTIONS

As metabolites pose a crucial part in the overall picture of their parent's PK and PD, they should be reflected effectively in the PBPK modeling process within MID_3. While the inclusion of PBPK modeling in D_3 is often done case-by-case and regulatory agencies mainly provide (non-binding) recommendations, neither FDA nor EMA guidelines mentioned the simulation of metabolites in their PBPK guidance documents [64, 65]. The decision on whether to include metabolites in the PBPK analyses would have to be assessed individually by the respective model developer. However, as parent-metabolites modeling holds an unbeknownst potential to improve understanding of a drugs behavior, there are several considerations that could be made to help decide whether simulation of metabolites could be useful towards the specific context of the intended model. At first, the model purpose indicates whether involvement of a metabolite, regardless of their pharmacological activity or pharmacokinetic interactivity, could be irrelevant and, therefore, excluded from the analyses. For example, if the PBPK model is planned to describe antibodies or physico-chemical drug interactions, where metabolites could be negligible. Although, the majority of model applications can be influenced by metabolites. Therefore, if the model purpose could be impacted by a metabolite, e.g. DDIs, not considering and investigating metabolites would be unfavorable and potentially extend the development process of the PBPK model, if considered too late.
Secondly, regulatory agencies already give recommendations on when

to test for metabolites *in vitro* or *in vivo*, hence, similar assumptions could be helpful to decide on whether and when to include metabolites in the PBPK model development process (*in silico*). These are, for example, (i) pharmacodynamic activity, e.g. activity at the target site, or association with ADRs and toxicity, or (ii) pharmacokinetic interactivity, such as enzyme or transporter inhibition and induction [29, 69, 71–74]. In these cases, metabolites participate actively in shaping the PD and PK profile of the parent drug. Thus, future PBPK models would benefit from including these metabolites as early as possible in the development process. Moreover, preclinically inactive metabolites are emphasized by the agencies as well, if they happen to be disproportionate metabolites. As they represent major metabolic pathways, they could hold a significant role in a parents PD and PK profile, when tested further in patients, that would fall into sub-populations susceptible towards changes in these metabolic pathways [71–74]. In this case, if an intended PBPK model was initially build to be applied in these sub-populations (differentiated by age, genetics or disease state), the ambiguous metabolite behavior *in vivo* could hold relevant effects, such as an increased occurrence of associated ADRs. Here, a parent-metabolite PBPK model analysis alongside additional nonclinical testing would help the assessment of an investigational drug's efficacy and safety. An overview on how to determine the role of a metabolite for a PBPK analysis is illustrated in Figure 5.1.

Lastly, if the investigational nature of PBPK modeling is of interest for the intended model, simulating metabolites, regardless of their activity, can attribute tremendously towards understanding the underlying research questions, such as for model-informed personalized medicine, where they could help derive novel treatment approaches, especially for already approved compounds. Here, PBPK modeling in general, parent-metabolites PBPK modeling in particular, can be beneficial, as parent-metabolites ratios already hold a strong position when it comes to dosing adaptions and optimizations [16, 112]. For example an administered compound and its metabolic ratio can give insights into the respective phenotype and the appropriate dosing of the medication in question. Parent-metabolite ratios being extensively used as a state-of-the-art phenotyping method and reflected in many dosing guidelines as established by the CPIC or DPWG [15, 17], could bear a similar potential when using model-based dose adaptation approaches. As an example, using the measured parent-metabolites ratios to estimate individual parameters of the respective PBPK model can help to give a personalized dosing recommendation for a patient susceptible for specific DGIs.

A similar approach was tackled within project III, however in this case the used parent-metabolite ratios were used to assess enzyme activity beyond genetic polymorphisms. While parent-metabolite ratios of uracil and dihydrouracil are well used in mandatory pretesting for

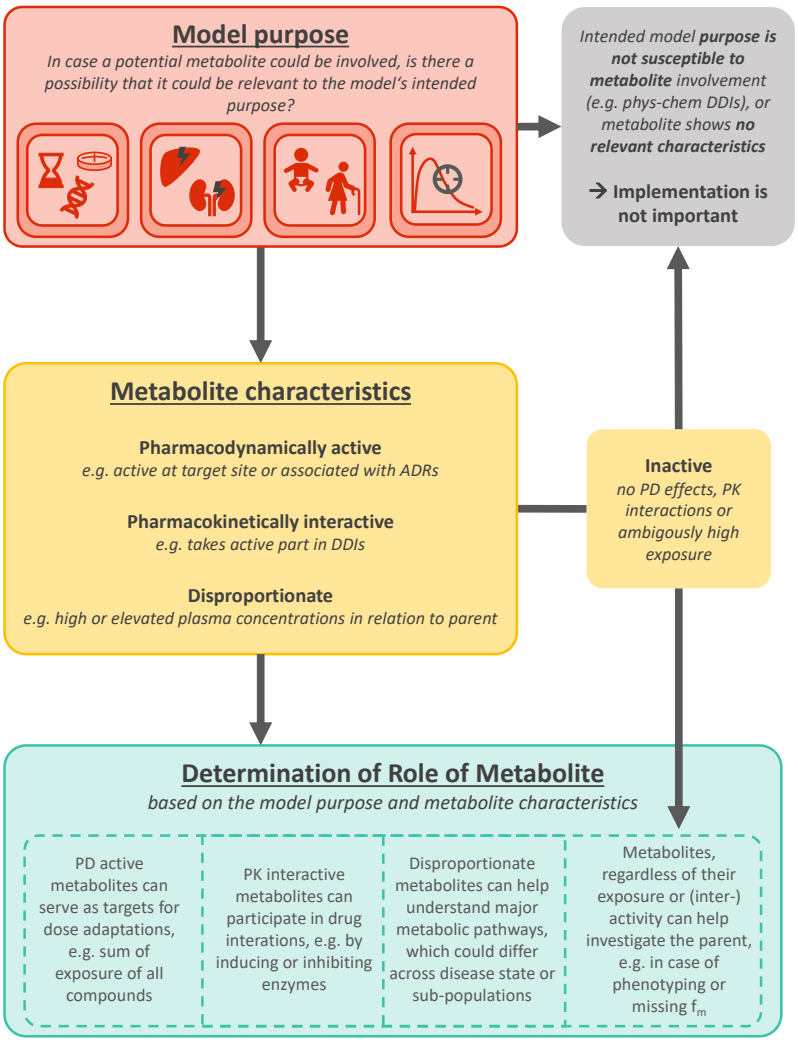

Figure 5.1: Determining the role of metabolites in MID3. In the first step to decide on whether to implement a metabolite in the PBPK model development, the model purpose needs to be discussed under the assumption that an active metabolite could be present (in red in the top row). If a present metabolite would be irrelevant, there is no need for an implementation. If the presence of a metabolite could be relevant towards the model purpose, the metabolite's characteristics should be investigated (in yellow in the middle row). Lastly, the role of the metabolite should be determined based on the model purpose and metabolite characteristics (in turquoise in the bottom row) to thoroughly plan their implementation into the PBPK model. ADRs: adverse drug reactions, DDIs: drug-drug interactions, f_m: fraction metabolized, PD: pharmacodynamics, PK: pharmacokinetics.

DPD activity to derive starting doses of 5-fluorouracil [15–17], we used

endogenous DHU/U as a means to assess the DPD chronotype, which showed great IIV between investigated cancer patients. Individual parameter values, in this case for the DPD amplitude and acrophase, could potentially be estimated from observed DHU/U and used to predict and individualize chronomodulated 5-fluorouracil treatment in the respective patient [3]. This novel approach was developed through the parallel use of parent-metabolite PBPK modeling for the endogenous biomarker and the respective therapeutic drug. It's especially important to emphasize that the metabolites modeled in project III were inactive metabolites, with no PD or PK-relevant contributions, yet they bore great usefulness in the model-based investigation of novel 5-fluorouracil chronomodulated treatment [3].

To summarize, there are two key elements that can help identify the need for inclusion of a metabolite into the PBPK analyses. As shown in Figure 5.1, these are (i) the intended model use and the dynamics of the model's application, as well as (ii) the metabolite archetype and its characteristics that could already imply a need for its implementation, illustrating the potential role of a metabolite for PBPK model. Naturally, these should be determined early in the PBPK model development process, preferably during the literature search or *in vitro* and *in vivo* drug investigation. Hence, the true impact and value of a metabolite for PBPK model development can only be assessed when looking beneath the surface of the parent drug.

6

CONCLUSION

In this thesis, parent-metabolites PBPK models were presented for three drugs, the antidepressant bupropion (project I), the antimycotic ketoconazole (project II) and the anticancer drug 5-fluorouracil alongside its endogenous biomarker uracil (project III). While all three drugs show completely different clinical relevance, their PBPK model development greatly benefitted from inclusion of their metabolites. Here, parent-metabolites PBPK modeling proved itself to be effective in addressing drug interactions at various levels. However, as considerations of metabolites for a PBPK analysis are barely reflected in dedicated regulatory PBPK guidance documents, and their role could potentially be overlooked, the presented thesis discussed their usefulness for PBPK model analyses. Moreover, an initial guidance towards determination of the necessity and role of metabolites for PBPK development, especially in the context of D_3, was generated within this thesis, that could pose as resource for future decision-making in MID_3.

BIBLIOGRAPHY

[1] F. Z. Marok, L. M. Fuhr, N. Hanke, D. Selzer, and T. Lehr, "Physiologically Based Pharmacokinetic Modeling of Bupropion and Its Metabolites in a CYP2B6 Drug-Drug-Gene Interaction Network," *Pharmaceutics*, vol. 13, no. 3, p. 331, 2021. DOI: 10.3390/pharmaceutics13030331.

[2] F. Z. Marok, J. G. Wojtyniak, L. M. Fuhr, D. Selzer, M. Schwab, J. Weiss, W. E. Haefeli, and T. Lehr, "A Physiologically Based Pharmacokinetic Model of Ketoconazole and Its Metabolites as Drug–Drug Interaction Perpetrators," *Pharmaceutics*, vol. 15, no. 2, 2023. DOI: 10.3390/pharmaceutics15020679.

[3] F. Z. Marok, J.-G. Wojtyniak, D. Selzer, R. Dallmann, J. J. Swen, H.-j. Guchelaar, M. Schwab, and T. Lehr, "Personalized Chronomodulated 5-Fluorouracil Treatment: A Physiologically-Based Pharmacokinetic Precision Dosing Approach for Optimizing Cancer Therapy," *Clinical Pharmacology and Therapeutics*, vol. 0, no. 0, pp. 1–11, 2024. DOI: 10.1002/cpt.3181.

[4] A. Brand, L. Allen, M. Altman, M. Hlava, and J. Scott, "Beyond authorship: attribution, contribution, collaboration, and credit," *Learned Publishing*, vol. 28, no. 2, pp. 151–155, 2015, ISSN: 09531513. DOI: 10.1087/20150211. URL: http://doi.wiley.com/10.1087/20150211.

[5] R. Costa, N. G. Oliveira, and R. J. Dinis-Oliveira, "Pharmacokinetic and pharmacodynamic of bupropion: integrative overview of relevant clinical and forensic aspects," *Drug Metabolism Reviews*, vol. 51, no. 3, pp. 293–313, 2019. DOI: 10.1080/03602532.2019.1620763.

[6] M. P. Goetz, V. J. Suman, J. M. Reid, D. W. Northfelt, M. A. Mahr, A. T. Ralya, M. Kuffel, S. A. Visscher, B. R. Kipp, M. C. Liu, J. R. Hawse, M. M. Ames, J. N. Ingle Buhrow, S. L. Safgren, R. M. McGovern, J. Black, T. Dockter, T. Haddad, C. Erlichman, A. A. Adjei, D. Collins, H. Streicher, Z. R. Chalmers, G. Frampton, J. R. Hawse, J. H. Doroshow, and J. M. Collins, "First-in-human phase I Study of the tamoxifen metabolite Z-endoxifen in women with endocrine-refractory metastatic breast cancer," *Journal of Clinical Oncology*, vol. 35, no. 30, pp. 3391–3400, 2017. DOI: 10.1200/jco.2017.73.3246.

[7] P. Neven, L. Jongen, A. Lintermans, K. Van Asten, C. Blomme, D. Lambrechts, A. Poppe, H. Wildiers, A.-S. Dieudonne, O. Brouckaert, J. Decloedt, P. Berteloot, D. Verhoeven, M. Joerger, P. Vuylsteke, W. Wynendaele, M. Casteels, S. Van Huffel, W. Ly-

baert, J. Van Ginderachter, R. Paridaens, I. Vergote, V. O. Dezentje, B. Van Calster, and H.-J. Guchelaar, "Tamoxifen Metabolism and Efficacy in Breast Cancer: A Prospective Multicenter Trial," *Clinical Cancer Research*, vol. 24, no. 10, pp. 2312–2318, 2018. DOI: 10.1158/1078-0432.CCR-17-3028.

[8] A. Ahmad, S. Sheikh, M. A. Khan, A. Chaturvedi, P. Patel, R. Patel, B. C. Buch, R. S. Anand, T. C. Shah, V. N. Vora, V. Ramasubramanian, S. Rao, N. Kumar, B. S. V. Prasad, R. Sathianathan, K. K. Verma, V. G. Jhanwar, N. Kumar, S. Shah, P. K. Dalal, B. Sindhu, P. Talukdar, and I. Ahmad, "Endoxifen: A new, protein kinase C inhibitor to treat acute and mixed mania associated with bipolar I disorder," *Bipolar Disorders*, vol. 23, no. 6, pp. 595–603, 2021. DOI: 10.1111/bdi.13041.

[9] S. Matsumoto and Y. Yamazoe, "Involvement of multiple human cytochromes P450 in the liver microsomal metabolism of astemizole and a comparison with terfenadine," *British Journal of Clinical Pharmacology*, vol. 51, no. 2, p. 133, 2001. DOI: 10.1046/j.1365-2125.2001.01292.x.

[10] S. Pohjola-Sintonen, M Viitasalo, L Toivonen, and P. Neuvonen, "Itraconazole prevents terfenadine metabolism and increases risk of torsades de pointes ventricular tachycardia," *European Journal of Clinical Pharmacology*, vol. 45, no. 2, pp. 191–193, 1993. DOI: 10.1007/BF00315505.

[11] S. G. Meeves and S. Appajosyula, "Efficacy and safety profile of fexofenadine HCL," *Journal of Allergy and Clinical Immunology*, vol. 112, no. 4, S69–S77, 2003. DOI: 10.1016/S0091-6749(03)01879-7.

[12] Aventis Pharmaceuticals Inc., *Prescribing Information: Fexofenadine Hydrochloride - ALLEGRA Capsule and Tablets. Available online (accessed on 03.04.2024)*. URL: https://www.accessdata.fda.gov/drugsatfda_docs/label/2003/20786se8-014,20872se8-011,20625se8-012_allegra_lbl.pdf.

[13] E. O. Meltzer, N. A. Rosario, H. Van Bever, and L. Lucio, "Fexofenadine: review of safety, efficacy and unmet needs in children with allergic rhinitis," *Allergy, Asthma and Clinical Immunology*, vol. 17, no. 1, pp. 1–11, 2021. DOI: 10.1186/s13223-021-00614-6.

[14] J. Weiss, K. I. Foerster, M. Weber, J. Burhenne, G. Mikus, T. Lehr, and W. E. Haefeli, "Does the circulating ketoconazole metabolite N-deacetyl ketoconazole contribute to the drug-drug interaction potential of the parent compound?" *European Journal of Pharmaceutical Sciences*, vol. 169, p. 106 076, 2022. DOI: 10.1016/j.ejps.2021.106076.

[15] U. Amstutz, L. M. Henricks, S. M. Offer, J. Barbarino, J. H. Schellens, J. J. Swen, T. E. Klein, H. L. McLeod, K. E. Caudle, R. B. Diasio, and M. Schwab, "Clinical Pharmacogenetics Implementation Consortium (CPIC) Guideline for Dihydropyrimidine Dehydrogenase Genotype and Fluoropyrimidine Dosing: 2017 Update," *Clinical Pharmacology and Therapeutics*, vol. 00, no. 0, 2017. DOI: 10.1002/cpt.668.

[16] European Medicines Agency, "5-Fluorouracil (i.v.), capecitabine and tegafur containing products : Pre-treatment testing to identify DPD-deficient patients at increased risk of severe toxicity. Available online (accessed on 10.02.2024)," Tech. Rep. URL: https://www.ema.europa.eu/en/documents/dhpc/direct-healthcare-professional-communication-dhpc-5-fluorouracil-iv-capecitabine-and-tegafur-containing-products-pre-treatment-testing-identify-dpd-deficient-patients-increased-risk-severe-toxicity_en.pdf.

[17] C. A. T. C. Lunenburg, C. H. van der Wouden, M. Nijenhuis, M. H. Crommentuijn-van Rhenen, N. J. de Boer-Veger, A. M. Buunk, E. J. F. Houwink, H. Mulder, G. A. Rongen, R. H. N. van Schaik, J. van der Weide, B. Wilffert, V. H. M. Deneer, J. J. Swen, and H.-J. Guchelaar, "Dutch Pharmacogenetics Working Group (DPWG) guideline for the gene–drug interaction of DPYD and fluoropyrimidines," *European Journal of Human Genetics*, vol. 28, no. 4, pp. 508–517, 2020. DOI: 10.1038/s41431-019-0540-0.

[18] A. Judge and M. S. Dodd, "Metabolism," *Essays in Biochemistry*, vol. 64, no. 4, pp. 607–647, 2020. DOI: 10.1042/EBC20190041. URL: https://portlandpress.com/essaysbiochem/article/64/4/607/226177/Metabolism.

[19] T. Shroff, K. Aina, C. Maass, M. Cipriano, J. Lambrecht, F. Tacke, A. Mosig, and P. Loskill, "Studying Metabolism with Multi-Organ Chips: New Tools for Disease Modelling, Pharmacokinetics and Pharmacodynamics," in *Advances in Medical Imaging, Detection, and Diagnosis*, Jenny Stanford Publishing, 2023, pp. 1273–1315, ISBN: 9781000602043. DOI: 10.1201/9781003298038-52.

[20] G. Szakács, A. Váradi, C. Oezvegy-Laczka, and B. Sarkadi, "The role of ABC transporters in drug absorption, distribution, metabolism, excretion and toxicity (ADME–Tox)," *Drug Discovery Today*, vol. 13, no. 9-10, pp. 379–393, 2008. DOI: 10.1016/j.drudis.2007.12.010.

[21] U. A. Meyer, "Overview of enzymes of drug metabolism," *Journal of Pharmacokinetics and Biopharmaceutics*, vol. 24, no. 5, pp. 449–459, 1996. DOI: 10.1007/BF02353473.

[22] O. A. Almazroo, M. K. Miah, and R. Venkataramanan, "Drug Metabolism in the Liver," *Clinics in Liver Disease*, vol. 21, no. 1, pp. 1–20, 2017. DOI: 10.1016/j.cld.2016.08.001.

[23] A. Saravanakumar, A. Sadighi, R. Ryu, and F. Akhlaghi, "Physicochemical Properties, Biotransformation, and Transport Pathways of Established and Newly Approved Medications: A Systematic Review of the Top 200 Most Prescribed Drugs vs. the FDA-Approved Drugs Between 2005 and 2016," *Clinical Pharmacokinetics*, vol. 58, no. 10, pp. 1281–1294, 2019. DOI: 10.1007/s40262-019-00750-8.

[24] H. Wang and L. Tompkins, "CYP2B6: New Insights into a Historically Overlooked Cytochrome P450 Isozyme," *Current Drug Metabolism*, vol. 9, no. 7, pp. 598–610, 2008. DOI: 10.2174/138920008785821710.

[25] E. D. Kharasch and A. Crafford, "Common Polymorphisms of CYP2B6 Influence Stereoselective Bupropion Disposition," *Clinical Pharmacology and Therapeutics*, vol. 105, no. 1, pp. 142–152, 2019. DOI: 10.1002/cpt.1116.

[26] B. A. W. Jacobs, M. J. Deenen, D. Pluim, J. G. C. van Hasselt, M. D. Kraehenbuehl, R. M. J. M. van Geel, N. de Vries, H. Rosing, D. Meulendijks, A. M. Burylo, A. Cats, J. H. Beijnen, A. D. R. Huitema, and J. H. M. Schellens, "Pronounced between-subject and circadian variability in thymidylate synthase and dihydropyrimidine dehydrogenase enzyme activity in human volunteers," *British Journal of Clinical Pharmacology*, vol. 82, no. 3, pp. 706–716, 2016. DOI: 10.1111/bcp.13007.

[27] A. Tourancheau, M. Rouleau, S. Guauque-Olarte, L. Villeneuve, I. Gilbert, A. Droit, and C. Guillemette, "Quantitative profiling of the UGT transcriptome in human drug-metabolizing tissues," *The Pharmacogenomics Journal*, vol. 18, no. 2, pp. 251–261, 2018. DOI: 10.1038/tpj.2017.5.

[28] M. Markovic, S. Ben-Shabat, and A. Dahan, "Prodrugs for Improved Drug Delivery: Lessons Learned from Recently Developed and Marketed Products," *Pharmaceutics*, vol. 12, no. 11, p. 1031, 2020. DOI: 10.3390/pharmaceutics12111031.

[29] Committee for Medicinal Products for Human Use (CHMP). European Medicines Agency., *Guideline on the investigation of drug interactions. Available online (accessed on 03.01.2024)*. URL: https://www.ema.europa.eu/en/documents/scientific-guideline/guideline-investigation-drug-interactions-revision-1_en.pdf.

[30] D. Tuerk, L. M. Fuhr, F. Z. Marok, S. Ruedesheim, A. Kuehn, D. Selzer, M. Schwab, and T. Lehr, "Novel models for the prediction of drug-gene interactions," *Expert Opinion on Drug*

Metabolism and Toxicology, vol. 00, no. 00, pp. 1–18, 2021. DOI: 10.1080/17425255.2021.1998455.

[31] *Pharmgkb - CYP2B6 frequency table. Available online (accessed on 06.08.2023)*. URL: https://www.pharmgkb.org/page/cyp2b6RefMaterials.

[32] R. Cacabelos, N. Cacabelos, and J. C. Carril, "The role of pharmacogenomics in adverse drug reactions," *Expert Review of Clinical Pharmacology*, vol. 12, no. 5, pp. 407–442, 2019. DOI: 10.1080/17512433.2019.1597706.

[33] J. J. Swen *et al.*, "A 12-gene pharmacogenetic panel to prevent adverse drug reactions: an open-label, multicentre, controlled, cluster-randomised crossover implementation study," *The Lancet*, vol. 401, no. 10374, pp. 347–356, 2023. DOI: 10.1016/S0140-6736(22)01841-4.

[34] U. M. Zanger and M. Schwab, "Cytochrome P450 enzymes in drug metabolism: Regulation of gene expression, enzyme activities, and impact of genetic variation," *Pharmacology and Therapeutics*, vol. 138, no. 1, pp. 103–141, 2013. DOI: 10.1016/j.pharmthera.2012.12.007.

[35] Z. Desta, R. S. Gammal, L. Gong, M. Whirl-Carrillo, A. H. Gaur, C. Sukasem, J. Hockings, A. Myers, M. Swart, R. F. Tyndale, C. Masimirembwa, O. F. Iwuchukwu, S. Chirwa, J. Lennox, A. Gaedigk, T. E. Klein, and D. W. Haas, "Clinical Pharmacogenetics Implementation Consortium (CPIC) Guideline for CYP2B6 and Efavirenz-Containing Antiretroviral Therapy," *Clinical Pharmacology and Therapeutics*, vol. 106, no. 4, pp. 726–733, 2019. DOI: 10.1002/cpt.1477.

[36] K Loboz, A Gross, K Williams, W Liauw, R Day, J Blievernicht, U Zanger, and A McLachlan, "Cytochrome P450 2B6 activity as measured by bupropion hydroxylation: Effect of induction by rifampin and ethnicity," *Clinical Pharmacology and Therapeutics*, vol. 80, no. 1, pp. 75–84, 2006. DOI: 10.1016/j.clpt.2006.03.010.

[37] U.S.Food and Drug Adminstration - FDA, *Drug Development and Drug Interactions - Table of Substrates, Inhibitors and Inducers. Available online (accessed on 28.08.2023)*. URL: https://www.fda.gov/drugs/drug-interactions-labeling/drug-development-and-drug-interactions-table-substrates-inhibitors-and-inducers.

[38] P. H. Silverstone, R. Williams, L. McMahon, R. Fleming, and S. Fogarty, "Convulsive liability of bupropion hydrochloride metabolites in Swiss albino mice," *Annals of General Psychiatry*, vol. 7, no. 1, p. 19, 2008. DOI: 10.1186/1744-859X-7-19.

[39] L. Magro, E. Arzenton, R. Leone, M. G. Stano, M. Vezzaro, A. Rudolph, I. Castagna, and U. Moretti, "Identifying and Characterizing Serious Adverse Drug Reactions Associated With Drug-Drug Interactions in a Spontaneous Reporting Database," *Frontiers in Pharmacology*, vol. 11, no. January, 2021. DOI: 10.3389/fphar.2020.622862.

[40] S. E. Bronskill, S. S. Gill, J. M. Paterson, C. M. Bell, G. M. Anderson, and P. A. Rochon, "Exploring Variation in Rates of Polypharmacy Across Long Term Care Homes," *Journal of the American Medical Directors Association*, vol. 13, no. 3, 309.e15–309.e21, 2012. DOI: 10.1016/j.jamda.2011.07.001.

[41] U.S. Food and Drug Administration, *Clinical Drug Interaction Studies - Cytochrome P450 Enzyme- and Drug Interactions. Guidance for Industry. Available online (accessed on 12.11.2023)*. URL: https://www.fda.gov/media/134581/download.

[42] L. M. Fuhr, F. Z. Marok, M. Mees, F. Mahfoud, D. Selzer, and T. Lehr, "A Physiologically Based Pharmacokinetic and Pharmacodynamic Model of the CYP3A4 Substrate Felodipine for Drug–Drug Interaction Modeling," *Pharmaceutics*, vol. 14, no. 7, p. 1474, 2022. DOI: 10.3390/pharmaceutics14071474.

[43] L. M. Fuhr, F. Z. Marok, U. Fuhr, D. Selzer, and T. Lehr, "Physiologically Based Pharmacokinetic Modeling of Bergamottin and 6,7-Dihydroxybergamottin to Describe <scp>CYP3A4</scp> Mediated Grapefruit-Drug Interactions," *Clinical Pharmacology and Therapeutics*, vol. 114, no. 2, pp. 470–482, 2023. DOI: 10.1002/cpt.2968.

[44] L. M. Fuhr, F. Z. Marok, N. Hanke, D. Selzer, and T. Lehr, "Pharmacokinetics of the CYP3A4 and CYP2B6 Inducer Carbamazepine and Its Drug-Drug Interaction Potential: A Physiologically Based Pharmacokinetic Modeling Approach.," *Pharmaceutics*, vol. 13, no. 2, pp. 1–21, 2021. DOI: 10.3390/pharmaceutics13020270.

[45] E. D. Kharasch, S Vangveravong, N Buck, A London, T Kim, J Blood, and R. H. Mach, "Concurrent assessment of hepatic and intestinal cytochrome P450 3A activities using deuterated alfentanil.," *Clinical pharmacology and therapeutics*, vol. 89, no. 4, pp. 562–70, 2011. DOI: 10.1038/clpt.2010.313.

[46] S. A. Stoch, E. Friedman, A. Maes, K. Yee, Y. Xu, P. Larson, M. Fitzgerald, J. Chodakewitz, and J. A. Wagner, "Effect of Different Durations of Ketoconazole Dosing on the Single-Dose Pharmacokinetics of Midazolam: Shortening the Paradigm," *The Journal of Clinical Pharmacology*, vol. 49, no. 4, pp. 398–406, 2009. DOI: 10.1177/0091270008331133.

[47] *SafePolyMed project. Available online (accessed on 29.02.2024)*. URL: https://cordis.europa.eu/project/id/101057639).

[48] *Pharmgkb - Clinical guidelines annotations summary. Available online (accessed on 13.11.2023)*. URL: https://api.pharmgkb.org/v1/download/file/data/clinicalAnnotations.zip.

[49] U.S.Food and Drug Adminstration - FDA, *For Healthcare Professionals - FDA's Examples of Drugs that Interact with CYP Enzymes and Transporter Systems, Available online (accessed on 28.08.2023)*. URL: https://www.fda.gov/drugs/drug-interactions-labeling/healthcare-professionals-fdas-examples-drugs-interact-cyp-enzymes-and-transporter-systems.

[50] C. Xu and Z. Desta, "In vitro analysis and quantitative prediction of efavirenz inhibition of eight cytochrome P450 (CYP) enzymes: Major effects on CYPs 2B6, 2C8, 2C9 and 2C19," *Drug Metabolism and Pharmacokinetics*, vol. 28, no. 4, pp. 362–371, 2013. DOI: 10.2133/dmpk.DMPK-12-RG-124.

[51] D. Tuerk, N. Scherer, D. Selzer, C. Dings, N. Hanke, R. Dallmann, M. Schwab, P. Timmins, V. Nock, and T. Lehr, "Significant impact of time-of-day variation on metformin pharmacokinetics," *Diabetologia*, vol. 66, no. 6, pp. 1024–1034, 2023. DOI: 10.1007/s00125-023-05898-4.

[52] J. E. Sager, S. Tripathy, L. S. Price, A. Nath, J. Chang, A. Stephenson-Famy, and N. Isoherranen, "In vitro to in vivo extrapolation of the complex drug-drug interaction of bupropion and its metabolites with CYP2D6; simultaneous reversible inhibition and CYP2D6 downregulation," *Biochemical Pharmacology*, vol. 123, pp. 85–96, 2017. DOI: 10.1016/j.bcp.2016.11.007.

[53] I. Todor, A. Popa, M. Neag, D. Muntean, C. Bocsan, A. Buzoianu, L. Vlase, A. M. Gheldiu, and C. Briciu, "Evaluation of a potential metabolism-mediated drug-drug interaction between atomoxetine and bupropion in healthy volunteers," *Journal of Pharmacy and Pharmaceutical Sciences*, vol. 19, no. 2, pp. 198–207, 2016. DOI: 10.18433/J3H03R.

[54] M. Kotlyar, L. H. Brauer, T. S. Tracy, D. K. Hatsukami, J. Harris, C. A. Bronars, and D. E. Adson, "Inhibition of CYP2D6 Activity by Bupropion," *Journal of Clinical Psychopharmacology*, vol. 25, no. 3, pp. 226–229, 2005. DOI: 10.1097/01.jcp.0000162805.46453.e3.

[55] M. J. Reese, R. M. Wurm, K. T. Muir, G. T. Generaux, L. St. John-Williams, and D. J. Mcconn, "An in Vitro Mechanistic Study to Elucidate the Desipramine/Bupropion Clinical Drug-Drug Interaction," *Drug Metabolism and Disposition*, vol. 36, no. 7, pp. 1198–1201, 2008. DOI: 10.1124/dmd.107.020198.

[56] D. Dong, D. Yang, L. Lin, S. Wang, and B. Wu, "Circadian rhythm in pharmacokinetics and its relevance to chronotherapy," *Biochemical Pharmacology*, vol. 178, no. April, p. 114 045, 2020. DOI: 10.1016/j.bcp.2020.114045.

[57] D. Lu, M. Zhao, M. Chen, and B. Wu, "Circadian Clock–Controlled Drug Metabolism: Implications for Chronotherapeutics," *Drug Metabolism and Disposition*, vol. 48, no. 5, pp. 395–406, 2020. DOI: 10.1124/dmd.120.090472.

[58] F. Lévi, A. Okyar, S. Dulong, P. F. Innominato, and J. Clairambault, "Circadian Timing in Cancer Treatments," *Annual Review of Pharmacology and Toxicology*, vol. 50, no. 1, pp. 377–421, 2010. DOI: 10.1146/annurev.pharmtox.48.113006.094626.

[59] F. Levi and U. Schibler, "Circadian Rhythms: Mechanisms and Therapeutic Implications," *Annual Review of Pharmacology and Toxicology*, vol. 47, no. 1, pp. 593–628, 2007. DOI: 10.1146/annurev.pharmtox.47.120505.105208.

[60] P. F. Innominato, V. P. Roche, O. G. Palesh, A. Ulusakarya, D. Spiegel, and F. A. Lévi, "The circadian timing system in clinical oncology," *Annals of Medicine*, vol. 46, no. 4, pp. 191–207, 2014. DOI: 10.3109/07853890.2014.916990.

[61] M. Nováková, M. Sládek, and A. Sumová, "Human chronotype is determined in bodily cells under real-life conditions," *Chronobiology International*, vol. 30, no. 4, pp. 607–617, 2013. DOI: 10.3109/07420528.2012.754455.

[62] T. Roenneberg, T. Kuehnle, M. Juda, T. Kantermann, K. Allebrandt, M. Gordijn, and M. Merrow, "Epidemiology of the human circadian clock," *Sleep Medicine Reviews*, vol. 11, no. 6, pp. 429–438, 2007. DOI: 10.1016/j.smrv.2007.07.005.

[63] J. Lippert, R. Burghaus, A. Edginton, S. Frechen, M. Karlsson, A. Kovar, T. Lehr, P. Milligan, V. Nock, S. Ramusovic, M. Riggs, S. Schaller, J. Schlender, S. Schmidt, M. Sevestre, E. Sjoegren, J. Solodenko, A. Staab, and D. Teutonico, "Open Systems Pharmacology Community—An Open Access, Open Source, Open Science Approach to Modeling and Simulation in Pharmaceutical Sciences," *CPT: Pharmacometrics and Systems Pharmacology*, vol. 8, no. 12, pp. 878–882, 2019. DOI: 10.1002/psp4.12473.

[64] Committee for Medicinal Products for Human Use. European Medicines Agency., *Guideline on the reporting of physiologically based pharmacokinetic (PBPK) modelling and simulation. Available online (accessed on 03.01.2024)*. URL: https://www.ema.europa.eu/en/documents/scientific-guideline/guideline-reporting-physiologically-based-pharmacokinetic-pbpk-modelling-and-simulation_en.pdf.

[65] U.S. Food and Drug Administration., *Physiologically Based Pharmacokinetic Analyses - Format and Content. Guidance for Industry. Available online (accessed on 14.07.2022*. URL: https://www.fda.gov/media/101469/download.

[66] Open Systems Pharmacology Suite Community, *Open Systems Pharmacology Suite Manual. Available online (accessed on 29.02.2024*. URL: https://docs.open-systems-pharmacology.org/.

[67] *Step 3 in drug development process - U.S. Food and Drug Administration. Available online (accessed on 20.01.2024)*. URL: https://www.fda.gov/patients/drug-development-process/step-3-clinical-research.

[68] G. A. Van Norman, "Drugs, Devices, and the FDA: Part 1," *JACC: Basic to Translational Science*, vol. 1, no. 3, pp. 170–179, 2016. DOI: 10.1016/j.jacbts.2016.03.002.

[69] Committee for Medicinal Products for Human Use and (CHMP). European Medicines Agency., *Guideline on strategies to identify and mitigate risks for first-in-human and early clinical trials with investigational medicinal products. Available online (accessed on 03.01.2024)*. URL: https://www.ema.europa.eu/en/documents/scientific-guideline/guideline-strategies-identify-and-mitigate-risks-first-human-and-early-clinical-trials-investigational-medicinal-products-revision-1_en.pdf.

[70] Committee for Medicinal Products for Human Use (CHMP) - European Medicines Agency, *ICH guideline E8 (R1) on general considerations for clinical studies. Available online (accessed on 03.01.2024)*. URL: https://www.ema.europa.eu/en/documents/scientific-guideline/ich-e-8-general-considerations-clinical-trials-step-5_en.pdf.

[71] U.S. Department of Health and Human Services. Food and Drug Administration. Center for Drug Evaluation and Research (CDER)., *Guidance for Industry: Safety Testing of Metabolites. Available online (acceessed on 03.01.2024)*. URL: http://www.fda.gov/cder/guidance/index.htm.

[72] Committee for Medicinal Products for Human Use (CHMP). European Medicines Agency., *Guideline on the Evaluation of the Pharmacokinetics of Medicinal Products in Patients With Impaired Hepatic Function. Available online (accessed on 03.01.2024)*. URL: https://www.ema.europa.eu/en/documents/scientific-guideline/guideline-evaluation-pharmacokinetics-medicinal-products-patients-impaired-hepatic-function_en.pdf.

[73] Committee for Medicinal Products for Human Use (CHMP). European Medicines Agency., *Guideline on the use of pharmacogenetic methodologies in the pharmacokinetic evaluation of medicinal products. Available online (accessed on 03.01.2024)*. URL: https://www.ema.europa.eu/en/documents/scientific-guideline/guideline-use-pharmacogenetic-methodologies-pharmacokinetic-evaluation-medicinal-products_en.pdf.

[74] Committee for Medicinal Products for Human Use (CHMP). European Medicines Agency., *Guideline on the evaluation of the pharmacokinetics of medicinal products in patients with decreased renal function Available online (accessed on 03.01.2024)*. URL: https://www.ema.europa.eu/en/documents/scientific-guideline/guideline-evaluation-pharmacokinetics-medicinal-products-patients-decreased-renal-function_en.pdf.

[75] *Open-Source MOdellierungs- und Simulationsplattform mit automatisierter Qualitaetskontrolle fuer die Entwicklung komplexer Systemmodelle in den Lebenswissenschaften (OSMOSES) project. Available online (accessed on 29.02.2024)*. URL: https://www.gesundheitsforschung-bmbf.de/de/osmoses-open-source-modellierungs-und-simulationsplattform-mit-automatisierter-9163.php.

[76] *Ubiquitous Pharmacogenomics (U-PGx) project. Available online (accessed on 29.02.2024)*. URL: https://cordis.europa.eu/project/id/668353.

[77] *Chemicalize online tool by ChemAxon. Available online (accessed on 16.02.2024)*. URL: https://chemicalize.com/welcome.

[78] M. Nishimura and S. Naito, "Tissue-specific mRNA expression profiles of human phase I metabolizing enzymes except for cytochrome P450 and phase II metabolizing enzymes.," *Drug metabolism and pharmacokinetics*, vol. 21, no. 5, pp. 357–374, 2006. DOI: 10.2133/dmpk.21.357.

[79] N. Kolesnikov, E. Hastings, M. Keays, O. Melnichuk, Y. Tang, E. Williams, M. Dylag, N. Kurbatova, M. Brandizi, T. Burdett, K. Megy, E. Pilicheva, G. Rustici, A. Tikhonov, H. Parkinson, R. Petryszak, U. Sarkans, and A. Brazma, "ArrayExpress update-simplifying data submissions," *Nucleic Acids Research*, vol. 43, no. D1, pp. D1113–D1116, 2015. DOI: 10.1093/nar/gku1057.

[80] National Center for Biotechnology Information (NCBI), *Expressed Sequence Tags (EST) from UniGene*, 2019.

[81] National Center for Health Statistics Hyattsville MD 20782., *Third National Health and Nutrition Examination Survey, (NHANES III)*, 1997.

[82] G. Tanaka and H. Kawamura, *Anatomical and physiological characteristics for Asian reference man: Male and female of different ages: Tanaka model*, 1996.

[83] J. Valentin, "Basic anatomical and physiological data for use in radiological protection: reference values. A report of age- and gender-related differences in the anatomical and physiological characteristics of reference individuals. ICRP Publication 89.," *Annals of the ICRP*, vol. 32, no. 3-4, pp. 5–265, 2002. DOI: 10.1016/S0146-6453(03)00002-2.

[84] Open Systems Pharmacology Suite Community, *PK-Sim® Ontogeny Database Documentation, Version 7.3. Available online (accessed on 29.02.2024*. URL: https://github.com/Open-Systems-Pharmacology/OSPSuite.Documentation/blob/master/PK-SimOntogenyDatabaseVersion7.3.pdf.

[85] V. M. Fokina, M. Xu, E. Rytting, S. Z. Abdel-Rahman, H. West, C. Oncken, S. M. Clark, M. S. Ahmed, G. D. Hankins, and T. N. Nanovskaya, "Pharmacokinetics of bupropion and its pharmacologically active metabolites in pregnancy," *Drug Metabolism and Disposition*, vol. 44, no. 11, pp. 1832–1838, 2016. DOI: 10.1124/dmd.116.071530.

[86] J. N. Connarn, S. Flowers, M. Kelly, R. Luo, K. M. Ward, G. Harrington, I. Moncion, M. Kamali, M. McInnis, M. R. Feng, V. Ellingrod, A. Babiskin, X. Zhang, and D. Sun, "Pharmacokinetics and Pharmacogenomics of Bupropion in Three Different Formulations with Different Release Kinetics in Healthy Human Volunteers," *AAPS Journal*, vol. 19, no. 5, pp. 1513–1522, 2017. DOI: 10.1208/s12248-017-0102-8.

[87] H. R. Arias, F. Gumilar, A. Rosenberg, K. M. Targowska-Duda, D. Feuerbach, K. Jozwiak, R. Moaddel, I. W. Wainer, and C. Bouzat, "Interaction of Bupropion with Muscle-Type Nicotinic Acetylcholine Receptors in Different Conformational States," *Biochemistry*, vol. 48, no. 21, pp. 4506–4518, 2009. DOI: 10.1021/bi802206k.

[88] F. I. Carroll, B. E. Blough, P. Abraham, A. C. Mills, J. A. Holleman, S. A. Wolckenhauer, A. M. Decker, A. Landavazo, K. T. McElroy, H. A. Navarro, M. B. Gatch, and M. J. Forster, "Synthesis and biological evaluation of bupropion analogues as potential pharmacotherapies for cocaine addiction," *Journal of Medicinal Chemistry*, vol. 52, no. 21, pp. 6768–6781, 2009. DOI: 10.1021/jm901189z.

[89] S. M. Stahl, J. F. Pradko, B. R. Haight, J. G. Modell, C. B. Rockett, and S. Learned-Coughlin, "A Review of the Neuropharmacology of Bupropion, a Dual Norepinephrine and Dopamine Reuptake Inhibitor," *The Primary Care Companion to The Journal*

of Clinical Psychiatry, vol. 06, no. 04, pp. 159–166, 2004. DOI: 10.4088/pcc.v06n0403.

[90] J. A. Jonhnston, J. Fiedler-Kelly, E. D. Glover, D. P. Sachs, T. H. Grasela, and J. De Veaugh-Geiss, "Relationship between drug exposure and the efficacy and safety of bupropion sustained release for smoking cessation," *Nicotine and Tobacco Research*, vol. 3, no. 2, pp. 131–140, 2001. DOI: 10.1080/14622200110042852.

[91] C. Xu, E. T. Ogburn, Y. Guo, and Z. Desta, "Effects of the CYP2B6*6 allele on catalytic properties and inhibition of CYP2B6 in vitro: Implication for the mechanism of reduced efavirenz metabolism and other CYP2B6 substrates in vivo," *Drug Metabolism and Disposition*, vol. 40, no. 4, pp. 717–725, 2012. DOI: 10.1124/dmd.111.042416.

[92] P. F. Wang, A. Neiner, and E. D. Kharasch, "Stereoselective Bupropion Hydroxylation by Cytochrome P450 CYP2B6 and Cytochrome P450 Oxidoreductase Genetic Variants," *Drug metabolism and disposition: the biological fate of chemicals*, vol. 48, no. 6, pp. 438–445, 2020. DOI: 10.1124/dmd.119.090407.

[93] Y. Chen, H. F. Liu, L. Liu, K. Nguyen, E. B. Jones, and A. J. Fretland, "The in vitro metabolism of bupropion revisited: Concentration dependent involvement of cytochrome P450 2C19," *Xenobiotica*, vol. 40, no. 8, pp. 536–546, 2010. DOI: 10.3109/00498254.2010.492880.

[94] B. T. Gufford, J. B. L. Lu, I. F. Metzger, D. R. Jones, and Z. Desta, "Stereoselective glucuronidation of bupropion metabolites in vitro and in vivo," *Drug Metabolism and Disposition*, vol. 44, no. 4, pp. 544–553, 2016. DOI: 10.1124/dmd.115.068908.

[95] J. E. Sager, L. S. Price, and N. Isoherranen, "Stereoselective metabolism of bupropion to OH-bupropion, threohydrobupropion, erythrohydrobupropion, and 49-OH-bupropion in vitro," *Drug Metabolism and Disposition*, vol. 44, no. 10, pp. 1709–1719, 2016. DOI: 10.1124/dmd.116.072363.

[96] C. Biovial Corporation, *Wellbutrin XL ® (bupropion hydrochloride extended-release tablets) - Medicine Guide. Available online (accessed on 22 January 2021)*. URL: https://www.accessdata.fda.gov/drugsatfda_docs/label/2010/021515s022lbl.pdf.

[97] R. C. Heel, R. N. Brogden, A. Carmine, P. A. Morley, T. M. Speight, and G. S. Avery, "Ketoconazole: A Review of its Therapeutic Efficacy in Superficial and Systemic Fungal Infections," *Drugs*, vol. 23, no. 1, pp. 1–36, 1982. DOI: 10.2165/00003495-198223010-00001.

[98] European Medicines Agency European, "European Medicines Agency recommends suspension of marketing authorisations for oral ketoconazole Available online (accessed on 12.11.2022) https://www.ema.europa.eu/documents/press-release/european-medicines-agency-recommends-suspension-marketing-authorisations-oral-ketoconazol," Tech. Rep. URL: https://www.ema.europa.eu/documents/press-release/european-medicines-agency-recommends-suspension-marketing-authorisations-oral-ketoconazol.

[99] D. E. Nix, "Cardiotoxicity Induced by Antifungal Drugs," *Current Fungal Infection Reports*, vol. 8, no. 2, pp. 129–138, 2014. DOI: 10.1007/s12281-014-0183-0.

[100] T. K. Daneshmend, D. W. Warnock, A. Turner, and C. J. Roberts, "Pharmacokinetics of ketoconazole in normal subjects," *Journal of Antimicrobial Chemotherapy*, vol. 8, no. 4, pp. 299–304, 1981. DOI: 10.1093/jac/8.4.299.

[101] T. Fukami, A. Iida, K. Konishi, and M. Nakajima, "Human arylacetamide deacetylase hydrolyzes ketoconazole to trigger hepatocellular toxicity," *Biochemical Pharmacology*, vol. 116, pp. 153–161, 2016. DOI: 10.1016/j.bcp.2016.07.007.

[102] W. Fitch, T. Tran, M. Young, L. Liu, and Y. Chen, "Revisiting the Metabolism of Ketoconazole Using Accurate Mass," *Drug Metabolism Letters*, vol. 3, no. 3, pp. 191–198, 2009. DOI: 10.2174/187231209789352085.

[103] R. J. Rodriguez and D Acosta, "Metabolism of ketoconazole and deacetylated ketoconazole by rat hepatic microsomes and flavin-containing monooxygenases.," *Drug metabolism and disposition: the biological fate of chemicals*, vol. 25, no. 6, pp. 772–7, 1997.

[104] Janssen Pharmaceuticals, *Nizoral(R) (Ketoconazole) Tablets - Drug label. Available online (accessed on 12.11.2022)*. URL: https://www.accessdata.fda.gov/drugsatfda_docs/label/2013/018533s040lbl.pdf.

[105] J.-H. Kim, W.-G. Choi, S. Lee, and H. Lee, "Revisiting the Metabolism and Bioactivation of Ketoconazole in Human and Mouse Using Liquid Chromatography–Mass Spectrometry-Based Metabolomics," *International Journal of Molecular Sciences*, vol. 18, no. 3, p. 621, 2017. DOI: 10.3390/ijms18030621.

[106] R. B. Diasio and B. E. Harris, "Clinical Pharmacology of 5-Fluorouracil," *Clinical Pharmacokinetics*, vol. 16, no. 4, pp. 215–237, 1989. DOI: 10.2165/00003088-198916040-00002.

[107] J. D. Sara, J. Kaur, R. Khodadadi, M. Rehman, R. Lobo, S. Chakrabarti, J. Herrmann, A. Lerman, and A. Grothey, "5-fluorouracil and cardiotoxicity: A review," *Therapeutic Advances in Medical Oncology*, vol. 10, no. 2s, p. 175 883 591 878 014, 2018. DOI: 10.1177/1758835918780140.

[108] Meta-Analysis Group In Cancer, "Toxicity of fluorouracil in patients with advanced colorectal cancer: effect of administration schedule and prognostic factors.," *Journal of clinical oncology : official journal of the American Society of Clinical Oncology*, vol. 16, no. 11, pp. 3537–41, 1998. DOI: 10.1200/JCO.1998.16.11.3537.

[109] E. J. Derissen, B. A. Jacobs, A. D. Huitema, H. Rosing, J. H. Schellens, and J. H. Beijnen, "Exploring the intracellular pharmacokinetics of the 5-fluorouracil nucleotides during capecitabine treatment," *British Journal of Clinical Pharmacology*, vol. 81, no. 5, pp. 949–957, 2016. DOI: 10.1111/bcp.12877.

[110] G. D. Heggie, J. P. Sommadossi, D. S. Cross, W. J. Huster, and R. B. Diasio, "Clinical pharmacokinetics of 5-fluorouracil and its metabolites in plasma, urine, and bile.," *Cancer research*, vol. 47, no. 8, pp. 2203–6, 1987.

[111] R. A. Fleming, G. Milano, A. Thyss, M. C. Etienne, N Renée, M. Schneider, and F. Demard, "Correlation between dihydropyrimidine dehydrogenase activity in peripheral mononuclear cells and systemic clearance of fluorouracil in cancer patients.," *Cancer research*, vol. 52, no. 10, pp. 2899–902, 1992.

[112] J. E. Knikman, H. Gelderblom, J. H. Beijnen, A. Cats, H. J. Guchelaar, and L. M. Henricks, "Individualized Dosing of Fluoropyrimidine-Based Chemotherapy to Prevent Severe Fluoropyrimidine-Related Toxicity: What Are the Options?" *Clinical Pharmacology and Therapeutics*, vol. 109, no. 3, pp. 591–604, 2021. DOI: 10.1002/cpt.2069.

[113] S. Giacchetti, G. Bjarnason, C. Garufi, D. Genet, S. Iacobelli, M. Tampellini, R. Smaaland, C. Focan, B. Coudert, Y. Humblet, J. L. Canon, A. Adenis, G. L. Re, C. Carvalho, J. Schueller, N. Anciaux, M.-A. Lentz, B. Baron, T. Gorlia, and F. Lévi, "Phase III Trial Comparing 4-Day Chronomodulated Therapy Versus 2-Day Conventional Delivery of Fluorouracil, Leucovorin, and Oxaliplatin As First-Line Chemotherapy of Metastatic Colorectal Cancer: The European Organisation for Research and Treatment of Cancer Chronotherapy Group," *Journal of Clinical Oncology*, vol. 24, no. 22, pp. 3562–3569, 2006. DOI: 10.1200/JCO.2006.06.1440.

[114] F. Lévi, A. Karaboué, M.-C. Etienne-Grimaldi, G. Paintaud, C. Focan, P. Innominato, M. Bouchahda, G. Milano, and E. Chatelut, "Pharmacokinetics of Irinotecan, Oxaliplatin and

5-Fluorouracil During Hepatic Artery Chronomodulated Infusion: A Translational European OPTILIV Study," *Clinical Pharmacokinetics*, vol. 56, no. 2, pp. 165–177, 2017. DOI: 10.1007/s40262-016-0431-2.

[115] H. L. H. Loer, C. Kovar, S. Ruedesheim, F. Z. Marok, L. M. Fuhr, D. Selzer, M. Schwab, and T. Lehr, "Physiologically based pharmacokinetic modeling of imatinib and N-desmethyl imatinib for drug–drug interaction predictions," *CPT: Pharmacometrics and Systems Pharmacology*, no. 00, pp. 1–15, 2024. DOI: 10.1002/psp4.13127.

[116] C. Kovar, H. L. H. Loer, S. Rüdesheim, L. M. Fuhr, F. Z. Marok, D. Selzer, M. Schwab, and T. Lehr, "A physiologically-based pharmacokinetic precision dosing approach to manage dasatinib drug–drug interactions," *CPT: Pharmacometrics and Systems Pharmacology*, 2024. DOI: 10.1002/psp4.13146.

[117] "PBPK Models for CYP3A4 and P-gp DDI prediction: a modeling network of rifampicin, itraconazole, clarithromycin, midazolam, alfentanil, and digoxin," *CPT: pharmacometrics and systems pharmacology*, vol. 7, no. 10, pp. 647–59, 2018. DOI: 10.1002/psp4.12343.

Part I

APPENDIX

A

LIST OF PUBLICATIONS

A.1 ORIGINAL ARTICLES

1. Kovar C, Loer HLH, Rüdesheim S, Fuhr LM, Marok FZ, Selzer D, Schwab M, Lehr T. A physiologically-based pharmacokinetic precision dosing approach to manage dasatinib drug–drug interactions *CPT Pharmacometrics and Systems Pharmacology*. 2024. https://doi.org/10.1002/psp4.13146.

2. Loer HLH, Kovar C, Rüdesheim S, Marok FZ, Fuhr LM, Selzer D, Schwab M, Lehr T. Physiologically based pharmacokinetic modeling of imatinib and N-desmethyl imatinib for drug–drug interaction predictions *CPT Pharmacometrics and Systems Pharmacology*. 2024; 00:1-15. https://doi.org/10.1002/psp4.13127.

3. Marok FZ, Wojtyniak JG, Selzer D, Dallmann R, Swen JJ, Guchelaar HJ, Schwab M, Lehr T. Personalized chronomodulated 5-fluorouracil treatment: A physiologically-based pharmacokinetic precision dosing approach for optimizing cancer therapy. *Clinical Pharmacology and Therapeutics*. 2024; 0:1-11. https://doi.org/10.1002/cpt.3181.

4. Fuhr LM, Marok FZ, Fuhr U, Selzer D, Lehr T. Physiologically Based Pharmacokinetic Modeling of Bergamottin and 6,7-Dihydroxybergamottin to Describe CYP3A4 Mediated Grapefruit-Drug Interactions. *Clinical Pharmacology and Therapeutics*. 2023; 114(2): 470-482. https://doi.org/10.1002/cpt.2968.

5. Feick D, Rüdesheim S, Marok FZ, Selzer D, Loer HLH, Teutonico D, Frechen S, van der Lee M, Moes DJAR, Swen JJ, Schwab M, Lehr T. Physiologically-based pharmacokinetic modeling of quinidine to establish a CYP3A4, P-gp, and CYP2D6 drug–drug–gene interaction network. *CPT Pharmacometrics and Systems Pharmacology*. 2023; 00:1-14. https://doi.org/10.1002/psp4.12981.

6. Marok FZ, Wojtyniak JG, Fuhr LM, Selzer D, Schwab M, Weiss J, Haefeli WE, Lehr T. A Physiologically Based Pharmacokinetic Model of Ketoconazole and Its Metabolites as Drug–Drug Interaction Perpetrators. *Pharmaceutics*. 2023; 15(2):679. https://doi.org/10.3390/pharmaceutics15020679.

7. Fuhr LM, Marok FZ, Mees M, Mahfoud F, Selzer D, Lehr T. A Physiologically Based Pharmacokinetic and Pharmacodynamic

Model of the CYP3A4 Substrate Felodipine for Drug–Drug Interaction Modeling. *Pharmaceutics*. 2022; 14(7):1474. https://doi.org/10.3390/pharmaceutics14071474.

8. Marok FZ, Fuhr LM, Hanke N, Selzer D, Lehr T. Physiologically Based Pharmacokinetic Modeling of Bupropion and Its Metabolites in a CYP2B6 Drug-Drug-Gene Interaction Network. *Pharmaceutics*. 2021; 13(3):331. https://doi.org/10.3390/pharmaceutics13030331.

9. Fuhr LM, Marok FZ, Hanke N, Selzer D, Lehr T. Pharmacokinetics of the CYP3A4 and CYP2B6 Inducer Carbamazepine and Its Drug–Drug Interaction Potential: A Physiologically Based Pharmacokinetic Modeling Approach. *Pharmaceutics*. 2021; 13(2):270. https://doi.org/10.3390/pharmaceutics13020270.

A.2 REVIEW ARTICLES

1. Türk D, Fuhr LM, Marok FZ, Rüdesheim S, Kühn A, Selzer D, Schwab M, Lehr T. Novel models for the prediction of drug-gene interactions. *Expert Opinon Drug Metabolism and Toxicology*. 2021;17(11):1293-1310. https://doi.org/10.1080/17425255.2021.1998455.

A.3 CONFERENCE ABSTRACTS AND POSTERS

1. Marok FZ, Wojtyniak JG, Fuhr LM, Selzer D, Schwab M, Weiss J, Haefeli WE, Lehr T. A Physiologically-based pharmacokinetic modeling of drug-drug interactions with ketoconazole and its metabolite deacetyl-ketoconazole. In: 30th Population Approach Group Europe (PAGE) meeting, 2022, Ljubljana, Slovenia.

2. Fuhr LM, Marok FZ, Lehr T. Peeling the grapefruit – investigating the drug interaction potential of grapefruit juice as CYP3A4 inhibitor using physiologically-based pharmacokinetic modeling. In: 30th Population Approach Group Europe (PAGE) meeting, 2022, Ljubljana, Slovenia.

3. Marok FZ, Wojtyniak JG, Schwab M, Lehr T. Optimizing 5-fluorouracil chemotherapy with regard to DPD drug-gene interactions and circadian effects utilizing a physiologically based pharmacokinetic (PBPK) modeling approach. In: Annual Meeting of the German Pharmaceutical Society (DPhG), 2019, Heidelberg, Germany. *Received award for best poster*.

4. Marok FZ, Wojtyniak JG, Schwab M, Lehr T. Physiologically-based pharmacokinetic modeling of DPYD substrate 5-fluorouracil and its prodrug capecitabine. In: 28th Population

Approach Group Europe (PAGE) meeting, 2019, Stockholm, Sweden.

5. Wojtyniak JG, Britz H, Marok FZ, Türk D, Fuhr LM, Kovar L, Hanke N, Schwab M, Lehr T. Physiologically-based Pharmaokinetic (PBPK) Modelling of a CYP3A4/P-gp DDI Network with Ketoconazole, Midazolam, Alfentanil, Repaglinide and Digoxin. In: Doktorandentagung of the German Pharmaceutical Society (DPhG), 2019, Darmstadt, Germany.

A.4 ORAL PRESENTATIONS

1. Marok FZ, Wojtyniak JG, Swen JJ, Guchelaar HJ, Schwab M, Lehr T. Model Based Chronomodulated Precision Dosing of 5 Fluorouracil – A Physiologically Based Pharmacokinetic Modeling Approach. In: PK/PD Expert Meeting – Arbeitsgemeinschaft für angewandte Humanpharmakologie e.V., 2022, Saarbruecken, Germany. *Received award for best presentation*.

2. Marok FZ. Therapie und Biorhythmen – Ticken wir alle gleich? In: Science Slam – MS Wissenschaft, 2022, Saarbruecken, Germany. https://www.youtube.com/watch?v=Al0FqXunyVA.

ACKNOWLEDGMENTS

Hiermit möchte ich mich bei all denjenigen bedanken, die mich tatkräftig während meiner Promotion unterstützt haben.

Allen voran danke ich Prof. Dr. Thorsten Lehr, dass er mir die Möglichkeit geboten hat, meine Doktorarbeit unter seiner Führung zu realisieren. Besonders schätze ich seine Geduld, Unterstützung und Expertise sowie den kreativen Freiraum, den er mir oft einräumte. Diese Freiheiten ermöglichten es mir, verschiedene spannende Projekte zu verfolgen und zu verwirklichen. Darüber hinaus bin ich ihm auch sehr dankbar dafür, dass er mich und andere bereits während des Studiums für das Gebiet der pharmakometrischen Modellierung begeistern konnte.

Ich möchte mich auch bei Prof. Dr. Markus R. Meyer, meinem Zweitgutachter, für seine wissenschaftliche Unterstützung bedanken. Mein Dank gilt ebenso all meinen Ko-Autoren für ihren wertvollen Input bei der Realisierung und Anfertigung meiner Publikationen.

Besonders bedanken möchte ich mich bei all meinen Kolleginnen und Kollegen der Klinischen Pharmazie, vor allem bei Dr. Jan-Georg Wojtyniak, für seine intensive Betreuung, insbesondere während meiner Diplomzeit, die mir den Einstieg in die PBPK-Modellierung erleichtert hat. Mein Dank geht auch an Dr. Nina Hanke und Dr. Dominik Selzer, die sich gerne die Zeit nahmen, mir bei kniffeligen Fragestellungen fachlich beizustehen. Mein besonderer Dank gilt auch unserem "Team PBPK", allen voran Laura Fuhr, Dr. Denise Feick, Hannah Britz, Dr. Simeon Rüdesheim, Helena Loer sowie Christina Kovar und Dr. Lukas Kovar für die hervorragende Zusammenarbeit und die zahlreichen gemeinsamen Diskussionsrunden.

Zu guter Letzt möchte ich mich auch bei meinen Freunden bedanken, die mir vor allem mental zur Seite standen und immer ein offenes Ohr für mich hatten. Ein großer Dank gilt meiner Familie, meinen Geschwistern und meinen Eltern, Khadija und Abdelkader Marok, dafür dass sie viel auf sich genommen haben, um uns ein sicheres und herzliches Zuhause zu bieten und mich bei all meinen Entscheidungen unterstützt haben.

أشكركم من أعماق قلبي على دعمكم لي طوال هذه السنوات. لولاكم ولولا الله سبحانه وتعالى لما كان هذا ممكناً. شكراً جزيلاً

B

SUPPLEMENTARY MATERIALS

1. Supplementary Materials of project I: Marok FZ, Fuhr LM, Hanke N, Selzer D, Lehr T. Physiologically Based Pharmacokinetic Modeling of Bupropion and Its Metabolites in a CYP2B6 Drug-Drug-Gene Interaction Network. *Pharmaceutics*. 2021; 13(3):331. https://doi.org/10.3390/pharmaceutics13030331.

2. Supplementary Materials of project II: Marok FZ, Wojtyniak JG, Fuhr LM, Selzer D, Schwab M, Weiss J, Haefeli WE, Lehr T. A Physiologically Based Pharmacokinetic Model of Ketoconazole and Its Metabolites as Drug–Drug Interaction Perpetrators. *Pharmaceutics*. 2023; 15(2):679. https://doi.org/10.3390/pharmaceutics15020679.

3. Supplementary Materials of project III: Marok FZ, Wojtyniak JG, Selzer D, Dallmann R, Swen JJ, Guchelaar HJ, Schwab M, Lehr T. Personalized chronomodulated 5-fluorouracil treatment: A physiologically-based pharmacokinetic precision dosing approach for optimizing cancer therapy. *Clinical Pharmacology and Therapeutics*. 2024; 0:1-11. https://doi.org/10.1002/cpt.3181.

Pharmaceutics

Physiologically Based Pharmacokinetic Modeling of Bupropion and its Metabolites in a CYP2B6 Drug-Drug-Gene Interaction Network

Supplementary Materials

Fatima Zahra Marok[1], Laura Maria Fuhr[1], Nina Hanke[1], Dominik Selzer[1], and Thorsten Lehr[1]

[1]Clinical Pharmacy, Saarland University, Saarbrücken, Germany

Funding:
The project has received support from the project “Open-source modeling framework for automated quality control and management of complex life science systems models” (OSMOSES), which is funded by the German Federal Ministry of Education and Research (BMBF, grant ID: 031L0161C). We acknowledge support by the Deutsche Forschungsgemeinschaft (DFG, German Research Foundation) and Saarland University within the funding programe “Open Access Publishing”.

Conflict of Interest:
Thorsten Lehr has received research grants from the German Federal Ministry of Education and Research (grant 031L0161C). Fatima Zahra Marok, Laura Maria Fuhr, Nina Hanke and Dominik Selzer declare no conflict of interest. The funders had no role in the design of the study; in the collection, analyses, or interpretation of data; in the writing of the manuscript, or in the decision to publish the results.

Corresponding Author:
Prof. Dr. Thorsten Lehr
Clinical Pharmacy, Saarland University
Campus C2 2, 66123 Saarbrücken, Germany
Phone: +49 681 302 70255
Email: thorsten.lehr@mx.uni-saarland.de

Contents

1 PBPK modeling

1.1 PBPK model building

A parent-metabolite PBPK model for bupropion and its metabolites hydroxybupropion, erythrohydrobupropion and threohydrobupropion was developed. The metabolic pathways and interactions implemented to describe their pharmacokinetics in the CYP2B6 network are illustrated in Figure S1.1.1. Physiological parameters, such as tissue volumes or surface areas, are predefined in the PBPK modeling software PK-Sim® (Version 9.1) [1]. Further system-dependent parameters such as reference concentrations (concentration in the tissue with the highest expression) and tissue expression profiles of metabolizing enzymes and transporters, are listed in Table S1.1. Demographic data were derived from the collected clinical study reports and are listed in the study tables of the respective sections. The drug-dependent parameters of the developed bupropion parent-metabolite PBPK model are listed in Section 2.

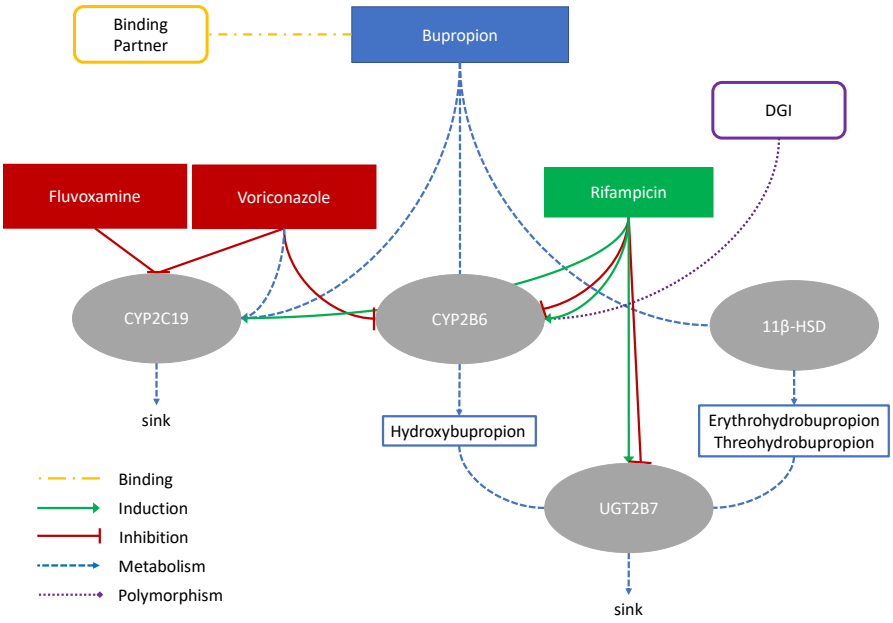

Figure S1.1.1: **Metabolic pathways and interactions implemented in the CYP2B6 network**. Bupropion is metabolized via CYP2B6 to hydroxybupropion and via 11β-HSD to erythrohydrobupropion and threohydrobupropion. Additionally, CYP2C19-mediated metabolism was included. Since bupropion binds to different therapeutic targets, binding to an unspecific protein (Binding Partner) was implemented as well. The metabolites are further degraded by UGT2B7. Drug-gene-interactions (DGIs), drug-drug-interactions (DDIs) as well as drug-drug-gene-interactions (DDGIs) were simulated for CYP2B6 with the perpetrators rifampicin, fluvoxamine and voriconazole. **11β-HSD**, 11β-hydroxysteroid dehydrogenase; **CYP**, cytochrome P450; **DGI**, drug-gene-interaction; **UGT**, uridine 5'-diphosphoglucuronosyltransferase.

Bupropion formulations

For simulation of oral tablets with different bupopion release, the weibull function was used according to Equation S1 [73], to describe immediate, sustained, and extended release formulations, as well as the cocktail capsule formulation (Geneva cocktail [74]) used in the Bosilkovska et al. 2014 and 2016 studies [24, 74].

Weibull model

$$m = 1 - exp\left(\frac{-(t - T_{lag}^{b})}{a}\right) \text{ with } a = (T_d)^b \tag{S1}$$

a = scale parameter
b = shape paramter
m = fraction of the dissolved drug at time t
T_d = time needed to dissolve 63% of the formulation
T_{lag} = lag time before the onset of dissolution

The parameters used in the presented model are listed in the drug-dependent parameter table (Table S2.2).

1.2 Quantitative PBPK model evaluation

The model performance was evaluated by comparing predicted plasma concentration-time profiles to observed data which are displayed in the following sections in linear and semilogarithmic scale (Figures S2.4.2-S2.4.15) and in goodness-of-fit plots (Figure S2.5.16). Furthermore, the models were evaluated by comparing predicted to observed area under the plasma concentration-time curve (AUC) and maximum plasma concentration (C_{max}) values (Figures S2.5.17-S2.5.18). Figures S2.5.19-S2.5.22 illustrate results of local sensitivity analyses as bar graphs.
As quantitative performance measures, the mean relative deviation (MRD) was calculated for all profiles from their respective predicted and observed plasma concentrations (Equation (S2)). Furthermore, the geometric mean fold errors (GMFE) of the AUC_{last} (AUC from the first time point to the last time point of concentration measurement of drug administration) and C_{max} were calculated according to Equation (S3).

Equation: Mean relative deviation

$$MRD = 10^x \text{ with } x = \sqrt{\frac{1}{n}\sum_{i=1}^{n}(\log_{10}\hat{c}_i - \log_{10} c_i)^2} \tag{S2}$$

c_i = the i^{th} observed plasma concentration
$\hat{c}_i$ = the respective predicted plasma concentration
n = number of observed values

Overall MRD values of ≤ 2 were considered reasonable predictions.
The GMFE was calculated for all AUC_{last} and C_{max} values according to Equation (S3).

Equation: Geometric mean fold error

$$GMFE = 10^x \text{ with } x = \frac{1}{n}\sum_{i=1}^{n}|\log_{10}(\frac{\hat{a}_i}{a_i})| \tag{S3}$$

a_i = the i^{th} observed AUC_{last} or C_{max} value
$\hat{a}_i$ = the respective predicted AUC_{last} or C_{max} value
n = number of studies

Overall GMFE values of ≤ 2 were considered reasonable predictions.

1.3 Sensitivity analysis

Sensitivity of the final models to single parameter changes (local sensitivity analysis) was calculated as relative change of the AUC_{last}. It was carried out using a relative perturbation of 1000% (variation range 10.0, maximum number of 9 steps). Parameters were included into the analysis if they were optimized or assumed to have an impact on AUC. Sensitivity to a parameter was calculated as the ratio of relative

change of the simulated AUC_{last} to the relative variation of the parameter value used in the final model according to Equation (S4).

Equation: Sensitivity analysis

$$S = \frac{\Delta AUC_{last}}{\Delta p} * \frac{p}{AUC_{last}} \tag{S4}$$

ΔAUC = change of the AUC_{last}
AUC = simulated AUC_{last} with the original parameter value
Δp = change of the examined parameter value
p = original parameter value
S = sensitivity of the AUC_{last} to the examined model parameter

A sensitivity of + 1.0 signifies that a 10% increase of the examined parameter value causes a 10% increase of the simulated AUC_{last}.

1.4 System-dependent parameters

System-dependent parameters, such as reference concentrations and tissue expression profiles of metabolizing enzymes and transporters, are listed in Table S1.1.

Table S1.1: System-dependent parameters.

Protein (*Gene*)	Reference concentration		Relative expression [a]	Localization	Half-life [h]	
	Mean[b] [µmol/l]	GeoSD[c]			Liver	Intestine
CYP2B6 (*CYP2B6*)	1.56	[d]1.40	RT-PCR [2]	intracellular	32	23
CYP2C19 (*CYP2C19*)	0.76	1.79 [16]	RT-PCR [2]	intracellular	26	23
11β-HSD (*HSD11B1*)	[e]1.0	[d]1.40	Array [3]	intracellular	36	23
UGT2B7 (*UGT2B7*)	[f]0.28 [4]	1.56 [16]	EST [5]	intracellular	36	23
NRT[g] (*SLC6A2*)	[e]1.0	[d]1.40	EST [5]	[h]membrane	36	23

11β-HSD, 11β-hydroxysteroid dehydrogenase 1; **conc.**, concentration **CYP**, cytochrome P450; **Array**, microarray expression profile; **EST**, expressed sequence tag expression profiles from UniGene; **NRT**, noradrenaline reuptake transporter; **RT-PCR**, reverse transcription-polymerase chain reaction measured expression profile; **UGT**, uridine 5'-diphospho-glucuronosyltransferase.
[a], in the different organs (PK-Sim® expression database profile)
[b], µmol protein/l in the tissue of highest expression
[c], geometric standard deviation of the reference concentration
[d], if no information was available, a moderate variability of 35% CV was assumed (1.40 GeoSD)
[e], no information was available, thus, the mean reference concentration was set to 1.0 µmol/l and the catalytic rate constant (k^{cat}) was optimized according to Meyer et al. 2012 [6].
[f], calculated from transporter per mg membrane protein times 26.2 mg human kidney microsomal protein per g kidney tissue [7]
[g], expression profile used for general binding partner
[h], extracellular membrane

Virtual individual

Proteins were implemented for every modeled individual. The individuals were created based on the demographics mentioned in the respective clinical study report. If no data was available a standard individual was used. This standard individual, similar to the Standard European Male implemented in OSP®, is based on the demographic databases used in the modeling software. Additionally, every individual had an activated enterohepatic circulation (EHC continuous fraction = 1). The characteristics of the standard individuals are compared in Table S1.2.

Virtual population

Virtual population were created based on 500 individuals, with their demographic information (age range, sex composition, ethnicity) derived from the respective clinical study report. If no information on ethnicity and sex composition was given, a 100% European male population with and age range of 20-50 years was assumed. System-dependent parameters, e.g. weight, height, organ volumes or blood flow rates, were varied by the implementd algorithm in PK-Sim® based on the limits of the following databases: American: Third National Health and Nutrition Examination Survey (NHANES)[15] database, Asian: Tanaka model [9], European: International Commission on Radiological Protection (ICRP) database [8]. The reference concentrations of the metaolizing enzymes and transporters as listed in Table S1.1, were log-normaly distributedmaccording to the variabilty reported in the ontogeny database implemented in PK-Sim® [16]. If no information could be found, reference concentrations were distributed with a variability of 35% CV (geometric standard deviation of 1.4).

Table S1.2: Standard individual demographics.

Individual	Age [years]	Weight [kg]	Height [cm]	BSA [m²]	BMI [kg/m²]	Reference
OSP® - Standard European Male[a]	30	73	176	1.89	23.57	[8]
European Female[b]	30	60	163	1.65	22.58	[8]
Asian Male[c]	30	60	170	1.68	20.78	[9]

BMI, body mass index; **BSA**, body surface area; **OSP®**, open systems pharmacology®.
[a], standard individual implemented in the modeling software, used for every study where demographical data was missing
[b], only used for Palovaara 2003 [10]
[c], only used for Fan 2009 [11], Gao 2012 [12], Gao 2016 [13] and Qin 2012 [14], since asian populations was assumed.

1.5 Implementation - Interaction modeling

1.5.1 Drug-gene-interaction

In order to describe the effect of different *CYP2B6* genotypes on the compounds' PK, the enzyme activity was implemented as two enzymes for each allele. The single alleles were modeled with Michaelis-Menten constant (K_M) values from literature (after correction for microsomal binding). For two genetic variants (*CYP2B6*4* and *CYP2B6*5*), the catalytic rate constant, k_{cat} was calculated from reported maximum velocity (V_{max}) in vitro measurements. For *CYP2B6*1* and *CYP2B6*6*, k_{cat} was optimized with reported plasma concentration-time profiles of populations with homozygous expression of the respective haplotype. All DGI parameters are shown in Table S3.2 in Section 3.1.

1.5.2 Drug-drug-interaction

DDIs were simulated for bupropion as the victim drug. For the CYP2B6 interaction network, the investigated perpetrators included rifampicin as inducer and fluvoxamine and voriconazole as inhibitors. Interaction parameters were informed from the literature and are listed in the respective parameter tables (Table S4.1,S4.2 and S4.3).

Mathematical implementation of induction

Drug-induced increase of gene expression and therefore, enzyme activity, was calculated as shown in Equations (S5) and (S6).

Implementation of enzyme induction

$$\frac{d[E]}{dt} = R_{syn,app} - k_{deg} * [E] \tag{S5}$$

$$R_{syn,app} = R_{syn} * (1 + \frac{E_{max} * [I]}{EC_{50} + [I]}) \tag{S6}$$

$\frac{d[E]}{dt}$ = enzyme turnover rate
$[E]$ = enzyme concentration
EC_{50} = inducer concentration to reach half-maximal induction in vivo
E_{max} = maximum induction effect in vivo
$[I]$ = free inducer concentration
k_{deg} = degradation rate constant
R_{syn} = enzyme synthesis rate in absence of inducer
$R_{syn,app}$ = enzyme synthesis rate in presence of inducer

Mathematical implementation of inhibition

Inhibition of enzyme activites was implemented as a competitive inhibition process. Competitive inhibition occurs if the inhibitor binds reversibly to the active site of an enzyme and hence, competes with

the substrate over the binding spot. Since the inhibitor binds reversibly to the enzyme, high substrate concentrations can overcome its inhibition. The process is calculated as shown in Equations (S7) and (S8).

Implementation of enzyme inhibition

$$v = \frac{V_{max} * [S]}{K_{M,app} + [S]} \tag{S7}$$

$$K_{M,app} = K_M * (1 + \frac{[I]}{K_I}) \tag{S8}$$

I = free inhibitor concentration
K_I = dissociation constant of the inhibitor-enzyme complex
K_M = Michaelis-Menten constant in absence of inhibitor
$K_{M,app}$ = apparent Michaelis-Menten constant in presence of inhibitor
S = free substrate concentration
v = reaction velocity
V_{max} = maximum reaction velocity

1.5.3 Drug-drug-gene-interaction

Drug-drug-gene-interactions (DDGIs) were simulated for various genotypes after concomitant rifampicin intake. The underlying effects on the PK were implemented according to the Sections 1.5.1 and 1.5.2.

1.6 Evaluation - Interaction modeling

1.6.1 Drug-gene-interaction

In addition to Section 1.2, the effect of DGIs was evaluated by calculation of the ratio of hydroxybupropion to bupropion AUC_{last} and C_{max} values in plasma as shown in Equation (S9).The calculated ratios are illustrated in Figure S3.5.4.

DGI effect ratio

$$PK_{HBup/Bup} = \frac{PK(HBup)}{PK(Bup)} \tag{S9}$$

Bup = PK parameter of bupropion
$HBup$ = PK parameter of hydroxybupropion
$PK_{HBup/Bup}$ = HBup/Bup ratio of the PK parameter
PK = PK parameter such as AUC_{last} or C_{max}

Additionally, DGI effect ratios for the ratio of hydroxybupropion to bupropion AUC_{last} and C_{max} values were calculated according to Equation (S10) for predicted and observed concentrations. The calculated ratios are illustrated in Figure S3.5.4.

DGI effect hydroxybupropion/bupropion ratio

$$DGI\ PK_{HBup/Bup} = \frac{PK_{HBup/Bup}(Effect)}{PK_{HBup/Bup}(Control)} \text{ with } PK_{HBup/Bup} = \frac{PK_{HBup}}{PK_{Bup}} \tag{S10}$$

Bup = bupropion
$HBup$ = hydroxybupropion
$PK_{HBup/Bup}(Control)$ = HBup/Bup ratio of the PK parameter of wildtype CYP2B6
$PK_{HBup/Bup}(Effect)$ = HBup/Bup ratio of the PK parameter of a variant CYP2B6 genotype
PK = PK parameter such as AUC_{last} or C_{max}

1.6.2 Drug-drug-interaction

Similar to the DGIs, the effect of DDIs was evaluated by calculation of the ratio of hydroxybupropion to bupropion AUC_{last} and C_{max} values according to Equation (S9). The calculated ratios are illustrated in Figure S4.6.4. Additionally, DDI effect ratios for the ratio of hydroxybupropion to bupropion AUC_{last} and C_{max} were calculated as shown in Equation (S11) for predicted and observed concentrations. The calculated DDI ratios are illustrated in Figure S4.6.4.

DDI effect hydroxybupropion/bupropion ratio

$$DDI\ PK_{HBup/Bup} = \frac{PK_{HBup/Bup}(Effect)}{PK_{HBup/Bup}(Control)} \text{ with } PK_{HBup/Bup} = \frac{PK_{HBup}}{PK_{Bup}} \quad \text{(S11)}$$

Bup = bupropion
$HBup$ = hydroxybupropion
$PK_{HBup/Bup}(Control)$ = HBup/Bup ratio of the PK parameter without perpetrator
$PK_{HBup/Bup}(Effect)$ = HBup/Bup ratio of the PK parameter with perpetrator
PK = PK parameter such as AUC_{last} or C_{max}

1.6.3 Drug-drug-gene-interaction

The majority of compiled DDGI data only included AUC_{inf} (AUC extrapolated to infinity) ratios of hydroxybupropion and bupropion, with only one study showing plasma concentration-time profile. Hence, the effect of DDGIs was evaluated by calculation of DDGI effect ratios for $AUC_{HBup/Bup}$ (AUC_{last} or AUC_{inf}) in plasma as shown in Equation (S12). The calculated DDGI effect ratios for the ratio of hydroxybupropion to bupropion are illustrated in Figure S5.4.2.

DDGI effect hydroxybupropion/bupropion ratio

$$DDGI\ AUC_{inf,HBup/Bup} = \frac{AUC_{inf,HBup/Bup}(Effect)}{AUC_{inf,HBup/Bup}(Control)} \text{ with } AUC_{inf,HBup/Bup} = \frac{AUC_{inf,HBup}}{AUC_{inf,Bup}} \quad \text{(S12)}$$

Bup = bupropion
$HBup$ = hydroxybupropion
$AUC_{inf,HBup/Bup}(Control)$ = HBup/Bup ratio of AUC_{inf} of wildtype CYP2B6 without perpetrator
$AUC_{inf,HBup/Bup}(Effect)$ = HBup/Bup ratio of AUC_{inf} of a variant CYP2B6 genotype with perpetrator

2 Bupropion model development

2.1 Background

Bupropion is a noradrenaline and dopamine reuptake inhibitor used in the treatment of major depressive disorder and to aid smoking cessation [17]. In therapy, the compound is either administered as monotherapy or in combination with additional anti-depressant agents [17, 18]. Bupropion is pharmacologically active, but is also transformed to three active metabolites [19].
One metabolite, hydroxybupropion, is formed by CYP2B6 mediated hydroxylation of bupropion. Erythro- and threohydrobupropion are formed through several metabolic steps of which reduction by carbonyl reductase 11β-HSD metabolizes is the rate-limiting step [20]. To some extent, further CYP enzymes, i.e. CYP2C19, are also involved in bupropion degradation [21]. Therefore, the presented model includes transformation via CYP2B6, 11β-HSD and CYP2C19. The three metabolites are subsequently glucuronidated via UGT2B7, which is also implemented in the model.
Bupropion binds and inhibits reuptake transporters for noradrenaline, dopamine and acetylcholine [22, 23]. This target-mediated binding was modeled by implementation of a surrogate binding parther, representing various different targets. An expression profile of the noradrenaline reuptake transpoter 1 was used for the surrogate binding partner.
Data from 48 clinical studies were used for model development and split into a training dataset, used for model building and parameter optimization, and a test dataset, used for model evaluation. Here, bupropion (20 mg to 450 mg) was administered as oral formulations with different release kinetics (Table S2.1). Drug-dependent parameters for the parent-metabolite model featuring bupropion, hydroxybupropion, erythorhydrobupropion and threohydrobupropion are listed in Table S2.2.
Several model input parameters that could not be informed from the literature, were optimized, including k_{cat} values for all metabolic reactions. To model the target-binding of bupropion, binding to various pharmacological targets was summarized by including one target protein as a binding partner.
Figure S2.1.1 illustrates a quantitative mass-balance diagram of the elimination pathways of bupropion. Bupropion is predicted to be absorbed completely. Metabolism via CYP2B6 accounts for 58 %, 11β-HSD for 28% and CYP2C19 for 13% of total bupropion. In urine, 1% of unchanged bupropion is predicted to be excreted, while almost no bupropion can be simulated in faeces. Influence of the first pass metabolism could not be determined, as data of intravenous administration of bupropion were not available and therefore, not evaluated.
The good performance of the model is demonstrated in linear (Fig. S2.4.2, S2.4.3, S2.4.8, S2.4.9 and S2.4.14) and semilogarithmic plots (Fig. S2.4.5, S2.4.6, S2.4.11, S2.4.12 and S2.4.15) of predicted compared to observed plasma concentration-time profiles of all clinical studies. Furthermore, goodness-of-fit plots comparing predicted to their corresponding observed plasma concentrations are presented (Fig. S2.5.16) and calculated MRD values for each study are listed in Table S2.4. Additionally, correlation plots of predicted versus observed AUC_{last} and C_{max} values are shown in Figures S2.5.17 and S2.5.18. A summary of the respective PK parameters, including calculated GMFE values, is shown in Table S2.4. Local sensitivity analysis results for simulations of 300 mg bupropion administered as immediate release (100 mg three times daily), sustained release (150 mg two times daily) or extended release (300 mg once daily) tablets are presented in Section 2.5.5.

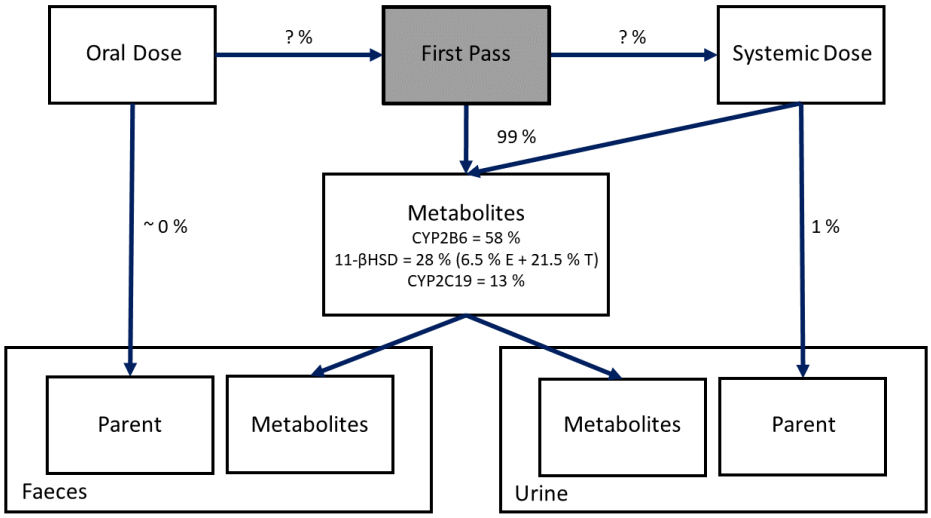

Figure S2.1.1: **Quantitative mass-balance diagram of the elimination pathways of bupropion**. Metabolism via CYP2B6, via 11β-HSD and CYP2C19 accounts for 99% of total bupropion. One % of bupropion is excreted unchanged to urine, while no bupropion is predicted to be in feces. **11β-HSD**, 11β-hydroxysteroid dehydrogenase; **CYP**, cytochrome P450; **E**, erythrohydrobupropion; **T**, threohydrobupropion.

2.2 Clinical studies

In Table S2.1, all clinical studies used for model development are listed. Virtual individuals were built according to the demographics published in the respective study reports. If no data on the demographics were reported, a standard individual was used as described in Section 1.4.

Table S2.1: Clinical studies used for bupropion model development.

Dosing	n	Age [years]	Weight [kg]	BMI [kg/m²]	Females [%]	*CYP2B6* genotype (n)	Dataset	Reference
20 mg Cap (s.d.)	30	23.5 (18–36)	-	21.7 (18.4–27.7)	50	**1/*6* (16), **6/*6* (1)	ta	Bosilkovska 2016 [24]
25 mg Cap (s.d.)	10	23 (20–36)	-	22 (19.9–24.4)	0	**1/*6* (4), **6/*6* (2)	te	Bosilkovska 2014 [25]
50 mg IR (s.d.)	24	19–43	-	-	50	-	ta	Findlay 1981 [26]
75 mg IR (s.d.)	20	18–55	72.3 (53.6–88.9)	19.5–28.3	50	-	ta	Zahner 2014 [27]
75 mg IR (s.d.)	7	18–45	-	-	100	-	te	Hesse 2006 [28]
75 mg IR (s.d.)	33	25–55	67.5 (56.3–107)	18.5–35	51.5	-	te	Connarn 2017 [18]
100 mg IR (s.d.)	33	25–55	67.5 (56.3–107)	18.5–35	51.5	-	ta	Connarn 2017 [18]
100 mg IR (s.d.)	24	19–43	-	-	50	-	ta	Findlay 1981 [26]
100 mg IR (s.d.)	15	24 (19–47)	74.8	25	40	-	te	Masters 2016 [29]
100 mg IR (s.d.)	24	43.5	72.9	26.5	45.8	-	te	Yamazaki 2017 [30]
100 mg IR (s.d.)	8	20-35	-	-	0	-	te	Posner 1984 [31]
100 mg IR (s.d.)	8	29.5 (22–42)	80 (66–101)	-	-	-	te	Posner 1985 [32]
100 mg IR (m.d.)	8	29.5 (22–42)	80 (66–101)	-	-	-	te	Posner 1985 [32]
100 mg IR (m.d.)	30	-	-	-	-	-	ta	Patent 1a (US2006/0228415A1) [33]
150 mg IR (s.d.)	10	31 (21–40)	73 (57–84)	-	60	-	ta	Kharasch 2008 [34]
150 mg IR (s.d.)	13	29 (23–39)	67 (53–84)	-	-	-	te	Kharasch 2008b [35]
200 mg IR (s.d.)	24	19–43	-	-	50	-	ta	Findlay 1981 [26]
100 mg SR (s.d.)	33	25–55	67.5 (56.3–107)	18.5–35	51.5	-	te	Connarn 2017 [18]
100 mg SR (s.d.)	12	20–44	-	-	16.7	-	te	Hogeland 2007 [36]
150 mg SR (m.d.)	42	31.8 (19–64)	74.7 (56.2–105.4)	25.4 (18.7–39.5)	38	**1/*5* (2), **1/*6* (6), **5/*6* (3), **6/*6* (4)	te	Benowitz 2013 [37]
150 mg SR (s.d.)	22	22.7	65	-	27.3	**1/*4* (3), **1/*6* (11), **6/*6* (2)	ta	Chung 2011 [38]
150 mg SR (s.d.)	33	25–55	67.5 (56.3–107)	18.5–35	51.5	-	ta	Connarn 2017 [18]
150 mg SR (s.d.)	24	-	-	-	-	-	te	Dennison 2018 [39]
150 mg SR (s.d.)	17	-	-	-	-	**1/*6* (6), **6/*6* (5)	te	Fan 2009 [11]
150 mg SR (s.d.)	30	29 (18–53)	75 (56–96)	24 (20–30)	0	-	te	Farid 2008 [40]
150 mg SR (s.d.)	19	-	-	-	0	-	ta	Gao 2012 [12]
150 mg SR (s.d.)	34	26.2	66.5	-	47.1	-	te	Hsyu 1997 [41]
150 mg SR (s.d.)	14	21.3	61.3	-	0	-	te	Lei 2009 [42]
150 mg SR (s.d.)	18	21.3	62.7	-	0	-	te	Lei 2010 [43]
150 mg SR (s.d.)	18	22 (19–34)	72 (53–99)	23.1 (18.4–26.9)	0	**1/*4* (1), **1/*5* (1), **1/*6* (6), **5/*5* (1), **4/*6* (1), **6/*6* (1), **6/*14* (1)	ta	Loboz 2006 [44]
150 mg SR (s.d.)	12	20–25	50–75	18–27	100	-	ta	Palovaara 2003 [10]
150 mg SR (m.d.)	49	-	-	-	-	-	ta	Patent 1b (US2006/0228415A1) [33]
150 mg SR (m.d.)	7	-	-	-	-	-	te	Patent 2 (US8545880B2) [45]
150 mg SR (s.d.)	16	20–23	62–85	21–26	0	**1/*6* (6), **6/*6* (4)	te	Qin 2012 [14]
150 mg SR (s.d.)	13	39 (21–54)	86	-	23.1	-	te	Robertson 2008 [46]
150 mg SR (s.d.)	12	22–27	67–95	21–26	0	-	te	Turpeinen 2005 [47]

Table S2.1: Clinical studies used for bupropion model development. (continued)

Dosing	n	Age [years]	Weight [kg]	BMI [kg/m²]	Females [%]	*CYP2B6* genotype (n)	Dataset	Reference
150 mg SR (s.d.)	17	27.3 (21–50)	73.9 (±8.9)	23.5 (±2.0)	41.7	-	te	Turpeinen 2007 [48]
150 mg SR (s.d.)	10	39.6 (32–43)	78.2 (±18.6)	26.4 (±5.3)	50	-	te	Turpeinen 2007 [48]
150 mg SR (s.d.)	16	61.9 (50–70)	-	-	100	-	te	Turpeinen 2013 [49]
300 mg SR (s.d.)	24	29 (18–45)	77 (56–96)	-	0	-	te	Kustra 1999 [50]
150 mg ER (s.d.)	33	25–55	67.5 (56.3–107)	18.5–35	51.5	-	ta	Connarn 2017 [18]
300 mg ER (s.d.)	33	25–55	67.5 (56.3–107)	18.5–35	51.5	-	te	Connarn 2017 [18]
300 mg ER (m.d.)	30	-	-	-	-	-	te	Patent 1a (US 2006/0228415 A1) [33]
300 mg ER (m.d.)	49	-	-	-	-	-	ta	Patent 1b (US 2006/0228415 A1) [33]
300 mg ER (m.d.)	38	-	-	-	-	-	te	Patent 3 (US7,645,802B2) [51]
300 mg ER (m.d.)	16	24.3	-	22.7	50	-	te	Schmid 2012 [52]
300 mg ER (m.d.)	-	-	-	-	-	-	ta	Woodcock 2012 [53]
450 mg ER (m.d.)	20	-	-	-	-	-	te	Paiement 2012 [54]

BMI, body mass index; **Cap**, capsule (Geneva cocktail [25]); **CYP**, cytochrome P450; **ER**, extended release formulation; **IR**, immediate release formulation; **m.d.**, multiple dose; **n**, number of individuals studied; **s.d.**, single dose; **SR**, sustained release formulation; **ta**, training dataset; **te**, test dataset; **-**, no data available. Values are given as mean ± standard deviation (SD), the range of values is given in brackets.

2.3 Drug-dependent model parameters

Table S2.2 lists the drug-dependent parameters used in model development of the final parent-metabolite model.

Table S2.2: Drug-dependent parameters of the bupropion PBPK model.

Parameter	Unit	Value	Source	Reference	Value	Source	Reference	Value	Source	Reference	Description
		Bupropion			Hydroxybupropion			Erythro-/Threohydrobupropion			
MW	g/mol	239.74	lit.	[55]	255.74	lit.	[56]	241.76	lit.	[57]	Molecular weight
pKa (base)	-	8.75	lit.	[58]	7.65	lit.	[56]	9.71	lit.	[57]	Acid dissociation constant
Solubility (pH)	mg/ml	364.56 (7.4)	lit.	[59]	0.91 (7.4)	lit.	[56]	82.98 (7.4)	lit.	[57]	Solubility
logP	-	[a]2.70	3.27	[55]	[a]1.90	2.20	[60]	[a]1.76	2.88	[61]	Lipophilicity
fu	%	16.00	lit.	[62]	23.00	lit.	[62]	58.00	lit.	[62]	Fraction unbound
Spec. int. perm.	cm/min	[a]3.30E-5	[b]2.42E-4	-	[b]2.78E-5	[b]2.78E-5	-	[b]2.64E-5	[b]2.64E-5	-	Normalized to surface area
Org. perm.	cm/min	[b]0.14	[b]0.14	-	[b]0.01	[b]0.01	-	[b]0.01	[b]0.01	-	Normalized to surface area
GFR frac.	-	1.00	asm.	-	1	asm.	-	1	asm.	-	Fraction of filtered drug in urine
EHC cont. frac.	-	1.00	asm.	-	1	asm.	-	1	asm.	-	Bile fraction continuously released
Cell. perm.	cm/min	Ch. d. S.	-	[63]	Ch. d. S.	-	[63]	Ch. d. S.	-	[63]	Permeation across cell membranes
Part. coef.	-	PK-Sim	-	[1]	Berez.	-	[64]	Berez.	-	[64]	Organ-plasma partition coefficients
11β-HSD K_M	µmol/l	39.10	lit.	[65]	-	-	-	-	-	-	11β-HSD Michaelis-Menten constant
11β-HSD kcat (EBup)	1/min	[a]2.15	-	-	-	-	-	-	-	-	11β-HSD catalytic rate constant for formation of EBup
11β-HSD kcat (TBup)	1/min	[a]8.18	-	-	-	-	-	-	-	-	11β-HSD catalytic rate constant for formation of TBup
CYP2B6 K_M	µmol/l	[c]25.80	lit.	[66]	-	-	-	-	-	-	CYP2B6 Michaelis-Menten constant
CYP2B6 kcat	1/min	[a]21.74	-	-	-	-	-	-	-	-	CYP2B6 catalytic rate constant for wildtype
CYP2C19 K_M	µmol/l	8.30	lit.	[67]	-	-	-	-	-	-	CYP2C19 Michaelis-Menten constant
CYP2C19 kcat	1/min	[a]2.59	-	-	-	-	-	-	-	-	CYP2C19 catalytic rate constant
BP K_D	µmol/l	[a]0.44	[d] 0.35, 0.53, 0.87, 6.98	[68–70]	-	-	-	-	-	-	Dissociation constant for binding
BP koff	1/min	[a]0.05	-	-	-	-	-	-	-	-	Dissociation rate constant for binding
UGT2B7 K_M	µmol/l	-	-	-	[c]14.64	lit.	[71]	[c]9.33 (EBup), [c]6.22 (TBup)	lit.	[71]	UGT2B7 Michaelis-Menten constant
UGT2B7 kcat	1/min	-	-	-	[a]1.38	-	-	[a]0.38 (EBup), [a]0.10 (TBup)	-	-	UGT2B7 catalytic rate constant
Weibull shape	-	[a]4.43 (Cap)	-	-	-	-	-	-	-	-	Shape used for Weibull
	-	[a]0.75 (IR)	-	-	-	-	-	-	-	-	
	-	[a]1.00 (SR)	-	-	-	-	-	-	-	-	
	-	[a,f]0.60 (SR)	-	-	-	-	-	-	-	-	

Table S2.2: Drug-dependent parameters of the bupropion PBPK model. (continued)

Parameter	Unit	Value	Source	Reference	Value	Source	Reference	Value	Source	Reference	Description
	-	[e]1.88 (ER)	[e]1.88	[33]	-	-	-	-	-	-	
Weibull time	min	[a]10.64 (Cap)	-	-	-	-	-	-	-	-	Time of 50% dissolved
	min	[a]3.12 (IR)	-	-	-	-	-	-	-	-	
	min	[a]100.00 (SR)	-	-	-	-	-	-	-	-	
	min	[a,f]54.13 (SR)	-	-	-	-	-	-	-	-	
	min	[e]230.00 (ER)	[e]230.00	[33]	-	-	-	-	-	-	

11β-HSD, 11β-hydroxysteroid dehydrogenase 1; **asm.**, assumed; **Berez.**, Berezhkovskiy calculation method; **BP**, binding partner; **Cap**, capsule (Geneva cocktail [25]); **cell. perm.**, cellular permeabilities; **Ch. d. S.**, Charge dependent Schmitt calculation method; **CYP**, cytochrome P450; **EBup**, erythrohydrobupropion; **EHC**, enterohepatic circulation; **ER**, extended release formulation; **frac.**, fraction; **IR**, immediate release formulation; **GFR**, glomerular filtration rate; **lit.**, literature; **org. perm.**, organ permeability; **part. coeff.**, partition coefficients; **PK-Sim**, PK-Sim Standard calculation method; **spec. int. perm.**, specific intestinal permeability; **SR**, sustained release formulation; **TBup**, threohydrobupropion; **UGT**, uridine 5'-diphospho-glucuronosyltransferase; **-**, not available.

[a], optimized

[b], calculated parameter

[c], in vitro values corrected for binding in the assay using fraction unbound to microsomal protein measurements from the same study [72]

[d], range also includes inhibition constant values (K_i)

[e], calculated dissolution parameter after Langenbuchener et al. 1972 [73]

[f], used for Fan 2009 [11], Gao 2012 [12], Gao 2016 [13], Lei 2009 [42], Lei 2010 [43] and Qin 2012 [14]

2.4 Concentration-time profiles

The geometric means of the population predictions (n=500) are shown as solid lines and corresponding observed data as filled dots. Symbols represent the arithmetic mean values ± standard deviation, if available. The shaded areas indicate the geometric standard deviation. Details on dosing regimens, study populations and literature references are listed in Table S2.1.

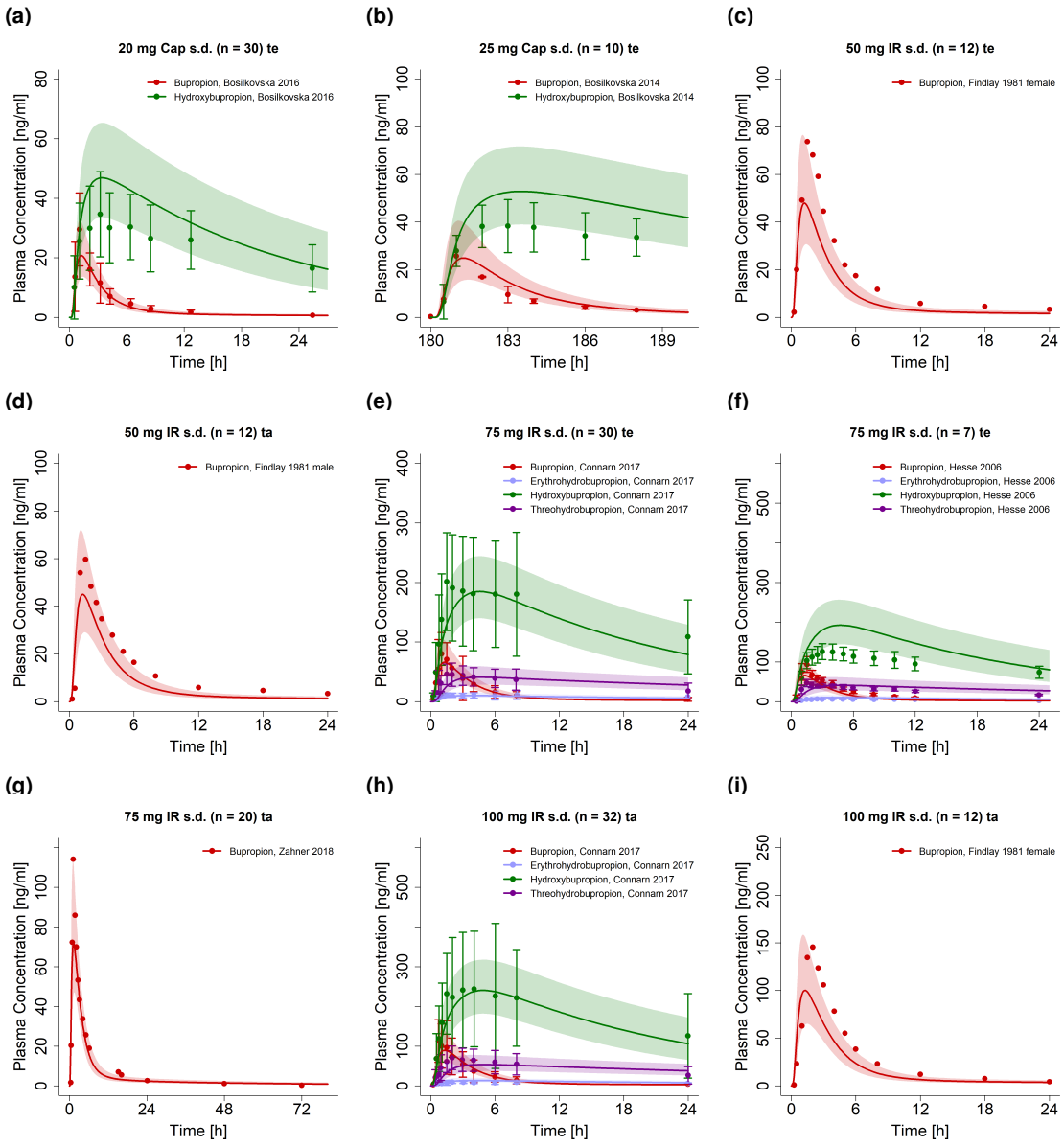

Figure S2.4.2: **Bupropion and metabolites after administration of single or multiple doses of bupropion as an immediate release formulation (part 1/3)** on a linear scale. **Cap**, capsule (Geneva cocktail [74]); **IR**, immediate release tablet; **m.d.**, multiple dose; **n**, number of individuals; **s.d.**, single dose; **ta**, training dataset; **te**, test dataset.

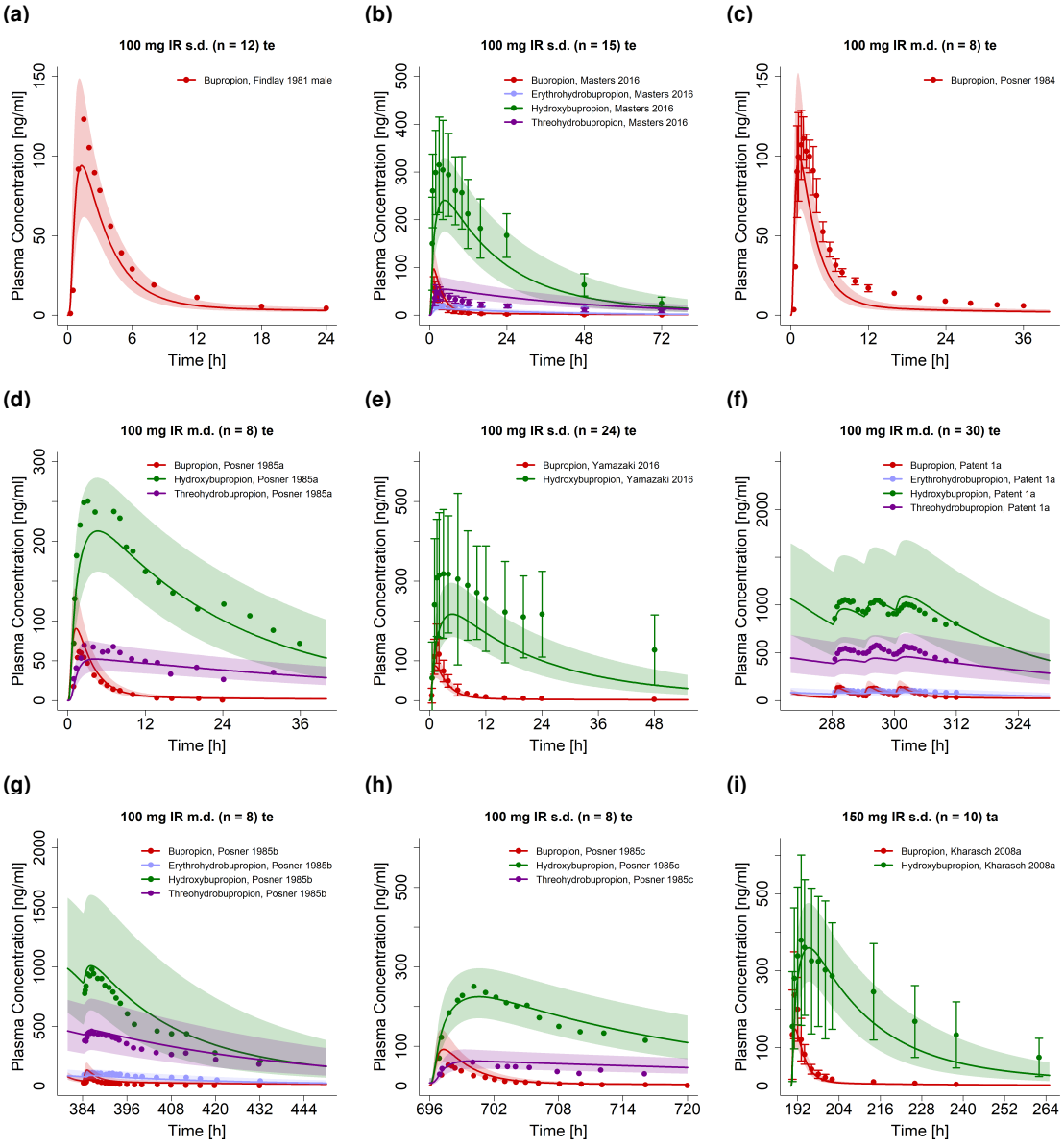

Figure S2.4.3: **Bupropion and metabolites after administration of single or multiple doses of bupropion as an immediate release formulation (part 2/3)** on a linear scale. **IR**, immediate release tablet; **m.d.**, multiple dose; **n**, number of individuals; **s.d.**, single dose; **ta**, training dataset; **te**, test dataset.

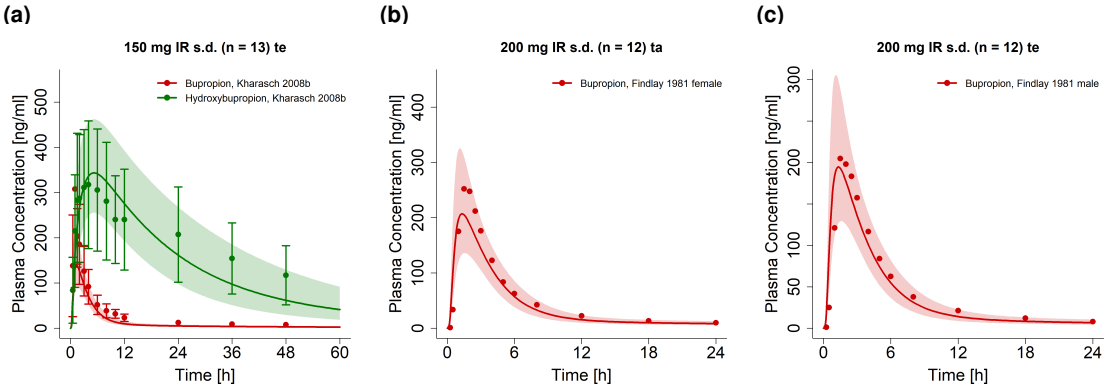

Figure S2.4.4: **Bupropion and metabolites after administration of single or multiple doses of bupropion as an immediate release formulation (part 3/3)** on a linear scale. **IR**, immediate release tablet; **m.d.**, multiple dose; **n**, number of individuals; **s.d.**, single dose; **ta**, training dataset; **te**, test dataset.

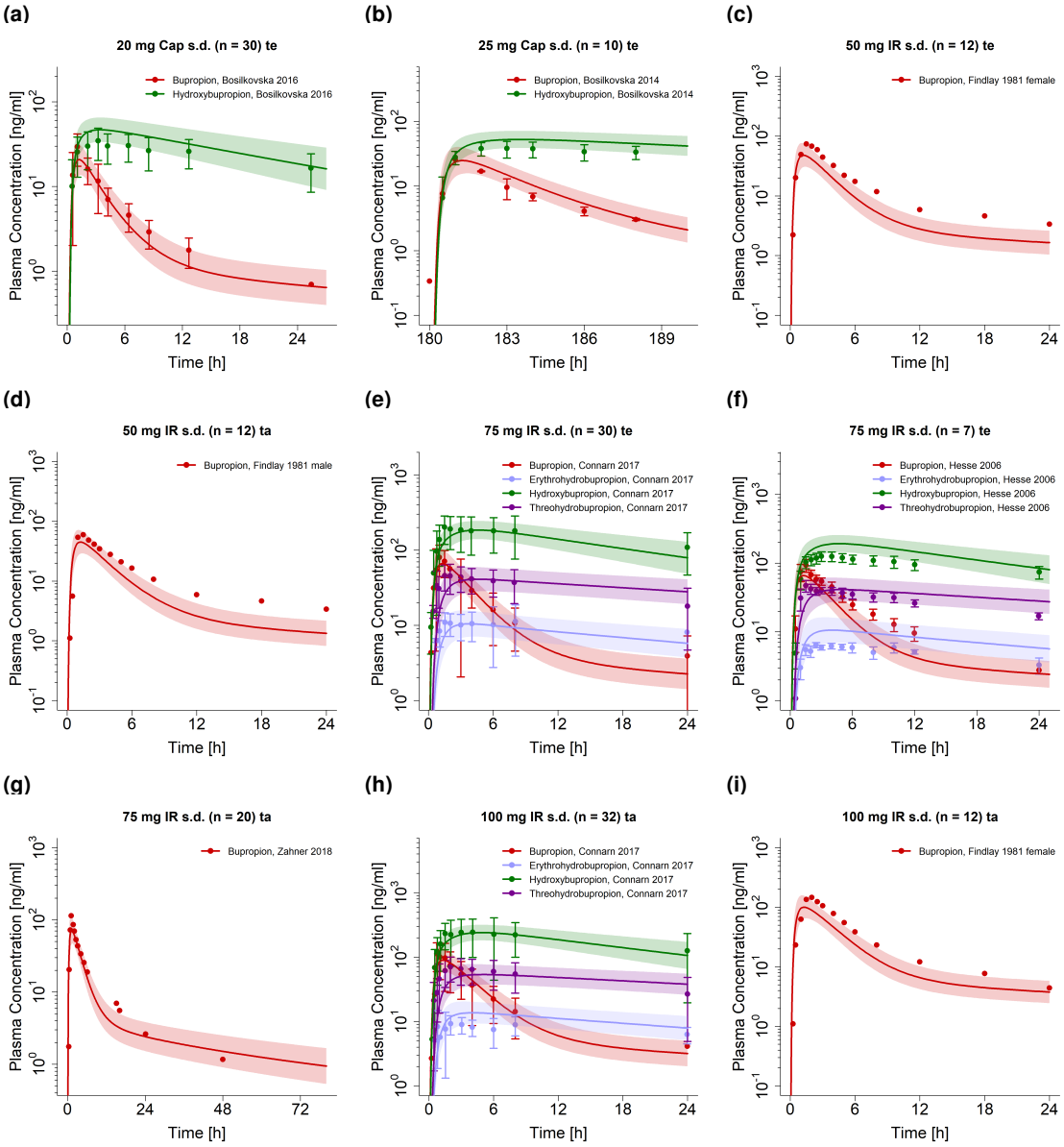

Figure S2.4.5: **Bupropion and metabolites after administration of single or multiple doses of bupropion as an immediate release formulation (part 1/3)** on a semi-logarithmic scale. **Cap**, capsule (Geneva cocktail [74]); **IR**, immediate release tablet; **m.d.**, multiple dose; **n**, number of individuals; **s.d.**, single dose; **ta**, training dataset; **te**, test dataset.

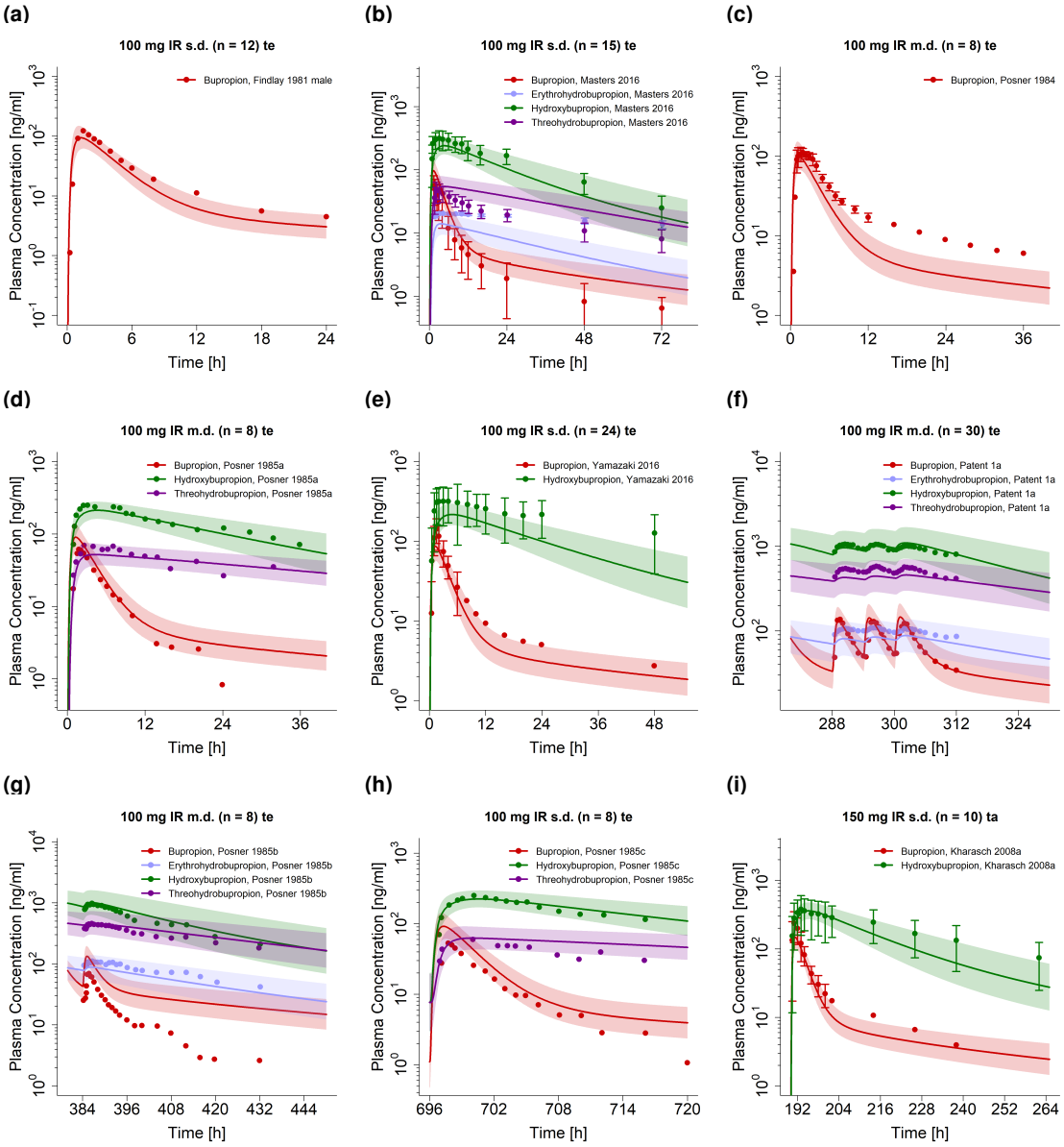

Figure S2.4.6: **Bupropion and metabolites after administration of single or multiple doses of bupropion as an immediate release formulation (part 2/3)** on a semi-logarithmic scale. **IR**, immediate release tablet; **m.d.**, multiple dose; **n**, number of individuals; **s.d.**, single dose; **ta**, training dataset; **te**, test dataset.

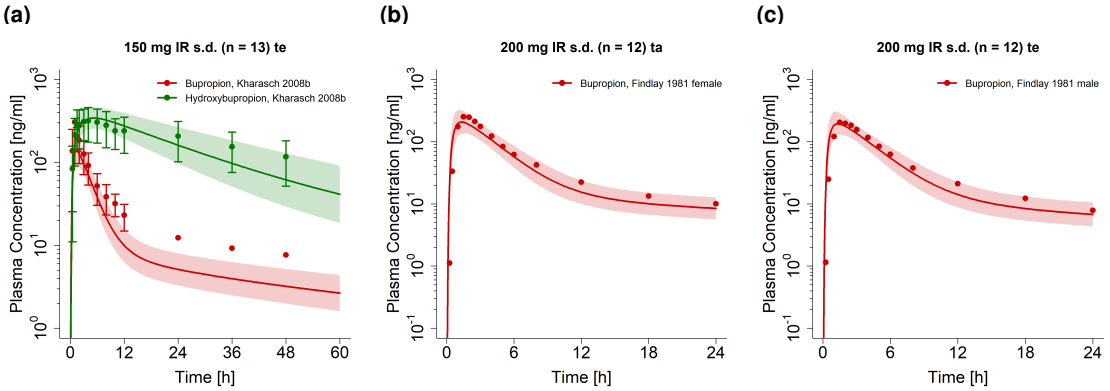

Figure S2.4.7: **Bupropion and metabolites after administration of single or multiple doses of bupropion as an immediate release formulation (part 3/3)** on a semi-logarithmic scale. **IR**, immediate release tablet; **m.d.**, multiple dose; **n**, number of individuals; **s.d.**, single dose; **ta**, training dataset; **te**, test dataset.

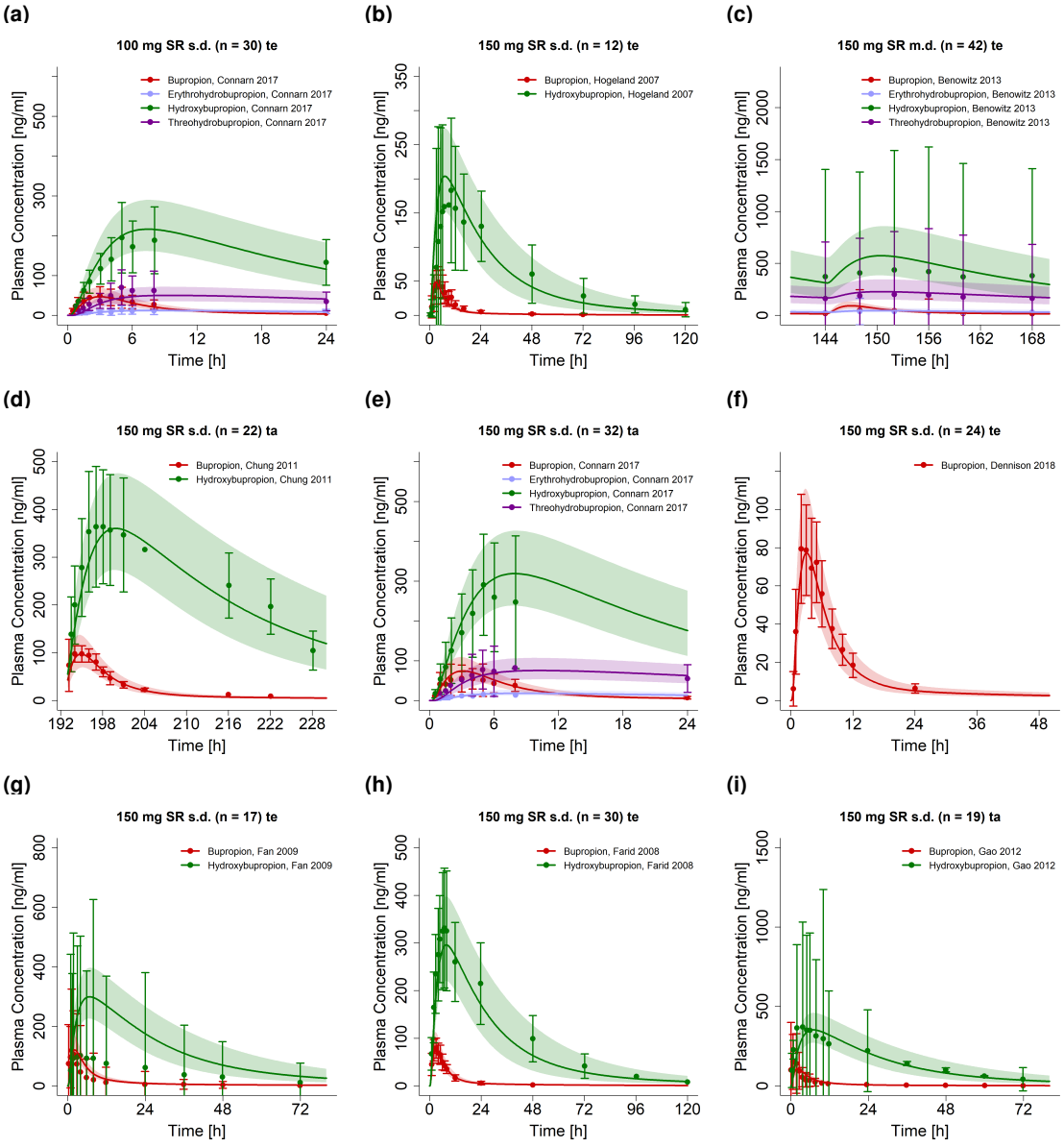

Figure S2.4.8: **Bupropion and metabolites after administration of single or multiple doses of bupropion as a sustained release formulation (part 1/3)** on a linear scale. **m.d.**, multiple dose; **n**, number of individuals; **s.d.**, single dose; **SR**, sustained release tablet; **ta**, training dataset; **te**, test dataset.

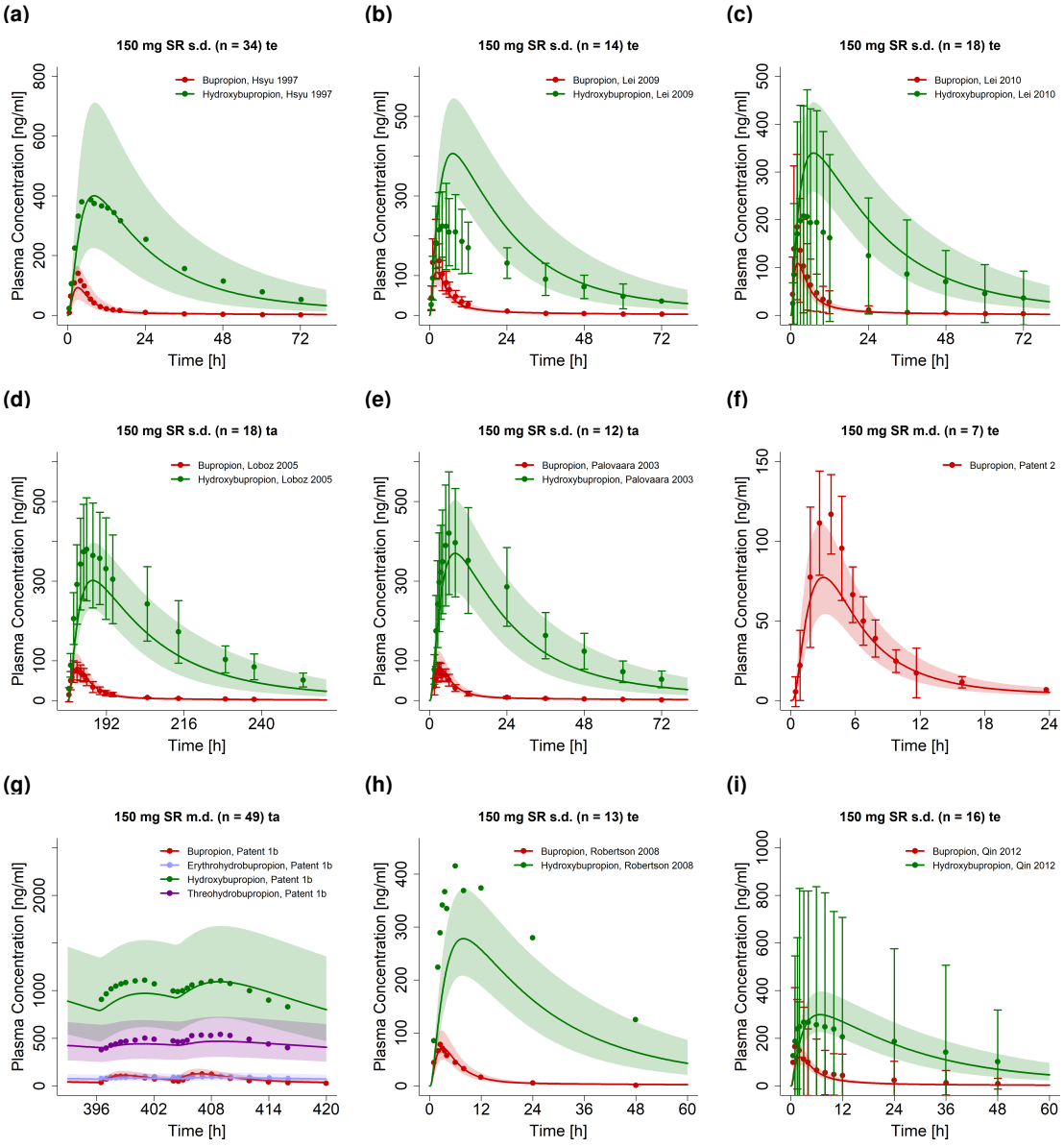

Figure S2.4.9: **Bupropion and metabolites after administration of single or multiple doses of bupropion as a sustained release formulation (part 2/3)** on a linear scale. **m.d.**, multiple dose; **n**, number of individuals; **s.d.**, single dose; **SR**, sustained release tablet; **ta**, training dataset; **te**, test dataset.

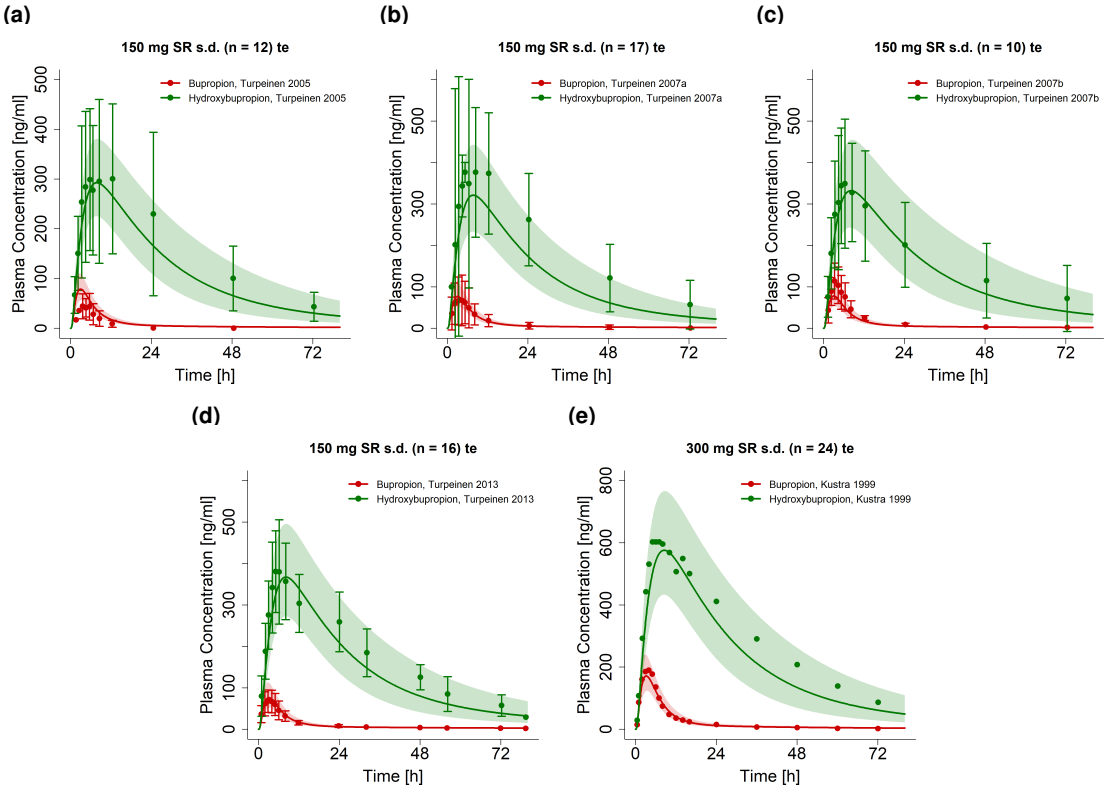

Figure S2.4.10: **Bupropion and metabolites after administration of single or multiple doses of bupropion as a sustained release formulation (part 3/3)** on a linear scale. **m.d.**, multiple dose; **n**, number of individuals; **s.d.**, single dose; **SR**, sustained release tablet; **ta**, training dataset; **te**, test dataset.

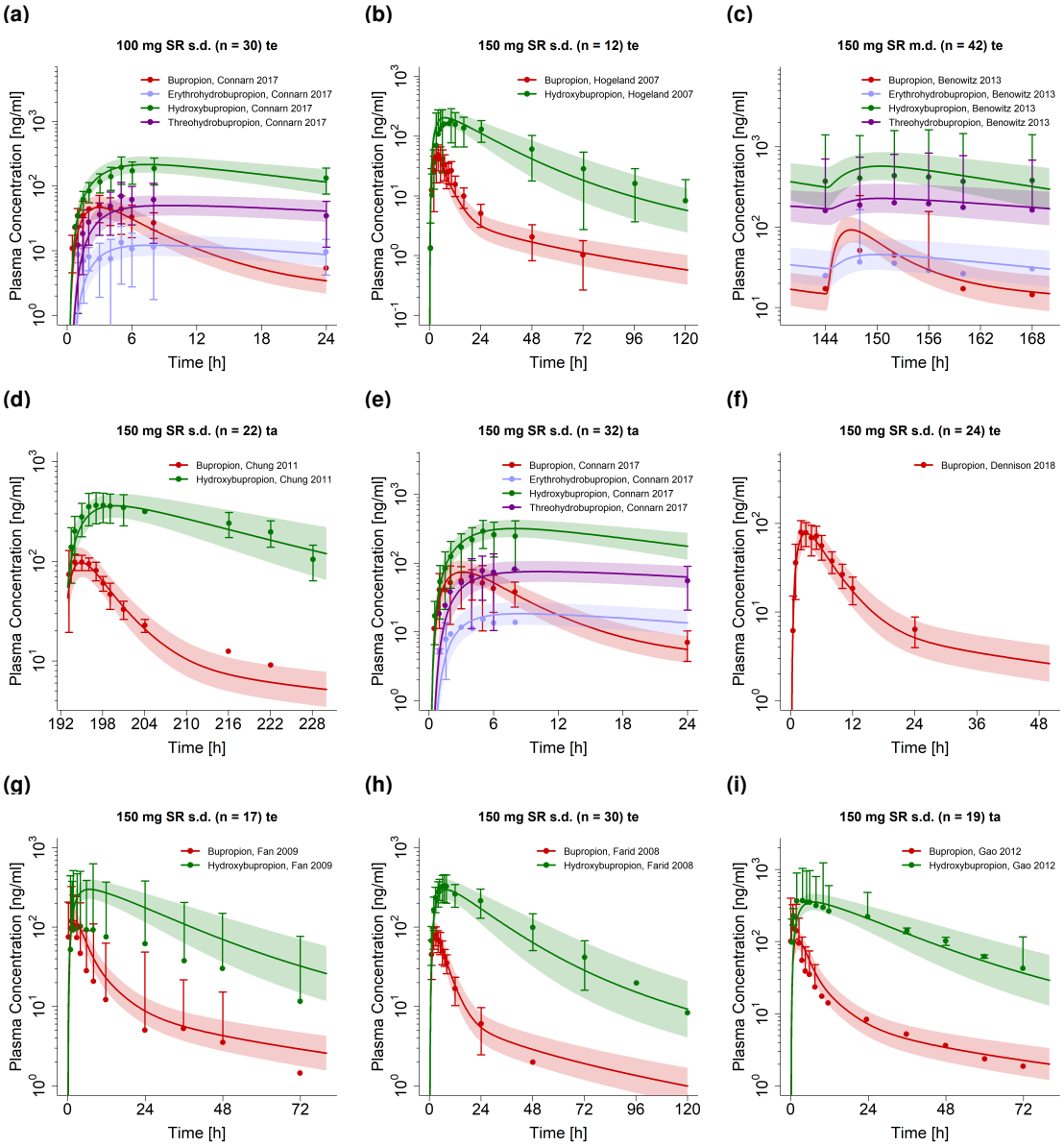

Figure S2.4.11: **Bupropion and metabolites after administration of single or multiple doses of bupropion as a sustained release formulation (part 1/3)** on a semi-logarithmic scale. **m.d.**, multiple dose; **n**, number of individuals; **s.d.**, single dose; **SR**, sustained release tablet; **ta**, training dataset; **te**, test dataset.

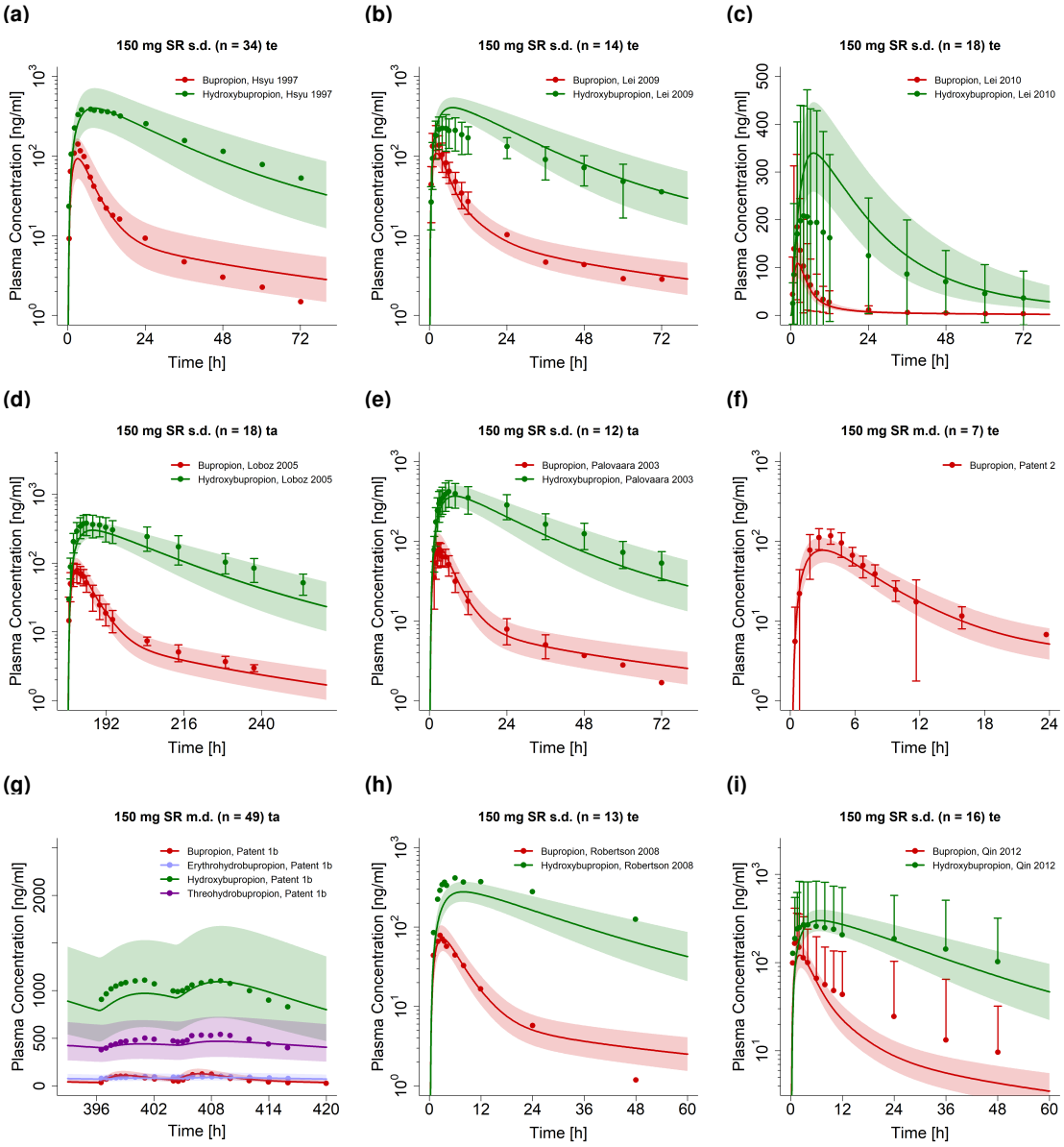

Figure S2.4.12: **Bupropion and metabolites after administration of single or multiple doses of bupropion as a sustained release formulation (part 2/3)** on a semi-logarithmic scale. **m.d.**, multiple dose; **n**, number of individuals; **s.d.**, single dose; **SR**, sustained release tablet; **ta**, training dataset; **te**, test dataset.

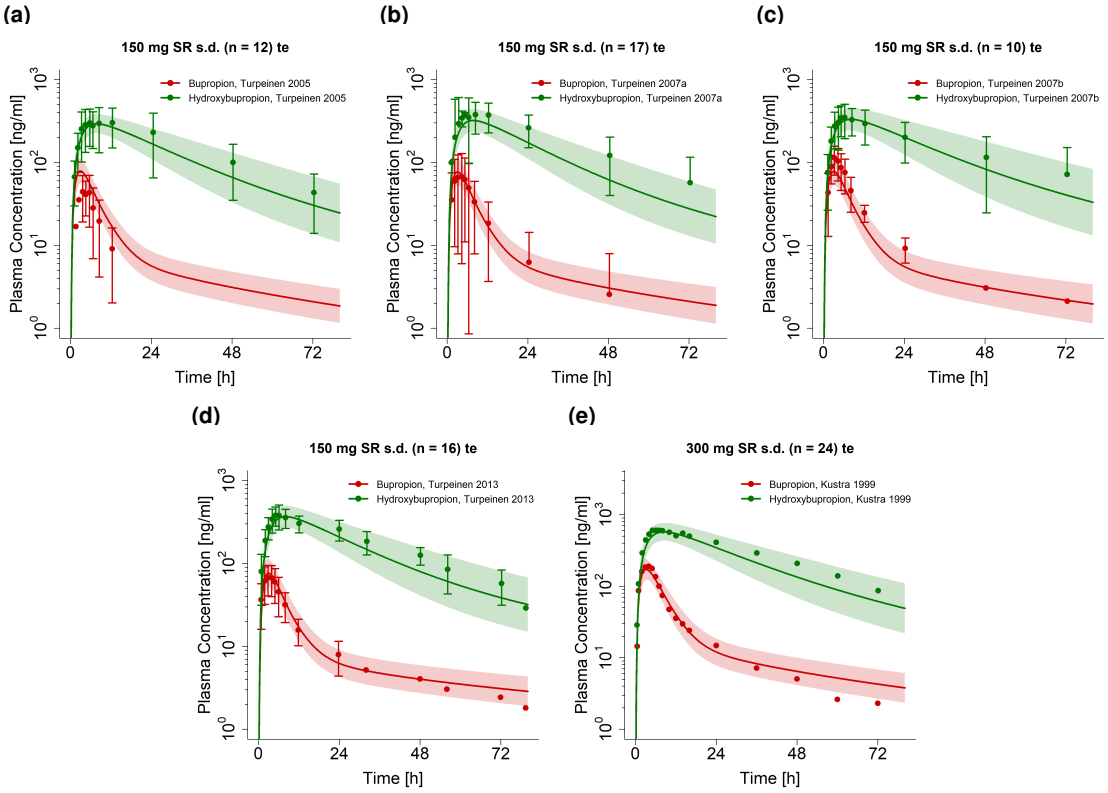

Figure S2.4.13: **Bupropion and metabolites after administration of single or multiple doses of bupropion as a sustained release formulation (part 3/3)** on a semi-logarithmic scale. **m.d.**, multiple dose; **n**, number of individuals; **s.d.**, single dose; **SR**, sustained release tablet; **ta**, training dataset; **te**, test dataset.

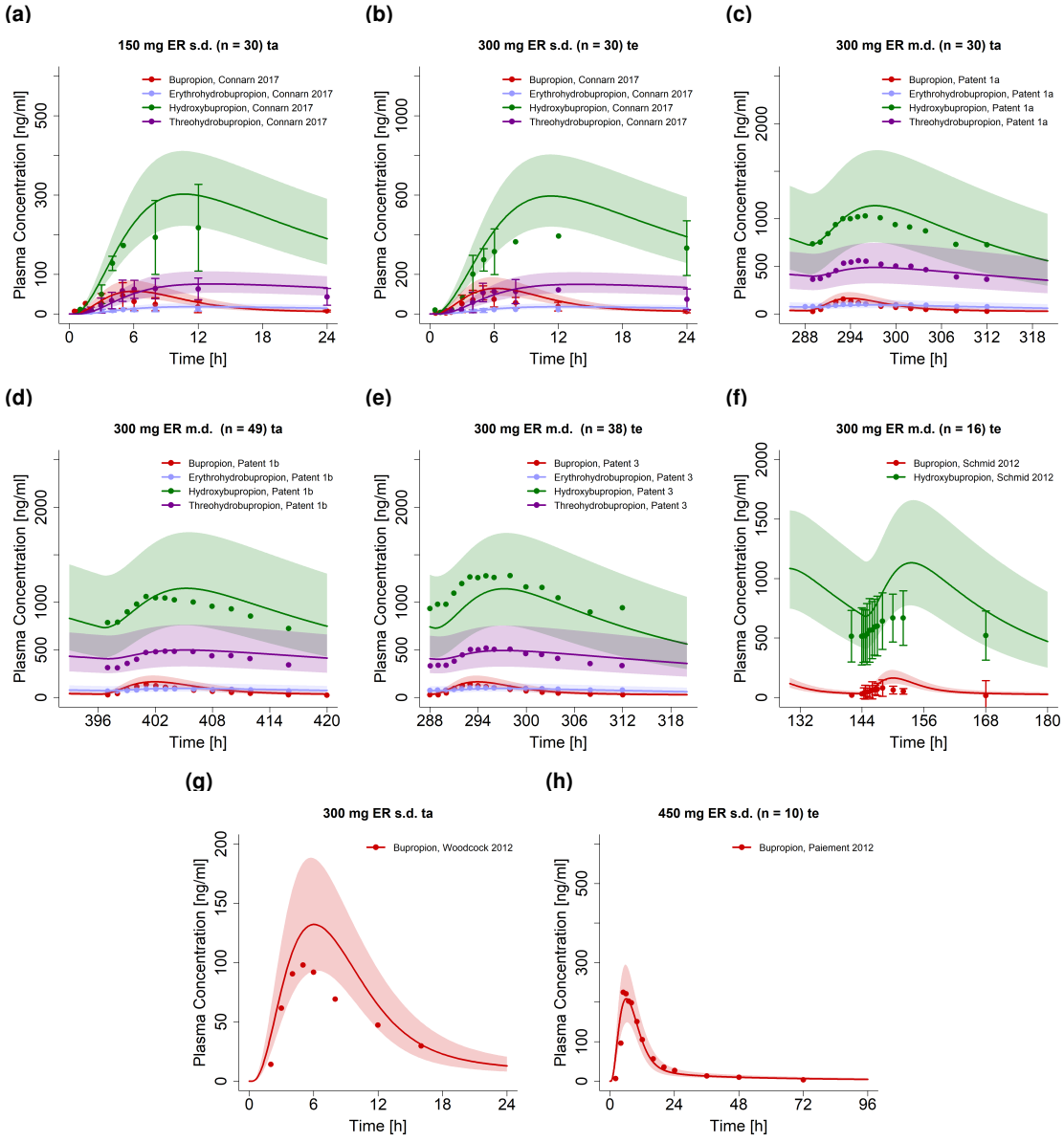

Figure S2.4.14: **Bupropion and metabolites after administration of single or multiple doses of bupropion as an extended release formulation** on a linear scale. **ER**, extended release tablet; **m.d.**, multiple dose; **n**, number of individuals; **s.d.**, single dose; **ta**, training dataset; **te**, test dataset.

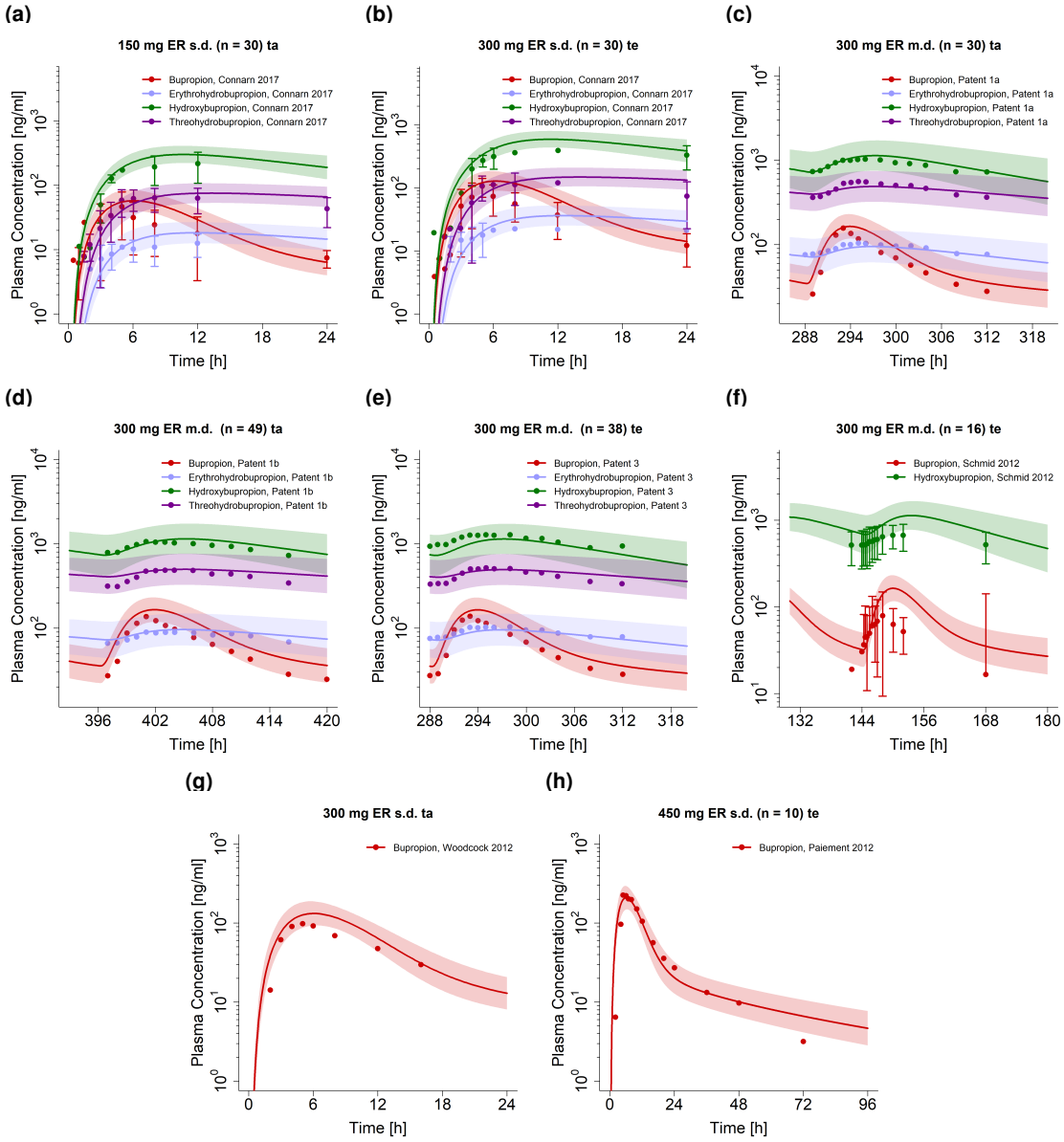

Figure S2.4.15: **Bupropion and metabolites after administration of single or multiple doses of bupropion as an extended release formulation** on a semi-logarithmic scale. **ER**, extended release tablet; **m.d.**, multiple dose; **n**, number of individuals; **s.d.**, single dose; **ta**, training dataset; **te**, test dataset.

2.5 Model evaluation

2.5.1 Predicted compared to observed concentrations goodness-of-fit plots

Following, goodness-of-fit plots of predicted compared to observed plasma concentrations of all four compounds are illustrated in Figure S2.5.16. Details on dosing regimens, study populations and literature references are listed in Table S2.1.

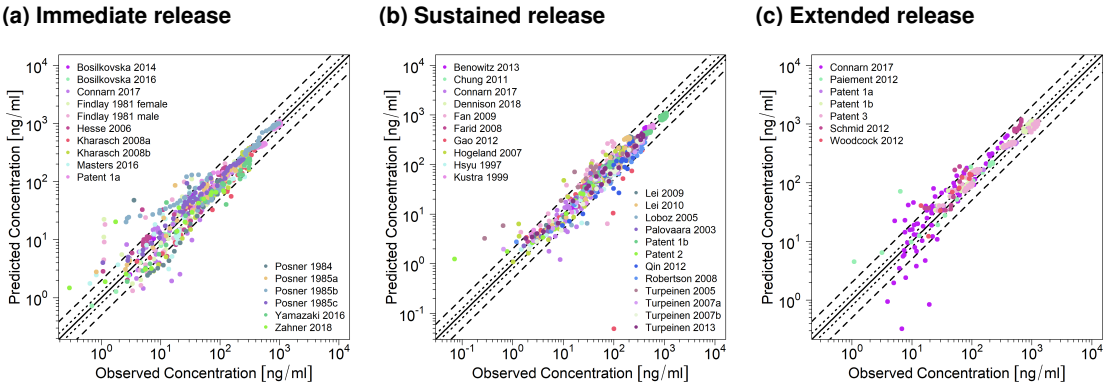

Figure S2.5.16: **Predicted compared to observed plasma concentration values.** Illustrated are values after application of (a) immediate release, (b) sustained release, and (c) extended release tablets. The solid line marks the line of identity. Dotted lines indicate 1.25-fold, dashed lines indicate 2-fold deviation.

2.5.2 Mean relative deviation of plasma concentration predictions

Table S2.3: Mean relative deviation values of bupropion, hydroxybupropion, erythrohydrobupropion and threohydrobupropion plasma concentration predictions.

Dosing	n	Compound	MRD	Compound	MRD	Dataset	Reference
20 mg Cap (s.d.)	30	Bup	1.86	HBup	1.18	ta	Bosilkovska 2016 [24]
25 mg Cap (s.d.)	10	Bup	1.40	HBup	1.36	te	Bosilkovska 2014 [25]
50 mg IR (s.d.)	12	Bup	2.03	HBup	-	te	Findlay 1981 (female) [26]
50 mg IR (s.d.)	12	Bup	2.64	HBup	-	ta	Findlay 1981 (male) [26]
75 mg IR (s.d.)	20	Bup	2.11	HBup	-	te	Zahner 2014 [27]
75 mg IR (s.d.)	7	Bup	1.62	HBup	1.57	te	Hesse 2006 [28]
75 mg IR (s.d.)	30	Bup	1.43	HBup	1.33	te	Connarn 2017 [18]
100 mg IR (s.d.)	32	Bup	1.59	HBup	1.22	ta	Connarn 2017 [18]
100 mg IR (s.d.)	12	Bup	2.10	HBup	-	ta	Findlay 1981 (female) [26]
100 mg IR (s.d.)	12	Bup	1.96	HBup	-	te	Findlay 1981 (male) [26]
100 mg IR (s.d.)	15	Bup	1.75	HBup	1.10	te	Masters 2016 [29]
100 mg IR (s.d.)	24	Bup	1.58	HBup	1.25	te	Yamazaki 2017 [30]
100 mg IR (s.d.)	8	Bup	2.30	HBup	-	te	Posner 1984 [31]
100 mg IR (s.d.)	8	Bup	1.59	HBup	1.08	te	Posner 1985a [32]
100 mg IR (m.d.)	8	Bup	2.50	HBup	1.03	te	Posner 1985b [32]
100 mg IR (s.d.)	8	Bup	1.92	HBup	1.08	te	Posner 1985c [32]
100 mg IR (m.d.)	30	Bup	1.79	HBup	1.08	ta	Patent 1a (US2006/0228415A1) [33]
150 mg IR (s.d.)	10	Bup	1.33	HBup	1.30	ta	Kharasch 2008 [34]
150 mg IR (s.d.)	13	Bup	1.71	HBup	1.14	te	Kharasch 2008b [35]
200 mg IR (s.d.)	12	Bup	2.22	HBup	-	ta	Findlay 1981 (female) [26]
200 mg IR (s.d.)	12	Bup	2.15	HBup	-	te	Findlay 1981 (male) [26]
100 mg SR (s.d.)	30	Bup	1.38	HBup	1.09	ta	Connarn 2017 [18]
100 mg SR (s.d.)	12	Bup	1.58	HBup	1.77	te	Hogeland 2007 [36]
150 mg SR (m.d.)	42	Bup	1.20	HBup	1.05	te	Benowitz 2013 [37]
150 mg SR (s.d.)	22	Bup	1.17	HBup	1.04	ta	Chung 2011 [38]
150 mg SR (s.d.)	32	Bup	1.25	HBup	1.11	ta	Connarn 2017 [18]
150 mg SR (s.d.)	24	Bup	1.13	HBup	-	te	Dennison 2018 [39]
150 mg SR (s.d.)	17	Bup	2.02	HBup	1.57	te	Fan 2009 [11]
150 mg SR (s.d.)	30	Bup	1.12	HBup	1.16	te	Farid 2008 [40]
150 mg SR (s.d.)	19	Bup	6.21	HBup	1.50	ta	Gao 2012 [12]
150 mg SR (s.d.)	34	Bup	1.25	HBup	1.33	te	Hsyu 1997 [41]
150 mg SR (s.d.)	14	Bup	1.26	HBup	1.14	te	Lei 2009 [42]
150 mg SR (s.d.)	18	Bup	1.19	HBup	1.20	te	Lei 2010 [43]
150 mg SR (s.d.)	18	Bup	1.25	HBup	1.37	ta	Loboz 2006 [44]
150 mg SR (s.d.)	12	Bup	1.22	HBup	1.16	ta	Palovaara 2003 [10]
150 mg SR (m.d.)	49	Bup	1.13	HBup	1.02	ta	Patent 1b (US2006/0228415A1) [33]
150 mg SR (m.d.)	7	Bup	1.49	HBup	-	te	Patent 2 (US8545880B2) [45]
150 mg SR (s.d.)	16	Bup	1.46	HBup	1.35	te	Qin 2012 [14]
150 mg SR (s.d.)	13	Bup	1.23	HBup	1.24	te	Robertson 2008 [46]
150 mg SR (s.d.)	12	Bup	4.02	HBup	1.12	te	Turpeinen 2005 [47]
150 mg SR (s.d.)	17	Bup	1.35	HBup	1.23	te	Turpeinen 2007a [48]
150 mg SR (s.d.)	10	Bup	1.37	HBup	1.15	te	Turpeinen 2007b [48]
150 mg SR (s.d.)	16	Bup	1.32	HBup	1.16	te	Turpeinen 2013 [49]
300 mg SR (s.d.)	24	Bup	1.35	HBup	1.13	te	Kustra 1999 [50]
150 mg ER (s.d.)	30	Bup	4.16	HBup	1.59	ta	Connarn 2017 [18]
300 mg ER (s.d.)	30	Bup	2.72	HBup	4.03	te	Connarn 2017 [18]
300 mg ER (m.d.)	30	Bup	1.16	HBup	1.02	te	Patent 1a (US2006/0228415A1) [33]
300 mg ER (m.d.)	49	Bup	1.22	HBup	1.02	ta	Patent 1b (US2006/0228415A1) [33]
300 mg ER (m.d.)	38	Bup	1.16	HBup	1.02	te	Patent 3 (US7,645,802B2) [51]
300 mg ER (m.d.)	16	Bup	1.42	HBup	1.04	te	Schmid 2012 [52]
300 mg ER (m.d.)	-	Bup	1.35	HBup	-	ta	Woodcock 2012 [53]
450 mg ER (s.d.)	10	Bup	1.97	HBup	-	te	Paiement 2012 [54]
75 mg IR (s.d.)	7	EBup	1.81	TBup	1.40	te	Hesse 2006 [28]
75 mg IR (s.d.)	32	EBup	1.55	TBup	2.39	te	Connarn 2017 [18]
100 mg IR (s.d.)	30	EBup	2.29	TBup	2.19	ta	Connarn 2017 [18]
100 mg IR (s.d.)	15	EBup	1.77	TBup	1.40	te	Masters 2016 [29]
100 mg IR (s.d.)	8	EBup	-	TBup	1.21	te	Posner 1985a [32]
100 mg IR (m.d.)	8	EBup	1.20	TBup	1.03	te	Posner 1985b [32]

Table S2.3: Mean relative deviation values of bupropion, hydroxybupropion, erythrohydrobupropion and threohydrobupropion plasma concentration predictions. (continued)

Dosing	n	Compound	MRD	Compound	MRD	Dataset	Reference
100 mg IR (m.d.)	8	EBup	-	TBup	1.19	te	Posner 1985c [32]
100 mg IR (m.d.)	30	EBup	1.13	TBup	1.03	ta	Patent 1a (US2006/0228415A1) [33]
100 mg SR (s.d.)	30	EBup	3.00	TBup	1.41	te	Connarn 2017 [18]
150 mg SR (m.d.)	42	EBup	1.13	TBup	1.04	te	Benowitz 2013 [37]
150 mg SR (s.d.)	32	EBup	1.87	TBup	1.39	ta	Connarn 2017 [18]
150 mg SR (m.d.)	49	EBup	1.05	TBup	1.01	ta	Patent 1b (US2006/0228415A1) [33]
150 mg ER (s.d.)	30	EBup	1.78	TBup	1.83	ta	Connarn 2017 [18]
300 mg ER (s.d.)	30	EBup	1.57	TBup	1.49	te	Connarn 2017 [18]
300 mg ER (m.d.)	30	EBup	1.04	TBup	1.02	te	Patent 1a (US2006/0228415A1) [33]
300 mg ER (m.d.)	49	EBup	1.10	TBup	1.05	ta	Patent 1b (US2006/0228415A1) [33]
300 mg ER (m.d.)	38	EBup	1.04	TBup	1.04	te	Patent 3 (US7,645,802B2) [51]
	Mean		**1.51 (1.01–6.21)**				
	Median		**1.24 (1.01–6.21)**				
			83.06% (103/124) $\leq$ **2**				

Bup, bupropion; **Cap**, capsule (Geneva cocktail capsule [74]); **EBup**, erythrohydrobupropion; **ER**, extended release tablet formulation, **HBup**, hydroxybupropion; **IR**, immediate release tablet formulation; **m.d.**, multiple dose; **MRD**, mean relative deviation; **n**, number of individuals studied; **s.d.**, single dose; **SR**, sustained release formulation; **TBup**, threohydrobupropion; **ta**, training dataset; **te**, test dataset; **-**, not available.

2.5.3 AUC and C_{max} goodness-of-fit plots

Following, goodness-of-fit plots of predicted compared to observed AUC and C_{max} values for every study are illustrated in Figures S2.5.17 and S2.5.18. Line of identity and 2.0-fold acceptance limits are shown as black dashed lines. The 1.25-fold limits are shown as black dotted lines.
Details on dosing regimens, study populations and literature references are listed in Table S2.1. Predicted and observed PK parameters are summarized in Table S2.4.

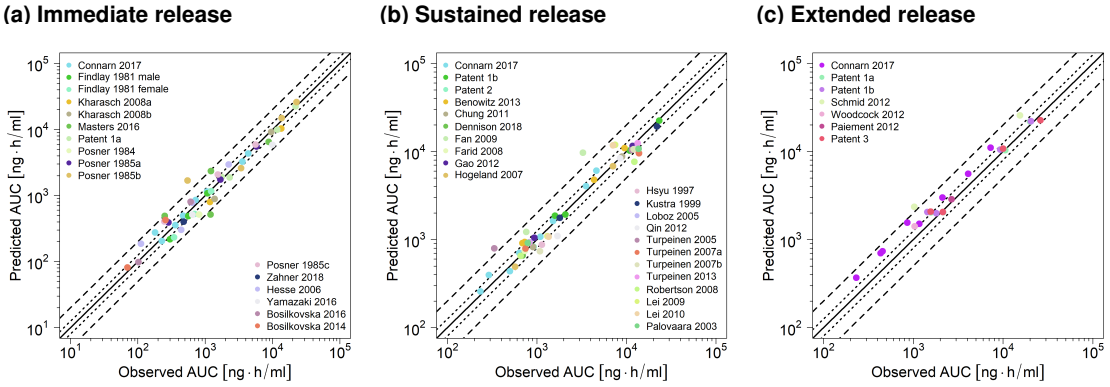

Figure S2.5.17: **Predicted compared to observed plasma AUC_{last} values.** Illustrated are values after application of (a) immediate release, (b) sustained release, and (c) extended release tablets. The solid line marks the line of identity. Dotted lines indicate 1.25-fold, dashed lines indicate 2-fold deviation. **AUC**, area under the plasma concentration-time curve.

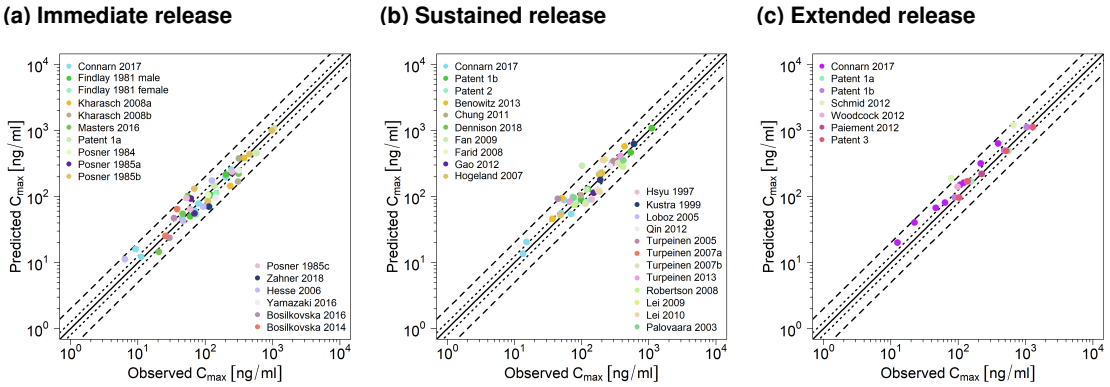

Figure S2.5.18: **Predicted compared to observed plasma C_{max} values.** Illustrated are values after application of (a) immediate release, (b) sustained release, and (c) extended release tablets. The solid line marks the line of identity. Dotted lines indicate 1.25-fold, dashed lines indicate 2-fold deviation. **C_{max}**, maximum plasma concentration.

2.5.4 Geometric mean fold error of predicted AUC and C_{max} values

Table S2.4: Predicted and observed AUC_{last} and C_{max} values of bupropion, hydroxybupropion, erythrohydrobupropion and threohydrobupropion plasma concentrations.

Dosing	n	Compound	AUC_{last} pred [ng*h/ml]	AUC_{last} obs [ng*h/ml]	AUC_{last} pred/obs	C_{max} pred [ng/ml]	C_{max} obs [ng/ml]	C_{max} pred/obs	Dataset	Reference
20 mg Cap (s.d.)	30	Bup	98.29	102.71	0.96	23.68	29.54	0.80	ta	Bosilkovska 2016 [24]
25 mg Cap (s.d.)	10	Bup	81.20	70.34	1.15	25.35	25.74	0.98	te	Bosilkovska 2014 [25]
50 mg IR (s.d.)	12	Bup	232.54	346.19	0.67	53.64	73.78	0.73	te	Findlay 1981 (female) [26]
50 mg IR (s.d.)	12	Bup	217.60	301.43	0.72	50.12	59.67	0.84	ta	Findlay 1981 (male) [26]
75 mg IR (s.d.)	20	Bup	401.99	481.30	0.84	70.29	114.17	0.62	te	Zahner 2014 [27]
75 mg IR (s.d.)	7	Bup	302.02	440.60	0.69	70.10	93.50	0.75	te	Hesse 2006 [28]
75 mg IR (s.d.)	30	Bup	354.49	361.90	0.98	78.04	80.17	0.97	te	Connarn 2017 [18]
100 mg IR (s.d.)	32	Bup	495.78	471.50	1.05	105.74	113.02	0.94	ta	Connarn 2017 [18]
100 mg IR (s.d.)	12	Bup	526.62	694.87	0.76	111.74	145.59	0.77	ta	Findlay 1981 (female) [26]
100 mg IR (s.d.)	12	Bup	489.31	562.72	0.87	104.48	123.13	0.85	te	Findlay 1981 (male) [26]
100 mg IR (s.d.)	15	Bup	491.78	250.82	1.96	101.26	55.38	1.83	te	Masters 2016 [29]
100 mg IR (s.d.)	24	Bup	512.69	648.61	0.79	96.95	143.0	0.68	te	Yamazaki 2017 [30]
100 mg IR (s.d.)	8	Bup	514.20	813.57	0.63	104.69	111.0	0.94	te	Posner 1984 [31]
100 mg IR (s.d.)	8	Bup	390.50	286.01	1.37	92.88	61.22	1.51	te	Posner 1985a [32]
100 mg IR (m.d.)	8	Bup	1681.00	549.73	3.06	131.59	69.30	1.90	te	Posner 1985b [32]
100 mg IR (s.d.)	8	Bup	404.32	248.92	1.62	94.40	52.89	1.78	te	Posner 1985c [32]
100 mg IR (m.d.)	30	Bup	1765.08	1765.08	1.08	145.51	136.69	1.06	ta	Patent 1a (US2006/0228415A1) [33]
150 mg IR (s.d.)	10	Bup	798.66	1182.40	0.68	144.23	235.94	0.61	ta	Kharasch 2008 [34]
150 mg IR (s.d.)	13	Bup	888.32	1386.28	0.64	168.77	307.63	0.55	te	Kharasch 2008b [35]
200 mg IR (s.d.)	12	Bup	1165.09	1225.94	0.95	230.57	252.23	0.91	ta	Findlay 1981 (female) [26]
200 mg IR (s.d.)	12	Bup	1165.09	1080.86	1.00	215.78	204.63	1.05	te	Findlay 1981 (male) [26]
100 mg SR (s.d.)	30	Bup	437.68	501.70	0.87	55.89	49.59	1.13	te	Connarn 2017 [18]
100 mg SR (s.d.)	12	Bup	492.31	572.17	0.86	52.32	48.77	1.07	te	Hogeland 2007 [36]
150 mg SR (m.d.)	42	Bup	910.01	689.79	1.32	95.34	51.32	1.86	te	Benowitz 2013 [37]
150 mg SR (s.d.)	22	Bup	822.18	909.01	0.90	88.34	55.37	1.60	ta	Chung 2011 [38]
150 mg SR (s.d.)	32	Bup	705.10	639.64	1.10	82.75	116.92	0.71	ta	Connarn 2017 [18]
150 mg SR (s.d.)	24	Bup	657.81	693.30	0.95	95.34	51.32	1.86	te	Dennison 2018 [39]
150 mg SR (s.d.)	17	Bup	1221.28	763.62	1.60	104.29	97.73	1.07	te	Fan 2009 [11]
150 mg SR (s.d.)	30	Bup	743.43	734.89	1.01	82.66	79.34	1.04	te	Farid 2008 [40]
150 mg SR (s.d.)	19	Bup	1048.12	941.59	1.11	126.61	118.63	1.07	ta	Gao 2012 [12]
150 mg SR (s.d.)	34	Bup	873.80	1141.13	0.77	114.07	151.68	0.75	te	Hsyu 1997 [41]
150 mg SR (s.d.)	14	Bup	1092.76	1319.17	0.83	90.21	140.82	0.64	te	Lei 2009 [42]
150 mg SR (s.d.)	18	Bup	1075.17	1358.91	0.79	178.25	189.50	0.94	te	Lei 2010 [43]
150 mg SR (s.d.)	18	Bup	932.99	832.02	1.12	98.22	74.04	1.33	ta	Loboz 2006 [44]
150 mg SR (s.d.)	12	Bup	916.46	793.90	1.15	96.64	76.52	1.26	ta	Palovaara 2003 [10]
150 mg SR (m.d.)	49	Bup	1861.39	1599.96	1.16	126.61	174.87	0.72	ta	Patent 1b (US2006/0228415A1) [33]
150 mg SR (m.d.)	7	Bup	827.72	920.60	0.90	92.50	44.25	2.09	te	Patent 2 (US8545880B2) [45]
150 mg SR (s.d.)	16	Bup	1097.92	1700.06	0.65	83.87	67.24	1.25	te	Qin 2012 [14]

Table S2.4: Predicted and observed AUC_{last} and C_{max} values of bupropion, hydroxybupropion, erythrohydrobupropion and threohydrobupropion plasma concentrations. (continued)

Dosing	n	Compound	AUC_{last} pred [ng*h/ml]	AUC_{last} obs [ng*h/ml]	AUC_{last} pred/obs	C_{max} pred [ng/ml]	C_{max} obs [ng/ml]	C_{max} pred/obs	Dataset	Reference
150 mg SR (s.d.)	13	Bup	651.49	659.39	0.99	77.90	113.75	0.68	te	Robertson 2008 [46]
150 mg SR (s.d.)	12	Bup	795.88	335.35	2.37	84.26	67.63	1.25	te	Turpeinen 2005 [47]
150 mg SR (s.d.)	17	Bup	788.51	746.66	1.06	95.34	53.56	1.78	te	Turpeinen 2007a [48]
150 mg SR (s.d.)	10	Bup	734.31	1082.42	0.68	73.91	78.49	0.94	te	Turpeinen 2007b [48]
150 mg SR (s.d.)	16	Bup	920.83	817.53	1.13	120.32	179.49	0.67	te	Turpeinen 2013 [49]
300 mg SR (s.d.)	24	Bup	1767.98	1803.47	0.98	52.32	48.77	1.07	te	Kustra 1999 [50]
150 mg ER (s.d.)	30	Bup	701.46	434.50	1.61	67.23	46.49	1.45	ta	Connarn 2017 [18]
300 mg ER (s.d.)	30	Bup	1552.49	860.70	1.80	150.08	106.61	1.41	te	Connarn 2017 [18]
300 mg ER (m.d.)	30	Bup	2031.86	1571.33	1.29	168.64	156.81	1.08	te	Patent 1a (US2006/0228415A1) [33]
300 mg ER (m.d.)	49	Bup	2051.28	1436.28	1.43	169.62	136.45	1.24	ta	Patent 1b (US2006/0228415A1) [33]
300 mg ER (m.d.)	38	Bup	2078.06	1565.12	1.33	169.15	138.19	1.22	te	Patent 3 (US7,645,802B2) [45]
300 mg ER (m.d.)	16	Bup	2355.85	1029.53	2.29	188.63	79.02	2.39	te	Schmid 2012 [52]
300 mg ER (m.d.)	-	Bup	1413.04	1036.09	1.36	140.19	97.94	1.43	ta	Woodcock 2012 [53]
450 mg ER (s.d.)	20	Bup	2870.69	2674.37	1.07	221.19	224.68	0.98	ta	Paiement 2012 [54]
20 mg Cap (s.d.)	30	HBup	801.40	607.74	1.32	195.62	201.48	0.97	ta	Bosilkovska 2016 [24]
25 mg Cap (s.d.)	10	HBup	427.83	257.69	1.66	256.21	244.02	1.05	te	Bosilkovska 2014 [25]
75 mg IR (s.d.)	7	HBup	2953.13	2239.20	1.32	1079.21	1055.87	1.02	te	Hesse 2006 [28]
75 mg IR (s.d.)	30	HBup	3269.46	3591.89	0.91	221.85	314.78	0.70	te	Connarn 2017 [18]
100 mg IR (s.d.)	32	HBup	4332.10	4370.16	0.99	383.99	379.17	1.01	ta	Connarn 2017 [18]
100 mg IR (s.d.)	15	HBup	6471.74	8796.79	0.74	237.18	250.64	0.95	te	Masters 2016 [29]
100 mg IR (s.d.)	24	HBup	5853.48	9995.87	0.59	64.28	38.33	1.68	te	Yamazaki 2017 [30]
100 mg IR (s.d.)	8	HBup	5498.67	5803.33	0.95	249.20	318.00	0.78	te	Posner 1985a [32]
100 mg IR (m.d.)	8	HBup	26056.97	22722.51	1.15	377.70	317.49	1.19	te	Posner 1985b [32]
100 mg IR (s.d.)	8	HBup	5890.56	5597.22	1.05	47.21	34.64	1.36	te	Posner 1985c [32]
100 mg IR (m.d.)	30	HBup	22454.16	22075.43	1.02	173.88	126.04	1.38	ta	Patent 1a (US2006/0228415A1) [33]
150 mg IR (s.d.)	10	HBup	9160.32	9618.74	0.95	227.45	250.39	0.91	ta	Kharasch 2008 [34]
150 mg IR (s.d.)	13	HBup	10351.70	13530.75	0.77	997.47	979.94	1.02	te	Kharasch 2008b [**?**]
100 mg SR (s.d.)	30	HBup	4045.70	3549.10	1.14	228.03	194.98	1.17	te	Connarn 2017 [18]
100 mg SR (s.d.)	12	HBup	6811.49	7084.82	0.96	216.14	182.94	1.18	te	Hogeland 2007 [36]
150 mg SR (m.d.)	42	HBup	10957.92	9547.77	1.15	573.84	436.84	1.31	te	Benowitz 2013 [37]
150 mg SR (s.d.)	22	HBup	8738.64	8936.26	0.98	366.16	363.64	1.01	ta	Chung 2011 [38]
150 mg SR (s.d.)	32	HBup	6041.12	4633.27	1.30	573.84	436.84	1.31	ta	Connarn 2017 [18]
150 mg SR (s.d.)	17	HBup	9661.12	3268.52	2.96	366.16	363.64	1.01	te	Fan 2009 [11]
150 mg SR (s.d.)	30	HBup	10502.50	12055.85	0.87	293.00	102.05	2.87	te	Farid 2008 [40]
150 mg SR (s.d.)	19	HBup	11539.68	11762.50	0.98	327.37	331.16	0.99	te	Gao 2012 [12]
150 mg SR (s.d.)	34	HBup	10166.26	13447.39	0.76	216.14	182.94	1.18	te	Hsyu [**?**]
150 mg SR (s.d.)	14	HBup	11893.87	7482.04	1.59	624.98	602.58	1.04	te	Lei 2009 [42]
150 mg SR (s.d.)	18	HBup	11704.75	7112.73	1.65	353.25	379.78	0.93	te	Lei 2010 [43]
150 mg SR (s.d.)	18	HBup	10854.40	12976.72	0.84	293.00	267.66	1.09	ta	Loboz 2006 [44]
150 mg SR (s.d.)	12	HBup	10727.87	13747.54	0.78	353.29	420.35	0.84	ta	Palovaara 2003 [10]

Table S2.4: Predicted and observed AUC_{last} and C_{max} values of bupropion, hydroxybupropion, erythrohydrobupropion and threohydrobupropion plasma concentrations. (continued)

Dosing	n	Compound	AUC_{last} pred [ng*h/ml]	AUC_{last} obs [ng*h/ml]	AUC_{last} pred/obs	C_{max} pred [ng/ml]	C_{max} obs [ng/ml]	C_{max} pred/obs	Dataset	Reference
150 mg SR (m.d.)	49	HBup	22365.49	23315.14	0.96	343.79	300.46	1.14	ta	Patent 1b (US2006/0228415A1) [33]
150 mg SR (s.d.)	16	HBup	8372.74	8540.70	0.98	315.19	376.14	0.84	te	Qin 2012 [14]
150 mg SR (s.d.)	13	HBup	7644.43	12305.92	0.62	322.75	348.93	0.92	te	Robertson 2008 [46]
150 mg SR (s.d.)	12	HBup	10397.75	11506.36	0.90	409.26	380.38	1.08	te	Turpeinen 2005 [47]
150 mg SR (s.d.)	17	HBup	9557.71	13862.09	0.69	573.84	435.00	1.32	te	Turpeinen 2007 [48]
150 mg SR (s.d.)	10	HBup	10597.39	12076.82	0.88	285.43	415.53	0.69	te	Turpeinen 2007 [48]
150 mg SR (s.d.)	16	HBup	12401.84	13350.60	0.93	364.92	223.79	1.63	te	Turpeinen 2013 [49]
300 mg SR (s.d.)	24	HBup	19212.14	21964.35	0.87	339.72	386.80	0.88	te	Kustra 1999 [50]
150 mg ER (s.d.)	30	HBup	5583.86	4088.58	1.37	318.33	217.43	1.46	ta	Connarn 2017 [18]
300 mg ER (s.d.)	30	HBup	11061.39	7266.99	1.52	635.02	392.91	1.62	te	Connarn 2017 [18]
300 mg ER (m.d.)	30	HBup	21885.82	20133.46	1.09	1123.03	1030.00	1.09	te	Patent 1a (US2006/0228415A1) [33]
300 mg ER (m.d.)	49	HBup	22072.35	20458.99	1.08	1130.27	1061.85	1.06	ta	Patent 1b (US2006/0228415A1) [33]
300 mg ER (m.d.)	38	HBup	22654.20	26187.27	0.87	1126.80	1280.80	0.88	te	Patent 3 (US7,645,802B2) [45]
300 mg ER (m.d.)	16	HBup	25727.64	15469.07	1.66	1196.56	668.29	1.79	te	Schmid 2012 [52]
75 mg IR (s.d.)	7	EBup	186.61	111.51	1.67	14.50	20.45	0.71	te	Hesse 2006 [28]
75 mg IR (s.d.)	30	EBup	204.83	228.25	0.90	12.19	11.26	1.08	te	Connarn 2017 [18]
100 mg IR (s.d.)	32	EBup	275.48	180.72	1.52	15.90	9.24	1.72	ta	Connarn 2017 [18]
100 mg IR (s.d.)	15	EBup	514.26	1205.83	0.43	88.37	108.50	0.81	te	Masters 2016 [29]
100 mg IR (m.d.)	30	EBup	1877.36	2312.75	0.81	83.97	110.63	0.76	ta	Patent 1a (US2006/0228415A1) [33]
100 mg IR (s.d.)	8	EBup	2586.00	3430.72	0.75	11.27	6.43	1.75	te	Posner 1985b [32]
100 mg SR (s.d.)	30	EBup	256.95	234.68	1.09	13.61	13.42	1.01	te	Connarn 2017 [18]
150 mg SR (m.d.)	42	EBup	936.91	733.66	1.28	45.94	36.84	1.25	te	Benowitz 2013 [37]
150 mg SR (s.d.)	32	EBup	394.99	292.35	1.35	20.47	15.15	1.35	ta	Connarn 2017 [18]
150 mg SR (m.d.)	49	EBup	1925.27	2084.16	0.92	89.99	98.09	0.92	ta	Patent 1b (US2006/0228415A1) [33]
150 mg ER (s.d.)	30	EBup	369.29	231.71	1.59	20.01	12.54	1.60	ta	Connarn 2017 [18]
300 mg ER (s.d.)	30	EBup	737.65	456.12	1.62	40.29	22.44	1.79	te	Connarn 2017 [18]
300 mg ER (m.d.)	30	EBup	2041.89	2144.43	0.95	95.75	103.90	0.92	te	Patent 1a (US2006/0228415A1) [33]
300 mg ER (m.d.)	49	EBup	1992.83	1807.20	1.10	96.76	89.23	1.08	ta	Patent 1b (US2006/0228415A1) [33]
300 mg ER (m.d.)	38	EBup	2050.67	2143.29	0.96	96.28	103.42	0.93	ta	Patent 3 (US2006/0228415A1) [45]
75 mg IR (s.d.)	7	TBup	777.19	644.82	1.21	42.87	47.04	0.91	te	Hesse 2006 [28]
75 mg IR (s.d.)	30	TBup	855.38	723.62	1.18	46.53	45.94	1.01	te	Connarn 2017 [18]
100 mg IR (s.d.)	32	TBup	1147.99	1072.29	1.07	60.66	70.73	0.86	ta	Connarn 2017 [18]
100 mg IR (s.d.)	15	TBup	2339.96	1220.23	1.92	54.62	46.64	1.17	te	Masters 2016 [29]
100 mg IR (s.d.)	8	TBup	1742.91	1681.44	1.04	55.59	69.63	0.80	te	Posner 1985a [32]
100 mg IR (m.d.)	8	TBup	14825.56	13696.52	1.08	438.38	458.40	0.96	te	Posner 1985b [32]
100 mg IR (s.d.)	8	TBup	2074.02	1548.84	1.34	64.15	59.95	1.07	te	Posner 1985 [32]
100 mg IR (m.d.)	30	TBup	9898.68	11793.82	0.84	454.37	579.14	0.78	te	Patent 1a (US2006/0228415A1) [33]
100 mg SR (s.d.)	30	TBup	1072.66	1097.26	0.98	54.17	70.09	0.77	te	Connarn 2017 [18]
150 mg SR (m.d.)	42	TBup	4781.47	4372.26	1.09	224.52	201.32	1.12	te	Benowitz 2013 [37]
150 mg SR (s.d.)	32	TBup	1623.87	1518.32	1.07	81.37	82.05	0.99	ta	Connarn 2017 [18]

Table S2.4: Predicted and observed AUC_{last} and C_{max} values of bupropion, hydroxybupropion, erythrohydrobupropion and threohydrobupropion plasma concentrations. (continued)

Dosing	n	Compound	AUC_{last} pred [ng*h/ml]	AUC_{last} obs [ng*h/ml]	AUC_{last} pred/obs	C_{max} pred [ng/ml]	C_{max} obs [ng/ml]	C_{max} pred/obs	Dataset	Reference
150 mg SR (m.d.)	49	TBup	10243.07	10905.15	0.94	466.39	539.88	0.86	ta	Patent 1b (US2006/0228415A1) [33]
150 mg ER (s.d.)	30	TBup	1507.34	1169.41	1.29	80.79	63.89	1.26	ta	Connarn 2017 [18]
300 mg ER (s.d.)	30	TBup	3000.24	2113.31	1.42	161.42	121.15	1.33	te	Connarn 2017 [18]
300 mg ER (m.d.)	30	TBup	10332.95	10585.97	0.98	488.69	560.01	0.87	te	Patent 1a (US2006/0228415A1) [33]
300 mg ER (m.d.)	49	TBup	10525.00	9316.26	1.13	495.81	486.37	1.02	ta	Patent 1b (US2006/0228415A1) [33]
300 mg ER (m.d.)	38	TBup	10784.29	10055.56	1.07	492.44	518.18	0.95	te	Patent 3 (US2006/0228415A1) [45]
GMFE (range)					**1.31 (1.00–3.06)**			**1.29 (1.00–2.87)**		
pred/obs within twofold (range)					**95.97%; 119/124 (0.43–3.06)**			**97.58%; 121/124 (0.55–2.87)**		

AUC_{last}, area under the concentration-time curve calculated from the first time point to the last time point; **Bup**, bupropion; **Cap**, capsule (Geneva cocktail [74]); **C_{max}**, maximum concentration; **EBup**, erythrohydrobupropion; **ER**, extended release tablet formulation; **GMFE**,geometric mean fold error; **HBup**, hydroxybupropion; **IR**, immediate release tablet formulation; **m.d.**, multiple dose; **n**, number of individuals studied; **obs**, observed; **pred** predicted; **s.d.**, single dose; **SR**, sustained release formulation; **TBup**, threohydrobupropion; **ta**, training dataset; **te**, test dataset; **-**, not available.

2.5.5 Local sensitivity analysis

Figures S2.5.19-S2.5.22 show the results of the local sensitivity analyses on the AUC of the compounds bupropion, hydroxybupropion, erythrohydrobupropion and threohydrobupopion. Sensitivity of the model to single parameter changes was determined as change of the simulated AUC extrapolated to infinity from the time of bupropion application after the last application of a 14 day multiple dose regimen of 100 mg IR (three times daily), 150 mg SR (twice daily) or 300 mg ER (once daily). A sensitivity value of -0.5 indicates a 5% decrease of the simulated AUC if the examined parameter is incraeased by 10%. Meaningful differences between formulations were only visible for the bupropion AUC. For all modeled compounds, fraction unbound in plasma (nonoptimized value) had the strongest impact. Lipophilicity of bupropion (optimized value) was more impactful for extended release administrations than for immediate release and sustained release formulations. In general, metabolite AUC is less sensitive to changes in bupropion lipophilicity than to metabolic pathways. Among the alteration of kinetics of the implemented metabolic pathways, CYP2B6 as well as 11β-HSD kinetics show a more profound influence on bupropion AUC than CYP2C19 kinetics, which reflects the key role of CYP2B6 in bupropion metabolism as described in literature [21]. Binding parameters K_D and k_{off} show no impact AUC of bupropion and metabolites after multiple dose application.

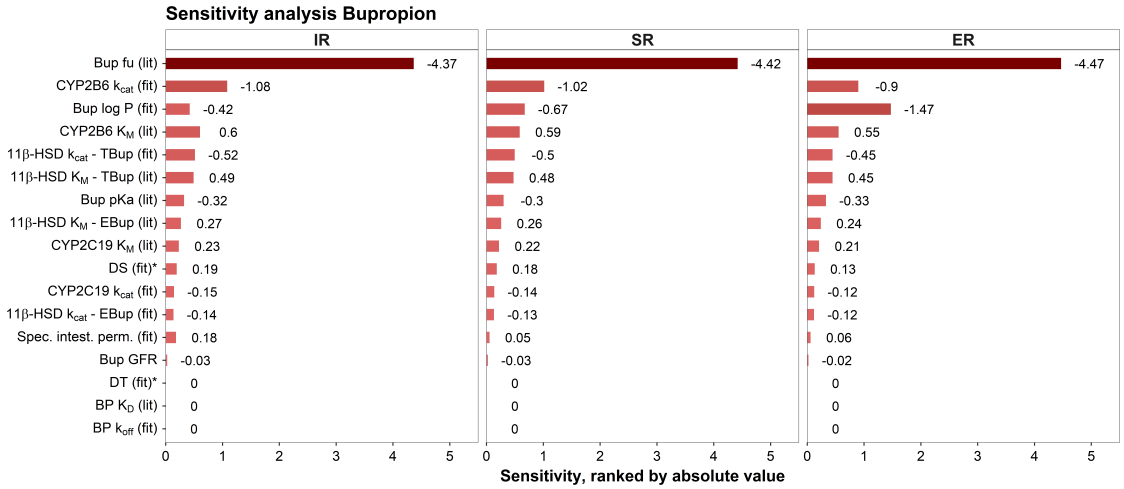

Figure S2.5.19: **Bupropion PBPK model sensitivity analyses - bupropion**. *, fitted for IR and SR; **11β-HSD**, 11β-hydroxysteroid dehydrogenase 1; **BP**, binding partner; **Bup**, bupropion; **CYP**, cytochrome P450; **DS**, dissolution shape; **DT**, dissolution time; **EBup**, erythrohydrobupropion; **ER**, extended release; **fit.**, fitted in parameter optimization; **GFR**, glomerular filtration rate; **IR**, immediate release; **K_D**, dissociation constant for binding; **k_{cat}**, catalytic rate constant; **K_M**, Michaelis-Menten constant; **k_{off}**, dissociation rate constant for binding; **lit.**, literature; **log P**, lipophilicity; **pKa**, acidic dissociation constant; **Spec. intest. perm.**, specific intestinal permeability; textbfSR, sustained release; **TBup**, threohydrobupropion.

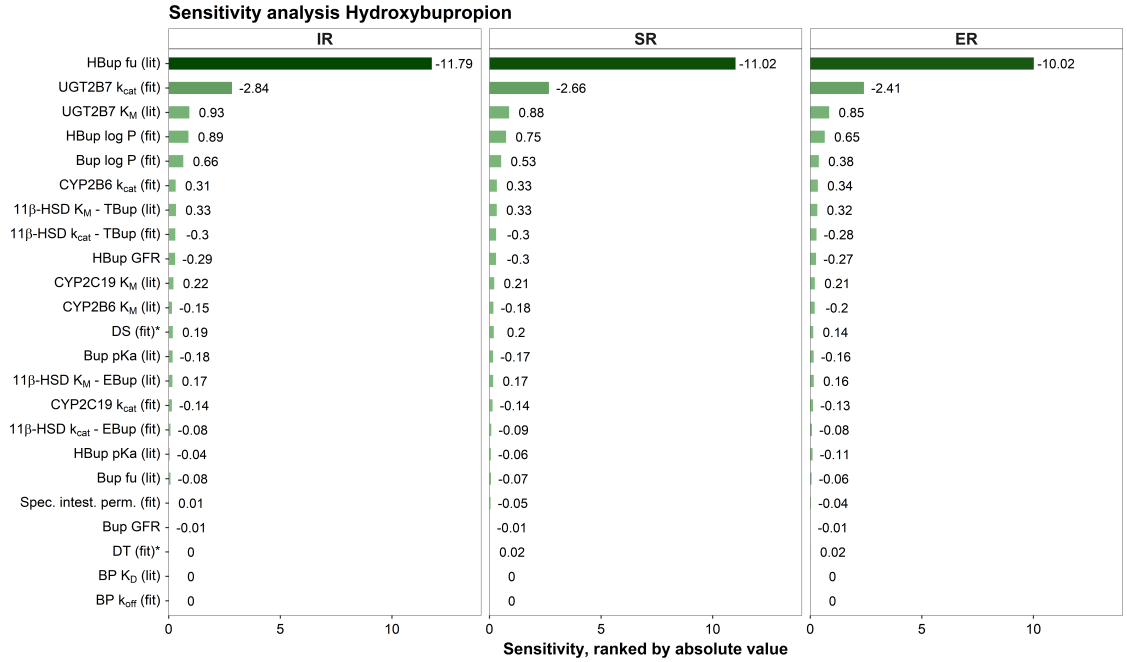

Figure S2.5.20: **Bupropion PBPK model sensitivity analyses - hydroxybupropion**. *****, fitted for IR and SR; **11β-HSD**, 11β-hydroxysteroid dehydrogenase 1; **BP**, binding partner; **Bup**, bupropion; **CYP**, cytochrome P450; **DS**, dissolution shape; **DT**, dissolution time; **EBup**, erythrohydrobupropion; **ER**, extended release; **fit.**, fitted in parameter optimization; **GFR**, glomerular filtration rate; **HBup**, hydroxybupropion; **IR**, immediate release; $\mathbf{K_D}$, dissociation constant for binding; $\mathbf{k_{cat}}$, catalytic rate constant; $\mathbf{K_M}$, Michaelis-Menten constant; $\mathbf{k_{off}}$, dissociation rate constant for binding; **lit.**, literature; **log P**, lipophilicity; **pKa**, acidic dissociation constant; **Spec. intest. perm.**, specific intestinal permeability; textbfSR, sustained release; **TBup**, threohydrobupropion.

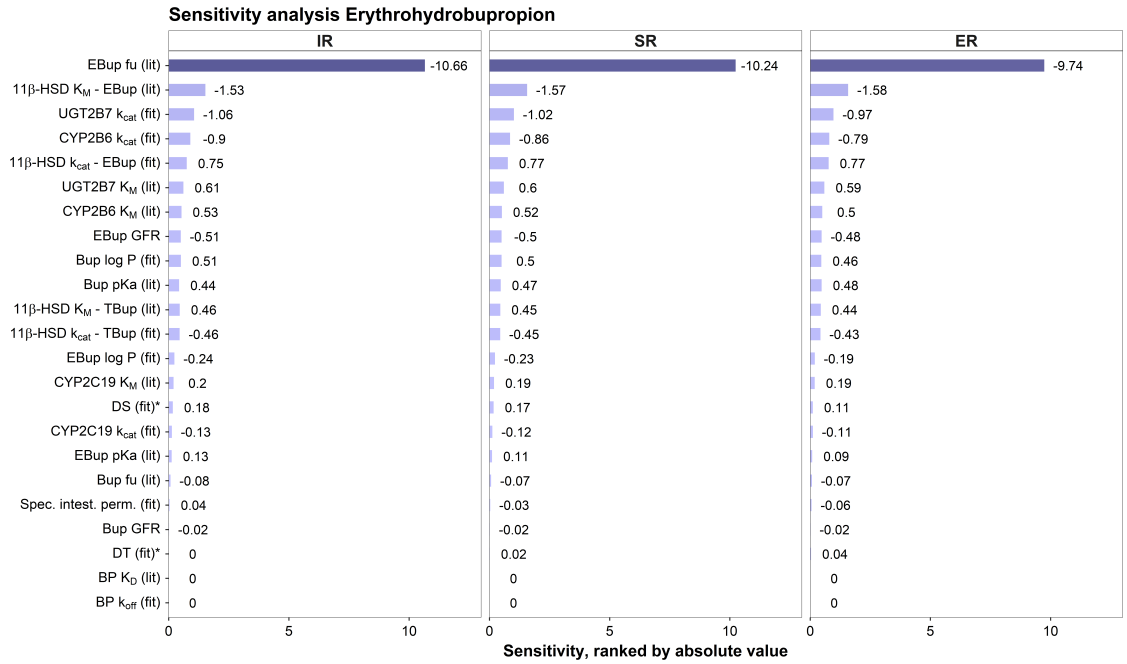

Figure S2.5.21: **Bupropion PBPK model sensitivity analyses - erythrohydrobupropion**. *****, fitted for IR and SR; **11β-HSD**, 11β-hydroxysteroid dehydrogenase 1; **BP**, binding partner; **Bup**, bupropion; **CYP**, cytochrome P450; **DS**, dissolution shape; **DT**, dissolution time; **EBup**, erythrohydrobupropion; **ER**, extended release; **fit.**, fitted in parameter optimization; **GFR**, glomerular filtration rate; **IR**, immediate release; $\mathbf{K_D}$, dissociation constant for binding; $\mathbf{k_{cat}}$, catalytic rate constant; $\mathbf{K_M}$, Michaelis-Menten constant; $\mathbf{k_{off}}$, dissociation rate constant for binding; **lit.**, literature; **log P**, lipophilicity; **pKa**, acidic dissociation; **Spec. intest. perm.**, specific intestinal permeability; textbfSR, sustained release; **TBup**, threohydrobupropion.

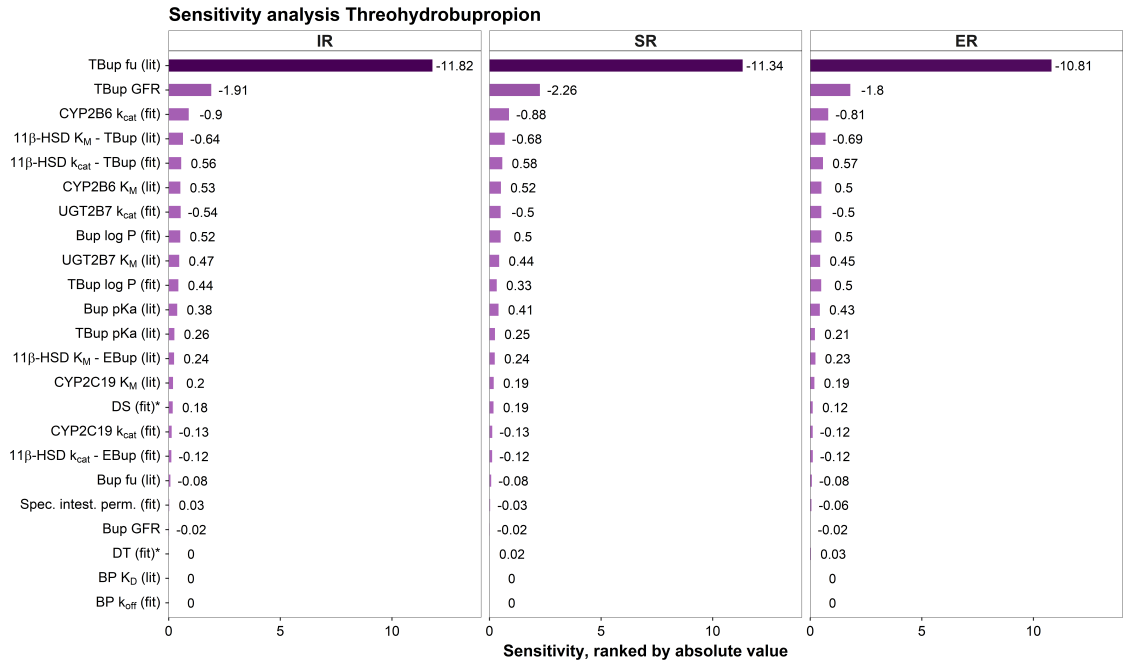

Figure S2.5.22: **Bupropion PBPK model sensitivity analyses - threohydrobupropion**. *****, fitted for IR and SR; **11β-HSD**, 11β-hydroxysteroid dehydrogenase 1; **BP**, binding partner; **Bup**, bupropion; **CYP**, cytochrome P450; **DS**, dissolution shape; **DT**, dissolution time; **EBup**, erythrobupropion; **ER**, extended release; **fit.**, fitted in parameter optimization; **GFR**, glomerular filtration rate; **IR**, immediate release; $\mathbf{K_D}$, dissociation constant for binding; $\mathbf{k_{cat}}$, catalytic rate constant; $\mathbf{K_M}$, Michaelis-Menten constant; $\mathbf{k_{off}}$, dissociation rate constant for binding; **lit.**, literature; **log P**, lipophilicity; **pKa**, acidic dissociation; **Spec. intest. perm.**, specific intestinal permeability; textbfSR, sustained release; **TBup**, threohydrobupropion.

3 DGI prediction

3.1 Background

CYP2B6 expression can be influenced by polymorphisms, especially single nucleotide polymorphisms [21]. Several genetic variants for the gene encoding for CYP2B6 have been reported [75]. According to dose recommendations published by the clinical pharmacogenetics implementation consortium (CPIC), these can lead to different phenotypes, i.e. poor metabolizers (PM), intermediate metabolizers (IM), normal metabolizers (NM) and rapid metabolizers (RM) [75]. For bupropion, dose recommendation based on CYP2B6 genotype are not established yet. Genetic polymorphisms that were included in the model were: *CYP2B6*1*, *CYP2B6*4*, *CYP2B6*5* and *CYP2B6*6*. Various combinations as homo- or heterozygous expressions of these polymorphisms were simulated. Polymorphisms were chosen based on their frequency and functionality in order to describe various investigated phenotypes (*CYP2B6*1*: 49.07%, *CYP2B6*4*: 4.09%, *CYP2B6*5*: 11.55% and *CYP2B6*6*: 23.30% in European populations).
For the description of different allele combinations, the enzyme was integrated twice. For the variants *CYP2B6*4* and *CYP2B6*5*, necessary parameters (K_M and k_{cat}) were obtained from literature. Furthermore, K_M values for the *CYP2B6*1* and *CYP2B6*6* genotypes were also derived from the literature, whereas the k_{cat} value for *CYP2B6*1* was optimized with data on mostly wildtype subjects and the k_{cat} value for *CYP2B6*6* by fitting plasma concentration-time profiles to a study including only *CYP2B6*6*/**6* subjects. Tabls S3.1 lists the clinical studies and Table S3.2 the model parameter used for DGI prediction. DGI $AUC_{HBup/Bup}$ and $C_{max\ HBup/Bup}$ ratios calculated from predictions were compared to observed values described in the literature.

3.2 Clinical studies

Clinical studies listed in Table S3.1 include data of patients with *CYP2B6* variants. Virtual individuals were built according to the demographics published in the respective study reports. If no data on demographics was reported, a standard individual were used as described in Section 1.4.

Table S3.1: Clinical studies used for DGI model development.

Dosing	n	Age [years]	Weight [kg]	BMI [kg/m²]	Females [%]	*CYP2B6* genotype (n)	Dataset	Reference
150 mg IR (s.d.)	21	28 (±7)	72 (±14)	-	57	**1/*1*	te	Kharasch 2019 [21]
150 mg IR (s.d.)	4	29 (±7)	68 (±14)	-	50	**1/*4* and **4/*6*	te	Kharasch 2019 [21]
150 mg IR (s.d.)	20	28 (±8)	78 (±12)	-	30	**1/*6*	te	Kharasch 2019 [21]
150 mg IR (s.d.)	2	28 (±1)	84 (±0)	-	0	**5/*5*	te	Kharasch 2019 [21]
150 mg IR (s.d.)	17	32 (±9)	71 (±13)	-	59	**6/*6*	ta	Kharasch 2019 [21]
150 mg SR (s.d.)	22	22.7	65	-	27.3	**1/*1* (19), **1/*4* (3)	ta	Chung 2011 [38]
150 mg SR (s.d.)	13	22.7	65	-	27.3	**1/*6* (11), **6/*6* (2)	te	Chung 2011 [38]
150 mg SR (s.d.)	19	-	-	-	-	**1/*1*	te	[a]Gao 2016 [13]
150 mg SR (s.d.)	11	-	-	-	-	**1/*6*	te	[a]Gao 2016 [13]
150 mg SR (s.d.)	6	-	-	-	-	**6/*6*	te	[a]Gao 2016 [13]
150 mg SR (s.d.)	6	22 (19–34)	72 (53–99)	23.1 (18.4–26.9)	0	**1/*1*	te	Loboz 2006 [44]
150 mg SR (s.d.)	1	22 (20–32)	64 (53–76)	21.4 (18.4–24.4)	0	**1/*4*	te	Loboz 2006 [44]
150 mg SR (s.d.)	1	22 (19–34)	80 (60–99)	24.8 (19.7–26.9)	0	**1/*5*	te	Loboz 2006 [44]
150 mg SR (s.d.)	6	22 (19–34)	72 (53–99)	23.1 (18.4–26.9)	0	**1/*6*	te	Loboz 2006 [44]
150 mg SR (s.d.)	1	22 (19–34)	80 (60–99)	24.8 (19.7–26.9)	0	**5/*5*	te	Loboz 2006 [44]
150 mg SR (s.d.)	1	22 (20–32)	64 (53–76)	21.4 (18.4–24.4)	0	**4/*6*	te	Loboz 2006 [44]
150 mg SR (s.d.)	1	22 (20–32)	64 (53–76)	21.4 (18.4–24.4)	0	**6/*6*	te	Loboz 2006 [44]

BMI, body mass index; **CYP**, cytochrome P450; **IR**, immediate release formulation; **n**, number of individuals studied; **s.d.**, single dose; **SR**, sustained release formulation; **ta**, training dataset; **te**, test dataset; **-**, no data available. Values are given as mean ± standard deviation (SD), the range of values is given in brackets.
[a], reported as SR but simulated as IR due to early C_{max} vales observed.

3.3 Drug-dependent model parameters

For implementation of the DGIs, model parameters were used as for the general model listed previously in Table S2.2. Table S3.2 lists the parameters that were adapted for different genotype scenarios. Details on DGI implementation can be found in Section 1.5.1.

Table S3.2: Model parameter adapted for DGI implementation.

Parameter	Unit	Value	Source	Reference	Description
CYP2B6 K_M **1*	µmol/l	25.80	lit.	[66]	Michaelis-Menten constant for the **1* allele
CYP2B6 k_{cat} **1*	1/min	10.87	opt.	[66]	Catalytic rate constant for the **1* allele
CYP2B6 K_M **6*	µmol/l	61.62	lit.	[66]	Michaelis-Menten constant for the **6* allele
CYP2B6 k_{cat} **6*	1/min	9.52	opt.	[66]	Catalytic rate constant for the **6* allele
CYP2B6 K_M **4*	µmol/l	12.70	lit.	[76]	Michaelis-Menten constant for the **4* allele
CYP2B6 k_{cat} **4*	1/min	18.12	lit.	[76]	Catalytic rate constant for the **4* allele
CYP2B6 K_M **5*	µmol/l	15.59	lit.	[76]	Michaelis-Menten constant for the **5* allele
CYP2B6 k_{cat} **5*	1/min	11.28	lit.	[76]	Catalytic rate constant for the **5* allele

CYP, cytochrome P450; **lit.**, literature; **opt.**, optimized.

3.4 Concentration-time profiles

The geometric means of the population predictions (n=500) are shown as solid lines and corresponding observed data as filled dots. Symbols represent the arithmetic mean values ± standard deviation, if available. The shaded areas indicate the geometric standard deviation. Details on dosing regimens, study populations and literature references are listed in Table S3.1.

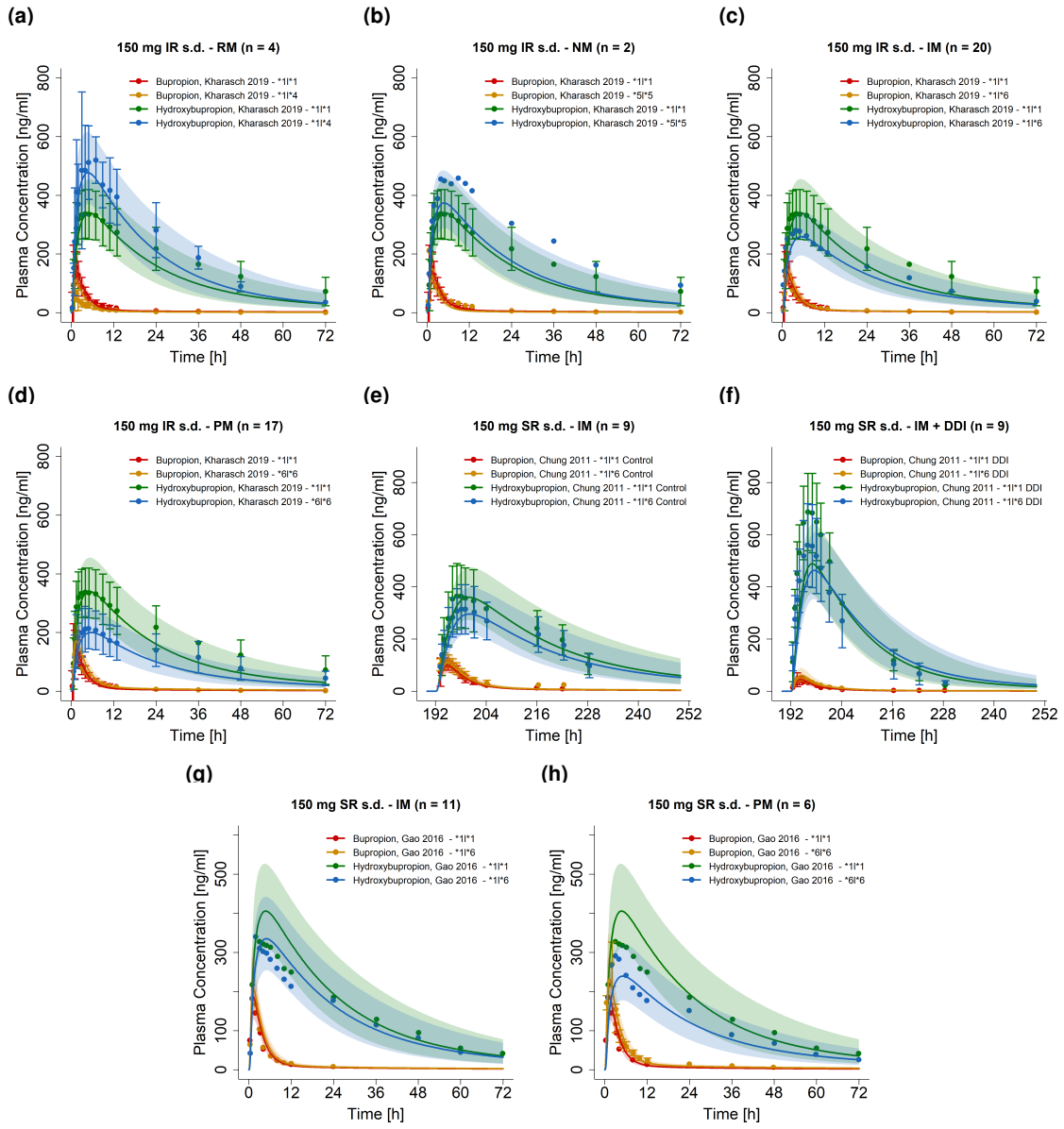

Figure S3.4.1: **Plasma concentration-time profiles of DGI predictions** on a linear scale. **Control**, without perpetrator; **DDI**, drug-drug-interaction with rifampicin; **IM**, intermediate metabolizers; **IR**, immediate release tablet; **NM**, normal metabolizers; **PM**, poor metabolizers; **RM**, rapid metabolizers; **s.d.**, single dose; **SR**, sustained release.

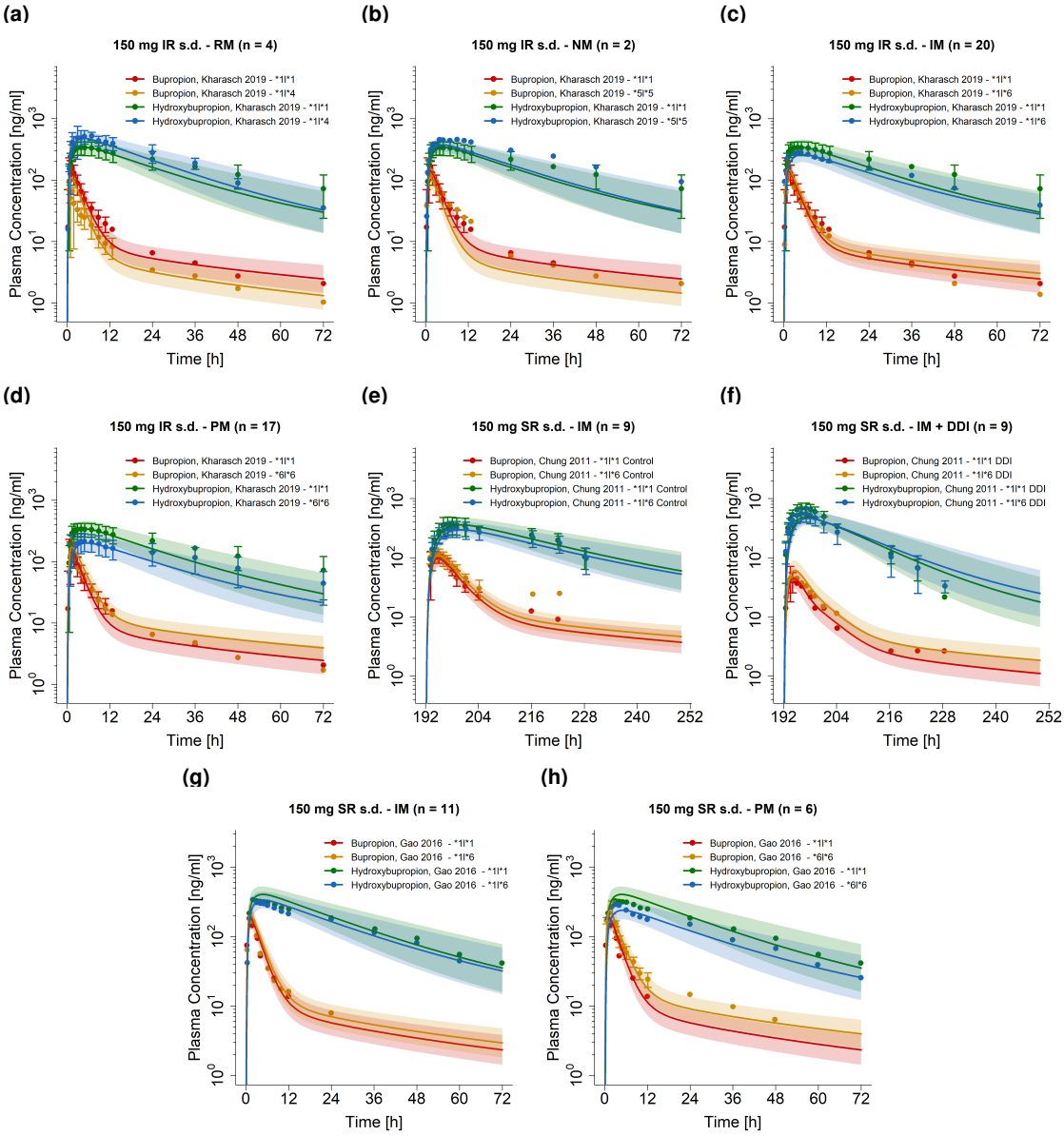

Figure S3.4.2: **Plasma concentration-time profiles of DGI predictions** on a semi-logarithmic scale. **Control**, without perpetrator; **DDI**, drug-drug-interaction with rifampicin; **IM**, intermediate metabolizers; **IR**, immediate release tablet; **NM**, normal metabolizers; **PM**, poor metabolizers; **RM**, rapid metabolizers; **s.d.**, single dose; **SR**, sustained release.

3.5 Model evaluation

3.5.1 Predicted compared to observed concentrations goodness-of-fit plots

Following, goodness-of-fit plots of predicted compared to observed plasma concentrations are illustrated in Figure S3.5.3. Details on dosing regimens, study populations and literature references are listed in Table S3.1. Predicted and observed PK parameters are summarized in Table S3.4.

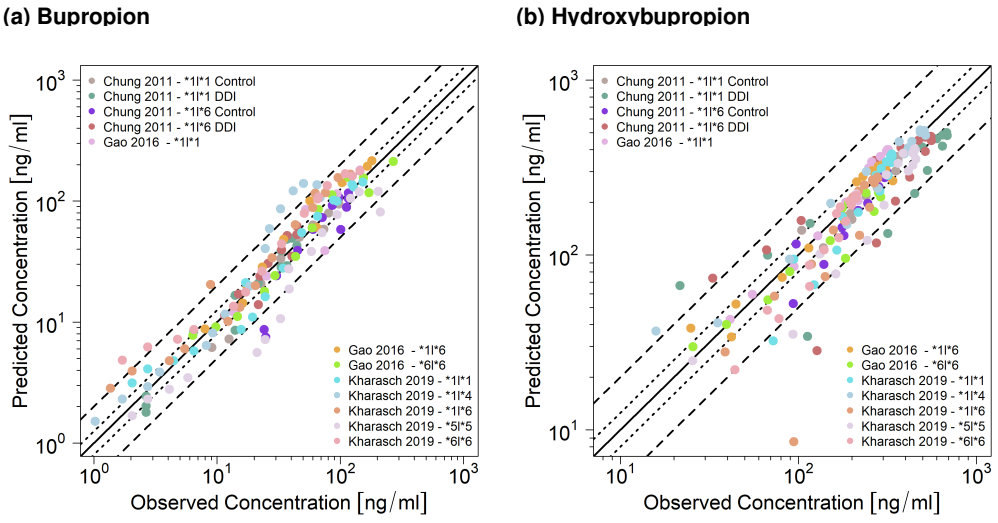

Figure S3.5.3: **DGI predicted compared to observed plasma concentrations of (a) bupropion and (b) hydroxybupropion.** The solid line marks the line of identity. Dotted lines indicate 1.25-fold, dashed lines indicate 2-fold deviation. **Control**, without perpetrator; **DDI**, drug-drug-interaction with perpetrator; **DGI**, drug-gene-interaction.

3.5.2 Mean relative deviation of plasma concentration predictions

Table S3.3: Mean relative deviation values of bupropion and hydroxybupropion DGI plasma concentration predictions.

Dosing	n	Compound	MRD	Compound	MRD	Dataset	Reference
150 mg IR (s.d.)	21	Bup	1.34	HBup	1.16	te	Kharasch 2019 **1/*1* [21]
150 mg IR (s.d.)	4	Bup	1.63	HBup	1.29	te	Kharasch 2019 **1/*4* & **4/*6* [21]
150 mg IR (s.d.)	20	Bup	1.86	HBup	1.48	te	Kharasch 2019 **1/*6* [21]
150 mg IR (s.d.)	2	Bup	1.58	HBup	1.17	te	Kharasch 2019 **5/*5* [21]
150 mg IR (s.d.)	17	Bup	1.91	HBup	1.16	ta	Kharasch 2019 **6/*6* [21]
150 mg SR (s.d.)	13	Bup	1.14	HBup	1.10	ta	Chung 2011 **1/*1* Control [38]
150 mg SR (s.d.)	13	Bup	1.47	HBup	1.42	ta	Chung 2011 **1/*1* DDI [38]
150 mg SR (s.d.)	9	Bup	1.28	HBup	1.11	te	Chung 2011 **1/*6* Control [38]
150 mg SR (s.d.)	9	Bup	1.37	HBup	1.39	te	Chung 2011 **1/*6* DDI [38]
150 mg SR (s.d.)	19	Bup	1.33	HBup	1.17	te	Gao 2016 **1/*1* [13]
150 mg SR (s.d.)	11	Bup	1.43	HBup	1.18	te	Gao 2016 **1/*6* [13]
150 mg SR (s.d.)	6	Bup	1.28	HBup	1.15	te	Gao 2016 **6/*6* [13]
		Mean	**1.33 (1.10–1.91)**				
		Median	**1.29 (1.10–1.91)**				
			100% (24/24) $\leq$ 2				

Bup, bupropion; **Control**, without perpetrator; **DDI**, drug-drug-interaction with perpetrator; **HBup**, hydroxybupropion; **IR**, immediate release formulation; **m.d.**, multiple dose; **MRD**, mean relative deviation; **n**, number of individuals studied; **s.d.**, single dose; **SR**, sustained release formulation; **ta**, training dataset; **te**, test dataset.

3.5.3 AUC and C_{max} goodness-of-fit plots

Following, predicted compared to observed AUC and C_{max} values are shown for individual bupropion and hydroxybupropion profiles, their metabolite-parent AUC and C_{max} ratio and their DGI effect metabolite-parent AUC and C_{max} ratio, respectively. Details on dosing regimens, study populations and literature references are listed in Table S3.1. Predicted and observed PK parameters are summarized in Tables S3.4, S3.5 and S3.6.

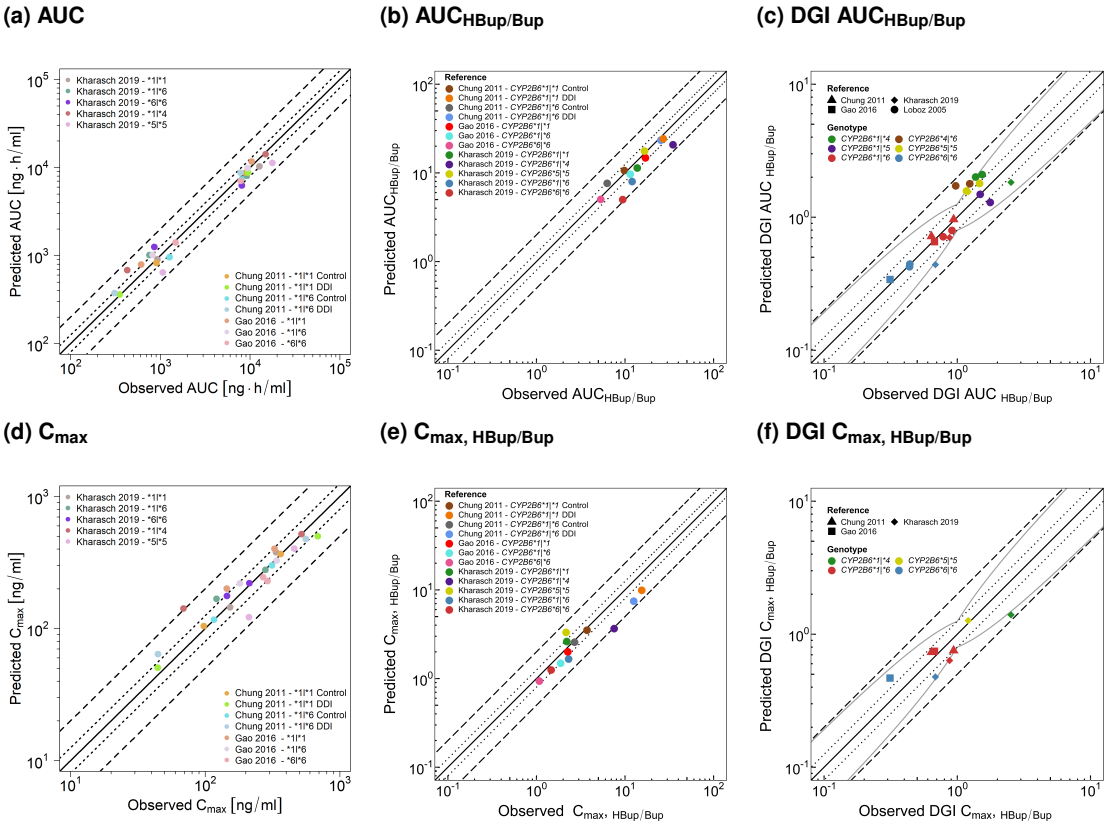

Figure S3.5.4: **Predicted compared to observed (a) AUC values, (b) $AUC_{HBup/Bup}$ ratios, (c) DGI $AUC_{HBup/Bup}$, (d) C_{max} values, (e) $C_{max,\ HBup/Bup}$ ratios and (f) DGI $C_{max,\ HBup/Bup}$ ratios.** The solid line marks the line of identity. Dotted lines indicate 1.25-fold, dashed lines indicate 2-fold deviation. The curved gray lines show the prediction success limits suggested by Guest et al. allowing a 1.25-fold variability [77]. **AUC**, area under the plasma concentration-time curve; **Bup**, bupropion; **C_{max}**, maximum plasma concentration; **Control**, without perpetrator; **DDI**, drug-drug-interaction with perpetrator; **DGI**, drug-gene-interaction; **HBup**, hydroxybupropion.

3.5.4 Geometric mean fold error of predicted AUC and C_{max} values, $AUC_{HBup/Bup}$ and $C_{max,\ HBup/Bup}$ ratios, and DGI $AUC_{HBup/Bup}$ and DGI $C_{max,\ HBup/Bup}$ ratios

Table S3.4: Predicted and observed AUC_{last} and C_{max} values of bupropion and hydroxybupropion DGI plasma concentrations.

Dosing	n	Compound	AUC_{last} pred [ng*h/ml]	AUC_{last} obs [ng*h/ml]	AUC_{last} pred/obs	C_{max} pred [ng/ml]	C_{max} obs [ng/ml]	C_{max} pred/obs	Dataset	Reference
150 mg IR (s.d.)	21	Bup	907.72	928.90	0.98	144.55	153.01	0.94	te	Kharasch 2019 **1/*1* [21]
150 mg IR (s.d.)	4	Bup	683.07	429.31	1.59	141.71	68.99	2.05	te	Kharasch 2019 **1/*4* & **4/*6* [21]
150 mg IR (s.d.)	20	Bup	1014.16	759.08	1.34	167.69	121.58	1.38	te	Kharasch 2019 **1/*6* [21]
150 mg IR (s.d.)	2	Bup	640.82	1070.57	0.60	121.60	212.09	0.57	te	Kharasch 2019 **5/*5* [21]
150 mg IR (s.d.)	17	Bup	1251.29	860.49	1.45	176.61	145.49	1.21	ta	Kharasch 2019 **6/*6* [21]
150 mg SR (s.d.)	13	Bup	823.49	909.01	0.91	104.29	97.73	1.07	ta	Chung 2011 **1/*1* Control [38]
150 mg SR (s.d.)	13	Bup	360.82	351.52	1.03	50.49	44.49	1.13	ta	Chung 2011 **1/*1* DDI [38]
150 mg SR (s.d.)	9	Bup	958.22	1268.88	0.76	116.76	116.63	1.00	te	Chung 2011 **1/*6* Control [38]
150 mg SR (s.d.)	9	Bup	373.58	309.15	1.21	63.99	44.66	1.43	te	Chung 2011 **1/*6* DDI [38]
150 mg SR (s.d.)	19	Bup	790.62	613.15	1.29	200.62	144.96	1.38	te	Gao 2016 **1/*1* [13]
150 mg SR (s.d.)	11	Bup	1016.99	820.34	1.24	219.70	181.33	1.21	te	Gao 2016 **1/*6* [13]
150 mg SR (s.d.)	6	Bup	1402.08	1483.80	0.94	244.27	269.84	0.91	te	Gao 2016 **6/*6* [13]
150 mg IR (s.d.)	28	HBup	10298.60	12764.00	0.81	378.25	336.77	1.12	te	Kharasch 2019 **1/*1* [21]
150 mg IR (s.d.)	4	HBup	14169.45	14938.93	0.95	518.15	520.08	1.00	te	Kharasch 2019 **1/*4* and **4/*6* [21]
150 mg IR (s.d.)	20	HBup	8093.83	9126.07	0.89	278.28	280.29	0.99	te	Kharasch 2019 **1/*6* [21]
150 mg IR (s.d.)	2	HBup	11293.90	17774.72	0.64	402.75	458.17	0.88	te	Kharasch 2019 **5/*5* [21]
150 mg IR (s.d.)	17	HBup	6250.18	8101.38	0.77	220.67	213.17	1.04	ta	Kharasch 2019 **6/*6* [21]
150 mg SR (s.d.)	13	HBup	8744.70	8936.26	0.98	366.16	363.64	1.01	ta	Chung 2011 **1/*1* Control [38]
150 mg SR (s.d.)	13	HBup	8750.56	9498.00	0.92	499.27	687.07	0.73	ta	Chung 2011 **1/*1* DDI [38]
150 mg SR (s.d.)	9	HBup	7304.46	7976.41	0.92	300.13	314.03	0.96	te	Chung 2011 **1/*6* Control [38]
150 mg SR (s.d.)	9	HBup	8726.17	7838.55	1.11	476.89	559.91	0.85	te	Chung 2011 **1/*6* DDI [38]
150 mg SR (s.d.)	19	HBup	11675.08	10421.81	1.12	401.09	327.24	1.23	te	Gao 2016 **1/*1* [13]
150 mg SR (s.d.)	11	HBup	9827.62	9404.32	1.05	326.93	340.08	0.96	te	Gao 2016 **1/*6* [13]
150 mg SR (s.d.)	6	HBup	7045.71	7886.01	0.89	228.64	291.04	0.79	te	Gao 2016 **6/*6* [13]
GMFE (range)				**1.22 (1.02–1.59)**			**1.21 (1.00–2.05)**			
pred/obs within twofold (range)				**100%; 24/24 (0.60–1.59)**			**95.83%; 23/24 (0.57–2.05)**			

AUC, area under the plasma concentration-time curve; **Bup**, bupropion; **C_{max}**, maximum plasma concentration; **Control**, without perpetrator; **DDI**, drug-drug-interaction with perpetrator; **GMFE**, geometric mean fold error; **HBup**, hydroxybupropion; **IR**, immediate release formulation; **n**, number of individuals studied; **obs**, observed; **pred**, predicted; **s.d.**, single dose; **SR**, sustained release formulation; **ta**, training dataset; **te**, test dataset.

Table S3.5: Predicted and observed $AUC_{HBup/Bup}$ and $C_{max,\ HBup/Bup}$ ratios of bupropion and hydroxybupropion DGI plasma concentrations.

Dosing	n	$AUC_{HBup/Bup}$ pred	$AUC_{HBup/Bup}$ obs	$AUC_{HBup/Bup}$ pred/obs	$C_{max,\ HBup/Bup}$ pred	$C_{max,\ HBup/Bup}$ obs	$C_{max,\ HBup/Bup}$ pred/obs	Dataset	Reference
150 mg IR (s.d.)	28	11.35	13.74	0.83	2.62	2.20	1.19	te	Kharasch 2019 **1/*1* [21]
150 mg IR (s.d.)	4	20.74	34.80	0.60	3.66	7.54	0.49	te	Kharasch 2019 **1/*4* and **4/*6* [21]
150 mg IR (s.d.)	20	7.98	12.02	0.66	1.66	2.31	0.72	te	Kharasch 2019 **1/*6* [21]
150 mg IR (s.d.)	2	17.62	16.60	1.06	3.31	2.16	1.53	te	Kharasch 2019 **5/*5* [21]
150 mg IR (s.d.)	17	4.99	9.41	0.53	1.25	1.47	0.85	ta	Kharasch 2019 **6/*6* [21]
150 mg SR (s.d.)	13	10.62	9.83	1.08	3.51	3.72	0.94	ta	Chung 2011 **1/*1* Control [38]
150 mg SR (s.d.)	13	24.25	27.02	0.90	9.89	15.44	0.64	ta	Chung 2011 **1/*1* DDI [38]
150 mg SR (s.d.)	9	7.62	6.29	1.21	2.57	2.69	0.95	te	Chung 2011 **1/*6* Control [38]
150 mg SR (s.d.)	9	23.36	25.36	0.92	7.45	12.54	0.59	te	Chung 2011 **1/*6* DDI [38]
150 mg SR (s.d.)	19	14.77	17.00	0.87	2.00	2.26	0.89	te	Gao 2016 **1/*1* [13]
150 mg SR (s.d.)	11	9.66	11.46	0.84	1.49	1.88	0.79	te	Gao 2016 **1/*6* [13]
150 mg SR (s.d.)	6	5.03	5.31	0.95	0.94	1.08	0.87	te	Gao 2016 **6/*6* [13]
150 mg SR (s.d.)	6	11.76	18.50	0.64	-	-	-	te	Loboz 2006 **1/*1* Control [44]
150 mg SR (s.d.)	6	21.78	30.90	0.70	-	-	-	te	Loboz 2006 **1/*1* DDI [44]
150 mg SR (s.d.)	1	22.75	25.40	0.90	-	-	-	te	Loboz 2006 **1/*4* Control [44]
150 mg SR (s.d.)	1	45.56	47.50	0.96	-	-	-	te	Loboz 2006 **1/*4* DDI [44]
150 mg SR (s.d.)	1	15.47	32.70	0.47	-	-	-	te	Loboz 2006 **1/*5* Control [44]
150 mg SR (s.d.)	1	32.36	45.90	0.71	-	-	-	te	Loboz 2006 **1/*5* DDI [44]
150 mg SR (s.d.)	6	8.38	14.50	0.58	-	-	-	te	Loboz 2006 **1/*6* Control [44]
150 mg SR (s.d.)	6	17.32	28.20	0.61	-	-	-	te	Loboz 2006 **1/*6* DDI [44]
150 mg SR (s.d.)	1	19.58	18.00	1.09	-	-	-	te	Loboz 2006 **4/*6* Control [44]
150 mg SR (s.d.)	1	38.87	38.30	1.01	-	-	-	te	Loboz 2006 **4/*6* DDI [44]
150 mg SR (s.d.)	1	18.87	21.70	0.87	-	-	-	te	Loboz 2006 **5/*5* Control [44]
150 mg SR (s.d.)	1	39.06	45.40	0.86	-	-	-	te	Loboz 2006 **5/*5* DDI [44]
150 mg SR (s.d.)	1	4.98	8.10	0.61	-	-	-	te	Loboz 2006 **6/*6* Control [44]
150 mg SR (s.d.)	1	9.69	13.60	0.71	-	-	-	te	Loboz 2006 **6/*6* DDI [44]
GMFE (range)			**1.33 (1.01–2.14)**			**1.31 (1.04–2.06)**			
pred/obs within twofold (range)			**96.15%; 25/26 (0.47–1.21)**			**91.67%; 11/12 (0.49–1.53)**			

AUC, area under the plasma concentration-time curve; **Bup**, bupropion; **C_{max}**, maximum plasma concentration; **Control**, without perpetrator; **DDI**, drug-drug-interaction with perpetrator; **GMFE**, geometric mean fold error; **HBup**, hydroxybupropion; **IR**, immediate release formulation; **n**, number of individuals studied; **obs**, observed; **pred**, predicted; **s.d.**, single dose; **SR**, sustained release formulation; **ta**, training dataset; **te**, test dataset; **-**, no data available.

Table S3.6: Predicted and observed DGI $AUC_{HBup/Bup}$ and DGI $C_{max,\ HBup/Bup}$ ratios of bupropion and hydroxybupropion DGI plasma concentrations.

Dosing	n	DGI $AUC_{HBup/Bup}$ pred	DGI $AUC_{HBup/Bup}$ obs	DGI $AUC_{HBup/Bup}$ pred/obs	DGI $C_{max,\ HBup/Bup}$ pred	DGI $C_{max,\ HBup/Bup}$ obs	DGI $C_{max,\ HBup/Bup}$ pred/obs	Dataset	Reference
150 mg IR (s.d.)	4	1.83	2.53	0.72	1.40	3.43	0.41	te	Kharasch 2019 **1/*4* and **4/*6* [21]
150 mg IR (s.d.)	20	0.70	0.87	0.80	0.63	1.05	0.60	te	Kharasch 2019 **1/*6* [21]
150 mg IR (s.d.)	2	1.55	1.21	1.28	1.26	0.98	1.29	te	Kharasch 2019 **5/*5* [21]
150 mg IR (s.d.)	17	0.44	0.68	0.64	0.48	0.67	0.71	ta	Kharasch 2019 **6/*6* [21]
150 mg SR (s.d.)	9	0.72	0.64	1.13	0.73	0.64	1.12	te	Chung 2011 **1/*6* Control [38]
150 mg SR (s.d.)	9	0.96	0.94	1.02	0.75	0.94	1.02	te	Chung 2011 **1/*6* DDI [38]
150 mg SR (s.d.)	11	0.65	0.67	0.97	0.75	0.83	0.90	te	Gao 2016 **1/*6* [13]
150 mg SR (s.d.)	6	0.34	0.31	1.09	0.47	0.48	0.98	te	Gao 2016 **6/*6* [13]
150 mg SR (s.d.)	1	2.01	1.37	1.46	-	-	-	te	Loboz 2006 **1/*4* Control [44]
150 mg SR (s.d.)	1	2.09	1.54	1.36	-	-	-	te	Loboz 2006 **1/*4* DDI [44]
150 mg SR (s.d.)	1	1.29	1.77	0.73	-	-	-	te	Loboz 2006 **1/*5* Control [44]
150 mg SR (s.d.)	1	1.49	1.49	1.00	-	-	-	te	Loboz 2006 **1/*5* DDI [44]
150 mg SR (s.d.)	6	0.71	0.78	0.91	-	-	-	te	Loboz 2006 **1/*6* Control [44]
150 mg SR (s.d.)	6	0.80	0.91	0.87	-	-	-	te	Loboz 2006 **1/*6* DDI [44]
150 mg SR (s.d.)	1	1.72	0.97	1.77	-	-	-	te	Loboz 2006 **4/*6* Control [44]
150 mg SR (s.d.)	1	1.78	1.24	1.44	-	-	-	te	Loboz 2006 **4/*6* DDI [44]
150 mg SR (s.d.)	1	1.58	1.17	1.34	-	-	-	te	Loboz 2006 **5/*5* Control [44]
150 mg SR (s.d.)	1	1.79	1.47	1.22	-	-	-	te	Loboz 2006 **5/*5* DDI [44]
150 mg SR (s.d.)	1	0.42	0.44	0.97	-	-	-	te	Loboz 2006 **6/*6* Control [44]
150 mg SR (s.d.)	1	0.44	0.44	1.01	-	-	-	te	Loboz 2006 **6/*6* DDI [44]
GMFE (range)			**1.25 (1.00–1.77)**			**1.35 (1.05–2.44)**			
pred/obs within twofold (range)			**100%; 20/20 (0.64–1.77)**			**87.5%; 7/8 (0.41–1.29)**			

AUC, area under the plasma concentration-time curve; **Bup**, bupropion; **C_{max}**, maximum plasma concentration; **Control**, without perpetrator; **DDI**, drug-drug-interaction with perpetrator; **GMFE**, geometric mean fold error; **HBup**, hydroxybupropion; **IR**, immediate release formulation; **n**, number of individuals studied; **obs**, observed; **pred**, predicted; **s.d.**, single dose; **SR**, sustained release formulation; **ta**, training dataset; **te**, test dataset; **-**, no data available.

4 DDI prediction

4.1 PBPK modeling of rifampicin

The antibiotic rifampicin exhibits a strong DDI potential. As an agonist of the pregnane X receptor, rifampicin induces multiple metabolizing enzymes, i.e. CYPs (CYP2B6 or CYP2C19) and UGTs (UGT2B7) [38]. The rifampicin PBPK model was developed and applied for several DDI predictions in previous publications [78–80]. For prediction of rifampicin-bupropion DDIs, interaction parameters were gathered from literature for implementation of rifampicins' influence on the following enzymes: CYP2B6, CYP2C19 and UGT2B7. Drug-dependent parameters of the rifampicin model are listed in Table S4.1.

Table S4.1: Drug-dependent parameters of the rifampicin PBPK model.

Parameter	Unit	Value	Source	Reference	Description
MW	g/mol	822.94	lit.	[a]DB01045	Molecular weight
pKa (acid)	-	1.70	lit.	[81]	Acid dissociation constant
pKa (base)	-	7.90	lit.	[81]	Acid dissociation constant
Solubility (pH)	g/l	2.80 (7.5)	lit.	[82–85]	Solubility
logP	-	[b]2.50	1.30, 2.70	[82, 86]	Lipophilicity
fu	%	17.0	lit.	[87]	Fraction unbound
B/P ratio	-	0.89	[c], [d]0.89	[88]	Blood/plasma ratio
Specific intest. perm.	cm/min	[b]1.24E-05	[d]3.84E-07	PK-Sim®	Normalized to surface area
Organ perm.	cm/min	2.93E-05	[d]2.93E-05.	PK-Sim®	Normalized to surface are
GFR fraction	-	1.00	asm.	-	Fraction of filtered drug in the urine
EHC cont. fraction	-	1.00	asm.	-	Fraction of bile continually released
Cellular permeabilities	cm/min	PK-Sim std.	-	[1]	Permeation across cell membranes
Partition coefficients	-	R&R	-	[89, 90]	Organ-plasma partition coefficients
AADAC K_M	µmol/l	195.10	lit.	[91]	AADAC Michaelis-Menten constant
AADAC kcat	1/min	[b]9.87	-	-	AADAC catalytic rate constant
OATP1B1 K_M	µmol/l	1.50	lit.	[92]	OATP1B1 Michaelis-Menten constant
OATP1B1 kcat	1/min	[b]105.41	-	-	OATP1B1 catalytic rate constant
Pgp K_M	µmol/l	55.0	lit.	[93]	Pgp Michaelis-Menten constant
Pgp kcat	1/min	[b]0.61	-	-	Pgp catalytic rate constant
Induction EC_{50}	µmol/l	0.34	lit.	[87, 94]	Conc. for half-maximal induction
AADAC E_{max}	-	[b]0.99	-	-	Maximum in vivo induction effect
OATP1B1 E_{max}	-	[b]0.38	-	-	Maximum in vivo induction effect
Pgp E_{max}	-	2.50	lit.	[95]	Maximum in vivo induction effect
CYP2B6 E_{max}	-	3.60	lit.	[96]	Maximum in vivo induction effect
CYP2C19 E_{max}	-	1.07	lit.	[97]	Maximum in vivo induction effect
UGT2B7 E_{max}	-	1.79	lit.	[98]	Maximum in vivo induction effect
OATP1B1 K_i	µmol/l	0.48	lit.	[99]	Conc. for half-maximal inhibition
Pgp K_i	µmol/l	169.00	lit.	[100]	Conc. for half-maximal inhibition
CYP2B6 K_i	µmol/l	[e]118.5	lit.	[101]	Conc. for half-maximal inhibition
UGT2B7 K_i	µmol/l	[e]554.0	lit.	[102]	Conc. for half-maximal inhibition
Formulation		Solution			

asm., assumed; **conc.**, concentration; **cont.**, continuous; **CYP**, cytochrome P450; **EHC**, enterohepatic circulation; **intest.**, intestinal; **GFR**, glomerular filtration rate; **lit.**, literature; **OATP**, organic anion transporting polypeptide; **perm.**, permeability; **Pgp**, P-glycoprotein; **PK-Sim std.**, PK-Sim Standard calculation method; **R&R**, Rodgers and Rowland calculation method; **UGT**, uridine 5'-diphosphoglucuronosyltransferase; **-**, not available.

[a], https://www.drugbank.ca/drugs/DB01045, 22 October 2018

[b], optimized

[c], blood/serum concentration ratio

[d], calculated parameter

[e], in vitro values corrected for binding in the assay using fraction unbound to microsomal protein [72]

4.2 PBPK modeling of fluvoxamine

The selective serotonin reuptake inhibitor fluvoxamine exhibits a strong inhibitory activity on several CYP enzymes, especially on CYP1A2, CYP2C19 and CYP3A4 [103, 104]. The fluvoxamine PBPK model was developed and applied for DDI predictions in a previous publication [103]. To describe a DDI cocktail study conducted by Bosilkovska et al. [25], the fluvoxamine model was used to predict the reported fluvoxamine-voriconazole-bupropion DDI, by implementing competitive inhibition on CYP2C19 and CYP3A4 using interaction parameters from the literature. Drug-dependent parameters of the fluvoxamine model are listed in Table S4.2.

Table S4.2: Drug-dependent parameters of the fluvoxamine PBPK model.

Parameter	Unit	Value	Source	Reference	Description
MW	g/mol	318.34	lit.	[a]DB00176	Molecular weight
pKa (base)	-	9.40	lit.	[105]	Acid dissociation constant
Solubility (pH)	mg/ml	14.66 (7.0)	lit.	MSDS	Solubility
logP	-	[b]3.57	3.20	[a]DB00176	Lipophilicity
fu	%	23	lit.	[106]	Fraction unbound
Specific intest. perm.	dm/min	[b]2.74E-06	[c]3.03E-5	PK-Sim®	Normalized to surface are
Specific organ perm.	dm/min	[c]0.02	[c]0.02	PK-Sim®	Normalized to surface are
GFR fraction	-	1.00	asm.	-	Fraction of filtered drug in the urine
EHC cont. fraction	-	1.00	asm.	-	Fraction of bile continually released
Cellular permeabilities	cm/min	PK-Sim std.	-	[1]	Permeation across cell membranes
Partition coefficients	cm/min	Schmitt	-	[107]	Organ-plasma partition coefficients
CYP1A2 K_M	µmol/l	[b]0.0074	-	-	CYP1A2 Michaelis-Menten constant
CYP1A2 kcat	1/min	[b]0.016	opt.	-	CYP1A2 catalytic rate constant
CYP2D6 K_M	µmol/l	76.30	lit.	[108]	CYP2D6 Michaelis-Menten constant
CYP2D6 kcat	1/min	[b]110.51	-	-	CYP2D6 catalytic rate constant
CYP2C19 K_i	µmol/l	0.013	lit.	[104]	Conc. for half-maximal inhibition
CYP3A4 K_i	µmol/l	1.60	lit.	[**? ?**]	Conc. for half-maximal inhibition
Formulation		Solution			

asm., assumed; **calc.**, calculated; **conc.**, concentration; **cont.**, continuous; **CYP**, cytochrome P450; **EHC**, enterohepatic circulation; **intest.**, intestinal; **GFR**, glomerular filtration rate; **lit.**, literature; **MSDS**, material safety data sheet; **perm.**, permeability; **PK-Sim std.**, PK-Sim Standard calculation method; **Schmitt**, Schmitt calculation method; **-**, not available.

[a], https://www.drugbank.ca/drugs/DB00176, 22 October 2018

[b], optimized

[c], calculated parameter

4.3 PBPK modeling of voriconazole

The antifungal voriconazole exhibits a strong inhibitory activity on several CYP enzymes, i.e. its mechanism-based autoinhibition of CYP3A4 [109]. Regarding CYP2B6 inhibition, voriconazole is known for its high interaction potential with the CYP2B6 substrate and inducer efavirenz [110]. As a CYP2C19 substrate and inhibitor, voriconazole also engages in CYP2C19 DDIs [111]. The voriconazole PBPK model was developed and applied for DDI predictions in a previous publication [112]. To describe a DDI cocktail study conducted by Bosilkovska et al. [25], the voriconazole model was used to predict the reported fluvoxamine-voriconazole-bupropion DDI, by implementing competitive inhibition on CYP2B6 and CYP2C19 using literature values. Drug-dependent parameters of the voriconazole model are listed in Table S4.3.

Table S4.3: Drug-dependent parameters of the voriconazole PBPK model.

Parameter	Unit	Value	Source	Reference	Description
MW	g/mol	349.30	lit.	[a]DB00582	Molecular weight
pKa (base)	-	1.60	lit.	[113]	Acid dissociation constant
Solubility (pH)	mg/ml	3.2 (1.0)	lit.	[113]	Solubility
		2.7 (1.2)	lit.	[114]	
		0.1 (7.0)	lit.	[a]DB00582	
logP	-	1.80	lit.	[14, 115]	Lipophilicity
fu	%	42.0	lit.	[115–117]	Fraction unbound
Specific intest. perm.	cm/s	[b]2.71E-04	2.81E-5	[116]	Normalized to surface are
Specific organ perm.	cm/s	4.30E-05	[c]4.30E-05	PK-Sim®	Normalized to surface are
GFR fraction	-	1.00	asm.	-	Fraction of filtered drug in the urine
EHC cont. fraction	-	1.00	asm.	-	Fraction of bile continually released
Cellular permeabilities	cm/s	PK-Sim std.	-	[1]	Permeation across cell membranes
Partition coefficients	cm/s	P. and T.	-	[115, 116]	Organ-plasma partition coefficients
CYP3A4 K_M	µmol/l	15.00	lit.	[115]	CYP3A4 Michaelis-Menten constant
CYP3A4 kcat	1/min	[b]2.12	0.31	[115]	CYP3A4 catalytic rate constant
CYP2C19 K_M	µmol/l	3.50	lit.	[115]	CYP2C19 Michaelis-Menten constant
CYP2C19 kcat	1/min	1.19	lit.	[115]	CYP2C19 catalytic rate constant
CYP3A4 K_I	µmol/l	9.33	lit.	[109]	Conc. for half-maximal inhibition
CYP3A4 k_{inact}	1/min	[b]0.0015	0.04	[109]	Maximum inactivation rate constant
CYP2B6 K_I	µmol/l	[b]0.07	[d]0.30	[111]	Conc. for half-maximal inhibition
CYP2C19 K_I	µmol/l	[d]4.57	lit.	[111]	Conc. for half-maximal inhibition
Weibull shape	-	[a]1.29	-	-	Shape used for Weibull
Weibull time	min	[a]30	-	-	Time of 50% dissolved

asm., assumed; **calc.**, calculated; **conc.**, concentration; **cont.**, continuous; **CYP**, cytochrome P450; **EHC**, enterohepatic circulation; **intest.**, intestinal; **GFR**, glomerular filtration rate; **lit.**, literature; **perm.**, permeability; **P. and T.**, Poulin and Theil calculation method; **PK-Sim std.**, PK-Sim Standard calculation method; **-**, not available.

[a], https://go.drugbank.com/drugs/DB00582 03.12.2020

[b], optimized

[c], calculated parameter

[d], in vitro values corrected for binding in the assay using fraction unbound to microsomal protein [72]

4.4 Clinical studies

In Tables S4.4 and S4.5, clinical studies used for DDI model development are listed. Virtual individuals were built according to the demographics published in the respective study report. If no data on demographics were reported, a standard individual was used as described in Section 1.4.

Table S4.4: Clinical studies used for rifampicin-bupropion DDI model development.

Rifampicin application	Bupropion application	Dose gap [h]	n	Age [years]	Weight [kg]	Females [%]	Dataset	Reference
600 mg po (tab) q.d. (D1–D7)	25 mg po (Cap) s.d. (D8)	12	10	23 (20–36)	22 (19.9–24.4)	0	te	Bosilkovska 2014 [25]
600 mg po (tab) q.d. (D1–D7)	150 mg po (IR) s.d. (D8)	12	10	31 (21–40)	73 (57–84)	60	te	Kharasch 2008a [34]
600 mg po (tab) q.d. (D1–D7)	150 mg po (SR) s.d. (D8)	24	22	22.7	65	27.3	te	Chung 2011 [38]
600 mg po (tab) q.d. (D1–D10)	150 mg po (SR) s.d. (D8)	12	17	22 (19–34)	72 (53–99)	0	te	Loboz 2006 [44]

Cap, capsule (Geneva cocktail [25]); **D**, study day; **IR**, immediate release formulations; **n**, number of individuals studied; **po**, oral; **q.d.**, once daily; **s.d.**, single dose; **SR**, sustained release formulations; **tab**, tablet; **te**, test dataset. Values are given as mean, the range of values is given in brackets.

Table S4.5: Clinical studies used for fluvoxamine-voriconazole-bupropion DDI model development.

Fluvoxamine application	Voriconazole application	Bupropion application	Dose gap [h]	n	Age [years]	Females [%]	Dataset	Reference
50 mg po (tab) b.i.d.	400 mg po (tab) s.d.	25 mg po (Cap) s.d.	12 (F), 2 (F), 2 (V)	10	23 (20–36)	0	ta	Bosilkovska 2014 [25]

b.i.d., twice daily; **Cap**, capsule (Geneva cocktail [25]); **D**, study day; **F**, fluvoxamine; **n**, number of individuals studied; **po**, oral; **s.d.**, single dose; **ta**, training dataset; **tab**, tablet; **V**, voriconazole. Values are given as mean, the range of values is given in brackets.

4.5 Concentration-time profiles

The geometric means of the population predictions (n=500) are shown as solid lines and corresponding observed data as filled dots. Symbols represent the arithmetic mean values ± standard deviation, if available. The shaded areas indicate the geometric standard deviation. Details on dosing regimens, study populations and literature references are listed in Tables S4.4 and S4.5.

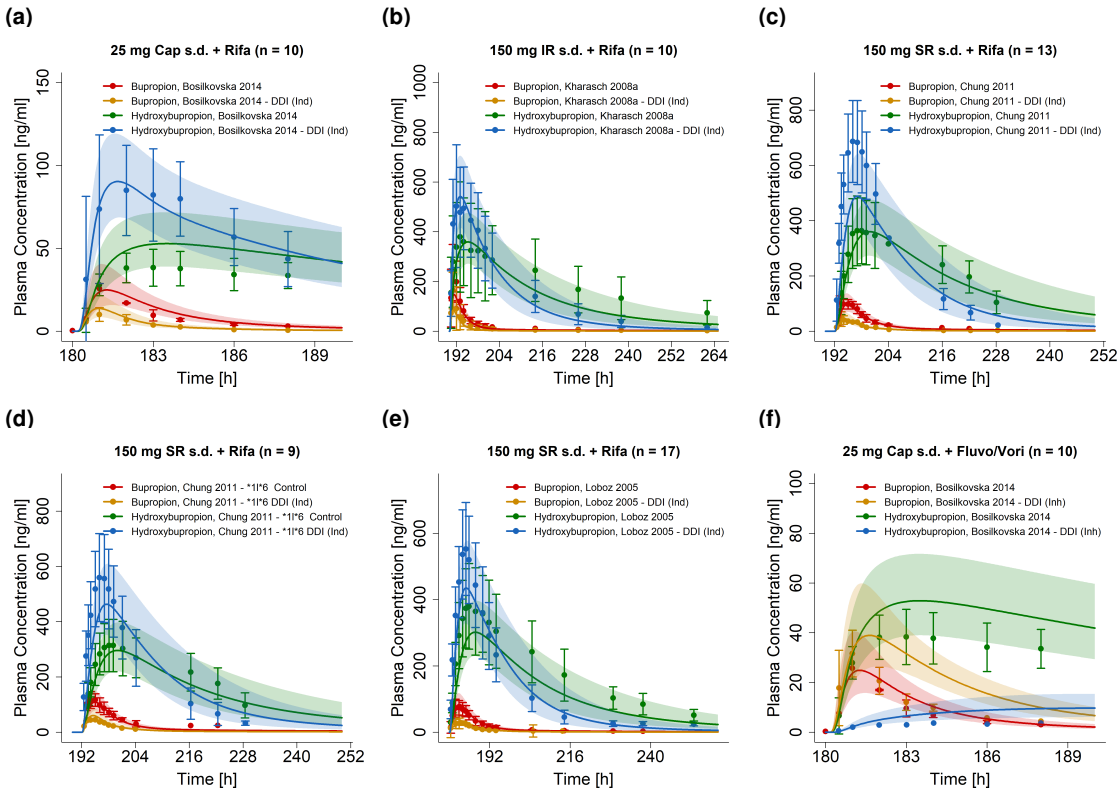

Figure S4.5.1: **Plasma concentration-time profiles of bupropion and hydroxybupropion DDI simulations** on a linear scale. **Cap**, capsule (Geneva cocktail [25]); **Control**, without perpetrator; **DDI (Ind)**, drug-drug-interaction with rifampicin as inducer; **DDI (Inh)**, drug-drug-interaction with fluvoxamine and voriconazole as inhibitors; **Fluvo/Vori**, fluvoxamine and voriconazole; **IR**, immediate release formulation; **Rifa**, rifampicin; **s.d.**, single dose; **SR**, sustained release formulation.

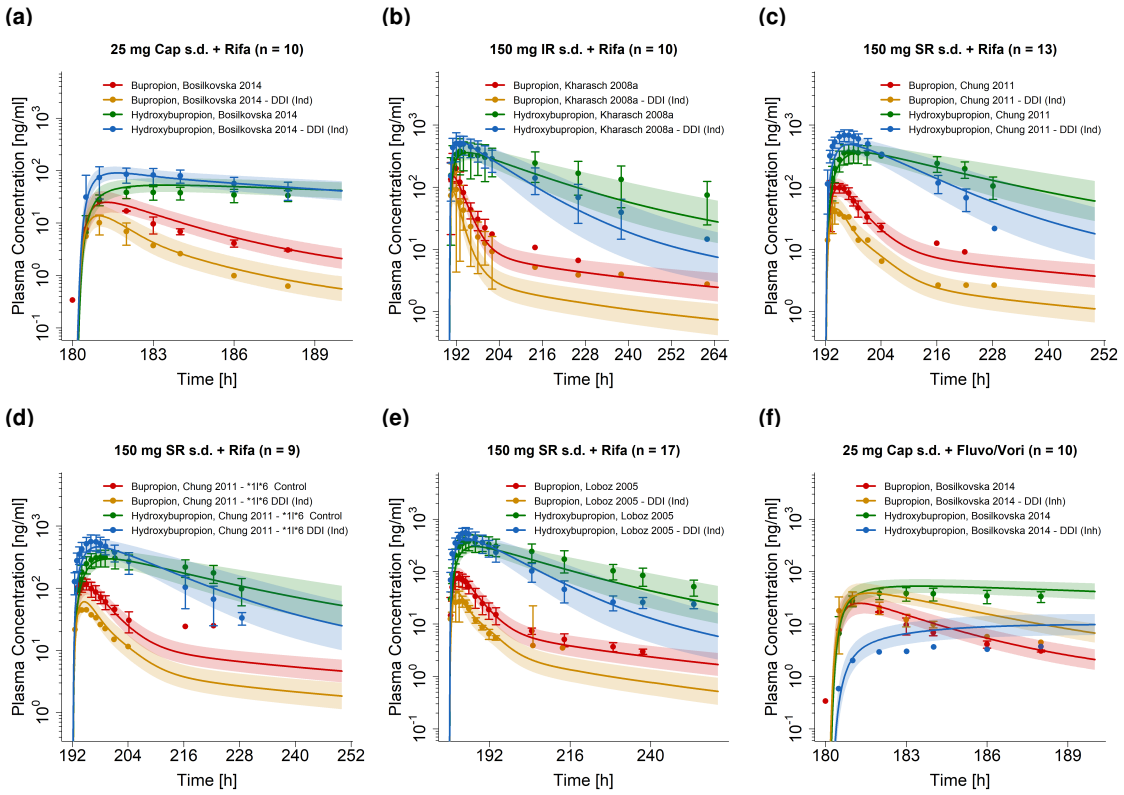

Figure S4.5.2: **Plasma concentration-time profiles of bupropion and hydroxybupropion DDI simulations** on a semi-logarithmic scale. **Cap**, capsule (Geneva cocktail [25]); **Control**, without perpetrator; **DDI (Ind)**, drug-drug-interaction with rifampicin as inducer; **DDI (Inh)**, drug-drug-interaction with fluvoxamine and voriconazole as inhibitors; **Fluvo/Vori**, fluvoxamine and voriconazole; **IR**, immediate release formulation; **Rifa**, rifampicin; **s.d.**, single dose; **SR**, sustained release formulation.

4.6 Model evaluation

4.6.1 Predicted compared to observed concentrations goodness-of-fit plots

Following, goodness-of-fit plots of predicted compared to observed plasma concentrations are illustrated in Figure S4.6.3. Details on dosing regimens, study populations and literature references are listed in Tables S4.4 and S4.5. Predicted and observed PK parameters are summarized in Table S4.7.

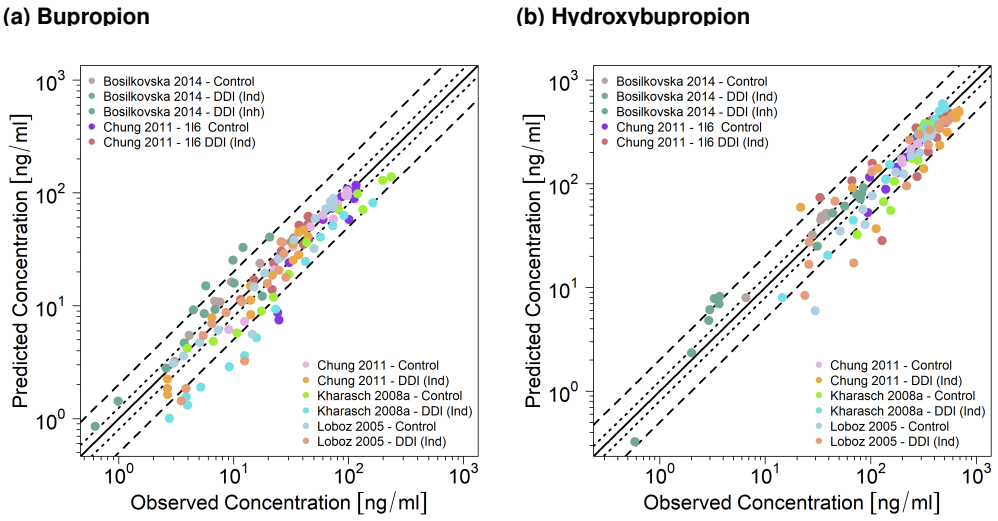

Figure S4.6.3: **DDI predicted compared to observed plasma concentrations of (a) bupropion and (b) hydroxybupropion.** The solid line marks the line of identity. Dotted lines indicate 1.25-fold, dashed lines indicate 2-fold deviation. **Control**, without perpetrators; **DDI (Ind)**, drug-drug-interaction with rifampicin as inducer; **DDI (Inh)**, drug-drug-interaction with fluvoxamine and voriconazole as inhibitors.

4.6.2 Mean relative deviation of plasma concentration predictions

Table S4.6: Mean relative deviation values of bupropion and hydroxybupropion DDI plasma concentration predictions.

Dosing	n	Compound	MRD	Compound	MRD	Dataset	Reference
				Rifampicin induction			
25 mg Cap (s.d.)	10	Bup	1.34	HBup	1.11	te	Bosilkovska 2014 Control [25]
25 mg Cap (s.d.)	10	Bup	1.65	HBup	1.07	te	Bosilkovska 2014 DDI [25]
150 mg IR (s.d.)	10	Bup	1.25	HBup	1.20	te	Kharasch 2008a Control [34]
150 mg IR (s.d.)	10	Bup	2.28	HBup	1.18	te	Kharasch 2008a DDI [34]
150 mg SR (s.d.)	13	Bup	1.15	HBup	1.04	ta	Chung 2011 **1*/**1* Control [38]
150 mg SR (s.d.)	13	Bup	1.31	HBup	1.26	ta	Chung 2011 **1*/**1* DDI [38]
150 mg SR (s.d.)	9	Bup	1.30	HBup	1.08	te	Chung 2011 **1*/**6* Control [38]
150 mg SR (s.d.)	9	Bup	1.12	HBup	1.26	te	Chung 2011 **1*/**6* DDI [38]
150 mg SR (s.d.)	18	Bup	1.30	HBup	1.35	ta	Loboz 2006 Control [44]
150 mg SR (s.d.)	18	Bup	1.57	HBup	1.26	te	Loboz 2006 DDI [44]
				Fluvoxamine and voriconazole inhibition			
25 mg Cap (s.d.)	10	Bup	1.69	HBup	2.68	ta	Bosilkovska 2014 DDI [25]
		Mean	**1.36 (1.04–2.68)**				
		Median	**1.26 (1.04–2.68)**				
			90.90% (20/22 $\leq$ 2)				

Bup, bupropion; **Cap**, capsule (Geneva cocktail [25]); **Control**, without perpetrators; **DDI**, drug-drug-interaction with perpetrators; **HBup**, hydroxybupropion; **IR**, immediate release formulation; **MRD**, mean relative deviation; **n**, number of individuals studied; **s.d.**, single dose; **SR**, sustained release formulation; **ta**, training dataset; **te**, test dataset.

4.6.3 AUC and C_{max} goodness-of-fit plots

Following, predicted compared to observed AUC and C_{max} values are shown for individual bupropion and hydroxybupropion profiles, their metabolite-parent AUC and C_{max} ratio and their DDI effect metabolite-parent AUC and C_{max} ratio, respectively. Details on dosing regimens, study populations and literature references are listed in Tables S4.4 and S4.5. Predicted and observed PK parameters are summarized in Tables S4.7, S4.8 and S4.9.

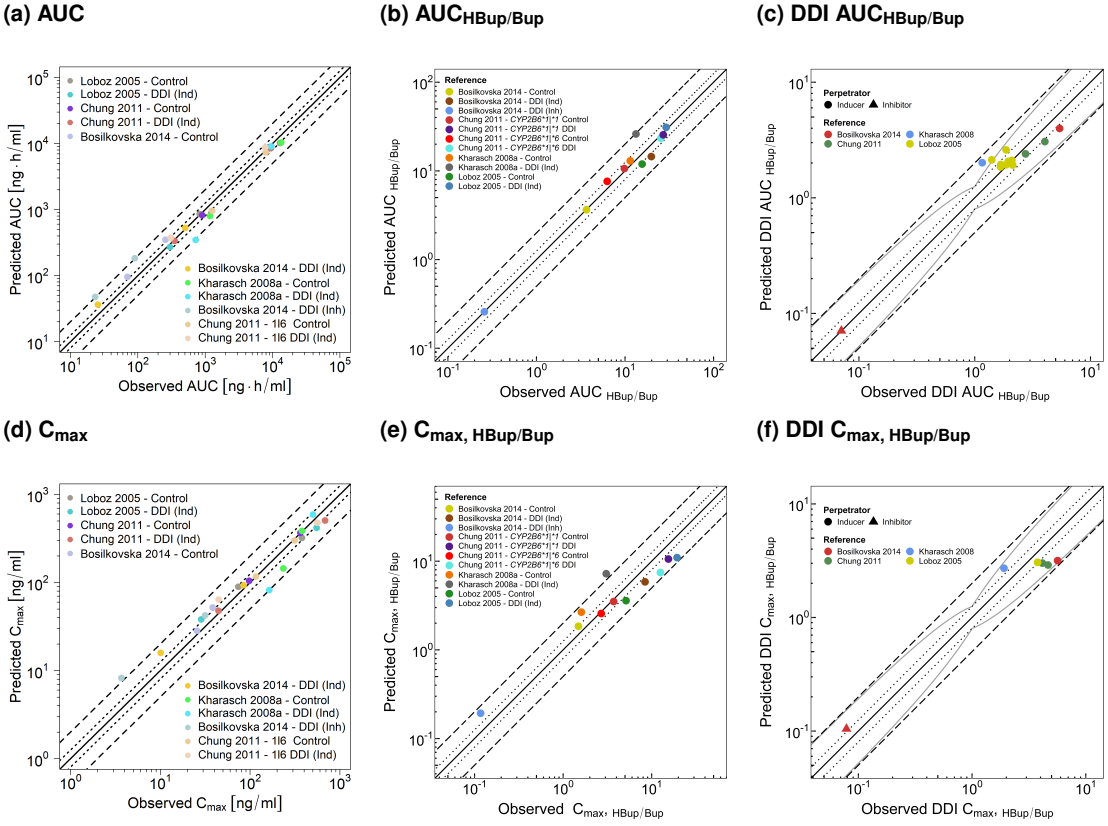

Figure S4.6.4: **Predicted compared to observed (a) AUC values, (b) $AUC_{HBup/Bup}$ ratios, (c) DDI $AUC_{HBup/Bup}$, (d) C_{max} values, (e) $C_{max, HBup/Bup}$ ratios and (f) DDI $C_{max, HBup/Bup}$ ratios.** The solid line marks the line of identity. Dotted lines indicate 1.25-fold, dashed lines indicate 2-fold deviation. The curved gray lines show the prediction success limits suggested by Guest et al. allowing a 1.25-fold variability [77]. **AUC**, area under the plasma concentration-time curve; **Bup**, bupropion; **C_{max}**, maximum plasma concentration; **Control**, without perpetrator; **DDI**, drug-drug-interaction with perpetrators; **DDI (Ind)**, drug-drug-interaction with rifampicin as inducer; **DDI (Inh)**, drug-drug-interaction with fluvoxamine and voriconazole as inhibitors; **HBup**, hydroxybupropion.

4.6.4 Geometric mean fold error of predicted AUC and C_{max} values, $AUC_{HBup/Bup}$ and $C_{max,\ HBup/Bup}$ ratios, and DDI $AUC_{HBup/Bup}$ and DDI $C_{max,\ HBup/Bup}$ ratios

Table S4.7: Predicted and observed AUC_{last} and C_{max} values of bupropion and hydroxybupropion DDI plasma concentrations.

Dosing	n	Compound	AUC_{last} pred [ng*h/ml]	AUC_{last} obs [ng*h/ml]	AUC_{last} pred/obs	C_{max} pred [ng/ml]	C_{max} obs [ng/ml]	C_{max} pred/obs	Dataset	Reference
Rifampicin induction										
25 mg Cap (s.d.)	10	Bup	95.61	70.34	1.36	28.20	25.74	1.10	te	Bosilkovska 2014 Control [25]
25 mg Cap (s.d.)	10	Bup	47.87	25.49	1.88	18.71	10.10	1.85	te	Bosilkovska 2014 DDI [25]
150 mg IR (s.d.)	10	Bup	798.66	1182.40	0.68	144.23	235.94	0.61	te	Kharasch 2008a Control [34]
150 mg IR (s.d.)	10	Bup	345.35	722.93	0.48	81.81	164.01	0.50	te	Kharasch 2008a DDI [34]
150 mg SR (s.d.)	13	Bup	822.18	909.01	0.90	104.29	97.73	1.07	ta	Chung 2011 **1/*1* Control [38]
150 mg SR (s.d.)	13	Bup	334.43	351.52	0.95	47.74	44.49	1.07	ta	Chung 2011 **1/*1* DDI [38]
150 mg SR (s.d.)	9	Bup	958.22	1268.88	0.76	116.76	116.63	1.00	te	Chung 2011 **1/*6* Control [38]
150 mg SR (s.d.)	9	Bup	354.09	309.15	1.15	61.23	44.66	1.37	te	Chung 2011 **1/*6* DDI [38]
150 mg SR (s.d.)	18	Bup	854.58	832.02	1.03	89.31	74.04	1.21	te	Loboz 2006 Control [44]
150 mg SR (s.d.)	18	Bup	269.42	300.93	0.90	37.95	28.60	1.33	te	Loboz 2006 DDI [44]
25 mg Cap (s.d.)	10	HBup	348.31	257.69	1.35	52.07	38.33	1.36	te	Bosilkovska 2014 Control [25]
25 mg Cap (s.d.)	10	HBup	449.48	505.31	0.89	75.50	84.97	0.89	te	Bosilkovska 2014 DDI [25]
150 mg IR (s.d.)	10	HBup	10351.70	13530.75	0.77	383.99	379.17	1.01	te	Kharasch 2008 Control [34]
150 mg IR (s.d.)	10	HBup	9004.53	9608.04	0.94	591.45	503.13	1.18	te	Kharasch 2008 DDI [34]
150 mg SR (s.d.)	13	HBup	8738.64	8936.26	0.98	366.16	363.64	1.01	ta	Chung 2011 **1/*1* Control [38]
150 mg SR (s.d.)	13	HBup	8533.25	9498.00	0.90	504.90	687.07	0.74	ta	Chung 2011 **1/*1* DDI [38]
150 mg SR (s.d.)	9	HBup	7304.46	7976.41	0.92	300.13	314.03	0.96	te	Chung 2011 **1/*6* Control [38]
150 mg SR (s.d.)	9	HBup	8894.42	7838.55	1.13	492.24	59.91	0.88	te	Chung 2011 **1/*6* DDI [38]
150 mg SR (s.d.)	18	HBup	10199.30	12976.72	0.79	320.63	379.78	0.84	ta	Loboz 2006 Control [44]
150 mg SR (s.d.)	18	HBup	8346.79	8767.25	0.95	416.72	552.73	0.75	te	Loboz 2006 DDI [44]
Fluvoxamine and voriconazole inhibition										
25 mg Cap (s.d.)	10	Bup	182.88	90.52	2.02	42.28	31.64	1.34	ta	Bosilkovska 2014 DDI [25]
25 mg Cap (s.d.)	10	HBup	47.14	23.37	2.02	8.16	3.70	2.21	ta	Bosilkovska 2014 DDI [25]
GMFE (range)					**1.30 (1.02–2.02)**			**1.30 (1.00–2.21)**		
pred/obs within twofold (range)					**86.36%; 19/22 (0.48–2.02)**			**95.45%; 21/22 (0.50–2.21)**		

AUC_{last}, area under the plasma concentration-time curve; **Bup**, bupropion; **Cap**, capsule (Geneva cocktail [25]); **C_{max}**, maximum plasma concentration; **Control**, without perpetrators; **DDI**, drug-drug-interaction with perpetrators; **GMFE**, geometric mean fold error; **HBup**, hydroxybupropion; **IR**, immediate release formulation; **n**, number of individuals studied; **obs**, observed; **pred**, predicted; **s.d.**, single dose; **SR**, sustained release formulation; **ta**, training dataset; **te**, test dataset.

Table S4.8: Predicted and observed $AUC_{HBup/Bup}$ and $C_{max,\ HBup/Bup}$ ratios of bupropion and hydroxybupropion DDI plasma concentrations.

Dosing	n	$AUC_{HBup/Bup}$ pred	$AUC_{HBup/Bup}$ obs	$AUC_{HBup/Bup}$ pred/obs	$C_{max,\ HBup/Bup}$ pred	$C_{max,\ HBup/Bup}$ obs	$C_{max,\ HBup/Bup}$ pred/obs	Dataset	Reference
Rifampicin induction									
25 mg Cap (s.d.)	10	3.64	3.66	0.99	1.85	1.49	1.24	te	Bosilkovska 2014 Control [25]
25 mg Cap (s.d.)	10	14.50	19.82	0.73	5.84	8.41	0.70	te	Bosilkovska 2014 DDI [25]
150 mg IR (s.d.)	10	12.96	11.44	1.13	2.66	1.61	1.66	ta	Kharasch 2008a Control [34]
150 mg IR (s.d.)	10	26.07	13.29	1.96	7.29	3.07	2.36	te	Kharasch 2008a DDI [34]
150 mg SR (s.d.)	13	10.62	9.83	1.08	3.51	3.72	0.94	ta	Chung 2011 **1/*1* Control [38]
150 mg SR (s.d.)	13	7.62	6.29	1.21	2.57	2.69	0.95	ta	Chung 2011 **1/*1* DDI [38]
150 mg SR (s.d.)	9	24.25	27.02	0.90	9.89	15.44	0.64	te	Chung 2011 **1/*6* Control [38]
150 mg SR (s.d.)	9	23.36	25.36	0.92	7.45	12.54	0.59	te	Chung 2011 **1/*6* DDI [38]
150 mg SR (s.d.)	18	11.93	15.60	0.76	3.59	5.13	0.70	ta	Loboz 2006 Control [44]
150 mg SR (s.d.)	18	30.98	29.13	1.06	10.98	19.33	0.57	te	Loboz 2006 DDI [44]
150 mg SR (s.d.)	6	11.76	18.50	0.64	-	-	-	te	Loboz 2006 **1/*1* Control [44]
150 mg SR (s.d.)	6	21.78	30.90	0.70	-	-	-	te	Loboz 2006 **1/*1* DDI [44]
150 mg SR (s.d.)	1	22.75	25.40	0.90	-	-	-	te	Loboz 2006 **1/*4* Control [44]
150 mg SR (s.d.)	1	45.56	47.50	0.96	-	-	-	te	Loboz 2006 **1/*4* DDI [44]
150 mg SR (s.d.)	1	15.47	32.70	0.47	-	-	-	te	Loboz 2006 **1/*5* Control [44]
150 mg SR (s.d.)	1	32.36	45.90	0.71	-	-	-	te	Loboz 2006 **1/*5* DDI [44]
150 mg SR (s.d.)	6	8.38	14.50	0.58	-	-	-	te	Loboz 2006 **1/*6* Control [44]
150 mg SR (s.d.)	6	17.32	28.20	0.61	-	-	-	te	Loboz 2006 **1/*6* DDI [44]
150 mg SR (s.d.)	1	19.58	18.00	1.09	-	-	-	te	Loboz 2006 **4/*6* Control [44]
150 mg SR (s.d.)	1	38.87	38.30	1.01	-	-	-	te	Loboz 2006 **4/*6* DDI [44]
150 mg SR (s.d.)	1	18.87	21.70	0.87	-	-	-	te	Loboz 2006 **5/*5* Control [44]
150 mg SR (s.d.)	1	39.06	45.40	0.86	-	-	-	te	Loboz 2006 **5/*5* DDI [44]
150 mg SR (s.d.)	1	4.98	8.10	0.61	-	-	-	te	Loboz 2006 **6/*6* Control [44]
150 mg SR (s.d.)	1	9.69	13.60	0.71	-	-	-	te	Loboz 2006 **6/*6* DDI [44]
Fluvoxamine and voriconazole inhibition									
150 mg IR (s.d.)	10	0.26	0.26	1.00	0.19	0.12	1.58	ta	Bosilkovska 2014 DDI [25]
GMFE (range)				**1.37 (1.00–2.14)**			**1.53 (1.05–2.36)**		
Pred/Obs within twofold (range)				**95.83%; 24/25 (0.47–1.96)**			**90.00%; 10/11 (0.57–2.36)**		

AUC_{last}, area under the plasma concentration-time curve; **Bup**, bupropion; **Cap**, capsule (Geneva cocktail [25]); **C_{max}**, maximum plasma concentration; **Control**, without perpetrators; **DDI**, drug-drug-interaction with perpetrators; **GMFE**, geometric mean fold error; **HBup**, hydroxybupropion; **IR**, immediate release formulation; **n**, number of individuals studied; **obs**, observed; **pred**, predicted; **s.d.**, single dose; **SR**, sustained release formulation; **ta**, training dataset; **te**, test dataset; **-**, no data available.

Table S4.9: Predicted and observed DDI $AUC_{HBup/Bup}$ and DDI $C_{max,\ HBup/Bup}$ ratios of bupropion and hydroxybupropion DDI plasma concentrations.

Dosing	n	DDI $AUC_{HBup/Bup}$ pred	DDI $AUC_{HBup/Bup}$ obs	DDI $AUC_{HBup/Bup}$ pred/obs	DDI $C_{max,\ HBup/Bup}$ pred	DDI $C_{max,\ HBup/Bup}$ obs	DDI $C_{max,\ HBup/Bup}$ pred/obs	Dataset	Reference
Rifampicin induction									
25 mg Cap (s.d.)	10	3.98	5.42	0.74	3.16	5.64	0.56	te	Bosilkovska 2014 [25]
150 mg IR (s.d.)	10	2.01	1.16	1.73	2.74	1.91	1.44	te	Kharasch 2008a [34]
150 mg SR (s.d.)	13	0.72	0.64	1.12	0.73	0.72	1.01	ta	Chung 2011 **1/*1* [38]
150 mg SR (s.d.)	9	0.96	0.94	1.03	0.75	0.81	0.93	te	Chung 2011 **1/*6* [38]
150 mg SR (s.d.)	18	2.60	1.87	1.39	3.06	3.77	0.81	te	Loboz 2006 [44]
150 mg SR (s.d.)	6	1.85	1.67	1.11	-	-	-	te	Loboz 2006 **1/*1* [44]
150 mg SR (s.d.)	1	1.93	1.87	1.03	-	-	-	te	Loboz 2006 **1/*4* [44]
150 mg SR (s.d.)	1	2.13	1.40	1.52	-	-	-	te	Loboz 2006 **1/*5* [44]
150 mg SR (s.d.)	6	2.07	1.94	1.06	-	-	-	te	Loboz 2006 **1/*6* [44]
150 mg SR (s.d.)	1	1.92	2.13	0.90	-	-	-	te	Loboz 2006 **4/*6* [44]
150 mg SR (s.d.)	1	1.10	2.09	1.01	-	-	-	te	Loboz 2006 **5/*5* [44]
150 mg SR (s.d.)	1	1.94	1.68	1.16	-	-	-	te	Loboz 2006 **6/*6* [44]
Fluvoxamine and voriconazole inhibition									
25 mg Cap (s.d.)	10	0.07	0.07	1.00	0.10	0.08	1.25	ta	Bosilkovska 2014 [25]
GMFE (range)				**1.23 (1.00–1.73)**			**1.46 (1.01–1.44)**		
Pred/Obs within twofold (range)				**100%; 13/13 (0.74–1.73)**			**100%; 6/6 (0.56–1.44)**		

AUC_{last}, area under the plasma concentration-time curve; **Bup**, bupropion; **Cap**, capsule (Geneva cocktail [25]); **C_{max}**, maximum plasma concentration; **DDI**, drug-drug-interaction with perpetrators; **GMFE**, geometric mean fold error; **HBup**, hydroxybupropion; **IR**, immediate release formulation; **n**, number of individuals studied; **obs**, observed; **pred**, predicted; **s.d.**, single dose; **SR**, sustained release formulation; **ta**, training dataset; **te**, test dataset; **-**, no data available.

5 DDGI prediction

5.1 Background

Drug-drug-gene interactions occur when subjects with variant *CYP2B6* variant genotypes receive bupropion with a potential perpetrator drug. In the following section, DDGIs were simulated for various CYP2B6 genotypes during concomitant bupropion and rifampicin intake. In the literature, plasma concentration-time profiles of this DDGI were only provided in the study of Chung et al. [38] (for the genotype *CYP2B6*1/*6* after rifampicin intake). However, Loboz et al. [44] also investigated DDGIs with rifampicin for several different genotypes and reported hydroxybupropion to bupropion AUC_{inf} ratios. Hence, for DDGI model evaluation, predicted $AUC_{inf\ HBup/Bup}$ ratios were calculated for DDGIs and compared to observed ratios. Model parameters to predict the rifampicin-bupropion DDGIs are listed in Tables S2.2 (bupropion), S3.2 (DGI) and S4.1 (rifampicin).

5.2 Clinical studies

In Table S5.1, clinical studies used for DDGI model development are listed. Virtual individuals were built according to the demographics published in the respective study reports. If no data on the demographics were reported, a standard individual was used as described in Section 1.4.

Table S5.1: Clinical studies used for DDGI model development.

Rifampicin application	Bupropion appliction	Dose gap [h]	n	*CYP2B6* genoytpe	Dataset	Reference
600 mg po (tab) q.d. (D1–D7)	150 mg po (SR) s.d. (D8)	24	13	**1/*1*	ta	Chung 2011 [38]
600 mg po (tab) q.d. (D1–D7)	150 mg po (SR) s.d. (D8)	24	9	**1/*6*	te	Chung 2011 [38]
600 mg po (tab) q.d. (D1–D10)	150 mg po (SR) s.d. (D8)	12	6	**1/*1*	te	Loboz 2006 [44]
600 mg po (tab) q.d. (D1–D10)	150 mg po (SR) s.d. (D8)	12	1	**1/*4*	te	Loboz 2006 [44]
600 mg po (tab) q.d. (D1–D10)	150 mg po (SR) s.d. (D8)	12	1	**1/*5*	te	Loboz 2006 [44]
600 mg po (tab) q.d. (D1–D10)	150 mg po (SR) s.d. (D8)	12	1	**1/*6*	te	Loboz 2006 [44]
600 mg po (tab) q.d. (D1–D10)	150 mg po (SR) s.d. (D8)	12	6	**4/*6*	te	Loboz 2006 [44]
600 mg po (tab) q.d. (D1–D10)	150 mg po (SR) s.d. (D8)	12	1	**5/*5*	te	Loboz 2006 [44]
600 mg po (tab) q.d. (D1–D10)	150 mg po (SR) s.d. (D8)	12	1	**6/*6*	te	Loboz 2006 [44]

CYP, cytochrome P450; **D**, study day; **n**, number of individuals studied; **po**, oral; **q.d.**, once daily; **s.d.**, single dose; **SR**, sustained release formulation; **tab**, tablet; **ta**, training dataset; **te**, test dataset.

5.3 Concentration-time profiles

Observed plasma concentration-time profiles were only published in the DDGI study by Chung et al. [38]. The profiles are shown on linear and semi-logarithmic scales in Figure S5.3.1. The geometric means of the population predictions (n=500) are shown as solid lines and corresponding observed data as filled dots. Symbols represent the arithmetic mean values ± standard deviation, if available. The shaded areas indicate the geometric standard deviation.

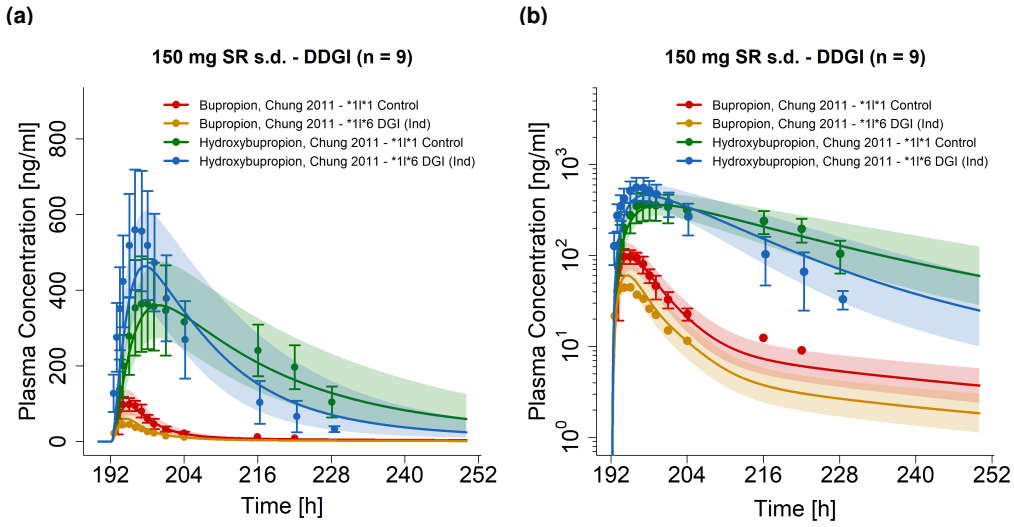

Figure S5.3.1: **Plasma concentration-time profiles of bupropion and hydroxybupropion for DDGI simulations** on (a) a linear and (b) a semi-logarithmic scale. **Control**, without perpetrator; **DDI (Ind)**, drug-drug-interaction with rifampicin as inducer; **DDGI**, drug-drug-gene-interaction; **s.d.**, single dose; **SR**, sustained release formulation.

5.4 Model evaluation

5.4.1 DDGI $AUC_{HBup/Bup}$ ratios goodness-of-fit plots

In Figure S5.4.2, predicted compared to observed DDGI $AUC_{HBup/Bup}$ ratios for different genotypes are shown. The DDGI $AUC_{HBup/Bup}$ ratios were calculated as described in Section 1.6.3. Details on dosing regimens, study populations and literature references are listed in Table S5.1. Predicted and observed PK parameters are summarized in Table S5.2.

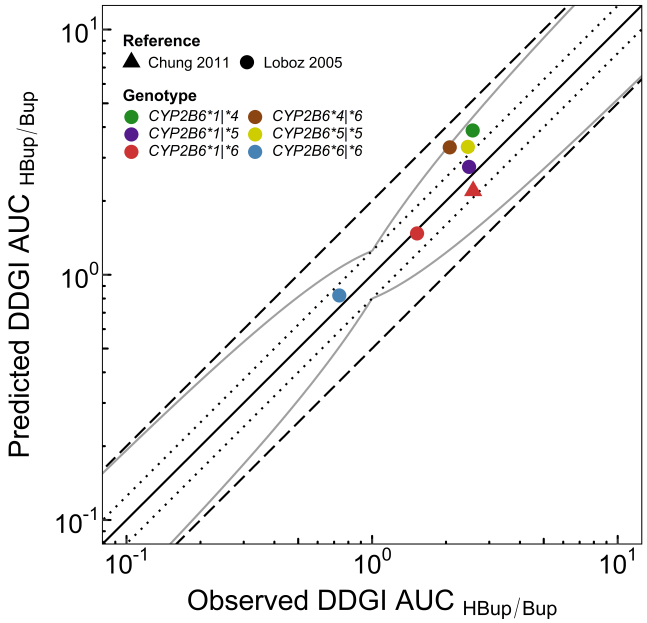

Figure S5.4.2: **Predicted compared to observed DDGI $AUC_{HBup/Bup}$ ratios.** The solid line marks the line of identity. Dotted lines indicate 1.25-fold, dashed lines indicate 2-fold deviation. The curved gray lines show the prediction success limits suggested by Guest et al. allowing a 1.25-fold variability [77]. **AUC**, area under the plasma concentration-time curve; **Bup**, bupropion; **DDGI**, drug-drug-gene-interaction; **HBup**, hydroxybupropion.

5.4.2 Geometric mean fold error of predicted DDGI $AUC_{HBup/Bup}$ ratios

Table S5.2 lists predicted and observed DDGI $AUC_{HBup/Bup}$ ratios for AUC_{last} (Chung 2011) and AUC_{inf} (Loboz 2006). Single $AUC_{HBup/Bup}$ ratios of the reference (*CYP2B6*1/*1* without perpetrator treatment) and the corresponding effect (CYP2B6 variant under perpetrator influence) are listed in Tables S3.5 and S4.8.

Table S5.2: Predicted and observed DDGI $AUC_{HBup/Bup}$ and DDGI $C_{max, HBup/Bup}$ ratios of bupropion and hydroxybupropion plasma concentrations.

Dosing	n	DDGI $AUC_{HBup/Bup}$ pred	DDGI $AUC_{HBup/Bup}$ obs	DDGI $AUC_{HBup/Bup}$ pred/obs	DDGI $C_{max, HBup/Bup}$ pred	DDGI $C_{max, HBup/Bup}$ obs	DDGI $C_{max, HBup/Bup}$ pred/obs	Dataset	Reference
150 mg SR (s.d.)	9	2.20	2.58	0.85	2.12	3.37	0.63	te	Chung 2011 **1/*6* DDI [38]
150 mg SR (s.d.)	1	3.87	2.57	1.51	-	-	-	te	Loboz 2006 **1/*4* DDI [44]
150 mg SR (s.d.)	1	2.75	2.48	1.11	-	-	-	te	Loboz 2006 **1/*5* DDI [44]
150 mg SR (s.d.)	6	1.47	1.52	0.97	-	-	-	te	Loboz 2006 **1/*6* DDI [44]
150 mg SR (s.d.)	1	3.31	2.07	1.60	-	-	-	te	Loboz 2006 **4/*6* DDI [44]
150 mg SR (s.d.)	1	3.32	2.45	1.36	-	-	-	te	Loboz 2006 **5/*5* DDI [44]
150 mg SR (s.d.)	1	0.82	0.74	1.12	-	-	-	te	Loboz 2006 **6/*6* DDI [44]
GMFE (range)				**1.27 (1.08–1.60)**			**1.59**		
pred/obs within twofold (range)				**100%; 7/7 (0.85–1.60)**			**100%; 1/1 (0.63)**		

AUC, area under the plasma concentration-time curve; **Bup**, bupropion; **C_{max}**, maximum plasma concentration; **DDI**, drug-drug-interaction with rifampicin; **DDGI**, drug-drug-gene-interaction with rifampicin in populations with *CYP2B6* varaints; **GMFE**, geometric mean fold error; **HBup**, hydroxybupropion; **n**, number of individuals studied; **obs**, observed; **pred**, predicted; **s.d.**, single dose; **SR**, sustained release formulation; **te**, test dataset; **-**, no data available.

5.4.3 DDGI scenarios of rifampicin-bupropion interactions

The change of $AUC_{HBup/Bup}$ during the rifampicin-bupropion DDGI for all CYP2B6 genotypes implemented into the model is illustrated in Figure S5.4.3. The values on the different bars represent the % change from *CYP2B6*1/*1* control conditions, for the different genotypes, with or without rifampicin coadministration. It should be noted, that DDIs for the genotypes *CYP2B6*4/*4* and *CYP2B6*5/*6* (shaded in gray) no clinical values were available to evaluate the presented model predictions. The rifampicin-bupropion coadministration protocol of Loboz et al. was applied for all simulations (see table S5.1).

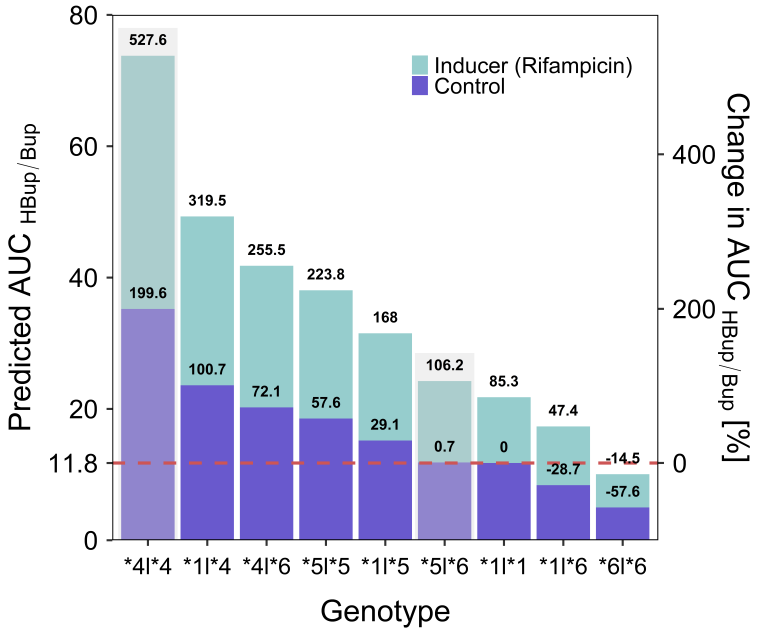

Figure S5.4.3: **Predicted $AUC_{HBup/Bup}$ for simulated DDGI scenarios. AUC**, area under the plasma concentration-time curve; **Bup**, bupropion; **Control**, without perpetrator; **HBup**, hydroxybupropion.

References

[1] Open Systems Pharmacology Suite Community, “Open Systems Pharmacology Suite Manual,” 2018.

[2] M. Nishimura and S. Naito, “Tissue-specific mRNA expression profiles of human phase I metabolizing enzymes except for cytochrome P450 and phase II metabolizing enzymes,” *Drug Metabolism and Pharmacokinetics*, vol. 21, no. 5, pp. 357–74, 2006.

[3] N. Kolesnikov, E. Hastings, M. Keays, O. Melnichuk, Y. A. Tang, E. Williams, M. Dylag, N. Kurbatova, M. Brandizi, T. Burdett, K. Megy, E. Pilicheva, G. Rustici, A. Tikhonov, H. Parkinson, R. Petryszak, U. Sarkans, and A. Brazma, “ArrayExpress update-simplifying data submissions,” *Nucleic Acids Research*, vol. 43, no. D1, pp. D1113–D1116, 2015.

[4] B. Prasad, K. Johnson, S. Billington, C. Lee, G. W. Chung, C. D. Brown, E. J. Kelly, J. Himmelfarb, and J. D. Unadkat, “Abundance of drug transporters in the human kidney cortex as quantified by quantitative targeted proteomics,” *Drug Metabolism and Disposition*, vol. 44, no. 12, pp. 1920–1924, 2016.

[5] National Center for Biotechnology Information (NCBI), “Expressed Sequence Tags (EST) from UniGene,” 2019.

[6] M. Meyer, S. Schneckener, B. Ludewig, L. Kuepfer, and J. Lippert, “Using expression data for quantification of active processes in physiologically based pharmacokinetic modeling,” *Drug metabolism and disposition: the biological fate of chemicals*, vol. 40, pp. 892–901, may 2012.

[7] D. Scotcher, S. Billington, J. Brown, C. R. Jones, C. D. Brown, A. Rostami-Hodjegan, and A. Galetin, “Microsomal and cytosolic scaling factors in dog and human kidney cortex and application for in vitro-in vivo extrapolation of renal metabolic clearance,” *Drug Metabolism and Disposition*, vol. 45, no. 5, pp. 556–568, 2017.

[8] J. Valentin, “Basic Anatomical and Physiological Data for Use in Radiological Protection: Reference Values,” *Annals of the ICRP*, vol. 32, jan 2002.

[9] G. Tanaka and H. Kawamura, “Anatomical and physiological characteristics for Asian reference man: Male and female of different ages: Tanaka model.,” 1996.

[10] S. Palovaara, O. Pelkonen, J. Uusitalo, and K. Laine, “Inhibition of cytochrome P450 2B6 activity by hormone replacement therapy and oral contraceptive as measured by bupropion hydroxylation,” *Clinical Pharmacology & Therapeutics*, vol. 74, no. 4, pp. 326–333, 2003.

[11] L. Fan, J. C. Wang, F. Jiang, Z. R. Tan, Y. Chen, Q. Li, W. Zhang, G. Wang, H. P. Lei, D. L. Hu, D. Wang, and H. H. Zhou, “Induction of cytochrome P450 2B6 activity by the herbal medicine baicalin as measured by bupropion hydroxylation,” *European Journal of Clinical Pharmacology*, vol. 65, no. 4, pp. 403–409, 2009.

[12] L. C. Gao, X. Huang, Z. R. Tan, L. Fan, and H. H. Zhou, “The effects of sodium ferulate on the pharmacokinetics of bupropion and its active metabolite in healthy men,” *European Review for Medical and Pharmacological Sciences*, vol. 16, no. 9, pp. 1192–1196, 2012.

[13] L. C. Gao, F. Q. Liu, L. Yang, L. Cheng, H. Y. Dai, R. Tao, S. P. Cao, D. Wang, and J. Tang, "The P450 oxidoreductase (POR) rs2868177 and cytochrome P450 (CYP) 2B6*6 polymorphisms contribute to the interindividual variability in human CYP2B6 activity," *European Journal of Clinical Pharmacology*, vol. 72, no. 10, pp. 1205–1213, 2016.

[14] W.-J. Qin, W. Zhang, Z.-Q. Liu, X.-P. Chen, Z.-R. Tan, D.-L. Hu, D. Wang, L. Fan, and H.-H. Zhou, "Rapid clinical induction of bupropion hydroxylation by metamizole in healthy Chinese men," *British Journal of Clinical Pharmacology*, vol. 74, pp. 999–1004, dec 2012.

[15] National Center for Health Statistics Hyattsville MD 20782., "Third National Health and Nutrition Examination Survey, (NHANES III)," tech. rep., 1997.

[16] "Open Systems Pharmacology Suite Community. Open Systems Pharmacology Suite Manual, Version 7.4, 2018. URLhttps://github.com/Open-Systems-Pharmacology/OSPSuite. Documentation/blob/master/OpenSystemsPharmacologySuite.pdf.," Available online (accessed on 27 November 2020).

[17] M. Fava, A. J. Rush, M. E. Thase, A. Clayton, S. M. Stahl, J. F. Pradko, and J. A. Johnston, "15 Years of Clinical Experience With Bupropion HCl," *The Primary Care Companion to The Journal of Clinical Psychiatry*, vol. 07, pp. 106–113, jun 2005.

[18] J. N. Connarn, S. Flowers, M. Kelly, R. Luo, K. M. Ward, G. Harrington, I. Moncion, M. Kamali, M. McInnis, M. R. Feng, V. Ellingrod, A. Babiskin, X. Zhang, and D. Sun, "Pharmacokinetics and Pharmacogenomics of Bupropion in Three Different Formulations with Different Release Kinetics in Healthy Human Volunteers," *AAPS Journal*, vol. 19, no. 5, pp. 1513–1522, 2017.

[19] V. M. Fokina, M. Xu, E. Rytting, S. Z. Abdel-Rahman, H. West, C. Oncken, S. M. Clark, M. S. Ahmed, G. D. Hankins, and T. N. Nanovskaya, "Pharmacokinetics of bupropion and its pharmacologically active metabolites in pregnancy," *Drug Metabolism and Disposition*, vol. 44, no. 11, pp. 1832–1838, 2016.

[20] J. E. Sager, L. S. Price, and N. Isoherranen, "Stereoselective metabolism of bupropion to OH-bupropion, threohydrobupropion, erythrohydrobupropion, and 49-OH-bupropion in vitro," *Drug Metabolism and Disposition*, vol. 44, no. 10, pp. 1709–1719, 2016.

[21] E. D. Kharasch and A. Crafford, "Common Polymorphisms of CYP2B6 Influence Stereoselective Bupropion Disposition," *Clinical Pharmacology and Therapeutics*, vol. 105, no. 1, pp. 142–152, 2019.

[22] J. E. Slemmer, B. R. Martin, and M. I. Damaj, "Bupropion is a nicotinic antagonist," *Journal of Pharmacology and Experimental Therapeutics*, vol. 295, no. 1, pp. 321–327, 2000.

[23] S. M. Stahl, J. F. Pradko, B. R. Haight, J. G. Modell, C. B. Rockett, and S. Learned-Coughlin, "A Review of the Neuropharmacology of Bupropion, a Dual Norepinephrine and Dopamine Reuptake Inhibitor," *The Primary Care Companion to The Journal of Clinical Psychiatry*, vol. 06, no. 04, pp. 159–166, 2004.

[24] M. Bosilkovska, C. Samer, J. Déglon, A. Thomas, B. Walder, J. Desmeules, and Y. Daali, "Evaluation of Mutual Drug-Drug Interaction within Geneva Cocktail for Cytochrome P450 Phenotyping using Innovative Dried Blood Sampling Method," *Basic & Clinical Pharmacology & Toxicology*, vol. 119, pp. 284–290, sep 2016.

[25] M. Bosilkovska, C. F. Samer, J. Déglon, M. Rebsamen, C. Staub, P. Dayer, B. Walder, J. A. Desmeules, and Y. Daali, "Geneva cocktail for cytochrome P450 and P-glycoprotein activity assessment using dried blood spots," *Clinical Pharmacology and Therapeutics*, vol. 96, no. 3, pp. 349–359, 2014.

[26] J. W. Findlay, J. Van Wyck Fleet, P. G. Smith, R. F. Butz, M. L. Hinton, M. R. Blum, and D. H. Schroeder, "Pharmacokinetics of bupropion, a novel antidepressant agent, following oral administration to healthy subjects," *European Journal of Clinical Pharmacology*, vol. 21, no. 2, pp. 127–135, 1981.

[27] C. Zahner, E. Kruttschnitt, J. Uricher, M. Lissy, M. Hirsch, S. Nicolussi, S. Krähenbühl, and J. Drewe, "No Clinically Relevant Interactions of St. John's Wort Extract Ze 117 Low in Hyperforin With Cytochrome P450 Enzymes and P-glycoprotein," *Clinical Pharmacology & Therapeutics*, vol. 106, pp. 432–440, aug 2019.

[28] L. M. Hesse, D. J. Greenblatt, L. L. von Moltke, and M. H. Court, "Ritonavir Has Minimal Impact on the Pharmacokinetic Disposition of a Single Dose of Bupropion Administered to Human Volunteers," *The Journal of Clinical Pharmacology*, vol. 46, pp. 567–576, may 2006.

[29] A. R. Masters, B. T. Gufford, J. B. L. Lu, I. F. Metzger, D. R. Jones, and Z. Desta, "Chiral Plasma Pharmacokinetics and Urinary Excretion of Bupropion and Metabolites in Healthy Volunteers," *Journal of Pharmacology and Experimental Therapeutics*, vol. 358, pp. 230–238, jun 2016.

[30] T. Yamazaki, A. Desai, R. Goldwater, D. Han, C. Howieson, S. Akhtar, D. Kowalski, C. Lademacher, H. Pearlman, D. Rammelsberg, and R. Townsend, "Pharmacokinetic Effects of Isavuconazole Coadministration With the Cytochrome P450 Enzyme Substrates Bupropion, Repaglinide, Caffeine, Dextromethorphan, and Methadone in Healthy Subjects," *Clinical Pharmacology in Drug Development*, vol. 6, pp. 54–65, jan 2017.

[31] J. Posner, A. Bye, S. Jeal, A. W. Peck, and P. Whiteman, "Alcohol and bupropion pharmacokinetics in healthy male volunteers," *European Journal of Clinical Pharmacology*, vol. 26, no. 5, pp. 627–630, 1984.

[32] J. Posner, A. Bye, K. Dean, A. W. Peck, and P. D. Whiteman, "The disposition of bupropion and its metabolites in healthy male volunteers after single and multiple doses," *European Journal of Clinical Pharmacology*, vol. 29, no. 1, pp. 97–103, 1985.

[33] W. Oberegger, O. Eradiri, F. Zhou, and P. Maes, "Patent No .: US 2006 / 0228415 A1," 2006.

[34] E. D. Kharasch, D. Mitchell, and R. Coles, "Stereoselective Bupropion Hydroxylation as an In Vivo Phenotypic Probe for Cytochrome P4502B6 (CYP2B6) Activity," *The Journal of Clinical Pharmacology*, vol. 48, pp. 464–474, apr 2008.

[35] E. D. Kharasch, D. Mitchell, R. Coles, and R. Blanco, "Rapid Clinical Induction of Hepatic Cytochrome P4502B6 Activity by Ritonavir," *Antimicrobial Agents and Chemotherapy*, vol. 52, pp. 1663–1669, may 2008.

[36] G. W. Hogeland, S. Swindells, J. C. McNabb, A. D. M. Kashuba, G. C. Yee, and C. M. Lindley, "Lopinavir/ritonavir Reduces Bupropion Plasma Concentrations in Healthy Subjects," *Clinical Pharmacology & Therapeutics*, vol. 81, pp. 69–75, jan 2007.

[37] N. L. Benowitz, A. Z. Zhu, R. F. Tyndale, D. Dempsey, and P. Jacob, “Influence of CYP2B6 genetic variants on plasma and urine concentrations of bupropion and metabolites at steady state,” *Pharmacogenetics and Genomics*, vol. 23, no. 3, pp. 135–141, 2013.

[38] J. Y. Chung, J. Y. Cho, H. S. Lim, J. R. Kim, K. S. Yu, K. S. Lim, S. G. Shin, and I. J. Jang, “Effects of pregnane X receptor (NR1I2) and CYP2B6 genetic polymorphisms on the induction of bupropion hydroxylation by rifampin,” *Drug Metabolism and Disposition*, vol. 39, no. 1, pp. 92–97, 2011.

[39] J. Dennison, A. Puri, S. Warrington, T. Endo, T. Adeloye, and A. Johnston, “Amenamevir: Studies of Potential CYP2C8- and CYP2B6-Mediated Pharmacokinetic Interactions With Montelukast and Bupropion in Healthy Volunteers,” *Clinical Pharmacology in Drug Development*, vol. 7, no. 8, pp. 860–870, 2018.

[40] N. A. Farid, C. D. Payne, C. S. Ernest, Y. G. Li, K. J. Winters, D. E. Salazar, and D. S. Small, “Prasugrel, a new thienopyridine antiplatelet drug, weakly inhibits cytochrome P450 2B6 in humans,” *Journal of Clinical Pharmacology*, vol. 48, no. 1, pp. 53–59, 2008.

[41] P.-H. Hsyu, A. Singh, T. D. Giargiari, J. A. Dunn, J. A. Ascher, and J. A. Johnston, “Pharmacokinetics of Bupropion and its Metabolites in Cigarette Smokers versus Nonsmokers,” *The Journal of Clinical Pharmacology*, vol. 37, pp. 737–743, aug 1997.

[42] H.-P. Lei, W. Ji, J. Lin, H. Chen, Z.-R. Tan, D.-L. Hu, L.-J. Liu, and H.-H. Zhou, “Effects of Ginkgo biloba extract on the pharmacokinetics of bupropion in healthy volunteers,” *British Journal of Clinical Pharmacology*, vol. 68, pp. 201–206, aug 2009.

[43] H. Lei, X. Yu, H. Xie, H. Li, L. Fan, L. Dai, Y. Chen, and H. Zhou, “Effect of St. John’s wort supplementation on the pharmacokinetics of bupropion in healthy male Chinese volunteers,” *Xenobiotica*, vol. 40, pp. 275–281, apr 2010.

[44] K. Loboz, A. Gross, K. Williams, W. Liauw, R. Day, J. Blievernicht, U. Zanger, and A. McLachlan, “Cytochrome P450 2B6 activity as measured by bupropion hydroxylation: Effect of induction by rifampin and ethnicity,” *Clinical Pharmacology & Therapeutics*, vol. 80, pp. 75–84, jul 2006.

[45] B. Li, A. Nangia, C. Ming, and X. X. Cheng, “Patent No.: US 8,545,880 B2,” 2013.

[46] S. M. Robertson, F. Maldarelli, V. Natarajan, E. Formentini, R. M. Alfaro, and S. R. Penzak, “Efavirenz induces CYP2B6-mediated hydroxylation of bupropion in healthy subjects,” *Journal of Acquired Immune Deficiency Syndromes*, vol. 49, no. 5, pp. 513–519, 2008.

[47] M. TURPEINEN, A. TOLONEN, J. UUSITALO, J. JALONEN, O. PELKONEN, and K. LAINE, “Effect of clopidogrel and ticlopidine on cytochrome P450 2B6 activity as measured by bupropion hydroxylation,” *Clinical Pharmacology & Therapeutics*, vol. 77, pp. 553–559, jun 2005.

[48] M. Turpeinen, N. Koivuviita, A. Tolonen, P. Reponen, S. Lundgren, J. Miettunen, K. Metsärinne, A. Rane, O. Pelkonen, and K. Laine, “Effect of renal impairment on the pharmacokinetics of bupropion and its metabolites,” *British Journal of Clinical Pharmacology*, vol. 64, pp. 165–173, aug 2007.

[49] M. Turpeinen, J. Uusitalo, T. Lehtinen, M. Kailajärvi, O. Pelkonen, J. Vuorinen, P. Tapanainen, C. Stjernschantz, R. Lammintausta, and M. Scheinin, “Effects of Ospemifene on Drug Metabolism Mediated by Cytochrome P450 Enzymes in Humans in Vitro and in Vivo,” *International Journal of Molecular Sciences*, vol. 14, pp. 14064–14075, jul 2013.

[50] R. Kustra, B. Corrigan, J. Dunn, B. Duncan, and P. H. Hsyu, “Lack of effect of cimetidine on the pharmacokinetics of sustained-release bupropion.,” *Journal of Clinical Pharmacology*, vol. 39, pp. 1184–8, nov 1999.

[51] W. Oberegger, P. Maes, M. Ashty Saleh, and G. Jackson, “Patent No.: US 7,645,802 B2,” 2010.

[52] Y. Schmid, A. Rickli, A. Schaffner, U. Duthaler, E. Grouzmann, C. M. Hysek, and M. E. Liechti, “Interactions between Bupropion and 3,4-Methylenedioxymethamphetamine in Healthy Subjects,” *Journal of Pharmacology and Experimental Therapeutics*, vol. 353, pp. 102–111, apr 2015.

[53] J. Woodcock, M. Khan, and L. X. Yu, “Withdrawal of Generic Budeprion for Nonbioequivalence,” *New England Journal of Medicine*, vol. 367, pp. 2461–2463, dec 2012.

[54] N. Paiement, P. K. Noonan, M. A. González, and H. Zerbe, “Steady State Plasma Levels of Bupropion After Administration of 3x150 Mg Extended Release Reference Tablets and Switching to 1x450 Mg Extended Release 450ER Tablets,” *International Journal of Clinical Pharmacology & Toxicology*, vol. 1, pp. 26–31, 2012.

[55] “ChemAxon Bupropion: https://chemicalize.com/app/calculation/bupropion,” Available online (accessed on 27 November 2020).

[56] “ChemAxon Hydroxybupropion: https://chemicalize.com/app/calculation/Hydroxybupropion,” Available online (accessed on 27 November 2020).

[57] “ChemAxon Erythro- and Threohydrobupropion: https://chemicalize.com/app/calculation/CC(NC(C)(C)C)C(O)C1%3
Available online (accessed on 27 November 2020).

[58] T. Takayanagi, D. Itoh, and H. Mizugushi, “Analysis of Acid Dissociation Equilibrium of Bupropion by Capillary Zone Electrophoresis After the Heat-Degradation,” *Chromatography*, vol. 37, no. 3, pp. 105–109, 2016.

[59] P. Muralidhar, E. Bhargav, and B. Srinath, “Formulation and optimization of bupropion HCl in microspongesby 2^3 factorial design,” *International Journal of Pharmaceutical Sciences and Research*, vol. 8, no. 3, pp. 1134–1144, 2017.

[60] “PubChem Hydroxybupropion: https://pubchem.ncbi.nlm.nih.gov/compound/446,” Available online (accessed on 27 November 2020).

[61] C. Xue, X. Zhang, and W. Cai, “Prediction of Drug-Drug Interactions with Bupropion and Its Metabolites as CYP2D6 Inhibitors Using a Physiologically-Based Pharmacokinetic Model,” *Pharmaceutics*, vol. 10, p. 1, dec 2017.

[62] M. J. Reese, R. M. Wurm, K. T. Muir, G. T. Generaux, L. St. John-Williams, and D. J. Mcconn, “An in Vitro Mechanistic Study to Elucidate the Desipramine/Bupropion Clinical Drug-Drug Interaction,” *Drug Metabolism and Disposition*, vol. 36, pp. 1198–1201, jul 2008.

[63] R. Kawai, M. Lemaire, J. L. Steimer, A. Bruelisauer, W. Niederberger, and M. Rowland, “Physiologically based pharmacokinetic study on a cyclosporin derivative, SDZ IMM 125.,” *Journal of pharmacokinetics and biopharmaceutics*, vol. 22, pp. 327–65, oct 1994.

[64] L. M. Berezhkovskiy, “Volume of Distribution at Steady State for a Linear Pharmacokinetic System with Peripheral Elimination,” *Journal of Pharmaceutical Sciences*, vol. 93, pp. 1628–1640, jun 2004.

[65] X. Wang, D. R. Abdelrahman, O. L. Zharikova, S. L. Patrikeeva, G. D. Hankins, M. S. Ahmed, and T. N. Nanovskaya, "Bupropion metabolism by human placenta," *Biochemical Pharmacology*, vol. 79, pp. 1684–1690, jun 2010.

[66] C. Xu, E. T. Ogburn, Y. Guo, and Z. Desta, "Effects of the CYP2B6*6 allele on catalytic properties and inhibition of CYP2B6 in vitro: Implication for the mechanism of reduced efavirenz metabolism and other CYP2B6 substrates in vivo," *Drug Metabolism and Disposition*, vol. 40, no. 4, pp. 717–725, 2012.

[67] Y. Chen, H. F. Liu, L. Liu, K. Nguyen, E. B. Jones, and A. J. Fretland, "The in vitro metabolism of bupropion revisited: Concentration dependent involvement of cytochrome P450 2C19," *Xenobiotica*, vol. 40, no. 8, pp. 536–546, 2010.

[68] F. I. Carroll, B. E. Blough, P. Abraham, A. C. Mills, J. A. Holleman, S. A. Wolckenhauer, A. M. Decker, A. Landavazo, K. T. McElroy, H. A. Navarro, M. B. Gatch, and M. J. Forster, "Synthesis and biological evaluation of bupropion analogues as potential pharmacotherapies for cocaine addiction," *Journal of Medicinal Chemistry*, vol. 52, no. 21, pp. 6768–6781, 2009.

[69] H. R. Arias, F. Gumilar, A. Rosenberg, K. M. Targowska-Duda, D. Feuerbach, K. Jozwiak, R. Moaddel, I. W. Wainer, and C. Bouzat, "Interaction of Bupropion with Muscle-Type Nicotinic Acetylcholine Receptors in Different Conformational States," *Biochemistry*, vol. 48, pp. 4506–4518, jun 2009.

[70] U. Simonsen, S. Comerma-Steffensen, and K. E. Andersson, "Modulation of Dopaminergic Pathways to Treat Erectile Dysfunction," *Basic and Clinical Pharmacology and Toxicology*, vol. 119, pp. 63–74, 2016.

[71] B. T. Gufford, J. B. L. Lu, I. F. Metzger, D. R. Jones, and Z. Desta, "Stereoselective glucuronidation of bupropion metabolites in vitro and in vivo," *Drug Metabolism and Disposition*, vol. 44, no. 4, pp. 544–553, 2016.

[72] R. P. Austin, P. Barton, S. L. Cockroft, M. C. Wenlock, and R. J. Riley, "The Influence of Nonspecific Microsomal Binding on Apparent Intrinsic Clearance, and Its Prediction from Physicochemical Properties," *Drug Metabolism and Disposition*, vol. 30, pp. 1497–1503, dec 2002.

[73] F. Langenbucher, "Linearization of dissolution rate curves by the Weibull distribution.," *The Journal of Pharmacy and Pharmacology*, vol. 24, pp. 979–81, dec 1972.

[74] M. Bosilkovska, C. F. Samer, J. Déglon, M. Rebsamen, C. Staub, P. Dayer, B. Walder, J. A. Desmeules, and Y. Daali, "Geneva Cocktail for Cytochrome P450 and P-Glycoprotein Activity Assessment Using Dried Blood Spots," *Clinical Pharmacology & Therapeutics*, vol. 96, pp. 349–359, sep 2014.

[75] Z. Desta, R. S. Gammal, L. Gong, M. Whirl-Carrillo, A. H. Gaur, C. Sukasem, J. Hockings, A. Myers, M. Swart, R. F. Tyndale, C. Masimirembwa, O. F. Iwuchukwu, S. Chirwa, J. Lennox, A. Gaedigk, T. E. Klein, and D. W. Haas, "Clinical Pharmacogenetics Implementation Consortium (CPIC) Guideline for CYP2B6 and Efavirenz-Containing Antiretroviral Therapy," *Clinical Pharmacology and Therapeutics*, vol. 106, no. 4, pp. 726–733, 2019.

[76] P. F. Wang, A. Neiner, and E. D. Kharasch, "Stereoselective Bupropion Hydroxylation by Cytochrome P450 CYP2B6 and Cytochrome P450 Oxidoreductase Genetic Variants," *Drug Metabolism and Disposition: The Biological Fate of Chemicals*, vol. 48, no. 6, pp. 438–445, 2020.

[77] E. J. Guest, L. Aarons, J. B. Houston, A. Rostami-Hodjegan, and A. Galetin, “Critique of the two-fold measure of prediction success for ratios: application for the assessment of drug-drug interactions.,” *Drug Metabolism and Disposition: The Biological Fate of Chemicals*, vol. 39, pp. 170–3, feb 2011.

[78] N. Hanke, S. Frechen, D. Moj, H. Britz, T. Eissing, T. Wendl, and T. Lehr, “PBPK models for CYP3A4 and P-gp DDI prediction: a modeling network of rifampicin, itraconazole, clarithromycin, midazolam, alfentanil and digoxin - Supplementary document,” *CPT: Pharmacometrics & Systems Pharmacology*, aug 2018.

[79] L. Kovar, C. Schräpel, D. Selzer, Y. Kohl, R. Bals, M. Schwab, and T. Lehr, “Physiologically-based pharmacokinetic (Pbpk) modeling of buprenorphine in adults, children and preterm neonates,” *Pharmaceutics*, vol. 12, no. 6, pp. 1–22, 2020.

[80] D. Türk, N. Hanke, S. Wolf, S. Frechen, T. Eissing, T. Wendl, M. Schwab, and T. Lehr, “Physiologically based pharmacokinetic models for prediction of complex CYP2C8 and OATP1B1 (SLCO1B1) drug–drug–gene interactions: a modeling network of gemfibrozil, repaglinide, pioglitazone, rifampicin, clarithromycin and itraconazole,” *Clinical Pharmacokinetics*, p. Supplementary document, may 2019.

[81] M. J. O’Neil, P. E. Heckelman, C. B. Koch, K. J. Roman, C. M. Kenny, and M. R. D’Arecca, *The Merck Index: An Encyclopedia of Chemicals, Drugs, and Biologicals 14th edn.* 2006.

[82] G. Baneyx, N. Parrott, C. Meille, A. Iliadis, and T. Lavé, “Physiologically based pharmacokinetic modeling of CYP3A4 induction by rifampicin in human: influence of time between substrate and inducer administration,” *European Journal of Pharmaceutical Sciences : Official Journal of the European Federation for Pharmaceutical Sciences*, vol. 56, pp. 1–15, 2014.

[83] R. Panchagnula, I. Gulati, M. Varma, and Y. A. Raj, “Dissolution methodology for evaluation of rifampicin-containing fixed-dose combinations using biopharmaceutic classification sytem based approach,” *Clinical Research and Regulatory Affairs*, vol. 24, no. 2-4, pp. 61–76, 2007.

[84] S. Agrawal and R. Panchagnula, “Implication of biopharmaceutics and pharmacokinetics of rifampicin in variable bioavailability from solid oral dosage forms,” *Biopharmaceutics & Drug Disposition*, vol. 26, no. 8, pp. 321–34, 2005.

[85] G. Boman and V. A. Ringberger, “Binding of rifampicin by human plasma proteins,” *European Journal of Clinical Pharmacology*, vol. 7, no. 5, pp. 369–73, 1974.

[86] D. S. Wishart, “DrugBank: a comprehensive resource for in silico drug discovery and exploration,” *Nucleic Acids Research*, vol. 34, pp. D668–D672, jan 2006.

[87] I. E. Templeton, J. B. Houston, and A. Galetin, “Predictive utility of in vitro rifampin induction data generated in fresh and cryopreserved human hepatocytes, Fa2N-4, and HepaRG cells,” *Drug Metabolism and Disposition: The Biological Fate of Chemicals*, vol. 39, no. 10, pp. 1921–9, 2011.

[88] U. Loos, E. Musch, J. C. Jensen, G. Mikus, H. K. Schwabe, and M. Eichelbaum, “Pharmacokinetics of oral and intravenous rifampicin during chronic administration,” *Klinische Wochenschrift*, vol. 63, pp. 1205–11, dec 1985.

[89] T. Rodgers, D. Leahy, and M. Rowland, “Physiologically based pharmacokinetic modeling 1: predicting the tissue distribution of moderate-to-strong bases.,” *Journal of Pharmaceutical Sciences*, vol. 94, pp. 1259–76, jun 2005.

[90] T. Rodgers and M. Rowland, "Physiologically based pharmacokinetic modelling 2: predicting the tissue distribution of acids, very weak bases, neutrals and zwitterions.," *Journal of Pharmaceutical Sciences*, vol. 95, pp. 1238–57, jun 2006.

[91] A. Nakajima, T. Fukami, Y. Kobayashi, A. Watanabe, M. Nakajima, and T. Yokoi, "Human arylacetamide deacetylase is responsible for deacetylation of rifamycins: Rifampicin, rifabutin, and rifapentine," *Biochemical Pharmacology*, vol. 82, no. 11, pp. 1747–1756, 2011.

[92] R. G. Tirona, B. F. Leake, A. W. Wolkoff, and R. B. Kim, "Human organic anion transporting polypeptide-C (SLC21A6) is a major determinant of rifampin-mediated pregnane X receptor activation.," *The Journal of Pharmacology and Experimental Therapeutics*, vol. 304, pp. 223–8, jan 2003.

[93] A. Collett, J. Tanianis-Hughes, D. Hallifax, and G. Warhurst, "Predicting P-glycoprotein effects on oral absorption: correlation of transport in Caco-2 with drug pharmacokinetics in wild-type and mdr1a(-/-) mice in vivo.," *Pharmaceutical Research*, vol. 21, pp. 819–26, may 2004.

[94] M. Shou, M. Hayashi, Y. Pan, Y. Xu, K. Morrissey, L. Xu, and G. L. Skiles, "Modeling, prediction, and in vitro in vivo correlation of CYP3A4 induction," *Drug metabolism and Disposition: The Biological Fate of Chemicals*, vol. 36, no. 11, pp. 2355–70, 2008.

[95] B. Greiner, M. Eichelbaum, P. Fritz, H. P. Kreichgauer, O. von Richter, J. Zundler, and H. K. Kroemer, "The role of intestinal P-glycoprotein in the interaction of digoxin and rifampin," *The Journal of Clinical Investigation*, vol. 104, no. 2, pp. 147–53, 1999.

[96] A. Ramamoorthy, Y. Liu, S. Philips, Z. Desta, H. Lin, C. Goswami, A. Gaedigk, L. Li, D. A. Flockhart, and T. C. Skaar, "Regulation of microRNA expression by rifampin in human hepatocytes," *Drug Metabolism and Disposition*, vol. 41, no. 10, pp. 1763–1768, 2013.

[97] H. Zhang, C. Sridar, C. Kenaan, H. Amunugama, D. P. Ballou, and P. F. Hollenberg, "Polymorphic variants of cytochrome P450 2B6 (CYP2B6.4-CYP2B6.9) exhibit altered rates of metabolism for bupropion and efavirenz: A charge-reversal mutation in the K139E variant (CYP2B6.8) impairs formation of a functional cytochrome P450-reductase complex," *Journal of Pharmacology and Experimental Therapeutics*, vol. 338, no. 3, pp. 803–809, 2011.

[98] M. G. Soars, D. M. Petullo, J. A. Eckstein, S. C. Kasper, and S. A. Wrighton, "An assessment of UDP-glucuronosyltransferase induction using primary human hepatocytes," *Drug Metabolism and Disposition*, vol. 32, no. 1, pp. 140–148, 2004.

[99] M. Hirano, K. Maeda, Y. Shitara, and Y. Sugiyama, "Drug-drug interaction between pitavastatin and various drugs via OATP1B1," *Drug Metabolism and Disposition*, vol. 34, no. 7, pp. 1229–1236, 2006.

[100] M. L. Reitman, X. Chu, X. Cai, J. Yabut, R. Venkatasubramanian, S. Zajic, J. A. Stone, Y. Ding, R. Witter, C. Gibson, K. Roupe, R. Evers, J. A. Wagner, and A. Stoch, "Rifampin's acute inhibitory and chronic inductive drug interactions: experimental and model-based approaches to drug-drug interaction trial design," *Clinical Pharmacology and Therapeutics*, vol. 89, no. 2, pp. 234–42, 2011.

[101] Y. Shimokawa, N. Yoda, S. Kondo, Y. Yamamura, Y. Takiguchi, and K. Umehara, "Inhibitory Potential of Twenty Five Anti-tuberculosis Drugs on CYP Activities in Human Liver Microsomes," *Biological & Pharmaceutical Bulletin*, vol. 38, no. 9, pp. 1425–1429, 2015.

[102] J. F. Rajaonarison, M. Placidi, and B. Lacarelle, “Screening in Human Liver Interactions for Inhibitors,” *Drug Metabolism and Disposition*, vol. 20, no. 4, 1994.

[103] H. Britz, N. Hanke, A.-K. Volz, O. Spigset, M. Schwab, T. Eissing, T. Wendl, S. Frechen, and T. Lehr, “PBPK models for CYP1A2 DDI prediction: a modelling network of fluvoxamine, theophylline, caffeine, rifampicin and midazolam,” *CPT: Pharmacometrics & Systems Pharmacology*, vol. XX, pp. 1–12, 2019.

[104] R. S. Foti, P. W. Swaan, J. Wang, H. Duan, Y. Pan, and T. Hu, “Potent and Selective Inhibition of Plasma Membrane Monoamine Transporter by HIV Protease Inhibitors,” *Drug Metabolism and Disposition*, vol. 43, no. 11, pp. 1773–1780, 2015.

[105] D. Hallifax and J. B. Houston, “Saturable Uptake of Lipophilic Amine Drugs into Isolated Hepatocytes: Mechanisms and Consequences for Quantitative Clearance Prediction,” *Drug Metabolism and Disposition*, vol. 35, pp. 1325–1332, aug 2007.

[106] V. Claassen, “Review of the animal pharmacology and pharmacokinetics of fluvoxamine.,” *British Journal of Clinical Pharmacology*, vol. 15, no. 3 S, pp. 349S–355S, 1983.

[107] W. Schmitt, “General approach for the calculation of tissue to plasma partition coefficients,” *Toxicology in Vitro*, vol. 22, pp. 457–467, mar 2008.

[108] M. Miura and T. Ohkubo, “Identification of human cytochrome P450 enzymes involved in the major metabolic pathway of fluvoxamine,” *Xenobiotica*, vol. 37, no. 2, pp. 169–179, 2007.

[109] X. Li, S. Frechen, D. Moj, T. Lehr, M. Taubert, C. hsuan Hsin, G. Mikus, P. J. Neuvonen, K. T. Olkkola, T. I. Saari, and U. Fuhr, “A Physiologically Based Pharmacokinetic Model of Voriconazole Integrating Time-Dependent Inhibition of CYP3A4, Genetic Polymorphisms of CYP2C19 and Predictions of Drug–Drug Interactions,” *Clinical Pharmacokinetics*, vol. 59, no. 6, pp. 781–808, 2020.

[110] P. F. Wang, A. Neiner, and E. D. Kharasch, “Efavirenz metabolism: Influence of polymorphic CYP2B6 variants and stereochemistry,” *Drug Metabolism and Disposition*, vol. 47, no. 10, pp. 1195–1205, 2019.

[111] S. Jeong, P. D. Nguyen, and Z. Desta, “Comprehensive in vitro analysis of voriconazole inhibition of eight cytochrome P450 (CYP) enzymes: Major effect on CYPs 2B6, 2C9, 2C19, and 3A,” *Antimicrobial Agents and Chemotherapy*, vol. 53, no. 2, pp. 541–551, 2009.

[112] X. Li, S. Frechen, D. Moj, T. Lehr, M. Taubert, C. hsuan Hsin, G. Mikus, P. J. Neuvonen, K. T. Olkkola, T. I. Saari, and U. Fuhr, “A Physiologically Based Pharmacokinetic Model of Voriconazole Integrating Time-Dependent Inhibition of CYP3A4, Genetic Polymorphisms of CYP2C19 and Predictions of Drug–Drug Interactions,” *Clinical Pharmacokinetics*, vol. 59, no. 6, pp. 781–808, 2020.

[113] Pfizer Canada ULC, “Product monograph: VFEND® voriconazole Tablets 50 mg and 200 mg For Injection 200 mg / Vial (10 mg/mL when reconstituted) Powder for Oral Suspension 3 g / bottle (40 mg/mL when reconstituted) Kirkland, Quebec; 2020.,” 2020.

[114] “Scientific Discussion-VFEND Procedure No. EMEA/H/ C/387/X/09. [London]: London; 2004.,” no. September, 2004.

[115] B. Damle, M. V. Varma, and N. Wood, “Pharmacokinetics of Voriconazole Administered Concomitantly with Fluconazole and Population-Based Simulation for Sequential Use,” *Antimicrobial Agents and Chemotherapy*, vol. 55, pp. 5172–5177, nov 2011.

[116] N. R. Zane and D. R. Thakker, “A Physiologically Based Pharmacokinetic Model for Voriconazole Disposition Predicts Intestinal First-pass Metabolism in Children,” *Clinical Pharmacokinetics*, vol. 53, pp. 1171–1182, dec 2014.

[117] F. Qi, L. Zhu, N. Li, T. Ge, G. Xu, and S. Liao, “Influence of different proton pump inhibitors on the pharmacokinetics of voriconazole,” *International Journal of Antimicrobial Agents*, vol. 49, pp. 403–409, apr 2017.

Pharmaceutics

A Physiologically based Pharmacokinetic Model of Ketoconazole and its Metabolites as Drug-Drug Interaction Perpetrators

Supplementary Material

Fatima Zahra Marok[1], Jan-Georg Wojtyniak[1,2], Laura Maria Fuhr[1], Matthias Schwab[2,3,4], Johanna Weiss[5,6], Walter Emil Haefeli[5,6], Thorsten Lehr[1]

[1]Clinical Pharmacy, Saarland University, Saarbruecken, Germany
[2]Dr. Margarete Fischer-Bosch-Institut of Clinical Pharmacology, Stuttgart, Germany
[3]Departments of Clinical Pharmacology, and of Biochemistry and Pharmacy, University Hospital Tuebingen, Germany
[4]Cluster of excellence iFIT (EXC2180) “Image-Guided and Functionally Instructed Tumor Therapies”, University Tuebingen, Germany
[5]Department of Clinical Pharmacology and Pharmacoepidemiology, University of Heidelberg, Germany
[6]German Center for Infection Research (DZIF), Heidelberg Partner Site, Germany

Funding:

M.S. was supported by the Robert Bosch Stiftung (Stuttgart, Germany), the European Commission Horizon 2020 UPGx grant 668353, a grant from the German Federal Ministry of Education and Research (BMBF 031L0188D), and the Deutsche Forschungsgemeinschaft (DFG, German Research Foundation) under Germany’s Excellence Strategy—EXC 2180—390900677. T.L. was supported by the the project “Open-source modeling framework for automated quality control and management of complex life science system models” (OSMOSES) funded by the German Federal Ministry of Education and Research (BMBF, grant ID:031L0161C).

Conflict of Interest:

Since January 2020 Jan-Georg Wojtyniak is an employe of Boehringer Ingelheim Pharma GmbH and Co. KG. All other authors declare no conflict of interest.

Corresponding Author:

Prof. Dr. Thorsten Lehr

Clinical Pharmacy, Saarland University

Campus C5 3, 66123 Saarbrücken, Germany

Phone: +49 681 302 70255

Email: thorsten.lehr@mx.uni-saarland.de

Contents

S1 PBPK Model Building

S1.1 System-dependent parameters

Table S1.1: System-dependent parameter

Protein	Reference concentration			Localization	Half-life	
	Mean[a]	GSD[b]	Relative expression[c]		liver [h]	intestine [h]
AADAC	[d]1.00 [1]	[e]1.40	RT-PCR [2]	Intracellular	36	23
CYP3A4	4.32 [3]	1.18 liver [4] 1.46 int. [4]	RT-PCR [5]	Intracellular	36 [6]	23 [7]
FMO3	[d]1.00	1.00 [1]	RT-PCR[2]	Intracellular	-	23
UGT1A4	[f]1.32 [8]	1.07[4]	RT-PCR [2]	Intracellular	36	23
P-gp	[h]1.41	1.60 [9]	RT-PCR [10]	Apical (Efflux)	36	23

AADAC: arylacetamide deacetylase, CYP: cytochrome P450, FMO: flavin-containing monooxygenase, P-gp: P-glycoprotein, RT-PCR: reverse transcription-polymerase chain reaction measured expression profile, UGT: UDP-glucuronosyltransferase.

[a] μmol protein/l in the tissue of highest expression

[b] geometric standard deviation of the reference concentration

[c] in the different organs (PK-Sim® expression database profile)

[d] if no information was available, the mean reference concentration was set to 1.00 µmol/l and the catalytic rate constant was optimized according to [1]

[e] if no information was available, a moderate variability of 35% CV was assumed (= 1.40 GSD)

[f] calculated from protein per mg microsomal protein x 40 mg microsomal protein per g liver [11]

[g] calculated from transporter per mg membrane protein x 26.2 mg human kidney microsomal protein per g kidney [11]

[h] optimized

S1.2 Mathematical implementation of drug interactions

S1.2.1 Drug-food interactions (DFIs)

DFIs were implemented by extending the gastric emptying time (GET). Extended GET was assumed for clincial studies with (i) reported food intake, (ii) a delayed observed time of maximum concentration (T_{max}) of more than two hours, (iii) multiple dose asministrations within a day and (iv) doses above 600 mg.

S1.2.2 Drug-drug interactions (DDIs)

The simulated DDIs included competitive inhibition of cytochrome P450 (CYP3A4) and P-glycoprotein (P-gp).

Equation: Competitive inhibition

$$K_{M,app} = K_M * (1 + \frac{[I]}{K_i}) \tag{S1}$$

$$v = \frac{v_{max} * [S]}{K_{M,app} + [S]} = \frac{k_{cat} * [E] * [S]}{K_{M,app} + [S]} \tag{S2}$$

$K_{M,app}$ = Michaelis-Menten constant in the presence of inhibitor
K_M = Michaelis-Menten constant
$[I]$ = free inhibitor concentration
K_i = dissociation constant of the inhibitor-protein complex
v = reaction velocity
$[S]$ = free substrate concentration
k_{cat} = catalytic/transport rate constant
$[E]$ = protein concentration

S1.3 Physiologically based pharmacokinetic (PBPK) model evaluation

The model performances were evaluated by illustrating predicted and observed plasma concentration-time profiles and goodness-of-fit plots. Furthermore, the models were evaluated by comparing predicted to observed area under the plasma concentration-time curve from the time of drug administration to the last concentration measuremente (AUC_{last}) and maximum plasma concentration (C_{max}) values.
As quantitative performance measures, a mean relative deviation (MRD) was calculated for all profiles from their respective predicted and observed plasma concentrations. Furthermore, the geometric mean fold error (GMFE) of the AUC_{last} and C_{max} were calculated.

S1.4 Sensitivity analysis

Sensitivity of the final models to single parameters (local sensitivity analysis) was calculated as relative change of the area under the plasma concentration-time curve extrapolated to infinity (AUC_{inf}). The analysis was carried out using a relative perturbation of 1000% (variation range 10.0, maximum number of 9 steps). Parameters were included into the analysis if they have been optimized, if they are associated with optimized parameters or if they might have a strong impact due to calculation methods used in the model. Sensitivity to a parameter changes was calculated according to Eq. (S3):

Equation: Sensitivity analysis

$$S = \frac{\Delta AUC_{inf}}{\Delta p} * \frac{p}{AUC_{inf}} \tag{S3}$$

S = sensitivity of the AUC_{inf} to the examined model parameter
ΔAUC_{inf} = change of the AUC_{inf}
AUC_{inf} = simulated, AUC_{inf} with the original parameter value
Δp = change of the examined parameter value
p = original parameter value

A sensitivity of + 1.0 signifies that a 10% increase of the examined parameter value causes a 10% increase of the simulated AUC.

S1.5 Ketoconazole – Clinical studies

Table S1.2: Clinical study data used for ketoconazole model development

Dose [mg]	Route	N	Age [years]	Weight [kg]	Height [cm]	BMI [kg/m²]	Females [%]	Dataset	Reference
200	sol s.d	12	-	-	-	-	-	training	Heel 1982 [12]
200	sol s.d	12	20 (18-25)	76.4 (61.2-95.3)	180 (167.6-188)	-	0	test	Huang 1986a [13]
200	sol s.d	23	20 (18-25)	76.4 (61.2-95.3)	180 (167.6-188)	-	0	test	Huang 1986b [13]
400	sol s.d	12	20 (18-25)	76.4 (61.2-95.3)	180 (167.6-188)	-	0	test	Huang 1986b [13]
800	sol s.d	12	20 (18-25)	76.4 (61.2-95.3)	180 (167.6-188)	-	0	training	Huang 1986b [13]
100	tab s.d	12	-	-	-	-	-	test	Heel 1982 [12]
200	tab s.d	9	(22-41)	-	-	-	33.34	test	Chin 1995 [14]
200	tab s.d	8	25 (21-46)	-	-	-	0	test	Daneshmend 1983 [15]
200	tab s.d	8	23 (20-31)	64 (50-75)	-	-	62.5	test	Daneshmend 1984a [16]
200	tab s.d	8	23 (20-31)	64 (50-75)	-	-	62.5	training	Daneshmend 1984b [16]
200	tab s.d	23	-	-	-	-	-	test	FDA 1998b [17]
200	tab s.d	39	-	-	-	-	-	test	FDA 1998a [17]
200	tab s.d	39	-	-	-	-	-	training	FDA 1998a [17]
200	tab s.d	12	-	-	-	-	-	test	Heel 1982 [12]
200	tab s.d	23	20 (18-25)	76.4 (61.2-95.3)	180 (167.6-188)	-	0	test	Huang 1986a [13]
200	tab s.d	12	30 (24-36)	78.8	180.7	-	0	test	Knupp 1993 [18]
200	tab s.d	10	24 (22-26)	62 (55-70)	-	-	50	test	Mannistoe 1982 [19]
400	tab s.d	12	(23-29)	(59-78)	-	-	0	test	Sadeghina 2005b [20]
400	tab s.d	12	(23-29)	(59-78)	-	-	0	test	Sadeghina 2005a [20]
200	tab s.d	24	23.2 (18-45)	-	-	22.5 (20-24)	0	test	Solomon 2007b [21]
200	tab s.d	24	23.2 (18-45)	-	-	22.5 (20-24)	0	test	Solomon 2007a [21]
200	tab s.d	3	(28-42)	-	-	-	-	test	Van der Meer 1980 [22]
200	tab s.d	18	-	-	-	-	-	test	Yuen 1999a [23]
200	tab s.d	18	-	-	-	-	-	test	Yuen 1999b [23]
400	tab s.d	8	23 (20-31)	64 (50-75)	-	-	62.5	test	Daneshmend 1984a [16]
400	tab s.d	8	23 (20-31)	64 (50-75)	-	-	62.5	test	Daneshmend 1984b [16]
400	tab s.d	12	-	-	-	-	-	test	Heel 1982 [12]
400	tab s.d	12	23 (19-41)	77.4 (64.2-99.8)	175.8 (163.2-185.4)	-	0	test	Polk 1999 [24]
400	tab s.d	6	(18-30)	-	-	-	0	test	Piscitelli 1991 [25]
400	cap s.d	12	33.7 (22-55)	-	-	22.56 (20.34-28.04)	75	test	Sriwiriyajan 2007 [26]
400	tab s.d	12	27.34 (20-48)	74.44 (57.5-100)	173.33 (162-180)	25.27 (21.9-29.9)	0	test	Weiss 2022 [27]
600	tab s.d	8	23 (20-31)	64 (50-75)	-	-	62.5	training	Daneshmend 1984a [16]
600	tab s.d	8	23 (20-31)	64 (50-75)	-	-	62.5	test	Daneshmend 1984b [16]
800	tab s.d	8	23 (20-31)	64 (50-75)	-	-	62.5	test	Daneshmend 1984a [16]
800	tab s.d	8	23 (20-31)	64 (50-75)	-	-	62.5	training	Daneshmend 1984b [16]
200	tab m.d	24	26.6 (18-39)	73.5 (53.8-98.8)	-	23.8 (18-28)	41.67	test	Boyce 2012b [28]

(Continued on next page...)

Table S1.2: Clinical study data used for Ketoconazole model development *(continued)*

Dose [mg]	Route	N	Age [years]	Weight [kg]	Height [cm]	BMI [kg/m²]	Females [%]	Dataset	Reference
200	tab m.d	24	26.6 (18-39)	73.5 (53.8-98.8)	-	23.8 (18-28)	41.67	test	Boyce 2012a [28]
200	tab m.d	8	25 (21-46)	-	-	-	0	test	Daneshmend 1983 [15]
200	tab m.d	15	36 (22-43)	74.7 (50.1-95)	168.8 (154-179)	26 (21.1-30.3)	19	test	Patel 2011 [29]
200	tab m.d	21	-	-	-	-	-	test	Tiseo 2002 [30]
200	tab m.d	15	-	-	-	-	-	training	Wire 2007 [31]
200	tab m.d	8	(18-38)	-	-	-	-	test	Greenblatt 1998 Control [32]
800	tab m.d	2	-	-	-	-	-	test	Craven 1983 [33]
1200	tab m.d	2	-	-	-	-	-	test	Craven 1983 [33]

BMI: body mass index, cap: capsule, m.d: multiple dose, N: number of individuals studied, Route: route of administration, tab: tablet, s.d: single dose, sol: solution
-: no data available. Values are means with ranges, if available.
* median

S1.6 Ketoconazole – Drug-dependent parameters

Table S1.3: Drug-dependent parameters of the ketoconazole PBPK model

Parameter	Unit	Value	Source	Literature	Reference
Ketoconazole					
MW	g/mol	531.43	lit.	531.43	[35]
logP	-	2.52	lit.	2.73	[36]
f_u	%	1	lit.	1	[12]
pka (base)	-	2.94, 6.51	lit.	2.94, 6.51	[35]
Solubility (pH)	mg/ml	$2.03{\cdot}10^4$ (1.2), $4.3{\cdot}10^4$ (3), 7.00 (6.8). 5.40 (7), 6.00 (7.5)	lit.	$2.03{\cdot}10^4$ (1.2), $4.3{\cdot}10^4$ (3), 7.00 (6.8). 5.40 (7), 6.00 (7.5)	[37]
Density	g/cm^3	1.40	lit.	1.40	[38]
Aqueous diffusion coefficient	dm^2/min	$3.75{\cdot}10^{-7}$	opt.	$*2.56{\cdot}10^{-6}$	[4]
Spec. intest. perm. fasted	cm/min	$1.56{\cdot}10^{-5}$	opt.	$*4.28{\cdot}10^{-6}$	[4]
Spec. intest. perm. fed	cm/min	$9.95{\cdot}10^{-6}$	opt.	$*4.28{\cdot}10^{-6}$	[4]
GET fasted	min	15	lit.	15	[4]
GET fed	min	45	asm.	45–120	[39]
Cellular permeabilities	-	PK-Sim	-	-	[4]
Partition coefficient	-	Berez.	-	-	[40]
GFR fraction	-	1	asm.	-	-
EHC fraction	-	1	asm.	-	-
AADAC K_M	nmol/l	1880	lit.	1880	[41]
AADAC k_{cat}	1/min	0.87	opt.	-	-
CYP3A4 K_M	nmol/l	8.46	asm.	-	[27]
CYP3A4 k_{cat}	1/min	0.10	opt.	-	-
UGT1A4 K_M	nmol/l	7000	asm.	-	[42]
UGT1A4 k_{cat}	1/min	0.31	opt.	-	-
P-gp K_M	nmol/l	35	asm.	-	[27]
P-gp k_{cat}	1/min	0.33	opt.	-	-
CYP3A4 K_i	nmol/l	8.46	lit.	[a]8.46	[27]
P-gp K_i	nmol/l	35	lit.	[a]35	[27]
Particle dissolution [b]r (Bin1)	nm	11.75	calc.	[b]11.75	[43]
Particle dissolution [c]r (Bin2)	nm	111.06	calc.	[c]111.06	[43]
Particle dissolution [d]r (Bin3)	nm	205.46	calc.	[d]205.46	[43]
N-Deacetylketoconazole					
MW	g/mol	489.40	lit.	489.40	[44]
logP	-	3.75	lit.	4.58	[44]
f_u	%	1	asm.	[e]1	[12]
pka (base)	-	0.20, 6.42, 8.90	lit.	0.20, 6.42, 8.90	[44]
Solubility (pH)	mg/ml	1240 (6.5)	lit.	1240 (6.5)	[44]
Cellular permeabilities	-	Ch.d.S.	-	-	[45]
Partition coefficient	-	R&R	-	-	[46]
GFR fraction	-	1	asm.	-	-
EHC fraction	-	1	asm.	-	-
FMO3 K_M	nmol/l	1170	lit.	1170	[47]
FMO3 k_{cat}	1/min	378.65	opt.	-	-
CYP3A4 K_i	nmol/l	22	lit.	[a]52	[27]
P-gp K_i	nmol/l	119	lit.	[a]119	[27]

(Continued on next page...)

Table S1.3: Drug-dependent parameters of the ketoconazole PBPK model *(continued)*

Parameter	Unit	Value	Source	Literature	Reference
N-Deacetyl-N-hydroxyketoconazole					
MW	g/mol	505.40	lit.	505.40	[48]
logP	-	4.20	lit.	4.20	[48]
f_u	%	1	asm.	[e]1	[12]
pka (base)	-	3.42, 6.42	lit.	3.42, 6.42	[48]
Solubility (pH)	mg/ml	4400 (6.5)	lit.	4400 (6.5)	[48]
Organ permeability	cm/min	0	asm.	*0.05	[4]
Cellular permeabilities	-	Ch.d.S.	-	-	[45]
Partition coefficient	-	Berez.	-	-	[40]
GFR fraction	-	1	asm.	-	-
EHC fraction	-	1	asm.	-	-
FMO3 Cl	l/µmol/min	0.09	opt.	-	-
CYP3A4 K_i	nmol/l	22	asm.	[a,f]52	[27]
P-gp K_i	nmol/l	119	asm.	[a,f]119	[27]

AADAC: arylacetamide deacetylase, asm.: assumed, Berez.: Berezhkovskiy calculation method, calc.: calculated, Ch.d.S.: charge dependent Schmitt calculation method, Cl: first order clearance rate constant,CYP3A4: cytochrome P450 3A4, EHC: enterohepatic circulation, FMO3: flavin-containing monooxygenase 3, f_u: fraction unbound, GET: gastric emptying time, GFR: glomerular filtration rate, intest.: intestinal, k_{cat}: catalytic/transport rate constant, K_i: concentration for half-maximal inhibition, K_M: Michaelis-Menten constant, lit.: literature, logP: lipophilicity, MW: molecular weight, opt.: optimized, P-gp: P-glycoprotein, perm.: permeability, pka: acid dissociation constant, PK-Sim: PK-Sim® standard calculation method , r: particle radii used for particle dissolution, R&R: Rodgers and Rowland, spec.: specific, tab: tablet, UGT1A4: uridine diphosphate glucuronosyltransferase 1A4,

* calculated by the software

[a] *in-vitro* values calculated from respective IC50 values. Inhibitions were implemented as competitive inhibitions.

[b] respective particle radii for 99.0025% of dose (calculated according to Dallmann et al. [34])

[c] respective particle radii for 0.895% of dose (calculated according to Dallmann et al. [34])

[d] respective particle radii for 0.1025% of dose (calculated according to Dallmann et al. [34])

[e] assumed from value for ketoconazole, as no data available

[f] assumed from value for N-deacetylketoconazole, as no data available

-: no data available.

S2 Ketoconazole – PBPK model evaluation

S2.1 Plasma concentration-time profiles (Linear)

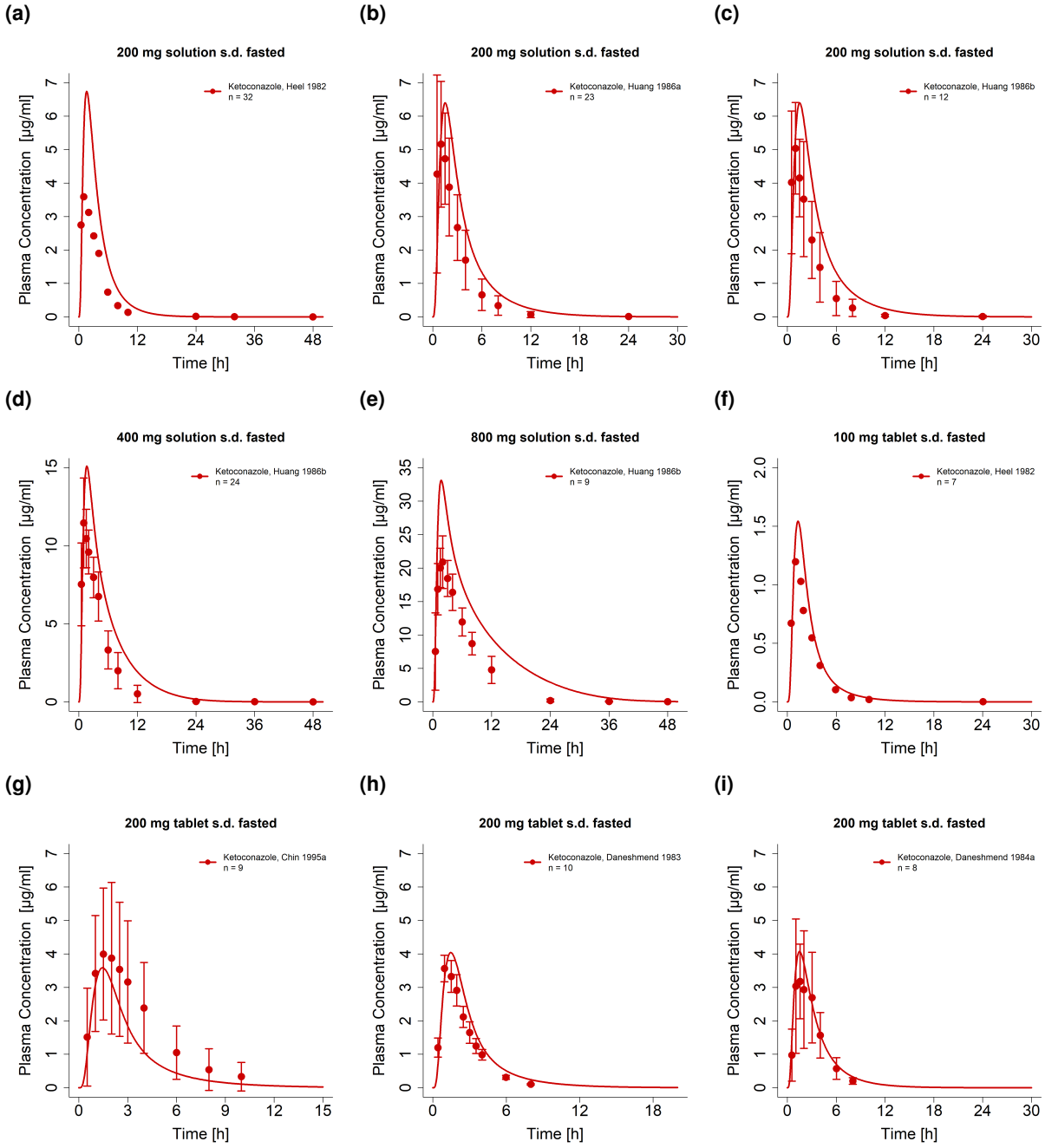

Figure S2.1: Ketoconazole plasma concentration-time profiles. Model predictions are shown as lines, observed data as dots (arithmetic mean ± SD). n: number of individuals studied, s.d: single dose

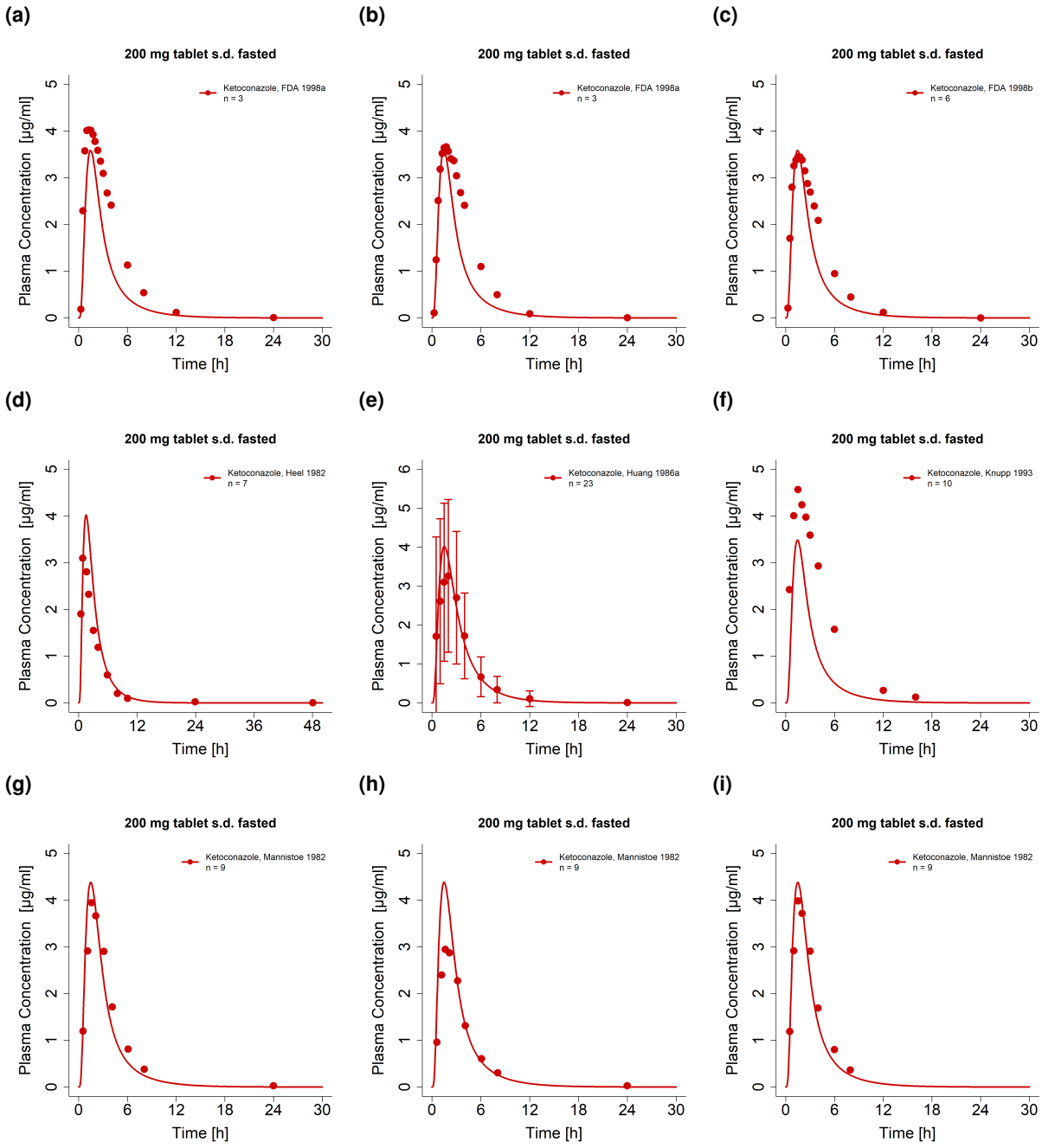

Figure S2.2: Ketoconazole plasma concentration-time profiles. Model predictions are shown as lines, observed data as dots (arithmetic mean ± SD). n: number of individuals studied, s.d: single dose

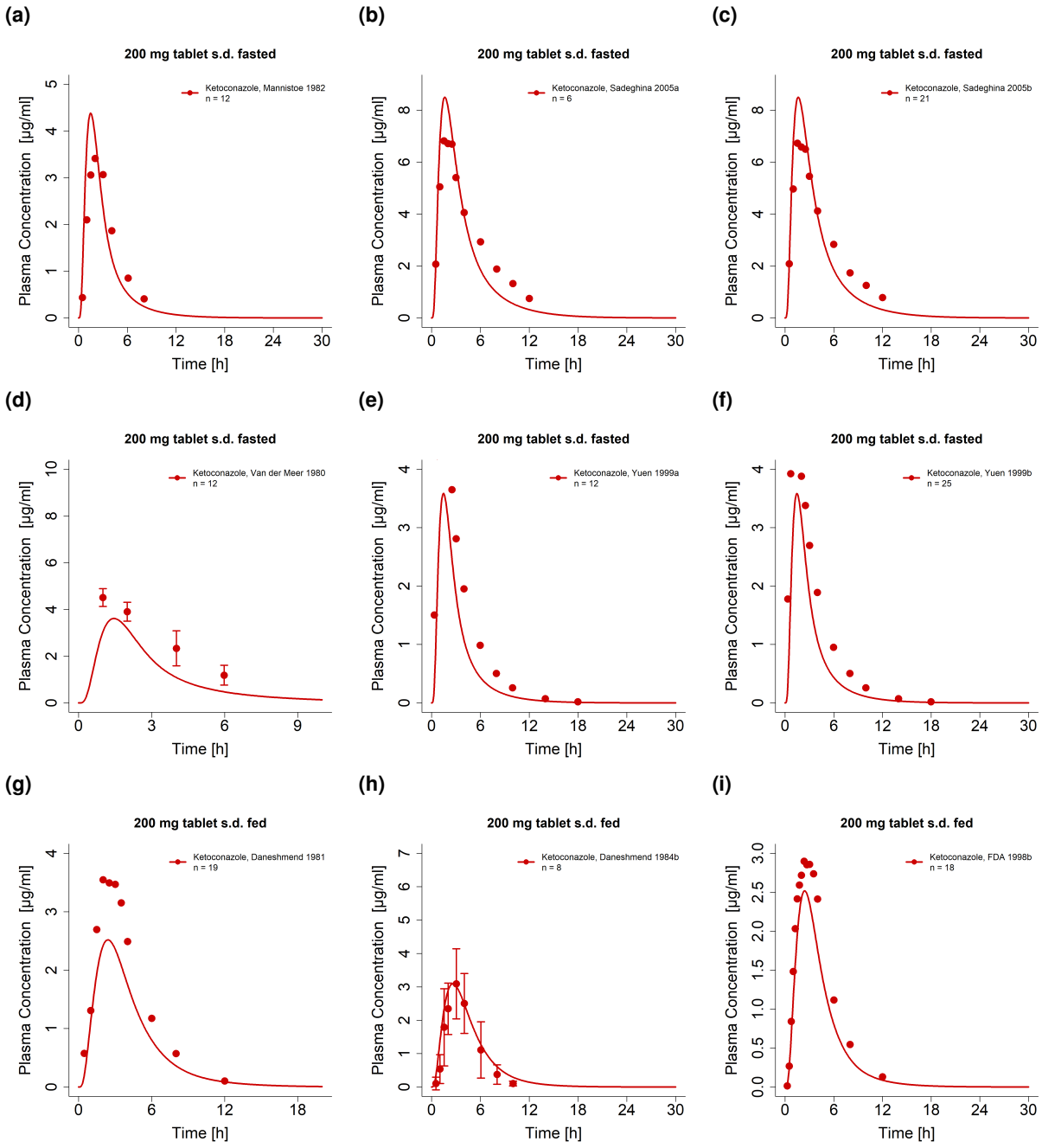

Figure S2.3: Ketoconazole plasma concentration-time profiles. Model predictions are shown as lines, observed data as dots (arithmetic mean ± SD). n: number of individuals studied, s.d: single dose

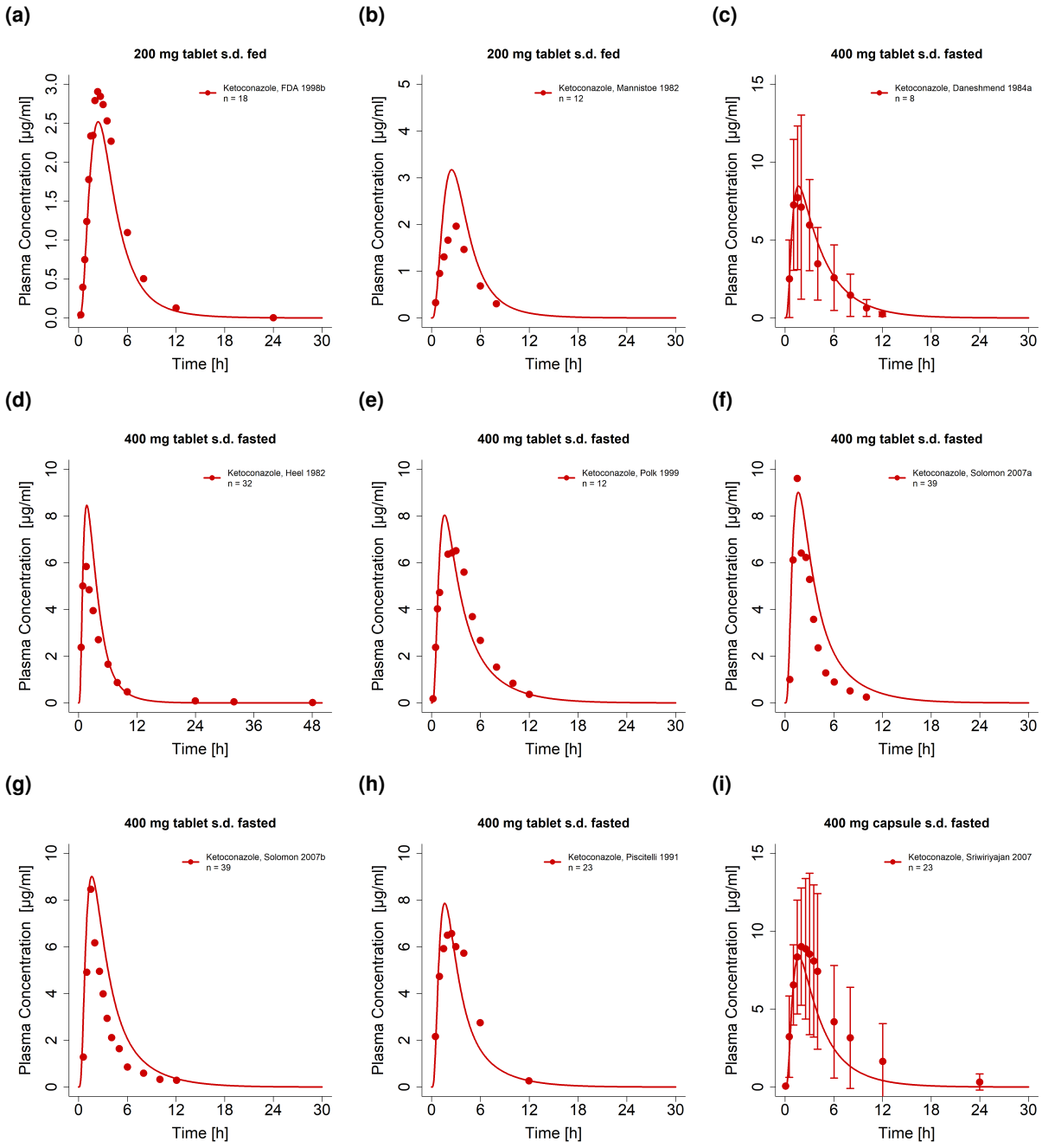

Figure S2.4: Ketoconazole plasma concentration-time profiles. Model predictions are shown as lines, observed data as dots (arithmetic mean ± SD). n: number of individuals studied, s.d: single dose

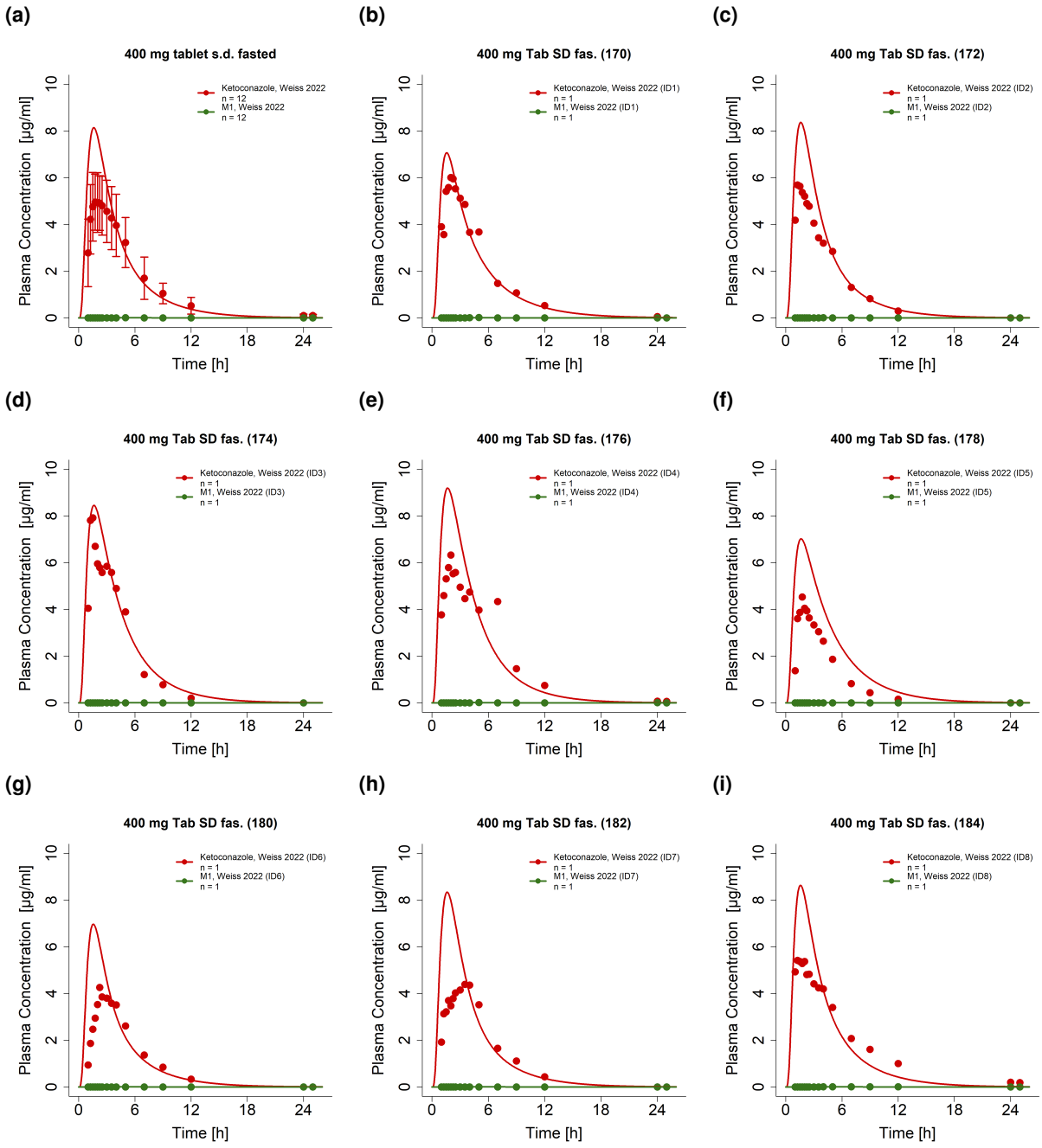

Figure S2.5: Ketoconazole plasma concentration-time profiles. Model predictions are shown as lines, observed data as dots (arithmetic mean ± SD). n: number of individuals studied, s.d: single dose

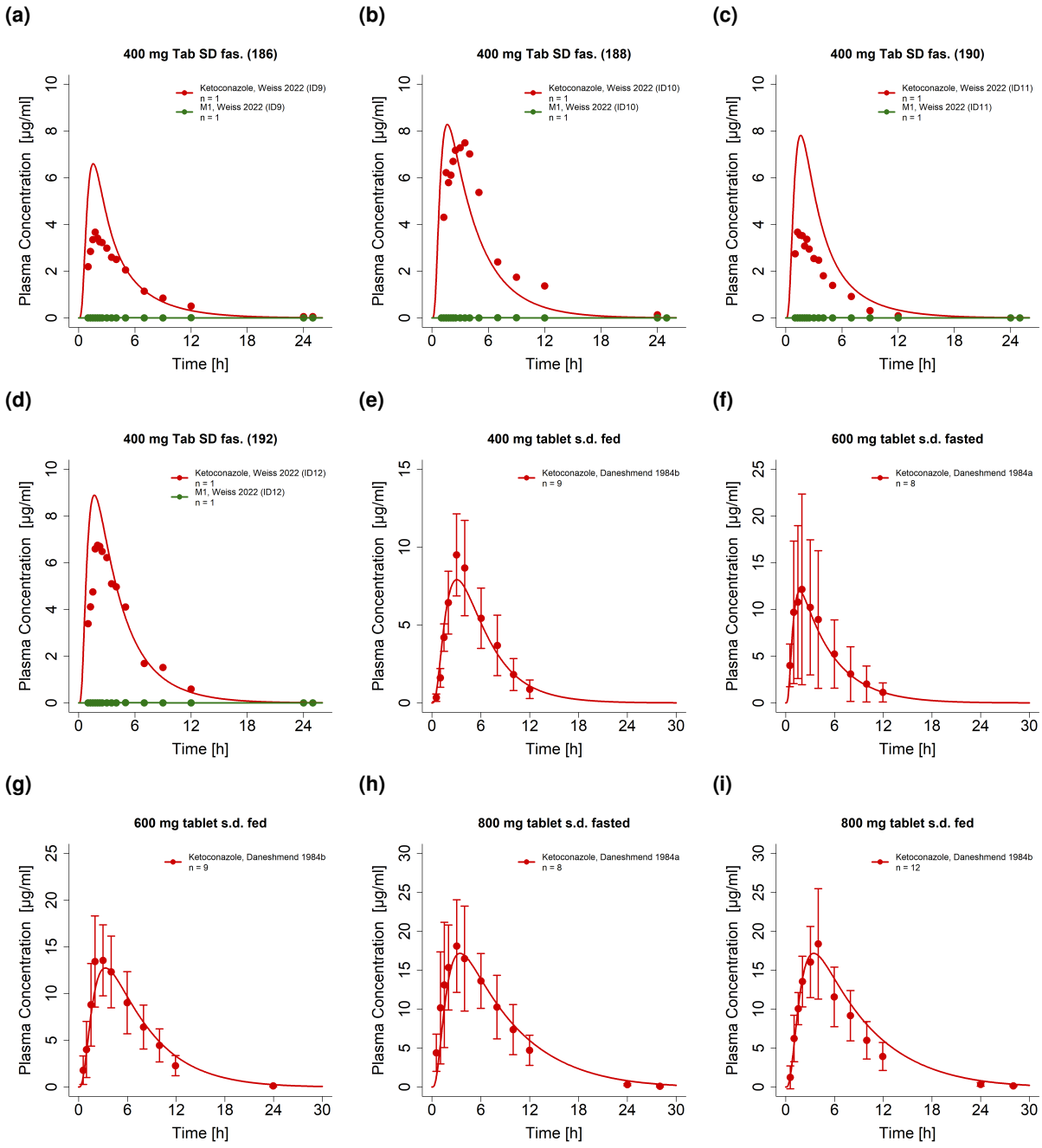

Figure S2.6: Ketoconazole plasma concentration-time profiles. Model predictions are shown as lines, observed data as dots (arithmetic mean ± SD). n: number of individuals studied, s.d: single dose

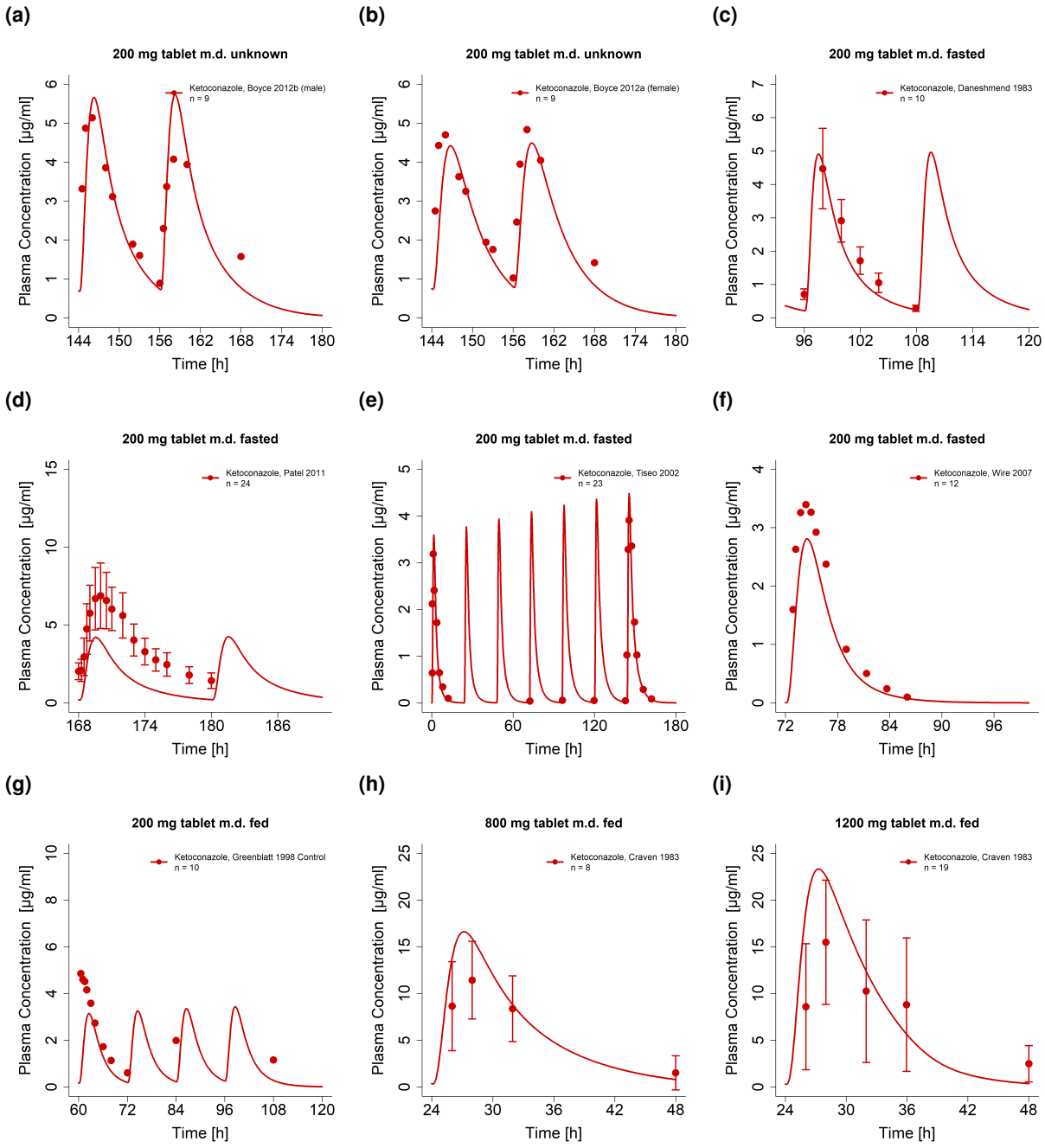

Figure S2.7: Ketoconazole plasma concentration-time profiles. Model predictions are shown as lines, observed data as dots (arithmetic mean ± SD). m.d: multiple dose, n: number of individuals studied, s.d: single dose

S2.2 Plasma concentration-time profiles (Semilogarhitmic)

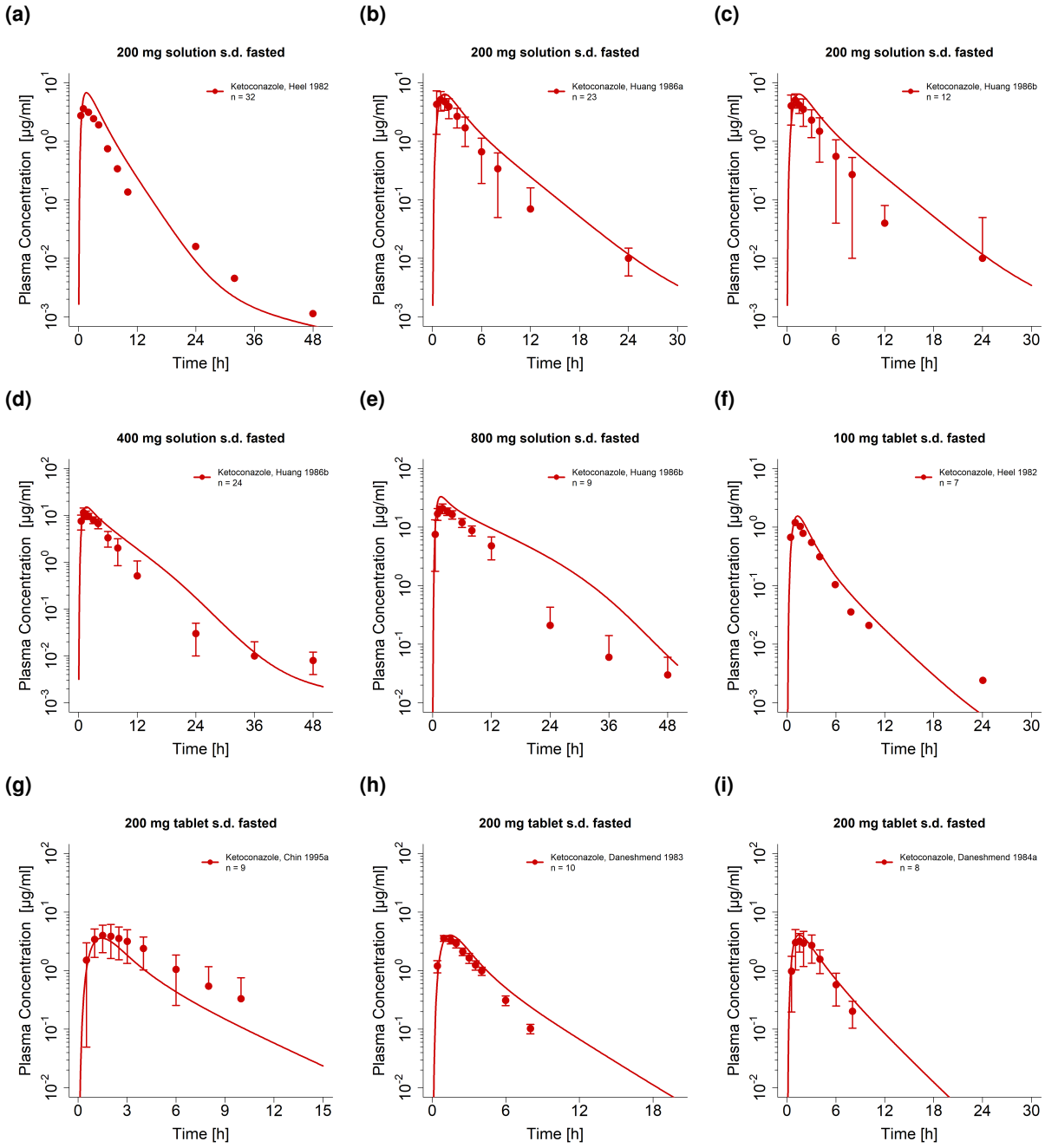

Figure S2.8: Ketoconazole plasma concentration-time profiles. Model predictions are shown as lines, observed data as dots (arithmetic mean ± SD). n: number of individuals studied, s.d: single dose

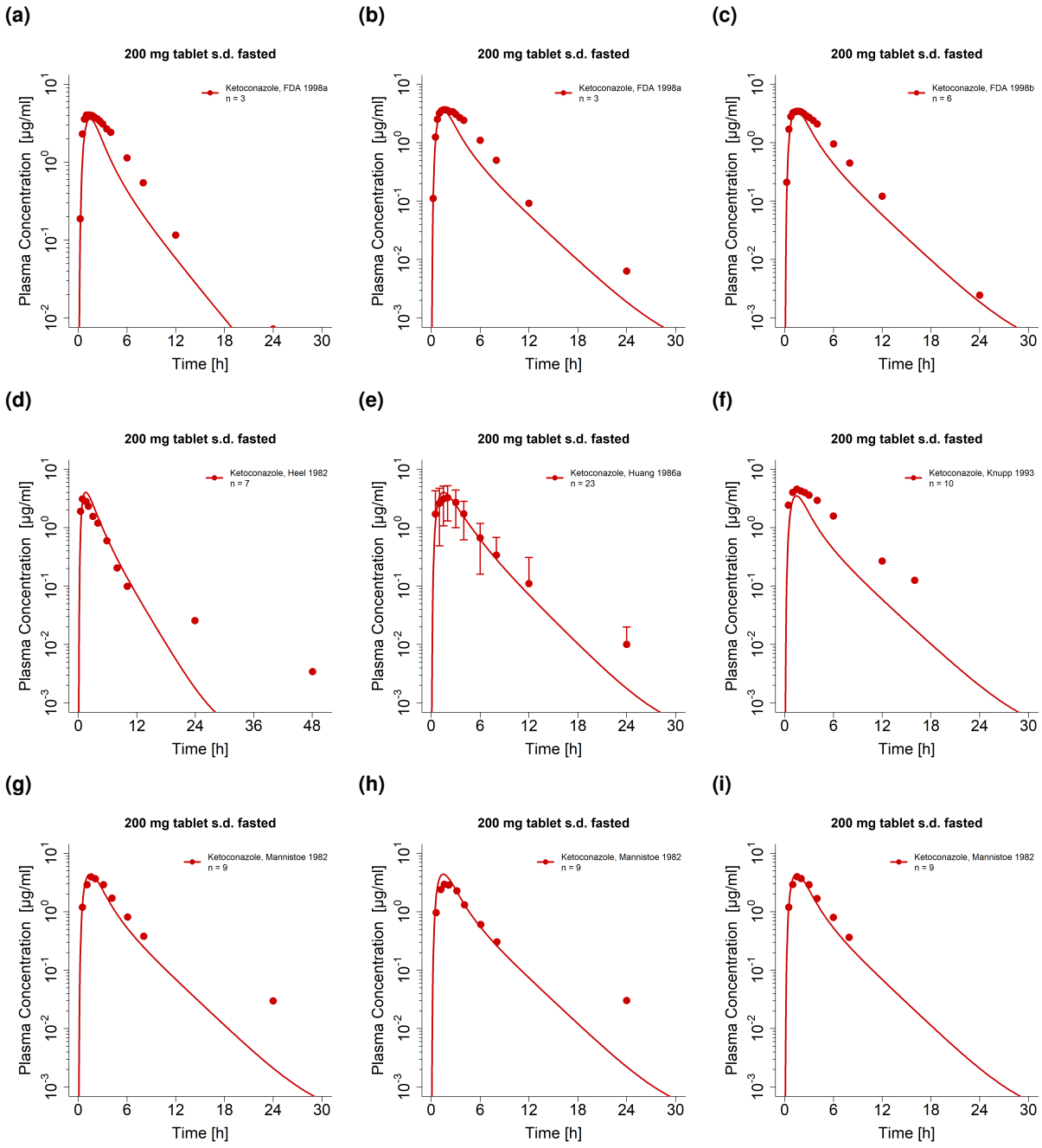

Figure S2.9: Ketoconazole plasma concentration-time profiles. Model predictions are shown as lines, observed data as dots (arithmetic mean ± SD). n: number of individuals studied, s.d: single dose

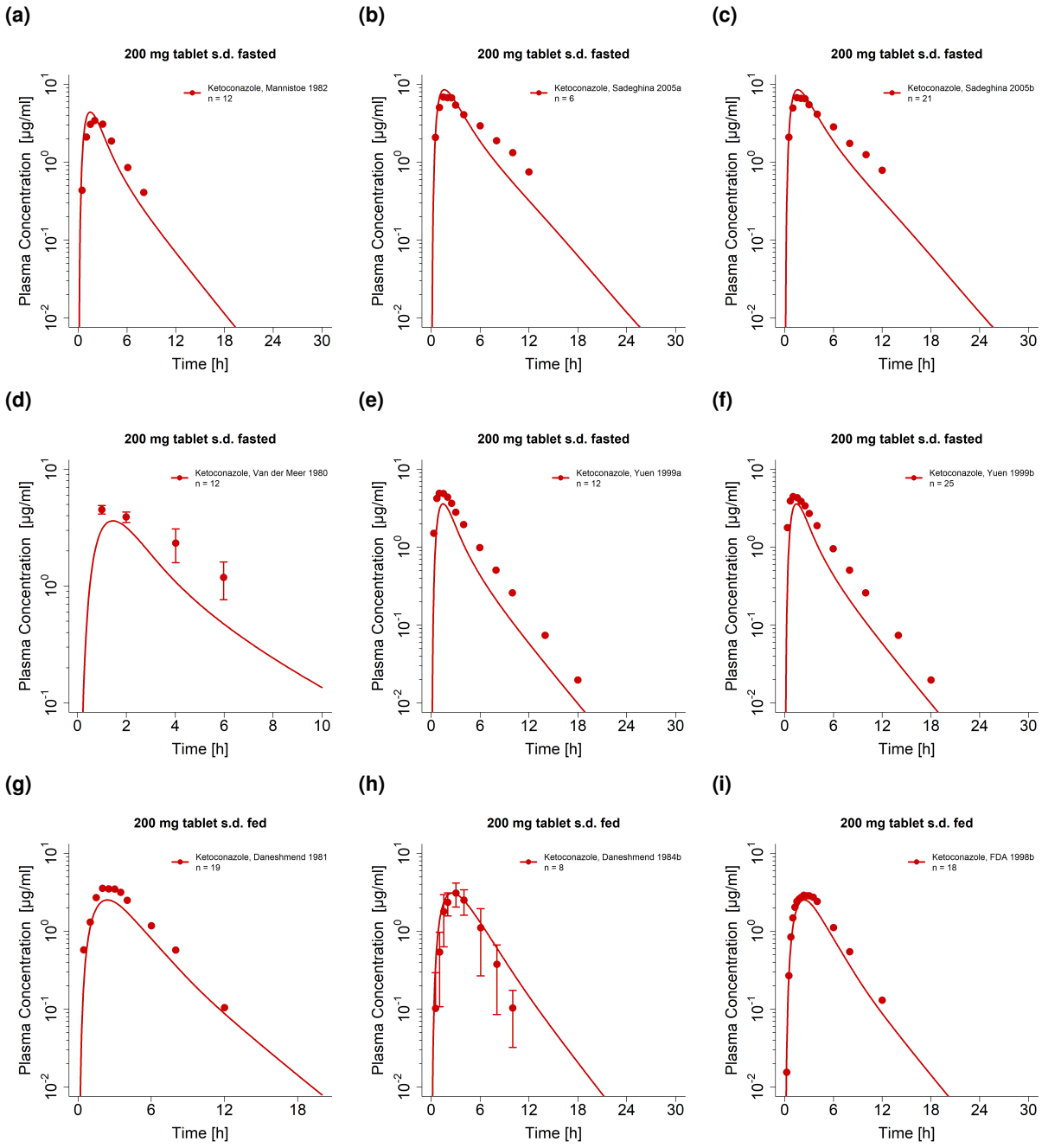

Figure S2.10: Ketoconazole plasma concentration-time profiles. Model predictions are shown as lines, observed data as dots (arithmetic mean ± SD). n: number of individuals studied, s.d: single dose

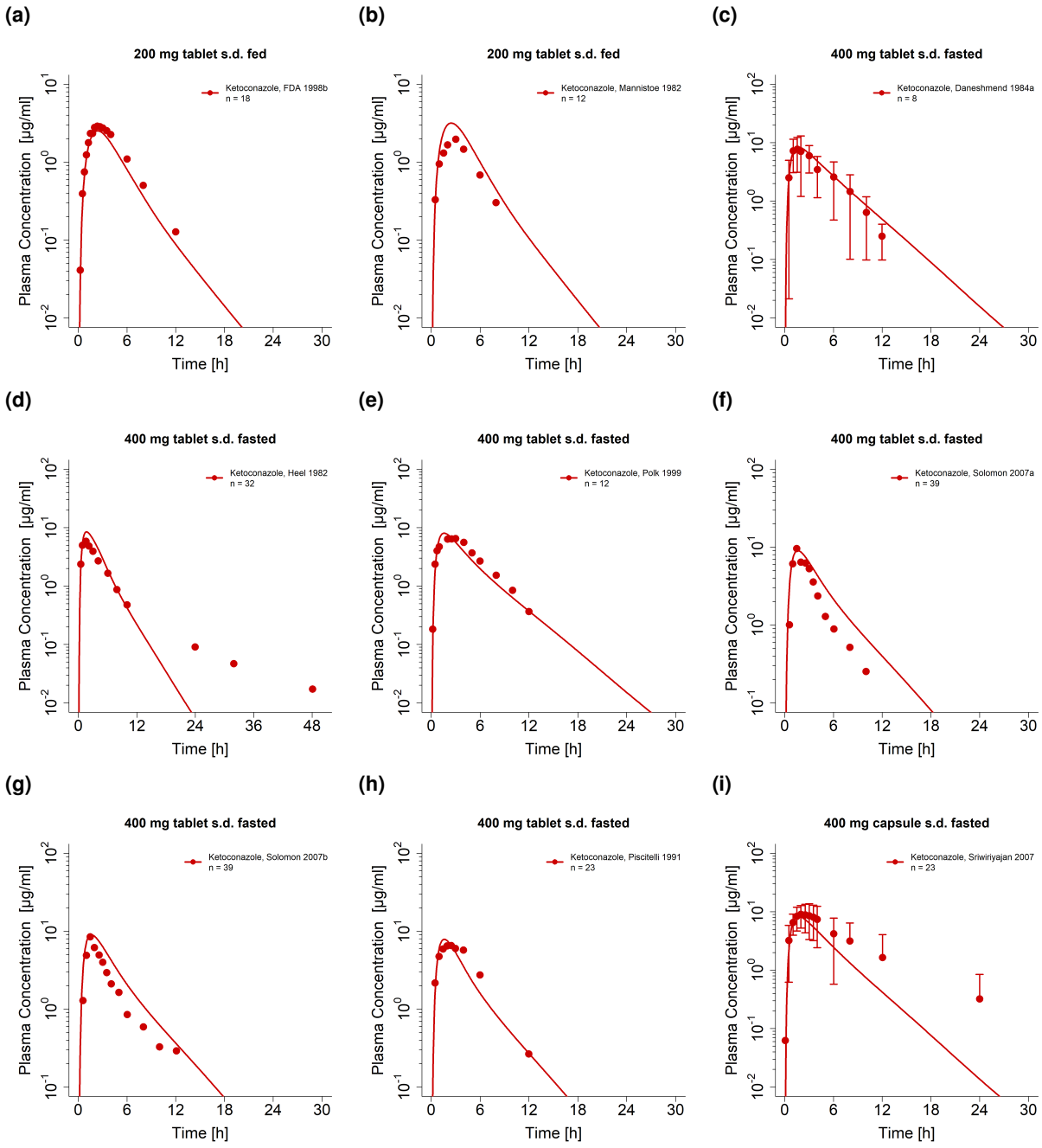

Figure S2.11: Ketoconazole plasma concentration-time profiles. Model predictions are shown as lines, observed data as dots (arithmetic mean ± SD). n: number of individuals studied, s.d: single dose

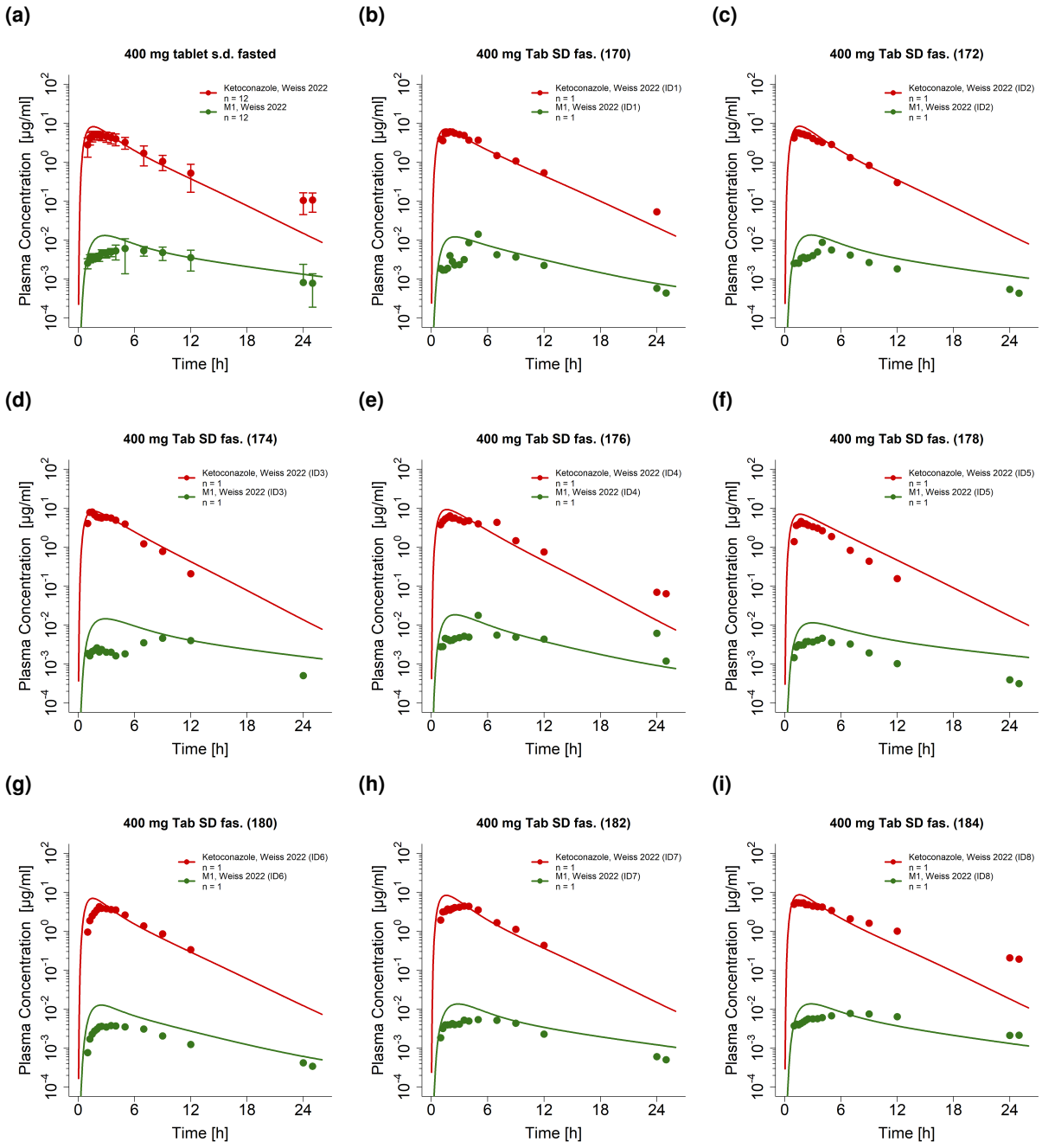

Figure S2.12: Ketoconazole plasma concentration-time profiles. Model predictions are shown as lines, observed data as dots (arithmetic mean ± SD). n: number of individuals studied, s.d: single dose

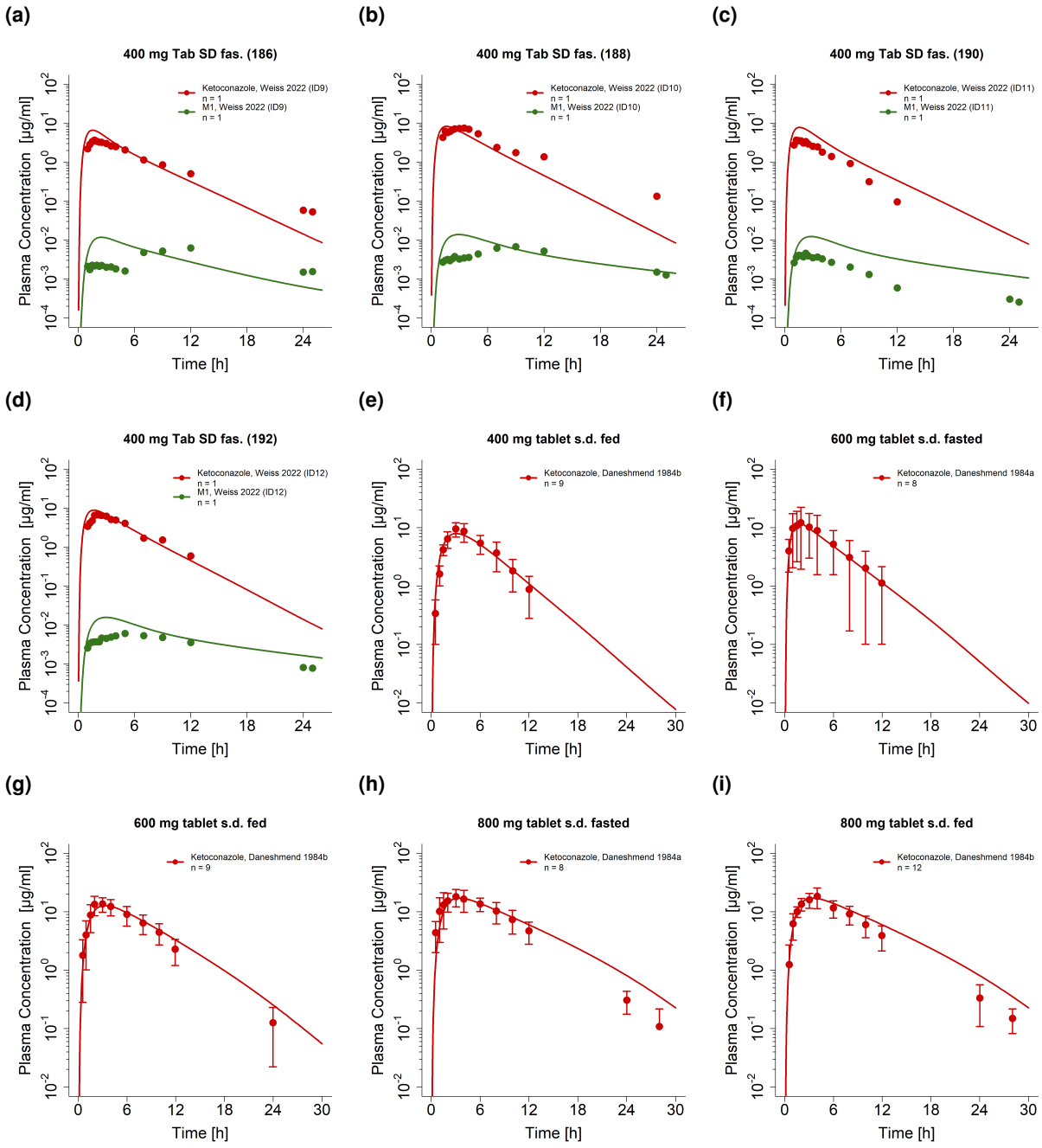

Figure S2.13: Ketoconazole plasma concentration-time profiles. Model predictions are shown as lines, observed data as dots (arithmetic mean ± SD). n: number of individuals studied, s.d: single dose

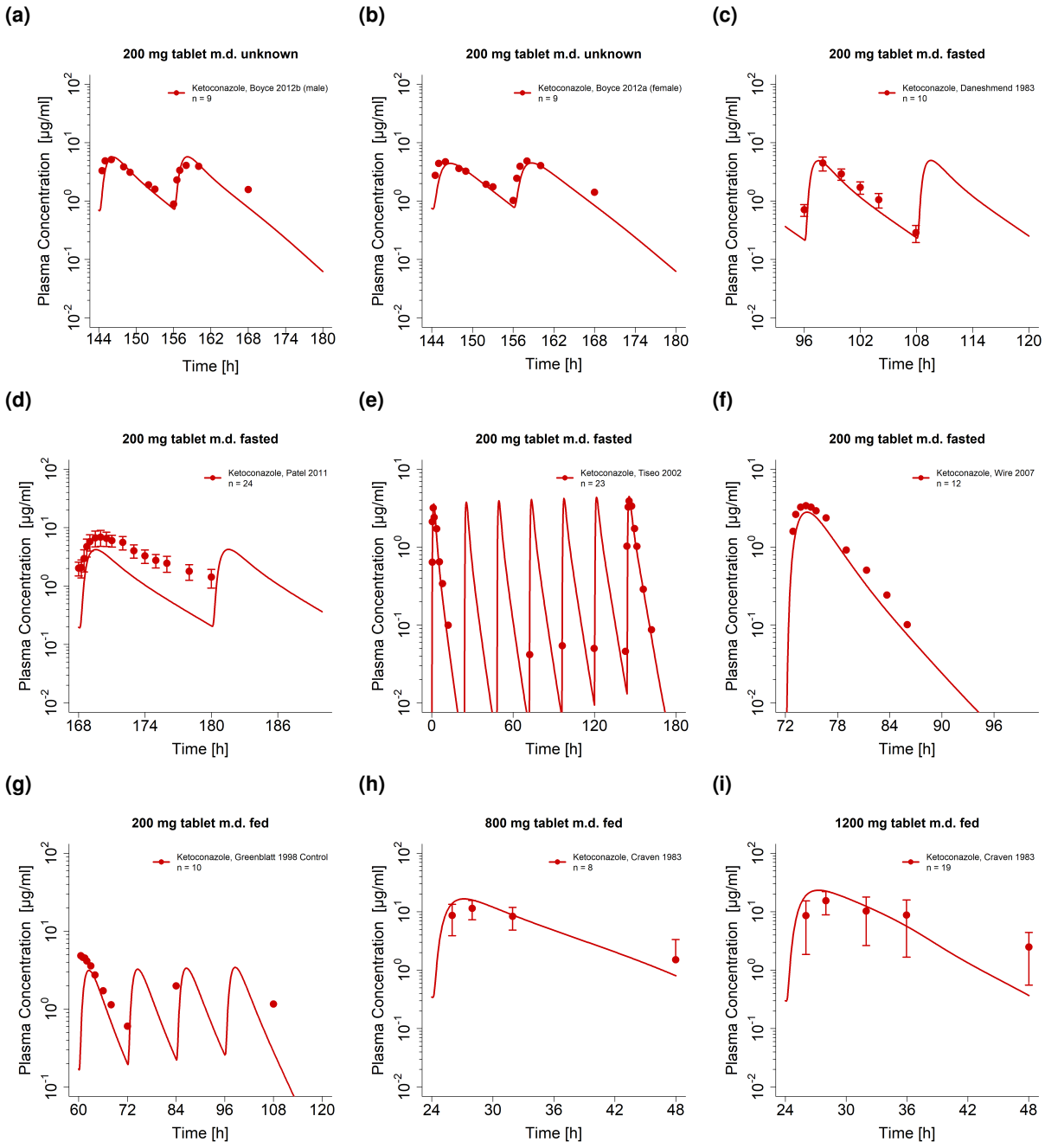

Figure S2.14: Ketoconazole plasma concentration-time profiles. Model predictions are shown as lines, observed data as dots (arithmetic mean ± SD). m.d.: multiple dose, n: number of individuals studied, s.d: single dose

S2.3 Predicted compared to observed concentrations goodness-of-fit plots

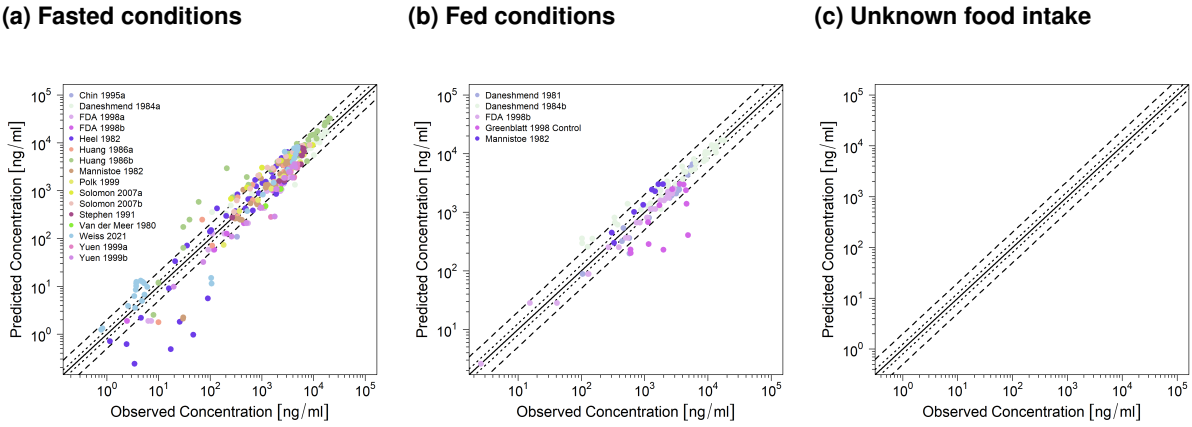

Figure S2.15: Predicted compared to observed ketoconazole plasma concentration values. The solid line marks the line of identity. Dotted lines indicate 1.25-fold, dashed lines indicate 2-fold deviation.

S2.4 AUC_{last} and C_{max} goodness-of-fit plots

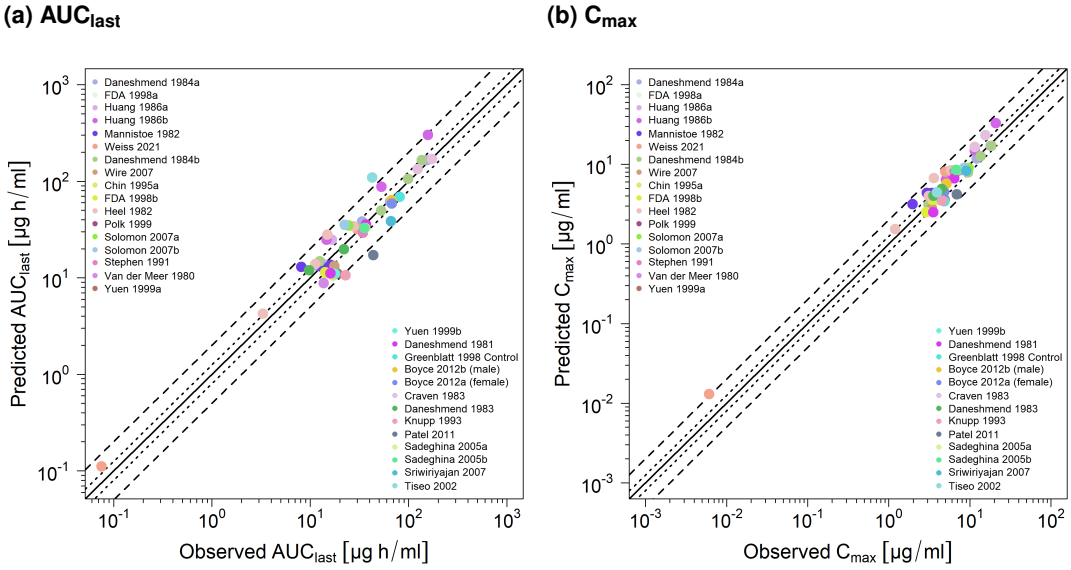

Figure S2.16: Predicted compared to observed ketoconazole AUC_{last} and C_{max} values. The solid line marks the line of identity. Dotted lines indicate 1.25-fold, dashed lines indicate 2-fold deviation. AUC_{last}: area under the plasma concentration-time curve from the time of drug administration to the last concentration measurement, C_{max}: maximum plasma concentration

S2.5 Mean relative deviation of plasma concentration predictions

Table S2.4: Mean relative deviation values of ketoconazole and N-deacetylketoconazole

Dose [mg]	Route	N	DFI	MRD	Dataset	Reference
Ketoconazole						
200	sol s.d	12	fasted	1.71	training	Heel 1982 [12]
200	sol s.d	23	fasted	1.30	test	Huang 1986a [13]
200	sol s.d	12	fasted	1.36	test	Huang 1986b [13]
400	sol s.d	12	fasted	1.63	test	Huang 1986b [13]
800	sol s.d	12	fasted	1.39	training	Huang 1986b [13]
100	tab s.d	12	fasted	2.08	training	Heel 1982 [12]
200	tab s.d	9	fasted	1.09	test	Chin 1995 [14]
200	tab s.d	8	unknown	1.24	test	Daneshmend 1983 [15]
200	tab s.d	8	fasted	1.23	test	Daneshmend 1984a [16]
200	tab s.d	39	fasted	1.48	training	FDA 1998a [17]
200	tab s.d	39	fasted	1.48	test	FDA 1998a [17]
200	tab s.d	23	fasted	1.16	test	FDA 1998b [17]
200	tab s.d	12	fasted	4.39	test	Heel 1982 [12]
200	tab s.d	23	fasted	1.30	test	Huang 1986a [13]
200	tab s.d	12	unknown	1.21	test	Knupp 1993 [18]
200	tab s.d	10	fasted	1.73	training	Mannistoe 1982 [19]
200	tab s.d	10	fasted	1.76	test	Mannistoe 1982 [19]
200	tab s.d	10	fasted	1.10	test	Mannistoe 1982 [19]
200	tab s.d	10	fasted	1.39	test	Mannistoe 1982 [19]
200	tab s.d	12	unknown	1.07	test	Sadeghina 2005 [20]
200	tab s.d	12	unknown	1.06	test	Sadeghina 2005 [20]
200	tab s.d	3	fasted	1.12	test	Van der Meer 1980 [22]
200	tab s.d	18	fasted	1.22	test	Yuen 1999a [23]
200	tab s.d	18	fasted	1.20	test	Yuen 1999b [23]
200	tab s.d	6	fed	1.10	test	Daneshmend 1981 [49]
200	tab s.d	8	fed	1.32	test	Daneshmend 1984b [16]
200	tab s.d	23	fed	1.11	training	FDA 1998b [17]
200	tab s.d	23	fed	1.18	test	FDA 1998b [17]
200	tab s.d	10	fed	1.35	test	Mannistoe 1982 [19]
400	tab s.d	8	fasted	1.18	test	Daneshmend 1984a [16]
400	tab s.d	12	fasted	4.66	test	Heel 1982 [12]
400	tab s.d	12	fasted	1.09	test	Polk 1999 [24]
400	tab s.d	24	fasted	1.38	test	Solomon 2007a [21]
400	tab s.d	24	fasted	1.34	test	Solomon 2007b [21]
400	tab s.d	6	fasted	1.11	test	Piscitelli 1991 [25]
400	cap s.d	12	unknown	3.23	test	Sriwiriyajan 2007 [26]
400	tab s.d	12	fasted	1.16	training	Weiss 2022 [27]
400	tab s.d	8	fed	1.20	test	Daneshmend 1984b [16]
600	tab s.d	8	fasted	1.08	training	Daneshmend 1984a [16]
600	tab s.d	8	fed	1.13	test	Daneshmend 1984b [16]
800	tab s.d	8	fasted	1.24	test	Daneshmend 1984a [16]
800	tab s.d	8	fed	1.18	training	Daneshmend 1984b [16]
200	tab m.d	24	unknown	1.16	training	Boyce 2012b [28]
200	tab m.d	24	unknown	1.12	test	Boyce 2012a [28]
200	tab m.d	8	unknown	1.07	test	Daneshmend 1983 [15]
200	tab m.d	15	unknown	1.39	test	Patel 2011 [29]
200	tab s.d	21	unknown	1.24	test	Tiseo 2002 [30]
200	tab m.d	15	unknown	1.09	training	Wire 2007 [31]
400	tab m.d	9	fed	1.39	test	Greenblatt 1998 Control [32]
800	tab m.d	2	unknown	1.05	test	Craven 1983 [33]

(Continued on next page...)

Table S2.4: Mean relative deviation values of ketoconazole and N-deacetylketoconazole *(continued)*

Dose [mg]	Route	N	DFI	MRD	Dataset	Reference
1200	tab m.d	2	unknown	1.23	test	Craven 1983 [33]
N-Deacetylketoconazole						
400	tab s.d	12	fasted	2.51	training	Weiss 2021 [27]
Mean MRD for ketoconazole				**1.42**		
Mean MRD for N-deacetylketoconazole				**2.51**		
Overall mean MRD (range)				**1.45 (1.09–2.69)**		
				92.45% (49/53) $\leq$ **2**		

cap: capsule, DFI: drug-food-interaction, m.d: multiple dose, MRD: mean relative deviation, N: number of individuals studied, Route: route of administration, s.d: single dose, sol: solution, tab: tablet

S2.6 Geometric mean fold error of predicted AUC_{last} and C_{max} values

Table S2.5: Predicted and observed AUC_{last} and C_{max} values of ketoconazole and N-deacetylketoconazole

Dose [mg]	Route	N	DFI	AUC_{last} [µg*h/ml]			C_{max} [µg/ml]			Dataset	Reference
				Pred	Obs	Pred/Obs	Pred	Obs	Pred/Obs		
Ketoconazole											
200	sol s.d	12	fasted	28.07	14.89	1.88	6.74	3.59	1.88	training	Heel 1982 [12]
200	sol s.d	23	fasted	24.91	16.58	1.50	6.40	5.16	1.24	test	Huang 1986a [13]
200	sol s.d	12	fasted	24.91	14.60	1.71	6.40	5.04	1.27	test	Huang 1986b [13]
400	sol s.d	12	fasted	87.95	52.96	1.66	15.09	11.46	1.32	test	Huang 1986b [13]
800	sol s.d	12	fasted	303.31	156.86	1.93	33.11	20.88	1.59	training	Huang 1986b [13]
100	tab s.d	12	fasted	4.27	3.29	1.30	1.54	1.20	1.29	training	Heel 1982 [12]
200	tab s.d	9	fasted	10.59	16.92	0.63	3.59	4.00	0.90	test	Chin 1995 [14]
200	tab s.d	8	unknown	11.99	9.73	1.23	4.04	3.56	1.13	test	Daneshmend 1983 [15]
200	tab s.d	8	fasted	13.45	11.63	1.16	4.07	3.18	1.28	test	Daneshmend 1984a [16]
200	tab s.d	39	fasted	11.12	18.68	0.60	3.59	4.02	0.89	training	FDA 1998a [17]
200	tab s.d	39	fasted	11.12	17.16	0.65	3.58	3.66	0.98	test	FDA 1998a [17]
200	tab s.d	23	fasted	11.12	15.94	0.70	3.58	3.44	1.04	test	FDA 1998b [17]
200	tab s.d	12	fasted	13.87	11.25	1.23	4.02	3.10	1.30	test	Heel 1982 [12]
200	tab s.d	23	fasted	13.79	13.76	1.00	4.02	3.26	1.23	test	Huang 1986a [13]
200	tab s.d	12	unknown	10.66	22.84	0.47	3.49	4.56	0.76	test	Knupp 1993 [18]
200	tab s.d	10	fasted	13.63	16.14	0.84	4.38	3.95	1.11	training	Mannistoe 1982 [19]
200	tab s.d	10	fasted	13.61	12.46	1.09	4.38	2.94	1.49	test	Mannistoe 1982 [19]
200	tab s.d	10	fasted	12.84	13.65	0.94	4.38	3.98	1.10	test	Mannistoe 1982 [19]
200	tab s.d	10	fasted	12.89	13.24	0.97	4.38	3.41	1.28	test	Mannistoe 1982 [19]
200	tab s.d	12	unknown	32.84	36.04	0.91	8.50	6.82	1.25	test	Sadeghina 2005 [20]
200	tab s.d	12	unknown	32.84	35.31	0.93	8.50	6.73	1.26	test	Sadeghina 2005 [20]
200	tab s.d	3	fasted	8.82	13.69	0.64	3.61	4.51	0.80	test	Van der Meer 1980 [22]
200	tab s.d	18	fasted	11.08	18.89	0.59	3.58	4.91	0.73	test	Yuen 1999a [23]
200	tab s.d	18	fasted	11.08	17.76	0.62	3.58	4.46	0.80	test	Yuen 1999b [23]
200	tab s.d	6	fed	11.11	15.96	0.70	2.52	3.55	0.71	test	Daneshmend 1981 [49]
200	tab s.d	8	fed	14.88	12.50	1.19	3.09	3.09	1.00	test	Daneshmend 1984b [16]
200	tab s.d	23	fed	11.13	14.40	0.77	2.52	2.90	0.87	training	FDA 1998b [17]
200	tab s.d	23	fed	11.41	14.14	0.81	2.52	2.90	0.87	test	FDA 1998b [17]
200	tab s.d	10	fed	12.99	8.10	1.60	3.17	1.96	1.61	test	Mannistoe 1982 [19]
400	tab s.d	8	fasted	38.44	33.67	1.14	8.46	7.71	1.10	test	Daneshmend 1984a [16]
400	tab s.d	12	fasted	34.20	27.62	1.24	8.46	5.83	1.45	test	Heel 1982 [12]
400	tab s.d	12	fasted	32.79	35.69	0.92	8.04	6.52	1.23	test	Polk 1999 [24]
200	tab s.d	24	fasted	34.90	24.30	1.44	9.01	9.61	0.94	test	Solomon 2007a [21]

(Continued on next page...)

Table S2.5: Mean relative deviation values of ketoconazole and N-deacetylketoconazole *(continued)*

Dose [mg]	Route	N	DFI	AUC_{last} [µg*h/ml]			C_{max} [µg/ml]			Dataset	Reference
				Pred	Obs	Pred/Obs	Pred	Obs	Pred/Obs		
200	tab s.d	24	fasted	35.46	22.40	1.58	9.01	8.46	1.06	test	Solomon 2007b [21]
400	tab s.d	6	fasted	29.48	34.32	0.86	7.86	6.57	1.20	test	Piscitelli 1991 [25]
400	cap s.d	12	unknown	38.61	65.85	0.59	8.34	9.02	0.93	test	Sriwiriyajan 2007 [26]
400	tab s.d	12	fasted	32.05	30.02	1.07	8.14	4.96	1.64	training	Weiss 2022 [27]
400	tab s.d	8	fed	35.64	36.91	0.97	6.70	6.44	1.04	test	Daneshmend 1984b [16]
600	tab s.d	8	fasted	61.56	64.92	0.95	11.93	12.15	0.98	training	Daneshmend 1984a [16]
600	tab s.d	8	fed	106.05	98.72	1.07	12.73	13.55	0.94	test	Daneshmend 1984b [16]
800	tab s.d	8	fasted	166.39	153.04	1.09	17.15	18.09	0.95	test	Daneshmend 1984a [16]
800	tab s.d	8	fed	166.38	135.94	1.22	17.15	18.37	0.93	training	Daneshmend 1984b [16]
200	tab m.d	24	unknown	58.75	67.41	0.87	4.49	4.83	0.93	training	Boyce 2012b [28]
200	tab m.d	24	unknown	63.94	66.77	0.96	5.73	5.14	1.12	test	Boyce 2012a [28]
200	tab m.d	8	unknown	19.74	21.94	0.90	4.91	4.47	1.10	test	Daneshmend 1983 [15]
200	tab m.d	15	unknown	17.19	43.67	0.39	4.21	6.87	0.61	test	Patel 2011 [29]
200	tab s.d	21	unknown	109.29	42.47	2.57	4.48	3.91	1.15	test	Tiseo 2002 [30]
200	tab m.d	15	unknown	13.25	17.51	0.76	2.81	3.40	0.83	training	Wire 2007 [31]
400	tab m.d	9	fed	68.89	81.00	0.85	3.44	4.86	0.71	test	Greenblatt 1998 Control [32]
800	tab m.d	2	unknown	170.53	172.40	0.99	23.32	15.48	1.51	test	Craven 1983 [33]
1200	tab m.d	2	unknown	134.16	123.24	1.09	16.61	11.43	1.45	test	Craven 1983 [33]
N-Deacetylketoconazole											
400	tab s.d	12	fasted	0.11	0.08	1.48	0.01	0.01	2.15	training	Weiss 2021 [27]
Mean GMFE for ketoconazole						**1.37**			**1.24**		
Mean GMFE for N-deacetylketoconazole						**1.48**			**2.15**		
Overall mean GMFE (range)						**1.37 (1.00–2.57)**			**1.26 (1.00–2.15)**		
						94.34% (50/53) $\leq$ 2			**98.11% (52/53) $\leq$ 2**		

AUC_{last}: area under the plasma concentration-time curve calculated from the first to last time point of measurement, cap: capsule, C_{max}: maximum plasma concentration, DFI: drug-food-interaction, GMFE: geometric mean fold error, m.d: multiple dose, N: number of individuals studied, obs: observed, pred: predicted, Route: route of administration, s.d: single dose, sol: solution, tab: tablet

S2.7 Ketoconazole – DFI model evaluation

S2.7.1 Plasma concentration-time profiles (Linear)

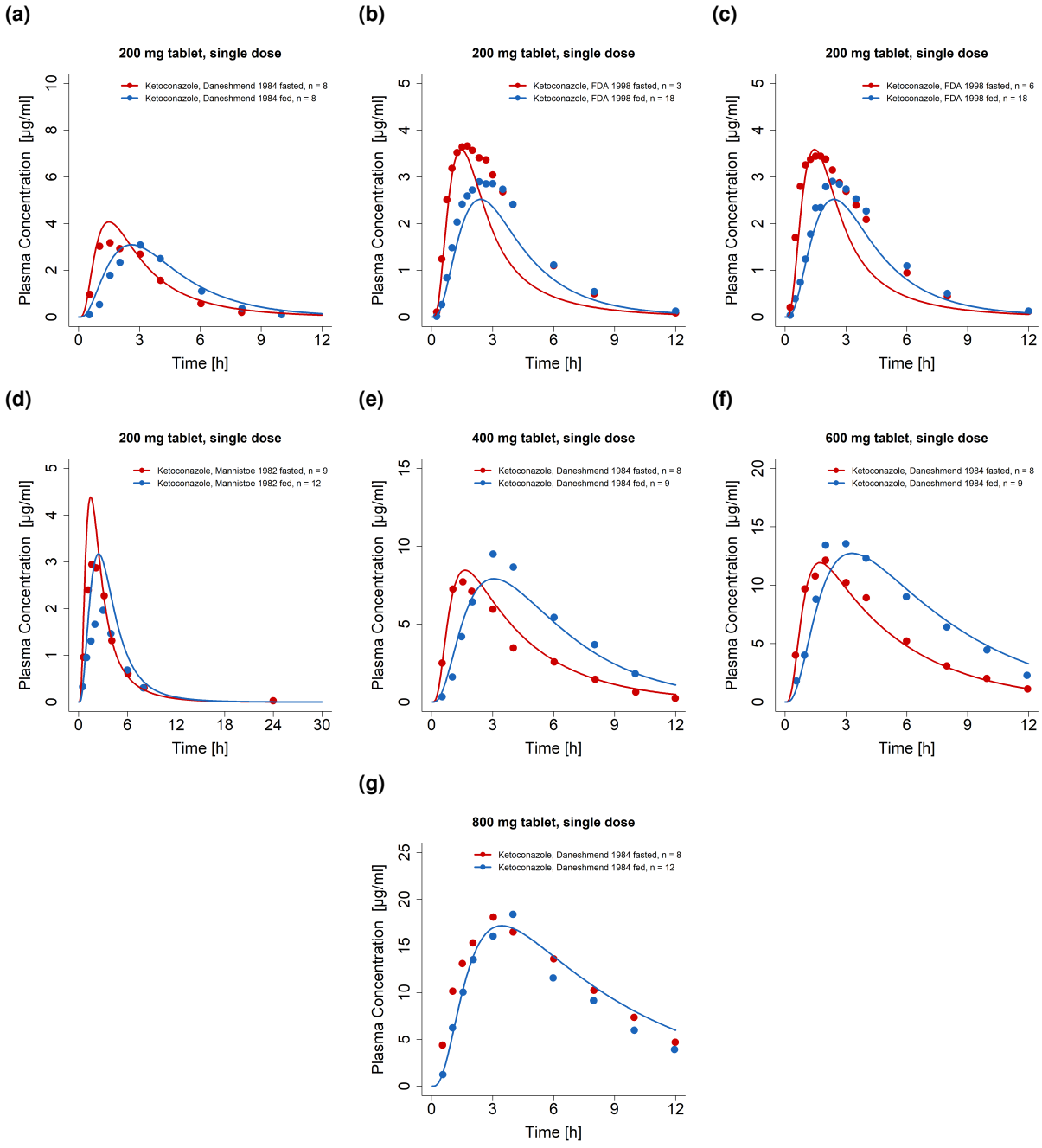

Figure S2.17: Comparison of predicted and observed ketoconazole plasma concentration-time profiles under fasted and fed conditions. Model predictions are shown as lines, observed data as dots (arithmetic mean ± SD). n: number of individuals studied.

S2.7.2 Plasma concentration-time profiles (Semilogarhitmic)

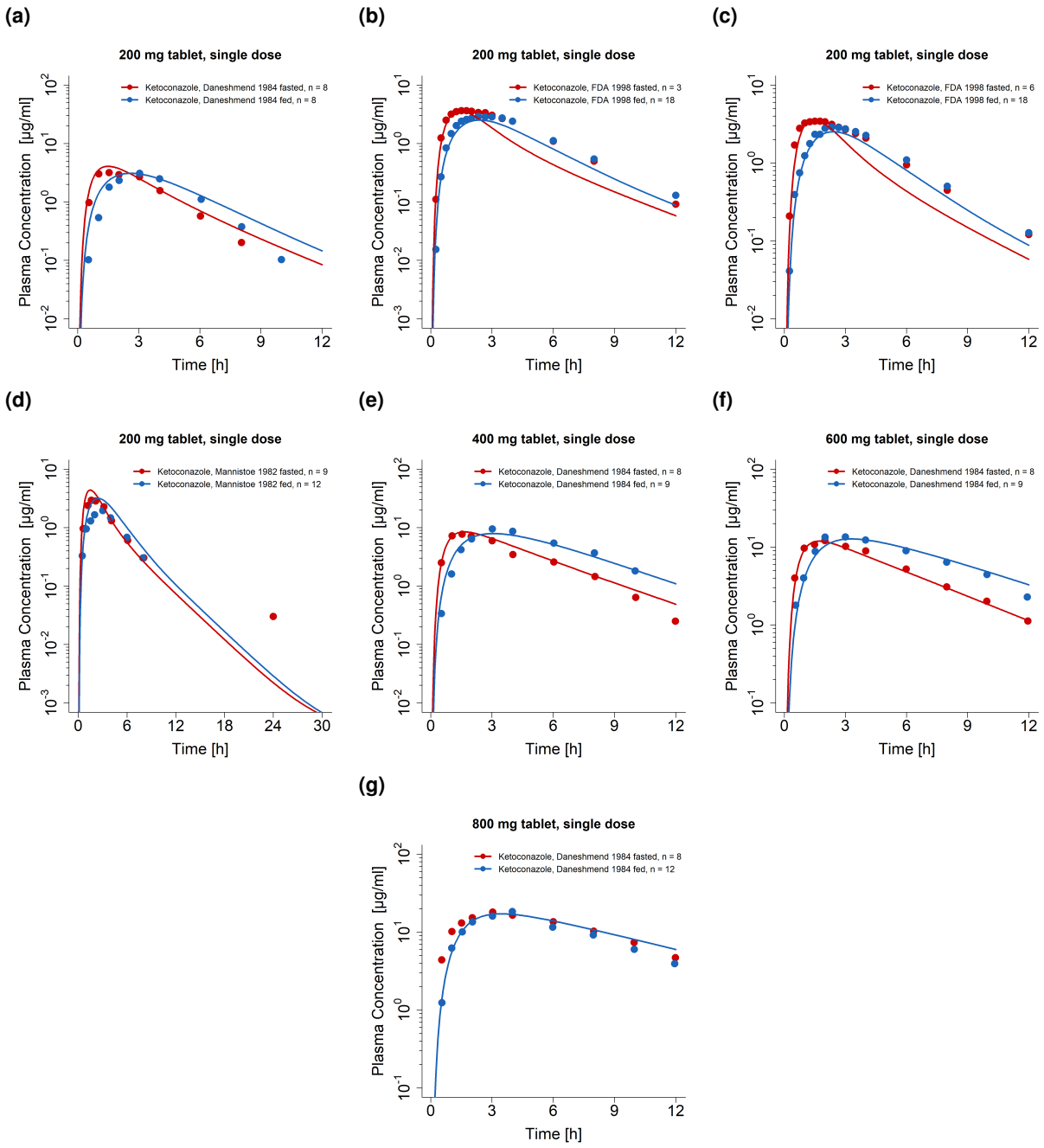

Figure S2.18: Comparison of predicted and observed ketoconazole plasma concentration-time profiles under fasted and fed conditions. Model predictions are shown as lines, observed data as dots (arithmetic mean ± SD). n: number of individuals studied.

S2.7.3 DFI AUC_{last} and DFI C_{max} goodness-of-fit plots

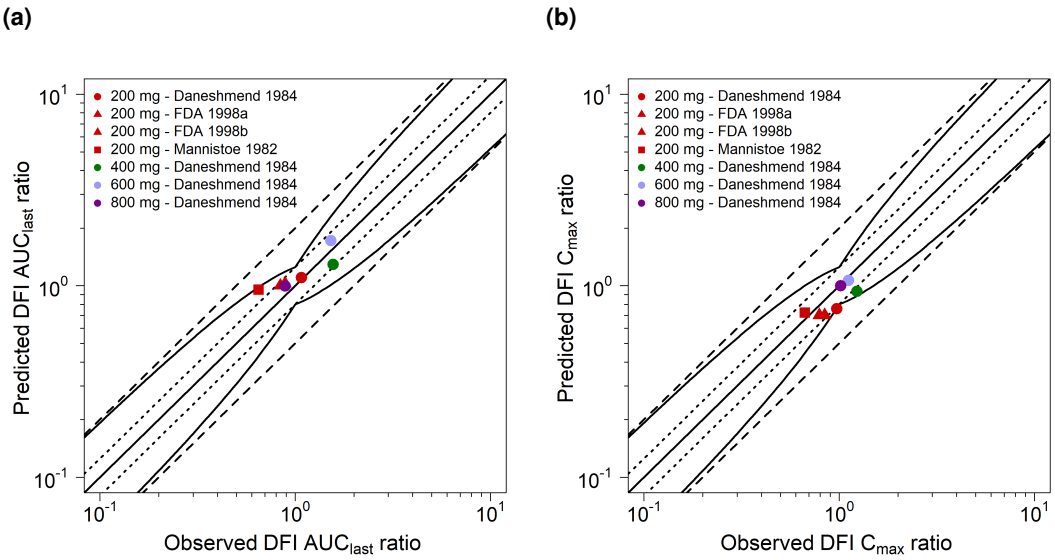

Figure S2.19: Predicted compared to observed DFI AUC_{last} and C_{max} ratios. The straight solid line marks the line of identity. The curved solid lines show the prediction acceptance limits proposed by Guest et al. including 1.25-fold variability [50]. Dotted lines indicate 1.25-fold, dashed lines indicate 2-fold deviation. AUC_{last}: area under the plasma concentration-time curve from the time of drug administration to the last concentration measurement, C_{max}: maximum plasma concentration, DFI: drug-food interaction

S2.7.4 Geometric mean fold error of predicted AUC_{last} and C_{max} values

Table S2.6: Predicted and observed DFI AUC_{last} and C_{max} ratios of ketoconazole

Dose [mg]	Route	N	DFI AUC_{last} ratio			DFI C_{max} ratio			Reference
			Pred	Obs	Pred/Obs	Pred	Obs	Pred/Obs	
200	tab s.d	8	1.11	1.08	1.03	0.76	0.97	0.78	Daneshmend 1984 [16]
200	tab s.d	39	1.00	0.84	1.19	0.70	0.79	0.89	FDA 1998 a [17]
200	tab s.d	23	1.03	0.89	1.16	0.70	0.84	0.83	FDA 1998 b [17]
200	tab s.d	10	0.95	0.65	1.47	0.72	0.67	1.08	Mannistoe 1982 [19]
400	tab s.d	8	1.29	1.56	0.83	0.94	1.23	0.76	Daneshmend 1984 [16]
600	tab s.d	8	1.72	1.52	1.13	1.07	1.12	0.96	Daneshmend 1984 [16]
800	tab s.d	8	1.00	0.89	1.13	1.00	1.02	0.98	Daneshmend 1984 [16]
Overall mean GMFE (range)					**1.19 (1.02–1.47)**			**1.15 (1.02–1.32)**	
					100.00% (7/7) $\leq$ 2			**100.00% (7/7) $\leq$ 2**	

AUC_{last}: area under the plasma concentration-time curve calculated from the first to last time point of measurement, cap: capsule, C_{max}: maximum plasma concentration, DFI: drug-food-interaction, GMFE: geometric mean fold error, n: number of individuals studied, obs: observed, pred: predicted, Route: route of administration, tab: tablet, s.d: single dose

S2.8 Sensitivity Analyses

Figures S2.20 and S2.21 show the results of the local sensitivity analyses on the AUC of the compounds ketoconazole and N-deacetylketoconazole. Sensitivity of the model to single parameter changes was determined after the last application of a 7 day multiple dose regimen of 200 mg once daily.

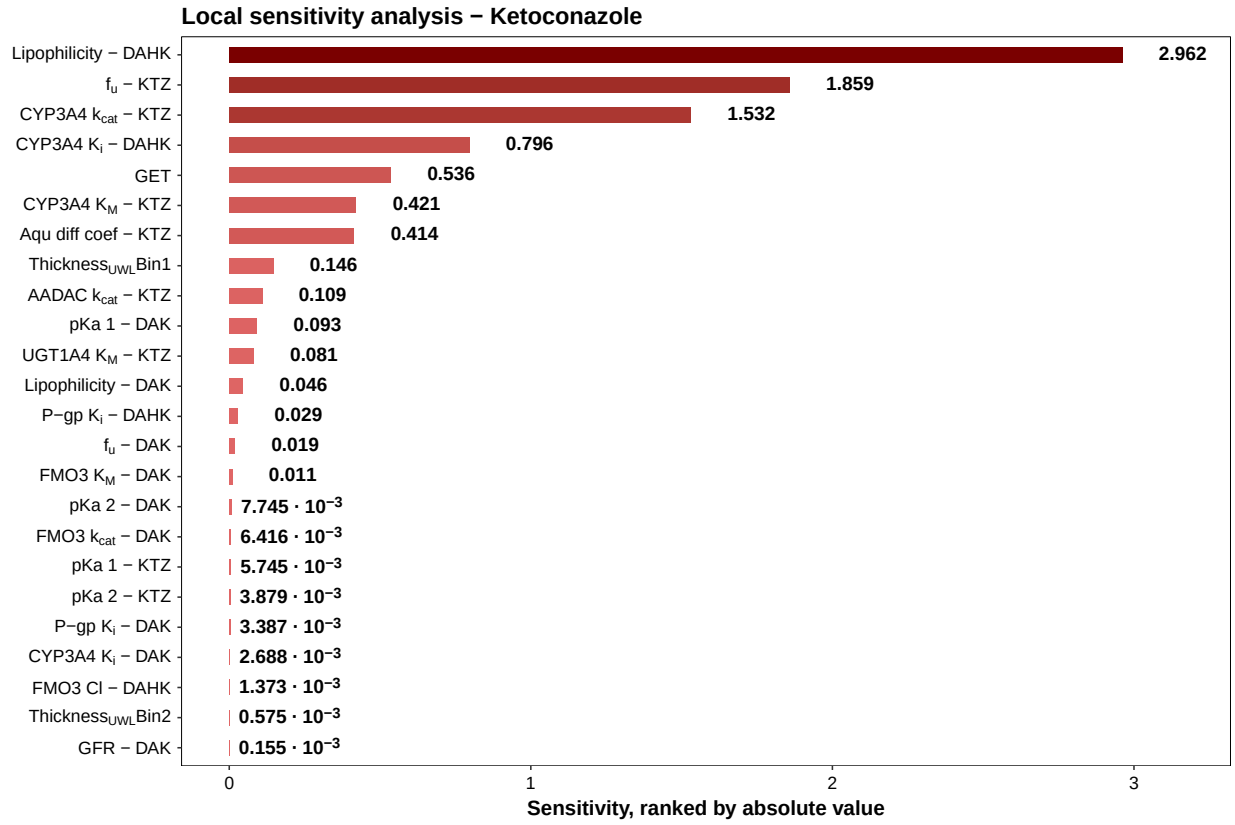

Figure S2.20: Local sensitivity analysis of ketoconazole PBPK model– calculated for sensitivity on ketoconazole plasma AUC_{inf}. AADAC: arylacetamide deacetylase, Aqu. diff. coef.: aqueous diffusion coeffecient, AUC_{inf}: area under the plasma concentration-time curve from the time of the last drug administration extrapolated to infinity, Cl: clearance, CYP: cytochrome P450, DAHK: N-deacetyl-N-hydroxyketoconazole, DAK: N-deacetylketoconazole, FMO: flavin-containing monooxygenase, f_u: fraction unbound, GET: gastric emptying time, GFR: fraction of glomerular filtration rate, k_{cat}: catalytic rate constant, K_i: concentration for half-maximal inhibition, K_M: Michaelis-Menten constant, pKa: acidic dissociation constant, P-gp: P-glycoprotein, $Thickness_{UWL}$: thickness of unstirred water layer for particle radii of the respective bin, UGT: uridine diphosphate glucuronosyltransferase

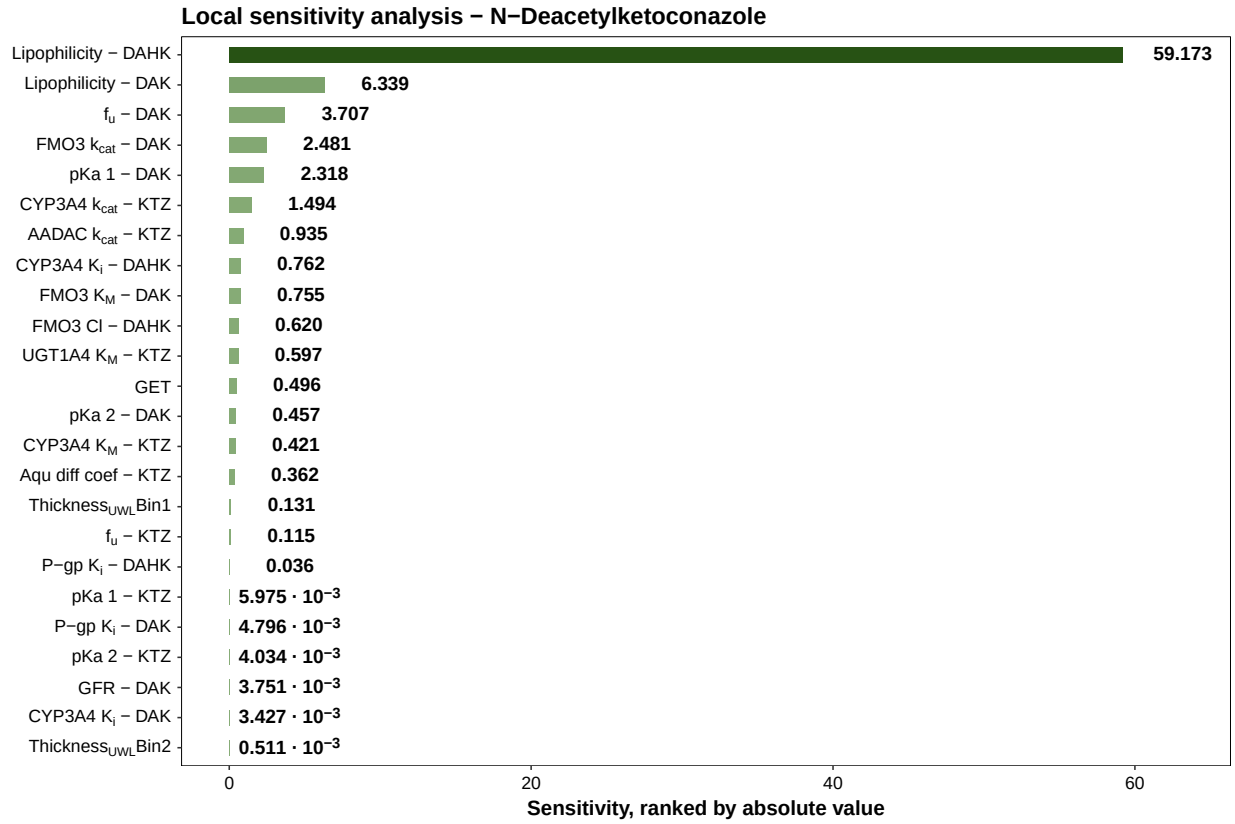

Figure S2.21: Local sensitivity analysis of ketoconazole PBPK model– calculated for sensitivity on N-deacetlyketoconazole plasma AUC_{inf}. AADAC: arylacetamide deacetylase, Aqu. diff. coef.: aqueous diffusion coefficient, AUC_{inf}: area under the plasma concentration-time curve from the time of the last drug administration extrapolated to infinity, Cl: clearance, CYP: cytochrome P450, DAHK: N-deacetyl-N-hydroxyketoconazole, DAK: N-deacetylketoconazole, FMO: flavin-containing monooxygenase, f_u: fraction unbound, GET: gastric emptying time, GFR: fraction of glomerular filtration rate, k_{cat}: catalytic rate constant, K_i: concentration for half-maximal inhibition, K_M: Michaelis-Menten constant, pKa: acidic dissociation constant, P-gp: P-glycoprotein, $Thickness_{UWL}$: thickness of unstirred water layer for particle radii of the respective bin, UGT: uridine diphosphate glucuronosyltransferase

S3 Ketoconazole – DDI Modeling

S3.1 Ketoconazole – Clinical studies

Table S3.7: Clinical study data used for ketoconazole DDI model development

Drug administration		Dose gap [h]	N	Age [years]	Weight [kg]	Females [%]	Dataset	Reference
Ketoconazole	Victim							
	Alfentanil							
-	1 mg iv bol seq (D0)	-	6	28 (21–33)	79 (63–106)	50.00	test	Kharash 2011 Control [51]
400 mg po tab qd (D1–D4)	0.5 mg iv bol seq (D5)	+8	6	28 (21–33)	79 (63–106)	50.00	test	Kharash 2011 DDI [51]
-	1 mg iv bol sim (D0)	-	6	28 (21–33)	79 (63–106)	50.00	test	Kharash 2011 Control [51]
400 mg po tab qd (D1–D4)	0.5 mg iv bol sim (D5)	+8	6	28 (21–33)	79 (63–106)	50.00	training	Kharash 2011 DDI [51]
-	4 mg po tab seq (D0)	-	6	28 (21–33)	79 (63–106)	50.00	test	Kharash 2011 Control [51]
400 mg po tab qd (D1–D4)	1 mg po tab seq (D5)	+8	6	28 (21–33)	79 (63–106)	50.00	test	Kharash 2011 DDI [51]
-	4 mg po tab sim (D0)	-	6	28 (21–33)	79 (63–106)	50.00	test	Kharash 2011 Control [51]
400 mg po tab qd (D1–D4)	1 mg po tab sim (D5)	+8	6	28 (21–33)	79 (63–106)	50.00	test	Kharash 2011 DDI [51]
-	1 mg iv bol & 4 mg po tab s.d. seq (D0)	-	6	28 (21–33)	79 (63–106)	50.00	test	Kharash 2011 Control [51]
400 mg po tab qd (D1–D4)	0.5 mg iv bol & 1 mg po tab seq (D5)	+8	6	28 (21–33)	79 (63–106)	50.00	test	Kharash 2011 DDI [51]
-	1 mg iv bol & 4 mg po tab s.d. sim (D0)	-	6	28 (21–33)	79 (63–106)	50.00	test	Kharash 2011 Control [51]
400 mg po tab qd (D1–D4)	0.5 mg iv bol & 1 mg po tab sim (D5)	+8	6	28 (21–33)	79 (63–106)	50.00	test	Kharash 2011 DDI [51]
	Alprazolam							
-	0.5 mg po tab (D0)	-	8	18–38	-	-	test	Boulenc 2016 Control [52]
200 mg po tab bid (D1–D6)	0.5 mg po tab (D4)	0	8	18–38	-	-	test	Boulenc 2016 DDI [52]
400 mg po tab qd (D1–D6)	0.5 mg po tab (D4)	0	8	18–38	-	-	test	Boulenc 2016 DDI [52]
-	1 mg po cap (D0)	-	8	18–38	-	-	test	Greenblatt 1998 Control[32]
200 mg po tab bid (D1–D3)	1 mg po cap (D3)	+1	7	21–44	-	-	training	Greenblatt 1998 DDI [32]
	Midazolam							
-	0.0003 mg po sol (D0)	-	6	18–50	-	41.67	test	Halama 2013 Control [53]
400 mg po tab qd (D1–D15)	0.0003 mg po sol (D2)	0	6	18–50	-	41.67	test	Halama 2013 DDI [53]
-	0.075 mg po sol (D0)	-	4	33 (23-55)	62 (50-78)	61.9	test	Eap 2004 Control [54]
200 mg po tab bid (D1–D4)	0.075 mg po sol (D4)	0	4	33 (23-55)	62 (50-78)	61.9	test	Eap 2004 DDI [54]
-	0.075 mg/kg po sol (D0)	-	19	38.7	73.4	52.63	test	Chung 2006 Control [55]
400 mg po tab qd (D1–D10)	0.075 mg/kg po sol (D6)	-2	19	38.7	73.4	52.63	training	Chung 2006 DDI [55]
-	0.4 mg iv bol (D0)	-	6	42.80 (28–53)	-	-	test	Krishna 2009 Control [56]
400 mg po tab qd (D1–D7)	0.4 mg iv bol (D7)	0	6	42.80 (28–53)	-	-	test	Krishna 2009 DDI [56]
-	2 mg po tab (D0)	-	8	18–38	-	-	test	Boulenc 2016 Control [52]
200 mg po tab bid (D1–D5)	2 mg po tab (D4)	0	8	18–38	-	-	test	Boulenc 2016 DDI [52]
400 mg po tab qd (D1–D5)	2 mg po tab (D4)	0	8	18–38	-	-	test	Boulenc 2016 DDI [52]
-	2 mg po tab (D0)	-	7	38.80 (21–54)	-	-	test	Stoch 2009 Control [57]

(Continued on Next Page...)

Table S3.7: Clinical study data used for ketoconazole DDI model development *(continued)*

Drug administration		Dose gap [h]	N	Age [years]	Weight [kg]	Females [%]	Dataset	Reference
Ketoconazole	Victim							
400 mg po tab qd (D1)	2 mg po tab (D1)	0	12	38.80 (21–54)	-	-	test	Stoch 2009 DDI [57]
400 mg po tab qd (D1–D2)	2 mg po tab (D2)	0	9	38.80 (21–54)	-	-	test	Stoch 2009 DDI [57]
400 mg po tab qd (D1–D5)	2 mg po tab (D5)	0	9	38.80 (21–54)	-	-	test	Stoch 2009 DDI [57]
-	2 mg po tab (D0)	-	6	42.80 (28–53)	-	-	test	Krishna 2009 Control [56]
400 mg po tab qd (D1–D7)	2 mg po tab (D6)	0	6	42.80 (28–53)	-	-	test	Krishna 2009 DDI [56]
-	2 mg iv bol (D0)	-	9	26 (19–41)	77.5	33.34	test	Tsunoda 1999 Control [58]
200 mg po tab bid (D1–D2)	2 mg iv bol (D1)	0	9	26 (19–41)	77.5	33.34	test	Tsunoda 1999 DDI [58]
-	3 mg po sol (D0)	-	6	18–50	-	41.67	test	Halama 2013 Control [53]
400 mg po tab qd (D1–D15)	3 mg po sol (D8)	0	6	18–50	-	41.67	test	Halama 2013 DDI [53]
100 mg po tab qd (D1)	5 mg po sol (D1)	0	9	24–54	56–85	22.22	test	Liu 2017 DDI [59]
200 mg po tab qd (D1)	5 mg po sol (D1)	0	9	24–54	56–85	22.22	test	Liu 2017 DDI [59]
400 mg po tab qd (D1)	5 mg po sol (D1)	0	9	24–54	56–85	22.22	test	Liu 2017 DDI [59]
400 mg po tab qd (D1)	5 mg po sol (D1)	+12	6	21–46	67–80	50.00	test	Liu 2017 DDI [59]
400 mg po tab qd (D1)	5 mg po sol (D1)	+2	6	21–46	67–80	50.00	test	Liu 2017 DDI [59]
400 mg po tab qd (D1)	5 mg po sol (D1)	0	6	21–46	67–80	50.00	test	Liu 2017 DDI [59]
400 mg po tab qd (D1)	5 mg po sol (D1)	-2	6	21–46	67–80	50.00	test	Liu 2017 DDI [59]
400 mg po tab qd (D1)	5 mg po sol (D1)	-4	6	21–46	67–80	50.00	test	Liu 2017 DDI [59]
-	6 mg po sol (D0)	-	9	26 (19–41)	77.5	33.34	test	Tsunoda 1999 Control [58]
200 mg po tab bid (D1–D2)	6 mg po sol (D1)	0	9	26 (19–41)	77.5	33.34	test	Tsunoda 1999 DDI [58]
-	7.5 mg po sol (D0)	-	9	(19-26)	(52-85)	77.78	test	Olkkolla 1994 Control [60]
400 mg po tab qd (D1–D4)	7.5 mg po sol (D4)	+1	9	(19-26)	(52-85)	77.78	test	Olkkolla 1994 DDI [60]
-	10 mg po sol (D0)	-	10	34.20	72.10	57.50	test	Lam 2003 Control [61]
200 mg po tab qd (D1–D12)	10 mg po sol (D12)	+1	10	34.20	72.10	57.50	test	Lam 2003 DDI [61]
	Triazolam							
-	0.25 mg po cap (D0)	-	8	18–38	-	-	test	Greenblatt 1998 Control[32]
200 mg po tab bid (D1–D3)	0.25 mg po cap (D3)	+1	6	21–44	-	-	test	Greenblatt 1998 DDI [32]
-	0.25 mg po tab (D0)	-	9	23.80 (20–26)	65.30 (50–86)	-	test	Varhe 1994 Control [62]
400 mg po tab qd (D1–D4)	0.25 mg po tab (D4)	+1	9	23.80 (20–26)	65.30 (50–86)	66.67	test	Varhe 1994 DDI [62]
	Digoxin							
-	0.5 mg po tab	-	10	24–34	53–115	50.00	test	Larsen 2007 Control [63]
200 mg po tab qd (D1–D4)	0.5 mg po tab (D4)	0	10	24–34	53–115	50.00	test	Larsen 2007 DDI [63]

bid: twice daily, bol: bolus injection, cap: capsule, D: day, iv: intravenous, m.d.: multiple dose, n: number of individuals studied, po: oral, qd: once daily, Route: route of administration, s.d.: single dose, seq: iv and po administration on D0 were either given sequentially with a three hour gap, sim: iv and po administration on D0 were either given simultaneously, sol: solution, tab: tablet

-: no data available. Values are means and ranges, if available.

S3.2 Ketoconazole – Drug-dependent parameters

The DDI partner models with their respective parameters were derived from literature for the victim drugs alfentanil [64], alprazolam [65], midazolam [64], triazolam [66] and digoxin [64].
For the alprazolam model, Weibull model parameters *Dissolution shape* and *Dissolution time (50%)* were adpated.

Table S3.8: Drug-dependent alprazolam parameters adapted for the ketoconazole-alprazolam DDI (fed state)

Parameter	Unit	Value	Source	Original model	Reference
Weibull Dissolution shape	-	2.09	opt.	1.12	[65]
Weibull Dissolution time (50%)	min	110.10	opt.	2.20	[65]

opt.: optimized

S3.3 Ketoconazole – DDI model evaluation

S3.3.1 Plasma concentration-time profiles (Linear)

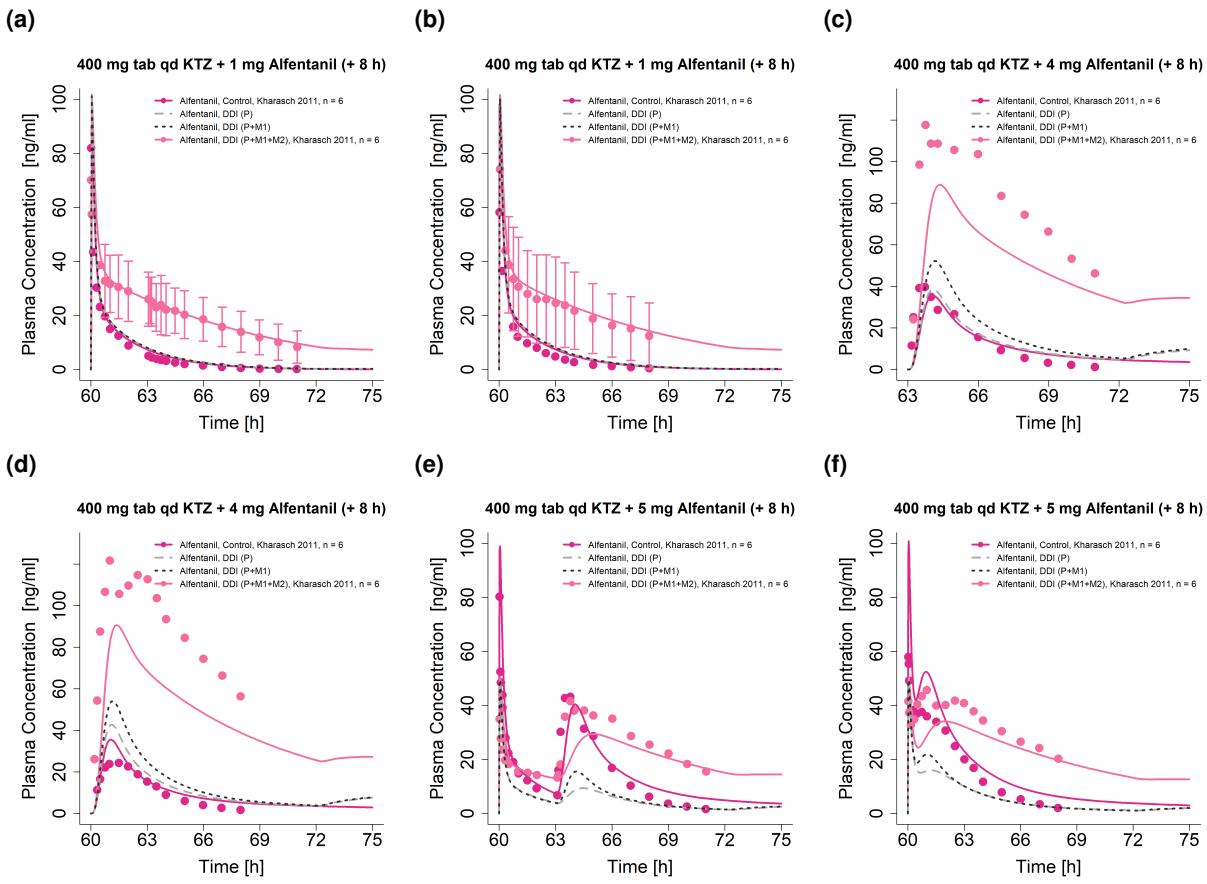

Figure S3.22: Comparison of predicted and observed ketoconazole-alfentanil DDI plasma concentration-time profiles for CYP3A4 DDIs with and without ketoconazole metabolites. Model predictions are shown as lines, observed data as dots (arithmetic mean ± SD). DDI: drug-drug interaction, KTZ: ketoconazole, M1: N-deacetylketoconazole, M2: N-hydroxy-N-deacetylketoconazole, n: number of participants, P: ketoconazole alone, qd: once daily, tab: tablet.

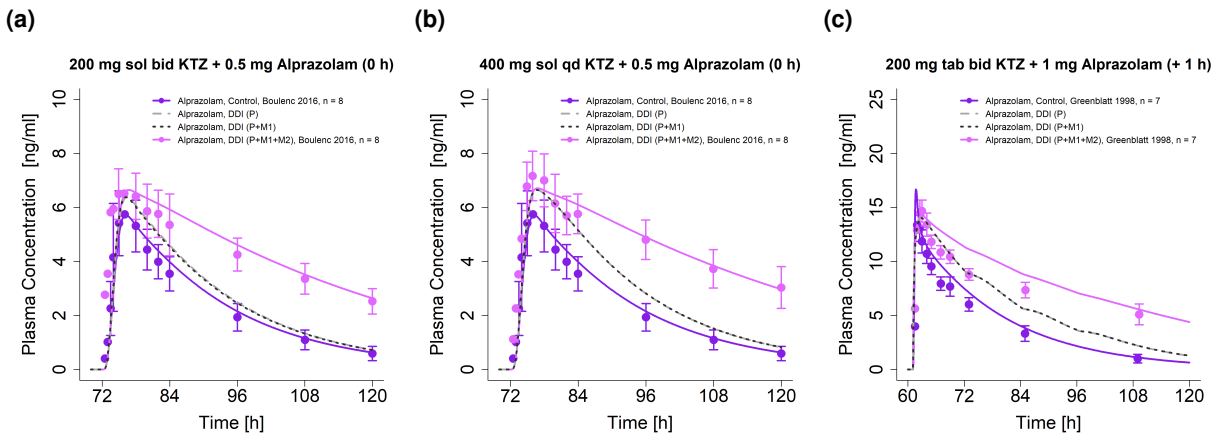

Figure S3.23: Comparison of predicted and observed ketoconazole-alprazolam DDI plasma concentration-time profiles for CYP3A4 DDIs with and without ketoconazole metabolites. Model predictions are shown as lines, observed data as dots (arithmetic mean ± SD). bid: twice daily, DDI: drug-drug interaction, KTZ: ketoconazole, M1: N-deacetylketoconazole, M2: N-hydroxy-N-deacetylketoconazole, n: number of participants, P: ketoconazole alone, qd: once daily, sol: solution, tab: tablet.

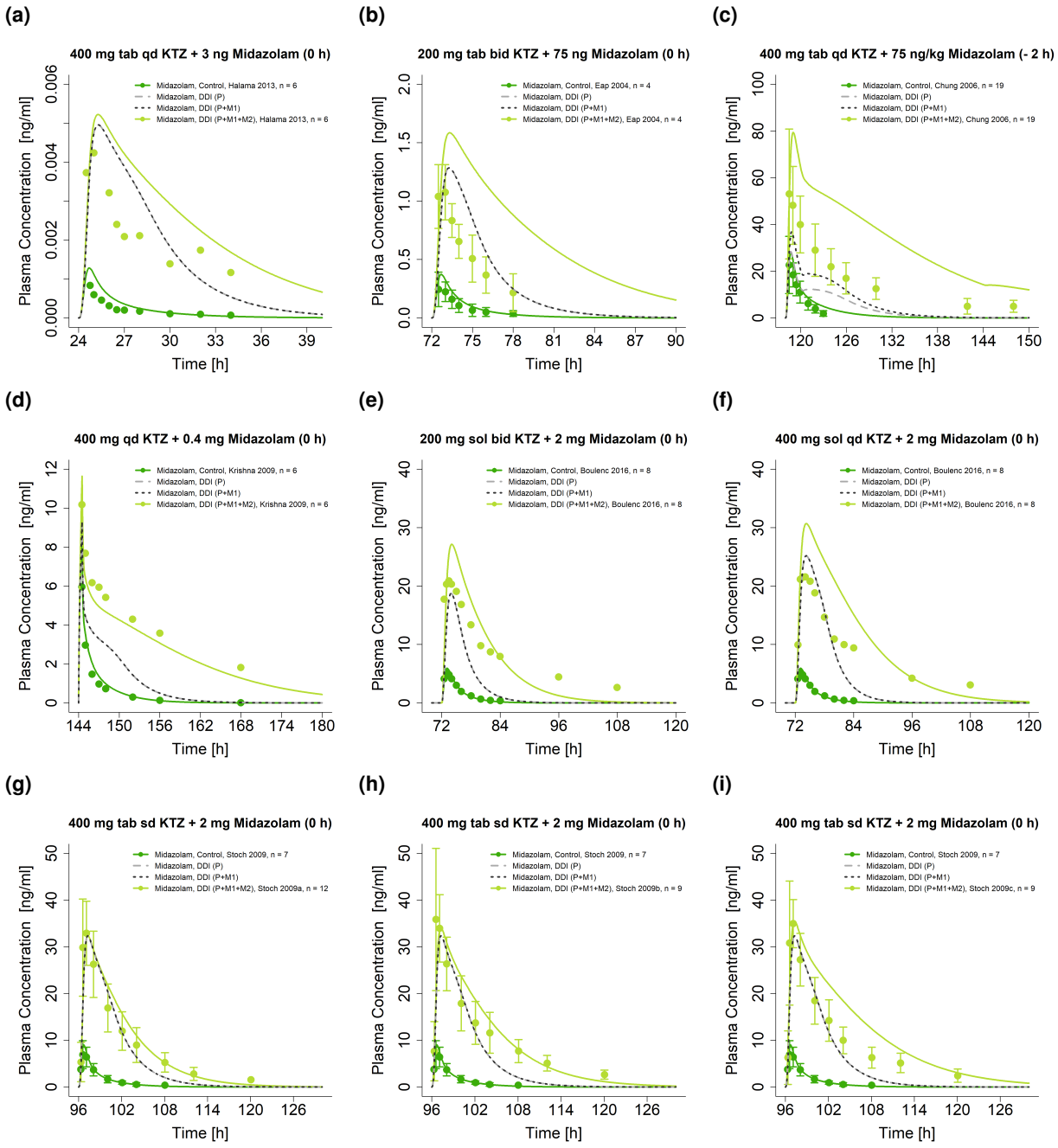

Figure S3.24: Comparison of predicted and observed ketoconazole-midazolam DDI plasma concentration-time profiles for CYP3A4 DDIs with and without ketoconazole metabolites. Model predictions are shown as lines, observed data as dots (arithmetic mean ± SD). bid: twice daily, DDI: drug-drug interaction, KTZ: ketoconazole, M1: N-deacetylketoconazole, M2: N-hydroxy-N-deacetylketoconazole, n: number of participants, P: ketoconazole alone, qd: once daily, sd: single dose, sol: solution, tab: tablet.

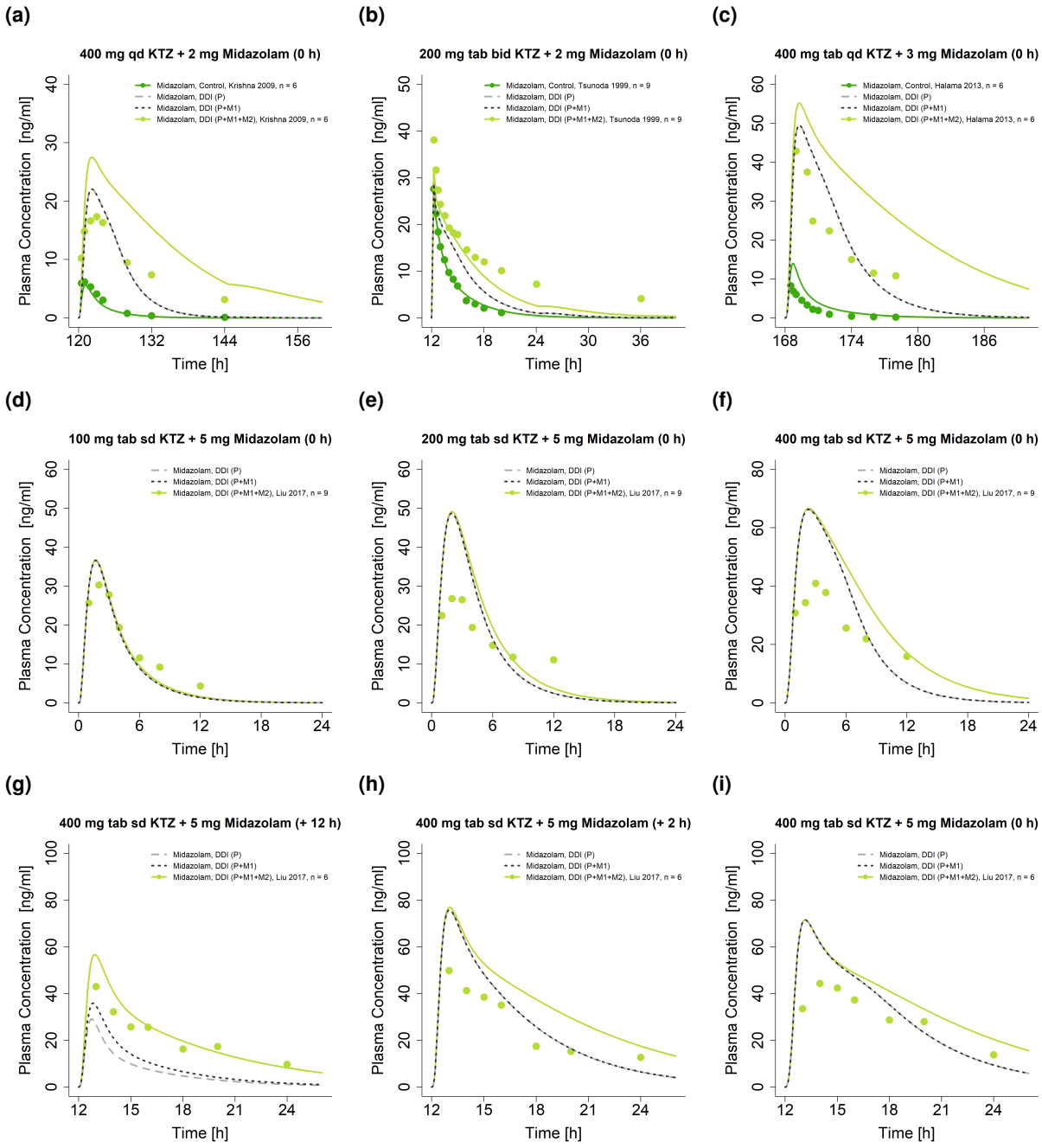

Figure S3.25: Comparison of predicted and observed ketoconazole-midazolam DDI plasma concentration-time profiles for CYP3A4 DDIs with and without ketoconazole metabolites. Model predictions are shown as lines, observed data as dots (arithmetic mean ± SD). bid: twice daily, DDI: drug-drug interaction, KTZ: ketoconazole, M1: N-deacetylketoconazole, M2: N-hydroxy-N-deacetylketoconazole, n: number of participants, P: ketoconazole alone, qd: once daily, sd: single dose, sol: solution, tab: tablet.

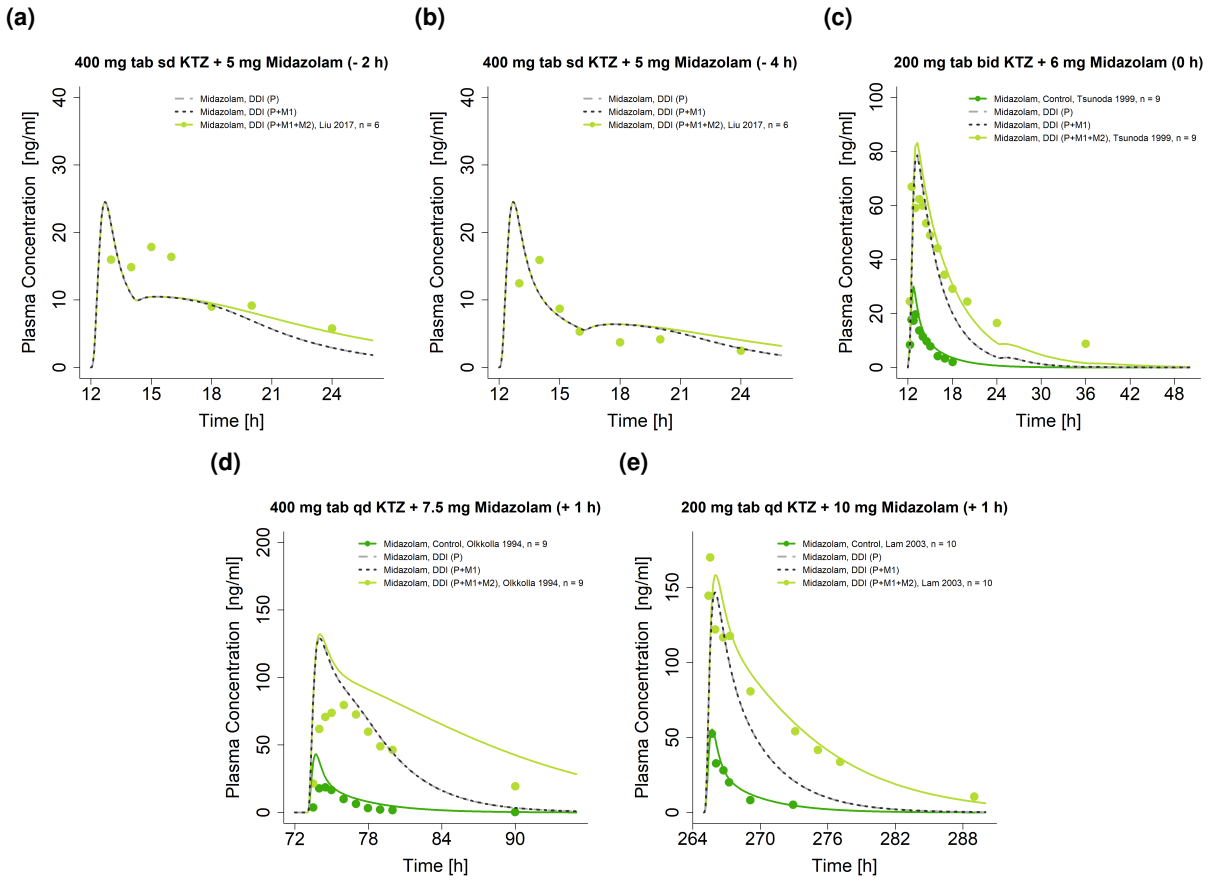

Figure S3.26: Comparison of predicted and observed ketoconazole-midazolam DDI plasma concentration-time profiles for CYP3A4 DDIs with and without ketoconazole metabolites. Model predictions are shown as lines, observed data as dots (arithmetic mean ± SD). bid: twice daily, DDI: drug-drug interaction, KTZ: ketoconazole, M1: N-deacetylketoconazole, M2: N-hydroxy-N-deacetylketoconazole, n: number of participants, P: ketoconazole alone, qd: once daily, sd: single dose, sol: solution, tab: tablet.

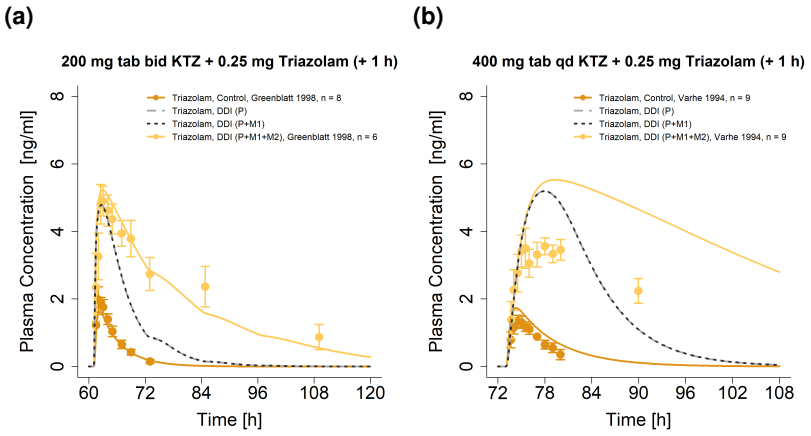

Figure S3.27: Comparison of predicted and observed ketoconazole-triazolam DDI plasma concentration-time profiles for CYP3A4 DDIs with and without ketoconazole metabolites. Model predictions are shown as lines, observed data as dots (arithmetic mean ± SD). bid: twice daily, DDI: drug-drug interaction, KTZ: ketoconazole, M1: N-deacetylketoconazole, M2: N-hydroxy-N-deacetylketoconazole, n: number of participants, P: ketoconazole alone, qd: once daily, tab: tablet.

(a)

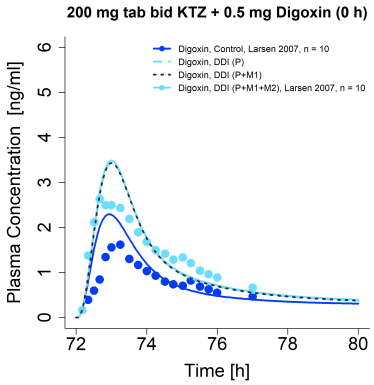

Figure S3.28: Comparison of predicted and observed ketoconazole-digoxin DDI plasma concentration-time profiles for P-gp DDIs with and without ketoconazole metabolites. Model predictions are shown as lines, observed data as dots (arithmetic mean). bid: twice daily, DDI: drug-drug interaction, KTZ: ketoconazole, M1: N-deacetylketoconazole, M2: N-hydroxy-N-deacetylketoconazole, n: number of participants, P: ketoconazole alone, tab: tablet.

S3.3.2 Plasma concentration-time profiles (Semilogarhitmic)

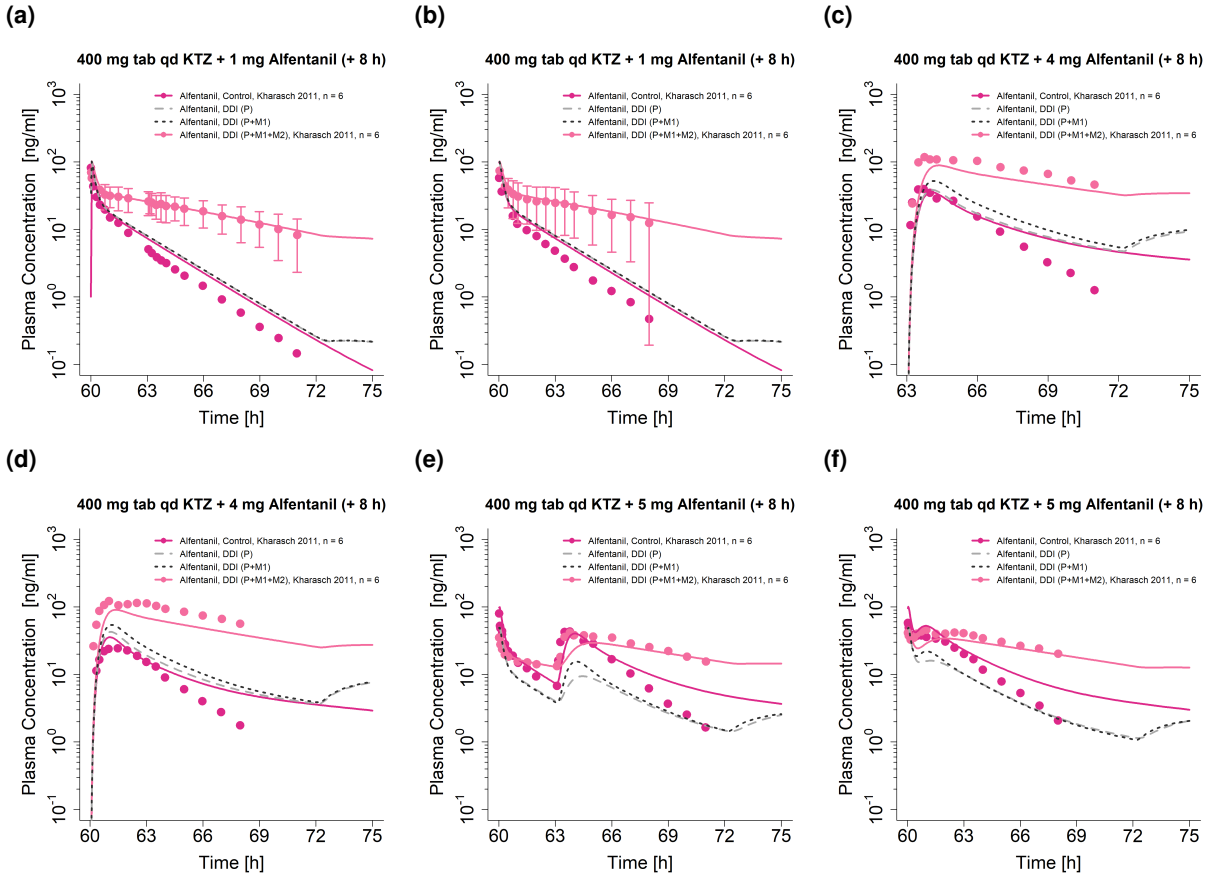

Figure S3.29: Comparison of predicted and observed ketoconazole-alfentanil DDI plasma concentration-time profiles for CYP3A4 DDIs with and without ketoconazole metabolites. Model predictions are shown as lines, observed data as dots (arithmetic mean ± SD). DDI: drug-drug interaction, KTZ: ketoconazole, M1: N-deacetylketoconazole, M2: N-hydroxy-N-deacetylketoconazole, n: number of participants, P: ketoconazole alone, qd: once daily, tab: tablet.

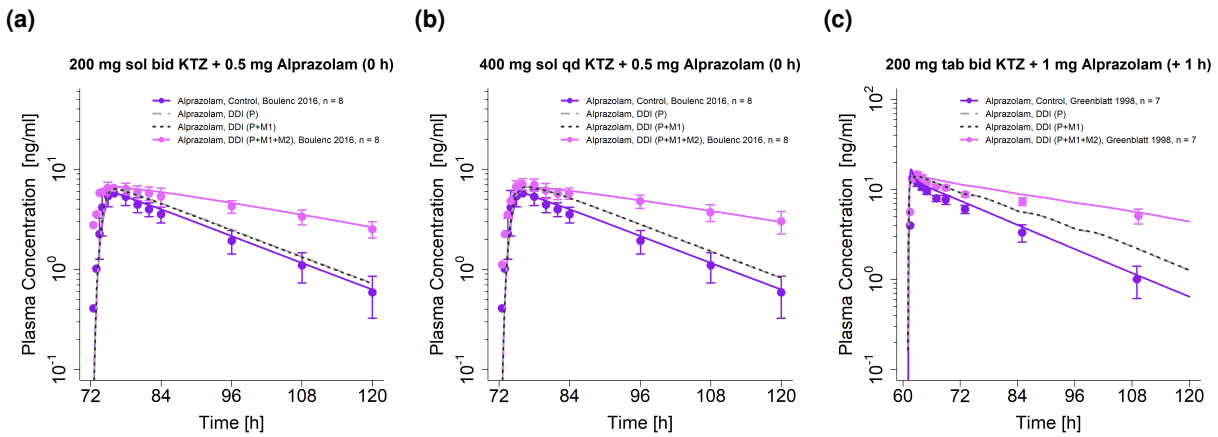

Figure S3.30: Comparison of predicted and observed ketoconazole-alprazolam DDI plasma concentration-time profiles for CYP3A4 DDIs with and without ketoconazole metabolites. Model predictions are shown as lines, observed data as dots (arithmetic mean ± SD). bid: twice daily, DDI: drug-drug interaction, KTZ: ketoconazole, M1: N-deacetylketoconazole, M2: N-hydroxy-N-deacetylketoconazole, n: number of participants, P: ketoconazole alone, qd: once daily, sol: solution, tab: tablet.

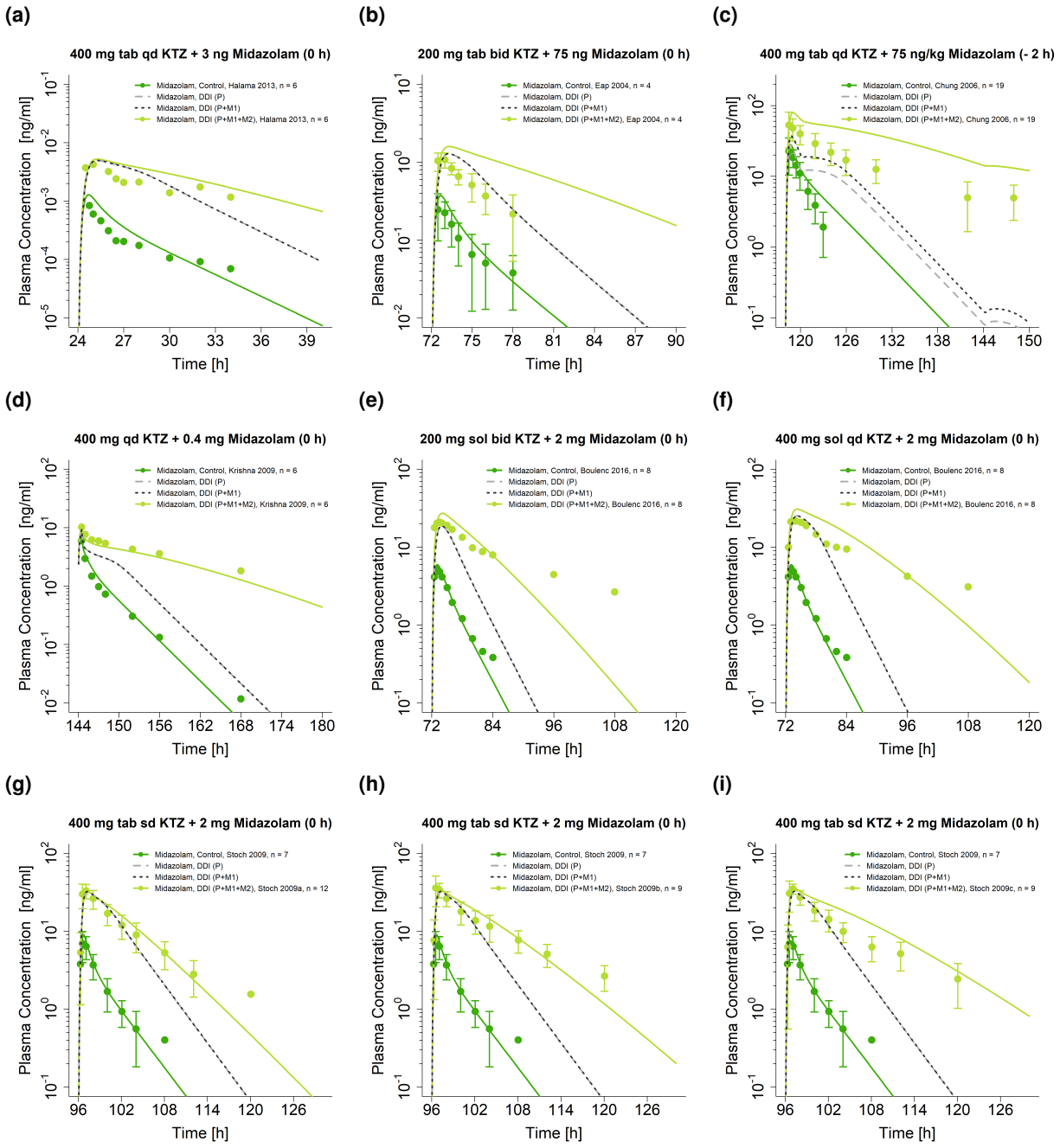

Figure S3.31: Comparison of predicted and observed ketoconazole-midazolam DDI plasma concentration-time profiles for CYP3A4 DDIs with and without ketoconazole metabolites. Model predictions are shown as lines, observed data as dots (arithmetic mean ± SD). bid: twice daily, DDI: drug-drug interaction, KTZ: ketoconazole, M1: N-deacetylketoconazole, M2: N-hydroxy-N-deacetylketoconazole, n: number of participants, P: ketoconazole alone, qd: once daily, sd: single dose, sol: solution, tab: tablet.

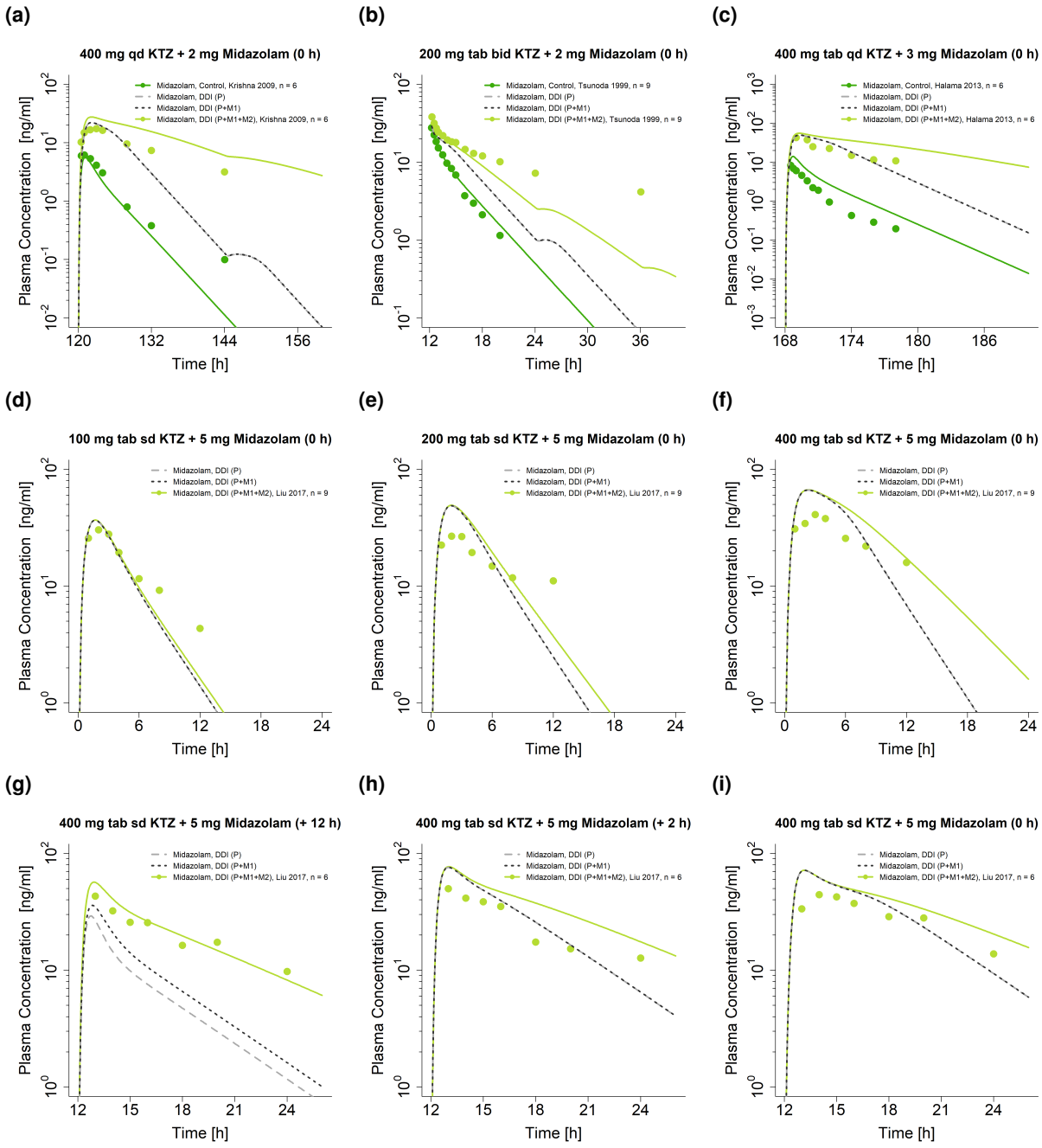

Figure S3.32: Comparison of predicted and observed ketoconazole-midazolam DDI plasma concentration-time profiles for CYP3A4 DDIs with and without ketoconazole metabolites. Model predictions are shown as lines, observed data as dots (arithmetic mean ± SD). bid: twice daily, DDI: drug-drug interaction, KTZ: ketoconazole, M1: N-deacetylketoconazole, M2: N-hydroxy-N-deacetylketoconazole, n: number of participants, P: ketoconazole alone, qd: once daily, sd: single dose, sol: solution, tab: tablet.

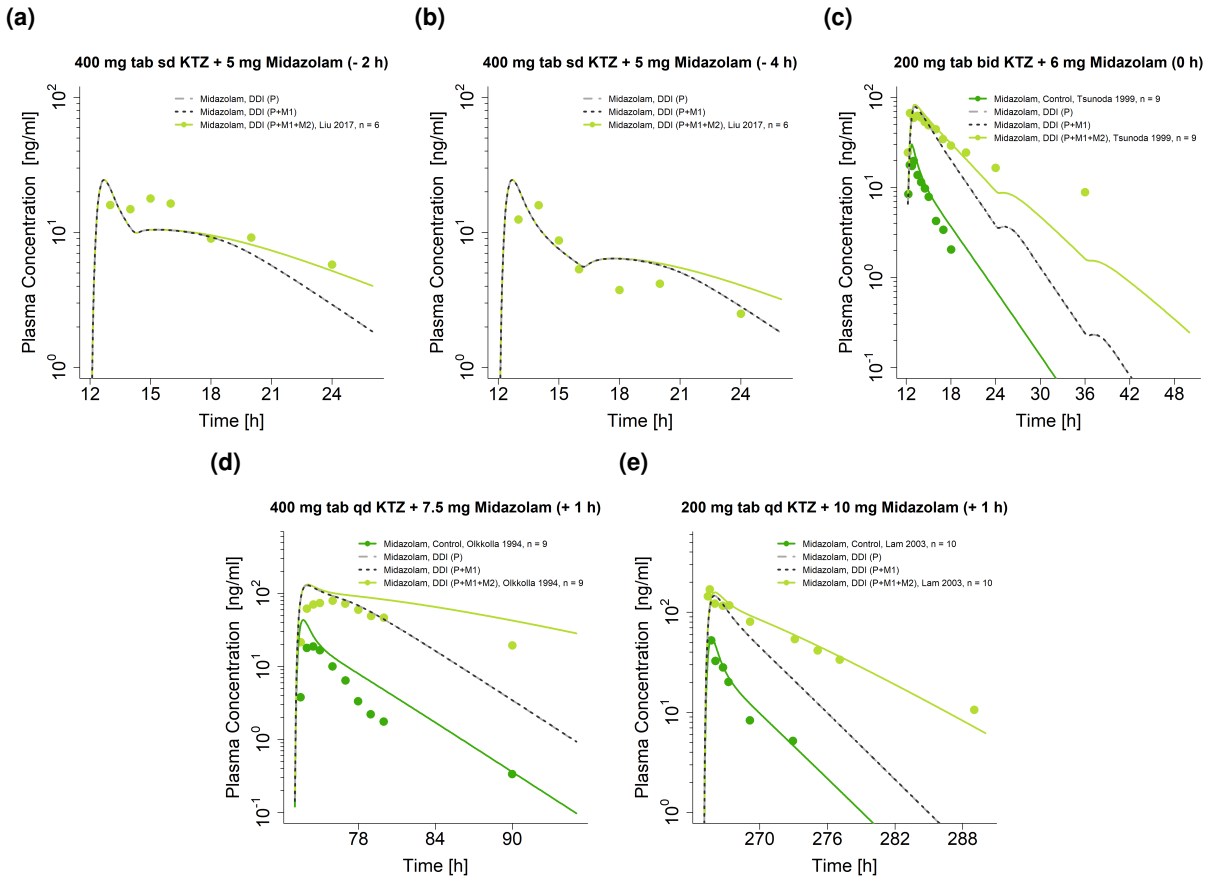

Figure S3.33: Comparison of predicted and observed ketoconazole-midazolam DDI plasma concentration-time profiles for CYP3A4 DDIs with and without ketoconazole metabolites. Model predictions are shown as lines, observed data as dots (arithmetic mean ± SD). bid: twice daily, DDI: drug-drug interaction, KTZ: ketoconazole, M1: N-deacetylketoconazole, M2: N-hydroxy-N-deacetylketoconazole, n: number of participants, P: ketoconazole alone, qd: once daily, sd: single dose, sol: solution, tab: tablet.

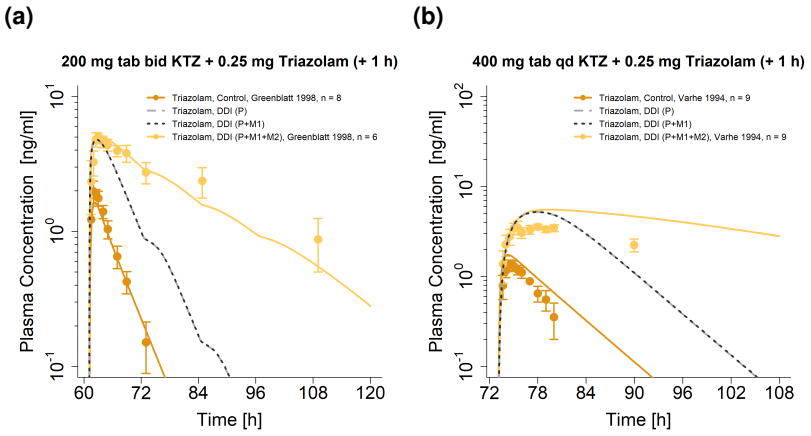

Figure S3.34: Comparison of predicted and observed ketoconazole-triazolam DDI plasma concentration-time profiles for CYP3A4 DDIs with and without ketoconazole metabolites. Model predictions are shown as lines, observed data as dots (arithmetic mean ± SD). bid: twice daily, DDI: drug-drug interaction, KTZ: ketoconazole, M1: N-deacetylketoconazole, M2: N-hydroxy-N-deacetylketoconazole, n: number of participants, P: ketoconazole alone, qd: once daily, tab: tablet.

(a)

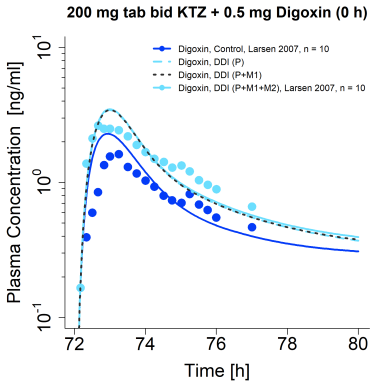

Figure S3.35: Comparison of predicted and observed ketoconazole-digoxin DDI plasma concentration-time profiles for P-gp DDIs with and without ketoconazole metabolites. Model predictions are shown as lines, observed data as dots (arithmetic mean ± SD). bid: twice daily, DDI: drug-drug interaction, KTZ: ketoconazole, M1: N-deacetylketoconazole, M2: N-hydroxy-N-deacetylketoconazole, n: number of participants, P: ketoconazole alone, tab: tablet.

S3.3.3 DDI AUC_{last} and DDI C_{max} goodness-of-fit plots

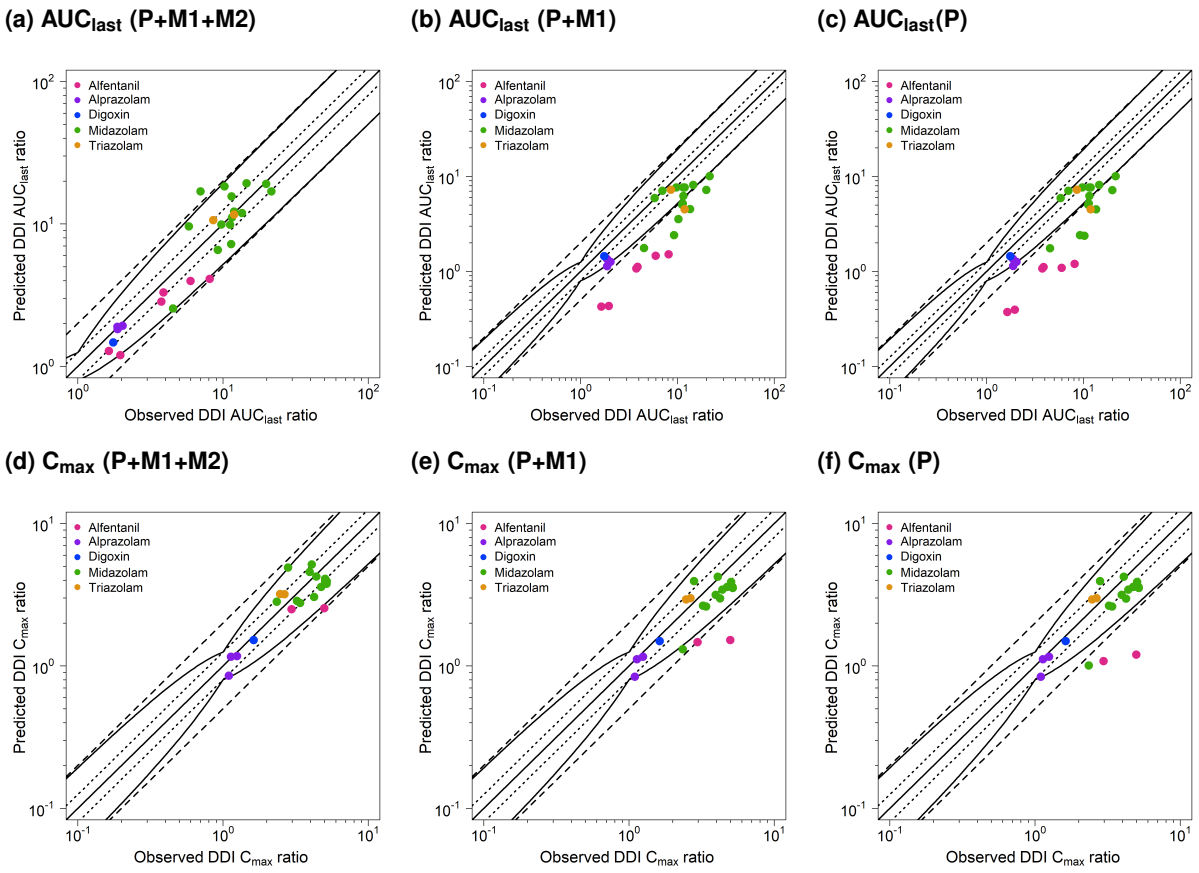

Figure S3.36: Predicted compared to observed victim drug DDI AUC_{last} and DDI C_{max} ratios for ketoconazole DDIs with and without its metabolites. The straight solid line marks the line of identity. The curved solid lines show the prediction acceptance limits proposed by Guest et al. including 1.25-fold variability [50]. Dotted lines indicate 1.25-fold, dashed lines indicate 2-fold deviation. AUC_{last}: area under the plasma concentration-time curve from the time of drug administration to the last concentration measurement, C_{max}: maximum plasma concentration, DDI: drug-drug interaction, M1: N-deacetylketoconazole, M2: N-hydroxy-N-deacetylketoconazole, P: ketoconazole alone.

S3.3.4 Geometric mean fold error of predicted DDI AUC_{last} and DDI C_{max} ratios

Table S3.9: Predicted and observed DDI AUC_{last} and C_{max} ratios of the victim drugs during DDIs, simulated with and without ketoconazole metabolite involvement

Drug administration			N	DDI AUC_{last} ratio			DDI C_{max} ratio			Reference
Ketoconazole	Victim	Gap [h]		Pred	Obs	Pred/Obs	Pred	Obs	Pred/Obs	
	Alfentanil									
400 mg po tab qd (D1–D4)	0.5 mg iv bol seq (D5)	+8	6	3.31	3.88	0.85	-	-	-	Kharash 2011 DDI (P+M1+M2) [51]
400 mg po tab qd (D1–D4)	0.5 mg iv bol seq (D5)	+8	6	1.12	3.88	0.29	-	-	-	Kharash 2011 DDI (P+M1) [51]
400 mg po tab qd (D1–D4)	0.5 mg iv bol seq (D5)	+8	6	1.12	3.88	0.29	-	-	-	Kharash 2011 DDI (P) [51]
400 mg po tab qd (D1–D4)	0.5 mg iv bol sim (D5)	+8	6	2.85	3.76	0.76	-	-	-	Kharash 2011 DDI (P+M1+M2) [51]
400 mg po tab qd (D1–D4)	0.5 mg iv bol sim (D5)	+8	6	1.08	3.76	0.29	-	-	-	Kharash 2011 DDI (P+M1) [51]
400 mg po tab qd (D1–D4)	0.5 mg iv bol sim (D5)	+8	6	1.07	3.76	0.29	-	-	-	Kharash 2011 DDI (P) [51]
400 mg po tab qd (D1–D4)	1 mg po tab seq (D5)	+8	6	3.98	5.97	0.67	2.50	2.96	0.84	Kharash 2011 DDI (P+M1+M2) [51]
400 mg po tab qd (D1–D4)	1 mg po tab seq (D5)	+8	6	1.46	5.97	0.25	1.47	2.96	0.50	Kharash 2011 DDI (P+M1) [51]
400 mg po tab qd (D1–D4)	1 mg po tab seq (D5)	+8	6	1.09	5.97	0.18	1.08	2.96	0.37	Kharash 2011 DDI (P) [51]
400 mg po tab qd (D1–D4)	1 mg po tab sim (D5)	+8	6	4.12	8.11	0.51	2.55	4.99	0.51	Kharash 2011 DDI (P+M1+M2) [51]
400 mg po tab qd (D1–D4)	1 mg po tab sim (D5)	+8	6	1.52	8.11	0.19	1.52	4.99	0.30	Kharash 2011 DDI (P+M1) [51]
400 mg po tab qd (D1–D4)	1 mg po tab sim (D5)	+8	6	1.20	8.11	0.15	1.20	4.99	0.24	Kharash 2011 DDI (P) [51]
400 mg po tab qd (D1–D4)	0.5 bol & 1 mg tab seq (D5)	+8	6	1.28	1.63	0.78	-	-	-	Kharash 2011 DDI (P+M1+M2) [51]
400 mg po tab qd (D1–D4)	0.5 bol & 1 mg tab seq (D5)	+8	6	0.43	1.63	0.26	-	-	-	Kharash 2011 DDI (P+M1) [51]
400 mg po tab qd (D1–D4)	0.5 bol & 1 mg tab seq (D5)	+8	6	0.37	1.63	0.23	-	-	-	Kharash 2011 DDI (P) [51]
400 mg po tab qd (D1–D4)	0.5 bol & 1 mg tab seq (D5)	+8	6	1.20	1.96	0.61	-	-	-	Kharash 2011 DDI (P+M1+M2) [51]
400 mg po tab qd (D1–D4)	0.5 bol & 1 mg tab seq (D5)	+8	6	0.43	1.96	0.22	-	-	-	Kharash 2011 DDI (P+M1) [51]
400 mg po tab qd (D1–D4)	0.5 bol & 1 mg tab seq (D5)	+8	6	0.40	1.96	0.20	-	-	-	Kharash 2011 DDI (P) [51]
	Mean GMFE DDI (P+M1+M2)					1.48			1.57	
	Mean GMFE DDI (P+M1)					4.12			2.65	
	Mean GMFE DDI (P)					4.76			3.44	
	Alprazolam									
200 mg po tab bid (D1–D6)	0.5 mg po tab (D4)	0	8	1.93	2.03	0.95	1.17	1.25	0.94	Boulenc 2016 DDI (P+M1+M2) [52]
200 mg po tab bid (D1–D6)	0.5 mg po tab (D4)	0	8	1.27	2.03	0.62	1.16	1.25	0.93	Boulenc 2016 DDI (P+M1) [52]
200 mg po tab bid (D1–D6)	0.5 mg po tab (D4)	0	8	1.26	2.03	0.62	1.16	1.25	0.93	Boulenc 2016 DDI (P) [52]
400 mg po tab qd (D1–D6)	0.5 mg po tab (D4)	0	8	1.83	1.88	0.97	1.16	1.13	1.02	Boulenc 2016 DDI (P+M1+M2) [52]

(Continued on next page...)

Table S3.9: Predicted and observed DDI AUC_{last} and C_{max} ratios of the victim drugs during DDIs, simulated with and without ketoconazole metabolite involvement *(continued)*

Drug administration			N	DDI AUC_{last} ratio			DDI C_{max} ratio			Reference
Ketoconazole	Victim	Gap [h]		Pred	Obs	Pred/Obs	Pred	Obs	Pred/Obs	
400 mg po tab qd (D1–D6)	0.5 mg po tab (D4)	0	8	1.14	1.88	0.61	1.12	1.13	0.98	Boulenc 2016 DDI (P+M1) [52]
400 mg po tab qd (D1–D6)	0.5 mg po tab (D4)	0	8	1.14	1.88	0.61	1.12	1.13	0.98	Boulenc 2016 DDI (P) [52]
200 mg po tab bid (D1–D3)	1 mg po cap (D3)	+1	7	1.90	1.87	1.01	0.85	1.10	0.78	Greenblatt 1998 DDI (P+M1+M2) [32]
200 mg po tab bid (D1–D3)	1 mg po cap (D3)	+1	7	1.36	1.87	0.72	0.84	1.10	0.77	Greenblatt 1998 DDI (P+M1) [32]
200 mg po tab bid (D1–D3)	1 mg po cap (D3)	+1	7	1.35	1.87	0.72	0.84	1.10	0.77	Greenblatt 1998 DDI (P) [32]
	Mean GMFE DDI (P+M1+M2)					1.03			1.12	
	Mean GMFE DDI (P+M1)					1.55			1.13	
	Mean GMFE DDI (P)					1.54			1.13	
	Midazolam									
400 mg po tab qd (D1–D15)	0.0003 mg po sol (D2)	0	6	16.91	21.56	0.78	4.09	5.06	0.81	Halama 2013 DDI (P+M1+M2) [53]
400 mg po tab qd (D1–D15)	0.0003 mg po sol (D2)	0	6	10.08	21.56	0.47	3.89	5.06	0.77	Halama 2013 DDI (P+M1) [53]
400 mg po tab qd (D1–D15)	0.0003 mg po sol (D2)	0	6	10.07	21.56	0.47	3.89	5.06	0.77	Halama 2013 DDI (P) [53]
200 mg po tab bid (D1–D4)	0.075 mg po sol (D4)	0	4	9.63	5.82	1.65	4.25	4.39	0.97	Eap 2004 DDI (P+M1+M2) [54]
200 mg po tab bid (D1–D4)	0.075 mg po sol (D4)	0	4	5.94	5.82	1.02	3.44	4.39	0.78	Eap 2004 DDI (P+M1) [54]
200 mg po tab bid (D1–D4)	0.075 mg po sol (D4)	0	4	5.93	5.82	1.02	3.44	4.39	0.78	Eap 2004 DDI (P) [54]
400 mg po tab qd (D1–D10)	0.075 mg/kg po sol (D6)	-2	19	18.39	10.24	1.80	2.82	2.34	1.20	Chung 2006 DDI (P+M1+M2) [55]
400 mg po tab qd (D1–D10)	0.075 mg/kg po sol (D6)	-2	19	3.56	10.24	0.35	1.31	2.34	0.56	Chung 2006 DDI (P+M1) [55]
400 mg po tab qd (D1–D10)	0.075 mg/kg po sol (D6)	-2	19	2.38	10.24	0.23	1.01	2.34	0.43	Chung 2006 DDI (P) [55]
400 mg po tab qd (D1–D7)	0.4 mg iv bol (D7)	0	6	6.57	9.21	0.71	-	-	-	Krishna 2009 DDI (P+M1+M2) [56]
400 mg po tab qd (D1–D7)	0.4 mg iv bol (D7)	0	6	2.41	9.21	0.26	-	-	-	Krishna 2009 DDI (P+M1) [56]
400 mg po tab qd (D1–D7)	0.4 mg iv bol (D7)	0	6	2.41	9.21	0.26	-	-	-	Krishna 2009 DDI (P) [56]
200 mg po tab bid (D1–D5)	2 mg po tab (D4)	0	8	19.30	14.55	1.33	5.17	4.08	1.27	Boulenc 2016 DDI (P+M1+M2) [52]
200 mg po tab bid (D1–D5)	2 mg po tab (D4)	0	8	8.15	14.55	0.56	4.24	4.08	1.04	Boulenc 2016 DDI (P+M1) [52]
200 mg po tab bid (D1–D5)	2 mg po tab (D4)	0	8	8.14	14.55	0.56	4.24	4.08	1.04	Boulenc 2016 DDI (P) [52]
400 mg po tab qd (D1–D5)	2 mg po tab (D4)	0	8	11.94	13.51	0.88	4.57	3.96	1.16	Boulenc 2016 DDI (P+M1+M2) [52]
400 mg po tab qd (D1–D5)	2 mg po tab (D4)	0	8	4.53	13.51	0.34	3.16	3.96	0.80	Boulenc 2016 DDI (P+M1) [52]
400 mg po tab qd (D1–D5)	2 mg po tab (D4)	0	8	4.52	13.51	0.33	3.15	3.96	0.80	Boulenc 2016 DDI (P) [52]
400 mg po tab qd (D1)	2 mg po tab (D1)	0	12	9.91	9.75	1.02	3.59	4.75	0.76	Stoch 2009 DDI (P+M1+M2) [57]
400 mg po tab qd (D1)	2 mg po tab (D1)	0	12	7.67	9.75	0.79	3.59	4.75	0.76	Stoch 2009 DDI (P+M1) [57]

(Continued on next page...)

Table S3.9: Predicted and observed DDI AUC_{last} and C_{max} ratios of the victim drugs during DDIs, simulated with and without ketoconazole metabolite involvement *(continued)*

Drug administration			N	DDI AUC_{last} ratio			DDI C_{max} ratio			Reference
Ketoconazole	Victim	Gap [h]		Pred	Obs	Pred/Obs	Pred	Obs	Pred/Obs	
400 mg po tab qd (D1)	2 mg po tab (D1)	0	12	7.66	9.75	0.79	3.58	4.75	0.76	Stoch 2009 DDI (P) [57]
400 mg po tab qd (D1–D2)	2 mg po tab (D2)	0	9	12.21	11.90	1.03	3.77	5.17	0.73	Stoch 2009 DDI (P+M1+M2) [57]
400 mg po tab qd (D1–D2)	2 mg po tab (D2)	0	9	7.67	11.90	0.64	3.59	5.17	0.69	Stoch 2009 DDI (P+M1) [57]
400 mg po tab qd (D1–D2)	2 mg po tab (D2)	0	9	7.67	11.90	0.64	3.59	5.17	0.69	Stoch 2009 DDI (P) [57]
400 mg po tab qd (D1–D5)	2 mg po tab (D5)	0	9	15.63	11.46	1.36	3.94	5.04	0.78	Stoch 2009 DDI (P+M1+M2) [57]
400 mg po tab qd (D1–D5)	2 mg po tab (D5)	0	9	7.68	11.46	0.67	3.59	5.04	0.71	Stoch 2009 DDI (P+M1) [57]
400 mg po tab qd (D1–D5)	2 mg po tab (D5)	0	9	7.67	11.46	0.67	3.59	5.04	0.71	Stoch 2009 DDI (P) [57]
400 mg po tab qd (D1–D7)	2 mg po tab (D6)	0	6	16.94	7.01	2.42	4.92	2.81	1.75	Krishna 2009 DDI (P+M1+M2) [56]
400 mg po tab qd (D1–D7)	2 mg po tab (D6)	0	6	7.09	7.01	1.01	3.95	2.81	1.41	Krishna 2009 DDI (P+M1) [56]
400 mg po tab qd (D1–D7)	2 mg po tab (D6)	0	6	7.09	7.01	1.01	3.95	2.81	1.41	Krishna 2009 DDI (P) [56]
200 mg po tab bid (D1–D2)	2 mg iv bol (D1)	0	9	2.55	4.53	0.56	-	-	-	Tsunoda 1999 DDI (P+M1+M2) [58]
200 mg po tab bid (D1–D2)	2 mg iv bol (D1)	0	9	1.76	4.53	0.39	-	-	-	Tsunoda 1999 DDI (P+M1) [58]
200 mg po tab bid (D1–D2)	2 mg iv bol (D1)	0	9	1.76	4.53	0.39	-	-	-	Tsunoda 1999 DDI (P) [58]
400 mg po tab qd (D1–D15)	3 mg po sol (D8)	0	6	19.14	19.85	0.96	3.94	5.18	0.76	Halama 2013 DDI (P+M1+M2) [53]
400 mg po tab qd (D1–D15)	3 mg po sol (D8)	0	6	7.21	19.85	0.36	3.54	5.18	0.68	Halama 2013 DDI (P+M1) [53]
400 mg po tab qd (D1–D15)	3 mg po sol (D8)	0	6	7.21	19.85	0.36	3.54	5.18	0.68	Halama 2013 DDI (P) [53]
200 mg po tab bid (D1–D2)	6 mg po sol (D1)	0	9	7.23	11.39	0.63	2.77	3.40	0.81	Tsunoda 1999 DDI (P+M1+M2) [58]
200 mg po tab bid (D1–D2)	6 mg po sol (D1)	0	9	5.21	11.39	0.46	2.62	3.40	0.77	Tsunoda 1999 DDI (P+M1) [58]
200 mg po tab bid (D1–D2)	6 mg po sol (D1)	0	9	5.21	11.39	0.46	2.62	3.40	0.77	Tsunoda 1999 DDI (P) [58]
400 mg po tab qd (D1–D4)	7.5 mg po sol (D4)	+1	9	11.12	11.53	0.96	3.05	4.24	0.72	Olkkolla 1994 DDI (P+M1+M2) [60]
400 mg po tab qd (D1–D4)	7.5 mg po sol (D4)	+1	9	6.24	11.53	0.54	2.98	4.24	0.70	Olkkolla 1994 DDI (P+M1) [60]
400 mg po tab qd (D1–D4)	7.5 mg po sol (D4)	+1	9	6.23	11.53	0.54	2.98	4.24	0.70	Olkkolla 1994 DDI (P) [60]
200 mg po tab qd (D1–D12)	10 mg po sol (D12)	+1	10	9.87	11.18	0.88	2.86	3.23	0.88	Lam 2003 DDI (P+M1+M2) [61]
200 mg po tab qd (D1–D12)	10 mg po sol (D12)	+1	10	5.05	11.18	0.45	2.65	3.23	0.82	Lam 2003 DDI (P+M1) [61]
200 mg po tab qd (D1–D12)	10 mg po sol (D12)	+1	10	5.05	11.18	0.45	2.65	3.23	0.82	Lam 2003 DDI (P) [61]
	Mean GMFE DDI(P+M1+M2)					1.40			1.30	
	Mean GMFE DDI (P+M1)					2.10			1.36	
	Mean GMFE DDI (P)					2.20			1.38	

(Continued on next page...)

Table S3.9: Predicted and observed DDI AUC_{last} and C_{max} ratios of the victim drugs during DDIs, simulated with and without ketoconazole metabolite involvement *(continued)*

Drug administration			N	DDI AUC_{last} ratio			DDI C_{max} ratio			Reference
Ketoconazole	Victim	Gap [h]		Pred	Obs	Pred/Obs	Pred	Obs	Pred/Obs	
	Triazolam									
200 mg po tab bid (D1–D3)	0.25 mg po cap (D3)	+1	6	11.67	11.90	0.98	3.20	2.47	1.29	Greenblatt 1998 DDI (P+M1+M2) [32]
200 mg po tab bid (D1–D3)	0.25 mg po cap (D3)	+1	6	4.52	11.90	0.38	2.93	2.47	1.19	Greenblatt 1998 DDI (P+M1) [32]
200 mg po tab bid (D1–D3)	0.25 mg po cap (D3)	+1	6	4.51	11.90	0.38	2.93	2.47	1.19	Greenblatt 1998 DDI (P) [32]
400 mg po tab qd (D1–D4)	0.25 mg po tab (D4)	+1	9	10.64	8.56	1.24	3.19	2.65	1.20	Varhe 1994 DDI (P+M1+M2)[62]
400 mg po tab qd (D1–D4)	0.25 mg po tab (D4)	+1	9	7.27	8.56	0.85	3.00	2.65	1.13	Varhe 1994 DDI (P+M1) [62]
400 mg po tab qd (D1–D4)	0.25 mg po tab (D4)	+1	9	7.26	8.56	0.85	3.00	2.65	1.13	Varhe 1994 DDI (P) [62]
	Mean GMFE DDI (P+M1+M2)					1.13			1.25	
	Mean GMFE DDI (P+M1)					1.91			1.16	
	Mean GMFE DDI (P)					1.91			1.16	
	Digoxin									
200 mg po tab qd (D1–D4)	0.5 mg po tab (D4)	0	10	1.47	1.75	0.84	1.52	1.63	0.93	Larsen 2007 DDI (P+M1+M2) [63]
200 mg po tab qd (D1–D4)	0.5 mg po tab (D4)	0	10	1.45	1.75	0.83	1.50	1.63	0.92	Larsen 2007 DDI (P+M1) [63]
200 mg po tab qd (D1–D4)	0.5 mg po tab (D4)	0	10	1.45	1.75	0.83	1.50	1.63	0.92	Larsen 2007 DDI (P) [63]
	Mean GMFE DDI(P+M1+M2)					1.19			1.07	
	Mean GMFE DDI (P+M1)					1.21			1.09	
	Mean GMFE DDI (P)					1.21			1.09	
	Overall mean GMFE (range) DDI (P+M1+M2)					**1.35 (1.01–2.41)**			**1.27 (1.02–1.96)**	
	pred/obs DDI ratios within two-fold					**96.30% (26/27) $\leq$ 2**			**100.00% (21/21) $\leq$ 2**	
	Overall mean GMFE (range) DDI (P+M1)					**2.44 (1.01–5.34)**			**1.42 (1.02–3.28)**	
	pred/obs DDI ratios within two-fold					**44.45% (12/27) $\leq$ 2**			**90.48% (19/21) $\leq$ 2**	
	Overall mean GMFE (range) DDI (P)					**2.64 (1.01–6.75)**			**1.52 (1.02–4.15)**	
	pred/obs DDI ratios within two-fold					**44.45% (12/27) $\leq$ 2**			**85.71% (18/21) $\leq$ 2**	

AUC_{last}: area under the plasma concentration-time curve calculated from the first to last time point of measurement, bid: twice daily, cap: capsule, C_{max}: maximum plasma concentration, DDI: drug-drug-interaction, GMFE: geometric mean fold error, iv: intravenous, M1: N-deacetylketoconazole, M2: N-hydroxy-N-deacetylketoconazle, N: number of individuals studied, obs: observed, pred: predicted, P: ketoconazole alone, seq: iv and po administration on D0 were either given sequentially with a three hour gap, sim: iv and po administration on D0 were either given simultaneously, sol: solution, tab: tablet

References

[1] M. Meyer, S. Schneckener, B. Ludewig, L. Kuepfer, and J. Lippert. Using expression data for quantification of active processes in physiologically based pharmacokinetic modeling. *Drug metabolism and disposition: the biological fate of chemicals*, 40(5):892–901, may 2012. doi: 10.1124/dmd.111.043174.

[2] M. Nishimura and S. Naito. Tissue-specific mRNA expression profiles of human phase I metabolizing enzymes except for cytochrome P450 and phase II metabolizing enzymes. *Drug metabolism and pharmacokinetics*, 21(5): 357–74, 2006. doi: 10.2133/dmpk.21.357.

[3] A. D. Rodrigues. Integrated cytochrome P450 reaction phenotyping: attempting to bridge the gap between cDNA-expressed cytochromes P450 and native human liver microsomes. *Biochemical pharmacology*, 57(5):465–80, mar 1999. doi: 10.1016/S0006-2952(98)00268-8.

[4] Open Systems Pharmacology Suite Community. Open Systems Pharmacology Suite Manual, 2018. URL https://docs.open-systems-pharmacology.org/.

[5] M. Nishimura, H. Yaguti, H. Yoshitsugu, S. Naito, and T. Satoh. Tissue distribution of mRNA expression of human cytochrome P450 isoforms assessed by high-sensitivity real-time reverse transcription PCR. *Journal of the Pharmaceutical Society of Japan*, 123(5):369–75, may 2003.

[6] K. Rowland Yeo, R. L. Walsky, M. Jamei, A. Rostami-Hodjegan, and G. T. Tucker. Prediction of time-dependent CYP3A4 drug-drug interactions by physiologically based pharmacokinetic modelling: Impact of inactivation parameters and enzyme turnover. *European Journal of Pharmaceutical Sciences*, 43(3):160–73, jun 2011. doi: 10.1016/j.ejps.2011.04.008.

[7] D. J. Greenblatt, L. L. Von Moltke, J. S. Harmatz, G. Chen, J. L. Weemhoff, C. Jen, C. J. Kelley, B. W. LeDuc, and M. A. Zinny. Time course of recovery of cytochrome P450 3A function after single doses of grapefruit juice. *Clinical Pharmacology and Therapeutics*, 74(2):121–29, aug 2003. doi: 10.1016/S0009-9236(03)00118-8.

[8] B. Achour, A. Dantonio, M. Niosi, J. J. Novak, J. K. Fallon, J. Barber, P. C. Smith, A. Rostami-Hodjegan, and T. C. Goosen. Quantitative characterization of major hepatic UDP-glucuronosyltransferase enzymes in human liver microsomes: Comparison of two proteomic methods and correlation with catalytic activity. *Drug metabolism and disposition: the biological fate of chemicals*, 45(10):1102–112, 2017.

[9] B. Prasad, R. Evers, A. Gupta, C. E. C. A. Hop, L. Salphati, S. Shukla, S. V. Ambudkar, and J. D. Unadkat. Interindividual variability in hepatic organic anion - transporting polypeptides and P-glycoprotein (ABCB1) protein expression: quantification by liquid chromatography tandem mass spectroscopy and influence of genotype, age, and sex. *Drug metabolism and disposition: the biological fate of chemicals*, 42(1):78–88, 2014. doi: 10.1124/dmd.113.053819.

[10] M. Nishimura and S. Naito. Tissue-specific mRNA expression profiles of human ATP-binding cassette and solute carrier transporter superfamilies. *Drug metabolism and pharmacokinetics*, 20(6):452–77, 2005.

[11] D. Scotcher, S. Billington, J. Brown, C. R. Jones, C. D. A. Brown, A. Rostami-Hodjegan, and A. Galetin. Microsomal and cytosolic scaling factors in dog and human kidney cortex and application for in vitro-in vivo extrapolation of renal metabolic clearance. *Drug Metabolism and Disposition*, 45(5):556–568, 2017.

[12] R. C. Heel, R. N. Brogden, A. Carmine, P. A. Morley, T. M. Speight, and G. S. Avery. Ketoconazole: A Review of its Therapeutic Efficacy in Superficial and Systemic Fungal Infections. *Drugs*, 23(1):1–36, 1982. doi: 10.2165/00003495-198223010-00001.

[13] Y. Huang, J. L. Colaizzi, R. H. Bierman, R. Woestenborghs, and J. Heykants. Pharmacokinetics and dose proportionality of ketoconazole in normal volunteers. *Antimicrobial agents and chemotherapy*, 30(2):206–10, aug 1986. doi: 10.1002/j.1552-4604.1986.tb02962.x.

[14] T. W. F. Chin, M. Loeb, and I. W. Fong. Effects of an acidic beverage (Coca-Cola) on absorption of ketoconazole. *Antimicrobial agents and chemotherapy*, 39(8):1671–5, aug 1995. doi: 10.1128/AAC.39.8.1671.

[15] T. K. Daneshmend, D. W. Warnock, M. D. Ene, E. M. Johnson, G. Parker, M. D. Richardson, and C. J.C. Roberts.

Multiple dose pharmacokinetics of ketoconazole and their effects on antipyrine kinetics in man. *Journal of Antimicrobial Chemotherapy*, 12(2):185–188, 1983. doi: 10.1093/jac/12.2.185.

[16] T. K. Daneshmend, D. W. Warnock, M. D. Ene, E. M. Johnson, M. R. Potten, M. D. Richardson, and P. J. Williamson. Influence of food on the pharmacokinetics of ketoconazole. *Antimicrobial agents and chemotherapy*, 25(1):1–3, jan 1984. doi: 10.1007/BF01061429.

[17] U.S. Food and Drug Administration. Bioequivalence - application number: 74-971, 1998.

[18] C. A. Knupp, D. C. Brater, J. Relue, and R. H. Barbhaiya. Pharmacokinetics of didanosine and ketoconazole after coadministration to patients seropositive for the human immunodeficiency virus. *Journal of clinical pharmacology*, 33(10):912–7, oct 1993.

[19] P. T. Männistö, R. Mäntylä, S. Nykänen, U. Lamminsivu, and P. Ottoila. Impairing effect of food on ketoconazole absorption. *Antimicrobial agents and chemotherapy*, 21(5):730–3, may 1982. doi: 10.1128/AAC.21.5.730.

[20] H. R Sadeghnia and M. Hassanzadeh-Khayyat. Bioequivalency Study of Two Formulations of Ketoconazole Tablet in Healthy Volunteers. *Iranian Journal of Pharmaceutical Sciences*, 1(4):209–215, 2005.

[21] W. D. S. Solomon, P. Senthamil Selvan, K. Yeeran Gowda, U. K. Mandal, and T. K. Pal. Evaluation of bioequivalence of two formulations containing 200 mg of ketoconazole. *Asian Journal of Chemistry*, 19(7):5365–5371, 2007. ISSN 09707077.

[22] J. W. M. Van Der Meer, J. J. Keuning, H. W. Scheijgrond, J. Heykants, J. Van Cutsem, and J. Brugmans. The influence of gastric acidity on the bio-availability of ketoconazole. *Journal of Antimicrobial Chemotherapy*, 6(4): 552–554, 1980. doi: 10.1093/jac/6.4.552.

[23] K. H. Yuen, J. W. Wong, N. Billa, W. P. Choy, and T. Julianto. Comparative bioavailability study of two ketoconazole tablet preparations. *The Medical journal of Malaysia*, 54(4):482–6, dec 1999.

[24] R. E. Polk, M. A. Crouch, D. S. Israel, A. Pastor, B. M. Sadler, G. E. Chittick, W. T. Symonds, W. Gouldin, and Y. Lou. Pharmacokinetic interaction between ketoconazole and amprenavir after single doses in healthy men. *Pharmacotherapy*, 19(12):1378–84, dec 1999. doi: 10.1592/phco.19.18.1378.30905.

[25] S. C. Piscitelli, T. F. Goss, J. H. Wilton, D. T. D'Andrea, H. Goldstein, and J. J. Schentag. Effects of ranitidine and sucralfate on ketoconazole bioavailability. *Antimicrobial Agents and Chemotherapy*, 35(9):1765–1771, sep 1991. doi: 10.1128/AAC.35.9.1765.

[26] S. Sriwiriyajan, W. Mahatthanatrakul, W. Ridtitid, and S. Jaruratanasirikul. Effect of efavirenz on the pharmacokinetics of ketoconazole in HIV-infected patients. *European Journal of Clinical Pharmacology*, 63(5):479–483, 2007. doi: 10.1007/s00228-007-0282-8.

[27] J. Weiss, K. I. Foerster, M. Weber, J. Burhenne, G. Mikus, T. Lehr, and W. E. Haefeli. Does the circulating ketoconazole metabolite N-deacetyl ketoconazole contribute to the drug-drug interaction potential of the parent compound? *European Journal of Pharmaceutical Sciences*, 169:106076, 2022. doi: 10.1016/j.ejps.2021.106076.

[28] M. J. Boyce, K. J. Baisley, and S. J. Warrington. Pharmacokinetic interaction between domperidone and ketoconazole leads to QT prolongation in healthy volunteers: a randomized, placebo-controlled, double-blind, crossover study. *British journal of clinical pharmacology*, 73(3):411–21, mar 2012. doi: 10.1111/j.1365-2125.2011.04093.x.

[29] C. G. Patel, L. Li, S. Girgis, D. M. Kornhauser, E. U. Frevert, and D. W. Boulton. Two-way pharmacokinetic interaction studies between saxagliptin and cytochrome P450 substrates or inhibitors: simvastatin, diltiazem extended-release, and ketoconazole. *Clinical pharmacology : advances and applications*, 3(1):13–25, 2011. doi: 10.2147/CPAA.S15227.

[30] Tiseo, Perdomo, and Friedhoff. Concurrent administration of donepezil HCl and ketoconazole: assessment of pharmacokinetic changes following single and multiple doses. *British Journal of Clinical Pharmacology*, 46(S1): 30–34, 2002. doi: 10.1046/j.1365-2125.1998.0460s1030.x.

[31] M. B. Wire, C. H. Ballow, J. Borland, M. J. Shelton, Y. Lou, G. Yuen, J. Lin, and E. W. Lewis. Fosamprenavir plus ritonavir increases plasma ketoconazole and ritonavir exposure, while amprenavir exposure remains unchanged. *Antimicrobial Agents and Chemotherapy*, 51(8):2982–2984, 2007. doi: 10.1128/AAC.00008-07.

[32] D. J. Greenblatt, C. E. Wright, L. L. Von Moltke, J. S. Harmatz, B. L. Ehrenberg, L. M. Harrel, K. Corbett, M. Counihan, S. Tobias, and R. I. Shader. Ketoconazole inhibition of triazolam and alprazolam clearance: Differential kinetic and dynamic consequences. *Clinical Pharmacology and Therapeutics*, 64(3):237–247, 1998. doi: 10.1016/S0009-9236(98)90172-2.

[33] P. C. Craven, J. R. Graybill, J. H. Jorgensen, W. E. Dismukes, and B. E. Levine. High-dose ketoconazole for treatment of fungal infections of the central nervous system. *Annals of internal medicine*, 98(2):160–7, feb 1983. doi: 10.7326/0003-4819-98-2-160.

[34] A. Dallmann. IVIC with the particle dissolution module implemented in OSP. Available online: https://github.com/AndreDlm/IVIVC-with-particle-dissolution-module-in-OSP (accessed on 30 June 2022).

[35] Chemicalize. Ketoconazole.

[36] F. Taneri, T. Güneri, Z. Aigner, and M. Kata. Improvement in the Physicochemical Properties of Ketoconazole through Complexation with Cyclodextrin Derivatives. *Journal of Inclusion Phenomena and Macrocyclic Chemistry*, (44):257–260, jul 2002. doi: https://doi.org/10.1023/A:1023013523416.

[37] H. S. Ghazal, A. M. Dyas, J. L. Ford, and G. A. Hutcheon. The impact of food components on the intrinsic dissolution rate of ketoconazole Authors. *Drug Development And Industrial Pharmacy*, 41(10):1647–54, 2015.

[38] Chemspider. Ketoconazole entry (accessed on 01 May 2021). URL https://www.chemspider.com/Chemical-Structure.401695.html.

[39] R. S. Fisher, E. Rock, and L. S. Malmud. Effects of meal composition on gallbladder and gastric emptying in man. *Digestive Diseases and Sciences*, 32(12):1337–1344, dec 1987. doi: 10.1007/BF01296658.

[40] L. M. Berezhkovskiy. Volume of Distribution at Steady State for a Linear Pharmacokinetic System with Peripheral Elimination. *Journal of Pharmaceutical Sciences*, 93(6):1628–1640, jun 2004. doi: 10.1002/jps.20073.

[41] T. Fukami, A. Iida, K. Konishi, and M. Nakajima. Human arylacetamide deacetylase hydrolyzes ketoconazole to trigger hepatocellular toxicity. *Biochemical Pharmacology*, 116:153–161, 2016. doi: 10.1016/j.bcp.2016.07.007.

[42] K. Bourcier, R. Hyland, S. Kempshall, R. Jones, J. Maximilien, N. Irvine, and B. Jones. Investigation into UDP-Glucuronosyltransferase (UGT) Enzyme Kinetics of Imidazole- and Triazole-Containing Antifungal Drugs in Human Liver Microsomes and Recombinant UGT Enzymes. *Drug Metabolism and Disposition*, 38(6):923–929, jun 2010. doi: 10.1124/dmd.109.030676.

[43] E. J. Elder, J. C. Evans, B. D. Scherzer, J. E. Hitt, G. B. Kupperblatt, S. A. Saghir, and D. A. Markham. Preparation, characterization, and scale-up of ketoconazole with enhanced dissolution and bioavailability. *Drug Development and Industrial Pharmacy*, 33(7):755–765, 2007. doi: 10.1080/03639040601031882.

[44] Chemicalize. N-deactylketoconazole entry (accessed on 01 May 2021), 2021.

[45] R. Kawai, M. Lemaire, J. L. Steimer, A. Bruelisauer, W. Niederberger, and M. Rowland. Physiologically based pharmacokinetic study on a cyclosporin derivative, SDZ IMM 125. *Journal of pharmacokinetics and biopharmaceutics*, 22(5):327–65, oct 1994.

[46] T. Rodgers and M. Rowland. Physiologically based pharmacokinetic modelling 2: predicting the tissue distribution of acids, very weak bases, neutrals and zwitterions. *Journal of pharmaceutical sciences*, 95(6):1238–57, jun 2006. doi: 10.1002/jps.20502.

[47] R. J. Rodriguez and D. Acosta. Metabolism of ketoconazole and deacetylated ketoconazole by rat hepatic microsomes and flavin-containing monooxygenases. *Drug metabolism and disposition: the biological fate of chemicals*, 25(6):772–7, jun 1997.

[48] Chemicalize. N-deacetyl-N-hydroxyketoconazole entry (accessed on 01 May 2021), 2022.

[49] T. K. Daneshmend, D. W. Warnock, A. Turner, and C. J.C. Roberts. Pharmacokinetics of ketoconazole in normal subjects. *Journal of Antimicrobial Chemotherapy*, 8(4):299–304, 1981. doi: 10.1093/jac/8.4.299.

[50] E. J. Guest, L. Aarons, J. B. Houston, A. Rostami-Hodjegan, and A. Galetin. Critique of the two-fold measure of prediction success for ratios: application for the assessment of drug-drug interactions. *Drug metabolism and disposition: the biological fate of chemicals*, 39(2):170–3, feb 2011. doi: 10.1124/dmd.110.036103.

[51] E. D. Kharasch, S. Vangveravong, N. Buck, A. London, T. Kim, J. Blood, and R. H. Mach. Concurrent assessment of hepatic and intestinal cytochrome P450 3A activities using deuterated alfentanil. *Clinical pharmacology and therapeutics*, 89(4):562–70, apr 2011. doi: 10.1038/clpt.2010.313.

[52] X. Boulenc, O. Nicolas, S. Hermabessière, I. Zobouyan, V. Martin, Y. Donazzolo, and doi = 10.1007/s13318-014-0235-4 file = :C /Users/Fatima Marok/AppData/Local/Mendeley Ltd./Mendeley Desktop/Downloaded/Boulenc et al. - 2016 - CYP3A4-based drug-drug interaction CYP3A4 substrates' pharmacokinetic properties and ketoconazole dose regime(2).pdf:pdf isbn = 2107-0180 (Electronic)ô378-7966 (Linking) journal = European Journal of Drug Metabolism and Pharmacokinetics keywords = Alprazolam,CYP3A4,Drug-drug interaction,Ketoconazole,Midazolam,PBPK simulation number = 1 pages = 45–54 pmid = 25374256 title = CYP3A4-based drug-drug interaction: CYP3A4 substrates' pharmacokinetic properties and ketoconazole dose regimen effect volume = 41 year = 2016 Ollier, C.

[53] B. Halama, N. Hohmann, J. Burhenne, J. Weiss, G. Mikus, and W. E. Haefeli. A nanogram dose of the CYP3A probe substrate midazolam to evaluate drug interactions. *Clinical Pharmacology and Therapeutics*, 93(6):564–571, 2013. ISSN 00099236. doi: 10.1038/clpt.2013.27.

[54] C. B. Eap, T. Buclin, G. Cucchia, D. Zullino, E. Hustert, G. Bleiber, K. Golay, A. Aubert, P. Baumann, A. Telenti, and R. Kerb. Oral administration of a low dose of midazolam (75 μg) as an in vivo probe for CYP3A activity. *European Journal of Clinical Pharmacology*, 60(4):237–246, 2004. doi: 10.1007/s00228-004-0762-z.

[55] E. Chung, A. N. Nafziger, D. J. Kazierad, and J. S. Bertino. Comparison of midazolam and simvastatin as cytochrome P450 3A probes. *Clinical Pharmacology and Therapeutics*, 79(4):350–361, 2006. doi: 10.1016/j.clpt.2005.11.016.

[56] G. Krishna, A. Moton, L. Ma, I. Savant, M. Martinho, M. Seiberling, and J. McLeod. Effects of oral posaconazole on the pharmacokinetic properties of oral and intravenous midazolam: A phase I, randomized, open-label, crossover study in healthy volunteers. *Clinical Therapeutics*, 31(2):286–298, 2009. doi: 10.1016/j.clinthera.2009.02.022.

[57] S. A. Stoch, E. Friedman, A. Maes, K. Yee, Y. Xu, P. Larson, M. Fitzgerald, J. Chodakewitz, and J. A. Wagner. Effect of different durations of ketoconazole dosing on the single-dose pharmacokinetics of midazolam: Shortening the paradigm. *Journal of Clinical Pharmacology*, 49(4):398–406, 2009. doi: 10.1177/0091270008331133.

[58] S. M. Tsunoda, R. L. Velez, L. L. von Moltke, and D. J. Greenblatt. Differentiation of intestinal and hepatic cytochrome P450 3A activity with use of midazolam as an in vivo probe: effect of ketoconazole. *Clinical pharmacology and therapeutics*, 66(5):461–71, nov 1999. doi: 10.1016/S0009-9236(99)70009-3.

[59] B. Liu, H. K. Crewe, M. Ozdemir, K. Rowland Yeo, G. Tucker, and A. Rostami-Hodjegan. The absorption kinetics of ketoconazole plays a major role in explaining the reported variability in the level of interaction with midazolam: Interplay between formulation and inhibition of gut wall and liver metabolism. *Biopharmaceutics and drug disposition*, 38(3):260–270, apr 2017. doi: 10.1002/bdd.2058.

[60] K. T. Olkkola, J. T. Backman, and P. J. Neuvonen. Midazolam should be avoided in patients receiving the systemic antimycotics ketoconazole or itraconazole. *Clinical pharmacology and therapeutics*, 55(5):481–5, may 1994.

[61] Y. W. F. Lam, C. L. Alfaro, L. Ereshefsky, and M. Miller. Pharmacokinetic and pharmacodynamic interactions of oral midazolam with ketoconazole, fluoxetine, fluvoxamine, and nefazodone. *Journal of clinical pharmacology*, 43(11): 1274–82, nov 2003. doi: 10.1177/0091270003259216.

[62] A. Varhe, K. T. Olkkola, and P. J. Neuvonen. Oral triazolam is potentially hazardous to patients receiving systemic antimycotics ketoconazole or itraconazole. *PHARMACOKINETICS AND DRUG DISPOSITION*, pages 601–607, 1994.

[63] U. L. Larsen, Hyldahl L. Olesen, Guldborg C. Nyvold, J. Eriksen, P. Jakobsen, M. Østergaard, H. Autrup, and V. Andersen. Human intestinal P-glycoprotein activity estimated by the model substrate digoxin. *Scandinavian Journal of Clinical and Laboratory Investigation*, 67(2):123–134, 2007. doi: 10.1080/00365510600986084.

[64] N. Hanke, S. Frechen, D. Moj, H. Britz, T. Eissing, T. Wendl, and T. Lehr. PBPK models for CYP3A4 and P-gp

DDI prediction: a modeling network of rifampicin, itraconazole, clarithromycin, midazolam, alfentanil and digoxin - Supplementary document. *CPT: pharmacometrics & systems pharmacology*, aug 2018.

[65] A. Frechen, S.; Dallmann. Building and Evaluation of a PBPK Model for Alprazolam in Healthy Adults. Available online: https://github.com/Open-Systems-Pharmacology/Alprazolam-Model/releases/tag/v1.1 (accessed on 30 June 2022).

[66] J.; Solodenko, S.; Frechen, and A. Dallmann. Building and Evaluation of a PBPK Model for Triazolam in Healthy Adults. Available online: https://github.com/Open-Systems-Pharmacology/Triazolam-Model/releases/tag/v1.1 (accessed on 30 June 2022).

Clinical Pharmacology & Therapeutics

Personalized Chronomodulated 5-Fluorouracil Treatment: A Physiologically Based Pharmacokinetic Modeling Precision Dosing Approach for Optimizing Cancer Therapy

Supplementary Material

Fatima Zahra Marok[1], Jan-Georg Wojtyniak[1,2], Dominik Selzer[1], Robert Dallmann[3], Jesse J Swen[4], Henk-Jan Guchelaar[4], Matthias Schwab[2,5,6], Thorsten Lehr[1]

[1]Clinical Pharmacy, Saarland University, Saarbruecken, Germany
[2]Dr. Margarete Fischer-Bosch-Institut of Clinical Pharmacology, Stuttgart, Germany
[3]Division of Biomedical Sciences, Warwick Medical School, University of Warwick, Coventry, United Kingdom
[4]Department of Clinical Pharmacy & Toxicology, Leiden University Medical Center, P.O. Box 9600, 2300 RC Leiden, The Netherlands
[5]Departments of Clinical Pharmacology, and of Biochemistry and Pharmacy, University Tuebingen, Tuebingen, Germany
[6]Cluster of excellence iFIT (EXC2180) “Image-Guided and Functionally Instructed Tumor Therapies”, University Tuebingen, Tuebingen, Germany

Funding:

RD’s work is supported by a grant from Cancer Research UK (C53720/A29468) and Anglo American Platinum. J.J.S., H.J.G. and M.S. were supported by the European Commission Horizon 2020 UPGx grant 668353. Moreover, M.S. was funded by the Robert Bosch Stiftung (Stuttgart, Germany), a grant from the German Federal Ministry of Education and Research (BMBF 031L0188D), and the Deutsche Forschungsgemeinschaft (DFG, German Research Foundation) under Germany’s Excellence Strategy—EXC 2180—390900677. T.L. was supported by the the project “Open-source modeling framework for automated quality control and management of complex life science system models” (OSMOSES) funded by the German Federal Ministry of Education and Research (BMBF, grant ID:031L0161C).

Conflict of Interest:

Since January 2020, Jan-Georg Wojtyniak is an employee of Boehringer Ingelheim Pharma GmbH and Co. KG. All other authors declare no conflict of interest.

Corresponding Author:

Prof. Dr. Thorsten Lehr
Clinical Pharmacy, Saarland University
Campus C5 3, 66123 Saarbruecken, Germany
Phone: +49 681 302 70255
Email: thorsten.lehr@mx.uni-saarland.de

Contents

S1 PBPK modeling

S1.1 Quantitative PBPK model evaluation

The models performance was evaluated by comparing predicted plasma concentration-time profiles with observed data which are displayed in the following sections in linear and semilogarithmic scale (Fig. S3.3.1-S3.3.22 and S2.3.1-S2.3.2). Furthermore, the models were evaluated by comparing predicted to observed plasma concentration values (Fig. S3.4.23 and S2.4.3), area under the plasma concentration-time curve calculated from the first time point to the last time point of measurements (AUC_{last}) values and maximum plasma concentration (C_{max}) values (Fig. S3.4.24,S3.4.25, S2.4.4 and S2.4.5). Fig. S3.4.26, S3.4.27, S2.4.6 and S2.4.7 illustrate results of local sensitivity analyses as bar graphs.
As quantitative performance measures, a mean relative deviation (MRD) and a median symmetric accuracy (MSA) were calculated for all profiles from their respective predicted and observed plasma concentrations (Eq. (S1) and Eq. (S2)). Furthermore, the geometric mean fold error (GMFE) of the AUC_{last} and C_{max} were calculated according to Eq. (S3).

Equation: Mean relative deviation

$$MRD = 10^{x} \text{ with } x = \sqrt{\frac{1}{n}\sum_{i=1}^{n}(\log_{10}\hat{c}_i - \log_{10} c_i)^2} \tag{S1}$$

c_i = the i^{th} observed plasma concentration
$\hat{c}_i$ = the respective predicted plasma concentration
n = number of observed values

Overall MRD values of ≤ 2 were considered reasonable predictions.

Equation: Median symmetric accuracy

$$MSA = 100(\mathrm{e}^{(\mathrm{M}(|\log_e(x_i)|))} - 1) \text{ with } x_i = c_i/\hat{c}_i \tag{S2}$$

c_i = the i^{th} observed plasma concentration
$\hat{c}_i$ = the respective predicted plasma concentration
M = median

The GMFE was calculated for all observed AUC_{last} and C_{max} values according to Eq. (S3).

Equation: Geometric mean fold error

$$GMFE = 10^x \text{ with } x = \frac{1}{n}\sum_{i=1}^{n}|\log_{10}(\frac{\hat{a}_i}{a_i})| \quad \text{(S3)}$$

a_i = observed AUC_{last} or C_{max} value
$\hat{a}_i$ = predicted AUC_{last} or C_{max} value
n = number of studies

S1.2 Sensitivity analysis

Sensitivity of the final models to single parameters (local sensitivity analysis) was calculated and measured as relative change of the AUC_{last}. The analysis was carried out using a relative perturbation of 1000% (variation range 10.0, maximum number of 9 steps). Parameters were included into the analysis if they have been optimized, if they are associated with optimized parameters or if they might have a strong impact due to calculation methods used in the model. Sensitivity to a parameter was calculated as the ratio of the relative change of the simulated AUC_{last} to the relative variation of the parameter around its value used in the final model according to Eq. (S4):

Equation: Sensitivity analysis

$$S = \frac{\Delta AUC_{0-24}}{\Delta p} * \frac{p}{AUC_{0-24}} \quad \text{(S4)}$$

S = sensitivity of the AUC to the examined model parameter
ΔAUC = change of the AUC
AUC = simulated, AUC with the original parameter value
Δp = change of the examined parameter value
p = original parameter value

A sensitivity of + 1.0 signifies that a 10% increase of the examined parameter value causes a 10% increase of the simulated AUC.

S1.3 System-dependent parameters

System-dependent parameters, such as reference concentrations and tissue expression profiles of metabolizing enzymes and transporters, are listed in Table S1.1 and S1.2.

Table S1.1: System-dependent parameter

Protein (*Gene*)	Mean reference concentration [µmol protein / l in the tissue of highest expression]	Geometric standard deviation of reference concentration	Half-life liver [hours]	Half-life intestine [hours]
DPD *DPYD*	[a]1.0	RT-PCR [1]	36	23
DPH *DPYS*	[a]1.0	Array [2]	36	23
MRP4 *ABCC4*	[b]0.024	Array [2]	36	23

Array, microarray expression profile; **DPD**, dihydropyrimidine dehydrogenase; **DPH**, dihydropyrimidinase; **MRP4**, multi drug resistance protein 4; **RT-PCR**, reverse transcription-polymerase chain reaction measured expression profile.
[a], default
[b], calculated from transporter per mg membrane protein times 26.2 mg human kidney microsomal protein per g kidney tissue [3, 4]

Table S1.2: Expression data of implemented proteins

	DPD (*DPYD*)	**DPH (*DPYS*)**	**MRP4 (*ABCC4*)**
Properties			
Localization	Intracellular	Intracellular	Cell membrane
Direction	n.a.	n.a.	Efflux
Half-life liver/intestine [h][a]	36/23	36/23	n.a.
Relative expression in various organs and tissues [%]			
Data source	RT-PCR [1]	Array [2]	Array [2]
Blood cells	100	0	0
Plasma	100	0	0
Bone	79	1	27
Brain	6	5	26
Fat	0	0	0
Gonads	9	3	50
Heart	28	8	24
Kidney	11	53	94
Liver periportal	38	100	45
Liver pericentral	38	100	45
Lung	56	4	72
Muscle	30	1	44
Pancreas	12	4	26
Skin	0	2	31
Spleen	49	5	44
Duodenum mucosa	15	1	32
Upper jejunum mucosa	15	1	32
Lower jejunum mucosa	15	1	32
Upper ileum mucosa	15	1	32
Lower ileum mucosa	15	1	32
Cecum	0	0	0
Colon ascendes mucosa	14	1	0
Colon transversum mucosa	14	1	0
Colon descendens mucosa	14	1	0
Colon sigmoid mucosa	14	1	0
Rectum	0	0	0
Stomach non-mucosal tissue	19	1	42
Small intestine non-mucosal tissue	15	1	32
Large intestine non-mucosal tissue	14	1	100

Array, microarray expression profile; **DPD**, dihydropyrimidine dehydrogenase; **DPH**, dihydropyrimidinase; **MRP4**, multi drug resistance protein 4; **RT-PCR**, reverse transcription-polymerase chain reaction measured expression profile.
[a], Information from PK-Sim® expression database

All of the above listed proteins were implemented in every modeled indiviual. The indivuals were created based on the demographics mentioned in the respective clinical study report. If no data was available a mean indiviual was used. This *mean individual* is based on the reported individuals in the accumulated studies, since the average patient was not reflected by the standard mean healthy induvidual implemented in PK-Sim®. The characteristics of the individuals are listed in Table S1.3.

Table S1.3: Standard indiviudal demographics

Indiviudual	Age [years]	Weight [kg]	Height [cm]	BSA [m²]	BMI [kg/m²]	Reference
OSP® - Standard european male[a]	30	73	176	1.89	23.57	[5]
European Male[b]	59.92	70.33	169.84	1.82	24.38	[5]
European Female[b]	59.90	70.30	169.80	1.82	24.38	[5]
Japanese Female[c]	59.90	51.73	156.12	1.50	21.23	[6]

BMI, body mass index; **BSA**, body surface area; **OSP®**, open systems pharmacology®.
[a], standard individual implemented in the modeling software, used for every study where demographical data was missing
[b], standard individual used for every study where demographical data was missing
[c], only used for Van Kuilenburg 2002 (ID =31) [7] and Wattanatorn 1997 (ID = 81) [8]
[c], only used for Yamada 2003 (ID=82) [9].

S1.4 Implementation of drug-time-of-day-interaction

S1.4.1 Diurnal enzyme activity

Diurnal variations in enzyme activity were implemented by implementing a sinusoidal relationship between tme-of-day and reaction for the metabolic transformation via DPD or DPH. Eq. (see S5).
The value for the amplitude (A) was derived from literature (Jacobs et al. 2016 [10] or Jiang et al. 2004 [11]) or was adjusted individually. The value T_{Acr} describes the shift from t=0 in maximum enzyme activity.

Circadian rythm in DPD activity

$$\frac{dN}{dt} = (1 + Amp * sin(2\pi(t + T_{Acr})/1440)) * kcat * V * Kwater * C(t)/(K_M + Kwater * C(t)) \quad \text{(S5)}$$

Amp = amplitude
C = concentration of 5-fluorouracil or uracil [µM]
$kcat$ = catalytic rate constant [1/min]
K_M = Michaelis-Menten constant [µM/l]
$Kwater$ = partition coefficient (water/organ)
N = amount of drug tranformed per time
t = simulation time [min]
T_{Acr} = shift in acrophase of enzyme activity [min]
V = volume of organ [ml]

S1.4.2 *In-Vitro-In-Vivo*-Extrapolation of diurnal patterns

Extrapolating diurnal patterns from *in-vitro* enzyme activity measurements to *in-vivo* predictions of drug concentrations was performed by fitting the parameters for Amp and T_{Acr} of Eq. (S5) to the respective observed data via Eq. (S6). Only Amp and T_{Acr} were needed to describe diurnal variations in enzyme activity. The baseline activity is calculated by the already implemented parameters described in Eq. (S5).

Estimation of diurnal variations in DPD activity

$$v(t) = (1 + Amp * sin(2\pi(t + T_{Acr})/1440)) * v_0 \quad \text{(S6)}$$

Amp = amplitude
t = time in minutes [min]
T_{Acr} = shift in acrophase of enzyme activity [min]
v = enzyme activity
v_0 = baseline enzyme activity

In case of *in-vitro* mRNA expression data derived from Raida et al. [12], mRNA expressions relative to the mean mRNA expression were translated to DPD activities by shifting the respective clock-times of mRNA expression measurements by a time of translation (Eq. (S7)). The mean DPD activtity from Jacobs et al. [10] and the relativ change in mRNA expressions were then used to estimate the DPD activities (Eq. S8).

Estimation of translation of *DPYD* mRNA

$$t = t_{obs} + \frac{a_{DPD}}{v_T} \tag{S7}$$

$$v = rel_{mRNA} * v_0 \tag{S8}$$

a_{DPD} = number of amino acids in DPD enzyme
rel_{mRNA} = relative change in mRNA expression
t = predicted time of DPD activity [min]
t_{obs} = observed time of *DPYD* mRNA expression [min]
v = predicted enzyme activity
v_0 = baseline enzyme activity
v_T = translation rate of 600 amino acids per minute [13] [1/min]

S1.4.3 Chronomodulated infusion rates

A sine function was used to describe chronomodulated application rates (see Eq. (S9)).

Equation: Chronomodulated application rates

$$v_{inf}(t) = Amp * sin(2\pi(t + T_{Acr})/1440) * (m/t_{inf}) \tag{S9}$$

Amp = amplitude
m = amount of drug applicated [µmol]
t = time [min]
T_{Acr} = shift in acrophase of infusion rate
t_{inf} = duration of infusion [min]
$v_{inf}(t)$ = chronomodulated infusion rate

S2 Uracil model development

S2.1 Clinical studies

Table S2.1: Clinical studies used for uracil model development

Dose absolute [mg]	Dose [mg/m^2]	Route	n	Age [years]	Weight [kg]	BSA [m^2]	Females [%]	Dataset	Reference
233.14	[a]6	po (sol), s.d.	19	-	-	-	-	te	Mattison 2006 [14]
-	500	po (sol), s.d.	11	38±9	74±10	-	54.5	ta	Van Staveren 2011 [15]
-	1000	po (sol), s.d.	11	38±9	74±10	-	54.5	te	Van Staveren 2011 [15]
-	-	syn	40	-	-	-	-	ta	Jacobs 2016 [10]

BSA, body surface area; **iv**, intravenous; **n**, number of individuals studied; **po**, oral; **Route**, route of administration; **s.d.**, single dose; **sol**, solution; **syn**, endogenous synthesis; **ta**, training dataset (parameter optimization); **te**, test dataset (model evaluation); **-**, no data available. Values are means ±standard deviation or ranges.
[a], dose relative in mg/kg bodyweight

S2.2 Drug-dependent model parameters

Table S2.2: Drug-dependent parameters of the uracil PBPK model

Parameter	Unit	Value	Source	Reference	Value	Source	Reference	Description
		uracil			**5,6-dihydrouracil**			
MW	g/mol	112.09	112.09	[16]	114.10	114.10	[17]	Molecular weight
pKa	-	(acidic) 8.80 and 13.76	(acidic) 8.80 and 13.76	[16]	(acidic) 11.73	(acidic) 11.73	[17]	Acid dissociation constant
Solubility (pH)	mg/ml	15.50 (7.4)	15.50 (7.4)	[16]	266.74 (7.4)	266.74 (7.4)	[17]	Solubility
logP	-	-0.86	-0.86	[16]	[a]1.92	-1.21	[17]	Lipophilicity
fu	%	[b]100	-	-	[b]100	-	-	Fraction unbound
Specific intest. perm.	cm/min	[c]$5.59 \cdot 10^{-5}$	[d]$1.32 \cdot 10^{-6}$	-	[d]$7.38 \cdot 10^{-4}$	[d]$7.38 \cdot 10^{-4}$	-	Normalized to surface area
Specific organ perm.	cm/min	[d]$2.00 \cdot 10^{-3}$	[d]$2.00 \cdot 10^{-3}$	-	[d]1.09	[d]1.09	-	Normalized to surface area
GFR fraction	-	[e]1	-	-	[e]1	-	-	Fraction of filtered drug in urine
Cellular permeabilities	-	Ch. d. S.	-	[18]	Ch. d. S.	-	[18]	Permeation across cell membranes
Partition coefficients	-	R&R	-	[19]	Berez.	-	[20]	Organ-plasma partition coefficients
Formulation	-	[c]dissolved	-	-	-	-		Formulation used in predictions
MRP4 K_M	µmol/l	[a]7.43	-	-	-	-	-	Michaelis-Menten constant
MRP4 k_{cat}	1/min	[a]31.67	-	-	-	-	-	MRP4 catalytic rate constant
DPD K_M	µmol/l	2.30	2.30	-	-	-	[21]	Michaelis-Menten constant
DPD k_{cat}	1/min	[a] 3.18	-	-	-	-	-	DPD catalytic rate constant
DPH K_M	µmol/l	-	-	-	9.75	9.75	[21]	Michaelis-Menten constant
DPH k_{cat}	1/min	-	-	-	[a]7.43	-	-	DPH catalytic rate constant

Berez., Berezhkovskiy calculation method; **Ch. d. S.**, Charge dependent Schmitt calculation method; **DPD**, dihydropyrimidine dehydrogenase; **DPH**, dihydropyrimidinase; **GFR**, glomerular filtration rate; **intest. perm.**, intestinal permeability; **MRP4**, multi drug resistence protein 4; **organ perm.**, organ permeability; **-**, not available.
[a], optimized
[b], assumed as no data on binding was found
[c], only used for oral solutions
[d], calculated value
[e], assumed

S2.2.1 Diurnal DPD activity

Table S2.3 lists all parameters used to predict the dirunal variations in DPD activity for endogenous uracil. Here, endogenous uracil was predicted for a European Male (see Table S1.3) with activities derived from individual DPD activity profiles estimated from DPD activities from Jacobs et al. [10] or *DPYD* mRNA measurements from Raida et al. [12].

Table S2.3: Diurnal parameters of the uracil PBPK model for time-of-day variation in DPD activity.

Study (ID)	Amplitude (DPD)	T_{Acr} (DPD) [min]	Reference
H#1	0.34	140.47	Jacobs et al. [10]
H#2	0.38	-139.30	Jacobs et al. [10]
H#3	0.35	117.82	Jacobs et al. [10]
H#4	0.40	2897.86	Jacobs et al. [10]
H#5	0.28	2935.33	Jacobs et al. [10]
H#6	0.23	68.51	Jacobs et al. [10]
H#7	0.33	23.87	Jacobs et al. [10]
H#8	0.23	-23.38	Jacobs et al. [10]
H#9	0.42	-135.54	Jacobs et al. [10]
H#10	0.30	-58.78	Jacobs et al. [10]
H#11	0.20	78.61	Jacobs et al. [10]
H#12	0.19	-19.43	Jacobs et al. [10]
H (mean)	0.24	0.00	Jacobs et al. [10]
D#1	0.33	323.21	Raida et al. [12]
D#2	0.28	2037.74	Raida et al. [12]
D#3	0.34	1555.45	Raida et al. [12]
D#4	0.36	1315.36	Raida et al. [12]
D#5	0.58	1276.63	Raida et al. [12]
D#6	0.16	1537.15	Raida et al. [12]
D#7	0.30	961.87	Raida et al. [12]
D#8	0.35	1758.55	Raida et al. [12]
D#9	0.25	599.99	Raida et al. [12]
D#10	0.42	2035.80	Raida et al. [12]
D(mean)	0.05	1727.43	Raida et al. [12]

D, cancer patient; **DPD**, dihydropyrimidine dehydrogenase; **H**, healthy individual; T_{Acr}, shift in time of maximum enzyme activity.

S2.3 Concentration-time profiles

Model predictions are shown as solid lines and corresponding observed data as filled dots. Symbols represent the mean values ± standard deviation, if available. For endogenous uracil where daily fluctuations are visible, day and night time were visualized with white and shaded areas. Here, a day and night cycle from 7 am to 7 pm was assumed.

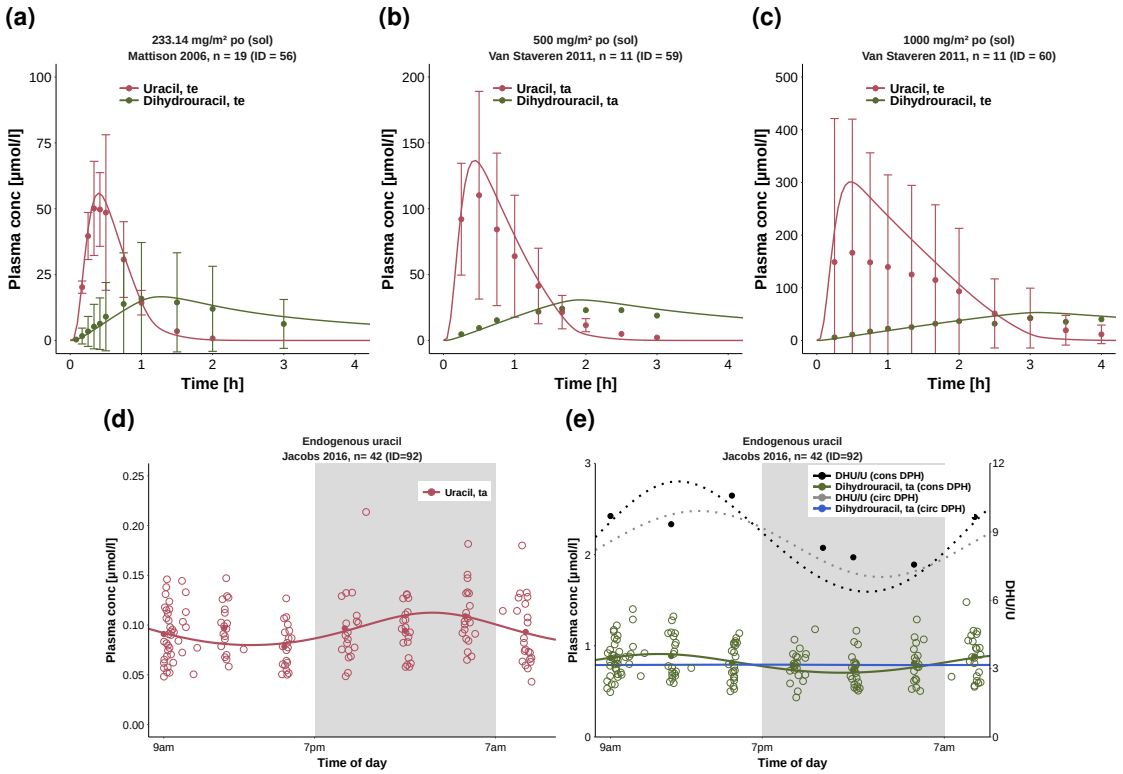

Figure S2.3.1: **Plasma uracil after oral administration of uracil including endogenous uracil** on a linear scale. The shaded areas illustrate nighttime. **circ**, circadian activity; **conc**, concentration; **cons**, constant activity; **DHU/U**, dihydrouracil-to-uracil plasma concentration ratio; **DPH**, dihydropyrimidinase; **n**, number of individuals; **po**, oral; **sol**, solution; **ta**, training dataset; **te**, test dataset.

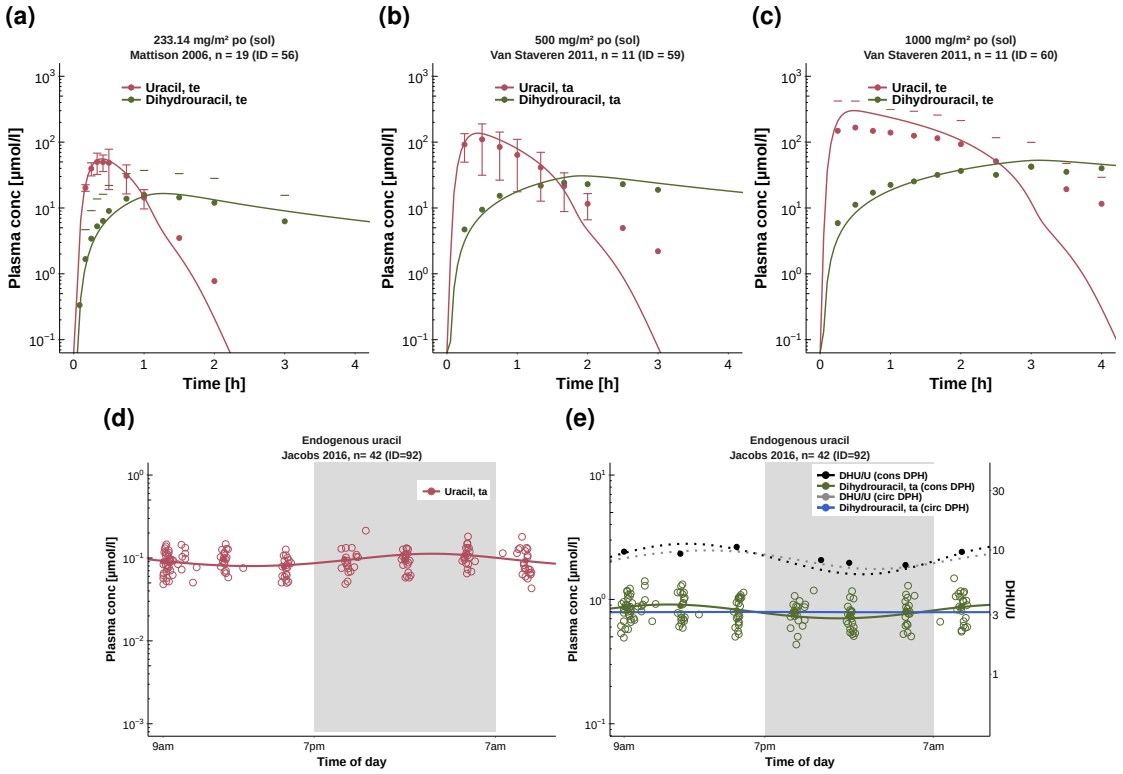

Figure S2.3.2: **Plasma uracil after oral administration of uracil including endogenous uracil** on a semi-logarithmic scale. The shaded areas illustrate nighttime. **circ**, circadian activity; **conc**, concentration; **cons**, constant activity; **DHU/U**, dihydrouracil-to-uracil plasma concentration ratio; **DPH**, dihydropyrimidinase; **n**, number of individuals; **po**, oral; **sol**, solution; **ta**, training dataset; **te**, test dataset.

S2.4 Model evaluation

S2.4.1 Predicted compared to observed concentrations goodness-of-fit plots

Following, goodness-of-fit plots of predicted compared to observed plasma concentrations for every study are illustrated in Fig. S2.4.3. Details on dosing regimens, study populations and literature references are listed in Table S2.1. Predicted and observed PK parameters are summarized in Table S2.5.

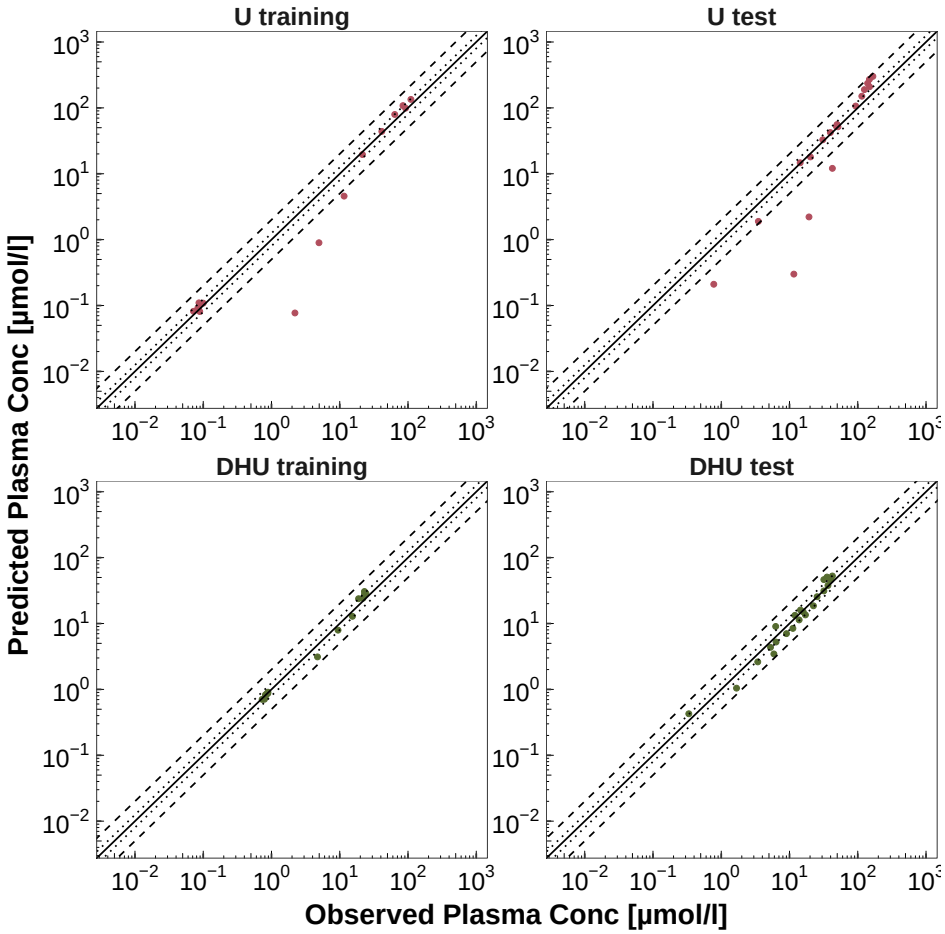

Figure S2.4.3: **Predicted compared to observed plasma concentrations**. Illustrated are values for uracil and 5,6-dihydrouracil for training and test data. The solid lines mark the line of identity. Dotted lines indicate 1.25-fold, dashed lines 2-fold deviation. **Conc**, concentration; **DHU**, 5,6-dihydrouracil; **U**, uracil.

S2.4.2 Mean relative deviation and median symmetric accuracy of plasma concentration predictions

Table S2.4: Mean relative deviation and median symmetric accuracy values of uracil and 5,6-dihydrouracil plasma concentrations

Dose [mg]	Route	n	Compound	MRD	MSA [%]	Dataset	Reference	Profile ID
422	po (sol), s.d.	19	**U**	1.63	9.02	te	Mattison 2006 [14]	56
500	po (sol), s.d.	11	**U**	3.67	24.26	ta	Van Staveren 2011 [15]	59
1000	po (sol), s.d.	11	**U**	3.98	69.40	te	Van Staveren 2011 [15]	60
	syn	40	**U**	1.14	10.28	ta	Jacobs 2016 [10]	92
422	po (sol), s.d.	19	**DHU**	1.28	21.99	ta	Mattison 2006 [14]	56
500	po (sol), s.d.	11	**DHU**	1.27	19.48	te	Van Staveren 2011 [15]	59
1000	po (sol), s.d.	11	**DHU**	1.31	24.01	te	Van Staveren 2011 [15]	60
	syn	40	**DHU**	1.05	2.25	ta	Jacobs 2016 [10]	92
			Mean	**1.92 (1.05–3.98)**	**84.01 (2.25–69.40)**			
			Median	**1.30 (1.05–3.98)**	**20.74 (2.25–69.40)**			
				6/8 < 2				

DHU, 5,6-dihydrouracil; **MRD**, mean relative deviation; **MSA**, median symmetric accuracy; **po**, oral; **Route**, route of administration; **s.d.**, single dose; **sol**, solution; **syn**, endogenous synthesis; **ta**, training dataset (parameter optimization); **te**, test dataset (model evaluation), **U**, uracil.
[a], dose relative in mg/kg bodyweight

S2.4.3 AUC_{last} and C_{max} goodness-of-fit plots

In the following section, goodness-of-fit plots of predicted compared to observed AUC_{last} and C_{max} values for every study are illustrated in Fig. S2.4.4-S2.4.5. Details on dosing regimens, study populations and literature references are listed in Table S2.1. Predicted and observed PK parameters are summarized in Table S2.5.

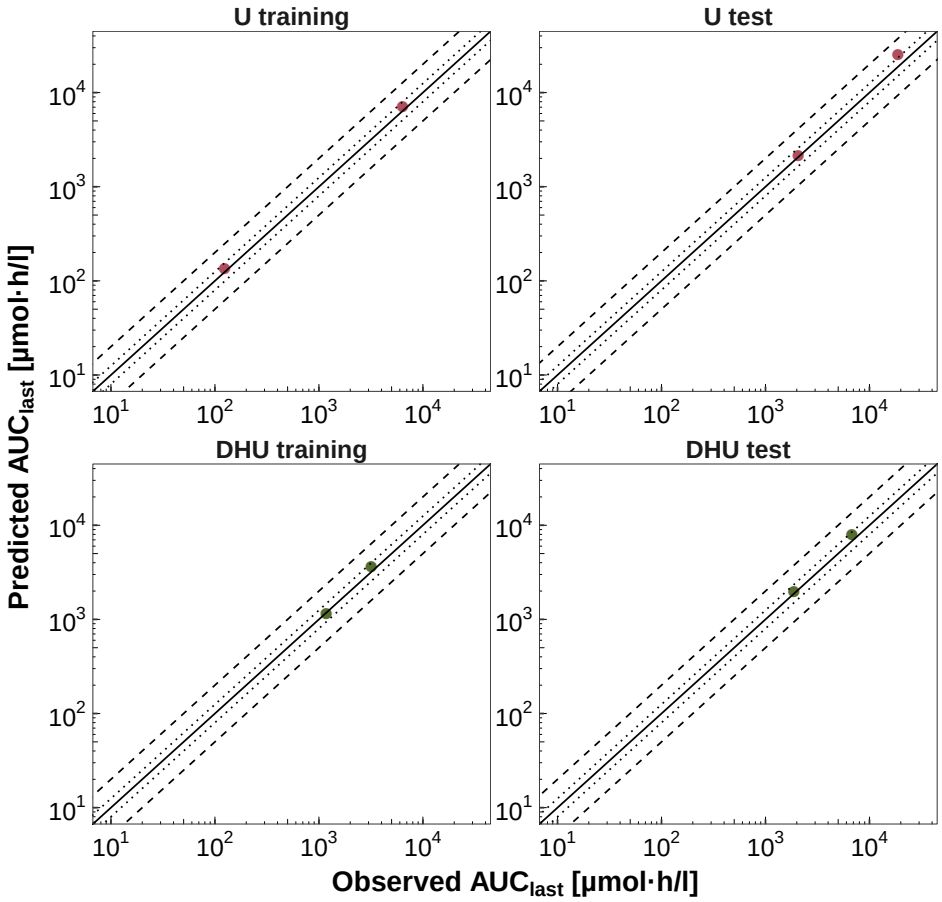

Figure S2.4.4: **Predicted compared to observed plasma AUC_{last} values**. Illustrated are values for uracil and 5,6-dihydrouracil for training and test data. The solid lines mark the line of identity. Dotted lines indicate 1.25-fold, dashed lines 2-fold deviation. **AUC_{last}**, area under the plasma concentration time curve from the first to last time point of concentration measurements; **DHU**, 5,6-dihydrouracil; **U**, uracil.

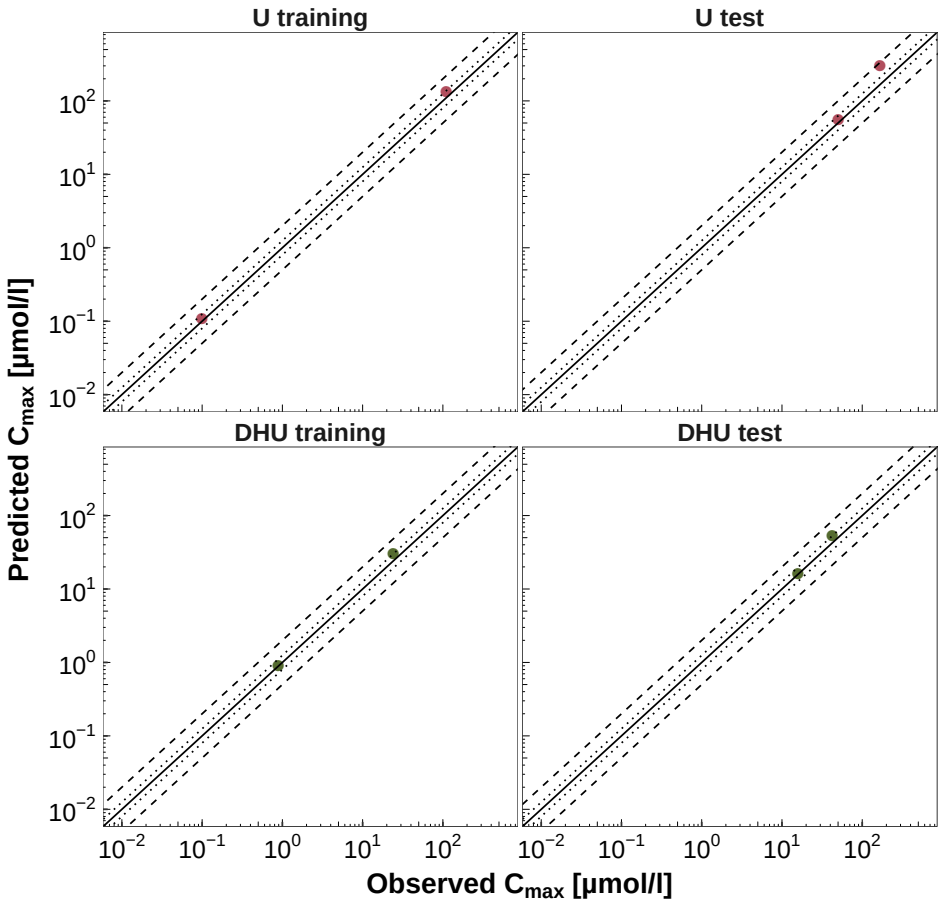

Figure S2.4.5: **Predicted compared to observed plasma C_{max} values**. Illustrated are values for uracil and 5,6-dihydrouracil for training and test data. The solid lines mark the line of identity. Dotted lines indicate 1.25-fold, dashed lines 2-fold deviation. **C_{max}**, maximum plasma concentration; **DHU**, 5,6-dihydrouracil; **U**, uracil.

S2.4.4 Geomentric mean fold error of predicted AUC_{last} and C_{max} values

Table S2.5: Predicted and observed AUC_{last} and C_{max} values of of uracil and 5,6-dihydrouracil plasma concentrations

Dose [mg/m²]	Route	n	Compound	AUC_{last} pred [µmol·h/l]	AUC_{last} obs [µmol·h/l]	Pred/Obs AUC_{last}	C_{max} pred [µmol/l]	C_{max} obs [µmol/l]	Pred/Obs C_{max}	Dataset	Reference	Profile ID
422	po (sol), s.d.	19	**U**	2116.18	2060.98	1.03	55.92	50.13	1.12	te	Mattison 2006 [14]	56
500	po (sol), s.d.	11	**U**	7049.29	6374.09	1.11	134.55	110.26	1.22	ta	Van Staveren 2011 [15]	59
1000	po (sol), s.d.	11	**U**	25379.77	18832.97	1.35	300.80	166.50	1.81	te	Van Staveren 2011 [15]	60
	syn	40	**U**	136.44	123.97	1.10	0.11	0.10	1.10	ta	Jacobs 2016 [10]	92
422	po (sol), s.d.	19	**DHU**	1987.53	1881.78	1.06	16.02	15.86	1.01	te	Mattison 2006 [14]	56
500	po (sol), s.d.	11	**DHU**	3652.33	3190.62	1.14	30.63	24.19	1.27	ta	Van Staveren 2011 [15]	59
1000	po (sol), s.d.	11	**DHU**	7946.90	6808.32	1.17	52.67	42.47	1.24	ta	Van Staveren 2011 [15]	60
	syn	40	**DHU**	1154.69	1181.88	0.98	0.91	0.89	1.02	ta	Jacobs 2016 [10]	92
Pred/Obs within twofold (Range)					**100%; 8/8 (0.98–1.35)**			**100%; 8/8 (1.01–1.81)**				
GMFE (Range)					**1.12 (1.02–1.35)**			**1.20 (1.01–1.81)**				

AUC_{last}, area under the plasma concentration-time curve calculated from the first to the last measurement; **C_{max}**, maximum concentration; **DHU**, 5,6-dihydrouracil ; **GMFE**, geometric meand fold error; **obs**, observed; **po**, oral; **pred** predicted; **Route**, route of administration; **s.d.**, single dose; **sol**, solution; **syn**, endogenous synthesis; **te**, test dataset (model evaluation); **ta**, training dataset (parameter optimization); **U**, uracil.
[a], dose relative in mg/kg bodyweight

S2.4.5 Local sensitivity analysis

Figures S2.4.6 and S2.4.7 show the local sensitivity analysis of the AUC to single parameter changes of the compounds uracil and 5,6-dihydrouracil. Sensitivity of the model to single parameters was determined as change of the simulated AUC extrapolated to infinity from starting time of uracil synthesis or uracil application of 500 mg/m² as a single oral solution. A sensitivity value of -0.5 indicates a 5% decrease of the simulated AUC if the examined parameter is incraeased by 10%. Depending on whether uracil was synthesized or administered, fraction unbound (plasma) or the acidic dissociation constant were the most sensitive parameters for both the parent and the metabolite.

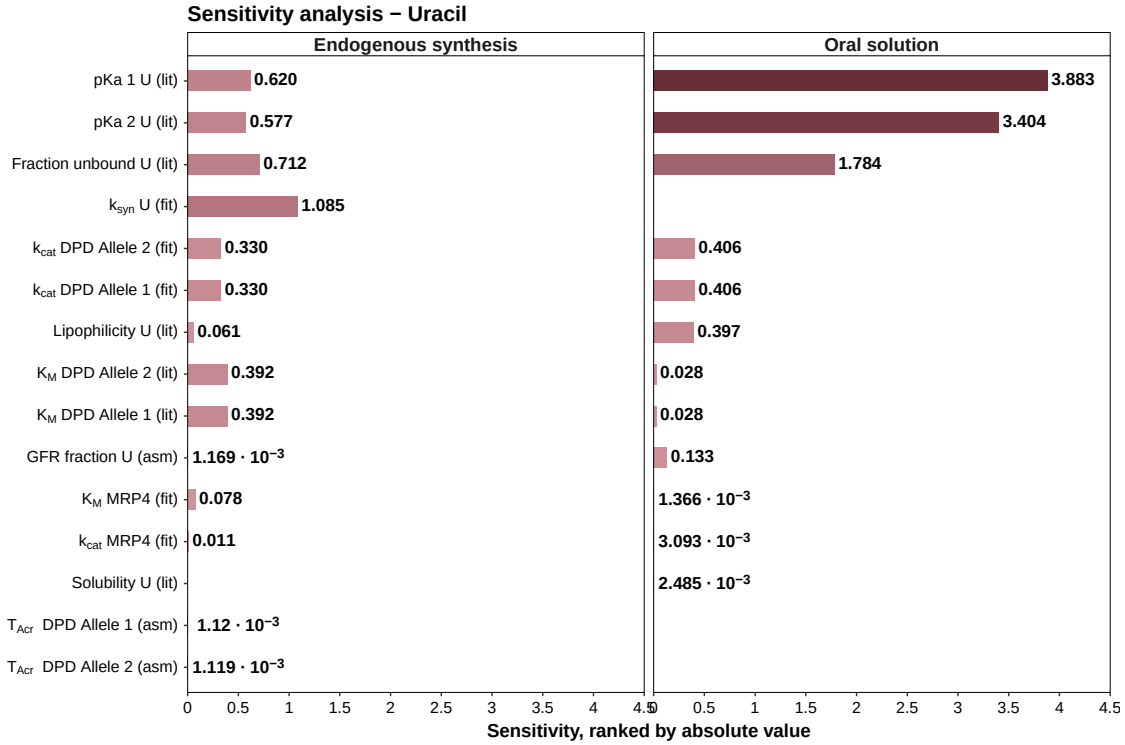

Figure S2.4.6: **Uracil PBPK model sensitivity analysis - Uracil.** **Amp**, amplitude; **asm**, assumed; **DPD**, dihydropyrimidine dehydrogenase; **fit**, fitted; **GFR**, glomerular filtration rate; $\mathbf{k_{cat}}$, catalytic rate constant; $\mathbf{K_M}$, Michaelis-Menten constant; $\mathbf{k_{syn}}$, synthesis constant; **MRP4**, multi drug resistence protein 4; **lit**, literature; **pKa**, acidic dissociation constant; $\mathbf{T_{Acr}}$, shift in time of maximum enzyme activity; **U**, uracil.

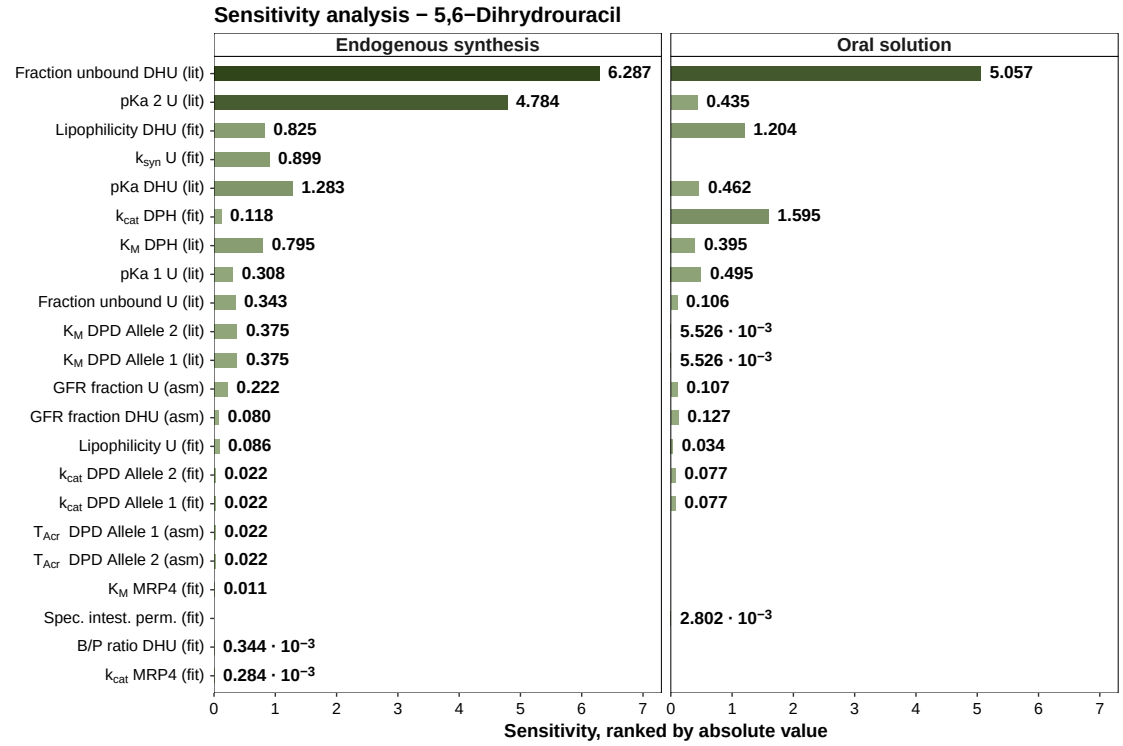

Figure S2.4.7: **Uracil PBPK model sensitivity analysis - 5,6-dihydrouracil.** **Amp**, amplitude; **asm**, assumed; **DHU**, 5,6-dihydrouracil; **DPD**, dihydropyrimidine dehydrogenase; **DPH**, dihydropyrimidinase; **fit**, fitted; **GFR**, glomerular filtration rate; $\mathbf{k_{cat}}$, catalytic rate constant; $\mathbf{K_M}$, Michaelis-Menten constant; $\mathbf{k_{syn}}$, synthesis constant; **MRP4**, multi drug resistence protein 4; **lit**, literature; **pKa**, acidic dissociation constant; $\mathbf{T_{Acr}}$, shift in time of maximum enzyme activity; **U**, uracil.

S2.5 Individual prediction of DHU/U with *IVIVE*

As described in Section S1.4.2, parameters were estimated for individual data (listed in Table S2.3).

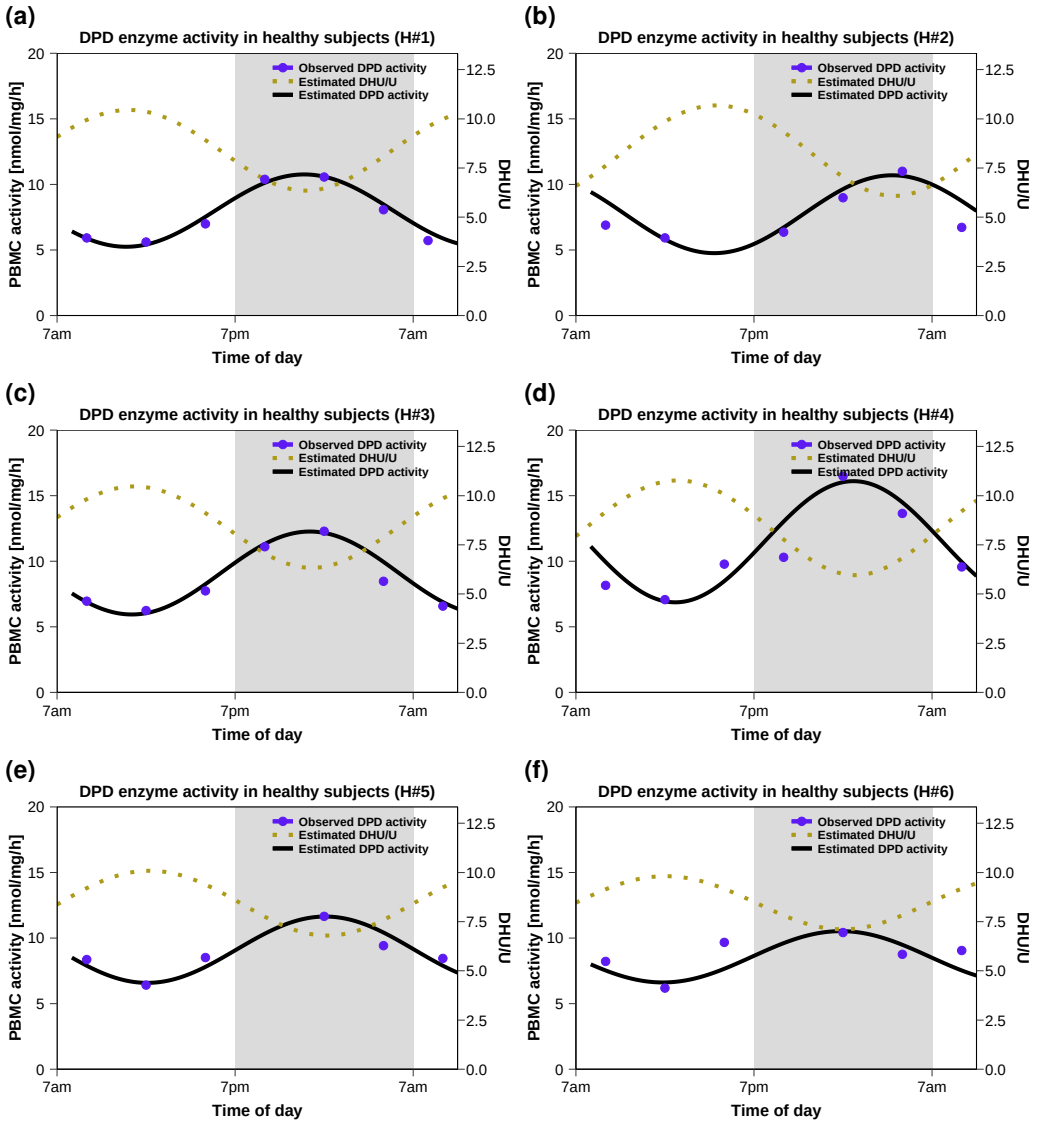

Figure S2.5.8: **DPD activities in PBMC cells and DHU/U ratios in plasma** for healthy individuals on a linear scale. The shaded areas illustrate night time. **DHU/U**, dihydrouracil-to-uracil plasma concentration ratio; **DPD**, dihydropyrimidine dehydrogenase, **PBMC**, peripheral blood mononuclear cell.

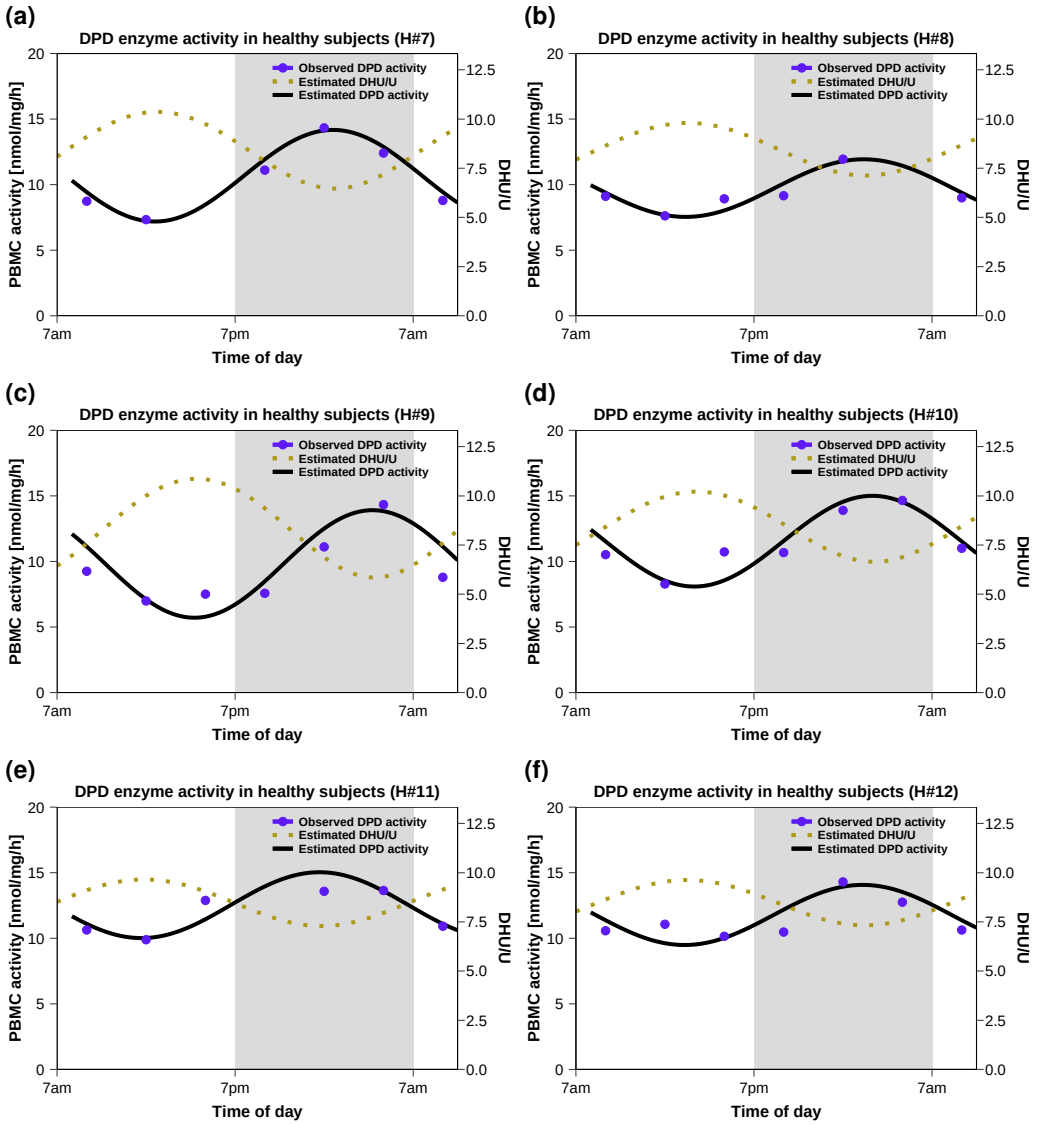

Figure S2.5.9: **DPD activities in PBMC cells and DHU/U ratios in plasma** for healthy individuals on a linear scale. The shaded areas illustrate night time. **DHU/U**, dihydrouracil-to-uracil plasma concentration ratio; **DPD**, dihydropyrimidine dehydrogenase, **PBMC**, peripheral blood mononuclear cell.

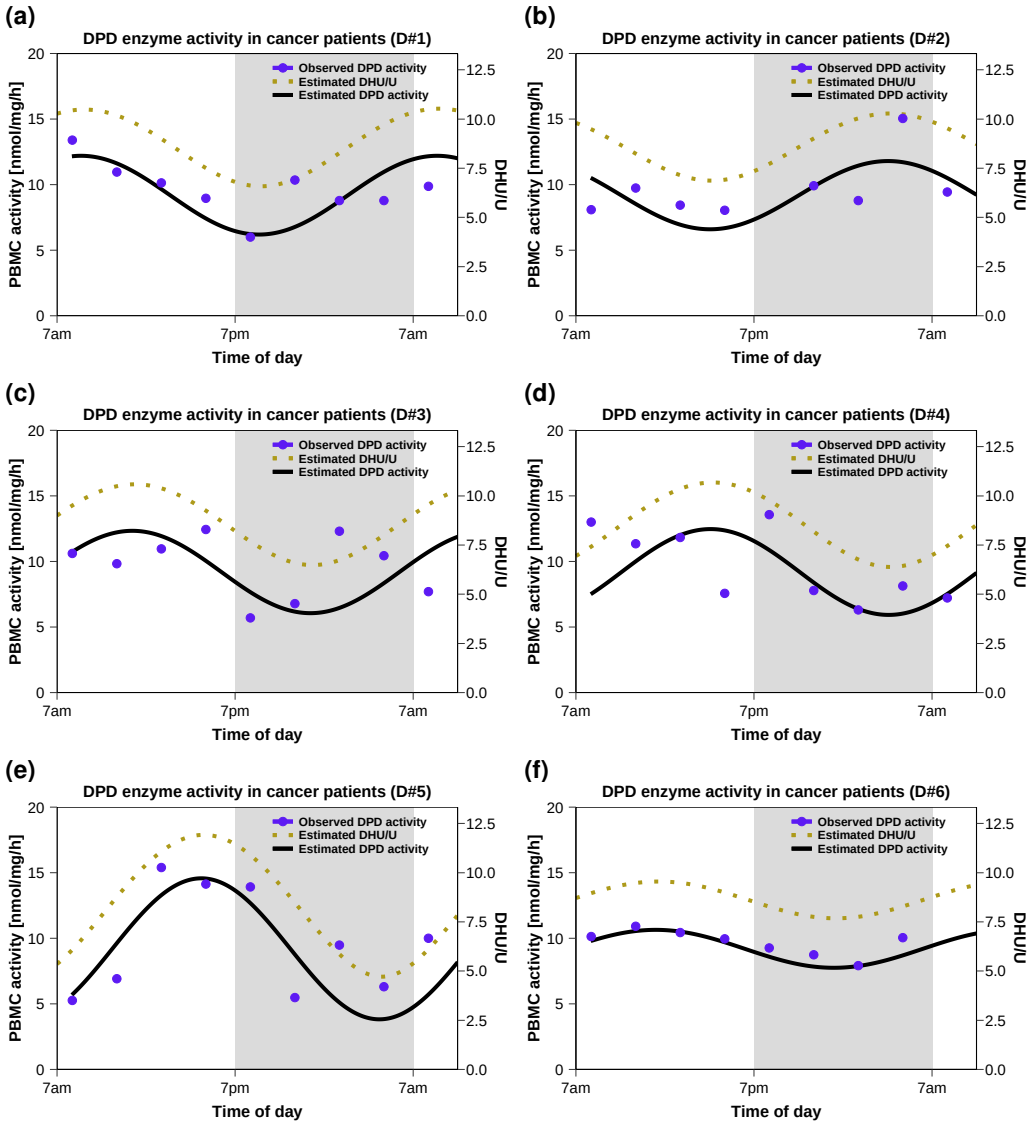

Figure S2.5.10: **DPD activities in PBMC cells and DHU/U ratios in plasma** for cancer patients on a linear scale. The shaded areas illustrate night time. DPD activities were estimated from relative *DPYD* mRNA expressions [12] as described in Section S1.4.2. **DHU/U**, dihydrouracil-to-uracil plasma concentration ratio; **DPD**, dihydropyrimidine dehydrogenase, **PBMC**, peripheral blood mononuclear cell.

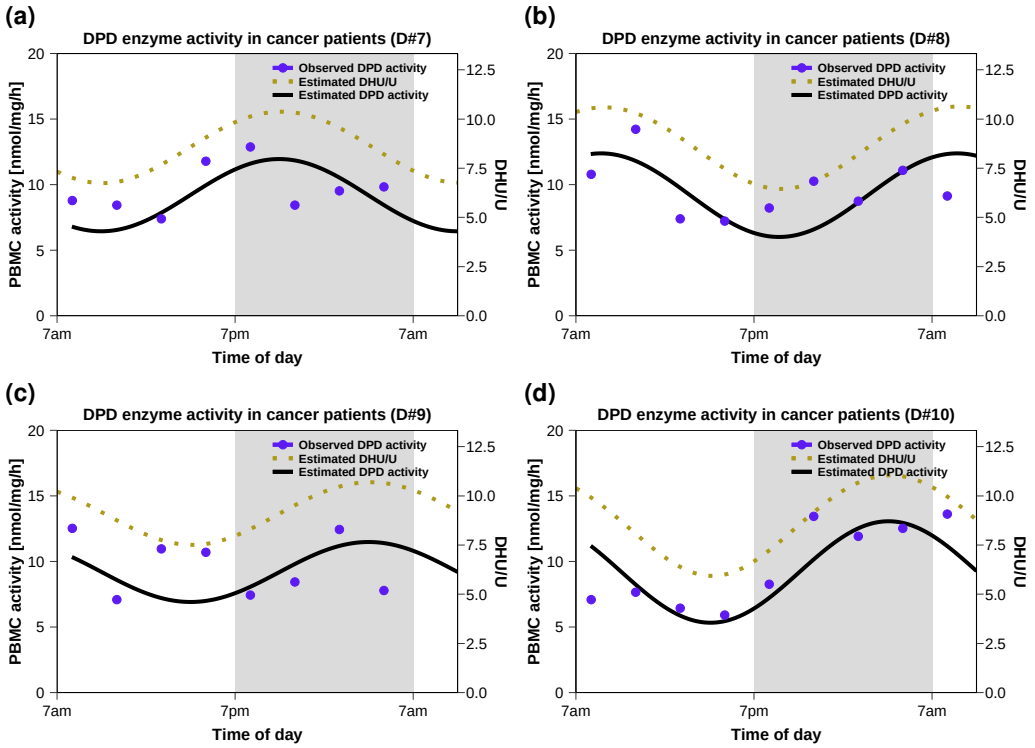

Figure S2.5.11: **DPD activities in PBMC cells and DHU/U ratios in plasma** for cancer patients on a linear scale. The shaded areas illustrate night time. DPD activities were estimated from relative *DPYD* mRNA expressions [12] as described in Section S1.4.2. **DHU**/**U**, dihydrouracil-to-uracil plasma concentration ratio; **DPD**, dihydropyrimidine dehydrogenase, **PBMC**, peripheral blood mononuclear cell.

S3 5-Fluorouracil model development

S3.1 Clinical studies

Table S3.1: Clinical studies used for 5-fluorouracil model development

Dose absolute [mg]	Dose [mg/m²]	Route	n	Age [years]	Weight [kg]	BSA [m²]	Females [%]	Dataset	Reference
250	-	iv (bol), s.d.	5	50.8 (40–61)	68.6 (55–77)	-	100	ta	Phillips 1980 [22]
427.5	250	iv (bol), s.d.	20	[m]66 (41–75)	-	[m]1.71	30	te	Bocci 2000 [23]
425	250	iv (bol), s.d.	188	[m]65 (37–85)	[m]66.5 (41–107)	[m]1.7 (1.35–2.8)	46.3	te	Bocci 2006 [24]
-	300	iv (bol), s.d.	8	-	-	-	-	ta	Van Kuilenburg 2008 [25]
632.7	370	iv (bol), s.d.	20	[m]66 (41–75)	-	[m]1.71	30	ta	Bocci 2000 [23]
684.5	370	iv (bol), s.d.	110	[m]61 (36–79)	-	-	43.6	te	Paolo 2001 [26]
600	400	iv (bol), s.d.	18	[m]58.5 (40–71)	[m]57.5 (48–85)	[m]1.5	39	te	Casale 2004 [27]
-	425	iv (bol), s.d.	6	-	-	-	33	te	Maring 2002 [28]
-	425	iv (bol), s.d.	18	[m]66 (45–80)	[m]73 (56–85)	-	28	ta	Maring 2003 [29]
850.2	[a]10.9	iv (bol), s.d.	8	56 (36–72)	78 (65–115)	-	25	te	MacMillan 1978 [30]
-	450	iv (bol), s.d.	8	-	-	-	-	te	Van Kuilenburg 2008 [25]
-	500	iv (bol), s.d.	14	70	-	-	43	te	Larsson 1996 [31]
-	500	iv (bol), s.d.	10	27-63	-	-	30	te	Heggie 1987 [32]
-	[a]15	iv (bol), s.d.	17	-	-	-	-	ta	Harvey 1984 [33]
-	600	iv (bol), s.d.	10	-	-	-	-	te	Bardakji 1986 [34]
500	-	po (sol), s.d.	6	55.3 (50–62)	68.3 (55–90)	-	100	ta	Phillips 1980 [22]
-	[a]15	po (sol), s.d.	17	-	-	-	-	te	Harvey 1984 [33]
-	[a]7.5	iv (inf), 0.4h	6	40–64	48.6–82.4	-	33	te	Schaaf 1987 [35]
-	425	iv (inf), 0.25h	12	47–78	-	-	25	te	Hoekstra 2005 [36]
-	[a]15	iv (inf), 0.4h	6	40–64	48.6–82.4	-	33	ta	Schaaf 1987 [35]
-	1250	iv (inf) 96h	10	62 (45–75)	-	-	-	te	Ho 1998 [37]
-	1250	iv (inf) 96h	10	-	-	-	-	te	Yamada 2003 [9]
1080	600	iv (inf) 24h	4	[m]36 (34–47)	-	[m]1.8 (1.7–2.0)	0	te	Metzger 1994 [38]
-	1071	iv (inf) 24h	7	58-81	30–65	1.1–1.8	14	te	Petit 1988 [39]
-	1750	iv (inf) 72h	27	[m]50 (37–78)	-	-	22	te	Grem 2001 [40]
-	1750	iv (inf) 72h	14	[m]46 (28–71)	-	-	21	ta	Takimoto 1999 [41]
-	300	iv (inf) 10h	3	56.8 (35–68)	-	-	33	te	Furuya 1995 [42]
-	300	iv (inf) 10h	6	56.8 (35–68)	-	-	50	te	Furuya 1995 [42]
-	4000	iv (inf) 96h	10	58.2 (48–75)	-	1.66 (1.36–1.97)	0	te	Thiberville 1994 [43]
-	2400	iv (inf) 46h	9	56 (36–74)	-	-	33	te	Matsumoto 2015 [44]
-	400	iv (bol), LD	33	[m]61 (34–76)	-	-	27	te	Eatock 2005 [45]
	600	iv (inf) 22h, MD							
760	400	iv (bol), LD	9	[m]68 (54–73)	-	[m]1.9 (1.4–2.0)	11	te	Joel 2004 [46]

Table S3.1: Clinical studies used for 5-FU model development (continued)

Dose absolute [mg]	Dose [mg/m²]	Route	n	Age [years]	Weight [kg]	BSA [m²]	Females [%]	Dataset	Reference
1140	600	iv (inf) 22h, MD							
-	400	iv (bol), LD	18	^{m}62 (43–77)	^{m}71 (43–107)	-	29	te	Joulia 1999 [47]
	600	iv (inf) 22h, MD							
-	400	iv (bol), LD	6	^{m}62 (43–77)	^{m}71 (43–107)	-	29	te	Joulia 1999 [47]
	900	iv (inf) 22h, MD							
-	400	iv (bol), LD	8	^{m}62 (43–77)	^{m}71 (43–107)	-	29	te	Joulia 1999 [47]
	1200	iv (inf) 22h, MD							
-	600	iv (inf) 0.5h, LD	5	^{m}67 (57–76)	-	-	80	ta	Wattanatorn 1997 [8]
	600	iv (inf) 22h, MD							
720	400	iv (bol), LD	10	^{m}65 (54–77)	-	^{m}1.8 (1.6–2.1)	20	te	Joel 2004 [46]
4320	2400	iv (inf) 46h, MD							
-	400	iv (bol), LD	53	^{m}60.5 (41–80)	-	-	36	te	Leong 2012 [48]
	2400	iv (inf) 46h, MD							
-	400	iv (bol), LD	16	^{m}59.5 (39–80)	-	-	38	te	Sharma 2010 [49]
	2400	iv (inf) 46h, MD							

bol, bolus injection; **BSA**, body surface area; **inf**, infusion; **iv**, intravenous; **LD**, loading dose; **MD**, multiple dose; **n**, number of individuals studied; **po**, oral; **Route**, route of administration; **s.d.**, single dose; **sol**, solution; **ta**, training dataset (parameter optimization); **te**, test dataset (model evaluation); **-**, no data available. Values are means ±standard deviation or ranges.
^{a}, dose relative in mg/kg bodyweight
^{m}, median

S3.2 Drug-dependent model parameters

Table S3.2: Drug-dependent parameters of the 5-fluorouracil PBPK model

Parameter	Unit	Value	Source	Reference	Value	Source	Reference	Description
		5-fluorouracil			**5,6-dihydrofluorouracil**			
MW	g/mol	130.08	130.08	[50]	132.09	132.09	[51]	Molecular weight
pKa	-	(acidic) 8.02	(acidic) 8.02	[50]	(acidic) 10.66	(acidic) 10.66	[51]	Acid dissociation constant
Solubility (pH)	mg/ml	40 (7)	40 (7)	[52]	89.47 (7.4)	89.47 (7.4)	[51]	Solubility
logP	-	[a]-1.40	-0.78	[52]	[a]-0.06	-1	[51]	Lipophilicity
fu	%	90	90	[53]	[b]100	-	-	Fraction unbound
Specific intest. perm.	cm/min	[c]$8.46 \cdot 10^{-4}$	[d]$3.65 \cdot 10^{-7}$	-	$7.37 \cdot 10^{-6}$	calc.	-	Normalized to surface are
Specific organ perm.	cm/min	[d]$5.48 \cdot 10^{-4}$	[d]$5.48 \cdot 10^{-4}$	-	[d]0.01	[d]0.01	-	Normalized to surface are
GFR fraction	-	[e]1	-	-	[e]1	-	-	Fraction of filtered drug in urine
Cellular permeabilities	-	Ch. d. S.	-	[18]	Ch. d. S.	-	[18]	Permeation across cell membranes
Partition coefficients	-	R&R	-	[19]	Berez.	-	[20]	Organ-plasma partition coefficients
Formulation	-	[c]dissolved	-	-	-	-		Formulation used in predictions
MRP4 K_M	µmol/l	[a]16.77	-	-	-	-	-	Michaelis-Menten constant
MRP4 k_{cat}	1/min	[a]27.66	-	-	-	-	-	MRP4 catalytic rate constant
DPD K_M	µmol/l	23.0	23	-	-	-	[54]	Michaelis-Menten constant
DPD k_{cat}	1/min	[a] 11.34	-	-	-	-	-	DPD catalytic rate constant
DPH K_M	µmol/l	-	-	-	21.61	21.61	[21]	Michaelis-Menten constant
DPH k_{cat}	1/min	-	-	-	[a]47.60	-	-	DPH catalytic rate constant

Berez., Berezhkovskiy calculation method; **calc.**, calculated; **Ch. d. S.**, Charge dependent Schmitt calculation method; **DPD**, dihydropyrimidine dehydrogenase; **DPH**, dihydropyrimidinase; **GFR**, glomerular filtration rate; **intest. perm.**, intestinal permeability; **MRP4**, multi drug resistence protein 4; **organ perm.**, organ permeability; **R&R**, Rodgers and Rowland calculation method; **-**, not available.

[a], optimized

[b], assumed as no data on binding was found

[c], only used for oral solutions

[d], calculated value

[e], assumed

S3.2.1 Diurnal DPD activity

Table S3.3 lists all parameters used to predict the dirunal variations in DPD activity in studies during 5-fluorouracil infusion at a constant rate. In most cases, the amplitude derived from the literature was sufficient to predict the oscillation of the plasma concentration curve. T_{Acr} had to be adapted individually. Parameters used for the prediction of 5-fluorouracil in individual healthy subjects or cancer patients are listed in Table S2.3 with the respective DPD activities illustrated in Figures S2.5.8-S2.5.11.

Table S3.3: Diurnal parameters of the 5-fluorouracil PBPK model for time-of-day variation in DPD activity.

Study (ID)	Amplitude (DPD)	T_{Acr} (DPD) [min]	Reference
Ho 1998 (70)	[a]0.245	94.33	Ho 1998 [37]
Yamada 2003 (82)	[a]0.245	136.13	Shimida 2003 [9]
Metzger 1994 (77)	0.84	71.43	Metzger 1994 [38]
Petit 1988 (78)	0.56	0.74	Petit 1988 [39]
Grem 2001 (86)	[b]0.124	1218.52	Grem 2001 [40]
Takimoto 1999 (80)	[b]0.124	1285	Takimoto 1999 [41]
Furuya 1995 (141)	[b]0.245	720	Furuya 1995 [42]
Furuya 1995 (141)	[b]0.124	451.83	Furuya 1995 [42]
Thiberville 1994 (130)	0.39	256.24	Thiberville 1994 [43]
Matsumoto 2015 (131)	0.18	0	Matsumoto 2015 [44]
Matsumoto 2015 (132)	0.42	5.64	Matsumoto 2015 [44]
Matsumoto 2015 (133)	[b]0.124	0	Matsumoto 2015 [44]
Matsumoto 2015 (134)	0.40	720	Matsumoto 2015 [44]
Matsumoto 2015 (135)	[a]0.245	237.54	Matsumoto 2015 [44]
Matsumoto 2015 (136)	[a]0.245	1236.83	Matsumoto 2015 [44]
Matsumoto 2015 (137)	[a]0.245	100	Matsumoto 2015 [44]
Matsumoto 2015 (138)	0.17	2.94	Matsumoto 2015 [44]
Matsumoto 2015 (139)	[b]0.124	0	Matsumoto 2015 [44]
Eatock 2005 (68)	[a]0.245	729.33	Eatock 2005 [45]
Joel 2004 (71)	[a]0.245	1291.44	Joel 2004 [46]
Joulia 1999 (73)	[a]0.245	34.31	Joulia 1999 [47]
Joulia 1999 (74)	[a]0.245	4.77	Joulia 1999 [47]
Joulia 1999 (75)	[a]0.245	97.34	Joulia 1999 [47]
Wattanatorn 1997 (81)	[a]0.245	1247.85	Wattanatorn 1997 [8]
Joel 2004 (72)	[a]0.245	1277.22	Joel 2004 [46]
Leong 2012 (76)	[a]0.245	702.68	Leong 2012 [48]
Sharma 2010 (79)	[a]0.245	120	Sharma 2010 [49]

DPD, dihydropyrimidine dehydrogenase; **T_{Acr}**, shift in time of maximum enzyme activity.
[a], Mean amplitude of DPD activity measured in human preipheral blood mononclear cells derived from Jacobs et al. 2016 [10]
[b], Mean amplitude of DPD activity measured in human preipheral blood mononclear cells derived from Jiang et al. 2004 [11]

S3.3 Concentration-time profiles

Model predictions are shown as solid lines and corresponding observed data as filled dots. Symbols represent the mean values ± sd, if available. For continuous infusions where daily fluctuations are visible, day and night time were visualized with white and shaded areas, if the respective study listed a specific clock time in which the infusion was started. Here, a day and night cycle from 7 am to 7 pm was assumed.

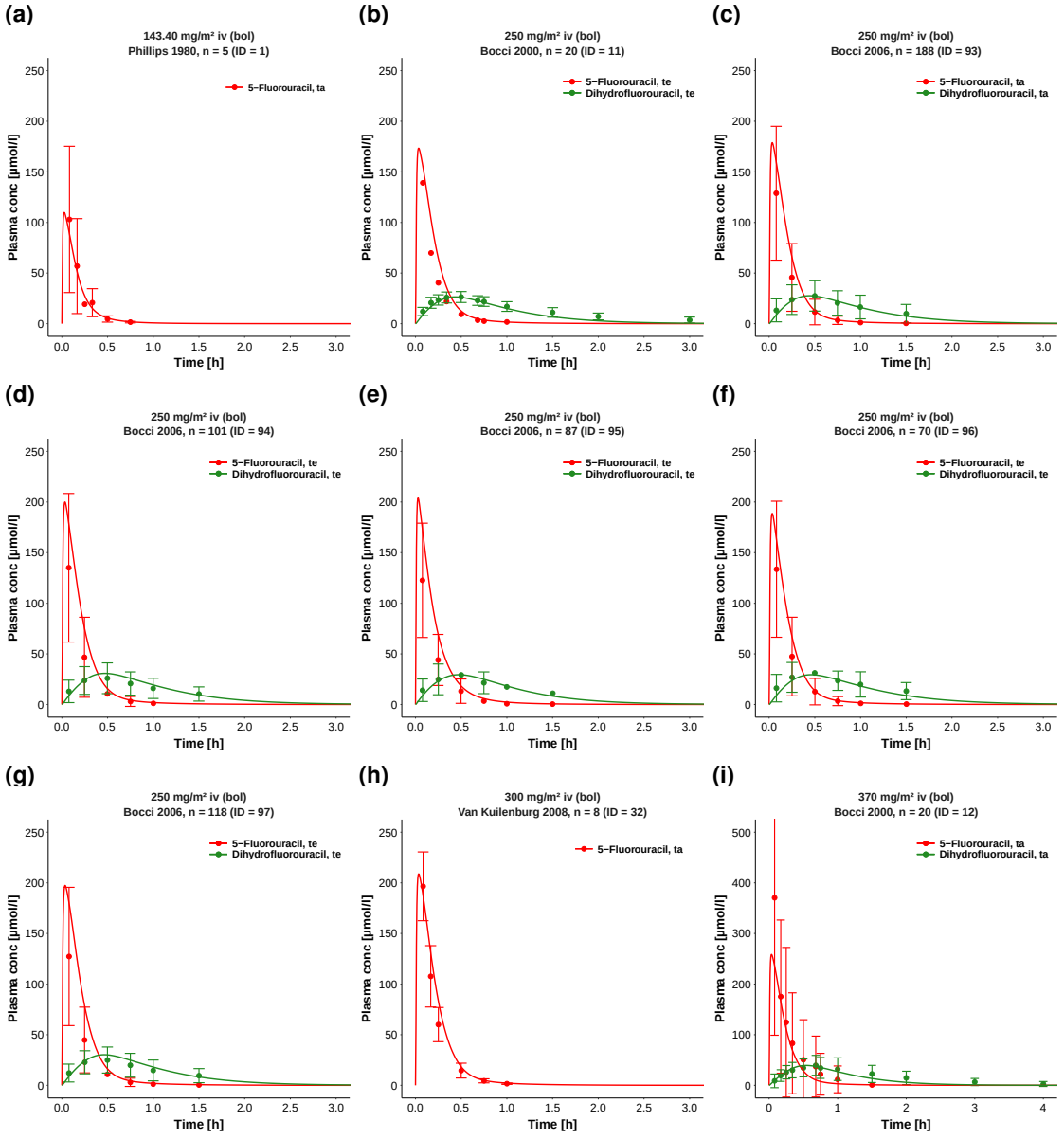

Figure S3.3.1: **Plasma 5-fluorouracil and 5,6-dihydrouracil after intravenous administration of 5-fluorouracil (part 1/10)** on a linear scale. **bol**, bolus injection; **iv**, intravenous; **n**, number of individuals; **ta**, training dataset; **te**, test dataset.

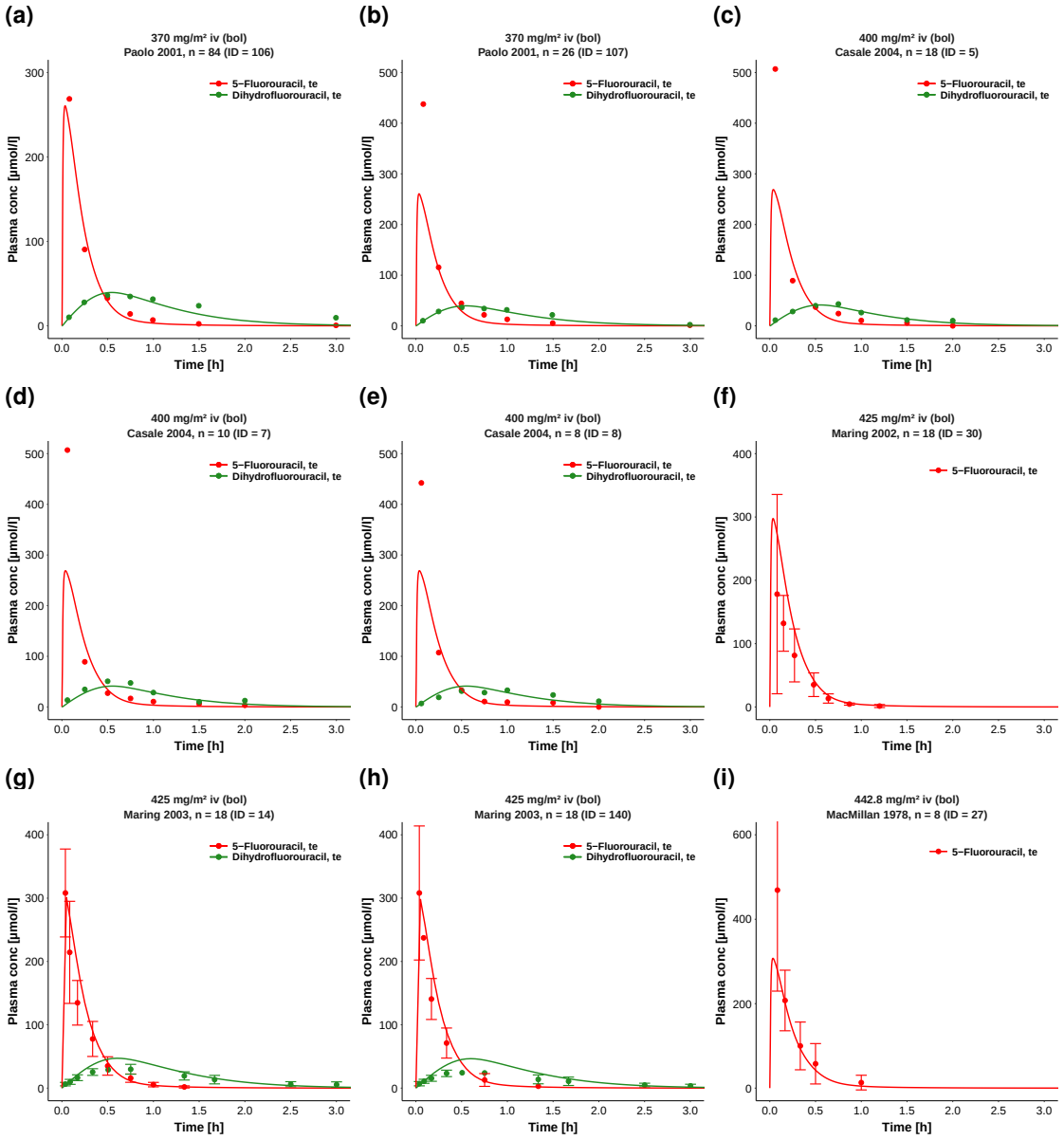

Figure S3.3.2: **Plasma 5-fluorouracil and 5,6-dihydrouracil after intravenous administration of 5-fluorouracil (part 2/10)** on a linear scale. **bol**, bolus injection; **iv**, intravenous; **n**, number of individuals **te**, test dataset.

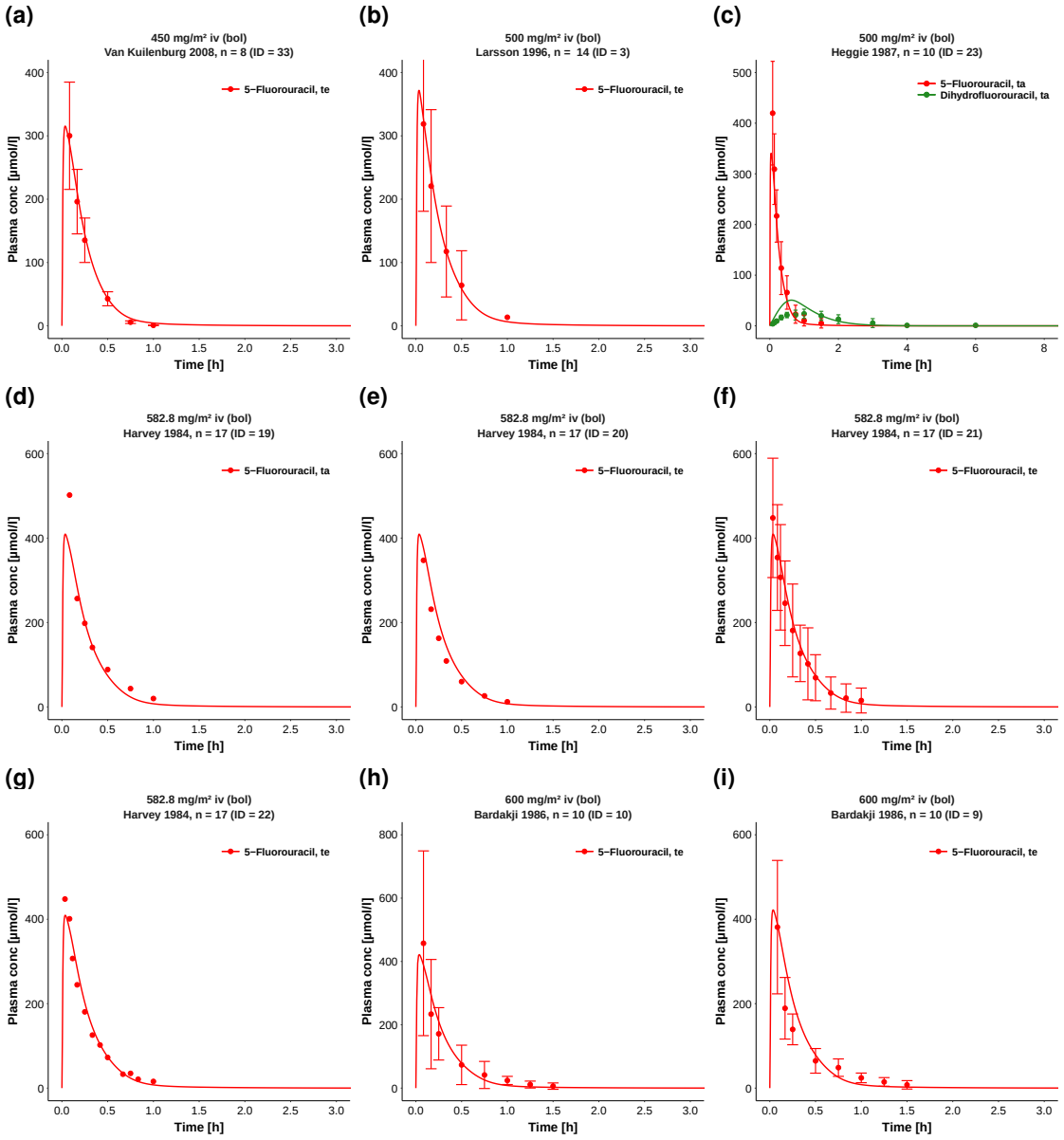

Figure S3.3.3: **Plasma 5-fluorouracil and 5,6-dihydrouracil after intravenous administration of 5-fluorouracil (part 3/10)** on a linear scale. **bol**, bolus injection; **iv**, intravenous; **n**, number of individuals; **ta**, training dataset; **te**, test dataset.

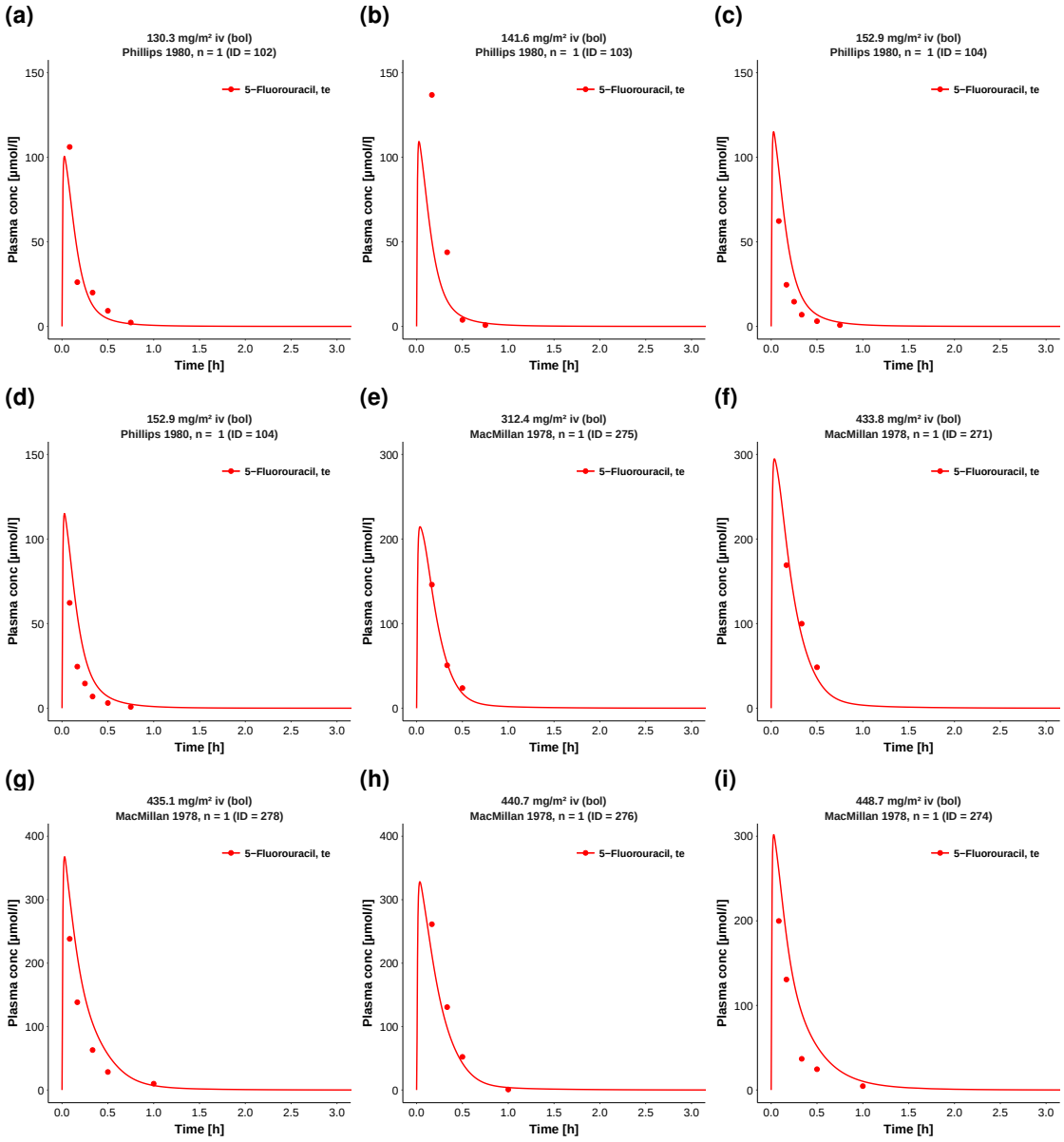

Figure S3.3.4: **Plasma 5-fluorouracil after intravenous administration of 5-fluorouracil (part 4/10)** on a linear scale. **bol**, bolus injection; **iv**, intravenous; **n**, number of individuals; **te**, test dataset.

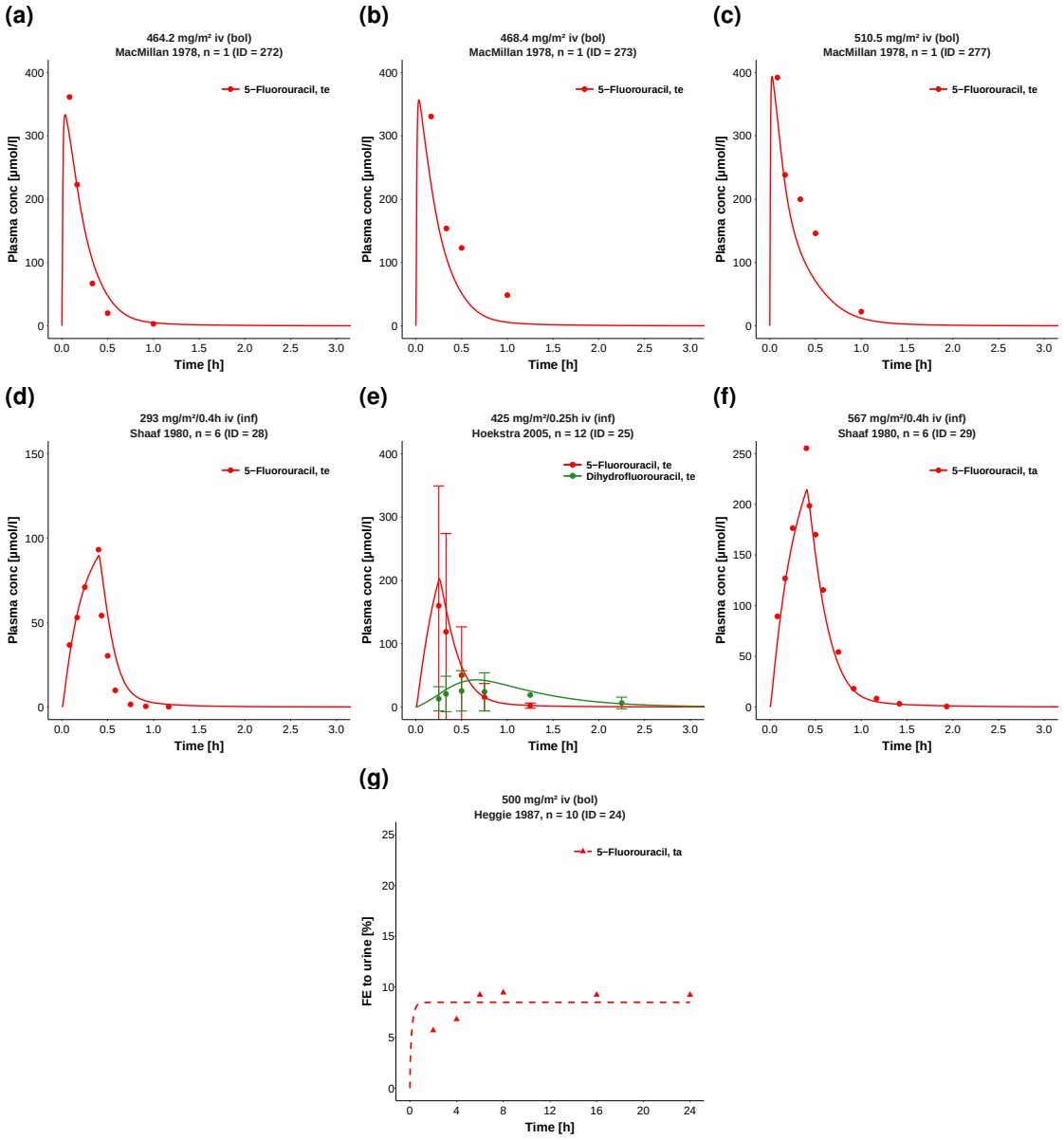

Figure S3.3.5: **Plasma and urine 5-fluorouracil and 5,6-dihydrouracil after intravenous administration of 5-fluorouracil (part 5/10)** on a linear scale. **bol**, bolus injection; **FE**, fraction of dose excreted; **inf**, infusion; **iv**, intravenous; **n**, number of individuals; **ta**, training dataset; **te**, test dataset.

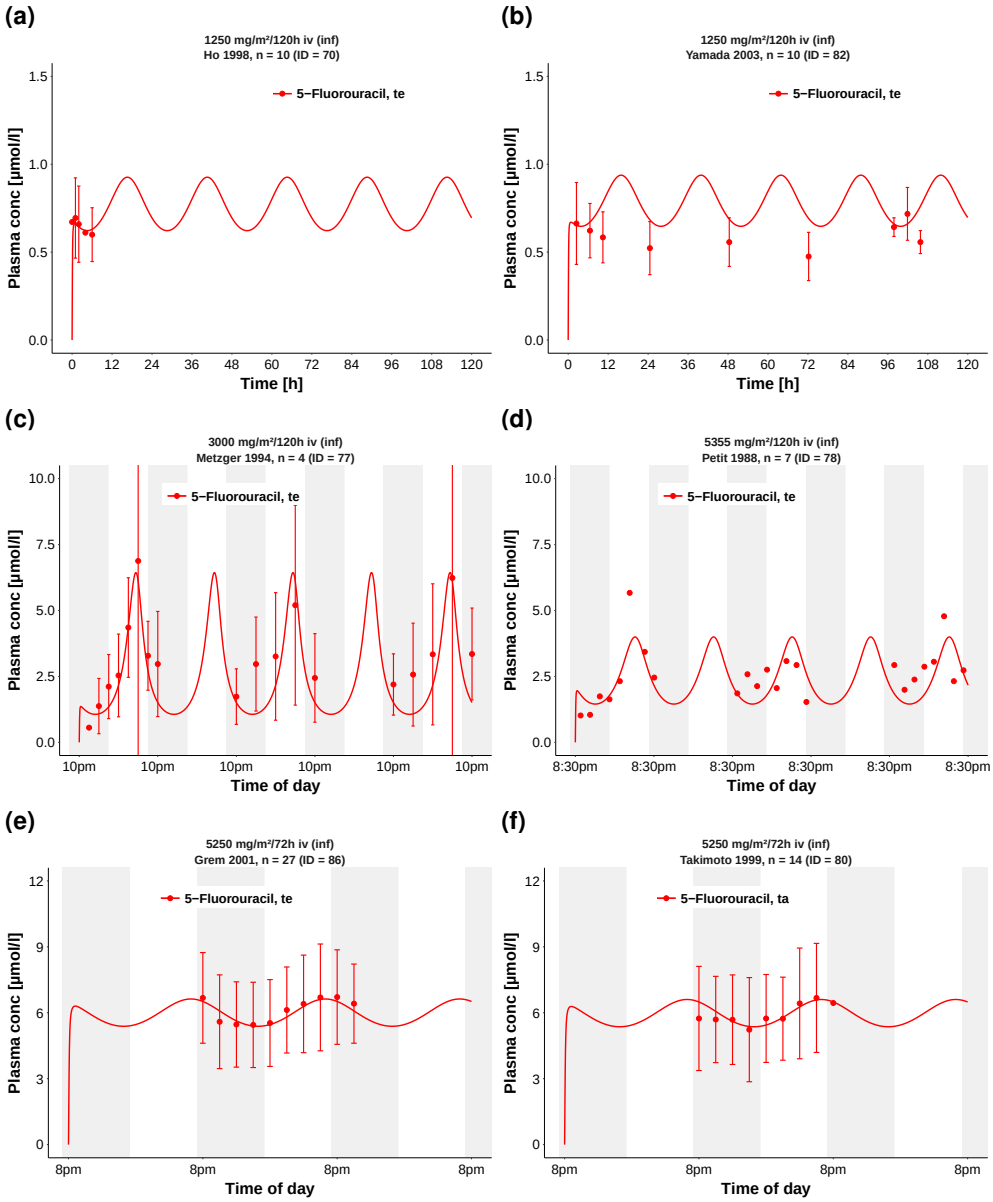

Figure S3.3.6: **Plasma 5-fluorouracil during intravenous administration of 5-fluorouracil (part 6/10)** on a linear scale. The shaded areas illustrate night time. **inf**, infusion; **iv**, intravenous; **n**, number of individuals; **ta**, training dataset; **te**, test dataset.

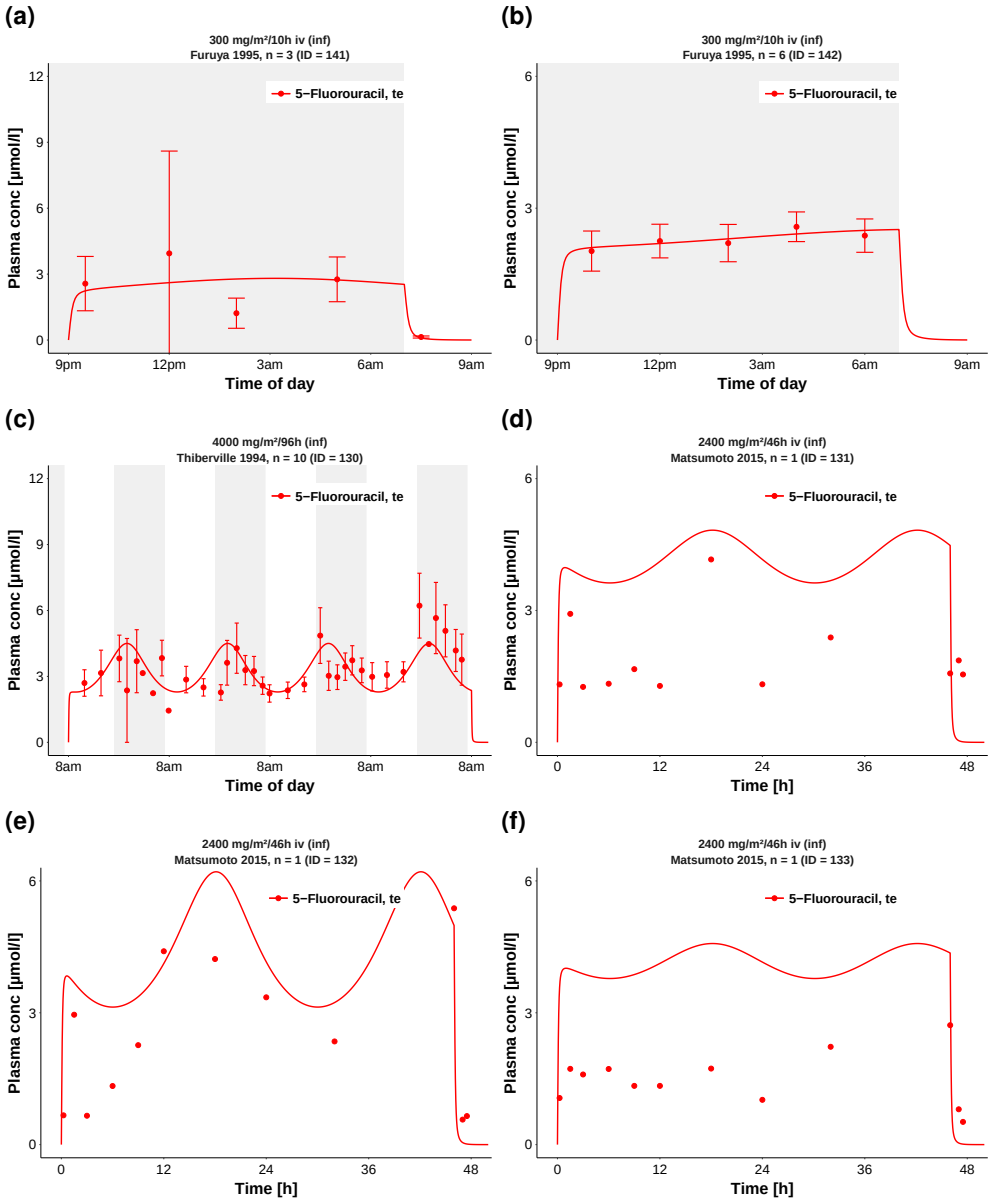

Figure S3.3.7: **Plasma 5-fluorouracil during intravenous administration of 5-fluorouracil (part 7/10)** on a linear scale. The shaded areas illustrate night time.**inf**, infusion; **iv**, intravenous; **n**, number of individuals; **te**, test dataset.

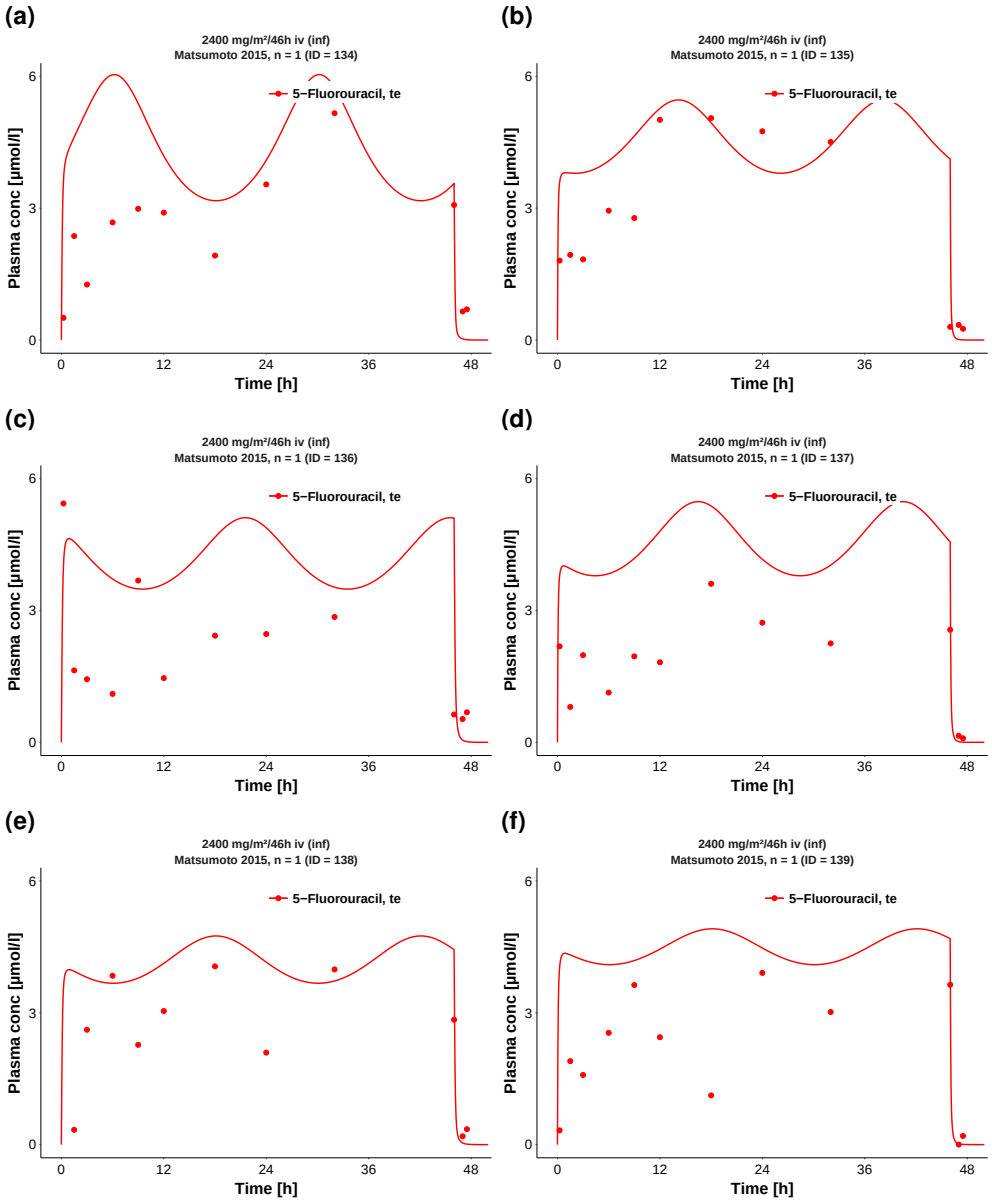

Figure S3.3.8: **Plasma 5-fluorouracil during intravenous administration of 5-fluorouracil (part 8/10)** on a linear scale. **inf**, infusion; **iv**, intravenous; **n**, number of individuals; **ta**, training dataset; **te**, test dataset.

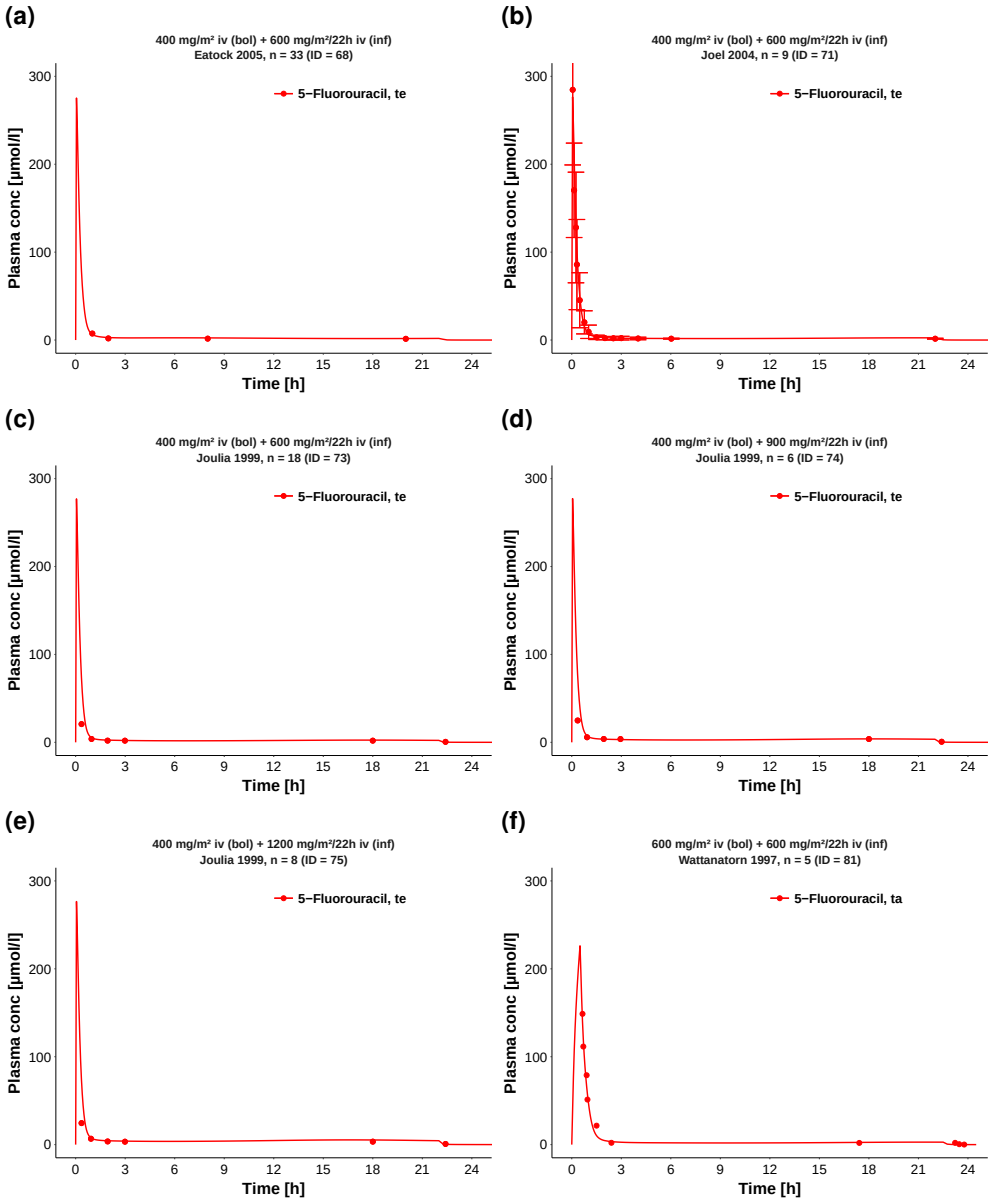

Figure S3.3.9: **Plasma 5-fluorouracil during intravenous administration of 5-fluorouracil (part 9/10)** on a linear scale. **bol**, bolus injection; **inf**, infusion; **iv**, intravenous; **n**, number of individuals; **ta**, training dataset; **te**, test dataset.

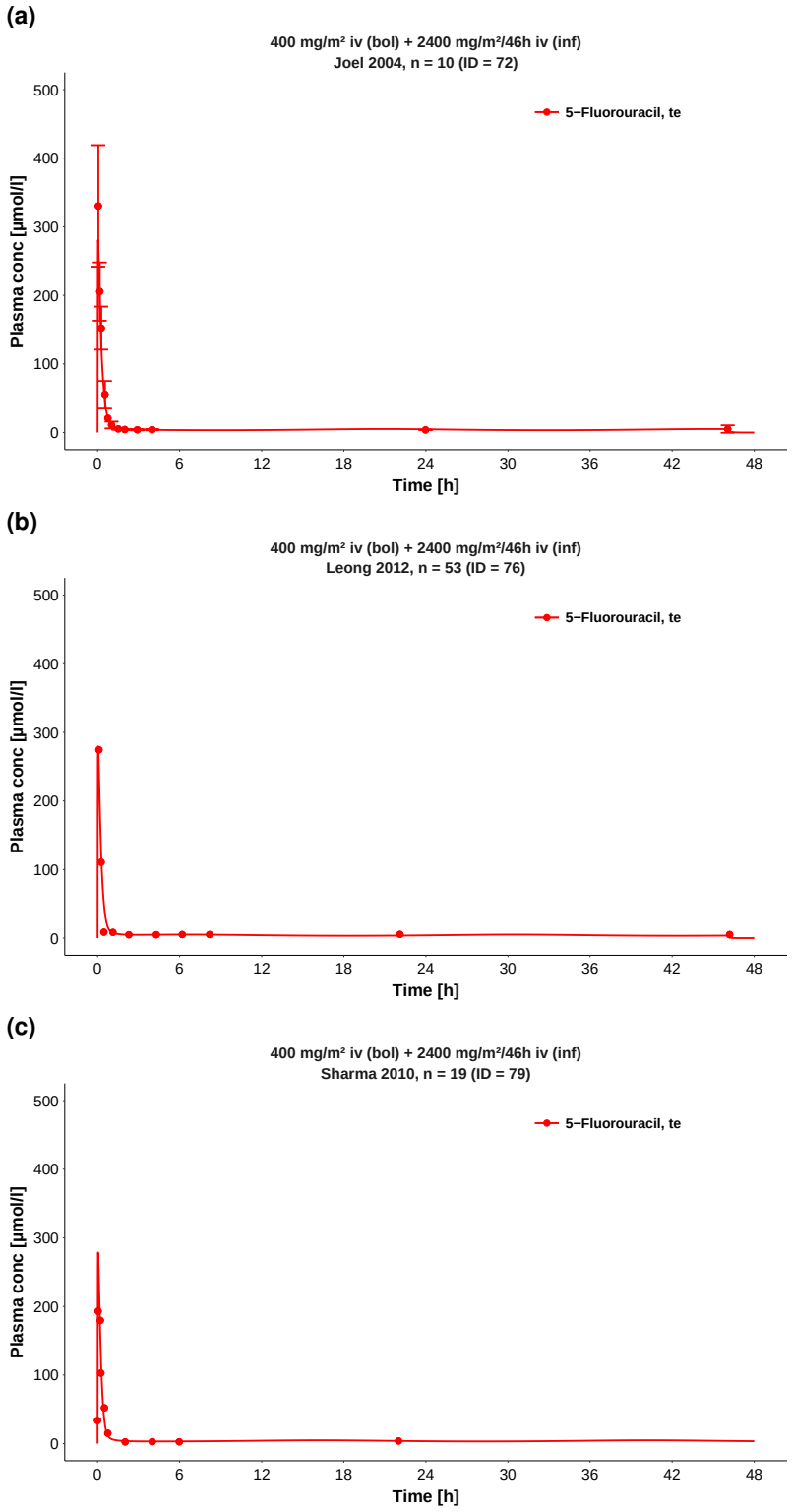

Figure S3.3.10: **Plasma 5-fluorouracil during intravenous administration of 5-fluorouracil (part 10/10)** on a linear scale. **inf**, infusion; **iv**, intravenous; **n**, number of individuals; **te**, test dataset.

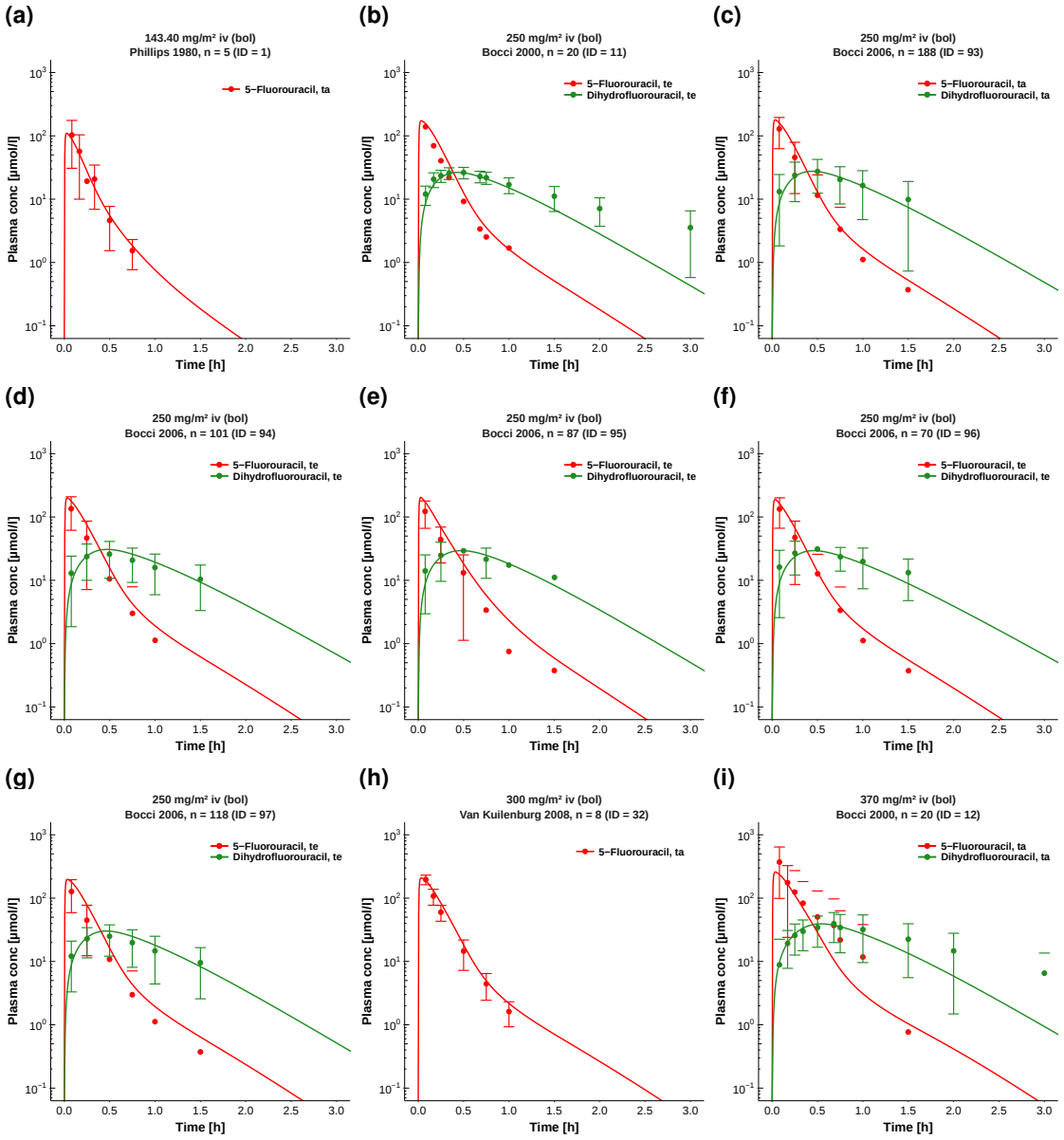

Figure S3.3.11: **Plasma 5-fluorouracil and 5,6-dihydrouracil after intravenous administration of 5-fluorouracil (part 1/10)** on a semi-logarithmic scale. **bol**, bolus injection; **iv**, intravenous; **n**, number of individuals; **ta**, training dataset; **te**, test dataset.

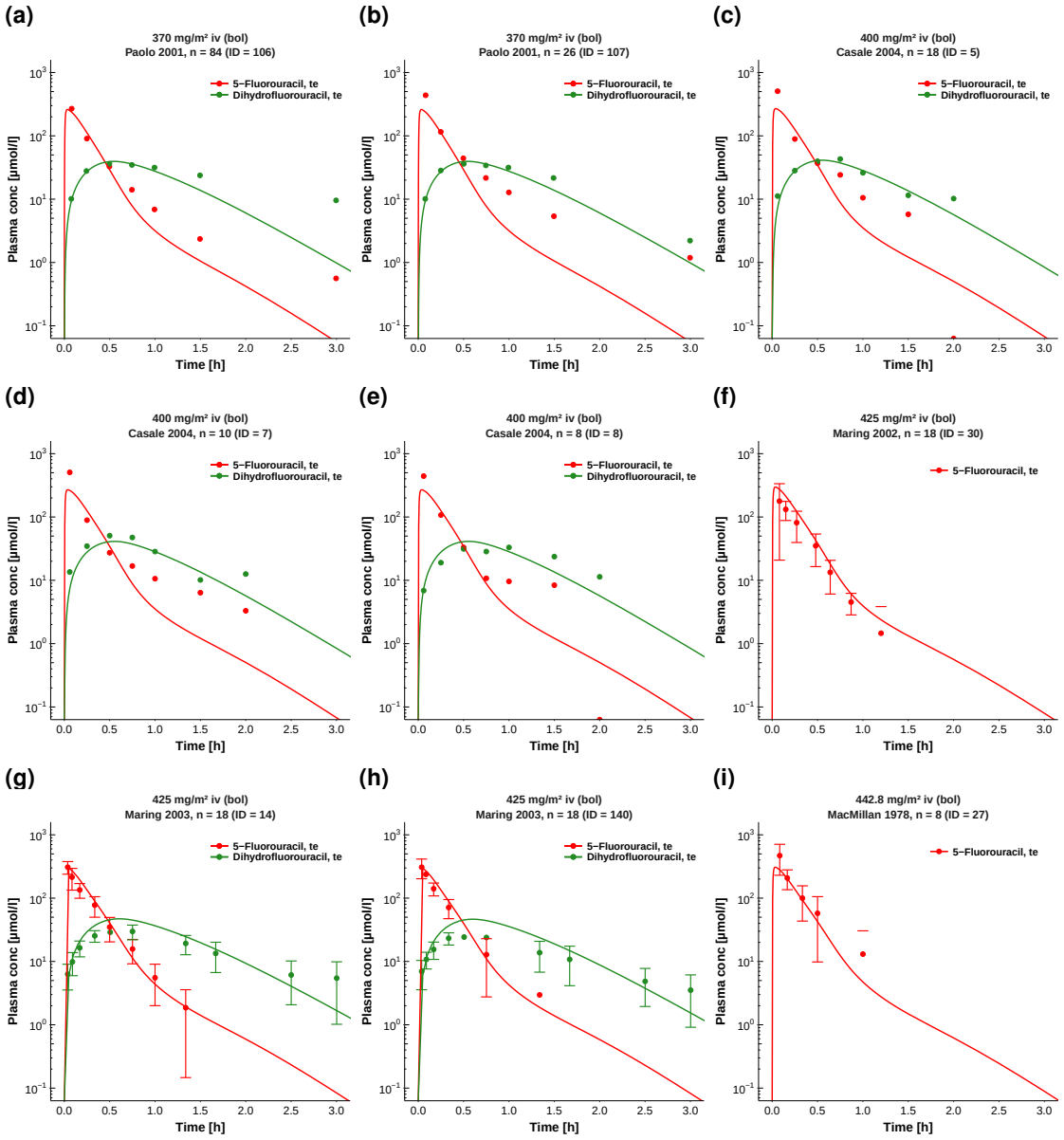

Figure S3.3.12: **Plasma 5-fluorouracil and 5,6-dihydrouracil after intravenous administration of 5-fluorouracil (part 2/10)** on a semi-logarithmic scale. **bol**, bolus injection; **iv**, intravenous; **n**, number of individuals; **te**, test dataset.

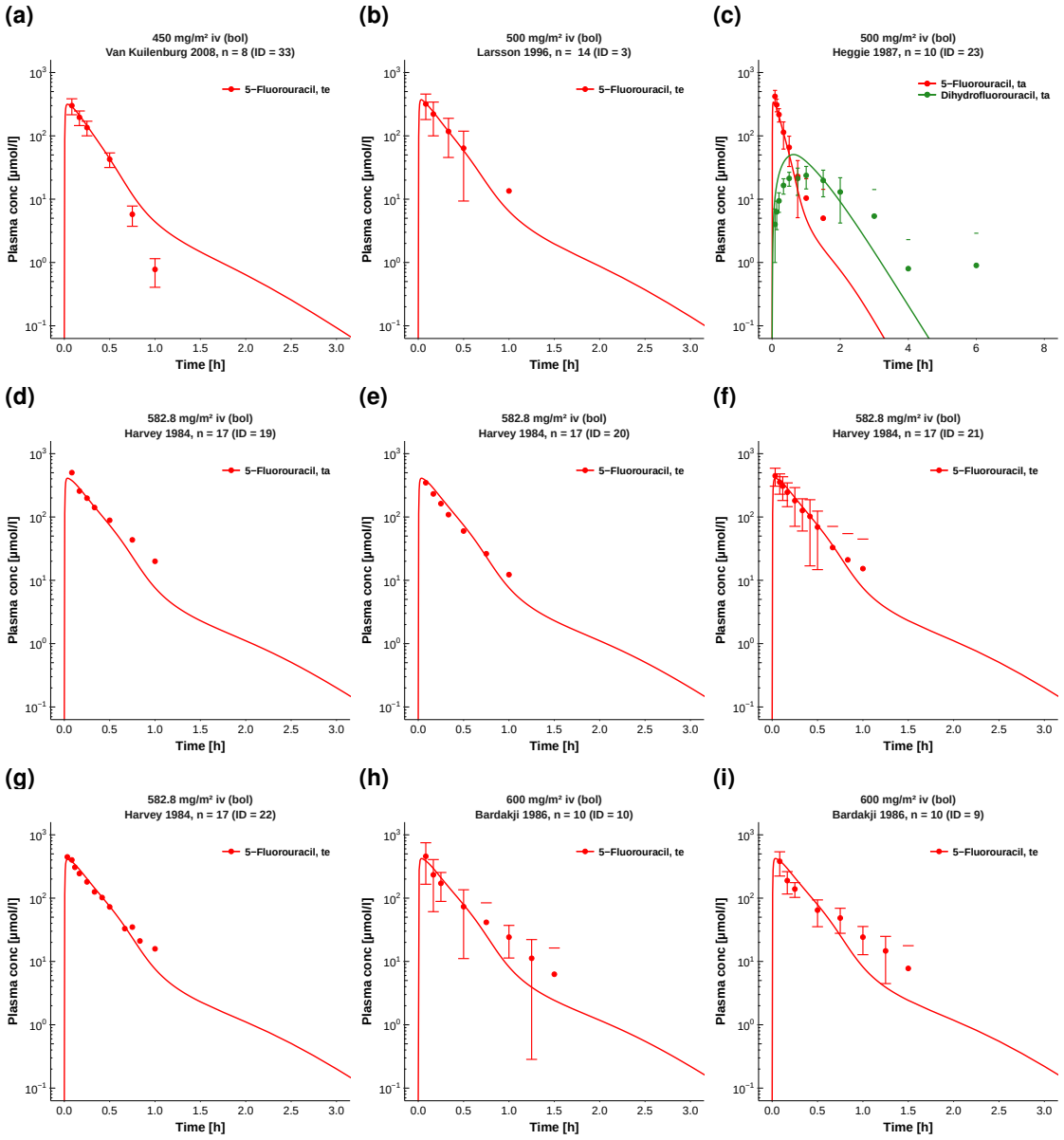

Figure S3.3.13: **Plasma 5-fluorouracil and 5,6-dihydrouracil after intravenous administration of 5-fluorouracil (part 3/10)** on a semi-logarithmic scale. **bol**, bolus injection; **iv**, intravenous; **n**, number of individuals; **ta**, training dataset; **te**, test dataset.

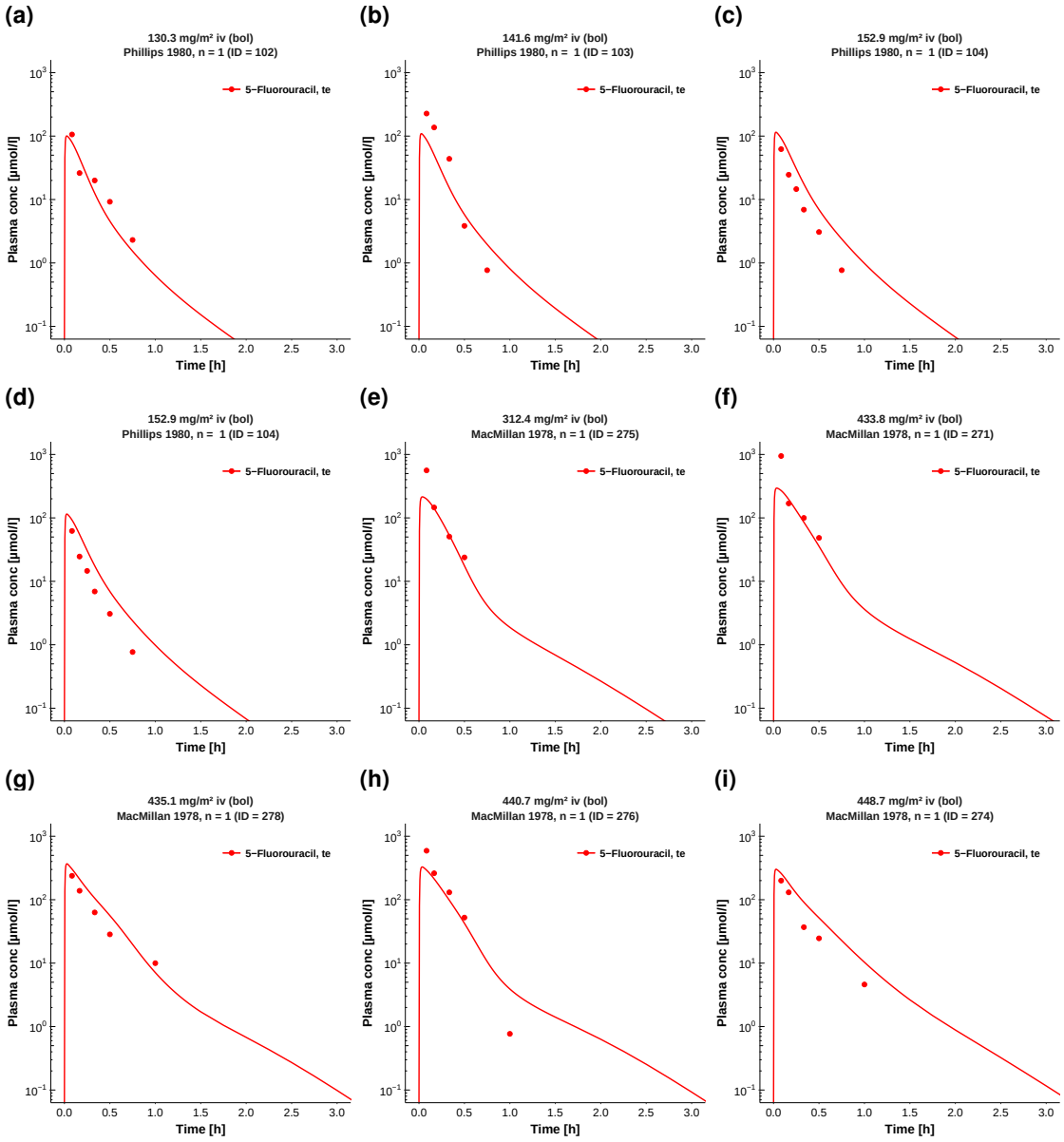

Figure S3.3.14: **Plasma 5-fluorouracil after intravenous administration of 5-fluorouracil (part 4/10)** on a semi-logarithmic scale. **bol**, bolus injection; **iv**, intravenous; **n**, number of individuals; **te**, test dataset.

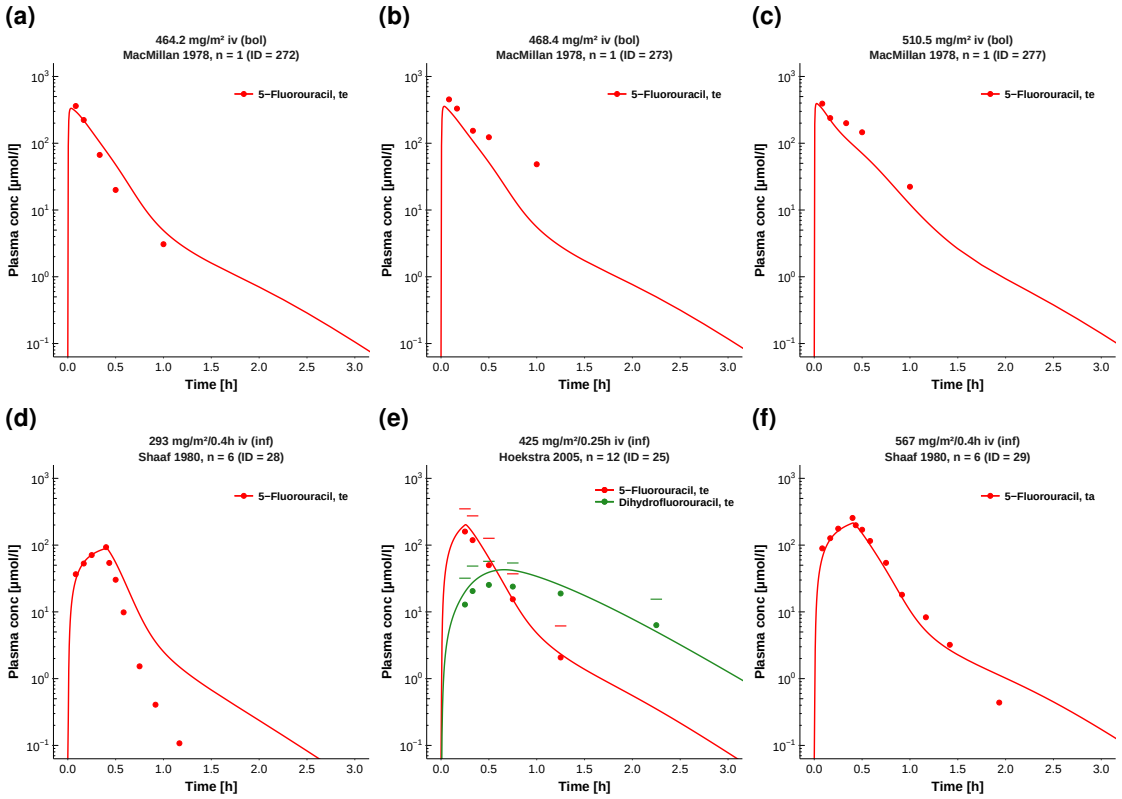

Figure S3.3.15: **Plasma and urine 5-fluorouracil and 5,6-dihydrouracil after intravenous administration of 5-fluorouracil (part 5/10)** on a semi-logarithmic scale. **bol**, bolus injection; **FE**, fraction of dose excreted; **iv**, intravenous; **n**, number of individuals; **ta**, training dataset; **te**, test dataset.

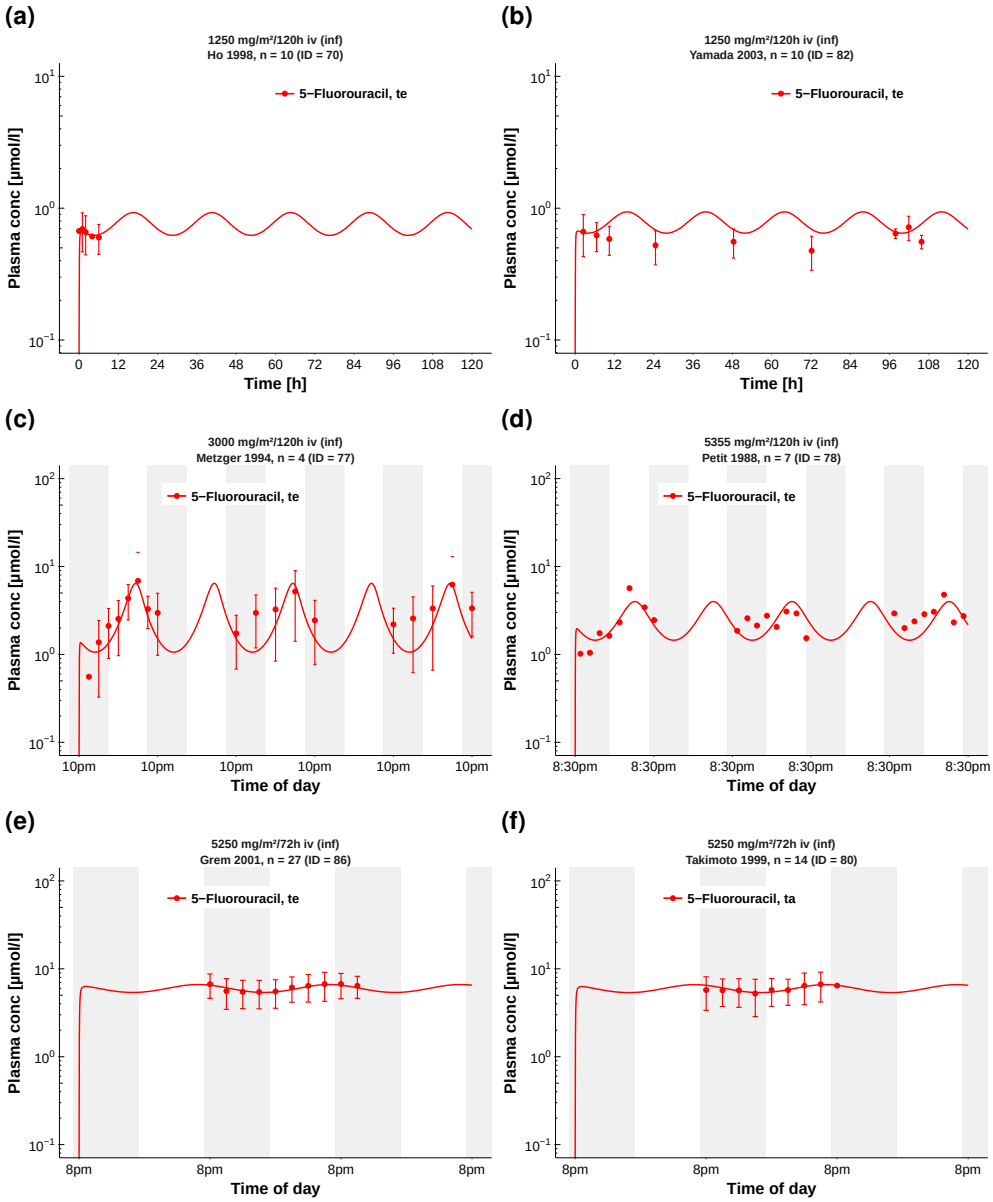

Figure S3.3.16: **Plasma 5-fluorouracil after intravenous administration of 5-fluorouracil (part 6/10)** on a semi-logarithmic scale. The shaded areas illustrate night time. **inf**, infusion; **iv**, intravenous; **n**, number of individuals; **ta**, training dataset; **te**, test dataset.

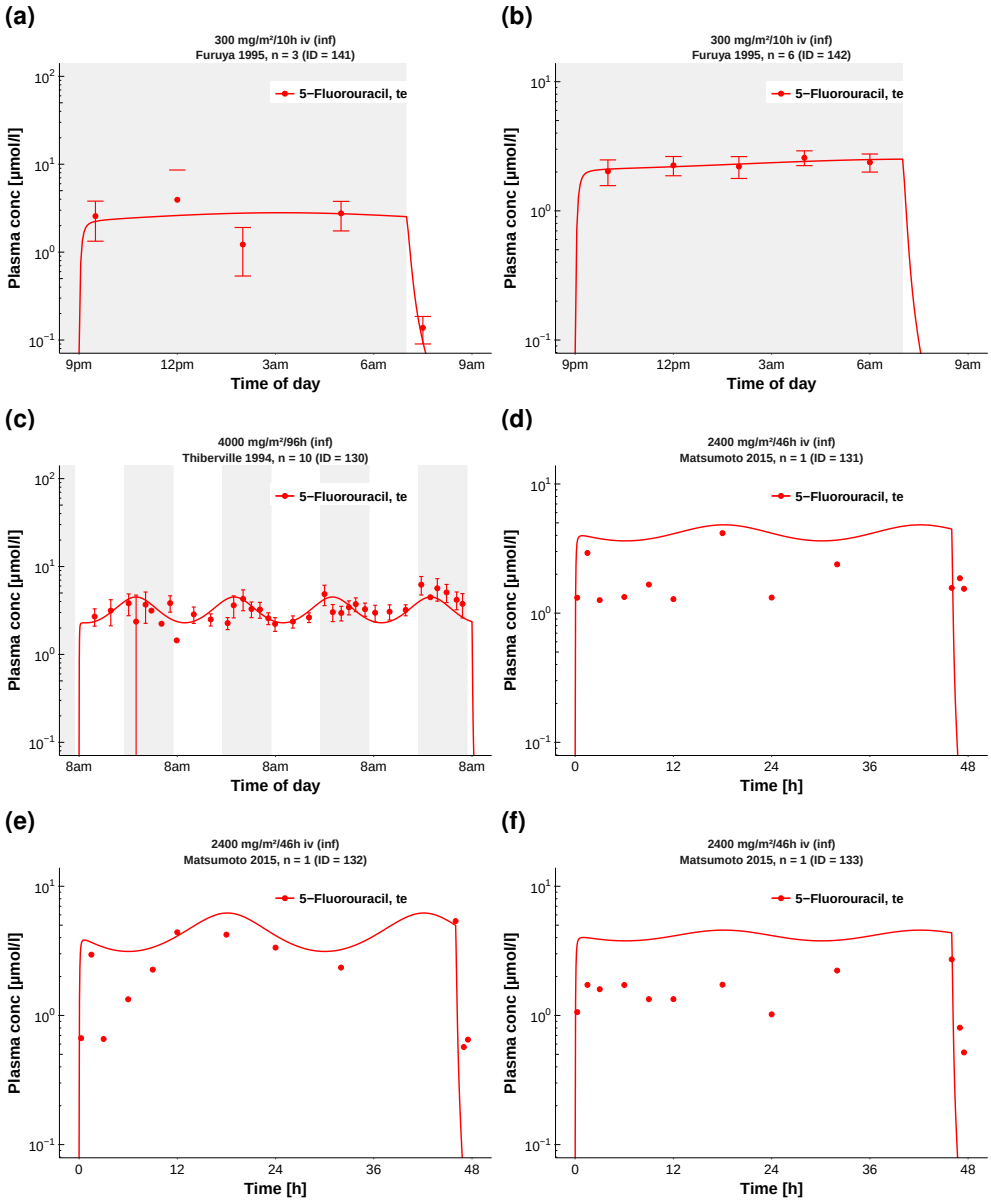

Figure S3.3.17: **Plasma 5-fluorouracil after intravenous administration of 5-fluorouracil (part 7/10)** on a semi-logarithmic scale. The shaded areas illustrate night time. **inf**, infusion; **iv**, intravenous; **n**, number of individuals; **ta**, training dataset; **te**, test dataset.

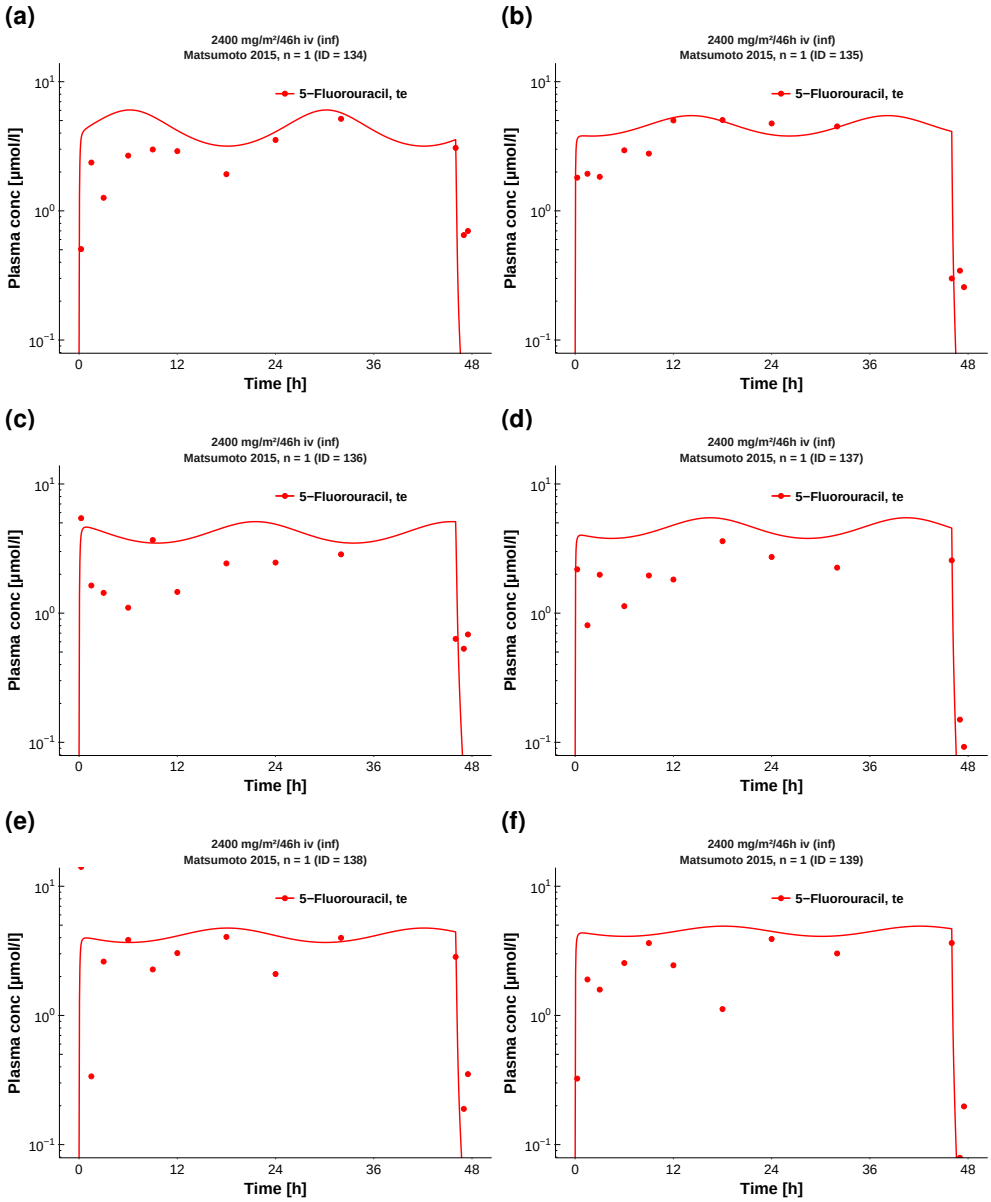

Figure S3.3.18: **Plasma 5-fluorouracil after intravenous administration of 5-fluorouracil (part 8/10)** on a semi-logarithmic scale. **inf**, infusion; **iv**, intravenous; **n**, number of individuals; **ta**, training dataset; **te**, test dataset.

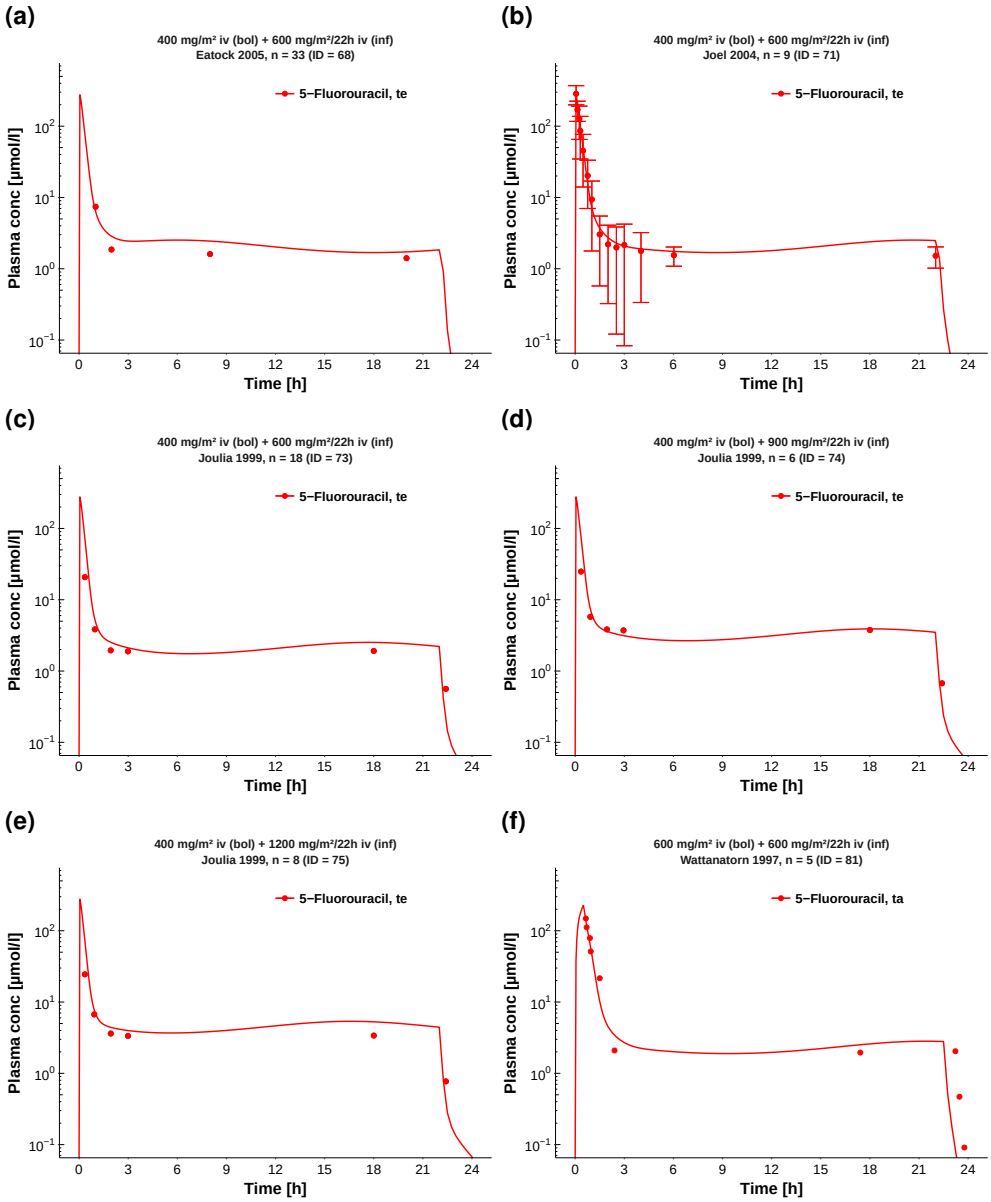

Figure S3.3.19: **Plasma 5-fluorouracil during intravenous administration of 5-fluorouracil (part 9/10)** on a semi-logarithmic scale. **bol**, bolus injection; **inf**, infusion; **iv**, intravenous; **n**, number of individuals; **ta**, training dataset; **te**, test dataset.

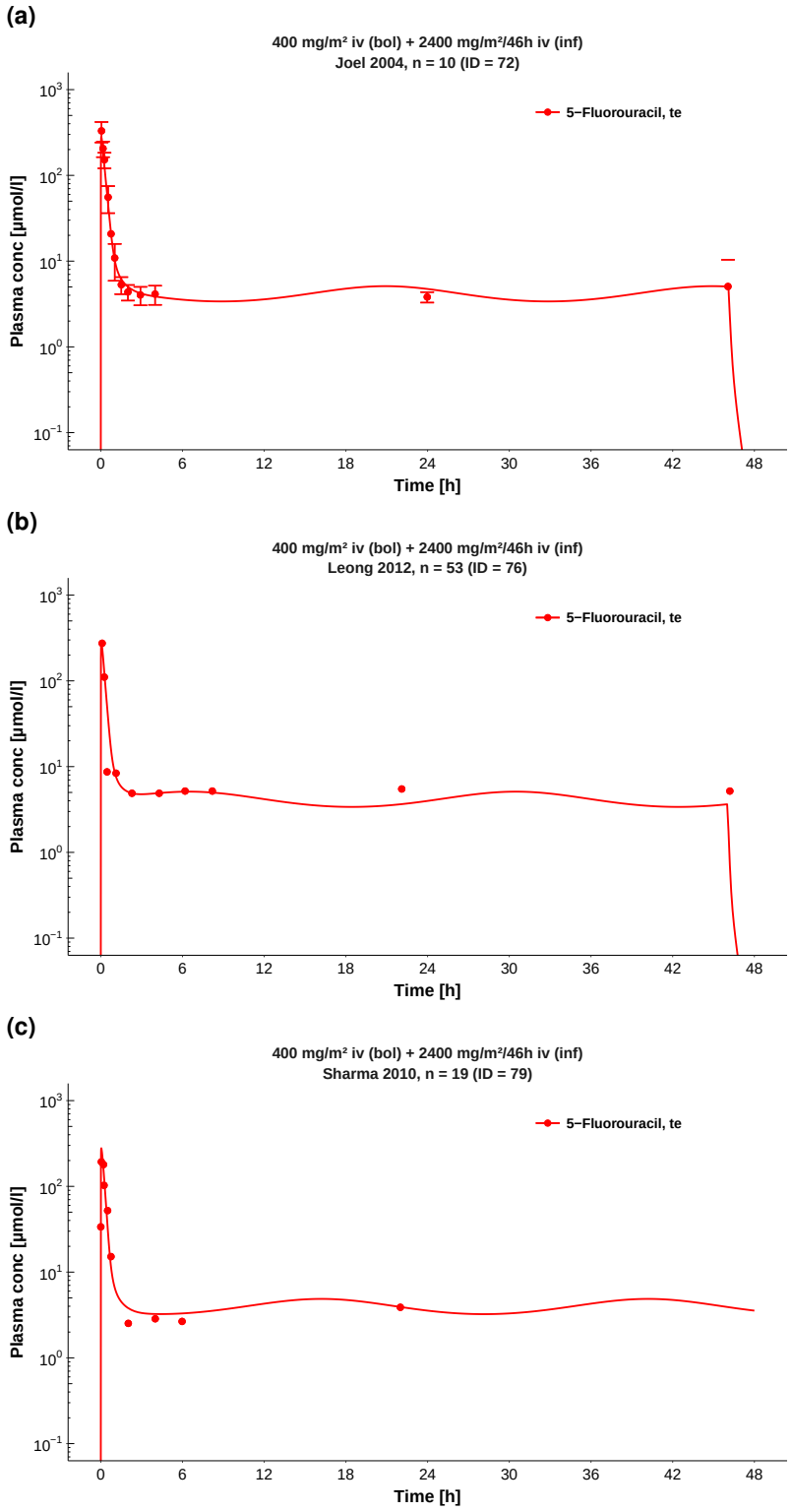

Figure S3.3.20: **Plasma 5-fluorouracil during intravenous administration of 5-fluorouracil (part 10/10)** on a semi-logarithmic scale. **bol**, bolus injection; **inf**, infusion; **iv**, intravenous; **n**, number of individuals; **te**, test dataset.

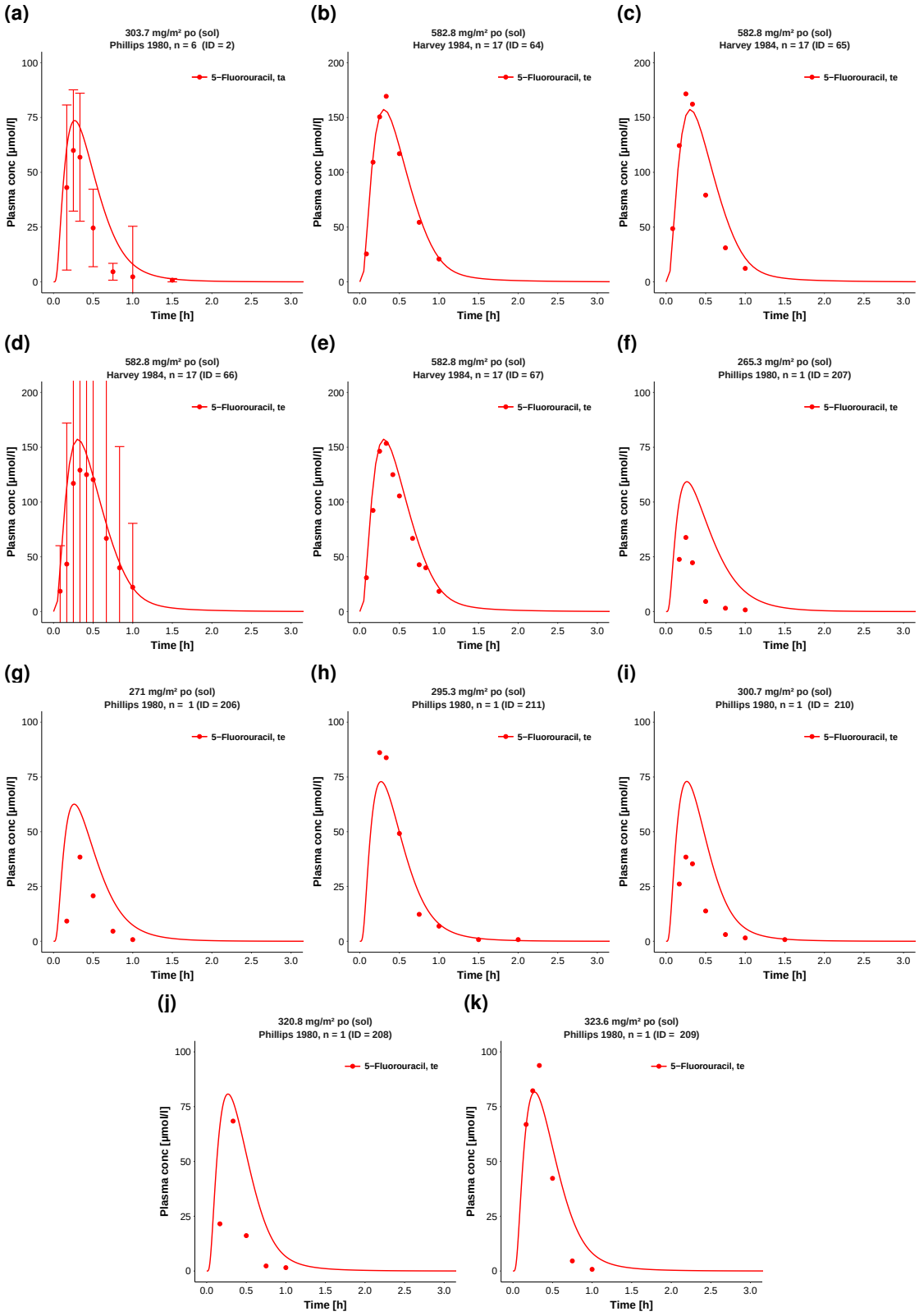

Figure S3.3.21: **Plasma 5-fluorouracil after oral administration of 5-fluorouracil** on a linear scale. **n**, number of individuals; **po**, oral; **sol**, solution; **ta**, training; **te**, test dataset.

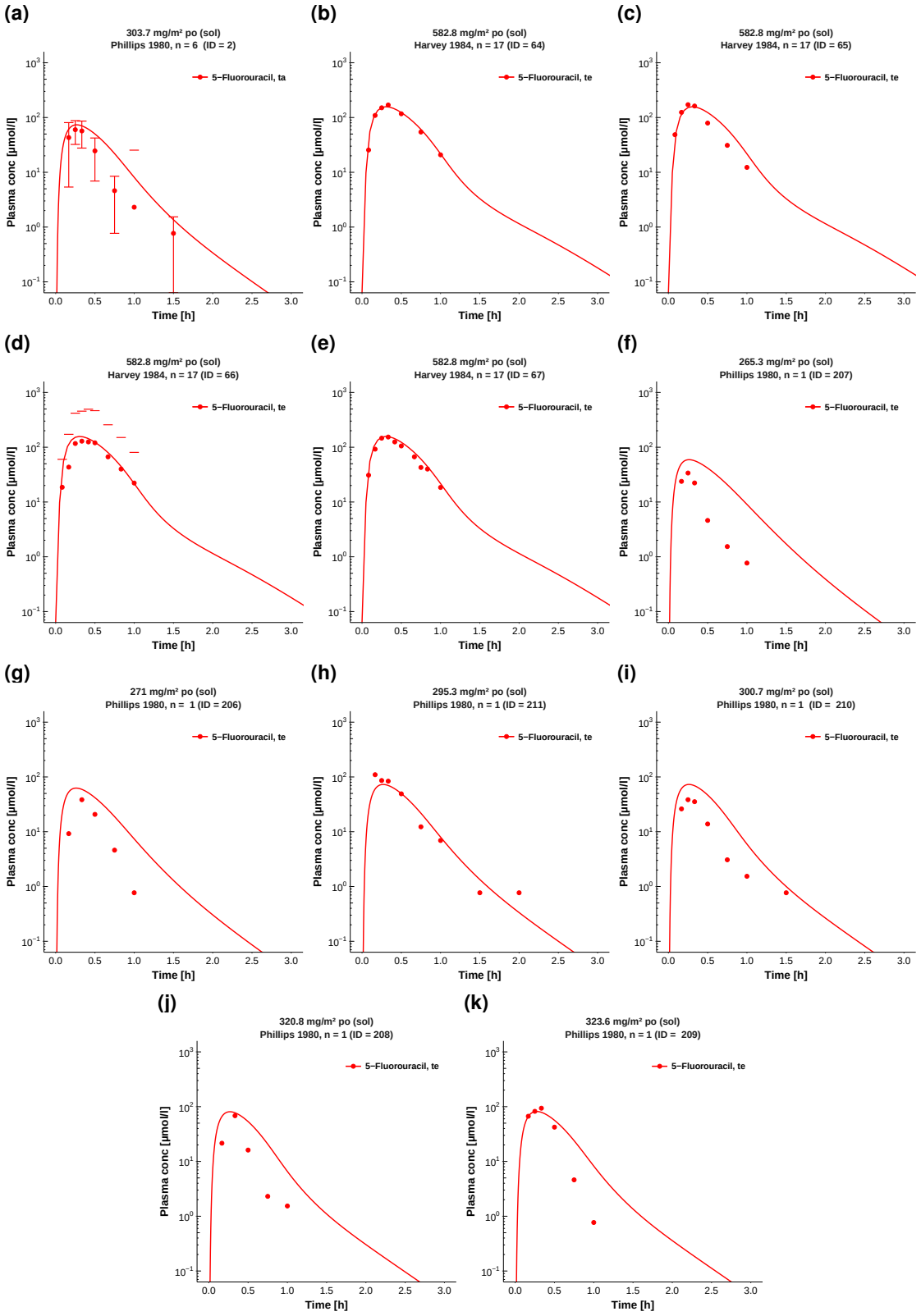

Figure S3.3.22: **Plasma 5-fluorouracil after oral administration of 5-fluorouracil** on a semi-logarithmic scale. **n**, number of individuals; **po**, oral; **sol**, solution; **ta**, training; **te**, test dataset.

S3.4 Model evaluation

S3.4.1 Predicted compared to observed concentrations goodness-of-fit plots

Following, goodness-of-fit plots of predicted compared to observed plasma concentrations for every study are illustrated in Fig. S3.4.23. Details on dosing regimens, study populations and literature references are listed in Table S3.1. Predicted and observed PK parameters are summarized in Table S3.5.

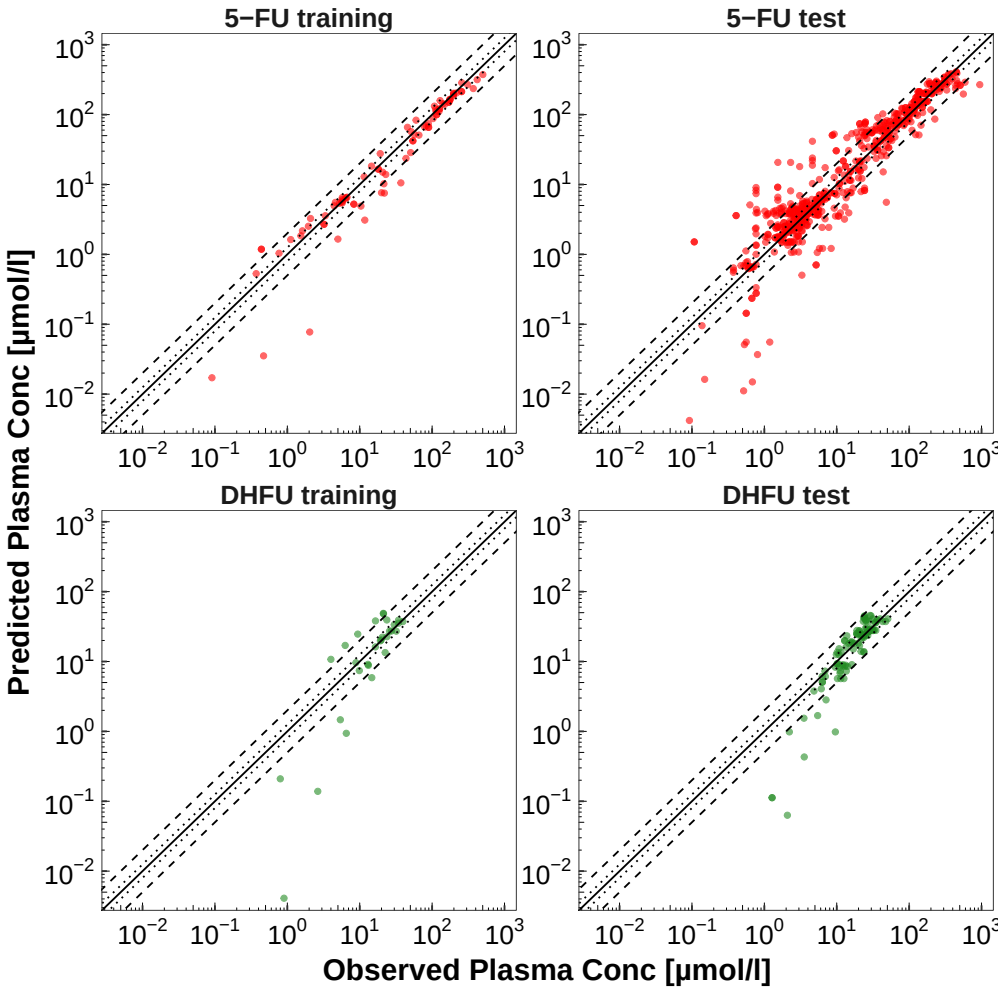

Figure S3.4.23: **Predicted compared to observed plasma concentrations**. Illustrated are values for 5-fluorouracil and 5,6-dihydrofluorouracil for training and test data. The solid lines mark the line of identity. Dotted lines indicate 1.25-fold, dashed lines 2-fold deviation. **5-FU**, 5-fluorouracil; **Conc**, concentration; **DHFU**, 5,6-dihydrofluorouracil.

S3.4.2 Mean relative deviation and median symmetric accuracy of plasma concentration predictions

Table S3.4: Mean relative deviation and median symmetric accuracy values of 5-fluorouracil and 5,6-dihydrofluorouracil plasma concentrations

Dose [mg/m²]	Route	n	Compound	MRD	MSA [%]	Dataset	Reference	ID
[a]**250**	iv (bol), s.d.	5	**5-FU**	1.27	19.99	ta	Phillips 1980 [22]	1
[a]**250**	iv (bol), s.d.	5	**5-FU**	1.59	33.42	te	Phillips 1980 [22]	101
[a]**250**	iv (bol), s.d.	5	**5-FU**	1.66	61.02	te	Phillips 1980 [22]	102
[a]**250**	iv (bol), s.d.	5	**5-FU**	2.47	162.88	te	Phillips 1980 [22]	103
[a]**250**	iv (bol), s.d.	5	**5-FU**	2.30	125.63	te	Phillips 1980 [22]	104
[a]**250**	iv (bol), s.d.	5	**5-FU**	1.34	13.42	te	Phillips 1980 [22]	105
250	iv (bol), s.d.	20	**5-FU**	1.41	40.65	te	Bocci 2000 [23]	11
250	iv (bol), s.d.	188	**5-FU**	1.32	32.52	ta	Bocci 2006 [24]	93
250	iv (bol), s.d.	101	**5-FU**	1.52	48.58	te	Bocci 2006 [24]	94
250	iv (bol), s.d.	87	**5-FU**	1.84	58.76	te	Bocci 2006 [24]	95
250	iv (bol), s.d.	70	**5-FU**	1.34	31.76	te	Bocci 2006 [24]	96
250	iv (bol), s.d.	118	**5-FU**	1.60	60.59	te	Bocci 2006 [24]	97
300	iv (bol), s.d.	8	**5-FU**	1.25	24.33	ta	Van Kuilenburg 2008 [25]	32
370	iv (bol), s.d.	20	**5-FU**	2.13	56.97	ta	Bocci 2000 [23]	12
370	iv (bol), s.d.	110	**5-FU**	2.73	81.72	te	Paolo 2001 [26]	106
370	iv (bol), s.d.	110	**5-FU**	4.47	179.76	te	Paolo 2001 [26]	107
400	iv (bol), s.d.	18	**5-FU**	4.52	234.91	te	Casale 2004 [27]	5
400	iv (bol), s.d.	18	**5-FU**	4.48	297.83	te	Casale 2004 [27]	7
400	iv (bol), s.d.	18	**5-FU**	5.11	437.88	te	Casale 2004 [27]	8
[b]**10.9**	iv (bol), s.d.	8	**5-FU**	1.69	35.58	te	MacMillan 1978 [30]	27
[b]**10.9**	iv (bol), s.d.	1	**5-FU**	1.93	26.41	te	MacMillan 1978 [30]	271
[b]**10.9**	iv (bol), s.d.	1	**5-FU**	1.63	53.69	te	MacMillan 1978 [30]	272
[b]**10.9**	iv (bol), s.d.	1	**5-FU**	2.95	47.43	te	MacMillan 1978 [30]	273
[b]**10.9**	iv (bol), s.d.	1	**5-FU**	1.93	110.25	te	MacMillan 1978 [30]	274
[b]**10.9**	iv (bol), s.d.	1	**5-FU**	1.73	18.74	te	MacMillan 1978 [30]	275
[b]**10.9**	iv (bol), s.d.	1	**5-FU**	2.26	33.96	te	MacMillan 1978 [30]	276
[b]**10.9**	iv (bol), s.d.	1	**5-FU**	1.64	70.63	te	MacMillan 1978 [30]	277
[b]**10.9**	iv (bol), s.d.	1	**5-FU**	1.59	53.80	te	MacMillan 1978 [30]	278
425	iv (bol), s.d.	6	**5-FU**	1.47	49.65	te	Maring 2002 [28]	30
425	iv (bol), s.d.	18	**5-FU**	1.26	18.18	te	Maring 2003 [29]	14
450	iv (bol), s.d.	8	**5-FU**	2.16	7.84	te	Van Kuilenburg 2008 [25]	33
500	iv (bol), s.d.	14	**5-FU**	1.40	8.60	te	Larsson 1996 [31]	3
500	iv (bol), s.d.	10	**5-FU**	1.69	30.94	ta	Heggie 1987 [32]	23
[a]**15**	iv (bol), s.d.	17	**5-FU**	1.57	19.62	ta	Harvey 1984 [33]	19
[a]**15**	iv (bol), s.d.	17	**5-FU**	1.29	23.52	te	Harvey 1984 [33]	20
[a]**15**	iv (bol), s.d.	17	**5-FU**	1.28	11.64	te	Harvey 1984 [33]	21
[a]**15**	iv (bol), s.d.	17	**5-FU**	1.31	11.86	te	Harvey 1984 [33]	22
600	iv (bol), s.d.	10	**5-FU**	2.22	71.54	te	Bardakji 1986 [34]	9
600	iv (bol), s.d.	10	**5-FU**	1.94	41.37	te	Bardakji 1986 [34]	10
[a]**7.5**	iv (inf), s.d.	6	**5-FU**	3.64	63.35	te	Schaaf 1987 [35]	28

Table S3.4: Mean relative deviation and median symmetric accuracy values of 5-fluorouracil and 5,6-dihydrofluorouracil plasma concentrations. (continued)

Dose [mg/m²]	Route	n	Compound	MRD	MSA [%]	Dataset	Reference	ID
425	iv (inf), s.d.	12	**5-FU**	1.22	25.34	te	Hoekstra 2005 [36]	25
b15	iv (inf), s.d.	6	**5-FU**	1.42	17.48	ta	Schaaf 1987 [35]	29
1250	iv (inf) 96h	10	**5-FU**	1.04	3.62	te	Ho 1998 [37]	70
1250	iv (inf) 96h	10	**5-FU**	1.25	23.98	te	Yamada 2003 [9]	82
600	iv (inf) 24h	4	**5-FU**	1.65	47.82	te	Metzger 1994 [38]	77
1071	iv (inf) 24h	7	**5-FU**	1.41	31.64	te	Petit 1988 [39]	78
1750	iv (inf) 72h	14	**5-FU**	1.04	2.77	te	Grem 2001 [40]	86
1750	iv (inf) 72h	14	**5-FU**	1.06	2.23	ta	Takimoto 1999 [41]	80
300	iv (inf) 10h	3	**5-FU**	1.56	44.52	te	Furuya 1995 [42]	141
300	iv (inf) 10h	6	**5-FU**	1.05	4.39	te	Furuya 1995 [42]	142
4000	iv (inf) 96h	10	**5-FU**	1.32	19.84	te	Thiberville 1994 [43]	130
2400	iv (inf) 46h	1	**5-FU**	7.21	178.68	te	Matsumoto 1994 [44]	131
2400	iv (inf) 46h	1	**5-FU**	4.57	47.82	te	Matsumoto 1994 [44]	132
2400	iv (inf) 46h	1	**5-FU**	5.34	176.61	te	Matsumoto 1994 [44]	133
2400	iv (inf) 46h	1	**5-FU**	5.94	87.54	te	Matsumoto 1994 [44]	134
2400	iv (inf) 46h	1	**5-FU**	5.88	81.07	te	Matsumoto 1994 [44]	135
2400	iv (inf) 46h	1	**5-FU**	4.86	162.19	te	Matsumoto 1994 [44]	136
2400	iv (inf) 46h	1	**5-FU**	3.85	103.21	te	Matsumoto 1994 [44]	137
2400	iv (inf) 46h	1	**5-FU**	4.05	61.43	te	Matsumoto 1994 [44]	138
2400	iv (inf) 46h	1	**5-FU**	4.56	82.02	te	Matsumoto 1994 [44]	139
400	iv (bol), LD	33	**5-FU**	1.38	36.59	te	Eatock 2005 [45]	68
600	iv (inf) 22h, MD							
400	iv (bol), LD	9	**5-FU**	1.22	17.55	te	Joel 2004 [46]	71
600	iv (inf) 22h, MD							
400	iv (bol), LD	18	**5-FU**	2.21	36.89	te	Joulia 1999 [47]	73
600	iv (inf) 22h, MD							
400	iv (bol), LD	6	**5-FU**	1.91	20.89	te	Joulia 1999 [47]	74
900	iv (inf) 22h, MD							
400	iv (bol), LD	8	**5-FU**	1.92	37.78	te	Joulia 1999 [47]	75
1200	iv (inf) 22h, MD							
600	iv (inf) 0.5h, LD	5	**5-FU**	2.91	38.50	ta	Wattanatorn 1997 [8]	81
600	iv (inf) 22h, MD							
400	iv (bol), LD	10	**5-FU**	1.14	10.82	te	Joel 2004 [46]	72
2400	iv (inf) 46h, MD							
400	iv (bol), LD	53	**5-FU**	2.35	11.04	te	Leong 2012 [48]	76
2400	iv (inf) 46h, MD							
400	iv (bol), LD	16	**5-FU**	1.32	24.08	te	Sharma 2010 [49]	79
2400	iv (inf) 46h, MD							
[b]**500**	po (sol), s.d.	6	**5-FU**	2.34	77.24	ta	Phillips 1980 [22]	2
[b]**500**	po (sol), s.d.	1	**5-FU**	4.36	308.99	te	Phillips 1980 [22]	206
[b]**500**	po (sol), s.d.	1	**5-FU**	6.04	377.78	te	Phillips 1980 [22]	207
[b]**500**	po (sol), s.d.	1	**5-FU**	4.00	230.62	te	Phillips 1980 [22]	208

Table S3.4: Mean relative deviation and median symmetric accuracy values of 5-fluorouracil and 5,6-dihydrofluorouracil plasma concentrations. (continued)

Dose [mg/m²]	Route	n	Compound	MRD	MSA [%]	Dataset	Reference	ID
[b]**500**	po (sol), s.d.	1	**5-FU**	3.28	26.11	te	Phillips 1980 [22]	209
[b]**500**	po (sol), s.d.	1	**5-FU**	2.93	132.48	te	Phillips 1980 [22]	210
[b]**500**	po (sol), s.d.	1	**5-FU**	1.60	44.87	te	Phillips 1980 [22]	211
[a]**15**	po (sol), s.d.	17	**5-FU**	1.35	6.62	te	Harvey 1984 [33]	64
[a]**15**	po (sol), s.d.	17	**5-FU**	1.47	21.40	te	Harvey 1984 [33]	65
[a]**15**	po (sol), s.d.	17	**5-FU**	1.62	19.85	te	Harvey 1984 [33]	66
[a]**15**	po (sol), s.d.	17	**5-FU**	1.28	17.13	te	Harvey 1984 [33]	67
250	iv (bol), s.d.	20	**DHFU**	3.40	17.73	te	Bocci 2000 [23]	11
250	iv (bol), s.d.	188	**DHFU**	1.22	6.80	ta	Bocci 2006 [24]	93
250	iv (bol), s.d.	101	**DHFU**	1.25	19.85	te	Bocci 2006 [24]	94
250	iv (bol), s.d.	87	**DHFU**	1.28	11.10	te	Bocci 2006 [24]	95
250	iv (bol), s.d.	70	**DHFU**	1.35	11.29	te	Bocci 2006 [24]	96
250	iv (bol), s.d.	118	**DHFU**	1.22	21.60	te	Bocci 2006 [24]	97
370	iv (bol), s.d.	20	**DHFU**	2.90	37.87	ta	Bocci 2000 [23]	12
370	iv (bol), s.d.	110	**DHFU**	2.42	9.33	te	Paolo 2001 [26]	106
370	iv (bol), s.d.	110	**DHFU**	1.43	9.33	te	Paolo 2001 [26]	107
400	iv (bol), s.d.	18	**DHFU**	1.33	15.40	te	Casale 2004 [27]	5
400	iv (bol), s.d.	18	**DHFU**	1.53	27.16	te	Casale 2004 [27]	7
400	iv (bol), s.d.	18	**DHFU**	1.49	31.13	te	Casale 2004 [27]	8
425	iv (bol), s.d.	18	**DHFU**	1.61	37.87	te	Maring 2003 [29]	14
500	iv (bol), s.d.	10	**DHFU**	5.91	146.19	ta	Heggie 1987 [32]	23
425	iv (inf), s.d.	12	**DHFU**	2.68	54.40	te	Hoekstra 2005 [36]	25
			Mean*	**1.83** (1.04–5.92)	**37.75** (2.58–174.13)			
			Median*	**1.51** (1.04–5-92)	**24.83** (2.58–174.13)			
				72.22% (52/72)* < 2				

5-FU, 5-fluorouracil; **bol**, bolus injection; **DHFU**, 5,6-dihydrofluorouracil ; **inf**, continuous infusion; **iv**, intravenous; **LD**, loading dose; **MD**, multiple dose; **MRD**, mean relative deviation; **MSA**, median symmetric accuracy; **n**, number of individuals studied; **po**, oral; **Route**, route of administration; **s.d.**, single dose; **sol**, solution; **te**, test dataset (model evaluation); **ta**, training dataset (parameter optimization).

*, MRD and MSA values are listed for individual profiles, but mean and median MRD and MSA values were only calculated for mean profiles.

[a], dose relative in mg/kg bodyweight

[b], absolute dose in mg

S3.4.3 AUC_{last} and C_{max} goodness-of-fit plots

In the following section, goodness-of-fit plots of predicted compared to observed AUC_{last} and C_{max} values for every study are illustrated in Fig. S3.4.23-S3.4.24. Details on dosing regimens, study populations and literature references are listed in Table S3.1. Predicted and observed PK parameters are summarized in Table S3.5.

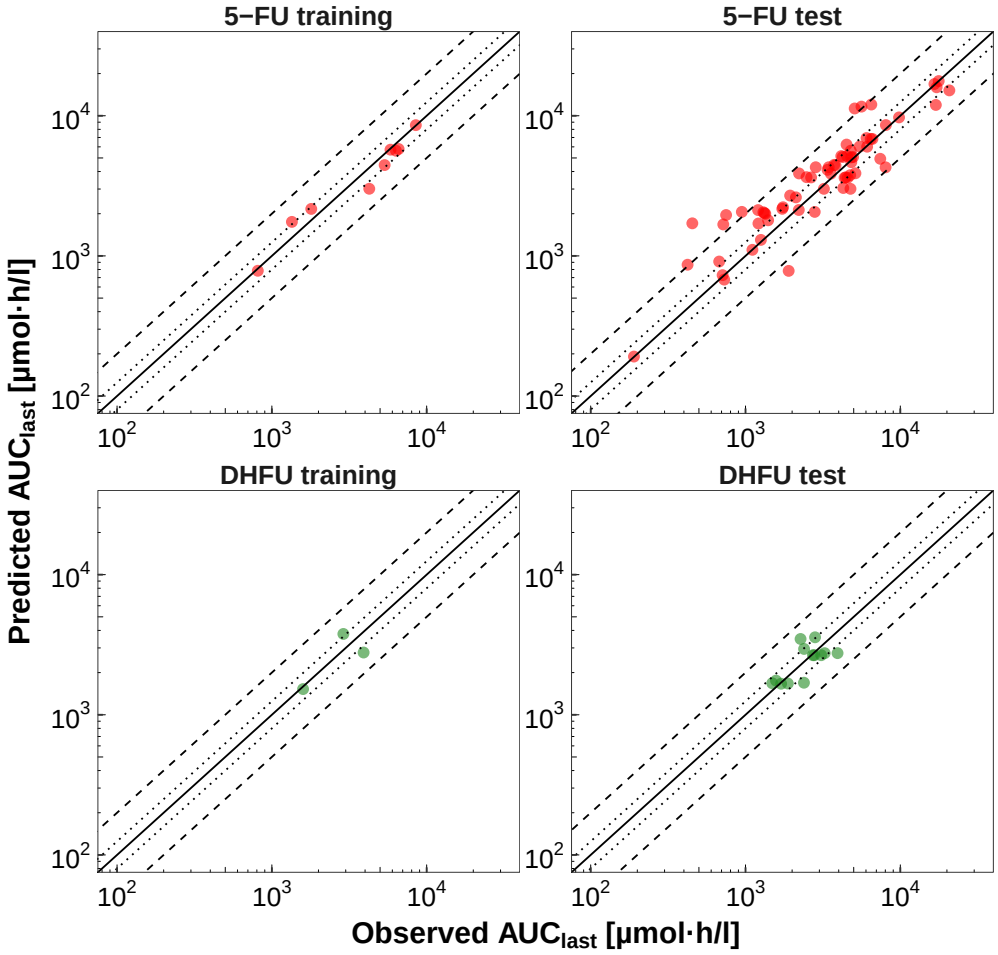

Figure S3.4.24: **Predicted compared to observed plasma AUC_{last} values**. Illustrated are values for 5-fluorouracil and 5,6-dihydrofluorouracil for training and test data. The solid lines mark the line of identity. Dotted lines indicate 1.25-fold, dashed lines 2-fold deviation. **5-FU**, 5-fluorouracil; **AUC_{last}**, area under the plasma concentration time curve from the first to last time point of concentration measurements; **DHFU**, 5,6-dihydrofluorouracil.

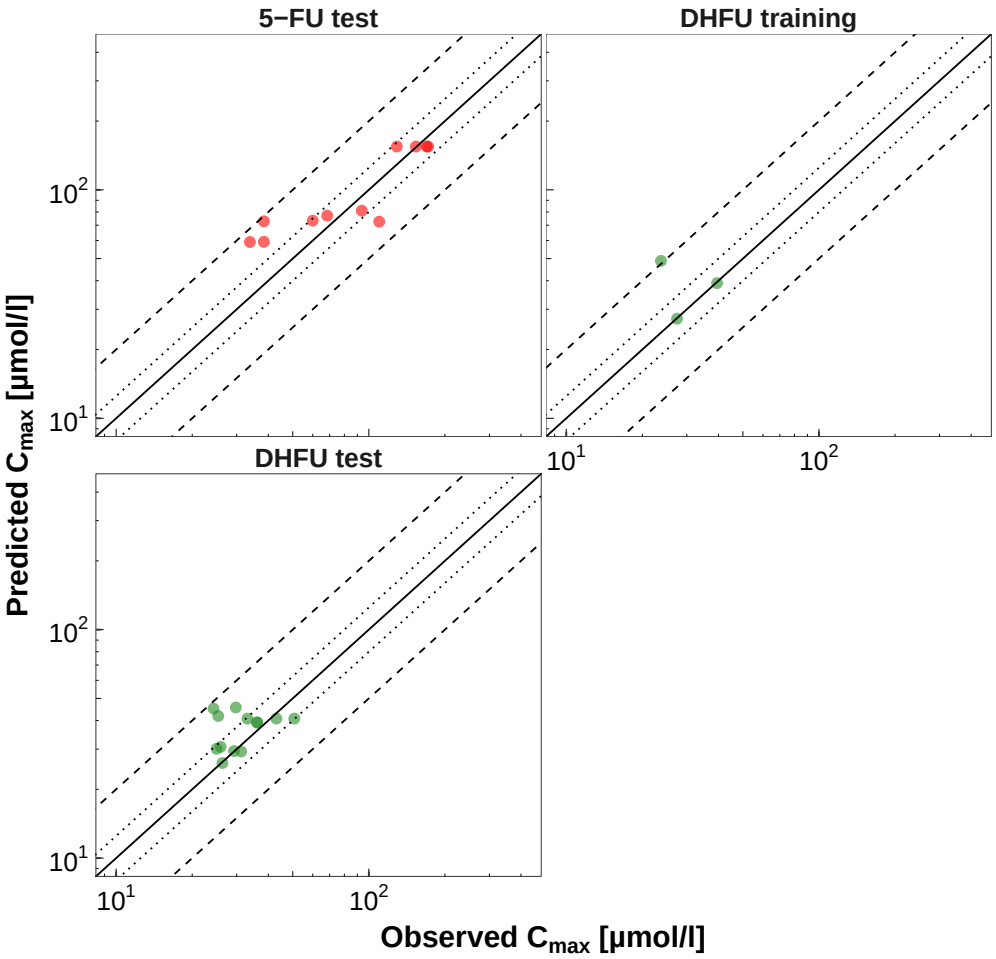

Figure S3.4.25: **Predicted compared to observed plasma C_{max} values**. Illustrated are values for 5-fluorouracil and 5,6-dihydrofluorouracil for training and test data. The solid lines mark the line of identity. Dotted lines indicate 1.25-fold, dashed lines 2-fold deviation. **5-FU**, 5-fluorouracil; **C_{max}**, maximum plasma concentration; **DHFU**, 5,6-dihydrofluorouracil.

S3.4.4 Geomentric mean fold error of predicted AUC_{last} and C_{max} values

Table S3.5: Predicted and observed AUC_{last} and C_{max} values of of 5-fluorouracil and 5,6-dihydrofluorouracil plasma concentrations

Dose [mg/m²]	Route	n	Compound	AUC_{last} pred [µmol·h/l]	AUC_{last} obs [µmol·h/l]	Pred/Obs AUC_{last}	C_{max} pred [µmol/l]	C_{max} obs [µmol/l]	Pred/Obs C_{max}	Dataset	Reference	ID
[a]**250**	iv (bol), s.d.	5	**5-FU**	783.35	811.23	0.97	-	-	-	ta	Phillips 1980 [22]	1
[a]**250**	iv (bol), s.d.	5	**5-FU**	728.88	711.29	1.02	-	-	-	te	Phillips 1980 [22]	101
[a]**250**	iv (bol), s.d.	5	**5-FU**	677.49	728.67	0.93	-	-	-	te	Phillips 1980 [22]	102
[a]**250**	iv (bol), s.d.	5	**5-FU**	781.93	1900.00	0.41	-	-	-	te	Phillips 1980 [22]	103
[a]**250**	iv (bol), s.d.	5	**5-FU**	865.04	422.45	2.05	-	-	-	te	Phillips 1980 [22]	104
[a]**250**	iv (bol), s.d.	5	**5-FU**	911.57	675.78	1.35	-	-	-	te	Phillips 1980 [22]	105
250	iv (bol), s.d.	20	**5-FU**	1703.13	1211.97	1.41	-	-	-	te	Bocci 2000 [23]	11
250	iv (bol), s.d.	188	**5-FU**	1748.99	1347.02	1.30	-	-	-	ta	Bocci 2006 [24]	93
250	iv (bol), s.d.	101	**5-FU**	1998.03	1342.04	1.49	-	-	-	te	Bocci 2006 [24]	94
250	iv (bol), s.d.	87	**5-FU**	2019.61	1325.57	1.52	-	-	-	te	Bocci 2006 [24]	95
250	iv (bol), s.d.	70	**5-FU**	1795.24	1399.76	1.28	-	-	-	te	Bocci 2006 [24]	96
250	iv (bol), s.d.	118	**5-FU**	2048.24	1304.55	1.57	-	-	-	te	Bocci 2006 [24]	97
300	iv (bol), s.d.	8	**5-FU**	2164.32	1796.36	1.20	-	-	-	ta	Van Kuilenburg 2008 [25]	32
370	iv (bol), s.d.	20	**5-FU**	3013.86	4257.86	0.71	-	-	-	ta	Bocci 2000 [23]	12
370	iv (bol), s.d.	110	**5-FU**	3010.45	3209.53	0.94	-	-	-	te	Paolo 2001 [26]	106
370	iv (bol), s.d.	110	**5-FU**	3010.52	4764.95	0.63	-	-	-	te	Paolo 2001 [26]	107
400	iv (bol), s.d.	18	**5-FU**	3610.66	4566.27	0.79	-	-	-	te	Casale 2004 [27]	5
400	iv (bol), s.d.	18	**5-FU**	3634.90	4441.69	0.82	-	-	-	te	Casale 2004 [27]	7
400	iv (bol), s.d.	18	**5-FU**	3610.66	4362.40	0.83	-	-	-	te	Casale 2004 [27]	8
[b]**10.9**	iv (bol), s.d.	8	**5-FU**	3768.83	4745.91	0.79	-	-	-	te	MacMillan 1978 [30]	27
[b]**10.9**	iv (bol), s.d.	1	**5-FU**	3051.38	4281.77	0.71	-	-	-	te	MacMillan 1978 [30]	271
[b]**10.9**	iv (bol), s.d.	1	**5-FU**	4112.79	3388.42	1.21	-	-	-	te	MacMillan 1978 [30]	272
[b]**10.9**	iv (bol), s.d.	1	**5-FU**	4285.62	8032.29	0.53	-	-	-	te	MacMillan 1978 [30]	273
[b]**10.9**	iv (bol), s.d.	1	**5-FU**	3876.43	2217.42	1.75	-	-	-	te	MacMillan 1978 [30]	274
[b]**10.9**	iv (bol), s.d.	1	**5-FU**	2060.65	2799.66	0.74	-	-	-	te	MacMillan 1978 [30]	275
[b]**10.9**	iv (bol), s.d.	1	**5-FU**	3885.90	5129.36	0.76	-	-	-	te	MacMillan 1978 [30]	276
[b]**10.9**	iv (bol), s.d.	1	**5-FU**	4931.61	7420.52	0.66	-	-	-	te	MacMillan 1978 [30]	277
[b]**10.9**	iv (bol), s.d.	1	**5-FU**	4292.81	2841.30	1.51	-	-	-	te	MacMillan 1978 [30]	278
425	iv (bol), s.d.	6	**5-FU**	3646.88	2477.32	1.47	-	-	-	te	Maring 2002 [28]	30
425	iv (bol), s.d.	18	**5-FU**	4466.01	3741.63	1.19	-	-	-	te	Maring 2003 [29]	14
425	iv (bol), s.d.	18	**5-FU**	4428.29	3813.08	1.16	-	-	-	te	Maring 2003 [29]	140
450	iv (bol), s.d.	8	**5-FU**	3862.77	3557.83	1.09	-	-	-	te	Van Kuilenburg 2008 [25]	33
500	iv (bol), s.d.	14	**5-FU**	4660.82	4822.09	0.97	-	-	-	te	Larsson 1996 [31]	3
500	iv (bol), s.d.	10	**5-FU**	4448.84	5350.47	0.83	-	-	-	ta	Heggie 1987 [32]	23
[a]**15**	iv (bol), s.d.	17	**5-FU**	5630.58	6333.62	0.89	-	-	-	te	Harvey 1984 [33]	19
[a]**15**	iv (bol), s.d.	17	**5-FU**	5630.59	4783.39	1.18	-	-	-	te	Harvey 1984 [33]	20
[a]**15**	iv (bol), s.d.	17	**5-FU**	6834.05	6433.07	1.06	-	-	-	te	Harvey 1984 [33]	21
[a]**15**	iv (bol), s.d.	17	**5-FU**	6834.28	6605.46	1.03	-	-	-	te	Harvey 1984 [33]	22
600	iv (bol), s.d.	10	**5-FU**	6032.89	5457.25	1.11	-	-	-	te	Bardakji 1986 [34]	9

Table S3.5: Predicted and observed AUC_{last} and C_{max} values of of 5-fluorouracil and 5,6-dihydrofluorouracil plasma concentrations. (continued)

Dose [mg/m²]	Route	n	Compound	AUC_{last} pred [µmol·h/l]	AUC_{last} obs [µmol·h/l]	Pred/Obs AUC_{last}	C_{max} pred [µmol/l]	C_{max} obs [µmol/l]	Pred/Obs C_{max}	Dataset	Reference	ID
600	iv (bol), s.d.	10	**5-FU**	6015.60	6104.77	0.99	-	-	-	te	Bardakji 1986 [34]	10
[a]**7.5**	iv (inf), s.d.	6	**5-FU**	2167.46	1727.94	1.25	-	-	-	te	Schaaf 1987 [35]	28
425	iv (inf), s.d.	12	**5-FU**	2616.53	2115.65	1.24	-	-	-	te	Hoekstra 2005 [36]	25
[a]**15**	iv (inf), s.d.	6	**5-FU**	5792.47	6586.32	0.88	-	-	-	ta	Schaaf 1987 [35]	29
1250	iv (inf) 96h	10	**5-FU**	191.32	190.24	1.01	-	-	-	te	Ho 1998 [37]	70
1250	iv (inf) 96h	10	**5-FU**	4291.36	3446.73	1.25	-	-	-	te	Yamada 2003 [9]	82
600	iv (inf) 24h	4	**5-FU**	15173.54	20734.96	0.73	-	-	-	te	Metzger 1994 [38]	77
1071	iv (inf) 24h	7	**5-FU**	15966.12	17160.11	0.93	-	-	-	te	Petit 1988 [39]	78
1750	iv (inf) 72h	14	**5-FU**	9735.10	9811.59	0.99	-	-	-	te	Grem 2001 [40]	86
1750	iv (inf) 72h	14	**5-FU**	8570.14	8509.16	1.01	-	-	-	ta	Takimoto 1999 [41]	80
300	iv (inf) 10h	3	**5-FU**	1300.95	1256.99	1.03	-	-	-	te	Furuya 1995 [42]	141
300	iv (inf) 10h	6	**5-FU**	1105.42	1108.07	1.00	-	-	-	te	Furuya 1995 [42]	142
4000	iv (inf) 96h	10	**5-FU**	17689.43	17697.20	1.00	-	-	-	te	Thiberville 1994 [43]	130
2400	iv (inf) 46h	1	**5-FU**	11253.41	5656.10	1.99	-	-	-	te	Matsumoto 2015 [44]	131
2400	iv (inf) 46h	1	**5-FU**	11411.05	9030.25	1.26	-	-	-	te	Matsumoto 2015 [44]	132
2400	iv (inf) 46h	1	**5-FU**	11273.40	5071.78	2.22	-	-	-	te	Matsumoto 2015 [44]	133
2400	iv (inf) 46h	1	**5-FU**	12513.07	9083.72	1.38	-	-	-	te	Matsumoto 2015 [44]	134
2400	iv (inf) 46h	1	**5-FU**	12052.04	9083.78	1.33	-	-	-	te	Matsumoto 2015 [44]	135
2400	iv (inf) 46h	1	**5-FU**	11621.24	5613.26	2.07	-	-	-	te	Matsumoto 2015 [44]	136
2400	iv (inf) 46h	1	**5-FU**	12026.19	6495.80	1.85	-	-	-	te	Matsumoto 2015 [44]	137
2400	iv (inf) 46h	1	**5-FU**	11254.37	8718.54	1.29	-	-	-	te	Matsumoto 2015 [44]	138
2400	iv (inf) 46h	1	**5-FU**	12167.92	7777.47	1.56	-	-	-	te	Matsumoto 2015 [44]	139
400	iv (bol), LD	33	**5-FU**	2659.19	1942.03	1.39	-	-	-	te	Eatock 2005 [45]	68
600	iv (inf) 22h, MD											
400	iv (bol), LD	9	**5-FU**	6932.09	6048.14	1.15	-	-	-	te	Joel 2004 [46]	71
600	iv (inf) 22h, MD											
400	iv (bol), LD	18	**5-FU**	3631.35	2652.72	1.37	-	-	-	te	Joulia 1999 [47]	73
600	iv (inf) 22h, MD											
400	iv (bol), LD	6	**5-FU**	5047.14	4819.01	1.05	-	-	-	te	Joulia 1999 [47]	74
900	iv (inf) 22h, MD											
400	iv (bol), LD	8	**5-FU**	6228.44	4494.74	1.39	-	-	-	te	Joulia 1999 [47]	75
1200	iv (inf) 22h, MD											
600	iv (inf) 0.5h, LD	5	**5-FU**	5727.93	5836.75	0.98	-	-	-	ta	Wattanatorn 1997 [8]	81
600	iv (inf) 22h, MD											
400	iv (bol), LD	10	**5-FU**	16849.49	16609.39	1.01	-	-	-	te	Joel 2004 [46]	72
2400	iv (inf) 46h, MD											
400	iv (bol), LD	53	**5-FU**	11945.13	16961.18	0.70	-	-	-	te	Leong 2012 [48]	76
2400	iv (inf) 46h, MD											
400	iv (bol), LD	16	**5-FU**	8583.33	8066.00	1.06	-	-	-	te	Sharma 2010 [49]	79
2400	iv (inf) 46h, MD											
[b]**500**	po (sol), s.d.	6	**5-FU**	2123.43	1205.74	1.76	73.33	59.96	1.22	ta	Phillips 1980 [22]	2
[b]**500**	po (sol), s.d.	1	**5-FU**	1676.75	718.44	2.33	59.20	38.44	1.54	te	Phillips 1980 [22]	206

Table S3.5: Predicted and observed AUC_{last} and C_{max} values of of 5-fluorouracil and 5,6-dihydrofluorouracil plasma concentrations. (continued)

Dose [mg/m²]	Route	n	Compound	AUC_{last} pred [µmol·h/l]	AUC_{last} obs [µmol·h/l]	Pred/Obs AUC_{last}	C_{max} pred [µmol/l]	C_{max} obs [µmol/l]	Pred/Obs C_{max}	Dataset	Reference	ID
[b]**500**	po (sol), s.d.	1	**5-FU**	1708.14	453.29	3.77	59.13	33.83	1.75	te	Phillips 1980 [22]	207
[b]**500**	po (sol), s.d.	1	**5-FU**	2061.27	946.82	2.18	81.09	93.79	0.86	te	Phillips 1980 [22]	208
[b]**500**	po (sol), s.d.	1	**5-FU**	2224.26	1746.68	1.27	73.33	59.96	1.22	te	Phillips 1980 [22]	209
[b]**500**	po (sol), s.d.	1	**5-FU**	1957.91	749.13	72.81	38.44	1.89	1.22	te	Phillips 1980 [22]	210
[b]**500**	po (sol), s.d.	1	**5-FU**	2125.98	2208.66	0.96	72.56	109.93	0.66	te	Phillips 1980 [22]	211
[a]**15**	po (sol), s.d.	17	**5-FU**	5075.09	4952.13	1.02	154.70	169.36	0.91	te	Harvey 1984 [33]	64
[a]**15**	po (sol), s.d.	17	**5-FU**	5075.09	4239.45	1.20	154.70	171.59	0.90	te	Harvey 1984 [33]	65
[a]**15**	po (sol), s.d.	17	**5-FU**	5075.09	4154.66	1.24	154.70	129.07	1.20	te	Harvey 1984 [33]	66
[a]**15**	po (sol), s.d.	17	**5-FU**	5075.09	4525.01	1.14	154.70	153.52	1.0	te	Harvey 1984 [33]	67
250	iv (bol), s.d.	20	**DHFU**	1693.65	2384.84	0.71	26.07	26.35	0.99	te	Bocci 2000 [23]	11
250	iv (bol), s.d.	188	**DHFU**	1525.87	1590.87	0.96	27.28	27.43	0.99	ta	Bocci 2006 [24]	93
250	iv (bol), s.d.	101	**DHFU**	1753.46	1574.04	1.11	30.70	25.94	1.18	te	Bocci 2006 [24]	94
250	iv (bol), s.d.	87	**DHFU**	1665.87	1697.86	0.98	29.41	29.27	1.00	te	Bocci 2006 [24]	95
250	iv (bol), s.d.	70	**DHFU**	1672.34	1876.97	0.89	29.28	31.24	0.94	te	Bocci 2006 [24]	96
250	iv (bol), s.d.	118	**DHFU**	1678.90	1488.62	1.13	30.09	24.99	1.20	te	Bocci 2006 [24]	97
370	iv (bol), s.d.	20	**DHFU**	2781.78	3913.47	0.71	39.06	39.52	0.99	ta	Bocci 2000 [23]	12
370	iv (bol), s.d.	110	**DHFU**	2753.51	3931.06	0.70	39.21	36.14	1.08	te	Paolo 2001 [26]	106
370	iv (bol), s.d.	110	**DHFU**	2753.19	3245.92	0.85	39.26	36.14	1.09	te	Paolo 2001 [26]	107
400	iv (bol), s.d.	18	**DHFU**	2662.00	2724.58	0.98	40.79	43.08	0.95	te	Casale 2004 [27]	5
400	iv (bol), s.d.	18	**DHFU**	2662.00	3082.31	0.86	40.79	50.72	0.80	te	Casale 2004 [27]	7
400	iv (bol), s.d.	18	**DHFU**	2662.00	2782.16	0.96	40.79	33.08	1.23	te	Casale 2004 [27]	8
500	iv (bol), s.d.	10	**DHFU**	3774.53	2896.14	1.30	48.87	23.70	2.06	ta	Heggie 1987 [32]	23
425	iv (inf), s.d.	12	**DHFU**	2950.68	2389.62	1.23	41.87	25.36	1.65	te	Hoekstra 2005 [36]	25
Pred/Obs within twofold (Range)*					**97.22%; 70/72 (0.41–2.43)**			**95.00%; 19/20 (0.80–2.06)**				
GMFE (Range)*					**1.23 (1.00–2.43)**			**1.20 (1.00–2.06)**				

5-FU, 5-fluorouracil; **AUC_{last}**, area under the plasma concentration-time curve calculated from the first to the last measurement; **bol**, bolus injection; **C_{max}**, maximum concentration; **DHFU**, 5,6-dihydrofluorouracil ; **GMFE**, geometric meand fold error; **inf**, continuous infusion; **iv**, intravenous; **LD**, loading dose; **MD**, multiple dose; **obs**, observed; **po**, oral; **pred** predicted; **Route**, route of administration; **s.d.**, single dose; **sol**, solution; **te**, test dataset (model evaluation); **ta**, training dataset (parameter optimization).

*, AUC_{last} and C_{max} values are listed for individual profiles, but mean and median GMFE values were only calculated for mean profiles.

[a], dose relative in mg/kg bodyweight

[b], absolute dose in mg

S3.4.5 Local sensitivity analysis

Figures S3.4.26 and S3.4.27 show the local sensitivity analysis of the AUC to single parameter changes of the compounds 5-fluorouracil and 5,6-dihydrofluorouracil. Sensitivity of the model to single parameters was determined as change of the simulated AUC extrapolated to infinity from start time of 5-fluorouracil application of a continuous infusion of 5250 mg/m²/72h. A sensitivity value of -0.5 indicates a 5% decrease of the simulated AUC if the examined parameter is incraeased by 10%. For both compounds, fraction unbound was the most sensitive parameter.

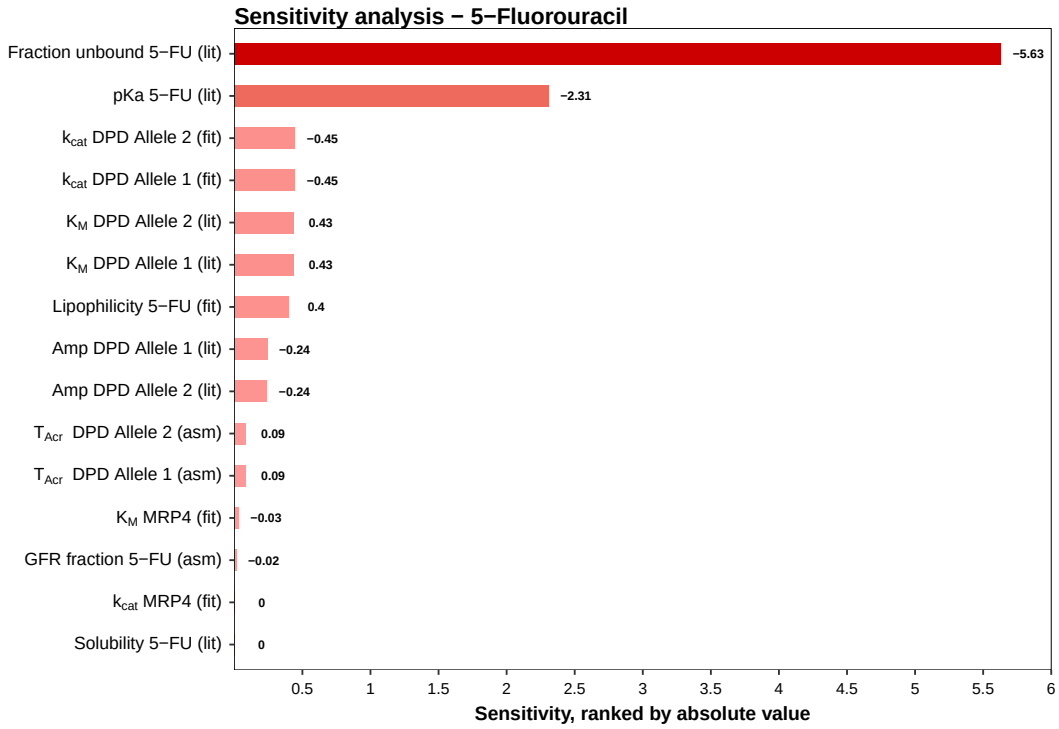

Figure S3.4.26: **5-Fluorouracil PBPK model sensitivity analysis - 5-fluorouracil.** **5-FU**, 5-fluorouracil; **Amp**, amplitude; **asm**, assumed; **DPD**, dihydropyrimidine dehydrogenase; **fit**, fitted; **GFR**, glomerular filtration rate; $\mathbf{k_{cat}}$, catalytic rate constant; $\mathbf{K_M}$, Michaelis-Menten constant; **MRP4**, multi drug resistence protein 4; **lit**, literature; **pKa**, acidic dissociation constant; $\mathbf{T_{Acr}}$, shift in time of maximum enzyme activity.

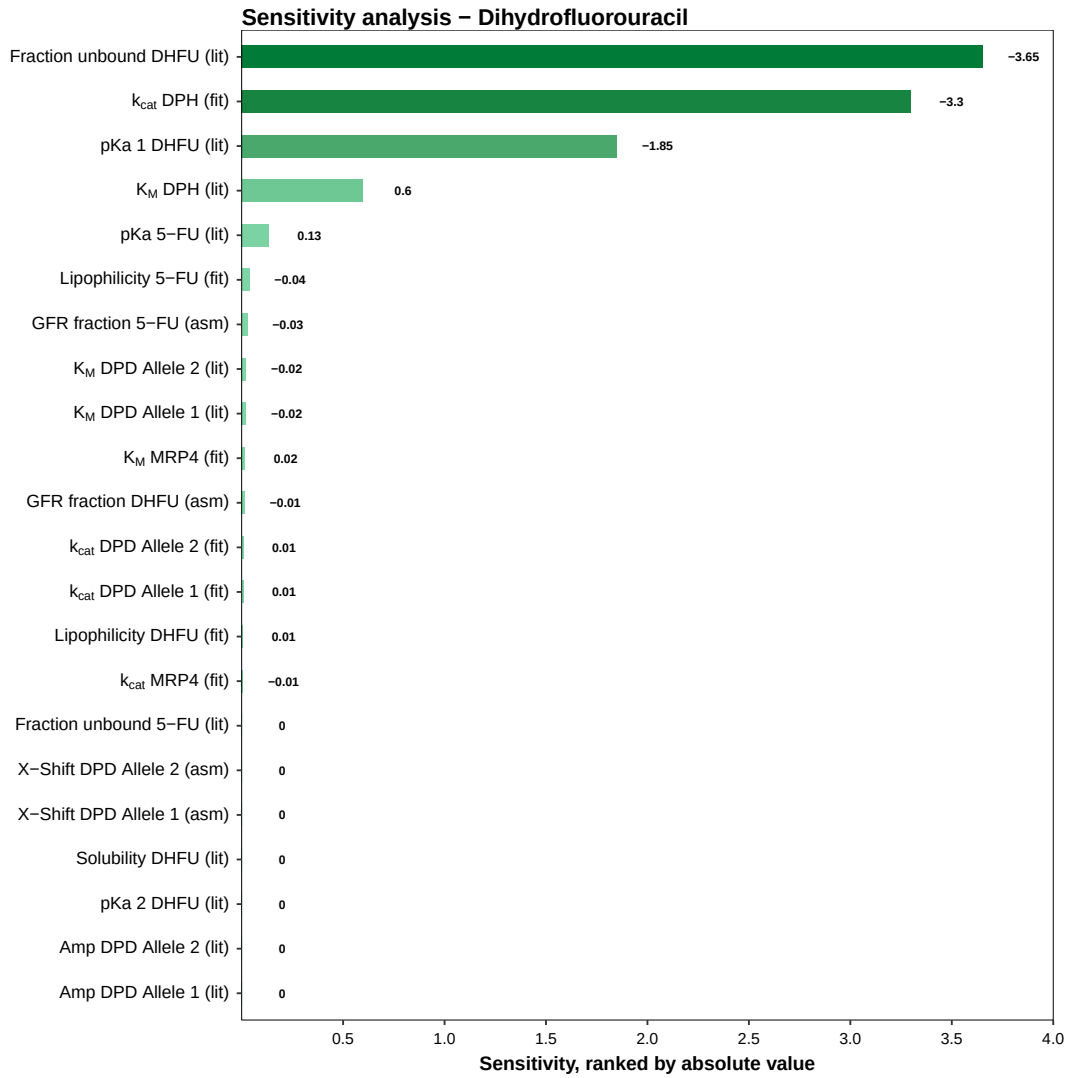

Figure S3.4.27: **5-Fluorouracil PBPK model sensitivity analysis - 5,6-dihydrofluorouracil.** **5-FU**, 5-fluorouracil; **Amp**, amplitude; **asm**, assumed; **DHFU**, 5,6-dihydrofluorouracil; **DPD**, dihydropyrimidine dehydrogenase; **DPH**, dihydropyrimidinase; **fit**, fitted; **GFR**, glomerular filtration rate; $\mathbf{k_{cat}}$, catalytic rate constant;$\mathbf{K_M}$, Michaelis-Menten constant; **MRP4**, multi drug resistence protein 4; **lit**, literature; **pKa**, acidic dissociation constant; $\mathbf{T_{Acr}}$, shift in time of maximum enzyme activity.

S3.5 Individual prediction of constant rate infusions with *IVIVE*

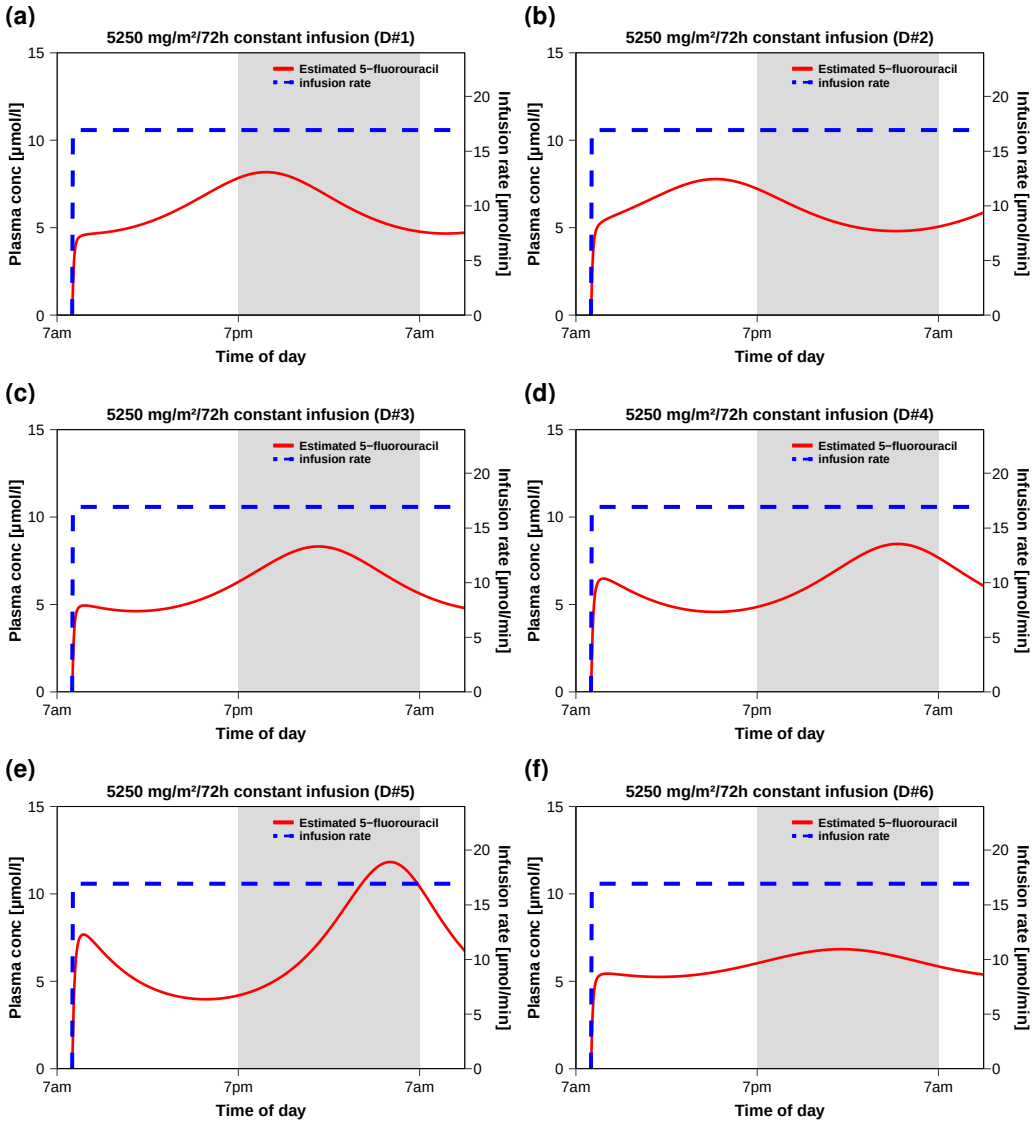

Figure S3.5.28: **Plasma 5-fluorouracil during constant rate infusions** in cancer patients on a linear scale. The shaded areas illustrate night time. DPD activities were estimated from relative *DPYD* mRNA expressions [12] as described in Section S1.4.2. **DHU**/**U**, dihydrouracil-to-uracil plasma concentration ratio; **DPD**, dihydropyrimidine dehydrogenase.

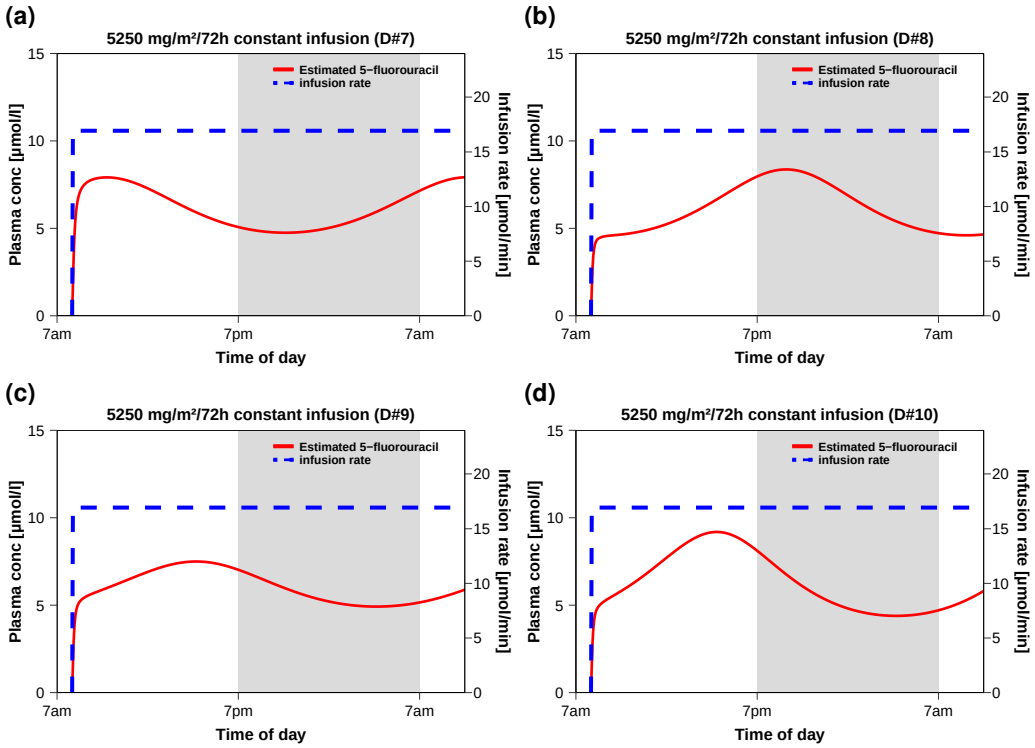

Figure S3.5.29: **Plasma 5-fluorouracil during constant rate infusions** in cancer patients on a linear scale. The shaded areas illustrate night time. DPD activities were estimated from relative *DPYD* mRNA expressions [12] as described in Section S1.4.2. **DHU**/**U**, dihydrouracil-to-uracil plasma concentration ratio; **DPD**, dihydropyrimidine dehydrogenase.

S4 Chronomodulated infusions

S4.1 Background

Chronomodulated infusion rates were simulated according to Eq. (S9). Here, infusion rates were informed by rates reported in the respective clinical study report. If no data were given, the amplitude of the chronomodulated rate was informed from a similar published rate, while $\mathbf{T_{Acr}}$ was adapted individually to fit the day time of the observed data. Further details on the parameters are provided in Table S4.2.

S4.2 Clinical studies

In the following Table S4.1 clinical studies are listed, where 5-fluorouracil was administered as a chronomodulated infusion. Indiviuals were modeled according to demographics reported in the respective study. If no data on the demographics was reported, a mean male individual was assumed as described in Section S1.3.

Table S4.1: Clinical studies used for chronomodulated 5-fluorouracil infusions

Dose [mg/m²]	Route	n	Age [years]	Females [%]	Dataset	Reference
1250	iv (inf) 96h	27	^{m}50 (37–78)	22	te	Grem 2001 [40]
1250	iv (inf) 96 h	14	^{m}46 (28–71)	21	ta	Takimoto 1999 [41]
2600	iv (inf), 48h	42	^{m}58 (34–74)	42.8	te	Falcone 2001 [55]
2600	iv (inf), 48h	41	^{m}57 (38–75)	41.4	te	Falcone 2001 [55]
2800	HAI (inf), 72h	11	^{m}60 (33–72)	36.36	te	Lévi 2017 [56]

BSA, body surface area; **HAI**, hepatic arterial infusion, **inf**, infusion; **iv**, intravenous; **n**, number of individuals studied; **Route**, route of administration; **ta**, training dataset (parameter optimization); **te**, test dataset (model evaluation); **-**, no data available. Values are median and ranges.
^{m}, median

S4.3 Drug-dependent model parameters

Table S4.2: Diurnal parameters of the 5-fluorouracil PBPK model for chronomodulated simulations.

Study (ID)	Amplitude (DPD)	T_{Acr} (DPD) [min]	Amplitude (inf)	T_{Acr} (inf) [min]	Reference
Grem 2001 (860)	^{b}0.124	1219	0.65	434.44	[40]
Takimoto 1999 (800)	^{b}0.124	1285	0.69	624.21	[41]
Falcone 2001 (98)	^{b}0.124	720	0.60	0	[55]
Falcone 2001 (980)	^{b}0.124	720	0.60	0	[55]
Falcone 2001 (99)	^{b}0.245	720	0.60	0	[55]
Falcone 2001 (990)	^{a}0.245	720	0.60	0	[55]
Levi 2017 (Lmean)	0.85	0	0.60	638	[56]
Levi 2017 (#1)	0.77	1415	0.60	638	[56]
Levi 2017 (#2)	0.95	1344	0.60	638	[56]
Levi 2017 (#3)	0.96	0	0.60	638	[56]
Levi 2017 (#4)	0.67	0	0.60	638	[56]
Levi 2017 (#5)	0.86	1356	0.60	638	[56]
Levi 2017 (#6)	1.1	638	0.60	638	[56]
Levi 2017 (#7)	0.58	0	0.60	638	[56]
Levi 2017 (#8)	0.82	28	0.60	638	[56]
Levi 2017 (#9)	0.73	1378	0.60	638	[56]
Levi 2017 (#10)	0.96	0	0.60	638	[56]

DPD, dihydropyrimidine dehydrogenase, **inf**, infusion; $\mathbf{T_{Acr}}$, shift in time of maximum enzyme activity.
^{a}, Mean amplitude of DPD activity measured in human preipheral blood mononclear cells derived from Jacobs et al. 2016 [10]
^{b}, Mean amplitude of DPD activity measured in human preipheral blood mononclear cells derived from Jiang et al. 2004 [11]

S4.4 Concentration-time profiles

Model predictions are shown as solid lines and corresponding observed data as filled dots. Symbols represent the mean values ± sd, if available. Day and night time were visualized with white and shaded areas, respectively.

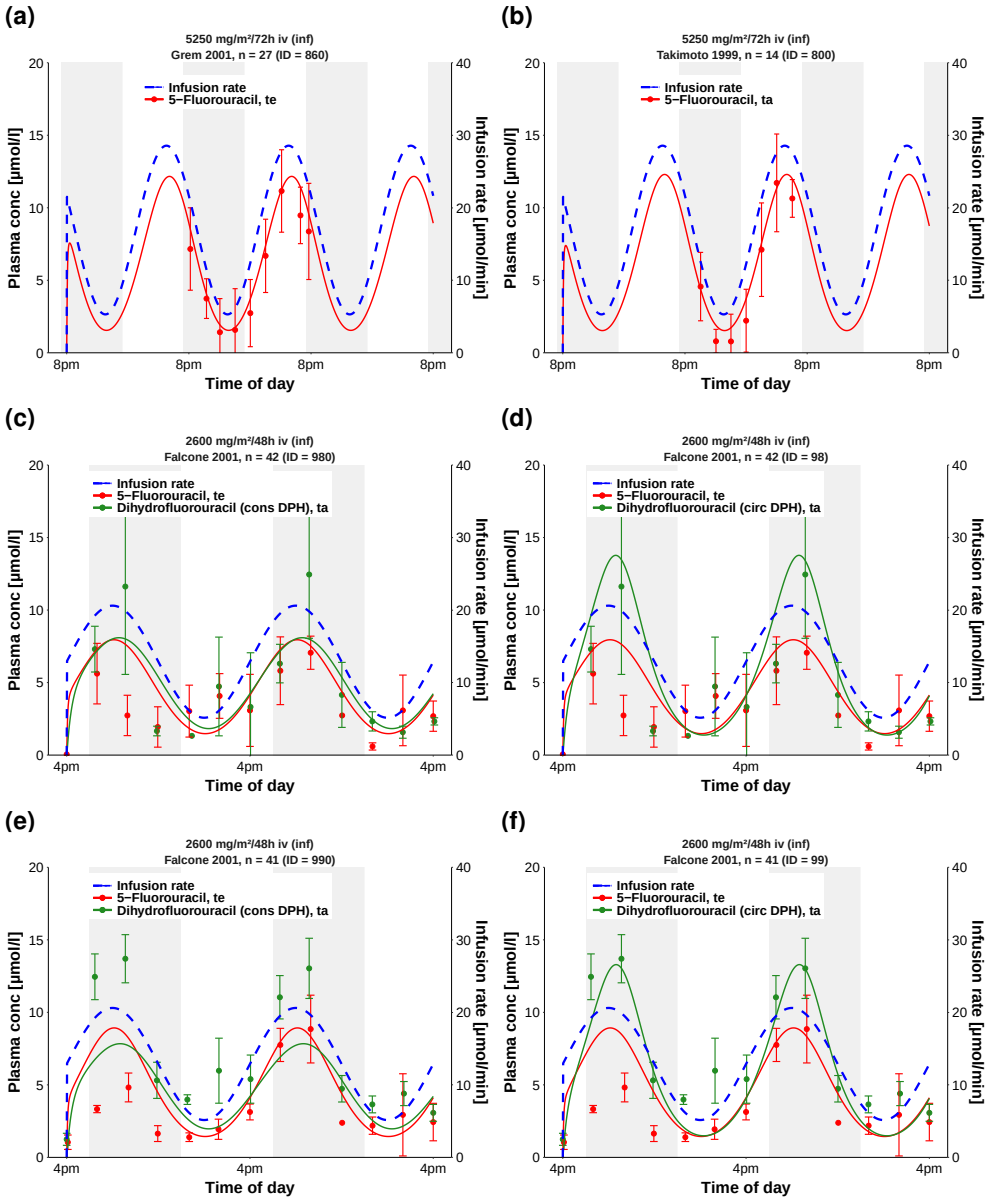

Figure S4.4.1: **Plasma 5-fluorouracil and 5,6-dihydrouracil during chronomodulated administration of 5-fluorouracil** on a linear scale. **circ DPH**, circadian diyhdropyrimidinase activity; **conc**, concentration; **cons DPH**, constant diyhdropyrimidinase activity; **inf**, infusion; **iv**, intavenous; **n**, number of individuals; **ta**, training dataset; **te**, test dataset.

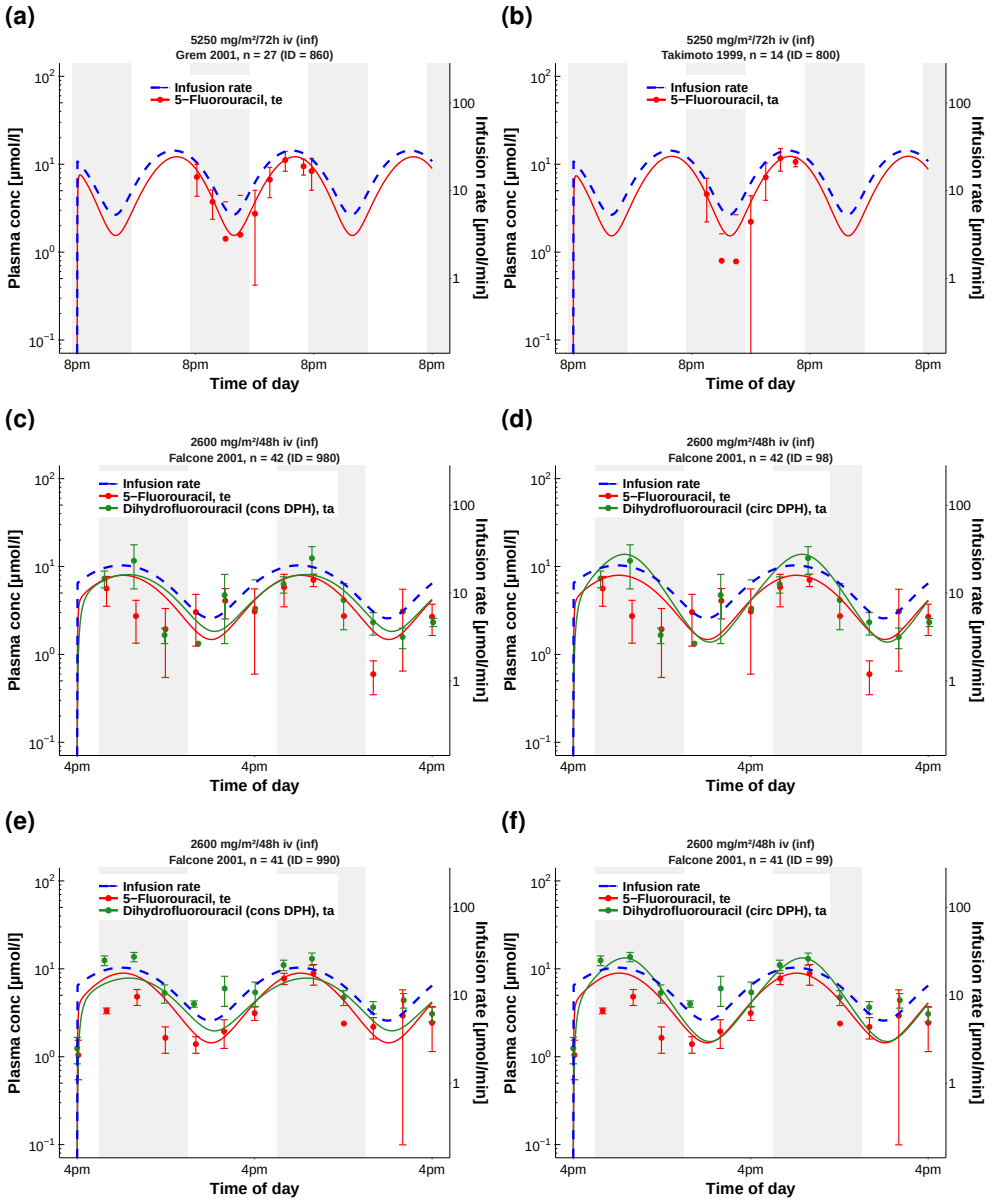

Figure S4.4.2: **Plasma 5-fluorouracil and 5,6-dihydrouracil during chronomodulated administration of 5-fluorouracil** on a semi-logarithmic scale. The shaded areas illustrate night time. **circ DPH**, circadian diyhdropyrimidinase activity; **conc**, concentration; **cons DPH**, constant diyhdropyrimidinase activity; **inf**, infusion; **iv**, intavenous; **n**, number of individuals; **ta**, training dataset; **te**, test dataset.

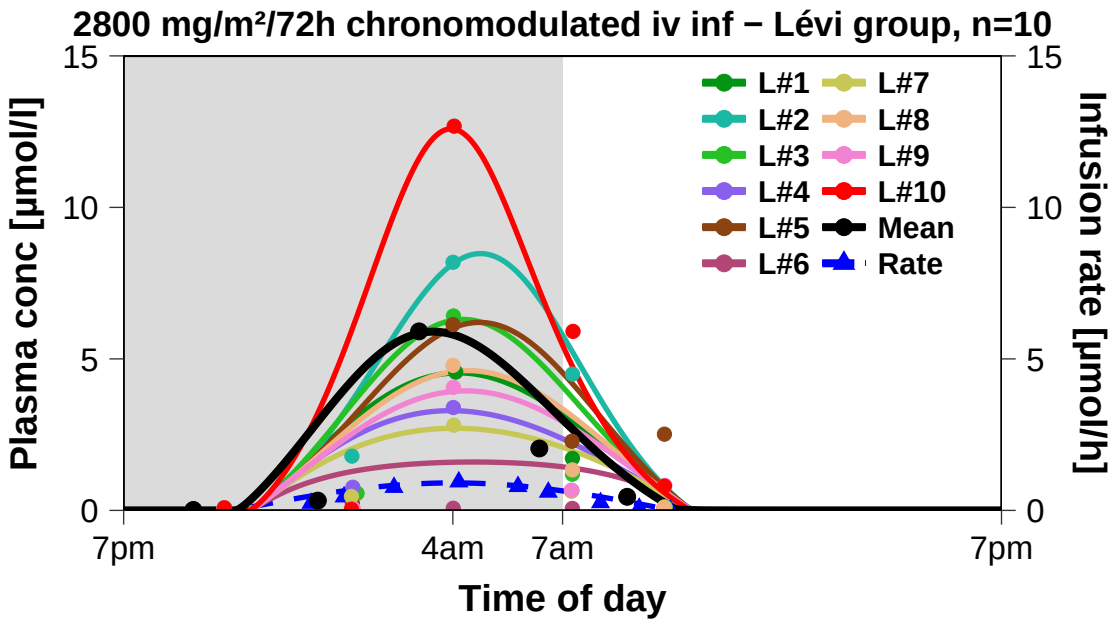

Figure S4.4.3: **Indiviual and mean plasma concentration during the application of a chronomodulated hepatic arterial infusion of Lévi 2017 The shaded area illustrates night time. [56] conc**, concentration;**inf**, infusion; **iv**, intravenous; **L**, individual from the Lévi cohort, **n**, number of individuals

S4.5 Model evaluation

S4.5.1 Predicted compared to observed concentrations goodness-of-fit plots

Following, goodness-of-fit plots of predicted compared to observed plasma concentrations for every study are illustrated in Fig. S4.5.4. Details on dosing regimens, study populations and literature references are listed in Table S4.1. Predicted and observed PK parameters are summarized in Table S4.4.

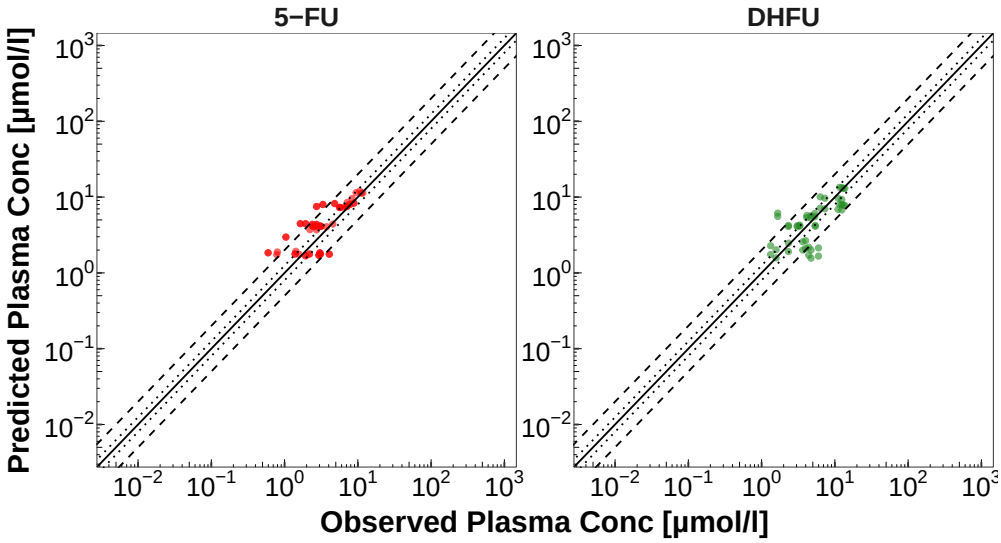

Figure S4.5.4: **Predicted compared to observed plasma concentrations**. Illustrated are values for 5-fluorouracil and 5,6-dihydrofluorouracil. The solid lines mark the line of identity. Dotted lines indicate 1.25-fold, dashed lines 2-fold deviation. **5-FU**, 5-fluorouracil; **DHFU**, 5,6-dihydrofluorouracil.

S4.5.2 Mean relative deviation and median symmetric accuracy of plasma concentration predictions

Table S4.3: Mean relative deviation and median symmetric accuracy values of 5-fluorouracil and 5,6-dihydrofluorouracil plasma concentrations

Dose [mg/m²]	Route	n	Compound	MRD	MSA [%]	Dataset	Reference	ID
1750	iv (inf) 72h	14	**5-FU**	1.19	14.40	te	Grem 2001 [40]	860
1750	iv (inf) 72h	14	**5-FU**	1.63	12.58	ta	Takimoto 1999 [41]	800
2600	iv (inf) 48h	42	**5-FU**	1.89	62.17	te	Falcone 2001 [55]	98
2600	iv (inf) 48h	42	**5-FU**	1.77	68.88	te	Falcone 2001 [55]	99
2600	iv (inf) 48h	42	**DHFU**	1.76	31.96	te	Falcone 2001 [55]	98
2600	iv (inf) 48h	42	**DHFU**	1.73	31.73	te	Falcone 2001 [55]	99
2600	iv (inf) 48h	42	**DHFU**	1.70	36.67	te	Falcone 2001 [55]	980
2600	iv (inf) 48h	42	**DHFU**	1.68	54.94	te	Falcone 2001 [55]	990
			Mean	**1.67** (1.20–1.89)	**34.32** (12.58–68.88)			
			Median	**1.72** (1.20–1.89)	**39.17** (12.58–68.88))			
				100% (10/10) < 2				

5-FU, 5-fluorouracil; **DHFU**, 5,6-dihydrofluorouracil ; **inf**, continuous infusion; **iv**, intravenous; **MRD**, mean relative deviation; **MSA**, median symmetric accuracy; **n**, number of individuals studied; **Route**, route of administration; **te**, test dataset (model evaluation); **ta**, training dataset (parameter optimization).

S4.5.3 AUC_{last} goodness-of-fit plots

In the following section, goodness-of-fit plots of predicted compared to observed AUC_{last} values for every study are illustrated in Fig. S4.5.5. Details on dosing regimens, study populations and literature references are listed in Table S4.1. Predicted and observed PK parameters are summarized in Table S4.4.

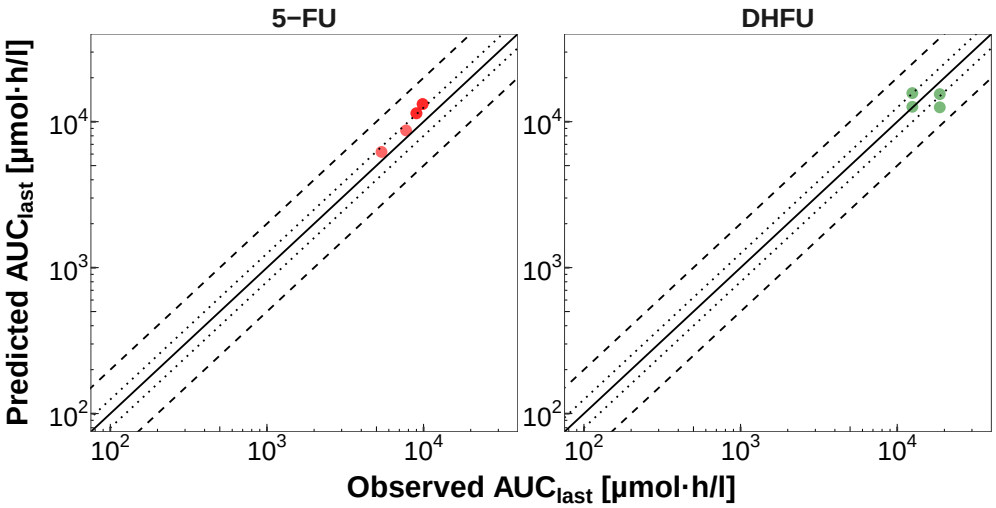

Figure S4.5.5: **Predicted compared to observed plasma AUC_{last} values**. Illustrated are values for 5-fluorouracil and 5,6-dihydrofluorouracil for training and test data. The solid lines mark the line of identity. Dotted lines indicate 1.25-fold, dashed lines 2-fold deviation. **5-FU**, 5-fluorouracil; **AUC_{last}**, area under the plasma concentration time curve from the first to last time point of concentration measurement; **DHFU**, 5,6-dihydrofluorouracil.

S4.5.4 Geomentric mean fold error of predicted AUC_{last} values

Table S4.4: Predicted and observed AUC_{last} and C_{max} values of of 5-fluorouracil and 5,6-dihydrofluorouracil plasma concentrations

Dose [mg/m²]	Route	n	Compound	AUC_{last} pred [µmol·h/l]	AUC_{last} obs [µmol·h/l]	Pred/Obs AUC_{last}	Dataset	Reference	ID
1750	iv (inf) 72h	14	**5-FU**	8716.98	7732.06	1.13	te	Grem 2001 [40]	860
1750	iv (inf) 72h	14	**5-FU**	6208.21	5386.58	1.15	ta	Takimoto 1999 [41]	800
2600	iv (inf) 48h	42	**5-FU**	11423.33	9001.56	1.27	te	Falcone 2001 [55]	98
2600	iv (inf) 48h	41	**5-FU**	13208.32	9863.52	1.34	te	Falcone 2001 [55]	99
2600	iv (inf) 48h	42	**DHFU**	15709.49	12487.03	1.26	te	Falcone 2001 [55]	98
2600	iv (inf) 48h	41	**DHFU**	15450.25	18694.87	0.83	te	Falcone 2001 [55]	99
2600	iv (inf) 48h	42	**DHFU**	12650.70	12487.03	1.01	ta	Falcone 2001 [55]	980
2600	iv (inf) 48h	41	**DHFU**	12546.43	18694.87	0.67	ta	Falcone 2001 [55]	990
Pred/Obs within twofold (Range)						**100%; 8/8 (0.67–1.34)**			
GMFE (range)						**1.18 (1.01–1.49)**			

5-FU, 5-fluorouracil; **AUC_{last}**, area under the plasma concentration-time curve calculated from the first to the last measurement; **DHFU**, 5,6-dihydrofluorouracil ; **GMFE**, geometric meand fold error; **inf**, continuous infusion; **iv**, intravenous; **n**, number of individuals studied; **obs**, observed; **pred** predicted; **Route**, route of administration; **te**, test dataset (model evaluation); **ta**, training dataset (parameter optimization).

S4.6 Individual prediction of chronomodulated infusions with *IVIVE*

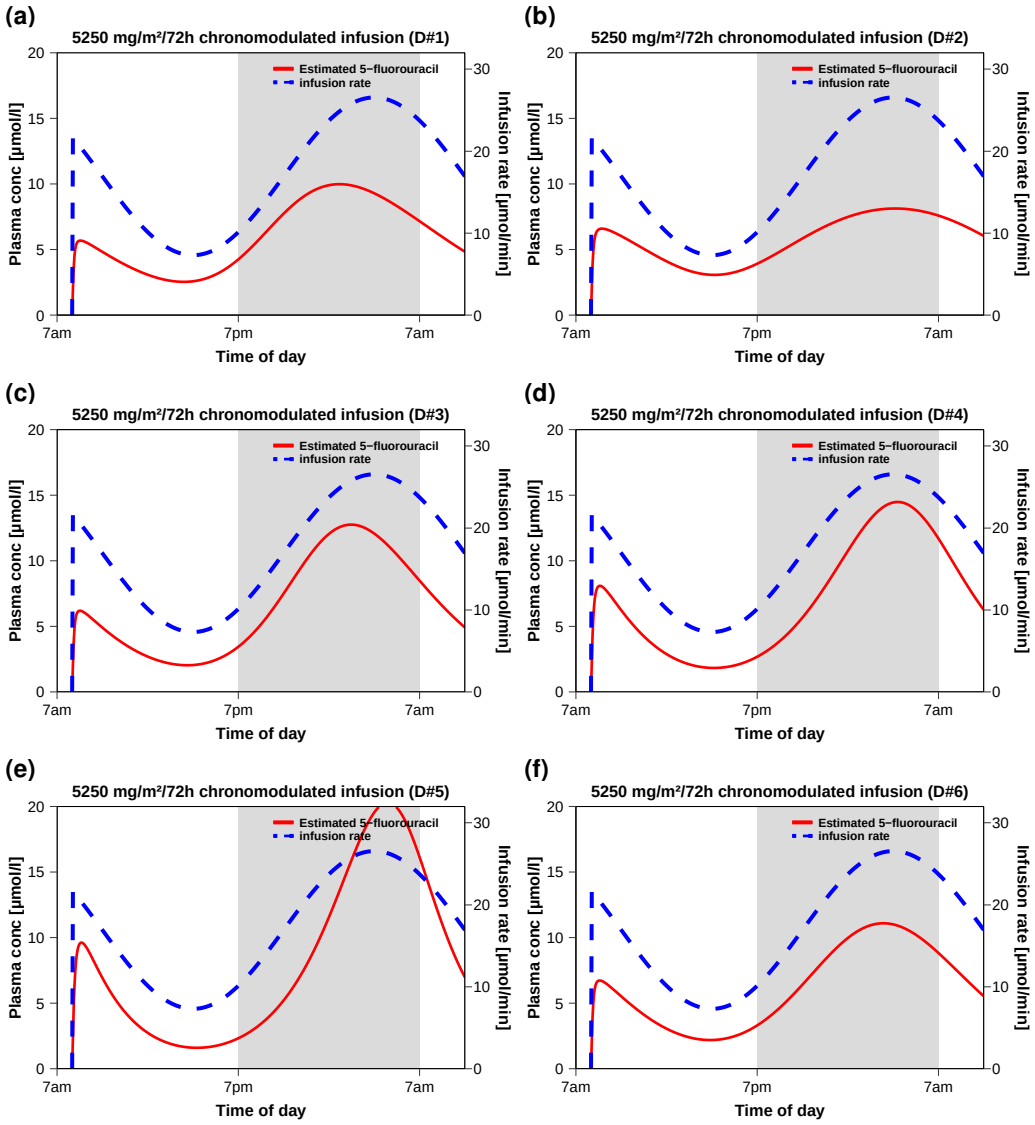

Figure S4.6.6: **Plasma 5-fluorouracil during chronomodulated rate infusions with uniformed peak rate at 4 am** in cancer patients on a linear scale. The shaded areas illustrate night time. DPD activities were estimated from relative *DPYD* mRNA expressions [12] as described in Section S1.4.2. **conc**, concentration; **D**, cancer patient.

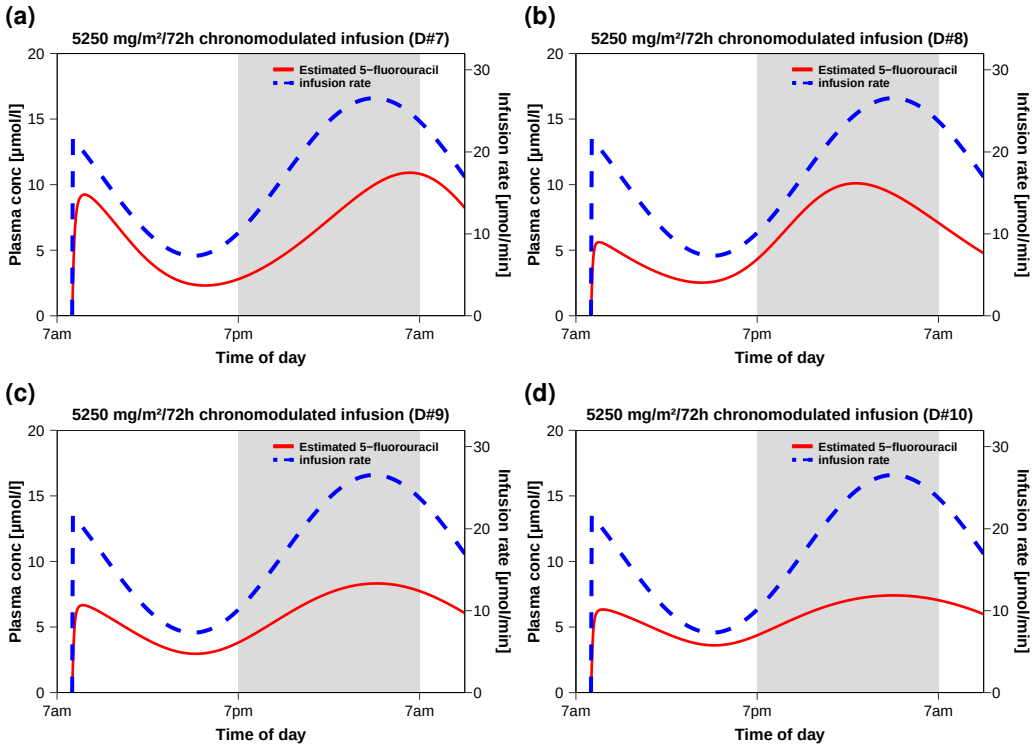

Figure S4.6.7: **Plasma 5-fluorouracil during chronomodulated rate infusions with uniformed peak rate at 4 am** in cancer patients on a linear scale. The shaded areas illustrate night time. DPD activities were estimated from relative *DPYD* mRNA expressions [12] as described in Section S1.4.2.**conc**, concentration; **D**, cancer patient.

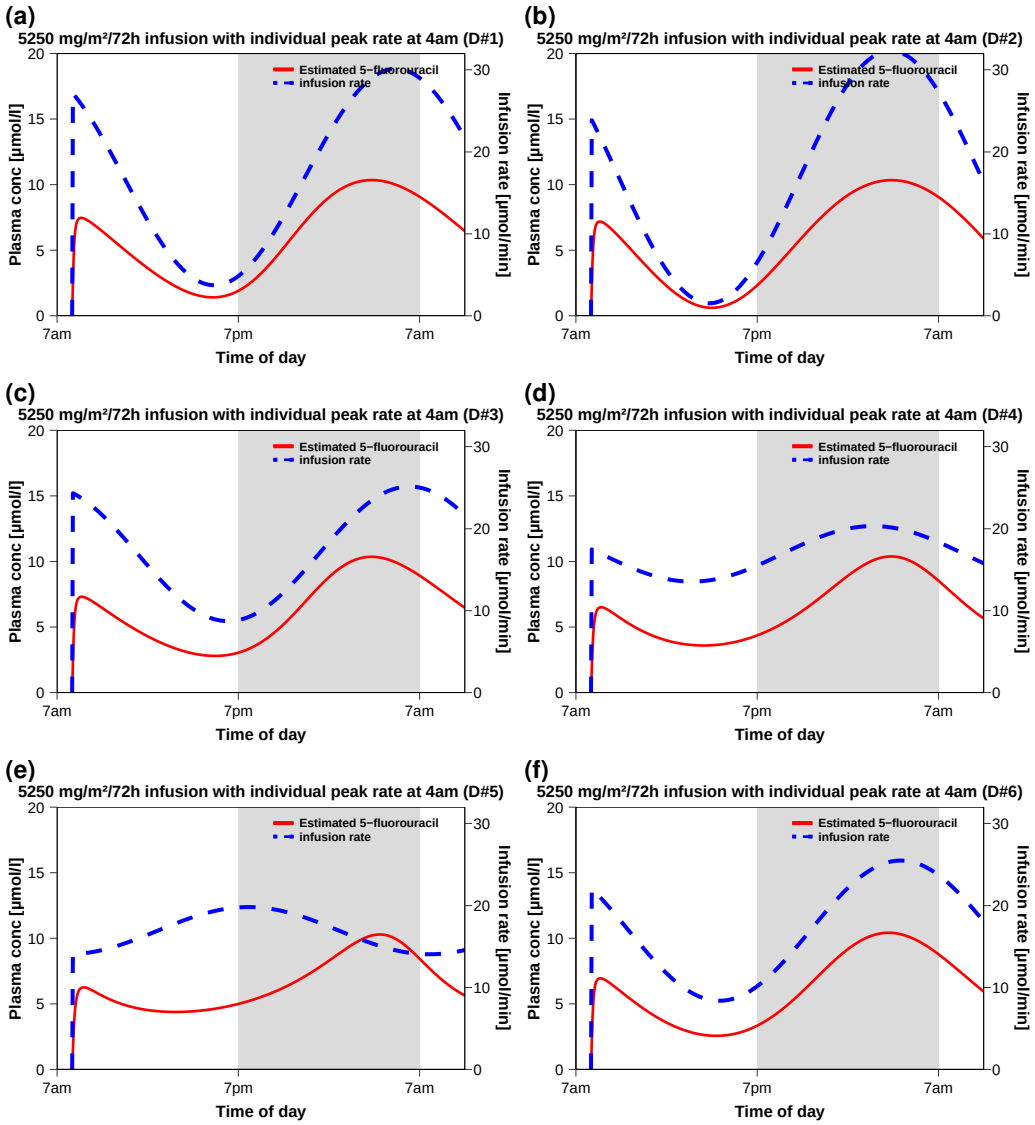

Figure S4.6.8: **Plasma 5-fluorouracil during chronomodulated rate infusions with individual peak rate at 4 am** in cancer patients on a linear scale. The shaded areas illustrate night time. DPD activities were estimated from relative *DPYD* mRNA expressions [12] as described in Section S1.4.2. **conc**, concentration; **D**, cancer patient.

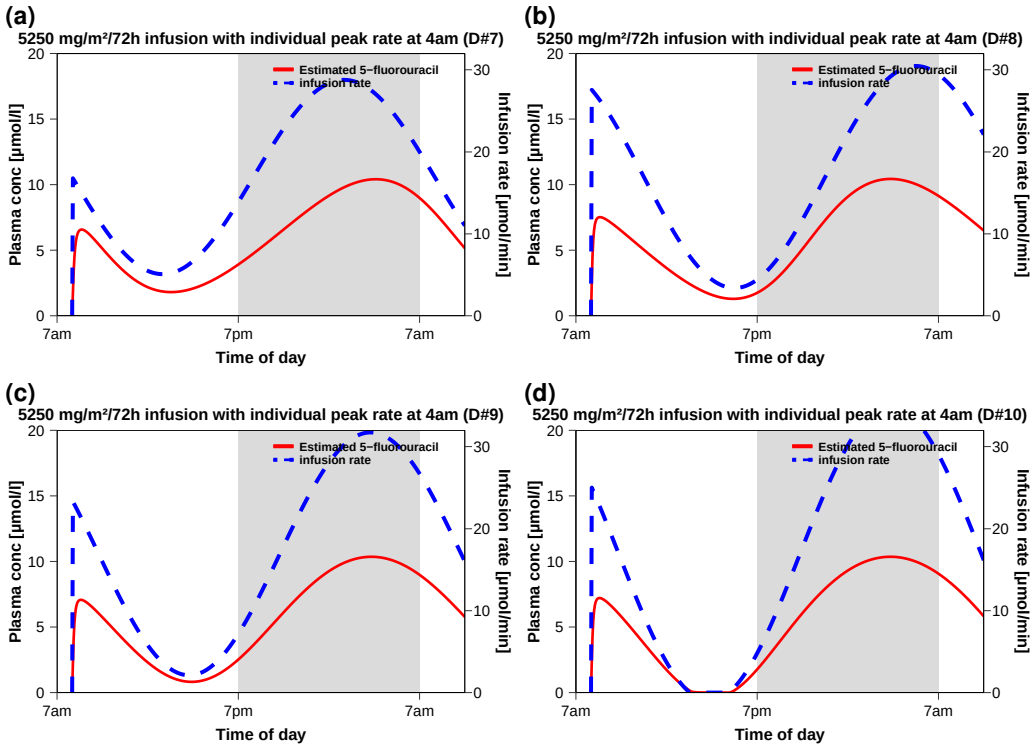

Figure S4.6.9: **Plasma 5-fluorouracil during chronomodulated rate infusions with individual peak rate at 4 am** in cancer patients on a linear scale. The shaded areas illustrate night time. DPD activities were estimated from relative *DPYD* mRNA expressions [12] as described in Section S1.4.2. **conc**, concentration; **D**, cancer patient.

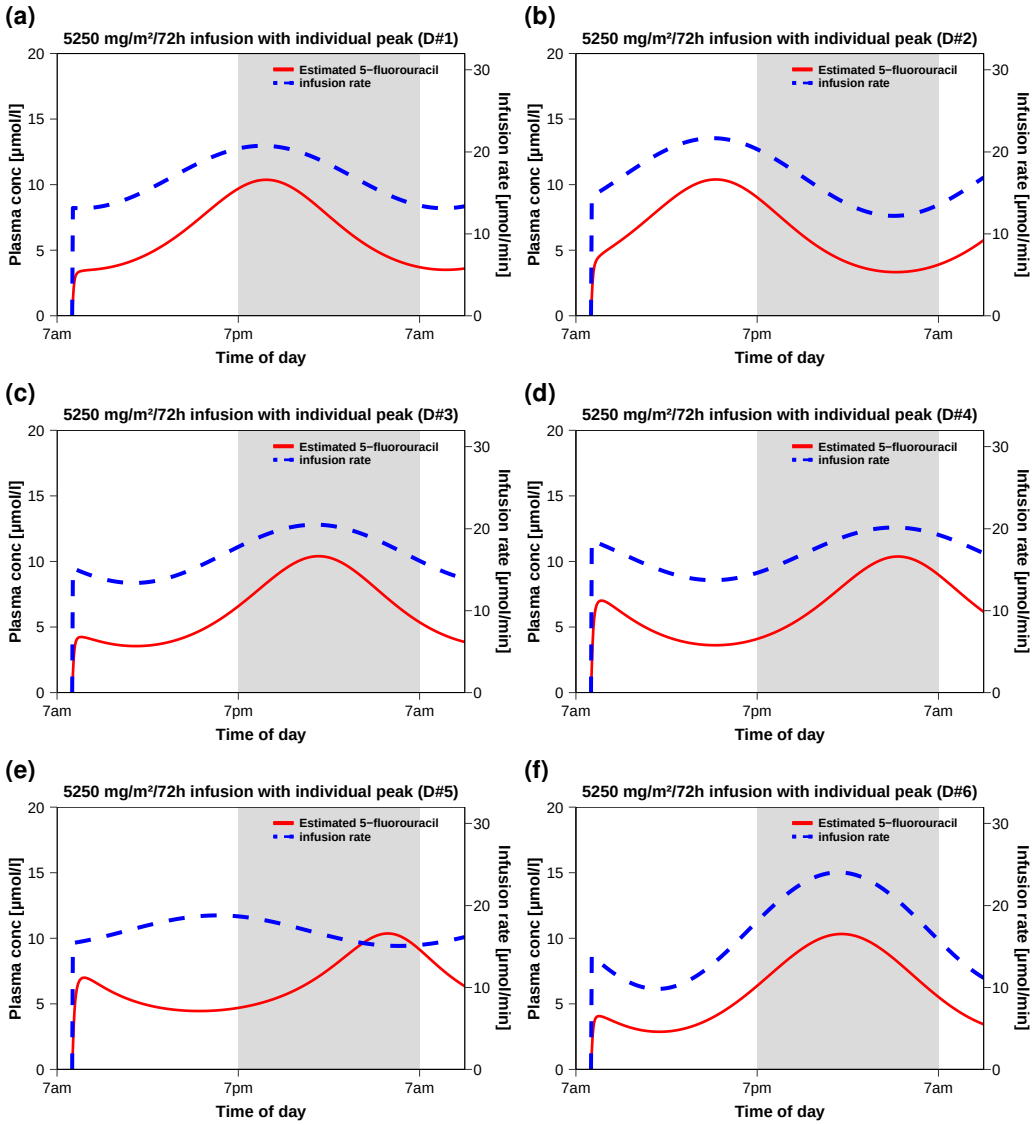

Figure S4.6.10: **Plasma 5-fluorouracil during chronomodulated rate infusions with individual peak rate at an individual time** in cancer patients on a linear scale. The shaded areas illustrate night time. DPD activities were estimated from relative *DPYD* mRNA expressions [12] as described in Section S1.4.2. **conc**, concentration; **D**, cancer patient.

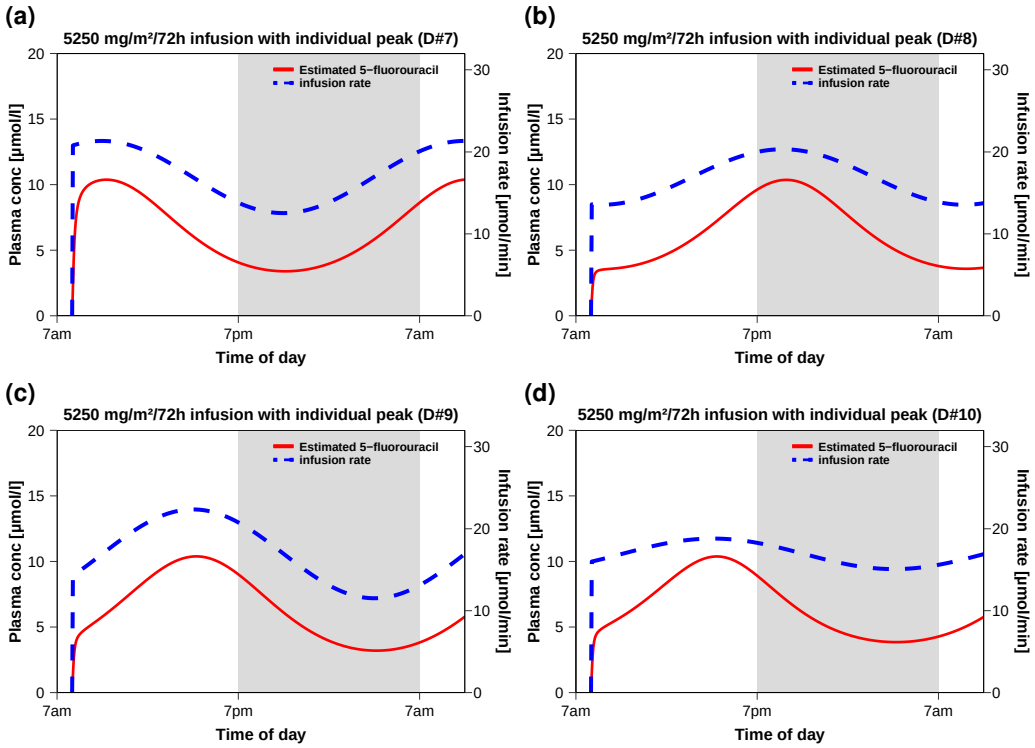

Figure S4.6.11: **Plasma 5-fluorouracil during chronomodulated rate infusions with individual peak rate at an individual time** in cancer patients on a linear scale. The shaded areas illustrate night time. DPD activities were estimated from relative *DPYD* mRNA expressions [12] as described in Section S1.4.2. **conc**, concentration; **D**, cancer patient.

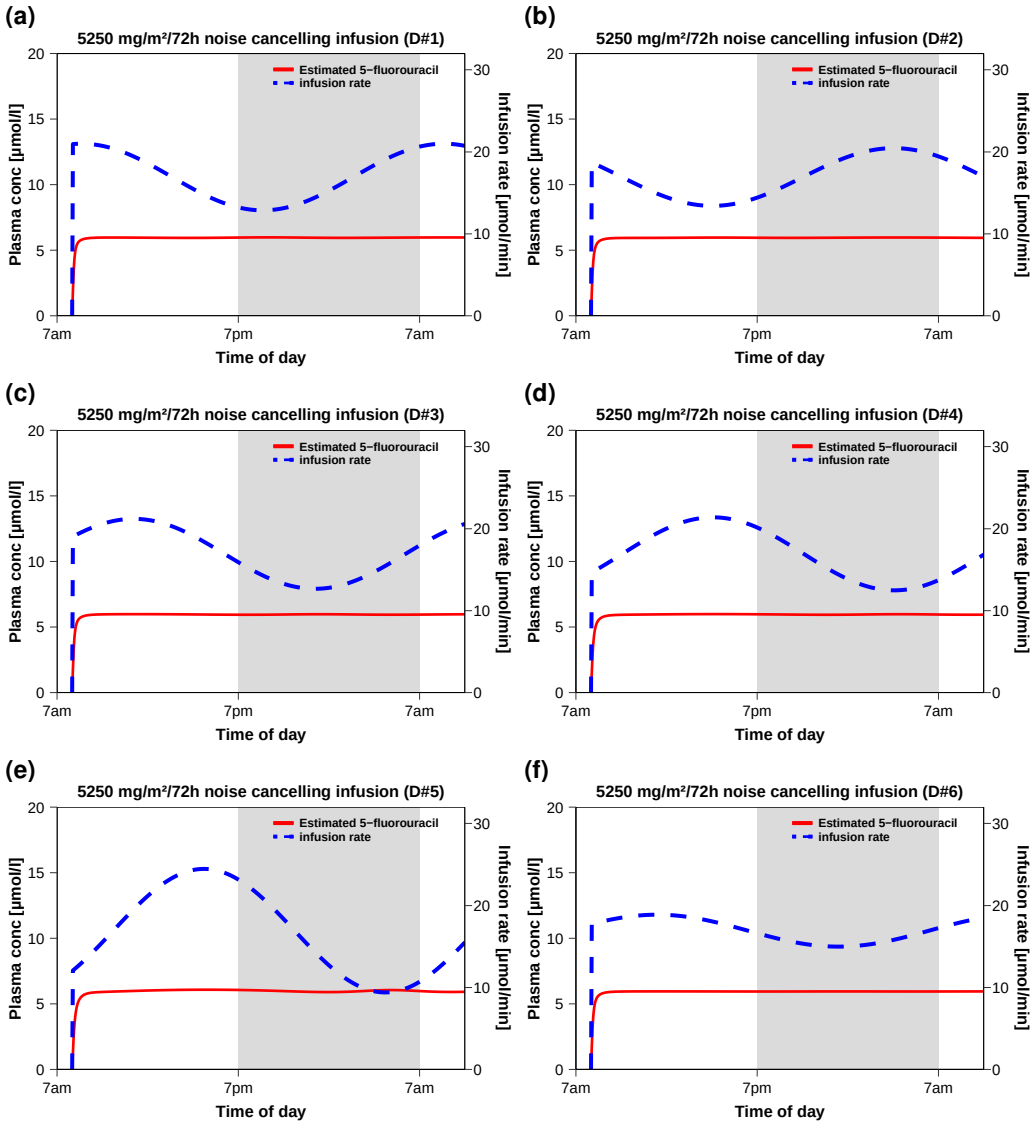

Figure S4.6.12: **Plasma 5-fluorouracil during chronomodulated rate infusions with noise cancelling infusion rate** in cancer patients on a linear scale. The shaded areas illustrate night time. DPD activities were estimated from relative *DPYD* mRNA expressions [12] as described in Section S1.4.2. **conc**, concentration; **D**, cancer patient.

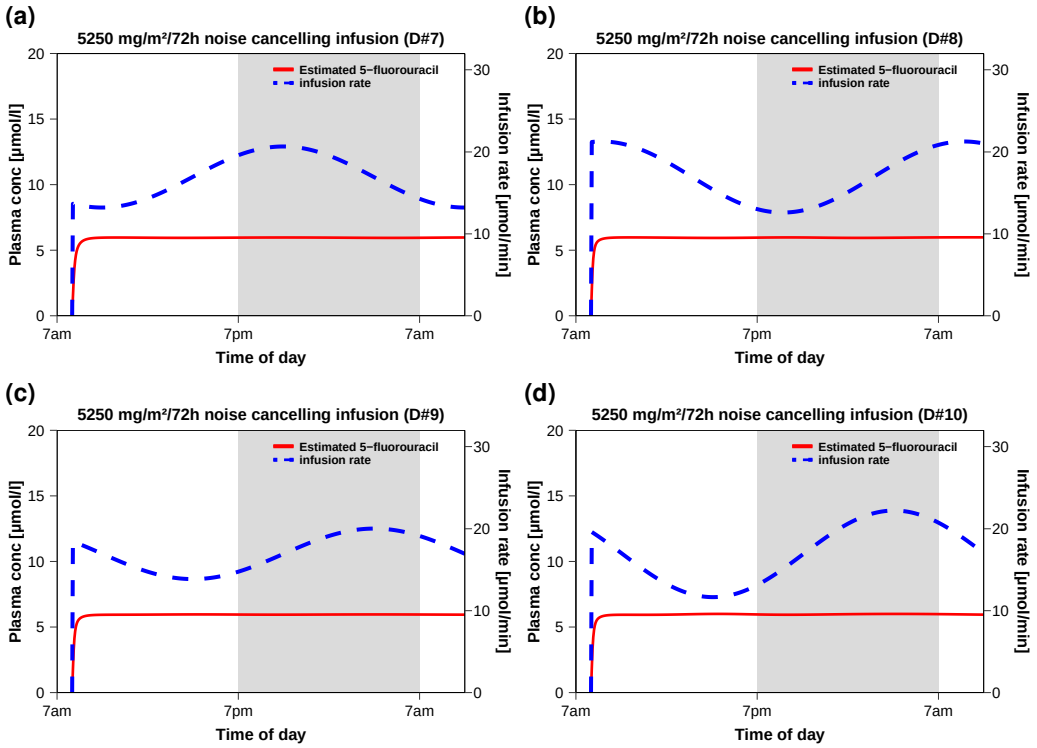

Figure S4.6.13: **Plasma 5-fluorouracil during chronomodulated rate infusions with noise cancelling infusion rate** in cancer patients on a linear scale. The shaded areas illustrate night time. DPD activities were estimated from relative *DPYD* mRNA expressions [12] as described in Section S1.4.2. **conc**, concentration; **D**, cancer patient.

Bibliography

[1] M. Nishimura and S. Naito. Tissue-specific mRNA expression profiles of human phase I metabolizing enzymes except for cytochrome P450 and phase II metabolizing enzymes. *Drug metabolism and pharmacokinetics*, 21(5):357–374, 2006.

[2] N. Kolesnikov, E. Hastings, M. Keays, O. Melnichuk, Y.A. Tang, E. Williams, M. Dylag, N. Kurbatova, M. Brandizi, T. Burdett, K. Megy, E. Pilicheva, G. Rustici, A. Tikhonov, H. Parkinson, R. Petryszak, U. Sarkans, and A. Brazma. ArrayExpress update-simplifying data submissions. *Nucleic Acids Research*, 43(D1):D1113–D1116, 2015.

[3] B. Prasad, K. Johnson, S. Billington, C. Lee, G.W. Chung, C.D.A. Brown, E.J. Kelly, J. Himmelfarb, and J.D. Unadkat. Abundance of drug transporters in the human kidney cortex as quantified by quantitative targeted proteomics. *Drug Metabolism and Disposition*, 44(12):1920–1924, 2016.

[4] D. Scotcher, S. Billington, J. Brown, C.R. Jones, C.D.A. Brown, A. Rostami-Hodjegan, and A. Galetin. Microsomal and cytosolic scaling factors in dog and human kidney cortex and application for in vitro-in vivo extrapolation of renal metabolic clearance. *Drug Metabolism and Disposition*, 45(5):556–568, 2017.

[5] J. Valentin. Basic Anatomical and Physiological Data for Use in Radiological Protection: Reference Values. *Annals of the ICRP*, 32(3-4), 2002. ISSN 0146-6453.

[6] G. Tanaka and H. Kawamura. Anatomical and physiological characteristics for Asian reference man: Male and female of different ages: Tanaka model, 1996.

[7] A.B.P. Van Kuilenburg, P. Häusler, A. Schalhorn, M.W.T. Tanck, J.H. Proost, C. Terborg, D. Behnke, W. Schwabe, K. Jabschinsky, and J.G. Maring. Evaluation of 5-fluorouracil pharmacokinetics in cancer patients with a c.19051G>A Mutation in DPYD by means of a bayesian limited sampling strategy. *Clinical Pharmacokinetics*, 51(3):163–174, 2012.

[8] W. Wattanatorn, H.L. McLeod, F. Macklon, M. Reid, K.E. Kendle, and J. Cassidy. Comparison of 5-fluorouracil pharmacokinetics in whole blood, plasma, and red blood cells in patients with colorectal cancer. *Pharmacotherapy*, 17(5):881–6, 1997.

[9] Y. Yamada, T. Hamaguchi, M. Goto, K. Muro, Y. Matsumura, Y. Shimada, K. Shirao, and S. Nagayama. Plasma concentrations of 5-fluorouracil and F-β-alanine following oral administration of S-1, a dihydropyrimidine dehydrogenase inhibitory fluoropyrimidine, as compared with protracted venous infusion of 5-fluorouracil. *British Journal of Cancer*, 89(5):816–820, 2003.

[10] B.A.W. Jacobs, M.J. Deenen, D. Pluim, J.G.C. Hasselt, M.D. Krähenbühl, R.M.J.M. Geel, N. Vries, H. Rosing, D. Meulendijks, A.M. Burylo, A. Cats, J.H. Beijnen, A.D.R. Huitema, and J.H.M. Schellens. Pronounced between-subject and circadian variability in thymidylate synthase and dihydropyrimidine dehydrogenase enzyme activity in human volunteers. *British Journal of Clinical Pharmacology*, 82 (3):706–716, 2016.

[11] H. Jiang, J. Lu, and J. Ji. Circadian rhythm of dihydrouracil/uracil ratios in biological fluids: A potential biomarker for dihydropyrimidine dehydrogenase levels. *British Journal of Pharmacology*, 141(4): 616–623, 2004.

[12] M. Raida, K.-O. Kliche, W. Schwabe, P. Häusler, J. Clement, D. Behnke, and K. Höffken. Circadian variation of dihydropyrimidine dehydrogenase mRNA expression in leukocytes and serum cortisol levels in patients with advanced gastrointestinal carcinomas compared to healthy controls. *Journal of Cancer Research and Clinical Oncology*, 128(2):96–102, 2002.

[13] M. Shamir, Y. Bar-On, R. Phillips, and R. Milo. SnapShot: Timescales in Cell Biology. *Cell*, 164(6): 1302–1302.e1, 2016.

[14] L. K. Mattison. The Uracil Breath Test in the Assessment of Dihydropyrimidine Dehydrogenase Activity: Pharmacokinetic Relationship between Expired 13CO2 and Plasma [2-13C]Dihydrouracil. *Clinical Cancer Research*, 12(2):549–555, 2006.

[15] M.C. Van Staveren, B. Theeuwes-Oonk, H.J. Guchelaar, A.B.P. Van Kuilenburg, and J.G. Maring. Pharmacokinetics of orally administered uracil in healthy volunteers and in DPD-deficient patients, a possible tool for screening of DPD deficiency. *Cancer Chemotherapy and Pharmacology*, 68(6): 1611–1617, 2011.

[16] Chemicalize entry for uracil: https://chemicalize.com/app/calculation/uracil (accessed on 09.07.2021), .

[17] Chemicalize entry fo dihydrouracil: https://chemicalize.com/app/calculation/dihydrouracil (accessed on 09.07.2021), .

[18] R. Kawai, M. Lemaire, J.L. Steimer, A. Bruelisauer, W. Niederberger, and M. Rowland. Physiologically based pharmacokinetic study on a cyclosporin derivative, SDZ IMM 125. *Journal of pharmacokinetics and biopharmaceutics*, 22(5):327–65, 1994.

[19] T. Rodgers and M. Rowland. Physiologically based pharmacokinetic modelling 2: predicting the tissue distribution of acids, very weak bases, neutrals and zwitterions. *Journal of Pharmaceutical Sciences*, 95(6):1238–57, 2006.

[20] L.M. Berezhkovskiy. Volume of Distribution at Steady State for a Linear Pharmacokinetic System with Peripheral Elimination. *Journal of Pharmaceutical Sciences*, 93(6):1628–1640, 2004.

[21] E. Hishinuma, F. Akai, Y. Narita, M. Maekawa, H. Yamaguchi, N. Mano, A. Oda, N. Hirasawa, and M. Hiratsuka. Functional characterization of 21 allelic variants of dihydropyrimidinase. *Biochemical Pharmacology*, 143:118–128, 2017.

[22] T.A. Phillips, A. Howell, R.J. Grieve, and P.G. Welling. Pharmacokinetics of oral and intravenous fluorouracil in humans. *Journal of Pharmaceutical Sciences*, 69(12):1428–1431, 1980.

[23] G. Bocci, R. Danesi, A.D. Di Paolo, F. Innocenti, G. Allegrini, A. Falcone, A. Melosi, M. Battistoni, G. Barsanti, P.F. Conte, and M. Del Tacca. Comparative pharmacokinetic analysis of 5-fluorouracil and its major metabolite 5-fluoro-5,6-dihydrouracil after conventional and reduced test dose in cancer patients. *Clinical cancer research : an official journal of the American Association for Cancer Research*, 6(8):3032–7, 2000.

[24] G. Bocci, C. Barbara, F. Vannozzi, A. Di Paolo, A. Melosi, G. Barsanti, G. Allegrini, A. Falcone, M. Del Tacca, and R. Danesi. A pharmacokinetic-based test to prevent severe 5-fluorouracil toxicity. *Clinical Pharmacology and Therapeutics*, 80(4):384–395, 2006.

[25] A.B.P. Van Kuilenburg, J.G. Maring, A. Schalhorn, C. Terborg, H. Schmalenberg, D. Behnke, W. Schwabe, K. Jabschinsky, and P. Hausler. Pharmacokinetics of 5-fluorouracil in patients heterozygous for the IVS14+1G > A mutation in the dihydropyrimidine dehydrogenase gene. *Nucleosides, nucleotides & nucleic acids*, 27(6):692–8, 2008.

[26] A. Di Paolo, R. Danesi, A. Falcone, L. Cionini, F. Vannozzi, G. Masi, G. Allegrini, E. Mini, G. Bocci, P.F. Conte, and M. Del Tacca. Relationship between 5-fluorouracil disposition , toxicity and. *Annals of Oncology*, 12(January):1301–1306, 2001.

[27] F. Casale, R. Canaparo, L. Serpe, E. Muntoni, C. D. Pepa, M. Costa, L. Mairone, G.P. Zara, G. Fornari, and M. Eandi. Plasma concentrations of 5-fluorouracil and its metabolites in colon cancer patients. *Pharmacological research*, 50(2):173–9, 2004.

[28] J.G. Maring, A.B.P. van Kuilenburg, J. Haasjes, H. Piersma, H.J.M. Groen, D.R.A. Uges, A.H. Van Gennip, and E.G.E De Vries. Reduced 5-FU clearance in a patient with low DPD activity due to heterozygosity for a mutant allele of the DPYD gene. *British Journal of Cancer*, 86(7):1028–1033, 2002.

[29] J.G. Maring, H. Piersma, A. Van Dalen, H.J.M. Groen, D.R.A. Uges, and E.G.E. De Vries. Extensive hepatic replacement due to liver metastases has no effect on 5-fluorouracil pharmacokinetics. *Cancer chemotherapy and pharmacology*, 51(2):167–73, 2003.

[30] W.E. MacMillan, W.H. Wolberg, and P.G. Welling. Pharmacokinetics of Fluorouracil in Humans. *Cancer Research*, 38(10):3479–3482, 1978.

[31] P.A. Larsson, G. Carlsson, B. Gustavsson, W. Graf, and B. Glimelius. Different intravenous administration techniques for 5-fluorouracil. Pharmacokinetics and pharmacodynamic effects. *Acta Oncol*, 35(2):207–212, 1996.

[32] G.D. Heggie, D.S. Cross, W.J. Huster, and R.B. Diasio. Clinical Pharmacokinetics Urine , and Bile1 of 5-Fluorouracil and Its Metabolites in Plasma ,. *Cancer Research*, (pH 8):2203–2206, 1987.

[33] V.J. Harvey, M.L. Slevin, M.R. Dilloway, P.I. Clark, A. Johnston, and A.F. Lant. The influence of cimetidine on the pharmacokinetics of 5-fluorouracil. *British Journal of Clinical Pharmacology*, 18(3): 421–430, 1984.

[34] Z. Bardakji, J. Jolivet, Y. Langelier, J.-G. Besner, and J. Ayoub. 5-Fluorouracil-metronidazole combination therapy in metastatic colorectal cancer. *Cancer chemotherapy and pharmacology*, 18(2): 140–144, 1986.

[35] L.J. Schaaf, B.R. Dobbs, I.R. Edwards, and D.G. Perrier. Nonlinear pharmacokinetic characteristics of 5-fluorouracil (5-FU) in colorectal cancer patients. *European Journal of Clinical Pharmacology*, 32 (4):411–418, 1987.

[36] R. Hoekstra, F.Y.F.L. De Vos, F.A.L.M. Eskens, E.G.E. de Vries, D.R.A. Uges, R. Knight, R.A. Carr, R. Humerickhouse, J. Verweij, and J.A. Gietema. Phase I study of the thrombospondin-1-mimetic angiogenesis inhibitor ABT-510 with 5-fluorouracil and leucovorin: a safe combination. *European journal of cancer (Oxford, England : 1990)*, 42(4):467–72, 2006.

[37] D.H. Ho, R. Pazdur, W. Covington, N. Brown, Y.Y. Huo, Y. Lassere, and J. Kuritani. Comparison of 5-fluorouracil pharmacokinetics in patients receiving continuous 5-fluorouracil infusion and oral uracil plus N1-(2'- tetrahydrofuryl)-5-fluorouracil. *Clinical Cancer Research*, 4(9):2085–2088, 1998.

[38] G. Metzger, C. Massari, M.-C. Etienne, M. Comisso, S. Brienza, Y. Touitou, G. Milano, G. Bastian, J.L. Misset, and F. Lévi. Spontaneous or imposed circadian changes in plasma concentrations of 5-fluorouracil coadministered with folinic acid and oxaliplatin: Relationship with mucosal toxicity in patients with cancer. *Clinical Pharmacology & Therapeutics*, 56(2):190–201, 1994.

[39] E. Petit, G. Milano, F. Lévi, A. Thyss, F. Bailleul, and M. Schneider. Circadian Rhythm-varying Plasma Concentration of 5-Fluorouracil during a Five-Day Continuous Venous Infusion at a Constant Rate in Cancer Patients. *Cancer Research*, 48(6):1676–1679, 1988.

[40] J.L. Grem, L.K. Yee, B. Schuler, J.M. Hamilton, A.P. Chen, C. Chabuk, F. Grollman, M. Grabenc, C.J. AJlegra, and C.H. Takimoto. N-(phosphonacetyl)-l-aspartate and calcium leucovorin modulation of fluorouracil administered by constant rate and circadian pattern of infusion over 72 hours in metastatic gastrointestinal adenocarcinoma. *Annals of Oncology*, 12(11):1581–1587, 2001.

[41] C.H. Takimoto, L.K. Yee, D.J. Venzon, B. Schuler, F. Grollman, C. Chabuk, J.M. Hamilton, A.P. Chen, C.J. Allegra, and J.L. Grem. High inter- and intrapatient variation in 5-fluorouracil plasma concentrations during a prolonged drug infusion. *Clinical Cancer Research*, 5(6):1347–1352, 1999.

[42] Yoshihiko Furuya, Kyousuke Yamamoto, Norio Kohno, Masahiro Yamamoto, and Yoichi Saitoh. Serum concentrations of 5-fluorouracil achieved with nocturnal constant-rate infusion in patients with disseminated cancer. *Cancer Letters*, 94(2):207–211, 1995. ISSN 03043835. doi: 10.1016/0304-3835(95)03851-M.

[43] Luc Thiberville, Patricia Compagnon, Nicholas Moore, Gerard Bastian, Marie Odile Richard, Marie France Hellot, Colette Vincent, M. M. Kannass, Stephane Dominique, Christian Thuillez, and Georges Nouvet. Plasma 5-fluorouracil and α-fluoro-β-alanin accumulation in lung cancer patients treated with continuous infusion of cisplatin and 5-fluorouracil. *Cancer Chemotherapy and Pharmacology*, 35(1):64–70, 1994. ISSN 03445704. doi: 10.1007/BF00686286.

[44] Hideo Matsumoto, Hideo Okumura, Haruaki Murakami, Hisako Kubota, Masaharu Higashida, Atsushi Tsuruta, Kaoru Tohyama, and Toshihiro Hirai. Fluctuation in plasma 5-fluorouracil concentration during continuous 5-fluorouracil infusion for colorectal cancer. *Anticancer Research*, 35(11):6193–6199, 2015. ISSN 17917530.

[45] M. Eatock, J. Cassidy, J. Johnson, R. Morrison, M. Devlin, R. Blackey, S. Owen, L. Choi, and C. Twelves. A dose-finding and pharmacokinetic study of the matrix metalloproteinase inhibitor MMI270 (previously termed CGS27023A) with 5-FU and folinic acid. *Cancer Chemotherapy and Pharmacology*, 55(1):39–46, 2005.

[46] S.P. Joel, D. Papamichael, F. Richards, T. Davis, V. Aslanis, E. Chatelut, K. Locke, M.L. Slevin, and M.T. Seymour. Lack of pharmacokinetic interaction between 5-fluorouracil and oxaliplatin. *Clinical pharmacology and therapeutics*, 76(1):45–54, 2004.

[47] J.M. Joulia, F. Pinguet, M. Ychou, J. Duffour, C. Astre, and F. Bressolle. Plasma and Salivary Pharmacokinetics of 5-Fluorouracil (5-FU) in Patients with Metastatic Colorectal Cancer Receiving 5-FU Bolus Plus Continuous Infusion with High-dose Folinic Acid. *Eur J Cancer*, 35(2):296–301, 1999.

[48] S. Leong, S.G. Eckhardt, E. Chan, W.A. Messersmith, J. Spratlin, D.R. Camidge, S. Diab, R. Khosravan, X. Lin, E. Chow Maneval, and A.C. Lockhart. A phase I study of sunitinib combined with modified FOLFOX6 in patients with advanced solid tumors. *Cancer chemotherapy and pharmacology*, 70(1):65–74, 2012.

[49] S. Sharma, V. Abhyankar, R.E. Burgess, J. Infante, R.C. Trowbridge, J. Tarazi, S. Kim, M. Tortorici, Y. Chen, and R.L. Robles. A phase I study of axitinib (AG-013736) in combination with bevacizumab plus chemotherapy or chemotherapy alone in patients with metastatic colorectal cancer and other solid tumors. *Annals of Oncology*, 21(2):297–304, 2010.

[50] Drugbank entry for 5-fluorouracil: https://go.drugbank.com/drugs/DB00544 (30.10.2018).

[51] Chemicalize entry for 5,6-dihydrofluorouacil: https://chemicalize.com/app/calculation/FC1CNC(on 07.07.2021, .

[52] Chemspider entry for 5-fluorouracil: http://www.chemspider.com/Chemical-Structure.3268.html (30.10.2018).

[53] B. Reigner, K. Blesch, and E. Weidekamm. Clinical Pharmacokinetics of Capecitabine. *Clinical Pharmacokinetics*, 40(2):85–104, 2001.

[54] S. Yamazaki, M. Hayashi, L.N. Toth, and N. Ozawa. Lack of interaction between bropirimine and 5-fluorouracil on human dihydropyrimidine dehydrogenase. *Xenobiotica*, 31(1):25–31, 2001.

[55] A. Falcone, G. Allegrini, G. Masi, M. Lencioni, E. Pfanner, I. Brunetti, R. Danesi, G. Bocci, M. Del Tacca, and P. Conte. 5-Fluorouracil Administered as a 48-Hour Chronomodulated Infusion in Combination with Leucovorin and Cisplatin: A Randomized Phase II Study in Metastatic Colorectal Cancer. *Oncology*, 61(1):28–35, 2001.

[56] F. Lévi, A. Karaboué, M.C. Etienne-Grimaldi, G. Paintaud, C. Focan, P. Innominato, M. Bouchahda, G. Milano, and E. Chatelut. Pharmacokinetics of Irinotecan, Oxaliplatin and 5-Fluorouracil During Hepatic Artery Chronomodulated Infusion: A Translational European OPTILIV Study. *Clinical Pharmacokinetics*, 56(2):165–177, 2017.